OECD DOCUMENTS

Advanced Monte Carlo Computer Programs for Radiation Transport

Organised by
the OECD *Nuclear Energy Agency*

in co-operation with
The Shielding Laboratory of French CEA, *Saclay* (*France*)

and
EPIC *Radiation Shielding Information Center* (*United States*)

PUBLISHER'S NOTE

The following texts are published in an unembellished form to permit faster distribution at a lower cost.
The views expressed are those of the authors,
and do not necessarily reflect those of the Organisation or of its Member countries.

NUCLEAR ENERGY AGENCY
ORGANISATION FOR ECONOMIC CO-OPERATION AND DEVELOPMENT

ORGANISATION FOR ECONOMIC CO-OPERATION AND DEVELOPMENT

Pursuant to Article 1 of the Convention signed in Paris on 14th December 1960, and which came into force on 30th September 1961, the Organisation for Economic Co-operation and Development (OECD) shall promote policies designed:

- to achieve the highest sustainable economic growth and employment and a rising standard of living in Member countries, while maintaining financial stability, and thus to contribute to the development of the world economy;
- to contribute to sound economic expansion in Member as well as non-member countries in the process of economic development; and
- to contribute to the expansion of world trade on a multilateral, non-discriminatory basis in accordance with international obligations.

The original Member countries of the OECD are Austria, Belgium,Canada, Denmark, France, Germany, Greece, Iceland, Ireland, Italy, Luxembourg, the Netherlands, Norway, Portugal, Spain, Sweden, Switzerland, Turkey, the United Kingdom and the United States. The following countries became Members subsequently through accession at the dates indicated hereafter: Japan (28th April 1964), Finland (28th January 1969), Australia (7th June 1971), New Zealand (29th May 1973) and Mexico (18th May 1994). The Commission of the European Communities takes part in the work of the OECD (Article 13 of the OECD Convention).

NUCLEAR ENERGY AGENCY

The OECD Nuclear Energy Agency (NEA) was established on 1st February 1958 under the name of the OEEC European Nuclear Energy Agency. It received its present designation on 20th April 1972, when Japan became its first non-European full Member. NEA membership today consists of all European Member countries of OECD as well as Australia, Canada, Japan, Republic of Korea, Mexico and the United States. The Commission of the European Communities takes part in the work of the Agency.

The primary objective of NEA is to promote co-operation among the governments of its participating countries in furthering the development of nuclear power as a safe, environmentally acceptable and economic energy source.

This is achieved by:

- *encouraging harmonization of national regulatory policies and practices, with particular reference to the safety of nuclear installations, protection of man against ionising radiation and preservation of the environment, radioactive waste management, and nuclear third party liability and insurance;*
- *assessing the contribution of nuclear power to the overall energy supply by keeping under review the technical and economic aspects of nuclear power growth and forecasting demand and supply for the different phases of the nuclear fuel cycle;*
- *developing exchanges of scientific and technical information particularly through participation in common services;*
- *setting up international research and development programmes and joint undertakings.*

In these and related tasks, NEA works in close collaboration with the International Atomic Energy Agency in Vienna, with which it has concluded a Co-operation Agreement, as well as with other international organisations in the nuclear field.

© OECD 1995
Applications for permission to reproduce or translate all or part of this publication should be made to:
Head of Publications Service, OECD
2, rue André-Pascal, 75775 PARIS CEDEX 16, France.

FOREWORD

New computer architectures such as those realised in vector and parallel machines, the increased availability of core storage and fast data communication have made the Monte Carlo method increasingly more attractive for production runs. Improved biasing schemes, automatic or semi-automatic, have been developed. Powerful graphic displays for both complex geometries and results from calculations are now an integral part of the advanced Monte Carlo program systems.

The Nuclear Science Committee of the OECD Nuclear Energy Agency has found it timely to organise a seminar in which state-of-the-art Monte Carlo programs for nuclear energy applications are presented, and the latest developments and performance of automatic biasing schemes discussed. This aims at speeding up progress towards advanced, user-friendly Monte Carlo systems featuring "intelligent" methods with self-adjusting procedures, that are readily usable by the non-specialist; and at increasing the domain of problems that can be treated with the Monte Carlo method through variance reduction.

There was also a perceived need to exchange views and to motivate progress on problems regarding to the implications of vector and/or parallel computer architectures on the Monte Carlo games and programming techniques, to decide which approaches should be used to make these programs compatible with, and portable to, the different architectures, to improve the exchange of experience and knowledge among experts in the use of the Monte Carlo techniques, and to foster new developments.

These Proceedings are published under the responsibility of the Secretary-General of the OECD.

Table of Contents

SUMMARY 9

SESSION I. **GENERAL PRESENTATION OF KEY FEATURES OF ADVANCED MONTE CARLO PROGRAMS INCLUDING THEIR VALIDATION**

MCNP4A: Features and Philosophy 13
(J. S. Hendricks, Los Alamos National Laboratory, USA)

Overview of Monte Carlo Methodologies in TRIPOLI-3 (French) 21
(T. Vergnaud, CEA, Saclay, France)

Status of the Morse Multigroup Monte Carlo Radiation Transport Code 31
(M. B. Emmet, Oak Ridge National Laboratory, USA)

The Development of the MONK and MCBEND Codes
within the New Monte Carlo Modular Code Scheme MCANO 39
(N. R. Smith & R. J. Brissenden, AEA Technology, UK)
(M. H. Watmough, British Nuclear Fuels plc, UK)

ITS Version 3.0: the Integrated TIGER Series of
Coupled Electron/Photon Monte Carlo Transport Codes 47
(J. A. Halbleib, R. P. Kensek, G. D. Valdez & T. A. Mehlhorn, Sandia National Laboratory, USA)
(S. M. Seltzer & M. J. Berger, National Institute of Standards and Technology, USA)

SESSION II. **AUTOMATIC/SEMI-AUTOMATIC BIASING SCHEMES, THEIR PERFORMANCE AND BENCHMARKING**

Present State of the Direct Statistical Approach
(Cell Model) to Semi-Automatic Variance Reduction 61
(K. W. Burn, ENEA, Italy)

Une Technique de Biaisage Automatique 71
(B. Morillon, CEA, Saclay, France)

Development and Application
of the Automated Monte Carlo Biasing Procedure in SAS4 81
(J. S. Tang & B. L. Broadhead, Oak Ridge National Laboratory, USA)

The Advanced Features of the Monte Carlo Code MCBEND 101
(S. J. Chucas, I. J. Curl & P. C. Miller, AEA Technology, UK)

Some Results concerning the Effect of Variance Reduction
Techniques on the Figure of Merit of Monte Carlo Calculations 119
(C. Oliveira & J. Salgado, ICEN-INETI, Portugal)

Automatic Generation of Biasing Parameters for MORSE Shielding Problems 133
(J. E. Hoogenboom, Delft University of Technology, The Netherlands)
(J. L. Kloosterman, Netherlands Energy Research Foundation, The Netherlands)

Variance Reduction Unique to Coupled Electron/Photon Monte Carlo Transport 141
(J. A. Halbleib, R. P. Kensek & G. D. Valdez, Sandia National Laboratory, USA)

Some Preliminary Remarks concerning the Proposal of an
International Benchmark on Variance Reduction Schemes
Employed in Monte Carlo Neutron and Photon Transport Codes 155
(K. W. Burn, ENEA, Italy)

Summary of Discussion on Variance Reduction Benchmark Proposal 159
(K. W. Burn, ENEA, Italy)

SESSION III. IMPACT OF NEW COMPUTER ARCHITECTURES, SPECIAL MONTE CARLO GAMES

MONTE-4 for Monte Carlo Simulations with High Performance 167
(K. Higuchi, JAERI, Japan)

Distributed Processor Monte Carlo: MCNP Results on a 16-Node IBM Cluster 177
(G. W. McKinney, Los Alamos National Laboratory, USA)

Capability and Performance of Vectorized Monte Carlo
Codes for Neutron and Photon Transport Calculations 185
(M. Nakagawa & T. Mori, JAERI, Japan)

A Communication Library for TRIPOLI-4 193
(J. P. Both, CEA, Saclay, France)

Monte Carlo Calculations on a Parallel Computer Using MORSE-C.G. 203
(J. Wood, University of London, UK)

Parallelism in Continuous Energy Monte Carlo Method for Neutron Transport 217
(Y. Uenohara, Toshiba Corporation, Japan)

SESSION IV. MONTE CARLO PERTUBATIONS, HYBRID METHODS, GEOMETRY MODELLING - ANY NEW MONTE CARLO DEVELOPMENT

Monte Carlo Perturbation Algorithms Exploit New Computer Architectures 231
(H. Rief, ISPRA, Italy)

Hybrid S_n Monte Carlo Research and Results 249
(R. S. Baker, Los Alamos National Laboratory, USA)

Recent Developments and Applications of the MORSE Code 261
(S. N. Cramer, Oak Ridge National Laboratory, USA)

The MASH 1.0 Code System: Utilization of MORSE in the Adjoint Mode 277
(J. A. Johnson & R. T. Santoro, Oak Ridge National Laboratory, USA)

A New Method to Assess Monte Carlo Convergence 295
(R. A. Forster, T. E. Booth & S. P. Pederson, Los Alamos National Laboratory, USA)

A New Approach to Geometry Modelling and Visualisation for MONK and MCBEND 305
(N. R. Smith, E. Shuttleworth, AEA Technology, UK)
(M. H. Watmough, British Nuclear Fuels plc, UK)

Monte Carlo Calculation of a "Quadratic Average" $\int q(x)\, W^2(x)\, dx$ 313
(W. K. Matthes, JRC Euratom, ISPRA)

SESSION V. PRESENTATION OF USER EXPERIENCE, APPLICATIONS, PERFORMANCE WITH EMPHASIS ON NEW ASPECTS

Various applications

A Comparison between the ITS-3 and EGS-4 Monte Carlo Codes in Radiation Physics 319
(P. Andreo, Karolinska Institute and University of Stockholm, Sweden)

Monte Carlo Activities at the Department of Reactor Physics, Chalmers University of Technology 331
(B. Dahl, Chalmers University of Technology, Sweden)

User Experience of the MCNP Code in Nuclear Power Plant Radiation Safety Analyses and Design 337
(T. Eurajoki, IVO International Ltd, Finland)

PETSI, A Package Based on Monte Carlo Techniques to Simulate the Positron Emission Tomography 341
(N. Cerullo & M. Bogliardi, University of Genoa, Italy)
(R. Guzzardi, CNR, Institute of Physical Physiology, Italy)
(P. Riscossa, ANSALDO, Italy)

Comments on Polarization Effects in Photon Transport 347
(J. E. Fernandez & M. Sumini, University of Bologna, Italy)

Comparison of MCNP Simulated and Measured Dose Rates from Depth Distributed Chernobyl $Cs^{134/137}$ in Russia and Ukraine 353
(L. E. De Geer, National Defence Research Establishment, Sweden)

Study of Neutron Spectra and Dose Rates Distribution in the VENUS Reactor Building with the Monte Carlo Code TRIPOLI-2 357
(G. Minsart, Centre d'Etude de l'Energie Nucléaire, Belgium)

Fusion Power Reactor Neutronic Analysis with TRIPOLI-3 367
(J. Ch. Sublet, AEA Technology, UK)

Cross sections and detectors

Probability Tables Cross Sections in Monte Carlo Code TRIPOLI-3 377
(S. H. Zheng, P. Ribon & J. C. Nimal, CEA, Saclay, France)

Monte Carlo Validation of Self-Shielding and Void Effect Calculations 389
(H. Tellier, M. Coste, C. Raepsaet, M. Soldevila & C. van der Gucht, CEA, Saclay, France)

Statistical Generating the Neutron Cross Sections in the Unresolved Resonance Energy Region for Monte Carlo Calculations 401
(A. G. Sboev & M. E. Tsitovich, I. V. Kurchatov Institute of Atomic Energy, Russia)

Use of MCNP in Fusion Blanket Design, ITER Magnet System Shielding Analysis, Benchmark of the EFF (European Fusion File) Neutron Data with the FNG (Frascati Neutron Generator) 14 MeV Neutron Facility 411
(P. Battistoni, L. Petrizzi, M. Pillon & V. Rado, ENEA, Italy)

Calculation of Radiation Fields Inside and Outside the NET Cryostat/Biological Shield during Operation 423
(A. Hogenbirk & K. Verschuur, Netherlands Energy Research Foundation, The Netherlands)

Use of Specific Purpose Monte Carlo Codes in Radiation Application Problems involving Finite Detectors 433
(R. P. Gardner & K. Verghese, North Carolina State University, USA)

Activity at ENEA-DRI (Bologna, Italy) on Monte Carlo Electron Transport 451
(R. Guaraldi & F. Padoani, ENEA, Italy)

CASCADE-5 Monte Carlo Code for Calculation of Average and Fluctuation Characteristics of Electron-Photon Transport 455
(A. V. Lappa & D. S. Burmistrov, Chelyabinsk State University, Russia)

APPENDIX A: Programme and Index 459

APPENDIX B: Organising Committee 466

and List of Participants 467

SUMMARY

The main objectives of the seminar were:

- Speed up progress towards real advanced, user-friendly Monte Carlo systems featuring "intelligent" methods with self adjusting procedures and readily usable by the non-specialist and increase the domain of problems that can be treated with Monte Carlo through variance reduction;

- Exchange views and motivate progress on problems relative to the implications of vector and/or parallel computer architectures on the Monte Carlo games and programming techniques, and as to which approaches should be used so that these programs are compatible with and portable to the different architectures;

- Improve among experts the exchange of experience and knowledge in the use of the Monte Carlo techniques; foster new developments.

A first analysis of the results of the seminar makes it clear that there are several general purpose Monte Carlo radiation transport codes that are well-maintained and under active development:

MCNP, MCANO (MONK and MCBEND), TRIPOLI, MORSE, and the Integrated Tiger Series (ITS).

What is new?

Certainly the codes have been refined and improved.
What is really new is how the field has matured. The emphasis has shifted from basic methods development, which all the codes now have, to engineering: making the codes better tools for users by focussing on quality, structure, new computer architectures, and user-interface.
What is also new is the rising importance of many new applications.

The seminar focussed upon new developments in the codes and their applications and data. The principal new code developments of the most interest and activity were:

1. ease of user interaction with the codes;

2. automatic biasing using diffusion or S_n adjoint solutions on orthogonal grids that overlay the 3D Monte Carlo geometry;

3. workstation and PC based program support including distributed processing;

4. code and data quality assurance (QA) including new statistical analyses of code output;

5. benchmarking.

These areas of development indicate how the Monte Carlo method has matured. A decade ago the emphasis of a Monte Carlo meeting would have been new mathematical sampling schemes, new variance reduction techniques, and new physics models. But these problems are largely solved for neutron and photon problems in nuclear reactor energy ranges, although physics development is still under way for electron codes. The new focus is upon "philosophy" type issues: quality, restructuring, and user-friendly interfaces.

Similarly, applications have changed. In addition to the field of nuclear reactor power generation, many other applications have risen to equal or greater prominence: high-energy physics, medical therapy (such as Boron Neutron Capture Therapy (BNCT) and Positron Emission Tomography (PET)), environmental analysis, nuclear well logging, bulk materials processing such as analysis of minerals (bauxite), nuclear safeguards, criticality safety, and other applications.

The objectives set out were ambitious and it turned out that more work is needed to achieve them. For instance, parallel processing in Monte Carlo seems to have come of age, so that generally distributed codes can be routinely parallelized, this also because computers are more widely available. However, there is still a lack of consensus on the choice of the hardware and software for parallel processing. This subject has been taken up by the NSC-WPAC Task Force on Supercomputing (TFSUP).

Variance reduction methods are not yet as automatic as one would wish or expect. There is still a need for comparing the whole spectrum of MC techniques with respect to efficiency, reliability, robustness and user-friendliness for some basic problem classes. Users still need guidance. There was a special discussion devoted to this, co-ordinated by K. Burn of ENEA. This resulted in a proposal for a benchmark on variance reduction techniques, which is the subject of a separate room document.

The seminar was a success in that it brought together the specialists in this field from all around the world to discuss their experience, views and projects. It has attracted many participants of which about 100 from 20 countries could be accepted. About sixty papers were presented and discussed and are printed in this proceedings.

This type of seminars, participants concluded, are of great value to ensure that users have a correct understanding of the use of codes and their modelling and contribute to user qualification.

Session I

GENERAL PRESENTATION OF KEY FEATURES OF ADVANCED MONTE CARLO PROGRAMS INCLUDING THEIR VALIDATION

CHAIR:

***J. C. NIMAL**, CEA - FRANCE*

MCNP4A: FEATURES AND PHILOSOPHY

John S. Hendricks
Los Alamos National Laboratory
Los Alamos, NM, 87545

ABSTRACT

In this paper we describe MCNP, state its philosophy, introduce a number of new features becoming available with version MCNP4A, and answer a number of questions asked by participants in the workshop.

MCNP is a general-purpose three-dimensional neutron, photon and electron transport code. Its philosophy is "Quality, Value, and New Features." Quality is exemplified by new software quality assurance practices and a program of benchmarking against experiments. Value includes a strong emphasis on documentation and code portability. New features are the third priority.

MCNP4A is now available at Los Alamos. New features in MCNP4A include enhanced statistical analysis, distributed processor multiprocessing, new photon libraries, ENDF/B-VI capabilities, X-Windows graphics, dynamic memory allocation, expanded criticality output, periodic boundaries, plotting of particle tracks via SABRINA, and many other improvements.

I. OVERVIEW OF MCNP

MCNP is a general purpose Monte Carlo code for calculating the time-dependent continuous-energy transport of neutrons, photons, and/or electrons in three-dimensional geometries. Both fixed source and k_{eff} criticality problems can be solved and a number of output tally options are available. Data representations either can be fully or partially continuous or multigroup. The code is rich in variance reduction techniques that improve the efficiency of difficult calculations. The documentation for MCNP is a 600-page manual[1] describing the Monte Carlo theory, geometry, physics, cross sections, variance reduction techniques, tallies, errors, input, and output.

MCNP is used for many applications: nuclear criticality safety, radiation shielding, nuclear safeguards, detector design and analysis, nuclear well logging, personnel dosimetry, health physics, accelerator target design, medical physics and radiotherapy, including BNCT, PET and neutron and photon oncology, aerospace applications, radiography, waste disposal, decontamination and decommissioning, and both fission and fusion reactor design. Recent major applications at Los Alamos include nuclear criticality safety, strategic nuclear materials safeguards, accelerator transmutation of nuclear waste, accelerator production of tritium, TOPAZ reactor analysis, facilities design, health physics, space exploration, environmental science, and reactor design.

MCNP is distributed for Los Alamos by the Radiation Shielding and Information Center (RSIC) in Oak Ridge, Tennessee, and, of course, OECD/Nuclear Energy Agency (NEA) in Saclay, France. We estimate that there are a thousand active users around the world at one hundred installations.

The Monte Carlo method was developed at Los Alamos during the Manhattan Project in the early 1940s. The current MCNP code is the heir to those early efforts. About 400 person-years have been invested into the research, development, programming, documentation, and data bases for MCNP. The first multipurpose code version, MCS, was written in 1963. In the mid-70's, neutron and photon codes were merged to form MCNP, which has undergone major upgrades approximately every two to three years since. MCNP3 was released in 1983 and rewritten in standard Fortran. MCNP3A was released in 1985 and featured a very flexible generalized source. MCNP3B was released in 1988, featuring a repeated structures and/or lattice capability, a multigroup option, and tally output plotting.

MCNP4 was released in July 1990 at Los Alamos and in March 1991 to the Reactor Shielding and Information Center at Oak Ridge (version MCNP4.2). In addition to being the first MCNP specifically designed for UNIX operating systems, MCNP4 had many new features including a continuous-energy electron transport package based on the Sandia National Laboratories Integrated Tiger Series (ITS),[2] a thick-target bremsstrahlung approximation incorporated to model electron-induced photon production using the ITS electron data, shared memory multitasking, a pulse-height tally model to record energy deposition, next-event estimators for $S(\alpha,\beta)$ thermal scattering[3,4] and better random number control.[5]

MCNP4A has just been released at Los Alamos (designated MCNP4XF) and should be available for international distribution next fall. New features in MCNP4A include enhanced statistical analysis[6] and distributed processor multiprocessing[7] which are described elsewhere at this meeting in papers by Art Forster and Gregg McKinney. Other features are new photon libraries, ENDF/B-VI capabilities, X-Windows graphics, dynamic memory allocation, expanded criticality output, periodic boundaries, plotting of particle tracks via SABRINA, and many smaller improvements.

MCNP has an active research program, some of which is described in papers by Ken Burn and Randy Baker at this meeting. Additional studies include investigations by Tom Booth in non-Boltzmann tallies,[8] phase space division,[9] automatic importance generation,[10] angle bias, and other topics.

II. MCNP PHILOSOPHY

The philosophy of MCNP is "Quality, Value and New Features." The highest priority for MCNP is quality, as exemplified by new software quality assurance practices and a validation program of benchmarking against experiments. The second priority is what we call value, which includes a strong emphasis on documentation and code portability. New features are the third priority.

As part of the emphasis upon quality, a fairly rigorous test set and verification procedure was made available starting with MCNP4. Since then every change in the code can be traced to a specific document as part of our Software Quality Assurance Program. Furthermore, the test set has been constantly upgraded and configuration management is stricter.

A major benchmarking program has been undertaken for MCNP as a second component of the quality control program. Los Alamos has made comparison with a wide variety of neutron[11] and photon[12] experiments. A comparison of MCNP to KENO using the KENO test problem set has just been released.[13] Still more benchmarks studies have been done as collaborations. In these collaborations, the benchmark reports are required to provide unambiguous input descriptions, specifically an MCNP input file, and are advertised and available via the MCNP E-mail network (mcnp@lanl.gov). As part of this coordinated effort, collaborators at General Electric have published light water reactor critical benchmarks[14] and collaborators at Westinghouse Idaho Nuclear Company have published several volumes[15,16,17,18] comparing MCNP to SCALE and experiments.

The "value" component of the MCNP development program includes better documentation and portability to various computer platforms. The MCNP manual is being rewritten. A primer is being written on how to use MCNP for criticality safety problems. The primer gives new users a step-by-step guide for setting up and interpreting MCNP problems starting with simple examples (critical spheres) and building up to more sophisticated problems likely to be encountered by criticality practitioners.

Also as part of "value" MCNP is maintained on many computer platforms. Actually, the source code is the same for all platforms with various portions turned on or off at compilation time. To further enhance the value of MCNP on different platforms or clusters of workstations, we have just added to MCNP4A X-Windows graphics, PVM multiprocessing (described by Gregg McKinney in a related paper at this meeting), and dynamic memory allocation on UNIX platforms. These and other new features will now be described.

III. NEW MCNP4A FEATURES

X-Windows Graphics: MCNP geometry and tally plotting now work with X-window based window systems (e.g., Open Windows, Motif, etc.) in addition to GKS, CGS, DISSPLA, and PLOT10. The X libraries are well-established and can be found on most workstations and mainframes. This capability has been tested on SUNs, IBM RS/6000s, HP, and Cray UNICOS. The graphics window can be easily resized, iconized, or printed and can be sent to or from other displays.

PVM Multiprocessing: MCNP can now be run in parallel on a cluster of workstations[7] using PVM (Parallel Virtual Machine) software. On the 16-machine IBM cluster at LANL, MCNP runs ten times as fast as a single-processor Cray YMP. PVM multiprocessing has also been demonstrated on a network of SUN workstations. PVM multiprocessing is described in more detail in another paper by Gregg McKinney at this meeting.

Dynamic Memory on UNIX systems: MCNP now dynamically adjusts its memory to problem size on UNIX systems. The new UNIX dynamic memory manager also works in conjunction with the distributed memory multiprocessing.

A New Means of Assessing Tally Quality: MCNP4A features a new, exclusive error analysis in addition to the usual estimate of tally variance. The variance of the variance and the underlying history score probability density function are calculated and analyzed as new aids to assess tally convergence.[6] Each tally is also subjected to ten statistical checks providing new confidence and insight into the statistical convergence process. Details are given in another paper at this meeting by Art Forster.

ENDF/B-VI Physics: The Kalbach-87 formalism (ENDF/B-VI file 6 LAW=1, LANG=2) and correlated energy-angle scattering (ENDF/B-VI file 6 LAW=7) have been incorporated in MCNP to handle new ENDF/B-VI data formats. A new algorithm has been developed for next event estimators so that collisions using these laws now contribute to point and ring detectors as well as the DXTRAN variance reduction method. Preliminary libraries are available and work is proceeding to process, test, and release entirely new ENDF/B-VI libraries.

Extended Photon Libraries and Electron Options: The photon libraries have been extended to 1000 MeV based upon the Livermore Evaluated Photon Data Library (EPDL).[19]

New Criticality Analysis and Output: Since the early 80's MCNP has had three estimates of k_{eff}: collision, absorption, and track length. MCNP has also had collision and absorption estimators of removal lifetime. These are calculated for every cycle and are averaged over the cycles as simple averages and covariance weighted averages. Correlation coefficients between estimators are also calculated.

In MCNP4A the following have been added:

- a check to determine if each cell with fissionable material had tracks entering, collisions, and fission source points to assess problem sampling.
- tests for normality of the active k_{eff} values for each estimator. We believe that this is the first normality check in any major criticality production code.
- a table of k_{eff} and confidence intervals if the largest value of k_{eff} for each estimator occurs on the next cycle.
- a fission neutron lifetime estimate.
- A table of k_{eff} and its variance as it would have been calculated with a different number of k_{eff} sources per batch and with different numbers of settling cycles.

Repeated Structures Tallies: MCNP tallies can now be made in individual lattice elements or repeated cells or combinations thereof in repeated structures geometries.

SABRINA Particle Tracks: History files are now optionally output from MCNP to describe particle trajectories which can be plotted with the three-dimensional

color graphics code SABRINA. This output can be filtered by cell and surface crossings, tally contributions, and various particle parameters. This new visualization capability will provide important insight into Monte Carlo solutions.

White and Periodic Boundaries: MCNP now models both white and periodic boundaries.

Case Insensitivity: For the first time MCNP is case insensitive which is particularly of interest on VMS systems.

Easing of Column Restrictions: The old fashioned requirement of input being required in certain columns of the input file is greatly relaxed.

IV. ANSWERS TO SPECIFIC QUESTIONS

The workshop participants have requested that a number of issues be addressed. Most questions had to do with parallel processing and automatic biasing. There were also many specific MCNP questions. Those that are not answered in the above text are now addressed here.

Vector and Parallel Processing: On an N-processor Cray or an N-node cluster of workstations, the MCNP speedup is almost a factor of N when parallel processing is used. See the PVM multiprocessing paper by Gregg McKinney at this meeting. However, MCNP is seldom run in parallel on the Crays at Los Alamos because a single job uses less cpu (no overhead) and less clock time because of time sharing and scheduling problems. PVM distributed multiprocessing appears more successful.

We are looking at massively parallel architectures, but feel that any successful commercial machines will soon look like desktop UNIX workstations with the parallelism invisible to both the programmer and user. Therefore, we do not feel it is prudent at this time to expend precious resources investigating massively parallel machines that will not resemble the machines most commonly used by our user community.

There were several questions about random number sequences for parallel processing. This is not a problem for MCNP since each history has always had its own unique random number seed.

Although vectorization has been successfully applied to special-purpose Monte Carlo computer codes, several attempts with MCNP have failed because of the code generality.

Automatic Biasing Schemes: MCNP has automatic biasing since the weight window generator was introduced a decade ago.[20] It does not yet work with electrons. Like similar schemes (see the paper by Ken Burn at this meeting) it requires user intervention and several iterations. When used correctly it can result in significant improvements in performance, but these improvements are difficult to quantify; it can be millions of times more efficient than analog Monte Carlo, and is usually about ten times more efficient than what a skilled Monte Carlo user could do by trial and error.

Charged Particle Transport: For high energy and charged particle transport we recommend the LAHET code system.[21] MCNP does have a continuous-energy electron transport capability taken from the Integrated Tiger series of codes and MCNP also has a Boltzmann-Fokker-Planck multigroup capability so one could transport charged particles if multigroup cross sections were provided.

Input of CT-scan Data: MCNP has to be modified ("patched") to input CT-scan data efficiently. We have proposals to provide for a regular-rectangular grid geometry which would enable direct mapping of such geometries into MCNP. Experience with prototypes indicates that large grids (> 1 million mesh points) perform as fast

as a few hundred general MCNP cells. Financial support is required for further development.

Graphics Plans: A new version of SABRINA is being prepared and MCNP4A now writes files for particle-track plotting. We continue to investigate a general graphical user interface for setting up MCNP problems but are not yet close to having something for the user community. Attempts to link MCNP or SABRINA graphics to CAD-CAM graphics have failed mostly because the details that a mechanical engineer includes in a CAD-CAM geometry are irrelevant to radiation transport and the details needed for radiation transport are irrelevant to mechanical engineering.

How does memory allocation depend upon input? The biggest demand on MCNP memory is continuous-energy neutron cross sections followed by multidimensional tallies: each tally bin requires five or more words of memory and a tally of 100 energy bins, 100 direction cosines, 100 time bins, etc., gets very big very fast. Note that the forthcoming MCNP4A has dynamic memory allocation on all UNIX systems.

Can both TTB and electron transport be in the same problem? No. If electron transport is turned on, the thick target bremsstrahlung (TTB) approximation is turned off, even if electron importance is zero.

What About Directional Biasing? We plan to add the DXANG[22] angle biasing technique to MCNP4B. Note that the exponential transform is a fairly effective angle biasing method by itself, and that most pure angle bias methods are unstable.[23]

Positron Emission Tomography: We are doing PET research in collaboration with University Hospital, Cleveland. Presently we cannot have positron sources in MCNP without patching the code. Also, non-Boltzmann Monte Carlo requires an entirely new variance reduction approach. Progress is being made but will not be generally available in MCNP for years.

Whatever happened to the MCMG Multigroup code? MCMG became part of MCNP3B. MCNP now has full multigroup and adjoint capabilities.

Other comments:

- We would like to, but have no funding for, perturbation Monte Carlo;
- Presently we have no plans for improving the plotting of tori;
- We have no plans to add combinatorial geometry. Note that SABRINA will translate combinatorial geometries to MCNP and any future graphical user interface will probably handle combinatorial geometries;
- We are not considering further investigation of or generation of multigroup cross sections until ENDF/B-VI is processed. Note that Randy Baker has done some work in this area and is presenting a related paper at this meeting.
- We are presently working on a modest description of the MCNP electron physics for the new MCNP manual. Unfortunately, a detailed description of our algorithm is beyond our present resources. The MCNP algorithm was adapted from the Integrated Tiger Series (ITS)[2] version 1. Because MCNP lags behind ITS, the only reason for using MCNP rather than ITS for electron transport is to do coupled neutron-photon-transport or because the user is already familiar with MCNP and not ITS. We believe ITS is the best electron transport code.

- MCNP has some preliminary ENDF/B-VI data for neutrons above 20 MeV, but we don't make it available. Running ANISN multigroup cross sections in MCNP is possible if someone converts the data to the proper format.

- Presently there are no plans for photon or electron transport in MCNP below 1 keV.

REFERENCES

1. J. F. Briesmeister, Editor, "MCNP - A General Purpose Monte Carlo Code for Neutron and Photon Transport," LA-7396-M, Rev. 2 (September 1986)

2. J. A. Halbleib and T. A. Mehlhorn, "ITS: The Integrated TIGER Series of Coupled Electron/Photon Monte Carlo Transport Codes," Sandia National Laboratory report SAND84-0573 (1984)

3. J. S. Hendricks and R. E. Prael, "Monte Carlo Next-Event Estimates from Thermal Collisions," *Nuclear Science and Engineering,* **109** (2) 150 - 157 (October 1991)

4. J. S. Hendricks, R. E. Prael, "MCNP $S(\alpha,\beta)$ Detector Scheme," Los Alamos National Laboratory report, LA-11952 (October, 1990)

5. J. S. Hendricks, "Effects of Changing the Random Number Stride in Monte Carlo Calculations," *Nuclear Science and Engineering,* **109** (1) 86 - 91 (September 1991)

6. R. A. Forster, S. P. Pederson, and T. E. Booth, "Two Proposed Convergence Criteria for Monte Carlo Solutions," *Trans. Am. Nucl. Soc.*, **66**, 277 (1992)

7. Gregg W. McKinney and James T. West, "Multiprocessing MCNP on an IBM RS/6000 Cluster," submitted to the ANS 1993 Annual Meeting, San Diego, California (June 20 - 24, 1993)

8. Thomas E. Booth,LA-12433 "Monte Carlo Variance Reduction Approaches for Non-Boltzmann tallies" Los Alamos National Laboratory Report LA-12433 (December 1992)

9. T. E. Booth, "Intelligent Monte Carlo Phase-Space Division and Importance Estimation," *Trans. Am. Nucl. Soc.,* **60**, 358 (1989)

10. T. E. Booth, "A Quasi-Deterministic Approximation of the Monte Carlo Importance Function," *Nuclear Science and Engineering,* **104** 374 - 384 (1990)

11. D. J. Whalen, D. A. Cardon, J. L. Uhle, J. S. Hendricks, "MCNP: Neutron Benchmark Problems," Los Alamos National Laboratory report, LA-12212 (November 1991)

12. D. J. Whalen, D. E. Hollowell, J. S. Hendricks, "MCNP: Photon Benchmark Problems," Los Alamos National Laboratory report, LA-12196 (September 1991)

13. John C. Wagner, James E. Sisolak, and Gregg W. McKinney, "MCNP: Criticality Safety Benchmark Problems," Los Alamos National Laboratory report, LA-12415 (October 1992)

14. Shiva Sitaraman, "MCNP: Light Water Reactor Critical Benchmarks," NEDO-32028, General Electric Nuclear Energy (March 1992)

15. Catherine Crawford and Brian Palmer, "Validation of MCNP, a Comparison with SCALE, Part 1: Highly Enriched Uranium Solutions," CSS-92-012 (October 1992)

16. Catherine Crawford and Brian Palmer, "Validation of MCNP, a Comparison with SCALE, Part 2: Highly Enriched Uranium Metal Systems," CSS-92-013 (October 1992)

17. Catherine Crawford and Brian Palmer, "Validation of MCNP, a Comparison with SCALE, Part 3: Highly Enriched Uranium Oxide Systems," CSS-92-014 (October 1992)

18. Catherine Crawford and Brian Palmer, "Validation of MCNP: SPERT-D and BORAX-V Fuel," CSS-92-015 (November 1992)

19. D. E. Cullen, M. H. Chen, J. H. Hubbell, S. T. Perkins, E. F. Plechaty, J. A. Rathkopf, and J. H. Scofield, "Tables and Graphs of Photon-Interaction Cross Sections from 10eV to 100 GeV Derived from the LLNL Evaluated Photon Data Library (EPDL)," Lawrence Livermore National Laboratory report, UCRL-50400, Vol. 6 (October 31, 1989)

20. T. E. Booth, J. S. Hendricks, "Importance Estimation in Forward Monte Carlo Calculations," *Nuclear Technology/Fusion,* **5** (1) 90 (January 1984)

21. R. E. Prael and H. Lichtenstein, "User Guide to LCS: The LAHET Code System," Los Alamos National Laboratory report, LA-UR-89-3014 (1989)

22. T. E. Booth, "A Weight Window/Importance Generator for Monte Carlo Streaming Problems," *Sixth International Conference on Radiation Shielding*, Tokyo, Japan (May 16-20, 1983)

23. J. S. Hendricks, L. L. Carter, "Anisotropic Angle Biasing of Photons," *Nuclear Science and Engineering,* **89** 118-130 (February 1985)

OVERVIEW of MONTE CARLO METHODOLOGIES

in TRIPOLI-3

T.VERGNAUD
Division des Reacteurs Nucléaires DMT / SERMA / LEPP
CEA Saclay 91191 Gif sur Yvette FRANCE

INTRODUCTION

Le code TRIPOLI, sous sa version TRIPOLI-2, a été utilisé depuis plus de 15 ans pour de nombreuses études dans des domaines divers : calculs de projet pour les réacteurs à fission et à fusion, sureté, démantèlement, dimensionnement de chateaux de transport, instrumentation, applications militaires ...

Depuis 1992 existe une nouvelle version : TRIPOLI-3, utilisable sur ordinateur centralisé (IBM, CRAY) et sur station de travail (SUN, RISC6000, HP...), dont le but principal est d'offrir à un utilisateur, non familier avec la méthode de Monte Carlo, un code facile d'utilisation.

La puissance grandissante des ordinateurs met en évidence la nécessité de réduire au maximum le temps passé par l'ingénieur pour préparer un calcul et en exploiter les résultats : un effort particulier a été fait pour simplifier l'entrée des données, clarifier les messages d'erreur, proposer des sorties graphiques et surtout pour automatiser le biaisage. Ce dernier point était souvent un point d'achoppement pour l'utilisateur car la définition d'un biaisage bien adapté au problème traité demandait une certaine expérience.

Toutes les potentialités du code TRIPOLI-2 ont été conservées :

- transport des neutrons et des gamma, calcul couplé neutron-gamma, dans des géométries tridimensionnelles, en fonction du temps ou non.

- étude de problèmes à source, avec ou sans prise en compte de la fission, caractérisés par une forte atténuation du flux pouvant atteindre 25 décades et nécessitant l'utilisation de techniques d'accélération.

- étude d'un problème "critique" (calcul de Keff) caractérisé par un gradient de flux nul ou faible mais nécessitant une description ponctuelle des sections efficaces. TRIPOLI est alors utilisé comme méthode de référence.

TRIPOLI-3 offre des possibilités supplémentaires et a été conçu pour faciliter la prise en compte de nouveaux developpements.

SECTIONS EFFICACES

Le code est couplé, par l'intermédiaire du module NJOY-THEMIS, aux bibliothèques ENDF/B4, JEF1 et EFF et dispose d'une bibliothèque de fonctions réponses, d'origines diverses, comprenant, en particulier, la compilation IRDF/85, décrites de façon multigroupe ou ponctuelle. Le couplage à ENF/B6 est en cours.

Plusieurs modes de description des sections efficaces sont possibles :

- mode multigroupe

un découpage à 315 groupes entre 19 MeV et 0. est généralement utilisé pour les problèmes de protection; un découpage à plusieurs milliers de groupes (par exemple 8000) est utilisé pour les calculs de benchmarks.

Les section efficaces sont pondérées par un spectre de fission au-dessus de 1 MeV, par un spectre en $1/E.\Sigma_t(E)$ jusqu'à 0.108 eV (où $\Sigma_t(E)$ est la section totale de la composition contenant l'isotope) et par un spectre de Maxwell au-dessous de 0.108 eV. La thermalisation des neutrons est traitée de façon exacte, en utilisant le modèle gaz libre ou les fonctions $S(\alpha,\beta)$ pour les noyaux légers.

- mode ponctuel

les sections sont décrites pour 33000 points entre 5KeV et 5eV avec interpolation linéaire

-tables de probabilité

ce point fait l'objet d'une autre communication du séminaire :

S.H.ZHENG : "Review of Cross-section Treatment in Monte Carlo - The Probability Table method"

La simulation du choc suit au plus près le processus physique et la particule est suivie de façon continue en espace, énergie et direction. L'anisotropie est décrite finement par aires d'égale probabilité (32 intervalles pour les neutrons et 60 intervalles pour les gamma entre -1 et +1)

Le couplage final à ENDF/B6 est prévu pour fin 93, avec prise en compte des sections doublement différentielles.

GEOMETRIE

La géométrie, tridimensionnelle, d'un problème est un ensemble de volumes finis, connexes, contenant une même composition isotopique. Un volume est défini par les surfaces analytiques, du premier ou du second degré, qui le limitent, ainsi que par le signe des équations de ces surfaces pour les points du volume. Un ensemble de surfaces est disponible : plan, sphère, cylindre, cône, quadrique quelconque. Les conditions aux limites peuvent être : fuite, réflexion, rotation ou translation.

Le problème peut comporter un grand nombre de volumes et des géométries complexes peuvent être ainsi décrites.

Le code dispose de modules de test de la géométrie : balayages dans les trois dimensions qui réalisent des tests approfondis et visualisation sur écran de coupes de la géométrie, ce qui permet de vérifier facilement le dimensionnement et l'association volume-composition. Plusieurs exemples sont présentés sur les figures 1 à 3.

figures 1 - calcul de l'activation du sodium secondaire dans l'échangeur de chaleur de Super-Phenix
coupes verticale et horizontale

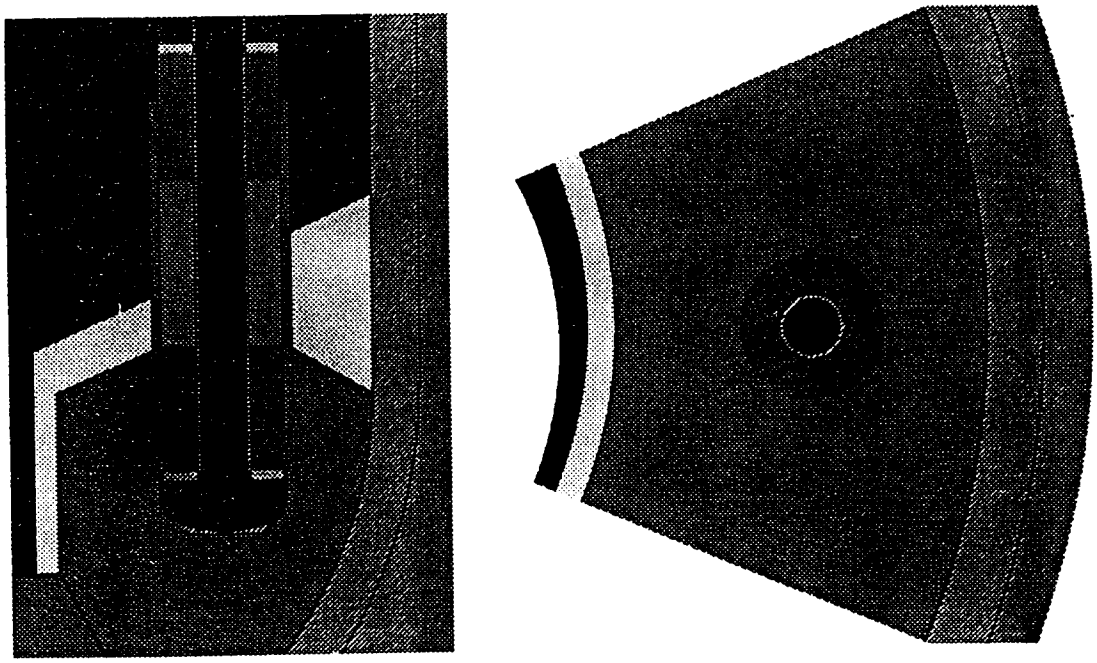

figure 2 - calcul de dose dans un chateau de transport - coupe horizontale

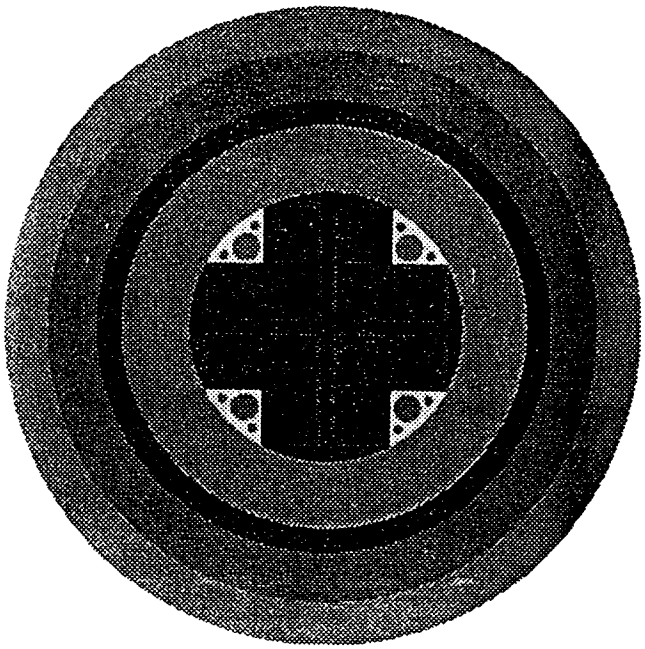

figures 3 - Tore ITER

chambre à plasma - coupe verticale

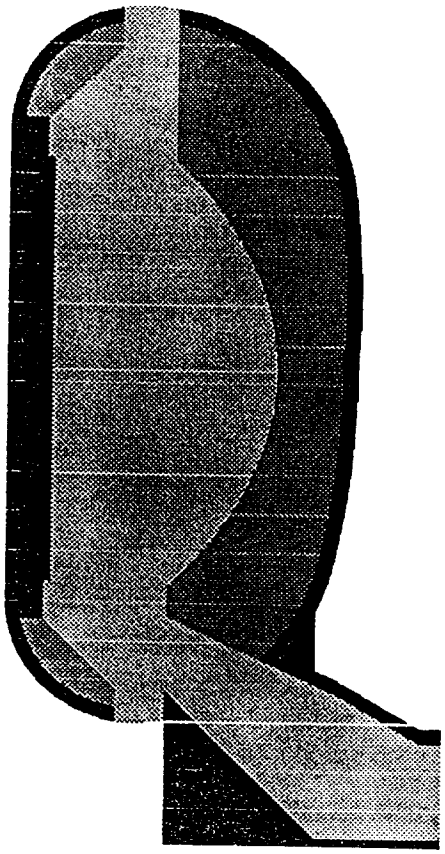

hall de pompage et divertor - coupe horizontale

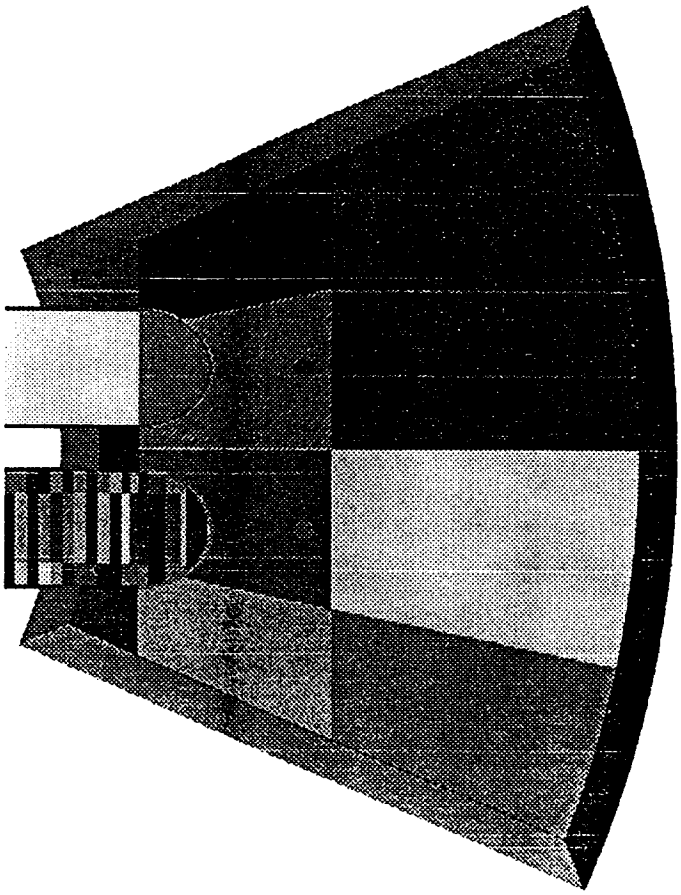

TECHNIQUES D'ACCELERATION : LE BIAISAGE

Les principes sur lesquels s'appuient les techniques d'accélération développées dans TRIPOLI sont exposés dans une autre communication : B.Morillon "Automatic Biasing Techniques in Monte Carlo". Seuls les caractéristiques principales sont ici présentées.

Le biaisage est basé sur la définition d'une fonction d'importance $I(\mathbf{r},E,\Omega)$ en tout point de l'espace des phases ($\mathbf{r}$ espace, E énergie, Ω direction), qui dépend du résultat (zone d'espace, domaine en énergie) que l'on veut optimiser. L'émission des particules et leur simulation sont réalisées avec des lois biaisées, de façon que le poids de la particule reste en accord avec l'inverse de l'importance.

Il est démontré que si l'importance $I(\mathbf{r},E,\Omega)$ est égale à la solution I_0 du problème adjoint, relative à la réponse d'un détecteur en un point, alors la réponse est estimée avec une variance nulle. La variance sera d'autant plus faible que l'importance choisie est plus proche de cette importance idéale I_0 .

Dans TRIPOLI l'importance est approximée par un produit de 3 facteurs :

$$I(x) = [\, I_1 (\vec{r})]^{F(E)} \; . \; I_2 (E) \; . \; I_3 (\vec{r},E,\vec{\Omega})$$

Deux quantités ont une signification physique importante :

$$K(\vec{r}) = \frac{F(E) \; . \; |\overrightarrow{gradI_1(\vec{r})}|}{I_1(\vec{r})} \qquad\qquad \vec{\Omega}_0(\vec{r}) = \frac{\overrightarrow{gradI_1(\vec{r})}}{K \; . I_1(\vec{r})}$$

K donne la variation de la partie spatiale de l'importance et caractérise "l'intensité" du biaisage;

$\Omega_0(\mathbf{r})$ peut être vue comme la direction d'intérêt au point $\mathbf{r}$, qui "pointe" vers la zone résultat où l'importance est la plus grande; c'est un vecteur perpendiculaire aux surfaces équi-importance.

Le biaisage du parcours ainsi que le biaisage de la collision sont réalisés avec une section totale biaisée :

$$\Sigma_t^*(\vec{r},E,\vec{\Omega}) = \Sigma_t(\vec{r},E) - K(\vec{r}) \; . \; F(E) \; . \; \vec{\Omega} . \overrightarrow{\Omega_0(\vec{r})}$$

La fonction $I_2(E)$ est facile à définir à partir de considérations physiques simples; de plus elle est ajustée par le code afin de conserver une taille de la population de particules adaptée à la réponse étudiée.

La fonction I_3 est conditionnée par l'utilisation de la transformation exponentielle et calculée automatiquement par le code.

La fonction $I_1(\mathbf{r})$ est la partie la plus significative de la fonction d'importance. Dans TRIPOLI-2 elle était définie par l'utilisateur et demandait une certaine expérience. Dans la version TRIPOLI-3, sa définition est maintenant prise en charge par le code de la manière suivante :

- un maillage recouvre l'ensemble de la géométrie; le centre de chaque maille définit le noeud d'un graphe; un élément du graphe est déterminé en joignant chaque noeud P à ses 26 voisins Q et la distance d(P,Q) lui est associée par intégration de K(r) le long de PQ.

- si l'on cherche l'estimation d'une réponse en un point D, on appelle D_0 le noeud du graphe le plus proche de D. L'algorithme de Djikstra est utilisé pour déterminer, parmi tous les chemins possibles, le plus court chemin entre P et D_0 , soit dist(P,D_0). La fonction I_1 en P est alors donnée par :

$$I_1(P) = e^{-dist(P,D_0)}$$

- $\Omega_0(P)$ est défini par l'estimation par différence finie du gradient de I_1

- le module INIPOND qui calcule la fonction I_1 est couplé à une bibliothèque de valeurs de K par isotope, dépendant du domaine en énergie étudié. Ces valeurs sont adaptées aux problèmes que nous traitons couramment avec des sources de fusion ou de fission. Une autre approche est en cours de développement par la méthode des probabilités de collision (cf exposé de B.Morillon)

Les technique de biaisages utilisées optimisent la simulation le long de "parcours préférentiels" des particules (espace x énergie). Cependant les résultats restent fiables dans une zone plus large; le module VISPAR, inclus dans TRIPOLI, permet de visualiser les zones où les résultats restent statistiquement valables : la simulation est réalisée pour un faible nombre de particules (par exemple 1000) et la densité de collision est visualisée sur des coupes 2D, par domaine d'énergie ou de temps.

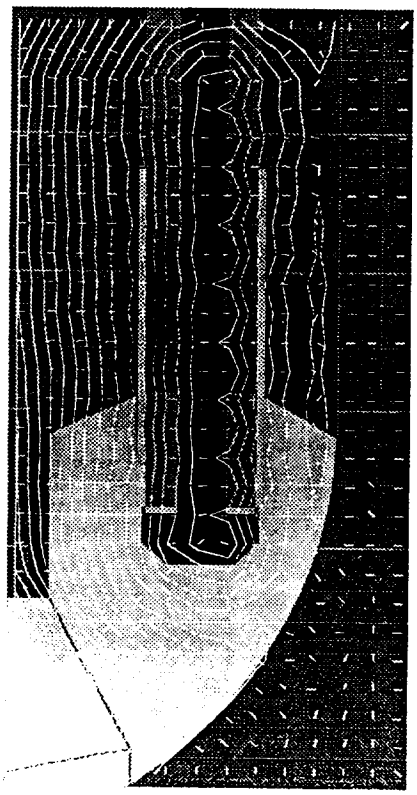

Les figures 4 et 5 montrent les surfaces équi-importance obtenues avec le module INIPOND

figure 4
calcul Super Phenix

la réponse optimisée est
l'activation du sodium
sur l'axe de l'échangeur

figure 5 - benchmark Jason

(cuve cylindrique de sodium entourée d'une ceinture de béton ménageant un vide annulaire)

la représentation de la densité de collision correspond à 150 neutrons

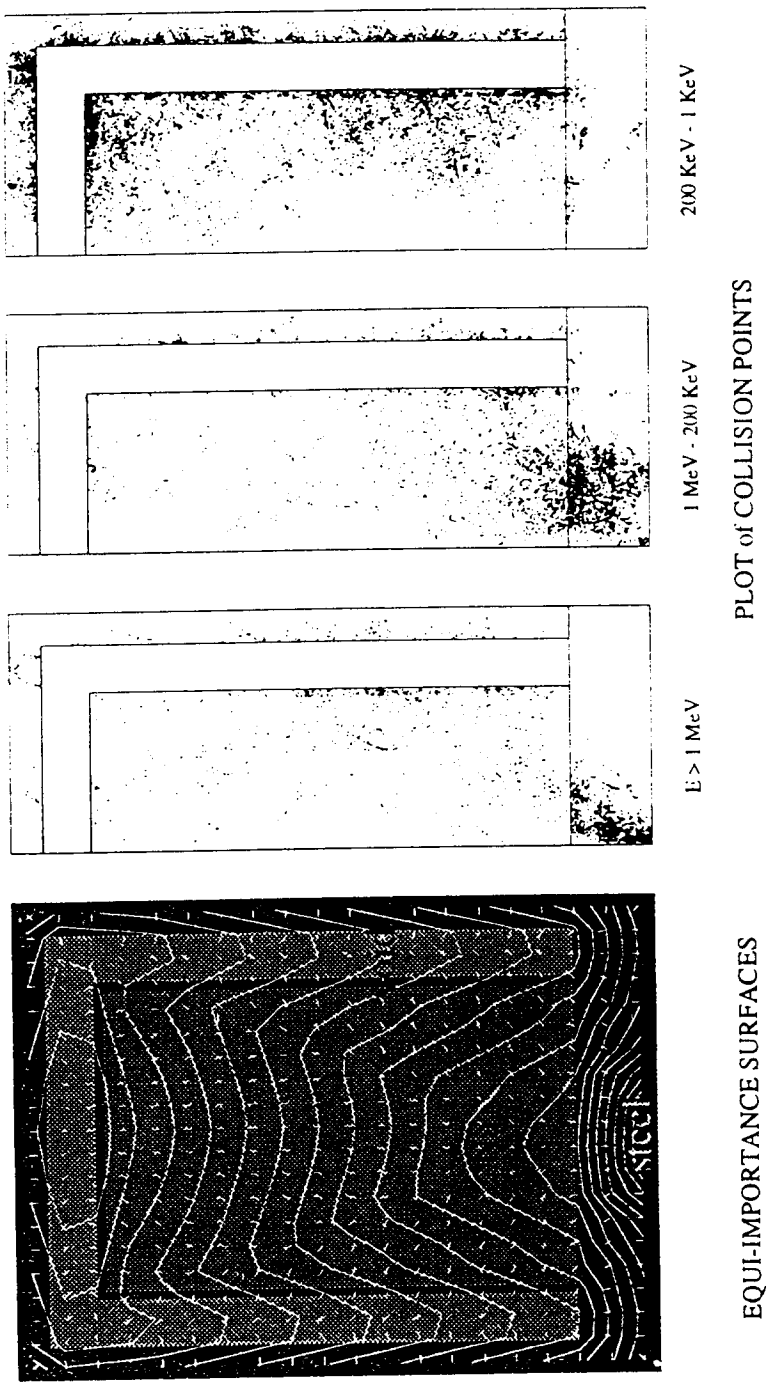

SOURCES

Les sources sont définies comme une combinaison linéaire de fonctions de l'espace, de l'énergie, de la direction et du temps :

$$S(\vec{r},E,\vec{\Omega}) = \sum_i c_{V(i)} \; . \; F_i(\vec{r}) \; . \; H_i(E) \; . \; G_i(\vec{\Omega}) \; . \; T_i(t)$$

Chaque systeme i est défini dans un repère cartésien, cylindrique ou sphérique.

Les particules sont émises proportionellement à $S^* = S \; . \; I(r,E,\Omega)$. La normalisation du calcul est réalisée automatiquement par le code.

Un module de couplage avec les codes Sn (DOT,BISTRO) permet d'utiliser les flux angulaires sur une surface comme source pour le calcul de Monte Carlo.

RESULTATS

Le code évalue

- soit des valeurs intégrées : flux dans un volume (estimation par densité de collision ou par longueur de cordes), flux et courant à travers une surface
- soit des valeurs ponctuelles de flux

ainsi que des réponses ou des taux de réaction associés :

$$R(E) = \int C(E) \; . \; \Phi(E) \; dE$$

les fonctions C(E) peuvent être des sections efficaces ou des réponses de détecteur, définies en mode multigroupe ou par valeurs ponctuelles.

Flux et réponses sont calculés dans des intervalles d'énergie, de temps ou d'angle (cosinus de la direction de la particule avec un vecteur normal à la surface ou avec un vecteur fixe)

Le Keff est évalué au cours d'un calcul critique.

A chaque résultat est associé l'écart type correspondant : la simulation est réalisée pour N batches de M particules; si R_k est le résultat du batch k, la moyenne et l'écart type sont évalués sur les N valeurs R_k

La figure 6 illustre certains des résultats fournis par le code pour le calcul du flux dans le hall de pompage du tore ITER (cf figure 3) :

figure 6a variation du flux neutronique dans le divertor

figure 6b distribution angulaire du flux à l'entrée du canal de pompage

figures 6

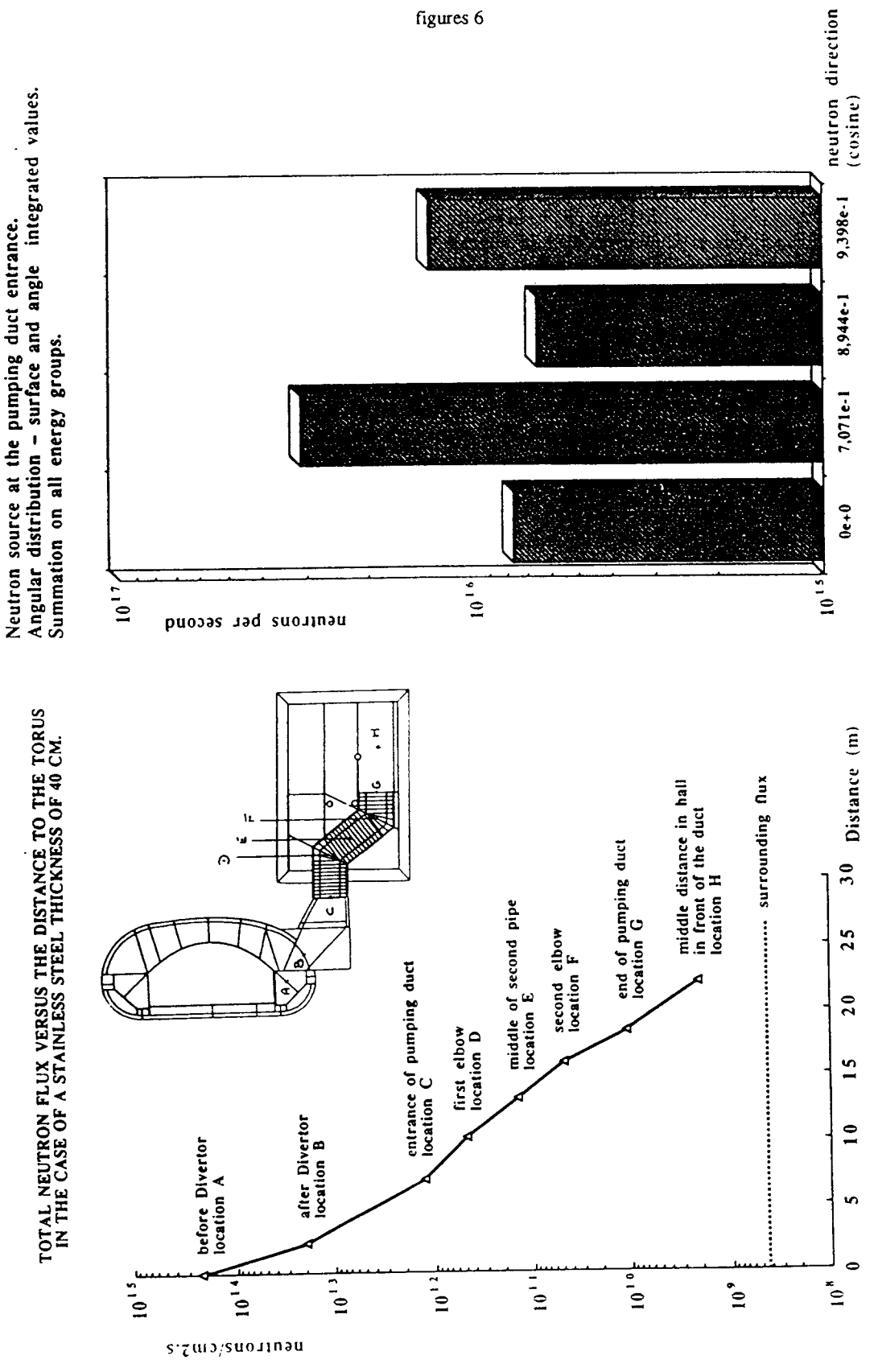
TOTAL NEUTRON FLUX VERSUS THE DISTANCE TO THE TORUS
IN THE CASE OF A STAINLESS STEEL THICKNESS OF 40 CM.
neutrons/cm2.s
before Divertor location A
after Divertor location B
entrance of pumping duct location C
first elbow location D
middle of second pipe location E
second elbow location F
end of pumping duct location G
middle distance in hall in front of the duct location H
surrounding flux
Distance (m)
Neutron source at the pumping duct entrance.
Angular distribution - surface and angle integrated values.
Summation on all energy groups.
neutrons per second
neutron direction (cosine)
0e+0
7,071e-1
8,944e-1
9,398e-1

Le code crée un fichier contenant l'ensemble des résultats par batch qui peut être utilisé en post-traitement pour, par exemple, regrouper des résultats dans différents volumes ou différents domaines en énergie et évaluer les écarts types correspondants, obtenir un histogramme des valeurs de Keff ou obtenir un tracé graphique d'un résultat en fonction de l'énergie ou du temps.

L'activation du sodium dans l'échangeur de Super-Phenix a été calculée dans chacun des 66 volumes représentant l'échangeur, qui ont été ensuite regroupés pour obtenir l'activation dans 12 zones, puis l'activation totale ainsi que l'écart type sur chacun de ces nouveaux résultats.

CALCULS de REFERENCE en NEUTRONIQUE

Une étude utilisant des sections efficaces décrites par points est détaillée dans un autre exposé :

H.Tellier M.Coste C.Raepsaet C.Van der Gucht :

"Monte Carlo Validation of the Self-shielding Formalism on Voids"

TRIPOLI est utilisé comme méthode de référence pour ce calcul où l'auto-protection est analysée de façon fine : on réalise une véritable "expérience sur ordinateur" et on peut ainsi valider un formalisme de calcul du flux en isolant certains paramètres qui sont à la disposition de l'utilisateur.

CONCLUSION

TRIPOLI-3 se présente comme un code convivial et portable, qui permet de traiter aussi bien des problèmes de pénétration profonde pour les calculs de protection, que les problèmes de physique fine rencontrés en neutronique.

STATUS OF THE MORSE MULTIGROUP MONTE CARLO RADIATION TRANSPORT CODE

Margaret B. Emmett
Computing Applications Division
Oak Ridge National Laboratory
P.O. Box 2008
Oak Ridge, Tennessee USA 37831-6370

ABSTRACT

Two versions of the MORSE multigroup Monte Carlo radiation transport computer code system are available at Oak Ridge National Laboratory. MORSE-CGA is widely known and has undergone extensive use for many years. MORSE-SGC was originally developed in about 1980 in order to restructure the cross-section handling and thereby save storage. However, with the advent of new computer systems having much larger storage capacity, that aspect of SGC has become unnecessary. Both versions use data from multigroup cross-section libraries, although in somewhat different formats. MORSE-SGC is the version of MORSE that is part of the SCALE system, but it can also be run in a stand-alone mode. Both CGA and SGC use the Multiple ARray System (MARS) geometry package.

In the last six months the main focus of the work on these two versions has been on making them operational on workstations, in particular, the IBM RISC 6000 family. A new version of SCALE for workstations is being released to the Radiation Shielding Information Center (RSIC). MORSE-CGA, Version 2.0, is also being released to RSIC. Both SGC and CGA have undergone other revisions recently. This paper reports on the current status of the MORSE code system.

HISTORY OF MORSE DEVELOPMENT

Two versions of the MORSE[1-3] Monte Carlo radiation transport computer code system are available at Oak Ridge National Laboratory: MORSE-CGA and MORSE-SGC. Both will be discussed in this presentation. MORSE-CGA is the most well-known version, and it has undergone extensive use for many years. Known simply as MORSE, originally it was developed in the 1968 time frame in response to the need for a Monte Carlo code with multigroup cross sections. This need came about partially because the discrete-ordinates codes ANISN[4] and DOT[5] used multigroup data, and a similar three-dimensional (3-D) code would allow direct comparison of results between these codes without having to determine whether cross-section differences were causing discrepancies. The original version of this multipurpose neutron and gamma-ray transport code used the O5R-type of geometry packages, such as general geometry, spherical geometry, cylindrical geometry, and slab geometry. MORSE solves neutron, gamma-ray, or coupled neutron-gamma-ray problems in both forward and adjoint modes. PICTURE, which makes two-dimensional (2-D) printer plots of the geometry mockups, was the only peripheral code available with this version. The MORSEC cross-section package and the SAMBO analysis package were installed in 1971. At about the same time, a collision density analysis package was made available to MORSE users.[6]

In 1973, the O5R geometry package was replaced with the combinational geometry package, and the code was renamed MORSE-CG. In 1975, this version was documented in the report, ORNL-4972. The combinational geometry package was based on one previously developed by MAGI and was originally installed in the UNIVAC version of MORSE by Dr. Edward Straker of the Huntsville SAIC office.[7] This new geometry package made modeling complex geometries much easier.

MORSE was being used primarily for radiation transport in reactors until 1973 when calculations of radiation exposure to crews of military vehicles were needed. At that time a Vehicle Code System[8] (VCS) made up of DOT, VISA, MORSE, and DRC (a detector response code) was developed and packaged. This code, documented in ORNL/TM-4648 in 1974, underwent major revisions to become MORSE Adjoint SHielding (MASH) code, which was published as ORNL/TM-11778 (ref. 9). This system used MORSE in the adjoint mode to solve problems where an event occurs a long distance from a vehicle that may have various orientations relative to the event. That is to say, a collision tape produced by adjoint MORSE may be coupled with several DOT flux results by running DRC specifying different orientations.

Early in the development of the MORSE code system, it became obvious that there was a need for the capability to couple a 2-D discrete-ordinates calculation to a MORSE Monte Carlo calculation. This allows users to solve the simpler part of a geometric structure in two dimensions with a code like DOT (DORT) and then produce a source distribution or a scoring function for use in MORSE. The code that processes the 2-D fluxes from the DOT runs to form probability tables for source or estimation selection is called the Discrete Ordinates to Monte Carlo INterface Operation (DOMINO-II).[10] Since the DOT family of codes has been revised and renamed to DORT, DOMINO needs to be altered to process the newer flux tapes and to run on newer computer architectures, such as workstations. This alteration is currently in the planning stages.

The ability to run an albedo calculation with MORSE was made available with the development of CARP (1978)[11] and BREESE-II (1979).[12] CARP processes DOT angular flux tapes to produce albedo data that are used as input for BREESE-II, which calculates cumulative distribution functions and writes an albedo tape used by MORSE. In 1991 a University of Tennessee graduate student modified the MORSE albedo option.[13] New albedo data were generated using the three-dimensional (3-D) discrete-ordinates code, TORT,[14] in order to remove the limitations on the data generated by the 2-D discrete-ordinates codes (DOT). These limitations involved the absence of a direction and a distance variable. Use of TORT allowed the inclusion of these two additional parameters. Several additional options were added to the MORSE/BREESE package, including the

capability of running an albedo problem in the adjoint mode. This work resulted in a computer code package, MORSE/STORM, which serves merely as a "proof of principle." Results for the chosen sample problem were good, but the code would require additional work for more general application. One major concern is that the volume of data could be too large for practical use.

In 1983, ORNL-4972/R1 was published. It included a section of advice on running MORSE and a description of some new options. In 1985, a set of nine sample problems, including the two original sample problems, was released and published in ORNL-4972/R2. Also, in 1985, a report detailing how to apply MORSE to various problems was published.[15]

MORSE-SGC, which was published in 1981, had as its primary purpose the restructuring of the cross-section handling to save storage, but the next generation of large core computers nullified this need. The MARS[16] geometry package was originally developed for SGC; however, because the SGC developers left ORNL before the code was thoroughly checked out, and because of various problems that arose when users attempted to apply it, a decision was made to add the MARS geometry module to MORSE-CG - a code thoroughly checked out over years of widespread use. Another factor was the desire to update and verify MARS. This development effort, which began in 1982, resulted in MORSE-CGA. MORSE-CGA has therefore been in use at ORNL since the early 1980s, and has been applied to extremely complicated geometries such as shipping casks and buildings.

In the last six months, the focus of the work on CGA and SGC has been on making them operational on workstations. Version 2.0 of MORSE-CGA, which will run on several mainframes as well as on personal computers and IBM workstations, and a SCALE 4.1 version of MORSE-SGC have recently been released. A workstation version of SCALE 4.1 for IBM RISC 6000 family will be available very soon.

FEATURES ASSOCIATED WITH MORSE SYSTEM

MORSE has many options and modes of operation. Some of the features associated with the MORSE system of computer codes are as follows:

- Applicable to both multiplying and non-multiplying media.
- Can operate in a fixed source or a k_{eff} eigenvalue mode.
- Operable in both forward and adjoint modes.
- Uses cross-section and/or albedo data in CGA.
- Treats regular and delta (fictitious) scattering.
- Can be coupled with discrete-ordinates codes (source and/or response mode coupling).
- Has available a general combinatorial geometry.
- Contains a multiple-array nesting feature for finite or infinite geometry lattices.
- Has a 2-D geometry picture drawing capability.
- Includes many standard variance reduction techniques.
- Uses ANISN library multigroup cross-section and anisotropic scattering formats, including upscatter for any number of thermal energy groups.
- Can treat Klein Nishina, pair production, and photoelectric reactions for gamma-ray next-event estimation.
- Can use a history file for post-processing of results by CGA.
- Has a "user friendly" framework of routines and other aids that alleviate much of the effort necessary for user-written routines.
- Has a large library of "standard" user routines that may be used directly or serve as models for further modification.

- Is supported by a plethora of related literature and documentation describing the code, multigroup and general theory, programming details, debugging aids, error messages, sample problems, applications, interpretation of results, and other capabilities and limitations.

SIMILARITIES AND DIFFERENCES IN CGA AND SGC

Both CGA and SGC use data from multigroup cross-section libraries although in somewhat different formats. CGA uses an ANISN-type library, whereas SGC uses an AMPX[17] working library. In either case the cross sections may be premixed (in earlier MORSE runs or, in the CGA case, by XCHEKR runs) and read from file IXTAPE. One difference in the two codes is that SGC contains no provision for running a neutron-gamma problem with a truncated number of neutron groups (e.g., CGA, when using a 22-group-neutron/18-group-gamma coupled cross-section set, could run 13 neutron groups and 17 gamma groups, but SGC must run all 22 neutron groups). The other major difference, as far as cross sections are concerned, is that CGA always has all cross-section data in core whereas SGC can have "n" groups in core at a time. Because of the availability of large amounts of core in the current generation of computers, it is unusual for SGC to fragment the groups.

Geometrically speaking, the two versions are identical—MARS is the geometry package in both. The MARS system allows the user to describe many rectangular cells of arbitrary content, called "universes." These universes can be arbitrarily combined to describe arrays. Arrays may contain sub-arrays, universes, and vacancies. Arrays may also be rotated.

One recent improvement to MARS was the implementation of a fix-up for fatal geometry errors which allows orderly termination of a problem for n-1 batches when such an error occurs in the *nth* batch. The change was initiated because of the occasional occurrence of geometry round-off errors that cause termination after significant amounts of CPU time have been expended. A new subroutine, RCOVER, was added to normalize results. Results printed for the "extra arrays of length ND" will include events that occurred in the current batch. There is no simple way to change this; and since these results are seldom, if ever, used, modification was not justified. Final tabulations of random walk statistics are not printed in this case because they would include the partial batch.

Another difference in SGC and CGA is that CGA requires user-written routines to describe the source and estimation techniques while SGC contains a set of default routines for these functions. Because of the long-time, widespread use of MORSE-CGA, many standard user routines exist and are distributed with the code; and they may be used directly or modified as needed. The user is responsible for altering subroutine BANKR in CGA to call the appropriate estimation routines (for example, RELCOL). Over the years of SGC use, occasions have arisen where its source and estimation routines have also required user intervention; therefore, this is no longer a clear-cut difference, although SGC allows the user to specify on input which routines to call rather than having the user alter a set of call statements.

Both codes are now in FORTRAN-77. They are executable on many different computers. A master file for MORSE-CGA is operated on by a preprocessor named CFLAG that configures it for the computer requested by the user's input. MORSE-SGC is handled in a similar way by the preprocessor code COMMENT. CGA will run on IBM mainframes with MVS, on CRAY mainframes with UNICOS or CTSS (where available), on VAX VMS, on personal computers under Silicon Valley FORTRAN or MICROSOFT FORTRAN, and on the (UNIX-based) IBM RISC 6000 family. SGC has not been run on any personal computers but will run on IBM mainframes, CRAYs and IBM RISC workstations. Although MORSE-SGC is part of the SCALE system, it can also be run stand-alone, and it is part of the SAS3[18] and SAS4[19] sequences in SCALE. CGA has

been converted to use all free-form FIDO-type input; SGC also uses a free-form FIDO-type input but allows some additional options. If the user executes the SAS3 or SAS4 sequence, the MORSE-SGC input utilizes a keyword input which allows the user to specify only the parameters that require change and utilizes default values for the others. A track-length estimator is now a standard estimator in CGA.

CONFIGURATION CONTROL

In the past there have been several versions of MORSE-CGA and MORSE-SGC that were set up as quality assured, or QA'd, systems. Efforts are currently under way to place both CGA and SGC under configuration control. A SCALE configuration control document exists, and many of the SCALE modules used for nuclear criticality safety are already handled in this way. Last year a verification was done for MORSE-SGC on a CRAY unicos system for the New Production Reactor (NPR) program, and a document was published describing that work.[20] A new effort is beginning related to software used for nuclear safety calculations at the facilities operated by Martin Marietta Energy Systems, Inc.

SAMPLE PROBLEMS

MORSE-CGA has a set of nine sample problems that illustrate neutron only, gamma only, combined neutron-gamma, adjoint mode, multiplying systems (k-effective calculations), several types of estimators, PICTURE, and XCHEKR. In 1992 four of these problems were adapted to MORSE-SGC and used to help verify the Unicos version of SGC. MORSE-SGC now has seven sample problems. Results of the sample problems are distributed with the code.

REFERENCES

1. M. B. Emmett, *The MORSE Monte Carlo Radiation Transport Code System*, ORNL-4972 (1975), ORNL-4972/R1 (1983), ORNL-4972/R2 (1984), Union Carbide Corp., Nucl. Div., Oak Ridge Natl. Lab.

2. M. B. Emmett, *MORSE-CGA, A Monte Carlo Radiation Transport Code With Array Geometry Capability*, ORNL-6174, Martin Marietta Energy Systems, Inc., Oak Ridge Natl. Lab., April 1985.

3. J. T. West, T. J. Hoffman, and M. B. Emmett, "MORSE-SGC/S for the SCALE System," Vol. II, Sect. F9 of *SCALE: A Modular Code System for Performing Standardized Computer Analyses for Licensing Evaluation*, NUREG/CR-0200, Rev. 4 (ORNL/NUREG/CSD-2/R4), Vols. I, II, and III (draft February 1990). Available from Radiation Shielding Information Center as CCC-545.

4. W. W. Engle, Jr., *A User's Manual for ANISN, A One-Dimensional Discrete-Ordinates Transport Code With Anisotropic Scattering*, K-1693, Union Carbide Corp., Nucl. Div., Oak Ridge Gaseous Diffusion Plant, March 1967.

5. W. A. Rhoades and R. L. Childs, *An Updated Version of the DOT-4 One- and Two-Dimensional Neutron/Photon Transport Code*, ORNL-5851, Union Carbide Corp., Nucl. Div., Oak Ridge Natl. Lab., 1982.

6. E. A. Straker and M. B. Emmett, *Collision Site Plotting Routines and Collision Density Fluence Estimates for the MORSE Monte Carlo Code*, ORNL/TM-3585, Union Carbide Corp., Nucl. Div., Oak Ridge Natl. Lab., October 1971.

7. E. A. Straker, W. H. Scott, Jr., and N. R. Byrn, *The MORSE Code with Combinatorial Geometry*, Defense Nuclear Agency DNA 2860T, SAI-72-511-LJ, Science Applications International Corp., May 1972.

8. W. A. Rhoades and M. B. Emmett et al., *Vehicle Code System (VCS) User's Manual*, ORNL/TM-4648, Union Carbide Corp., Nucl. Div., Oak Ridge Natl. Lab., August 1974.

9. J. O. Johnson, Ed., *A User's Manual for MASH 1.0—A Monte Carlo Adjoint Shielding Code System*, ORNL/TM-11778, Martin Marietta Energy Systems, Inc., Oak Ridge Natl. Lab., March 1992.

10. M. B. Emmett, *DOMINO-II, A General-Purpose Code for Coupling DOT-IV Discrete Ordinates and Monte Carlo Radiation Transport Calculations*, ORNL/TM-7771, Union Carbide Corp., Nucl. Div., Oak Ridge Natl. Lab., 1981.

11. M. B. Emmett and W. A. Rhoades, *CARP, A Computer Code and Albedo Data Library for Use by BREESE, the MORSE Albedo Package*, ORNL/TM-6503, Union Carbide Corp., Nucl. Div., Oak Ridge Natl. Lab., 1978.

12. V. R. Cain and M. B. Emmett, *BREESE-II: Auxiliary Routines for Implementing the Albedo Option in the MORSE Monte Carlo Code*, ORNL/TM-6807, Union Carbide Corp., Nucl. Div., Oak Ridge Natl. Lab., July 1979.

13. I. C. Gomes and P. N. Stevens, *MORSE/STORM: A Generalized Albedo Option for Monte Carlo Calculations*, ORNL/FEDC-91/1, Martin Marietta Energy Systems, Inc., Oak Ridge Natl. Lab., September 1991.

14. W. A. Rhoades and R. L. Childs, *The TORT Three-Dimensional Discrete Ordinates Neutron/Photon Transport Code*, ORNL-6268, Martin Marietta Energy Systems, Inc., Oak Ridge Natl. Lab., November 1987.

15. S. N. Cramer, *Applications Guide to the MORSE Monte Carlo Code*, ORNL/TM-9355, Martin Marietta Energy Systems, Inc., Oak Ridge Natl. Lab., May 1985.

16. J. T. West and M. B. Emmett, "MARS, A Multiple Array System Using Combinatorial Geometry," Sect. M9 of *SCALE: A Modular Code System for Performing Standardized Computer Analyses for Licensing Evaluation*, NUREG/CR-0200, Rev. 4 (ORNL/NUREG/CSD-2/R4), Vols. I, II, and III (draft February 1990). Available from Radiation Shielding Information Center as CCC-545.

17. N. M. Greene et al., *AMPX-77: A Modular Code System for Generating Coupled Multigroup Neutron-Gamma Cross-Section Libraries From ENDF/B-IV and/or ENDF/B-V*, ORNL/CSD/TM-283, Martin Marietta Energy Systems, Inc., Oak Ridge Natl. Lab., October 1992.

18. J. T. West, "SAS3: An Automated Monte Carlo Shielding Analysis Module," Sect. S3 of *SCALE: A Modular Code System for Performing Standardized Computer Analyses for Licensing Evaluation*, NUREG/CR-0200, Rev. 4 (ORNL/NUREG/CSD-2/R4), Vols. I, II, and III (draft February 1990). Available from Radiation Shielding Information Center as CCC-545.

19. J. S. Tang, "SAS4: A Monte Carlo Cask Shielding Analysis Module Using an Automated Biasing Procedure," Sect. S4 of *SCALE: A Modular Code System for Performing Standardized Computer Analyses for Licensing Evaluation*, NUREG/CR-0200, Rev. 4 (ORNL/NUREG/CSD-2/R4), Vols. I, II, and III (draft February 1990). Available from Radiation Shielding Information Center as CCC-545.

20. M. B. Emmett, *Verification of MORSE-SGC on the CRAY UNICOS System*, ORNL/NPR-92/5, Martin Marietta Energy Systems, Inc., Oak Ridge Natl. Lab., March 1992.

The Development of the MONK and MCBEND Codes within the New Monte Carlo Modular Code Scheme MCANO

N R Smith & R J Brissenden
AEA Technology, UK

M H Watmough
British Nuclear Fuels plc, UK

Summary

MONK and MCBEND are the major UK Monte Carlo particle transport codes for the criticality and shielding application areas respectively. Both codes have been developed and used for over twenty-five years in support of the design and operation of a wide range of nuclear plant. In order to prepare the foundations for future large-scale developments, a new modular code scheme called MCANO has been created from which new versions of both codes will emerge in 1993. In setting up MCANO the principal aims and objectives have included: creation of an effective common software development environment for the two main codes; optimisation of the use of the available mathematical modelling and software development expertise by removing unnecessary duplication; judicious rationalisation to produce a common user environment that would have significant efficiency benefits for users of both codes. This paper describes the design and development of the MCANO system and the resulting benefits that are beginning to emerge.

1. INTRODUCTION

In the fields of nuclear criticality safety and radiation shielding, Monte Carlo particle transport computer codes are important analytical tools. Indeed, in the criticality area, the Monte Carlo code is the principal calculational tool and, due to the high physical realism possible, forms the basis of the majority of criticality safety assessments. In the shielding area, the Monte Carlo method has been traditionally less extensively used. This has been due to the fact that many problems could be analysed with simpler, more approximate techniques as a lower level of absolute accuracy has been acceptable. In addition the wide-ranging requirements of a shielding study can make Monte Carlo a difficult to use and time-consuming method of solution. However improvements in recent year in code capabilities, user image and computer hardware, coupled with increasing accuracy requirements, are changing this situation to some extent and the Monte Carlo method is becoming established as a standard rigorous method in the shielding area as well.

The standard United Kingdom Monte Carlo particle transport codes are MONK [1] and MCBEND [2] for criticality and shielding respectively. These codes have been successfully used for over twenty-five years in support of the design and operation of a wide range of nuclear facilities covering the entire fuel cycle. They are now distributed and supported in use by the ANSWERS Software Service of AEA Technology, and the code development programme is performed and funded by the Nuclear Code Development Collaboration comprising AEA and British Nuclear Fuels Plc (BNFL).

The basic components of a Monte Carlo particle transport code are:

- nuclear data library
- material composition package
- source selection package
- geometry modelling and tracking package
- nuclear collision processing package
- scoring package

These are common requirements for codes for both criticality and shielding applications. In addition, the two areas each have their own individual requirements, such as variance reduction for shielding and fission powering for criticality. However the large overlap between the basic requirements of the two application areas suggests that some savings in efficiency could accrue, both for the code developers and the code users, if the codes MONK and MCBEND could be combined in some sensible way: this is the essence of the MCANO Monte Carlo modular code scheme. This paper describes the creation of the MCANO scheme and its current status.

2. HISTORICAL BACKGROUND

MCBEND was originally designed as a modular code. By modular, we mean that the distinct functions of the code are clearly separated as individual code units or modules, each comprising a number of FORTRAN subroutines. These function modules interact by using a standard suite of management routines which control the storage and flow of data. At the highest level a controlling module acts as the traditional main routine to define a sequence of function modules that form a complete code. The use of modular programming enables the code to be more easily maintained, developed and tested, and enables spin-off codes to be produced at minimal cost.

MONK on the other hand is not a modular code, although it does simulate the behaviour of a modular code in the collision processing area (the so-called DICE module). For all other parts of the code, MONK is typical of an ageing large scientific code with some inherent structure but with little in the way of formal data management as embodied in MCBEND. It has long been recognised as a requirement that some remedial action would be beneficial in order to facilitate the future development of MONK.

The MCANO project was set up with the following objectives:

- to provide a stable and effective software development environment for a range of application areas
- to rationalise and optimise the use of the available software development and maintenance resources
- to bring MONK into a modern programming environment to ease future development activity
- to enable future large scale developments to be more widely utilised with minimal additional overheads

3. THE MODULAR PROGRAMMING ENVIRONMENT

The modular structure used to create and develop MCBEND was originally devised by Bendall and Grimstone in the late 1960's. The system provides a suite of utility subroutines to manage the storage of data within a FORTRAN programme and defines conventions for the development of mutually consistent function modules.

For over twenty years this modular system has proved a valuable method of overcoming limitations with the FORTRAN language for the development of large complex codes with massive data management requirements. In addition by clearly breaking down a complex code into its basic functional units, the efficiency of many aspects of the software development life cycle have been improved. This is especially true when multiple concurrent developments are being performed.

The fundamental principles of the system remain as valid now as when they were first introduced, but experience and hindsight have led to the enhancement of the system over the years. For the purposes of the MCANO scheme it was decided to perform a review and revision of the system as a pre-requisite of the new project. This work led to the creation of WRMS (the Winfrith Revised Modular System) by Shuttleworth in 1991 and the MCANO code scheme is based around the WRMS system.

A computer code developed within the WRMS environment comprises three components: standard utility packages, to provide all the WRMS service requirements associated with reading, storing, manipulating and transferring data; a set of function modules, each of which performs a particular task; a control module, to control the execution of the computer code by calling appropriate function modules. Each function module consists of up to four separate sections accessible via distinct subroutine calls: an input section, to read any additional data or to access existing data; a set-up section, to process input data into a structure convenient for the calculation; a calculation section, to perform the particular task of the function module; and an output section, to process and possibly display the derived data.

Within a WRMS-based code all global data (that is data required by more than one function module) may be kept either as datagroups or scalars. A datagroup is a structured collection of elements (for example, an array) whereas a scalar is a single element of data.

A datagroup is attributed to a selection of modules and is catalogued against them by being assigned a unique number for each one. Normally only one of these modules will derive the given datagroup, the remainder will access and use it. However this situation will clearly alter is there are several methods of deriving the datagroup which arise at different times. Each scalar is named and kept in the data dictionary utility of the WRMS system. Communication of data between a control module and its function modules takes place solely by one or other of the following three methods: aliases created in the control module between datagroups in different function modules; the use of scalars by name, using the data dictionary routines; or the use of subroutine argument lists.

4. THE MCANO CODE SCHEME

4.1 Overview

MCANO is a Monte Carlo modular code scheme based on the WRMS principles outlined above. MCANO is therefore not a code in its own right but a library of modules from which codes are constructed. This library can comprise any number of function modules together with a controlling module for each code contained in the scheme. In the steady state, by adhering to the WRMS principles and employing a strict version control system, new issues of any code in the scheme can be readily constructed.

For a software environment involving multiple concurrent developments on different modules aimed at different codes, the environment needs to be carefully controlled in line with established QA principles. The administration and management of the MCANO scheme is performed by the Scheme Controller and the Scheme Custodian. The Scheme Controller is responsible: for co-ordinating and monitoring development activities for MCANO scheme modules; ensuring that the integrity of the modular scheme is maintained; and co-ordinating the investigation and correction of reported code errors. The Scheme Custodian is responsible for safeguarding the library of modules and supplying them to developers; creating ANSWERS code products from the MCANO scheme; and logging errors reported by ANSWERS customers for the MCANO-based codes.

The first step for the MCANO scheme was to produce a code scheme from which versions of MONK and MCBEND could be constructed. Given that earlier versions of MCBEND were constructed in a modular environment that was a predecessor of that employed for MCANO, the obvious starting point was to upgrade the existing MCBEND function modules and incorporate additional function modules to cover the additional requirements of MONK. Then new controlling modules for MCBEND and MONK could be produced to complete the codes.

4.2 Creating MCANO

We identified above the basic requirements of a Monte Carlo particle transport code. If we examine the basic functionality of MCBEND and MONK against these five requirements (together with an 'other major features' category) we can see the work plan emerge that has led to the creation of the MCANO scheme.

Feature	MCBEND	MONK
Nuclear data library	Continuous energy (multigroup for cross-checks)	Continuous energy (multigroup for cross-checks)
Material composition package	Individual isotopes, standard materials	Individual isotopes
Source selection package	Location, energy, direction	Location, material
Geometry modelling and tracking package	Simple bodies constructed using combinatorial geometry principles	Simple bodies in hierarchic combinations together with hole geometries (Woodcock tracking)
Nuclear collision processing package	Neutrons, gammas, electrons, positrons	Neutrons
Scoring package	Flux, energy deposition, charge, pulse height etc.	K-effective, reaction rates etc.
Other major features	Variance reduction techniques, sensitivities, time dependence	Fission powering, perturbations

In order to meet the MCANO objectives the following requirements needed to be addressed:

- rationalise similar options to remove unnecessary duplication of functionality
- streamline common options to remove any unnecessary code specific overheads
- combine related options into single functional modules
- maintain the existing user-images as far as is reasonably practicable
- develop the combined user-image for future developments

Of the main parts of a Monte Carlo code identified above, basic consistency between MCBEND and MONK already existed in the neutron nuclear data and collision processing areas prior to the MCANO project. The standard system employed in both MCBEND and MONK is the DICE continuous energy collision processing package and an ultra-fine energy mesh data library (8220 energy groups). This situation was reached as part of the MONK6 development project in the early 1980's and, although each version of DICE had minor code-specific interface differences, this was a first significant step towards rationalisation, pre-dating the MCANO project by some ten years. This has enabled a major part of the MCANO scheme to be set up at minimum cost. As it is only MCBEND that is interested in anything other than neutron interactions, the existing MCBEND capability could form another part of MCANO.

The commonality in the nuclear collision processing has enabled a new thermalisation treatment, comprising a $S(\alpha,\beta)$ representation of incoherent inelastic scattering and an incoherent elastic scattering capability for organic compounds of hydrogen, to be incorporated into both MCBEND and MONK with no code-specific overhead. In addition a common access route from the JEF nuclear data library has been established.

The main software development activity has been therefore concentrated on rationalising the other areas of geometry modelling, source selection and scoring. The most significant product from this work is the Fractal Geometry package [4] which combines the best features of the MONK and MCBEND geometry packages in a single entity. In fact what has been done is to retain the user-friendly concepts of the MONK user image and incorporate the MCBEND user image as a logical extension; however behind the scenes all of the geometry tracking is performed by a revised module based on the original MCBEND techniques, which are more efficient than the original MONK implementation.

For the source selection area the MCBEND source module has been used as a starting point for MCANO as with a small number of exceptions the MONK requirement are a sub-set of those for MCBEND. The additional requirements for MONK are being added as a natural extension to the existing MCBEND capability. For the scoring area the starting point was again the existing MCBEND module and this is sufficient for some of the criticality scoring requirements. However for scoring and calculating k-effective a new MONK module has been produced.

The programme of work summarised above has resulted in the creation of the first generation MCANO scheme. As a result a collaborative software development programme is now being performed within AEA and BNFL employing the MCANO scheme. This development programme will lead to the first code versions from MCANO later this year, namely MONK7 and MCBEND8.

4.3 Future Development Plans

The work on the MCANO code scheme to date has been aimed largely at rationalising and combining existing code facilities, with the notable exception of the new thermalisation treatment. This has been an essential process of laying down foundations to carry the UK Monte Carlo particle transport code development activity forward in a cost-effective manner. This initial stage of the MCANO project will be essentially complete once the release of the first MCANO-based codes has been performed. Subsequent development will then be aimed at enhancing and improving the functionality of the MCANO system.

The largest planned major development area is the renewal of the continuous energy collision processing package DICE, largely in order provide better access to the JEF nuclear data library formats. This work is currently at the design stage and the wide-ranging user requirements are being assembled. These include the requirements of a range of particle and collision types, both forward and adjoint modes of operation, sensitivity and perturbation facilities and, of course, the basic accuracy needs of the different application areas.

Coupled to this work will be a review of the continuous energy mesh used in MCANO. The use of continuous energy collision processing was one of the original requirements for UK Monte Carlo particle transport codes and the creation of the 8220 energy group scheme was made in the late 1970's. In 1993 the availability of cheap and powerful computer processing allied with ever increasing accuracy requirements, both from a safety and an efficiency point of view, suggest that even greater detail is possible and required in the nuclear data library.

Whilst the MCANO scheme so far only contains modules for the codes MCBEND and MONK, this is far from being the perceived final position. An existing code that would fit conveniently into the MCANO scheme is the RANKERN point kernel code [3], that already contains some MCBEND components. This is a logical extension of the scheme within an existing application area.

In addition MCBEND has been used to great effect in the oil industry for analysing both neutron and gamma-ray oil-well logging instruments. Here the modular construction of MCANO provides a convenient means of creating application-specific codes from a sub-set of the available modules at minimum cost. A further planned extension of the MCANO scheme is to include deterministic solution modules to enable survey codes to be created which employed a similar user image to that of the Monte Carlo codes.

4.4 Graphical User Interface

The above MCANO development plans are concerned with three distinct areas: increasing the physical realism of the existing codes to provide improved accuracy and confidence; enhancing the repertoire of the existing codes by providing additional features and facilities; and augmenting the scheme with additional codes, either directly or by the creation of spin-off codes based on existing modules. With the establishment of the MCANO scheme now essentially complete, attention is now also turning to the question of user interaction with the MCANO codes.

The use of MCBEND and MONK at present follows a traditional route: prepare an input text file using standard computer editing facilities; submit a batch calculation; examine an output text file. Despite the basic user-friendliness of the modelling packages, this leads to a situation where a lot of effort and experience can be required to employ the codes successfully. The geometric modelling is labour intensive and much duplication of effort can occur. In addition the interpretation and analysis of results is a time consuming and difficult process with the related uncertainties being difficult to quantify.

In order to meet the challenges of the coming years and to exploit the recent advances in computer technology, a parallel development project to that identified above has been set up which will make the codes significantly easier to use by developing a user oriented computer software environment within which the codes are embedded. The computer software environment will be produced in an integrated yet flexible way which can respond to a range of user interaction requirements and cope with extensions to meet new situations.

The intended features can be summarised as follows:

(a) Integrated Computer Desktop

Work has already started on producing a set of analysis tools to support and ease the use of the identified physics codes. At present work has been concerned solely with geometry model visualisation and has led to two- and three-dimensional interactive packages for the MCANO codes (VISAGE and VISTA). It is envisaged that additional tools will be developed to provide facilities such as multi-dimensional output display, auditable computer file management and window/menu based input data facilities.

(b) Engineering Design Link

There is an emerging requirement that the design and assessment of new plant be based directly on common engineering data. In order to achieve this, consideration is being given to the creation of formal two-way links between the MCANO codes and engineering computer aided design (CAD) databases.

(c) Expert System

Additional analysis tools that interact in a more intelligent way with the operation of the MCANO codes are now being investigated. It is envisaged that this set of tools will include intelligent pre- and post-processors, proactive diagnostic analysis, real time monitoring of calculational performance, integrated uncertainty analysis, optimum parameter searching and links to a range of supporting material and data.

Although clearly ambitious, the above plans are all feasible with existing technology and are aimed to bring the use of particle tracking Monte Carlo codes into a modern environment similar to that enjoyed by more conventional engineering disciplines for some time. By combining MCBEND and MONK in the MCANO scheme, and by aiming to extend the scheme to address new application areas, the user-oriented desktop environment can become less of a dream and more of a reality.

5. CONCLUSIONS

This paper has described the investment that has been made in the United Kingdom to improve both the user and software development environments for the major Monte Carlo particle transport computer codes. To accomplish this, a new modular code scheme called MCANO has been set up from which new generation versions of the criticality code MONK and the shielding code MCBEND will be developed. The benefits of the new arrangement are already being realised, with collaborative on-going developments being performed within both AEA and BNFL with minimal additional cost, and large-scale across-application development plans being proposed with little or no code specific overheads. For the code user, the ability to move readily between two major codes with a common user image will have a significant efficiency benefit from reduced costs of training and maintenance of code expertise, as well as reducing overall modelling effort. For the future it is envisaged that the MCANO scheme will continue to grow to extend the capability of the existing codes, to encompass other codes within the same application areas, and to meet the requirements of new application areas.

6 REFERENCES

[1] N R Smith
A Summary of the Current Status of the MONK6 Code and its Validation for Criticality Applications (International Conference on Nuclear Criticality Safety ICNC'91, Oxford, UK 1991)

[2] S J Chucas, I J Curl & P C Miller,
The Advanced Features of the Monte Carlo Code MCBEND (Seminar on Advanced Monte Carlo Computer Programs for Radiation Transport, Saclay, France 1993)

[3] P C Miller
RANKERN - A Point-Kernel Integration Code for Complicated Geometry Problems (Sixth International Shielding Conference, Tokyo, Japan 1983)

[4] N R Smith, E Shuttleworth & M H Watmough
A New Approach to Geometry Modelling and Visualisation for MONK and MCBEND (Seminar on Advanced Monte Carlo Computer Programs for Radiation Transport, Saclay, France 1993)

ITS VERSION 3.0:
THE INTEGRATED TIGER SERIES OF
COUPLED ELECTRON/PHOTON MONTE CARLO TRANSPORT CODES [1]

J. A. Halbleib, R. P. Kensek, G. D. Valdez & T. A. Mehlhorn
Sandia National Laboratory, USA

S. M. Seltzer & M. J. Berger
National Institute of Standards and Technology, USA

ABSTRACT

ITS is a powerful and user-friendly software package permitting state-of-the-art Monte Carlo solution of linear time-independent coupled electron/photon radiation transport problems, with or without the presence of macroscopic electric and magnetic fields. It combines operational simplicity and physical accuracy in order to provide experimentalists and theorists alike with a method for the routine but rigorous solution of sophisticated radiation transport problems. Flexibility of construction permits tailoring of the codes to specific applications and extension of code capabilities to more complex applications through simple update procedures.

[1]This work was supproted by the U. S. Department of Energy under Contract No. DE-AC04-76DP00789

1. Introduction

The Integrated TIGER Series (ITS), [2] - [3] - [4], is a system of time-independent, multimaterial and multidimensional coupled electron/photon Monte Carlo transport codes designed to provide a state-of-the-art description of the production and transport of the electron/photon cascade. It is based primarily on the ETRAN model, [4] - [5], which combines microscopic random walk, [6], for electron transport. Emphasis is on simplicity of application without sacrificing the rigor or sophistication of the physical model.

A brief description of the ITS system will be given in Section 2 before presenting sample results of extensive benchmarks in Section 3.

2. Overview of the System

Features / Geometry	Standard Codes	P Codes Enhanced Ionization/Relaxation	M Codes Macroscopic Fields
1-D	TIGER	TIGERP	
2-D/3-D	CYLTRAN	CYLTRANP	CYLTRANM
3-D	ACCEPT	ACCEPTP	ACCEPTM

TABLE 1. ITS Member Codes

From top to bottom, the member codes grouped by row in Table 1 will be referred to as the TIGER codes, the CYLTRAN codes, and the ACCEPT codes, respectively.

From left to right, the codes grouped by column will be referred to as the standard codes, the P codes and the M codes, respectively. All member codes of the ITS system allow transport over the range from 1.0 GeV to 1.0 keV.

Fluorescence and Auger processes in the standard codes are only allowed for the K shell of the highest atomic number element in a given material. For some applications, it is desirable to have a more detailed model of the low energy transport. In the P codes, a more elaborate ionization/ relaxation model from the SANDYL code, [7], was added to the standard codes.

In the M codes, the collisional transport of the standard codes is combined with transport in macroscopic electric and magnetic fields of arbitrary spatial dependence. A high order Runga-Kutta-Fehlberg algorithm, [8] - [9], is employed to integrate the Lorentz force equations.

The three objectives of the ITS development are:

1. to employ the most sophisticated and accurate physical model;

2. to provide a code system that can be used to address a wide range of scientific and engineering applications;

3. and to accomplish the first two objectives with robust software of exceptional user friendliness.

The physical model is outlined in Table 2.

PHYSICAL MODEL
• Production and Transport of $e^+/e^-/\gamma$ Cascade
(a) Electron/Positron Interactions
Energy loss straggling
Elastic scattering
Production of knock-on electrons
Impact ionization followed by production of fluorescence photons and/or Auger electrons
Bremsstrahlung production
Production of annihilation radiation
(b) Photon Interactions
Photoelectric absorption with the production of photoelectrons. Auger electrons, and fluorescence photons
Incoherent scattering with the production of scattered electrons
Coherent scattering
Pair production
• Transport in Macroscopic Electric (voids) and Magnetic Fields of Arbitrary Spatial Dependence

TABLE 2. ITS Physical Model

A model that includes this complex set of phenomena results in a very sophisticated simulation of the generation and transport of the electron/photon cascade. Much of the flexibility of application derives from the variety exhibited by the member codes of Table 1. This flexibility is further enhanced by the ease with which users can modify the member codes. Robustness is achieved through extensive internal error detection and by providing informative diagnostics. Flexibility and user friendliness is most easily perceived from a description of I/O, which we will now summarize.

There are four essential elements of the ITS system:

1. The atomic data file,

2. The program file for generating cross sections,

3. The Monte Carlo program file,

4. The update processor.

The atomic data file contains the data for generating cross sections for arbitrary mixtures or compounds of the first 100 elements. The two program files contain multiple machine versions of the multiple codes (Table 1 for the Monte Carlo program file), integrated in such a way as to minimize common coding. Their corresponding binary program libraries are input to the update processor, [10], which selects a particular code for a particular machine and makes any modifications requested by the user. The output of the processor is a code that is ready for compilation.

Apart from the atomic data file, which is read by the cross-section generator, and the cross section output file produced by the generator, which is read by the Monte Carlo code, there are two other types of input required for running either the cross-section generator code or the Monte Carlo code. First, there is the set of instructions to the processor that tells it how to produce a compile-ready code from either of the program libraries (see [2] for instructions on the on-time-only creation, or installation, of the binary program libraries for each of the two program files). This input involves a simple syntax for defining code, machine, and a few other options. An equally simple syntax allows the user to modify the Fortran via deletions, insertions, and replacements. The user may make no

such modifications, thus treating the selected code like a "black box", or he/she may make elaborate and lengthy changes. An example of the latter is the complex variance reduction coding required for the absorption experiments of Section 4 of the companion paper on variance reduction in electron/ photon Monte Carlo. The second type of input is that required by the resulting executable code. For example, the problem materials and energy range must be specified for the cross-section generator code, and the problem geometry and source distribution must be defined for the Monte Carlo code.This input consists of a set of order-independent, free-formatted, descriptive keywords with their attendant numerical parameters that makes maximum use of defaults.

The default output consists of:

a) energy and number escape fractions (leakage) for electrons, unscattered primary photons, and scattered photons,

b) charge and energy deposition profiles,

c) an explicit statement of energy conservation,

d) for the TIGER codes, the number and energy electron boundary currents for each layer.

In addition to the default output, a number of optional outputs may be selected. These are:

a) escape fractions that are differential in energy for electrons, scattered continuum photons, and line radiation;

b) escape fractions that are differential in angle for electrons, scattered continuum photons and line radiation;

c) coupled energy and angular distributions of escaping electrons, scattered continuum photons and line radiation;

d) volume averaged fluxes that are differential in energy for electrons, scattered continuum photons, and line radiation for selected regions of the problem geometry;

e) volume averaged fluxes that are differential in angle for electrons, scattered continuum photons, and line radiation for selected regions of the problem geometry;

f) coupled energy and angular distribution of volume averaged fluxes of electrons, scattered continuum photons, and line radiation for selected regions of the problem geometry;

g) a pseudo-pulse-height distribution for a selected region of the problem geometry - for example, the region corresponding to active detector elements;

h) geometry and trajectory plots.

Except for an initial diagnostic table containing accounting information on the various particle types, every output quantity is followed by an estimate of its one-sigma statistical uncertainty.

A more detailed description of the structure and operation of the ITS system can be found in reference [2].

3. ITS Benchmarks

In this section we present selected experimental benchmarks of the ITS codes. For the period up through about 1987, a more comprehensive survey of ITS experimental benchmarks and engineering applications, as well as the results of extensively modified research versions of the system, can be found in Chapter 11 of reference [4].

• Miller, [11], used the CYLTRANP code to simulate the measurements of Farley et al., [12], of the two-dimensional energy deposition by a 500-MeV electron beam in layered targets using thermoluminescent dosimeters.

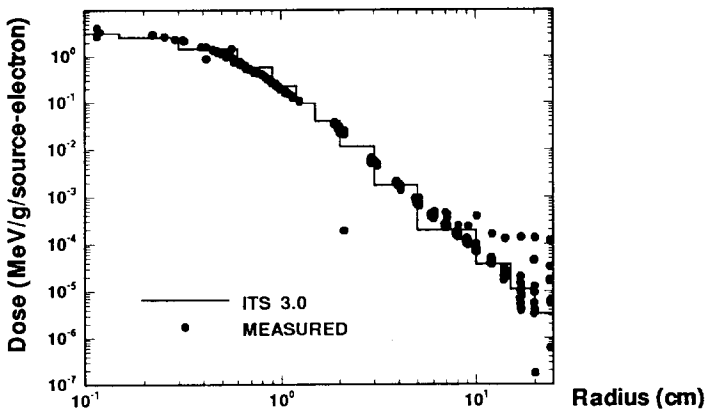

Figure 1. Radial deposition profile from a 500-MeV electron beam in LiF at a location 12 cm deep into an Al/Lucite/air configuration.

Figure 1 is a comparison of measured and predicted (CYLTRAN 3.0) radial profiles at a particular axial location in a configuration employing Al absorber plates. Using a modification of CYLTRAN for transport up to 100 GeV, Miller, [13], simulated the electron/photon cascade in a Pb/plastic scintillator stack at source electron energies of 10 and 15 GeV for comparison with the measurements of Müller, [14].

His results are shown in Figure 2.

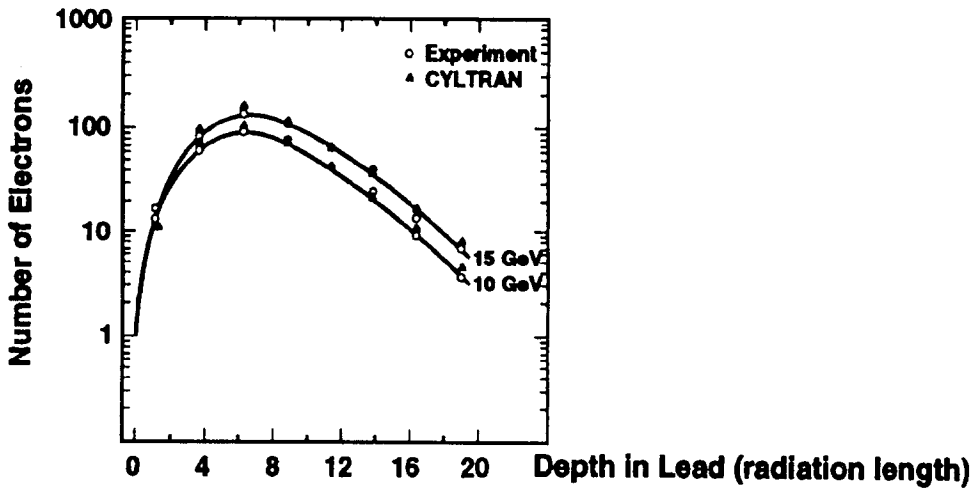

Figure 2. Scintillator deposition from 10- and 15-GeV electron beams in an alternating Pb/plastic scintillator configuration.

Theoretical and experimental depositions were normalized to the bare scintillator response to electrons at 7.4 MeV.

• Frederickson and Woolf, [15], measured charge deposition profiles in an electrically conductive carbon-filled polymer irradiated by monoenergetic electrons at kinetic energies from 0.4 to 1.4 MeV. Their results are compared with predictions of Version 3.0 of the TIGER code in Figure 3. At an order magnitude higher energy, Figure 4 compares TIGER code predictions with the measurements of Tabata et al., [16], in Be and Al.

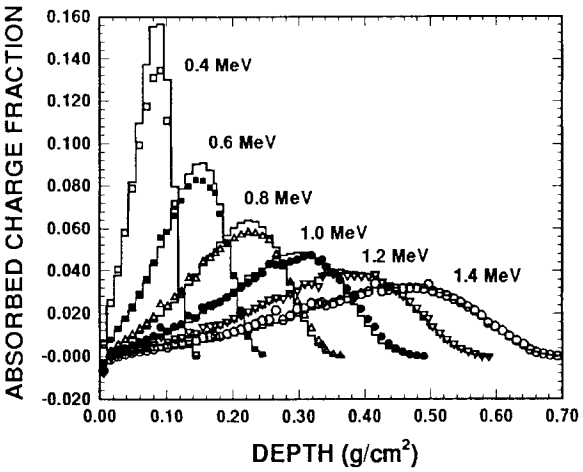

Figure 3. Comparison of measured (symbols) and predicted (histograms) charge deposition profiles in a carbon-filled polymer for various electron beam energies

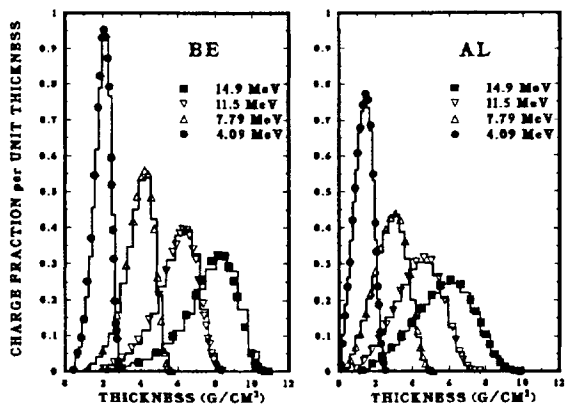

Figure 4. Comparison of measured (symbols) and predicted (histograms) charge deposition profiles in Be and Al for various electron beam energies.

• Considerable effort has been expended over the years to improve Monte Carlo transport of low energy electrons in high-Z media. Using an expanded scale to exaggerate the discrepancy, Figure 5 demonstrates this improvement by comparing predictions of the various versions of the TIGER code with the saturated backscatter data of Lockwood et al., [17] for Ta. This improvement has been achieved through the implementation of more accurate elastic scattering cross sections and energy-loss straggling distributions.

• Using a 1.0-MeV Van de Graaff accelerator, Beutler et al., [18], measured pulse-height distributions of hte X-rays from Ta converters in Ge detectors at a variety of energy. A measured distribution at an accelerator energy of 0.9 MeV is compared with the distribution predicted by Version 3.0 of the CYLTRANP code in Figure 6. Wender et al., [19], compared pulse-height distributions from monoenergetic photon sources calculated with CYLTRAN for a bismuth germanate scintillator with measured distributions. Figure 7 gives the results for a bare crystal at 6 MeV, and a crystal surrounded by Pb and with a ^{6}LiD absorber in front at 40 MeV. Mac Callum et al., [20], used the ACCEPT code to predict the spectrum, as measured by a bismuth germanate detector, of the bremsstrahlung backscattered when various materials were irradiated by 20-MeV electrons from a linac. Figure 8 compares their predictions with measured spectrum for a Pb target. Greenwood et al., [21], used the CYLTRAN code, in conjunction with a NaI(Ti)/Si coincidence configuration, to develop a total absorption gamma-ray spectrometer system for measuring the spectra of fission product nuclei. Figure 9 demonstrates the result of employing the system to derive a modified decay scheme for ^{141}Ba that is more consistent with the measured spectrum than that obtained using the published decay scheme.

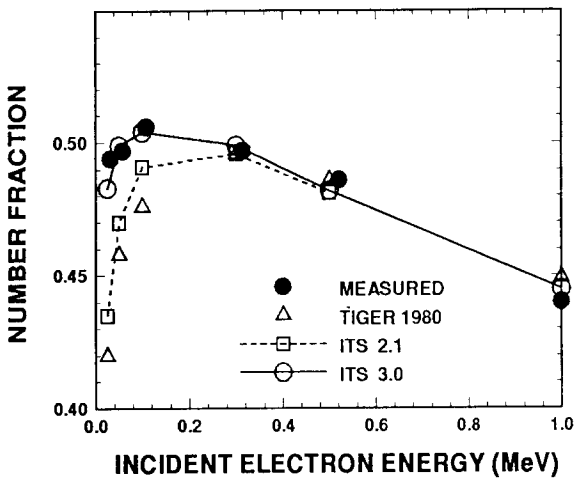

Figure 5. Comparison of measured electron backscatter from Ta with predictions of various versions of the TIGER code

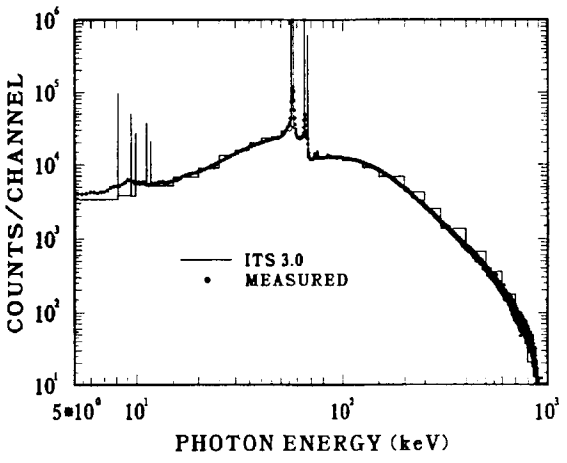

Figure 6. Measurements and CYLTRANP predictions of the pulse-height distribution in a Ge detector from the forward X-ray spectrum produced by a 0.9-MeV Van de Graaff electron beam on 0.089 mm of Ta

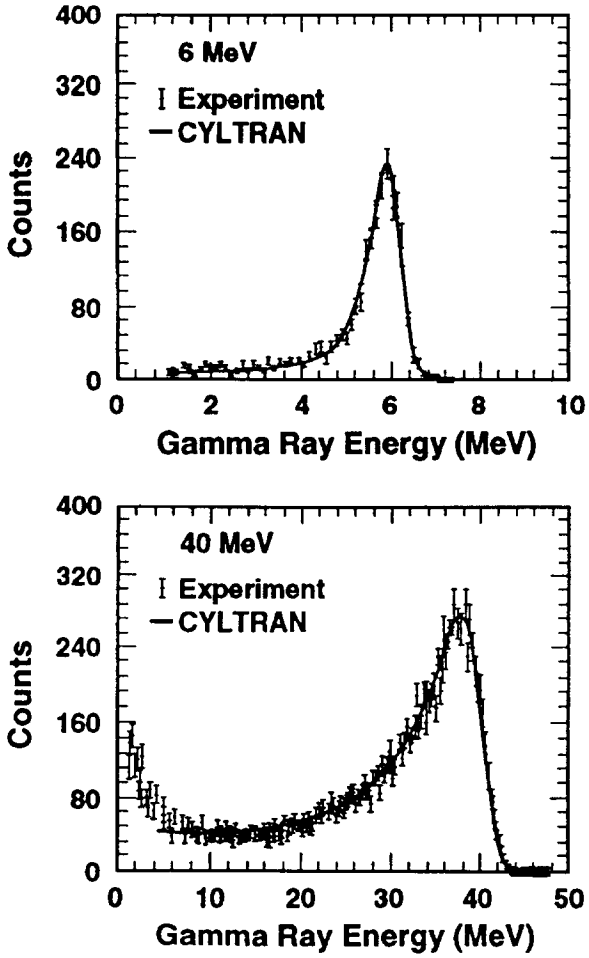

Figure 7. Measurements and CYLTRAN code predictions (solid lines) of the pulse-height distributions obtained using a bismuth germanate scintillator for monoenergetic photons. The upper curve is for 6.0-MeV photons incident on a bare crystal, and the lower curve is for 40.0-MeV photons incident on a crytal with a ^{6}LiD absorber in front and surrounded by Pb.

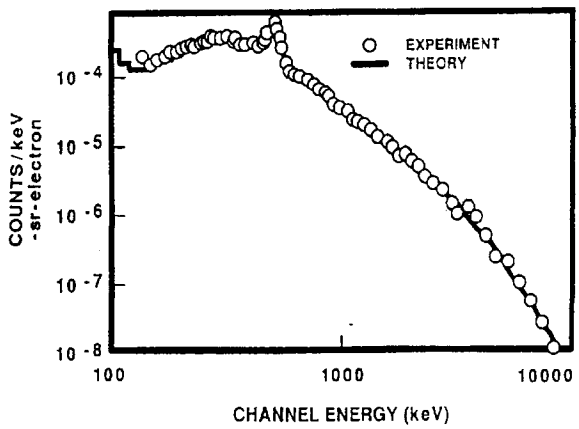

Figure 8. Measurements and ACCEPT code predictions of the pulse-height distributions obtained using a bismtuh germanate scintillator for the backdirected bremsstrahlung generated by 20-MeV electrons incident on a lead target.

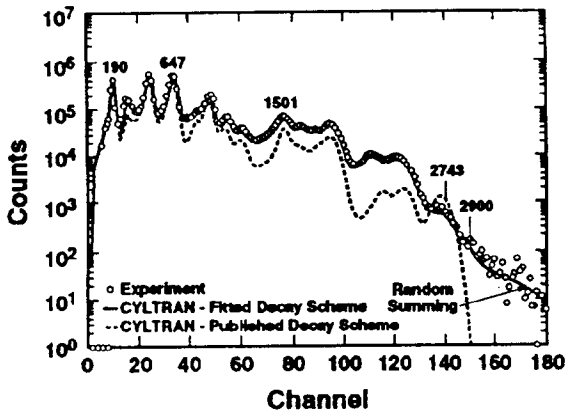

Figure 9. Measurements and CYLTRAN code predictions of the pulse-height distributions obtained using a NaI(Ti)/Si coincidence configuration for the decay spectrum of ^{141}Ba

The basic transport phenomenon that dominates most radiation effects requiring electron/photon simulation is photoemission, which determines the transport of charge and energy across material interfaces. Figure 10 is a comparison of a TIGER-code prediction, [22], of the forward photoemission spectrum from Cu foil with the measured data of Dolan, [23]. The source was a filtered 50-kV-peak X-ray spectrum. In Figure 11 are similar comparisons for a Ta foil, demonstrating the superiority of TIGERP over TIGER for this case. The photoemission is dominated by L-shell photoelectric, and, with its less sophisticated ionization/relaxation algorithms, the TIGER code gives too much energy to photoelectrons from the L shell. Users will probably find that it is only in the relatively small percentage of applications where ionization in shells other than the K shell, plays an important role that the slower running P codes will be required.

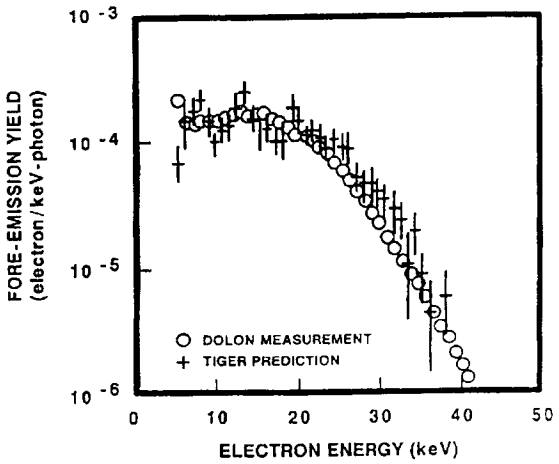

Figure 10. Measured and calculated forward photoemission from a Cu foil irradiated by a filtered 50-kV-peak bremsstrahlung spectrum

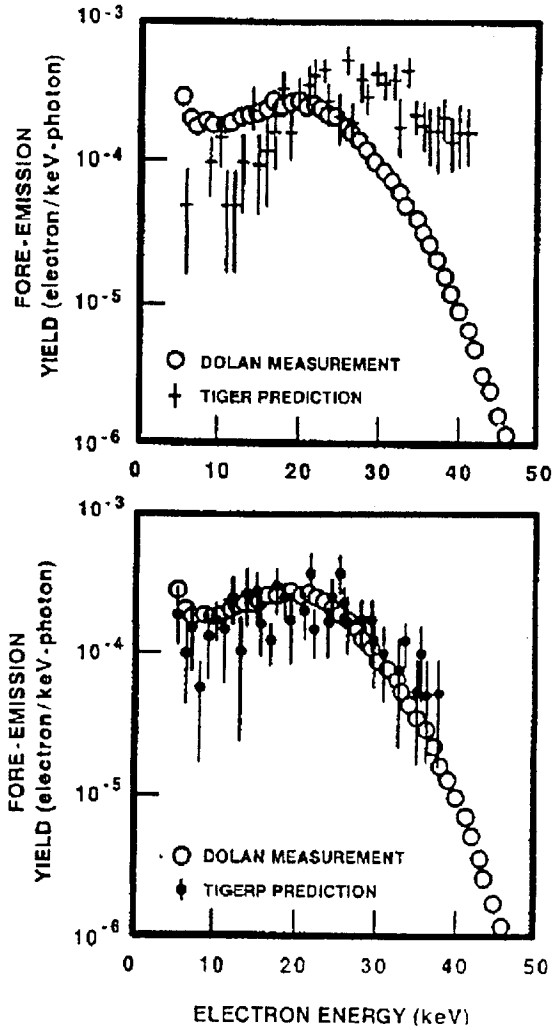

Figure 11. Measured and calculated forward photoemission from a Ta foil irradiated by a filtered 50-kV-peak bremsstrahlung spectrum, showing the superiority of TIGERP simulations (lower) over TIGER simulations (upper) for applications where ionization in shells other than the K shell plays a dominant role.

4. Concluding Remarks

Version 3.0 represents the first major upgrade of the ITS system, and the extensive improvements are as much a consequence of the many valuable suggestions by the user community as they are the results of our own limited experience. We continue to solicit feedback from the user community on further modifications that will enhance the utility and accuracy of the system. We sincerely hope that Version 3.0 of the ITS system will prove a successful tool for the design and analysis of that broad class of science and engineering applications in which the transport of electron, positron, and gamma radiation plays an important role.

References

[1] This work was supported by the U.S. Department of Energy under Contract No. DE8AC04876DP00789

[2] J. A. Halbleib, R. P. Kensek, T. A. Mehlhorn, G. D. Valdez, S. M. Seltzer & M. J. Berger, "ITS Version 3.0: The Integrated TIGER Series of Coupled Electron/Photon Monte Carlo Transport Codes", Sandia National Laboratories Report No. SAND91-1634, March 1992

[3] J. A. Halbleib, R. P. Kensek, T. A. Mehlhorn, G. D. Valdez, S. M. Seltzer & M. J. Berger, "ITS Version 3.0: The Integrated TIGER Series of Electron/Photon Transport Codes - Version 3.0", IEEE Trans. Nucl. Sci. 39, (1992) 1025

[4] M. Berger, S. M. Seltzer, J.A. Halbleib & R. Wang, "Monte Carlo Transport of Electrons and Photons", edited by T. M. Jenkins, W. R. Nelson & A. Rindi, (Plenum Publishing Corporation, 1988) Chapter 2-4 and 7-11

[5] M. J. Berger & S. M. Seltzer, "ETRAN Monte Carlo Code System for Electron and Photon Transport Through Extended Media", CCC-107, Radiation Shielding Information Center, Computer Code Collection, Oak Ridge National Laboratory, June 1968

[6] M. J. Berger, "Monte Carlo Calculation of the Penetration and Diffusion of Fast Charged Particles", Methods in Computational Physics, Vol. 1, (Academic, New York 1963)

[7] H. M. Colbert, "SANDYL: A Computer Code for Calculating Combined Photon/Electron Transport in Complex Systems", SLL-74-0012, Sandia National Laboratories, May 1974

[8] L. F. Shampine, H. A. Watts & S. Davenport, "Solving Nonstiff Ordinary Differential Equations - The State of the Art", SIAM Rev. 18, 376 (1976)

[9] K. L. Hiebert & L. F. Shampine, "Implicity Defined Output Points for Solutions of ODEs", SAND80-0180, Sandia National Laboratories, February 1980

[10] T. A. Mehlhorn & M. F. Young, "UPEML Version 3.0: A Machine-Portable CDC UPDATE Emulator", SAND92-0073, Sandia National Laboratories, March 1992

[11] S. G. Miller, "500 MeV Electron Beam Benchmark Experiment Revisited", DDV-88-0010, Lawrence Livermore National Laboratory, March 1988

[12] E. Farley, K. Crase & D. Selway, "500-MeV Electron Beam Benchmark Experiments and Calculations", UCRL-52871, Lawrence Livermore National Laboratory, December 1979

[13] G. Miller, "Extension of the Integrated TIGER Series (ITS) of Electron/Photon Monte Carlo Codes to 100 GeV", DDV-88-0019, Lawrence Livermore National Laboratory, July 1988

[14] D. Müller, "Electron Showers of High Primary Energy in Lead", Phys. Rev. 5, (1972) 2677

[15] A. R. Frederickson & S. Woolf, "Electron Beam Current Penetration in Semi-Infinite Slabs", IEEE Trans. Nucl. Sci. NS-28, (1981) 4186

[16] T. Tabata, R. Ito, S. Okabe & Y. Fujita, "Charge Distribution Produced by 4- to 24-MeV Electrons in Elemental Materials", Phys. Rev; B 3, (February 1971) 572

[17] G. J. Lockwood, L. E. Ruggles, G.H. Miller & J. A. Halbleib, "Electron Energy and Charge Albedos - Calometric Measurement vs Monte Carlo Theory", SAND80-1968, Sandia National Laboratories, Reprinted February 1987

[18] D. E. Beutler, J. A. Halbleib & D. P. Knott, "Comparison of Experimental Pulse-Height Distribution in Germanium Detectors with Integrated-TIGER-Series-Code Predictions", IEEE Trans. Nucl. Sci. 36, 1912 (December 1989)

[19] A. Wender, G. F. Auchampaugh, H. Hsu, P. T. Debevec, S. F. Lebrun & S. D. Hoblit, "Response Functions for Bismuth Germanate Detectors", Nucl. Instr. Meth. Phys. Res. A258, 225 (1987)

[20] Private Communication, C. J. MacCallum, University of New Mexico, Albuquerque, NM, USA

[21] R. C. Greenwood, R. G. Helmer, M. A. Lee, M. H. Putman, M. A. Oates, D. A. Stuttmann & K. D. Watts, "Total Absorption Gamma-Ray Spectrometer for Measurement of Beta-Decay Intensity Distributions for Fission Product Radionuclides", Nucl. Instr. Meth. Res. A314, 514 (1992)

[22] Private communication, K. J. Adams, Science Applications International Corporation McLean, VA 22102, USA

[23] K. W. Dolan, "X-Ray-Induced Electron Emission from Metals", J. Appl. Phys. 46, 2456 (June 1975).

Session II

AUTOMATIC / SEMI-AUTOMATIC BIASING SCHEMES - THEIR PERFORMANCE AND BENCHMARKING -

CHAIRS:

***G. LEDANOIS**, CEA - FRANCE*
***K. W. BURN**, ENEA - ITALY*

PRESENT STATE OF THE DIRECT STATISTICAL APPROACH (CELL MODEL) TO SEMI-AUTOMATIC VARIANCE REDUCTION

K.W.BURN

ENEA, Dipartimento Reattori Innovativi,
Via Martiri di Monte Sole, 4, 40129 Bologna, Italy

Abstract: The Direct Statistical Approach (DSA) represents a rigorous mathematical approach to optimizing surface splitting and Russian Roulette (RR) in Monte Carlo applied at present to fixed source neutron and photon transport. It is currently operational and provides optimized splitting/RR parameters in a wide variety of deep penetration problems, involving both bulk shielding and streaming. This paper summarizes the derivation and gives the present state of the DSA (cell model) and indicates contemporary and future directions of development.

1. SURFACE SPLITTING AND RUSSIAN ROULETTE

The surface splitting and Russian Roulette (RR) game is one of the oldest and easiest to use variance reduction techniques. It involves no change to the transport operator. A parameter $\nu(i)$ is assigned to each surface i (the surface may be in normal space, in energy and in angle). In the direction of crossing that is towards the detector, the particle is split $\nu(i)$-to-1 with the weight of each progeny updated by the factor $1/\nu(i)$. In the other direction of crossing, the particle is Russian Rouletted with survival probability $1/\nu(i)$. If it survives, its weight is updated by the factor $\nu(i)$:

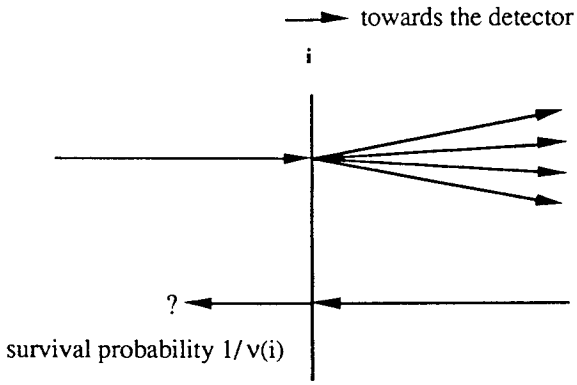

Fig. 1:
Surface Splitting/RR

The user must supply the parameters $\nu(i)$. Whilst leaving the expected value of the first moment unaltered, appropriate values of these parameters increase the efficiency of the calculation. (The parameters reduce the second moment S^2 and raise the time τ - both per source particle history. The efficiency of the calculation may be measured in terms of q^{-1} where $q = S^2.\tau$.) The Direct Statistical Approach (DSA) aims to supply optimized values of $\nu(i)$ that give a minimum value of q.

As a general rule, as well as being easier to use, this method is also less dangerous to use compared with methods that alter the transport operator, i.e. biasing methods. (The main danger is to produce an estimated response with a low estimated error, this estimated response being however much lower than the real response with a difference far greater than the estimated error. This because some contributing channels have not been sampled.) Nevertheless a method that alters the transport operator may be more efficient than surface splitting/RR if the operator is altered in an appropriate fashion - there is no way that the surface splitting/RR game can achieve zero variance whilst in theory the biasing game can.

Furthermore the surface splitting/RR method may not be efficient if used in

conjunction with fixed biasing techniques as the same degree of splitting/RR is carried out on all particles independent of their weight. In this case a weight window method that splits and Russian Roulettes according to the weight of the particle may be more efficient.

2. DEVELOPMENT OF THE VARIOUS DSA MODELS

The DSA, originated by Dubi (/1/, /2/, /3/), describes in a precise mathematical fashion the second moment per source history (also called the population second moment) and the time per source history, for the surface splitting/RR game. Of these two quantities the second moment is by far the more difficult both to express mathematically and to calculate, compared with the time.

The DSA applied to the game described in §1 has been named the DSA surface parameter model, splitting/RR being applied according to the value of the parameter $\nu(i)$ that is attached to each surface i. In the surface parameter model described in /3/, the surfaces may be in a general configuration:

Fig. 2: General Surface Configuration in the DSA Surface Parameter Model

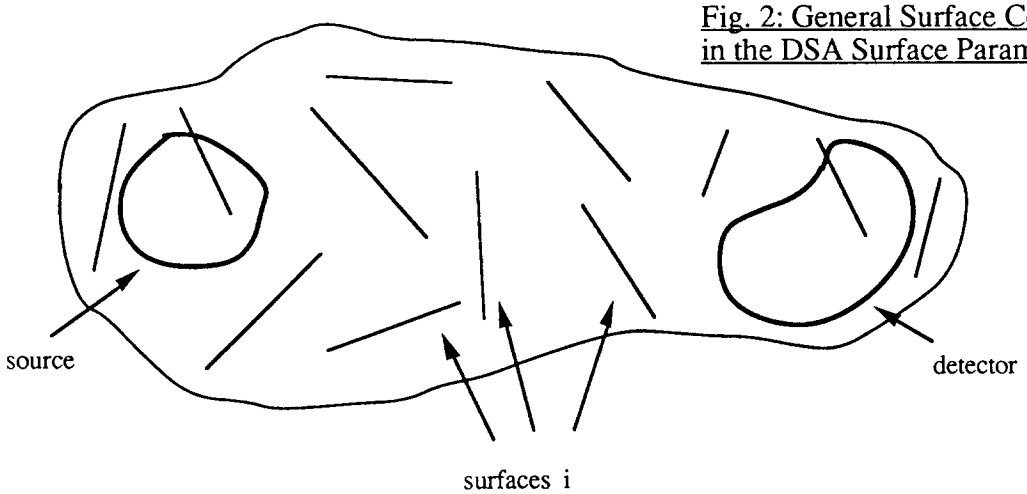

The DSA surface parameter model has been employed on a wide variety of problems /4/. The surfaces i may currently be defined in normal space and in energy.

The surface parameter model was then extended by allowing the parameter $\nu(i)$ to be non-integer (/5/). Now the procedure followed when crossing the surface in the direction towards the detector ($\nu(i)>1$) is as follows:

- divide $\nu(i)$ into its integer part $\eta^*(i)=\text{Int}(\nu(i))$ and decimal part $R(i)=\nu(i)-\eta^*(i)$.

Then:

- with probability $R(i)$ split $(\eta^*(i)+1)$-to-1
- with probability $(1-R(i))$ split $\eta^*(i)$-to-1.

These are exclusive. In either case the weight is updated by the factor $1/\nu(i)$. This has been called "expected value splitting" /6/. Russian Roulette is treated as before.

Because when $\nu(i)<1$, $\eta^*(i)=0$, splitting and RR have been unified in a single algorithm and it is no longer necessary to define *a priori* the "towards the detector" direction.

As it is now non-integer, $\nu(i)$ may be defined as the ratio of parameters assigned to the volumes on either side of the surface. If the particle is leaving volume j and entering volume k, with attached parameters F(j) and F(k), splitting/RR is performed at the surface i according to the value of F(k)/F(j). If this ratio is greater than 1, splitting ensues and if it is less than 1 Russian Roulette ensues:

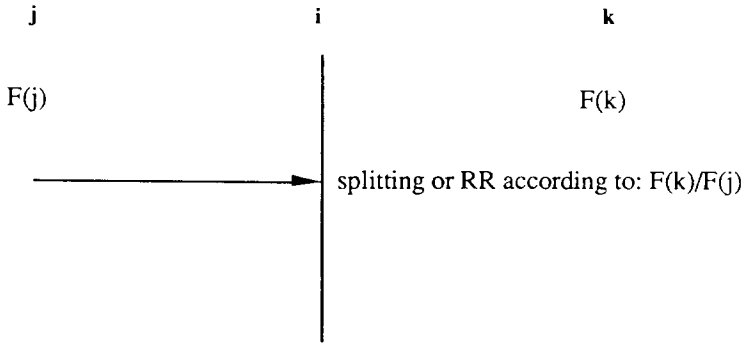

Fig. 3: Splitting/RR at Surfaces according to Cell Importances

This is the DSA volume parameter model /5/. A constraint was then introduced that all phase space should be covered by the volumes j and k:

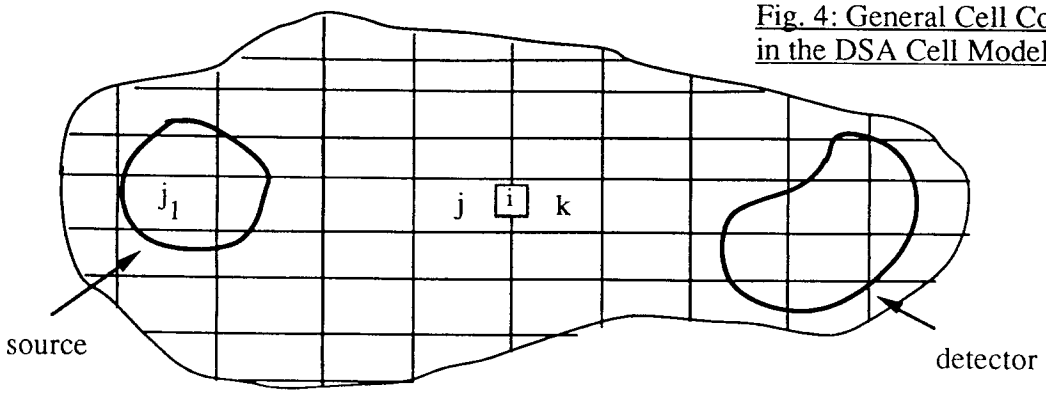

Fig. 4: General Cell Configuration in the DSA Cell Model

This is the DSA cell model (/5/, /7/ and /8/). The volumes j and k are called cells and the volume parameters, F, are called cell importances. Instead of providing optimized surface parameters, v(i), the DSA provides optimized cell importances F(j).

3. THE DSA CELL MODEL

The DSA cell model described above leads to important changes in the nature of the second moment and time functions compared with the functions resulting from the volume parameter model. The functions of the cell model are closed whilst those of the surface parameter and volume parameter models are open. (This has important consequences on the way that these functions are calculated.) The second moment function in the cell model is as follows (see expression (1) of /7/ and expression (5) of /8/):

$$S^2 = \sum_{j_1} \sum_{j,k} C_o(j_1,j,k) \cdot \frac{F(j_1)}{F(k)} \cdot \frac{Int(G(j,k))}{G(j,k)} \cdot \left[2.G(j,k) - Int(G(j,k)) - 1\right] + \sum_{j_1} \sum_{j} B_o(j_1,j) \cdot \frac{F(j_1)}{F(j)} \qquad (1)$$

where:

- j_1 is the source cell (see fig. 4)
- j and k are adjacent cells (see fig. 4)
- F( ) are the cell importances
- G(j,k) = F(k)/F(j)
- Int(G(j,k)) is the integer part of G(j,k)
- $C_o(j_1,j,k)$ is a coefficient that depends on the source-to-surface and surface-to-surface transition probabilities and squares of accumulated weights between a source cell j_1 and the boundary between cells j and k, and on the square of the adjoint flux at the same boundary
- $B_o(j_1,j)$ is a coefficient that depends on the source-to-surface, surface-to-surface and surface-to-detector transition probabilities and squares of accumulated weights between a source cell j_1 and a cell j in which a detector contribution is made (for the surface-to-detector transitions the accumulated weight includes the detector score)

The time function in the cell model is as follows (see expression (4) of /7/ and

expression (8) of /8/):

$$\tau = \sum_{j_1} \sum_{j} D_o(j_1,j) \cdot \frac{F(j)}{F(j_1)} \qquad (2)$$

where:

- $D_o(j_1,j)$ is a coefficient that depends on the source-to-surface and surface-to-surface transition probabilities between a source cell j_1 and a cell j, and on the average CPU time spent by tracks in cell j

The functions are closed because in any problem there is a finite and known number of source cells j_1, of cells j and of pairs of adjacent cells j and k. However the coefficients C_o, B_o and D_o consist in most problems of infinite (convergent) series, similar in structure to the first moment when written in terms of the DSA variables (the surface-to-surface transition probabilities and accumulated weights), the important difference compared to the first moment being the presence in the C_o coefficients of the term: $[\phi^*(p(j,k))]^2$ (where p is a phase space point on the boundary between cells j and k, and ϕ^* is the adjoint flux at p).

4. CALCULATING THE SECOND MOMENT AND TIME IN THE CELL MODEL

Monte Carlo is used to estimate the coefficients C_o, B_o and D_o. At present there are two algorithms that calculate the C_o coefficients. The first calculates the exact coefficients by estimating $[\phi^*(p(j,k))]^2$ at every phase space crossing point on every boundary between cells. This is carried out with a sample N that must be at least 2 (i.e. at every boundary between cells with some non-zero probability a splitting of at least 2-to-1 must be made). Also at least 2 samples out of N must give a non-zero detector score to give a non-zero estimate of $[\phi^*(p(j,k))]^2$ at that phase space crossing point (/7/ and /8/). The consequences of this are that a rather different population of tracks in the cells is required compared with a normal first moment calculation, and even then the requirement of at least 2 non-zero scores from each splitting event means that a large error on the estimate of the C_o coefficients and consequently on the second moment ensues. This is the core of the problem of directly estimating the second moment with Monte Carlo.

The difficulties in estimating the exact second moment lead to consideration of an approach in which approximate C_0 coefficients and therefore an approximate second moment was estimated. The approximation used was the "point-surface approximation" (p-s approximation) (/9/, /7/ and /8/). This includes within the sample N used to estimate $[\phi^*(p(j,k))]^2$ all tracks passing from cell j to cell k and not just those tracks leaving phase space point p(j,k). Thus all phase space points on the boundary between cells j and k are assumed to have the same adjoint flux and the boundary is assumed to behave like a point in phase space. Using the p-s approximation, phase space cells may be populated in a similar fashion to that of a normal first moment calculation and the C_0 coefficients may be estimated to a much greater accuracy (as N is now large). When the boundary between cells j and k is too extensive in phase space so that the adjoint flux varies considerably over the boundary, the p-s approximation breaks down and the final importances turn out not to be optimum. In this case the exact algorithm must be employed.

As far as the time is concerned, this is a first moment-like quantity and the exact time function may be estimated with a high statistical accuracy.

Given the second moment and time functions, a code based on a standard IMSL library minimization routine is employed to find the optimum cell importances F( ) /8/.

5. CURRENT PERFORMANCE OF THE DSA CELL MODEL

The DSA cell model has been tested on a range of problems involving neutron-only or photon-only transport /8/. Currently the cells are defined in normal space and in energy. The DSA codes are based on MCNP version 4 /10/. One obvious problem at present is that the exact algorithm performs better than the p-s approximation algorithm on a certain range of problems (due to a breakdown of the p-s approximation), whilst the p-s approximation algorithm performs better than the exact algorithm on a different range of problems (due to statistical errors on the second moment with the exact algorithm) /8/ and /11/.

Recently a comparison has been made /11/ between results obtained using the DSA cell model and results obtained using the quasi-deterministic weight window generator /12/. Both bulk and streaming neutron-only problems were considered and differences between the two methods were observed in the streaming problems. (In streaming problems the exact DSA cell model algorithm must be used as the p-s approximation breaks down.)

It was a surprising result to find that the exact algorithm actually worked in a range of problems (streaming, single energy group, etc. /8/, /11/); i.e. that for some problems, it is

less CPU time-consuming to calculate the exact second moment even with a quite high statistical error and to run with the subsequent cell importances, than to run with importances that are user-guessed or found by some other means. This may be a result peculiar to the surface splitting/RR technique.

The DSA cell model has not been tested on coupled neutron/photon transport as the theory does not yet cover this (there are uncontrolled particle bifurcations - see §6).

6. PRESENT AND FUTURE DEVELOPMENTS OF THE DSA CELL MODEL

The developments may be divided into two groups:

a) Improvements and generalizations in the model

The current DSA cell model (and the volume and surface parameter models) contain the following specific assumptions and general limitations:

a) Particles are split and Russian Rouletted at DSA cell boundaries independently of the particle's weight (as described previously).

b) No bifurcations be they natural (e.g. (n,xn), fission) or artificial (e.g. DXTRAN, forced collision) are allowed within the DSA phase space cells.

c) A source particle cannot make a score without passing at least once into a new DSA cell.

d) A particle cannot cross into a new DSA cell after making a detector score.

The aim is to eliminate as many of these limitations as possible.

As far as b) is concerned, the problem of bifurcations between the DSA surfaces has been considered for the limited case of coupled neutron/photon transport /13/. The main problem here is the correlation between γ's produced at a neutron collision and the neutron as it continues its transport. Recently the bifurcation problem between the DSA surfaces has been treated in complete generality /14/. Also the limitation c) was removed (which is trivial).

It is intended to remove limitation d).

Finally it is intended to examine the possibility of also removing limitation a).

b) Improvements in the second moment algorithm

As already remarked, the present situation of the two second moment algorithms - exact and p-s approximation - is unsatisfactory. These two algorithms actually represent approaches to calculating the second moment from opposite extremes. The exact algorithm estimates the square of the adjoint flux at each individual phase space crossing point at each cell boundary. The p-s approximation algorithm, for a reasonably large number of particles crossing the boundary, estimates the average adjoint flux over the whole boundary and squares this estimate.

Work is underway on developing an algorithm that represents a compromise between these two extremes and that should perform satisfactorily on all problems. Such an algorithm will involve discretizations in energy and angle at each cell boundary, these discretizations being made automatically within the code /11/.

REFERENCES

1. Dubi A., Elprin T. and Dudziak D.J. "Geometrical Splitting in Monte Carlo", *Nucl. Sci. Eng.* **80** 139 (1982)

2. Dubi A. and Dudziak D.J. "Extended Model of Geometrical Surface Splitting in Monte Carlo", *Nucl. Sci. Eng.* **83** 487 (1983)

3. Dubi A. "General Statistical Model for Geometrical Splitting in Monte Carlo - I and II", *Trans. Theory and Stat. Phys.* **14-2** 167 and 195 (1985)

4. Dubi A., Goldfeld A. and Burn K.W. "An Automatic Package for Optimization of Splitting in the MCNP Code", Int. Top. Meeting on Advances in Reactor Physics, Mathematics and Computation, CEC-OECD/NEA, Paris, p. 1699 (1987)

5. Burn K.W. "Extension of the Direct Statistical Approach to a Volume Parameter Model (Non-Integer Splitting)", *Ann. nucl. Energy* **17-6** 293 (1990)

6. Booth T.E. "Monte Carlo Variance Comparison for Expected-Value versus Sampled Splitting", *Nucl. Sci. Eng.* 89 305 (1984)

7. Burn K.W. "Optimizing Cell Importances using an Extension of the DSA - Theory,

Implementation, Preliminary Results", *Progress in Nuclear Energy* **24** 39 (1990) (part of the Proceedings of the Int. Conf. on Monte Carlo Methods for Neutron and Photon Transport Calculations, Budapest, Hungary, Sept.1990)

8. Burn K.W. "Complete Optimization of Space/Energy Cell Importances with the DSA Cell Importance Model", *Ann. nucl. Energy* **19-2** 65 (1992)

9. Dubi A., Goldfeld A. and Burn K.W. "Algorithms for the Calculation of the Second Moment of Geometrical Splitting in Monte Carlo", *Trans. Theory and Stat. Phys.* **16-8** 1149 (1987)

10. LANL (J.F. Briesmeister, Ed.) "MCNP - A General Monte Carlo Code for Neutron and Photon Transport Version 3A" LA-7396-M rev. 2 (1986) (updated with internal Los Alamos memoranda to version 4)

11. Booth T.E. and Burn K.W. "Some Sample Problem Comparisons between the DSA Cell Model and the Quasi-Deterministic Method", to be published

12. Booth T.E. "A Quasi-Deterministic Approximation of the Monte Carlo Importance Function", *Nucl. Sci. Eng.* 104 374 (1990)

13. Burn K.W., Dubi A., Goldfeld A. and Tinti R. "Developments in the Direct Statistical Approach to Monte Carlo Optimization", 7th. Int.Conf. on Radiation Shielding, Bournemouth, U.K., p.957 (1988)

14. Burn K.W. "Extending the DSA to include Particle Bifurcation between the Splitting Surfaces", to be published

Une Technique de Biaisage Automatique

B. Morillon

Commissariat à l'Énergie Atomique
CE/SACLAY, DRN/DMT/SERMA/LEPP
91191 Gif sur Yvette, FRANCE

Résumé

Le logiciel de simulation de particules neutres Tripoli posséde de nombreuses et puissantes techniques d'accélération de la convergence. Elles reposent essentiellement sur la modification des lois naturelles régissant le parcours et le choc des particules ainsi que l'emploie de méthodes de fractionnement et roulette Russe. La fonction d'importance, grandeur fondamentale à partir de laquelle on déduit l'ensemble des paramètres pour la simulation modifiée, est soit donnée par l'utilisateur soit directement calculée par le programme.

Tout d'abord sur un exemple simple, pour un même type de fonction d'importance, on compare différentes techniques d'accélération de la convergence et l'on montre la supériorité des méthodes modifiant les lois naturelles sur celles de fractionnement et roulette Russe.

Puis on indique une façon de calculer la fonction d'importance pour des problèmes plus compliqués. En cours de développement, cette technique s'appuie sur la résolution de l'équation adjointe par la méthode des probabilités de premiere collision. On montre un exemple de calcul de fonction d'importance pour un problème de contournement ainsi que les résultats obtenus au cours d'une simulation utilisant cette fonction pour modifier les lois naturelles. On compare alors la précision des résultats avec le logiciel Tripoli utilisant le module de pondération automatique Inipond pour un même nombre de particules simulées.

Cette nouvelle possibilité ne nécessite aucune expérience de la part de l'utilisateur et conduit donc à des calculs Monte Carlo non analogues complètement automatiques.

Modification des lois naturelles

Parcours

Le choix du parcours est réalisé à l'aide de la probabilité modifiée :

$$P^{\star}(\rho)\, d\rho \;=\; \Sigma_t^{\star}\, e^{-\Sigma_t^{\star}\,\rho}\, d\rho \qquad (1)$$

où $\Sigma_t^{\star}$ est la section totale macroscopique modifiée définie par la relation (2).

$$\Sigma_t^{\star}(\vec{r}, E, \vec{\Omega}) \;=\; \Sigma_t(\vec{r}, E) \;-\; K\, \vec{\Omega}\,.\,\vec{\Omega}_0 \qquad (2)$$

- $\vec{\Omega}$: direction du neutron d'énergie E.
- $\Sigma_t(\vec{r}, E)$: section totale macroscopique du milieu dans lequel se propage le neutron.
- $\vec{\Omega}_0$: direction pour laquelle l'espérance de la contribution au résultat auquel on s'intéresse est maximale.
- K : le paramètre de la transformation exponentielle.

Ainsi lorsque la direction du neutron est telle que $\vec{\Omega}\,.\,\vec{\Omega}_0 > 0$ le parcours est allongé alors que si $\vec{\Omega}\,.\,\vec{\Omega}_0 < 0$ il est diminué ; la propagation des neutrons est donc favorisée dans la direction $\vec{\Omega}_0$.

Choc et Source

On choisit la direction $\vec{\Omega}'$ et l'énergie E' après choc suivant la probabilité :

$$P^*(E, \vec{\Omega} \rightarrow E', \vec{\Omega}') = \frac{A\ \Sigma_t(E')}{\Sigma_t(E') - K\,\vec{\Omega}'.\vec{\Omega}_0} \frac{I(E')}{I(E)} \tag{3}$$

où A est une constante de normalisation, et $I(E)$ l'importance d'un neutron d'énergie E définie ci-après.

Ce procédé est également employé lors de la génération des sources.

Correction de poids

Lors de l'utilisation des probabilités modifiées (1) et (3) le poids de la particule est affecté d'une correction égale au rapport de la probabilité naturelle sur la probabilité modifiée.

Notons que dans un problème monocinétique, à une dimension avec l'hypothèse d'un choc isotrope et une probabilité de diffusion P_s, le poids d'un neutron situé à l'abscisse x après le parcours suivant le $n^{ème}$ choc s'écrit :

$$W_n(x) = \left(\frac{0.5\,P_s}{A}\right)^n e^{-K\,x} \tag{4}$$

Cette quantité est indépendante du nombre de chocs donc de l'histoire du neutron si $\frac{0.5\,P_s}{A} = 1$. On obtient alors la valeur du paramètre K optimal en résolvant l'équation de Placzek :

$$\frac{\Sigma_s}{2.K} \ln \frac{\Sigma_t + K}{\Sigma_t - K} = 1. \tag{5}$$

Les fluctuations sont alors réduites au nombre de fois que le neutron contribue au résultat.

De façon plus générale, lorsque les quantités K et $\vec{\Omega}_0$ sont déduites de la solution du problème adjoint (relations 6) on obtient théoriquement des résultats avec une variance nulle.

$$K(\vec{r}, E, \vec{\Omega}) = \frac{\left|\overrightarrow{grad}\, I(\vec{r}, E, \vec{\Omega})\right|}{I(\vec{r}, E, \vec{\Omega})} \qquad \vec{\Omega}_0 = \frac{\overrightarrow{grad}\, I(\vec{r}, E, \vec{\Omega})}{\left|\overrightarrow{grad}\, I(\vec{r}, E, \vec{\Omega})\right|} \tag{6}$$

Lors de la réalisation de simulations non analogues, la solution du problème adjoint est inconnue ; mais si on peut trouver une expression approchée de I la précision sur les résultats sera grande.

Fractionnement et roulette Russe

Sur l'ensemble du domaine où l'on étudie la propagation des neutrons, on se donne une fonction $I(\vec{r}, E, \vec{\Omega})$. A tous moments de la vie d'un neutron on peut décider de le fractionner en plusieurs neutrons fils (techniques de fractionnement ou "splitting") ou de le supprimer du système avec une certaine probabilité (techniques de la roulette Russe) suivant que le produit $W\,I$ est supérieur ou inférieur à 1. Dans les deux cas l'espérance du poids du neutron est conservé.

En ce qui concerne le logiciel Tripoli, au cours de la traversée de chaque surface délimitant un volume physique ainsi qu'après chaque choc, on utilise la technique de la roulette Russe si le poids du neutron est inférieur à $0.5\,I$; de plus si le poids du neutron W après choc est supérieur à deux fois la quantité I, celui-ci donne naissance à N descendants (N est la partie entière du produit $W\,I$) dont les parcours ρ_i sont choisis suivant la probabilité (1) et

un échantillonnage stratifié (appelé aussi "quota-sampling"). Un neutron supplémentaire est émis avec la probabilité $W\,I\,-\,N$ pour assurer la conservation du poids du neutron père.

$$\int_0^{\rho_i} P^{\star}(\rho)\,d\rho \;=\; \frac{i\,-\,1\,+\,\xi_i}{W\,I}$$

On obtient alors les parcours des N neutrons fils grâce à la relation suivante :

$$\rho_i \;=\; -\frac{1}{\Sigma_t^{\star}}\,\ln\Big(1\,-\,\frac{i\,-\,1\,+\,\xi_i}{W\,I}\Big)$$

ξ_i désigne un nombre aléatoire uniformément réparti dans l'intervalle $[0.\,,\,1.[$ et $i\,=\,1,2,\ldots N$.

Lorsqu'on utilise conjointement les techniques de modification des lois naturelles et celle de fractionnement et roulette Russe, plus la fonction d'importance I d'où l'on déduit les paramètres K et $\vec{\Omega}_0$ se trouve proche de la fonction d'importance optimale, plus la différence au cours de l'histoire d'un neutron, entre son poids et l'inverse de la fonction d'importance choisie est faible. Ainsi est-il possible d'ajuster la fonction afin de minimiser le fractionnement et le nombre de neutrons supprimés par roulette Russe : on s'approche alors de la fonction optimale.

Simulation non analogue

On propose d'évaluer sur un exemple monocinétique à une dimension les performances de diverses simulations non analogues. On considère une plaque d'épaisseur 20 λ où les neutrons diffusent suivant un choc isotrope et une probabilité de diffusion $P_s\,=\,0.9$. La source mono-directionnelle est placée en x = 20 λ comme indiquée figure (1). Ce type de problème a été

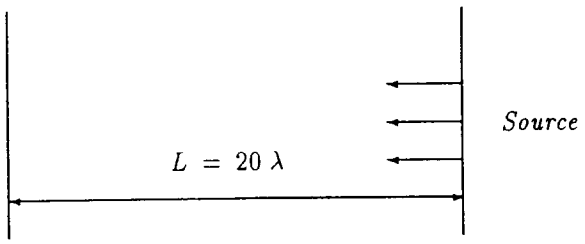

Figure 1: *Problème mono-cinétique à une dimension*

étudié à l'origine par Levitt [Lev 68] et plus récemment par Noack [Noa 91] avec estimation d'un flux point et une source isotrope. La fonction d'importance après choc $I\,(\vec{r},\vec{\Omega})$ est factorisée en une partie spatiale égale à l'importance avant choc $I\,(\vec{r})$ et une partie angulaire de la façon suivante :

$$I\,(\vec{r},\vec{\Omega}) \;=\; I\,(\vec{r})\;I\,(\vec{\Omega}) \;=\; e^{-K\,x}\;\frac{\Sigma_t}{\Sigma_t\,-\,K\,\vec{\Omega}'\,.\,\vec{\Omega}}$$

Lors des différentes simulations, on étudie 100000 neutrons. On s'intéresse à la probabilité pour un neutron de traverser cette plaque, à l'écart-type, au temps de calcul et au gain apporté par la méthode définie comme la figure de mérite de la simulation rapportée à celle de la simulation avec probabilité de non absorption seulement :

$$\text{Gain} \;=\; \frac{\frac{1}{\sigma^2\,T}}{\frac{1}{(\sigma^2\,T)_{P_s}}}$$

Pour chaque simulation on note également le nombre de chocs, le nombre de descendants et le nombre de neutrons supprimés par roulette Russe.

Parmi ces simulations on distingue trois types de simulations non analogues :

- Modification des lois naturelles : "biaisage" du parcours et du choc.
- Fractionnement et roulette Russe.
- Modification des lois naturelles + fractionnement et roulette Russe.

Lorsqu'on utilise les techniques de fractionnement et roulette Russe sur une surface, celles-ci sont placées tous les libres parcours moyen.

Pour chaque simulation, on effectue cinq calculs, avec des paramètres K encadrant la valeur optimale théorique donnée par la résolution de l'équation (5) soit $K_{opt} = 0.5245$. Tableau (1) sont reportés les différents résultats. On constate que si $K = 0.5$ et pour une simulation avec biaisage du choc et du parcours, on obtient un gain très important sur le facteur de qualité par rapport aux valeurs $K = 0.3$ et $K = 0.7$. Si l'on ajoute la technique du "quota sampling", pour $K = 0.5$ aucun neutron n'est fractionné au cours de son histoire et seules quelques particules disparaissent par roulette Russe : le neutron se déplace avec un poids très voisin de l'inverse de la fonction importance considérée. Cependant lorsque $K < 0.5$ il n'y a toujours pas de neutrons fractionnés mais beaucoup disparaissent par roulette Russe. Le temps de calcul est réduit ainsi que le nombre de contributions au résultat ; l'écart-type augmente et on constate que le produit $\sigma^2 T$ augmente. Pour $K > 0.5$ les effets s'inversent et lorsque $K = 0.7$ un neutron donne naissance en moyenne à 47 descendants, augmentant ainsi le temps de calcul, mais comme l'écart-type diminue de façon importante le terme $\sigma^2 T$ se trouve inférieur à celui obtenu en utilisant uniquement les lois modifiées du parcours et du choc. Ainsi lorsqu'on dispose d'une simulation modifiée quasi-optimale, l'apport des techniques de fractionnement et roulette Russe ne peut améliorer la figure de mérite. Par contre si on ajoute les techniques de fractionnement et roulette Russe celle-ci est d'une part diminuée pour une fonction d'importance trop faible ($K < K_{opt}$), on supprime injustement certaines particules, et d'autres part augmentée lorsque la fonction d'importance est trop forte ($K > K_{opt}$).

Enfin on remarque que le gain apporté par les techniques de fractionnement et roulette Russe reste très inférieur à celui des techniques modifiant les lois naturelles avec l'inconvénient supplémentaire d'exiger une mémoire importante pour stocker les neutrons fils. Ceci confirme les options de réduction de la variance adoptées dans le logiciel de Monte Carlo Tripoli.

Fonction importance et probabilités de collision

Dans l'exemple précédent, le gain apporté par l'utilisation d'une bonne approximation de la solution du problème adjoint nous incite à rechercher des méthodes pour trouver une forme approchée de l'équation de Boltzmann adjointe. Ces méthodes doivent répondre à deux critères contradictoires :

- Minimum d'approximation.
- Rapidité d'exécution.

Parmi l'ensemble des techniques bien connues appliquées en neutronique, la méthode des probabilités de collision semble satisfaire le premier critère. De plus si on utilise une simulation pour calculer les probabilités de collision, la méthode devient très simple même pour des configurations compliquées.

Equations adjointes

Le principe de la méthode des probabilités de collision est de discrétiser le domaine spatial et énergétique en éléments de petites tailles appelés mailles ou volumes, puis de calculer les probabilités de transition entre ces différentes mailles au cours d'un événement (choc ou parcours). Ensuite pour toutes les mailles du domaine, on étudie les différents chemins possibles jusqu'au détecteur via les probabilités de transition précédemment calculées ; en sommant les contributions au détecteur de chaque chemin pour une maille donnée, on obtient

la contribution moyenne de cette maille c'est-à-dire l'importance de la maille. L'équation s'écrit alors :

$$I_i^g = \sum_j P_{ij}^g \left(R_j^g + \sum_{g'} C_j^{g \to g'} I_j^{g'} \right) \tag{7}$$

Avec :

- P_{ij}^g probabilité pour un neutron émis uniformément en espace, direction et énergie dans le volume $\mathcal{V}_i$ et le groupe d'énergie g de subir son premier choc dans le volume $\mathcal{V}_j$.
- $C_i^{g \to g'}$ la probabilité pour un neutron ayant un choc dans le volume $\mathcal{V}_i$ dans le groupe g de diffuser dans le groupe g'.
- R_i^g la réponse à optimiser dans le groupe g et la maille i.

L'équation (7) représente l'importance d'un neutron situé après choc (ou à la naissance), et il est possible de construire une relation semblable pour calculer l'importance d'un neutron placé avant choc [Irv 70] :

$$I_i^g = R_j^g + \sum_{g'} C_i^{g \to g'} \sum_j P_{ij}^{g'} I_j^{g'} \tag{8}$$

Si en théorie ces deux fonctions sont nécessaires pour effectuer une simulation non analogue, l'importance avant choc pour biaiser le parcours et le rapport de l'importance après choc par l'importance avant choc pour biaiser la collision, on propose de calculer uniquement l'importance avant choc. Ensuite grâce aux relations (6) on calcule les quantités $\vec{\Omega}_0$ et K et on prend comme forme approchée de l'importance après choc :

$$\frac{\Sigma_{t\,g'}}{\Sigma_{t\,g'} - K\,\vec{\Omega}'\,.\,\vec{\Omega}_0} I_j^g$$

Une des principales approximations de la méthode est l'isotropie du choc. Par analogie avec la relation (7) on définit des probabilités de collision anisotropes puis on calcul une fonction d'importance multigroupe anisotrope approchée :

$$I_i^{g\,k} = \sum_j P_{ij}^{g\,k} \left(R_j^{g\,k} + \sum_{g'\,k'} C_j^{g\,k \to g'\,k'} I_j^{g'\,k'} \right) \tag{9}$$

L'indice k repère un angle solide, le terme $I_i^{g\,k}$ l'importance d'un neutron situé dans la maille i le groupe g, l'angle solide k, et $P_{ij}^{g\,k}$ la probabilité pour un neutron de la maille i, du groupe g, de l'angle solide k, de subir son prochain choc dans le maille j.

Calcul des probabilités de transfert

Avant de résoudre le système (7) il est nécessaire de calculer les probabilités de transfert en espace P_{ij}^g ou $P_{ij}^{g\,k}$ et en énergie $C_j^{g\,k \to g'\,k'}$.

Pour cela on génère uniformément dans chaque maille du domaine un ensemble de particules avec une direction isotrope. Puis en localisant la position après un unique parcours on compte le nombre de chocs dans les mailles voisines. On obtient ainsi les termes P_{ij}^g. Notons que pour un neutron de direction $\vec{\Omega}$ on peut calculer un parcours dans chaque groupe d'énergie et à l'aide d'un seul appel géométrique (calcul de la distance à la prochaine surface) obtenir le lieu du choc pour chaque groupes. Pour le calcul des $P_{ij}^{g\,k}$ on procède de manière similaire mais on note en plus l'angle solide auquel appartient la direction du neutron. Pour le calcul des probabilités de transfert on utilise une section totale modifiée $\Sigma_t^* = 0.6\,\Sigma_t$. Ceci permet de prendre en compte les interactions entre volumes éloignés.

Le calcul des quantités $C_i^{g\,k \to g'\,k'}$ se déroule de façon analogue. On génère uniformément des particules avec une énergie distribuée dans le groupe g et une direction dans l'angle

solide k. Après un choc réalisé de façon exacte sur chaque noyau appartenant à la maille i, on repère le groupe d'énergie et l'angle solide d'arrivée. On obtient ainsi la probabilité de transfert du groupe g de l'angle solide k vers le groupe g' et l'angle solide k' pour tous les noyaux. En sommant ces différents termes pondérés par la probabilité de choquer chaque noyau on obtient les quantités $C_i^{g\,k\to g'\,k'}$:

$$C_i^{g\,k\to g'\,k'} = \sum_{n=1}^{N} \frac{n_n\,\sigma_{in}^g}{\Sigma_{ti}^g}\,c_n^{g\,k\to g'\,k'}$$

Exemple de simulation non analogue multigroupe

Pour évaluer les possibilités de cette fonction importance on présente un exemple simple sur le plan géométrique (figure 2). C'est un problème à deux dimensions (X-Y) constitué de fer et d'eau : on impose une condition de fuite sur le pourtour de la géométrie et des conditions de réflexion pour deux plans en Z espacés de 10cm. Les dimensions sont indiquées sur la figure ainsi que la position des différents milieux. Tableau (2) on a reporté les concentrations des différents nuclides. On s'intéresse au flux situé dans les mailles 1 à 9 (ces mailles sont carrées et ont pour arrête 5cm) créé par une source uniforme entre les énergies 2.019 MeV et 1.9205 MeV, monodirectionnelle placée en $X = 100$cm et $85\text{cm} < Y < 90\text{cm}$.

Tout d'abord il faut procéder au calcul de la fonction importance. Pour cela on discrétise la géométrie en 20 mailles en x et 20 mailles suivant y. Puis on calcul les probabilités anisotropes avec 8 angles solides et 14 groupes d'énergie. Il reste à résoudre le système (9), if faut donc se donner une fonction réponse. Figure (3) sont représentées les iso-importances obtenues avec deux types de réponse. Pour la premiere réponse on a voulu optimiser le flux supérieur à 1 MeV pour les maille 1 à 9 alors que pour la seconde on désire calculer le flux supérieur à 4 KeV. On voit ainsi que pour une source placée comme indiquée figure (2) suivant le type de réponse à laquelle on s'intéresse les neutrons contournent ou traversent l'eau.

La figure (4) représente les iso-importances obtenu par Inipond, module de biaisage automatique du logiciel Tripoli présenté au cours de ce séminaire par T. Vergnaud : "Overview of Monte Carlo Methodologies in Tripoli-3". On a choisi comme valeurs du paramètre K 0.07 cm^{-1} pour le fer et 0.15 cm^{-1} pour l'eau. Ces valeurs sont obtenues après plusieurs essais de simulation où on désire optimiser le flux supérieur à 4 KeV toujours pour les même mailles.

Lors de la simulation on dispose de sections efficaces extraites de l'évaluation Jef2 définies en 315 groupes pour le fer ($^{56}F_e$), l'oxygène (^{16}O) et l'hydrogène (H). Seul le biaisage du parcours est utilisé ; la technique du "quota-sampling" est alors nécessaire pour assurer l'accord de poids du neutron avec l'inverse de la fonction importance.

Tableau (3) sont mentionnés les valeurs des flux et des écarts type obtenus par deux simulations différentes pour 100000 neutrons étudiés. La première est celle effectuée par le logiciel de Monte Carlo Tripoli-3 avec une pondération automatique assurée par le module Inipond, la seconde est obtenue par une simulation simplifiée du type Tripoli écrite spécialement pour recevoir et tester la fonction importance et les paramètres de biaisage provenant du calcul de probabilités de collisions. En outre le biaisage de la collision n'étant pas terminé dans cette simulation simplifiée il n'a pas été utilisé pour ces calculs.

Ce travail représente la première comparaison entre ces deux méthodes. Pour l'instant il n'est pas possible de comparer la figure de mérite car la simulation est différente en ce qui concerne le calcul de la distance à la prochaine surface. Cependant il indique que la précision pour un même nombre de particules est plus grande avec le biaisage par probabilité de collision et ceci sans aucune intervention de l'utilisateur. La connaissance de la valeur des paramètres de biaisage est nécessaire pour le module Inipond, par contre le temps de calcul est très court contrairement à celui de la méthode des probabilités de collision fonction de la précision demandée sur les termes de transfert spatiaux.

Conclusion

L'emploi simultané de probabilités modifiées pour le parcours et le choc des particules est une technique de réduction importante de la variance. L'ajout des méthodes de fractionnement et roulette Russe contribuent à la réduction de la variance lorsque la fonction importance utilisée n'est pas optimale. Cependant trouver une forme approchée de cette fonction optimale est une tâche difficile. Pour cela des techniques semi-automatiques ou complètement automatiques sont indispensables. La méthode des probabilités de collision semble possible pour de telles applications. Néanmoins, pour des problèmes de grandes dimensions le temps nécessaire au calcul des termes de transferts risque d'être prohibitif. If faut alors étudier l'impact de la variation du nombre de mailles pour la fonction importance sur la figure de mérite.

Références

[Lev 68] L.B. Levitt *The Use of Self-Optimized Exponential Biaising in Obtaining Monte Carlo Estimates of Transmission Probabilities.* N.S.E. 31, 500

[Irv 70] D. C. Irving *The Adjoint Boltzmann Equation and its Simulation by Monte Carlo.* O.R.N.L.-TM-2879 (1970)

[Nim 70] J.C. Nimal et al. *Programme de Monte-Carlo Polycinétique à trois Dimensions : TRIPOLI* C.E.A. (1970)

[Noa 91] K. Noack *Efficiency and Reliability in Deep-Penetration Monte-Carlo Calculations.* A.N.E. 18, 309 (1991)

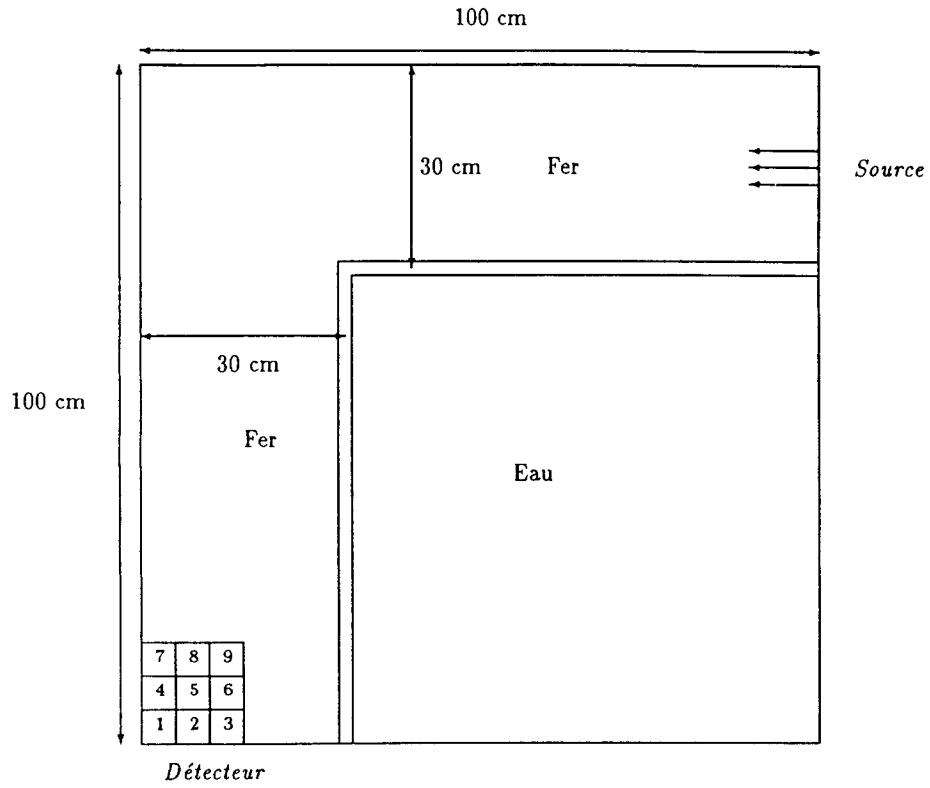

Figure 2: *Contournement Fer-Eau*

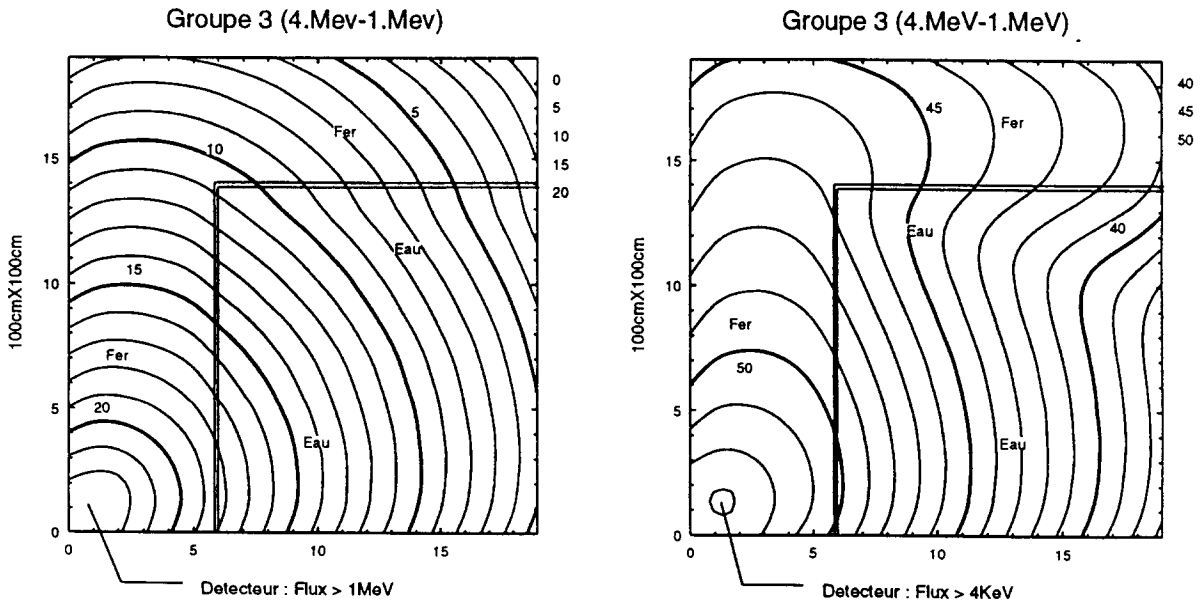

Figure 3: *Iso-Importance (log) Probabilités de collision*

Biaisage parcours + collision

K	Resultat	σ(%)	T (s)	Gain
0.3	$2.944\ 10^{-5}$	0.859	1079.	125
0.4	$2.928\ 10^{-5}$	0.392	917.	707
0.5	$2.932\ 10^{-5}$	0.164	760.	4886
0.6	$2.941\ 10^{-5}$	0.284	620.	1993
0.7	$2.896\ 10^{-5}$	1.194	480.	146

Biaisage parcours + collision
Quota sampling après choc
Roulette choc et surfaces

K	Resultat	σ(%)	T (s)	Gain
0.3	$2.850\ 10^{-5}$	2.453	325.	51
0.4	$2.944\ 10^{-5}$	0.842	496.	283
0.5	$2.933\ 10^{-5}$	0.167	773.	4614
0.6	$2.941\ 10^{-5}$	0.170	2379.	1449
0.7	$2.941\ 10^{-5}$	0.250	9326.	171

Biaisage parcours + collision
Splitting roulette avant choc

K	Resultat	σ(%)	T (s)	Gain
0.3	$2.850\ 10^{-5}$	2.453	329.	50
0.4	$2.944\ 10^{-5}$	0.842	502.	280
0.5	$2.933\ 10^{-5}$	0.167	783.	4572
0.6	$2.936\ 10^{-5}$	0.167	2345.	1524
0.7	$2.929\ 10^{-5}$	0.244	8899.	188

Biaisage parcours + collision
Splitting roulette avant choc et surfaces

K	Resultat	σ(%)	T (s)	Gain
0.3	$2.980\ 10^{-5}$	2.390	322.	54
0.4	$2.963\ 10^{-5}$	0.836	493.	289
0.5	$2.935\ 10^{-5}$	0.167	793.	4510
0.6	$2.936\ 10^{-5}$	0.169	2585.	1350
0.7	$2.939\ 10^{-5}$	0.239	10600.	165

Biaisage parcours
Splitting roulette avant choc et surfaces

K	Resultat	σ(%)	T (s)	Gain
0.3	$2.853\ 10^{-5}$	3.177	275.	36
0.4	$2.886\ 10^{-5}$	1.485	425.	106
0.5	$2.927\ 10^{-5}$	0.848	915.	151
0.6	$2.941\ 10^{-5}$	0.582	2789.	105
0.7	$2.934\ 10^{-5}$	0.479	11298.	38

Splitting roulette avant choc et surfaces

K	Resultat	σ(%)	T (s)	Gain
0.3	$2.826\ 10^{-5}$	4.609	268.	18
0.4	$3.015\ 10^{-5}$	2.543	445.	35
0.5	$2.892\ 10^{-5}$	1.488	933.	48
0.6	$2.904\ 10^{-5}$	1.182	2734.	26
0.7	$2.956\ 10^{-5}$	1.285	10687.	6

Splitting roulette avant choc

K	Resultat	σ(%)	T (s)	Gain
0.3	$2.787\ 10^{-5}$	5.023	245.	16
0.4	$2.838\ 10^{-5}$	2.837	385.	32
0.5	$2.902\ 10^{-5}$	1.920	768.	35
0.6	$2.900\ 10^{-5}$	1.670	2280.	16
0.7	*Trop grand nombre de descendants*			

Quota sampling après choc
Roulette choc et surfaces

K	Resultat	σ(%)	T (s)	Gain
0.3	$3.032\ 10^{-5}$	5.024	253.	16
0.4	$2.979\ 10^{-5}$	2.841	401.	31
0.5	$2.826\ 10^{-5}$	1.736	797.	41
0.6	$2.894\ 10^{-5}$	1.532	2268.	19
0.7	$2.964\ 10^{-5}$	1.319	9219.	6

Table 1: *Resultats simulations non anologues une dimension.*

Element	Nb. noyaux (cm^{-3})
^{56}Fe	$8.47\ 10^{-2}$
^{16}O	$3.37\ 10^{-2}$
H	$6.74\ 10^{-2}$

Table 2: *Nombre de noyaux.*

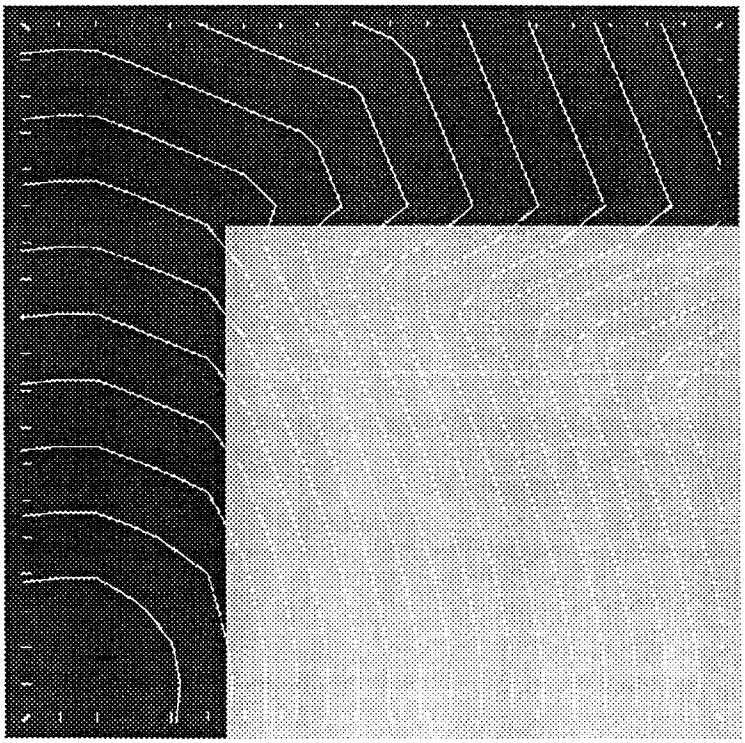

Figure 4: *Isi-Importance Inipond* $K_{fer} = 0.07$ $K_{eau} = 0.15$

Maille	Flux σ Inipond	Flux σ Pij
1	$6.799\ 10^{-5}$ 15.0 %	$6.608\ 10^{-5}$ 4.1 %
2	$6.044\ 10^{-5}$ 9.7 %	$7.379\ 10^{-5}$ 4.4 %
3	$8.953\ 10^{-5}$ 14.6 %	$7.017\ 10^{-5}$ 5.3 %
4	$8.605\ 10^{-5}$ 9.5 %	$8.819\ 10^{-5}$ 6.7 %
5	$9.283\ 10^{-5}$ 9.8 %	$9.716\ 10^{-5}$ 3.3 %
6	$1.154\ 10^{-4}$ 11.3 %	$1.198\ 10^{-4}$ 14.1 %
7	$9.774\ 10^{-5}$ 9.3 %	$1.018\ 10^{-4}$ 10.4 %
8	$1.241\ 10^{-4}$ 7.7 %	$1.133\ 10^{-4}$ 6.4 %
9	$1.548\ 10^{-4}$ 11.1 %	$1.170\ 10^{-4}$ 4.4 %

Table 3: *Résultats contournement fer-eau.*

DEVELOPMENT AND APPLICATION OF THE AUTOMATED MONTE CARLO BIASING PROCEDURE IN SAS4

J. S. Tang and B. L. Broadhead
Computing Applications Division
Oak Ridge National Laboratory
P.O. Box 2008
Oak Ridge, Tennessee USA 37831-6370

ABSTRACT

An automated approach for biasing Monte Carlo shielding calculations is described. In particular, adjoint fluxes from a one-dimensional discrete-ordinates calculation are used to generate biasing parameters for a three-dimensional Monte Carlo calculation. The automated procedure consisting of cross-section processing, adjoint flux determination, biasing parameter generation, and the initiation of a MORSE-SGC/S Monte Carlo calculation has been implemented in the SAS4 module of the SCALE computer code system.

The automated procedure has been used extensively in the investigation of both computational and experimental benchmarks for the Nuclear Energy Agency-Committee on Reactor Physics (NEACRP) working group on shielding assessment of transportation packages. The results of these studies indicate that with the automated biasing procedure, Monte Carlo shielding calculations of spent fuel casks can be easily performed with minimum effort and that accurate results can be obtained at reasonable computing cost. The systematic biasing approach described in this paper can also be applied to other similar shielding problems.

I. INTRODUCTION

SAS4[1] is a module in the SCALE computer code system[2] which was developed by the Computing Applications Division of Oak Ridge National Laboratory. The primary task of SAS4 is to perform a three-dimensional (3-D) Monte Carlo shielding analysis of a spent fuel cask using an automated biasing procedure. The automated procedure consists of cross-section processing, adjoint flux calculation, biasing parameter generation, and the initiation of a Monte Carlo calculation.

In Monte Carlo shielding analysis of a deep-penetration problem such as a spent fuel cask, variance reduction techniques must be employed in order to calculate reasonably good results at an affordable cost. Theoretically,[3,4] a single Monte Carlo history is sufficient to solve any problem if the adjoint flux is used to bias the selection of particle parameters (i.e., position, energy, and direction). However, from a practical standpoint, calculation of the adjoint flux and subsequent selection from the biased distributions would have required a greater computational expense than an unbiased solution to the original problem. Therefore, to achieve a reduction in the cost of the calculation, this optimal biasing procedure must be approximated.

In this work, the adjoint flux for the actual shipping cask is approximated by that obtained for a geometrically simplified [one-dimensional (1-D)] cask model. The adjoint flux for the simplified model is obtained from a discrete-ordinates calculation with the XSDRNPM-S code in the SCALE system.[2] Another practical problem associated with the use of the adjoint flux to bias Monte Carlo histories is that sampling from the adjoint-biased distribution must be carried out efficiently. This difficulty has been overcome by using the biasing schemes available in the MORSE-SGC/S code in the SCALE system, and the XSDRNPM-S adjoint fluxes are used to specify the biasing parameters needed to implement these techniques. The entire procedure for adjoint flux calculation, generation of Monte Carlo biasing parameters, and Monte Carlo calculation of radiation doses exterior to a spent fuel cask has been developed and described in this paper.

The automated biasing procedure is presented in the next section, followed by the description of the biasing techniques and generation of the biasing parameters. Application of the automated procedure to two recent studies on shipping casks dose-rate evaluations is described. The two studies are (1) a series of calculations for computational benchmarks for the Nuclear Energy Agency-Committee on Reactor Physics (NEACRP) working group on shielding assessment of transport packages[5] and (2) the analysis of a series of dose-rate measurements for a transport cask loaded with unconsolidated pressurized-water reactor (PWR) spent fuel.[6] Finally, conclusions and discussion are given in the last section.

II. AUTOMATED BIASING PROCEDURE

The automated biasing procedure in SAS4 basically consisted of five steps:

1. processing of multigroup cross-section data, which includes resonance self-shielding and optionally cell-weighting treatments;

2. calculation of adjoint fluxes of a simplified 1-D slab model of a cask using the XSDRNPM-S program;

3. processing of the adjoint fluxes into different biasing parameters;

4. application of the biasing parameters to the particle random walk in a Monte Carlo calculation with the MORSE-SGC/S code; and

5. estimation of radiation doses exterior to the cask.

This paper focuses on the discussion of the last four steps because they form the basis of this advanced Monte Carlo method. For Monte Carlo shielding analysis of a spent fuel cask, the purpose of biasing (or importance sampling) is to encourage and increase the propagation of radiation particles toward the outside of the cask so that better estimates of exterior dose rates can be obtained. Because nuclear fuel casks generally have a long cylindrical shape, it is difficult to effectively bias particles simultaneously toward all three sides of a cask. For this reason, the Monte Carlo cask geometry used in this work is assumed to be symmetrical about the midplane perpendicular to the axial dimension. Even with the axially symmetric cask model, the radial and axial characteristics of particle transport may be drastically different due to the geometric shape, the shielding materials, and possibly the streaming effect in the fuel. Because of these complications, separate Monte Carlo calculations with different biasing procedures are required for radial and axial detectors. For radial detectors, the particle random walk is biased radially toward the side. For axial detectors, the particle random walk is biased axially away from the midplane and toward the top or bottom surfaces.

The adjoint discrete-ordinates calculation, from which biasing parameters are generated, is a 1-D slab model of either the radial or axial geometry of the cask being analyzed. The slab geometry starts with a spent fuel material that has a specular reflective boundary on one side and layers of materials simulating the radial or axial geometry of the cask on the other. Each material layer is identified as a zone in XSDRNPM-S. The thickness of the first zone is the height of spent fuel measured from the midplane for the axial geometry or the radius of the spent fuel for the radial geometry. If the spent fuel geometry in the Monte Carlo calculation is not cylindrical, a nominal radius is used as the thickness of the first zone in XSDRNPM-S. An adjoint source with a response function as the source spectrum located on the outermost surface of the slab geometry starts the adjoint calculation. The response function is either a neutron or gamma-ray fluence-to-dose conversion factor.

In MORSE-SGC/S, biasing takes place at each collision site, and the biasing parameters are generally functions of energy group and spatial region (importance region). In the automated biasing procedure, a direct correspondence is made between the Monte Carlo importance regions and the zones in the adjoint discrete-ordinates calculation. Each zone in XSDRNPM-S corresponds to one or more importance regions in MORSE-SGC/S, depending on the optical thickness of the zone. The biasing parameters generated from adjoint fluxes are spatially averaged over the thickness of each importance region. During Monte Carlo random walk, biasings are implemented to each collision site according to the importance region in which the collision takes place. In this work, the importance region of a collision site is determined by the distance between the collision and the adjoint source surface. For radial responses, the adjoint source surface is the side surface; for axial responses, it is the top or bottom surface. Finally, the biasing parameters expressed as functions of energy group and/or spatial region are input or used directly in MORSE-SGC/S for calculation of external dose rates of the spent fuel cask.

III. BIASING TECHNIQUES AND GENERATION OF BIASING PARAMETERS

The MORSE-SGC/S biasing options used in this study are the source energy biasing, energy biasing at collision site, splitting and Russian roulette, and path-length stretching. The efficiency of a calculation is determined by the proper specification of these parameters. It has been shown[3,4] that a near-optimal importance function for selection of emergent particle parameters (i.e., energy and direction of a particle emerging from a source or a collision point) is the adjoint flux. The

event-value function has been shown[7] to be the proper biasing function for path-length selection. In this work, these adjoint functions are generated for a 1-D cask model with XSDRNPM-S and are used to specify the biasing parameters for the biasing options in MORSE-SGC/S.

The theoretical development of Monte Carlo importance sampling in MORSE-SGC/S is given elsewhere[7,8] and will not be repeated here. Instead, each biasing technique and biasing parameter evaluation in the automated procedure is described in detail.

III.A ENERGY BIASING PARAMETERS AT COLLISION SITE, EPROB, AND SOURCE ENERGY BIASING PARAMETERS, BFS

For selection of the energy of a particle emergent from a collision site, $\phi^*(IG,IR)$ (the region-averaged and energy-dependent adjoint flux calculated by XSDRNPM-S) is used directly as the importance function EPROB(IG,IR) in MORSE-SGC/S; that is,

$$\text{EPROB}(IG,IR) = \phi^*(IG,IR),$$

where

IG = energy group number,
IR = region number.

Since a source particle can be regarded as a particle emergent from the zeroth collision site, source energy biasing is treated in the same manner; that is,

$$\text{BFS}(IG) = \phi^*(IG,1),$$

where

BFS = source energy importance function,
$\phi^*(IG,1)$ = adjoint flux in group IG averaged over region 1, which contains the spent fuel.

Then, the biased source energy distribution is

$$\hat{S}(IG) = \frac{S(IG)\phi^*(IG,1)}{\sum_{IG} S(IG)\phi^*(IG,1)}, \qquad (1)$$

where $S(IG)$ is the natural source spectrum.

SAS4 allows axial dependence of the source distribution in order to account for the spent fuel burnup profile. For calculations involving radial detectors (radial calculations), source particle axial locations are sampled directly from the specified distribution. However, for calculations involving axial detectors (axial calculations), the axial location of source particles is biased by the adjoint flux when the source distribution is axially uniform, but is sampled from an exponential function e^{CZ} when the source has an axial profile. The constant C is chosen such that $CZ_{max} = 5$, where Z_{max} is the source height measured from the midplane. The selection of the source location is independent of the selection of the source energy from Eq. (1).

III.B RUSSIAN ROULETTE AND SPLITTING PARAMETERS *WTAV, WTHI, WTLO*

Because it has been shown[9] that in near-optimal calculations particle statistical weights are inversely proportional to the adjoint flux, we set the weights of particles in regions *IR* with energy group *IG* as

$$\mathrm{WTAV}(IG,IR) = \frac{\lambda}{\phi^*(IG,IR)} , \tag{2}$$

where

WTAV = group- and region-dependent Russian roulette survival weight,
λ = effect of interest or the total response.

The total response is the sum of responses of each group that, in turn, can be computed from the product of the group source strength and the corresponding adjoint flux in the source region; that is,

$$\lambda = \sum_{IG} \lambda(IG) \simeq \sum_{IG} S(IG)\phi^*(IG,1) .$$

Substituting Eq. (1) into the above, we have

$$\lambda \simeq \frac{S(IG)\phi^*(IG,1)}{\hat{S}(IG)} .$$

Substitution of λ into Eq. (2) gives

$$\mathrm{WTAV}(IG,IR) \simeq \frac{S(IG)\phi^*(IG,1)}{\hat{S}(IG)\phi^*(IG,IR)} . \tag{3}$$

In Eqs. (2) and (3), the quantities on the right side are known since the adjoint fluxes are calculated by XSDRNPM-S, and $\hat{S}(IG)$ is given by Eq. (1). Equation (2) or (3) is used to set the Russian roulette survival weight of each region and energy group throughout the entire system. Note from Eq. (3) that for the source region, WTAV is equal to $S(IG)/\hat{S}(IG)$, which is the statistical weight of source particles after source energy biasing. In a similar manner, the weight above which splitting occurs in zone *IR* and group *IG* is determined by the minimum adjoint flux in zone *IR* of group *IG*; that is,

$$\mathrm{WTHI}(IG,IR) = \frac{\lambda}{\phi^*_{\min}(IG,IR)} . \tag{4}$$

The weight below which Russian roulette is played is determined by the maximum ϕ^* in zone *IR* of group *IG*; that is,

$$\text{WTLO}(IG,IR) = \frac{\lambda}{\phi^*_{max}(IG,IR)} . \tag{5}$$

Finally, to regulate the values of WTHI and WTLO, limits had been set on ϕ^*_{max} and ϕ^*_{min} so that WTHI would be <100 * WTAV and WTLO would be >WTAV/100.

III.C PATH-LENGTH STRETCHING PARAMETERS, PATH

In MORSE-SGC/S, path-length stretching is accomplished by selecting the number of mean-free paths η to the next collision site from the probability density function (pdf)

$$\hat{f}(\eta) = [1 - \text{PATH}(IG,IR) * DIREC] \times \exp \{ - [1 - \text{PATH}(IG,IR) * DIREC]\eta \} , \tag{6}$$

where *DIREC* is the cosine of the angle between the particle direction and a vector specifying the most important direction of particle transport. Both *DIREC* and PATH(*IG,IR*) are input parameters, each with values between -1 and 1. For positive values of PATH, particle path lengths are stretched toward the most important direction; for negative values of PATH, path lengths are shrunk toward this direction. If either PATH or *DIREC* equals 0, no path-length biasing takes place, and η is sampled from the natural pdf, $\exp(-\eta)$.

In this work, PATH(*IG,IR*) is determined by considering only those particles traveling in the most important direction (i.e., *DIREC* = 1). Then, PATH(*IG,IR*) is used in Eq. (6) for selection of η for all particles. For spent fuel cask problems, the most important directions are the outward radial vector for radial detectors and axially toward the top or bottom surfaces for axial detectors. For particles traveling in the most important direction, the path length is selected from the pdf,

$$\hat{f}_1(\eta) = [1 - \text{PATH}(IG,IR)] \times \exp \{ - [1 - \text{PATH}(IG,IR)]\eta \} . \tag{7}$$

A good approximation to the optimal pdf (Ref. 7) is

$$\hat{f}_2(\eta) = \frac{W(IG,IM)\exp(-\eta)}{\int W(IG,IM)\exp(-\eta)d\eta} , \tag{8}$$

where *W(IG,IM)* is the event-value function from the adjoint discrete-ordinates XSDRNPM-S calculation for a particle at spatial interval *IM* and energy group *IG* traveling in the most forward direction.

To illustrate the procedure for determination of PATH, let $W \sim \exp(c\eta)$, where $c < 1$. Then, from Eq. (8),

$$\hat{f}_2(\eta) = (1 - c)\exp[-(1 - c)\eta] \ . \tag{9}$$

Comparison of Eq. (9) with Eq. (7) shows that PATH = c. Of course, the event-value function will not have this simple exponential form. However, determination of PATH in such a manner that the error between exp(PATH * η) and W is minimized should result in appropriate values of PATH. This determination is done using the least-squares procedure outlined below.

Initially, consider the determination of $PATH_k$, where k is a spatial interval index in the XSDRNPM-S calculation as shown in Fig. 1. (The energy dependency is implied.) Let $\eta_{k,i}$ be the number of mean-free paths between intervals k and i. The following data points are available to estimate appropriate values of PATH: $[\eta_{k,i}; W(i)]$ for $i = k$ to IMAX.

We want to fit these data to

$$W(i) = W(k)\exp(\mathrm{PATH}_k * \eta_{k,i}) \quad \text{for } i = k \text{ to IMAX} \tag{10}$$

or

$$\mathrm{PATH}_k * \eta_{k,i} = \ln[W(i)/W(k)] \ .$$

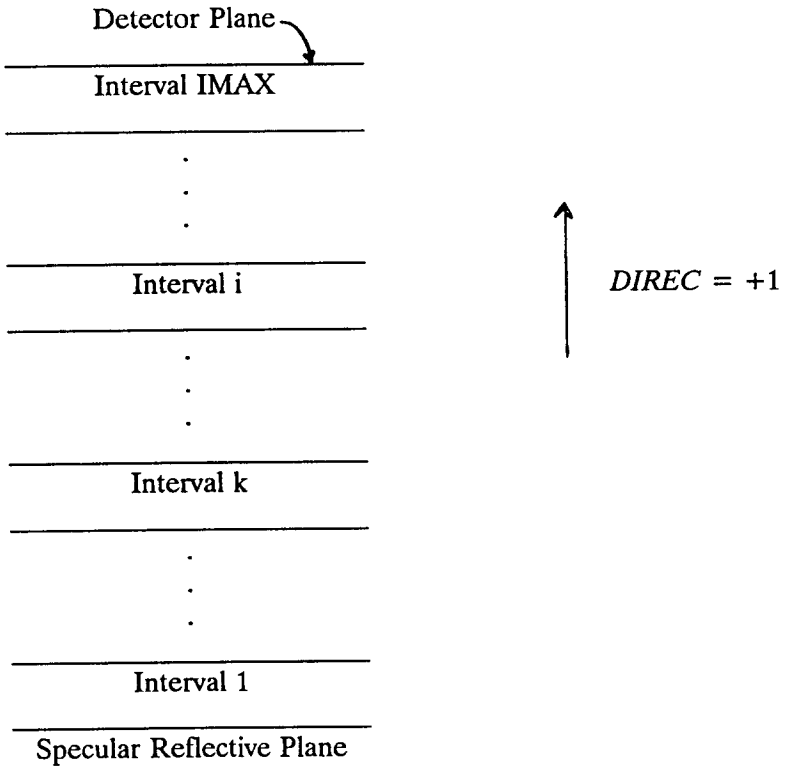

Fig. 1. The XSDRNPM-S interval notation used to obtain path-length stretching parameters, PATH.

The sum of the square errors will be

$$\epsilon_k^2 = \sum_{i=k}^{IMAX} [\ln W(i) - \ln W(k) - \text{PATH}_k * \eta_{k,i}]^2 . \quad (11)$$

Setting the derivative of ϵ_k^2 with respect to PATH_k to 0 leads to the following expression:

$$\text{PATH}_k = \frac{\sum_{i=k}^{IMAX} \eta_{k,i}[\ln W(i) - \ln W(k)]}{\sum_{i=k}^{IMAX} \eta_{k,i}^2} . \quad (12)$$

The values of PATH_k are calculated for each interval in a given region, and an average is taken to obtain the region-dependent PATH parameters. This procedure is done for all energy groups.

III.D FISSION NEUTRON WEIGHTS, FWLO

In MORSE-SGC/S, the population of fission neutrons can be regulated by the statistical weights given to fission neutrons at their birth. To have an efficient Monte Carlo calculation, the region- and energy-dependent fission neutron weights should be consistent with the biasing schemes used in a calculation. The Russian roulette survival weights, WTAV(*IG,IR*) of Eq. (2), are the appropriate values to use. However, the current version of MORSE-SGC/S does not allow input of these parameters as a function of energy group. Therefore, a group-averaged value of WTAV is needed. If the simple average is used for a given region, FWLO will be primarily determined by the WTAV value corresponding to low-importance particles because energy groups with low ϕ^* have high WTAV values [see Eq. (2)]. To avoid this problem, we weight WTAV with the fission spectrum of the spent fuel, FSE(*IG*,1); that is,

$$\text{FWLO}(IR) = \sum_{IG} \text{WTAV}(IG,IR) * \text{FSE}(IG,1) . \quad (13)$$

Although the fission spectrum corresponding to the medium in region *IR* would be more appropriate, the fission spectrum in the spent fuel region is usually similar enough to that of region *IR* that this approximation has no significant effect on the calculation. This approximation enables one to calculate FWLO without first determining the fission medium in region *IR* and avoids the problem that would be encountered if more than one fissionable medium were present in region *IR*.

III.E NEXT-EVENT ESTIMATION PROBABILITIES, PROB

The idea of the next-event estimation probabilities is not new and has been an option in major Monte Carlo transport codes such as TRIPOLI[10] and MCNP[11] for some time. When one uses a next-event estimator to point detectors or other types of detectors, an estimate to each detector position is made at all collision sites. The computational time required for this estimation process often exceeds the time required to generate and process the particle histories. This estimation from all collision sites can be very wasteful. For example, in the source region where a large number of collisions occur, the next-event contribution of the particle to detectors outside a

cask is often insignificant. This inefficiency can be reduced without biasing the effect of interest, λ, by estimating from a given region, *IR*, with a probability PROB(*IR*) and, if the estimation is made, dividing the contribution by PROB(*IR*); that is,

$$\begin{aligned}\lambda &= \sum_{IR} N(IR)\xi(IR) \\ &= \sum_{IR} [N(IR) * \mathrm{PROB}(IR)]\left(\frac{\xi(IR)}{\mathrm{PROB}(IR)}\right) \\ &= \sum_{IR} M(IR)\hat{\xi}(IR) \ , \end{aligned} \tag{14}$$

where

$N(IR)$ = collisions per history in region *IR*,
$\xi(IR)$ = average, next-flight contributions of a particle having a collision in *IR* in standard game,
$M(IR)$ = $N(IR)$ * PROB(*IR*) = number of estimates from region *IR* in the modified game,
$\hat{\xi}(IR)$ = $\xi(IR)$/PROB(*IR*) = contribution in the modified game.

Although estimation probabilities are not normally used in MORSE-SGC/S, their implementation is simple and their effectiveness is apparent. Reasonable values for PROB can be determined from mean-free-path, WTAV, and response function considerations—all quantities can be calculated before the Monte Carlo calculation.

In this work, we set PROB(*IR*) such that the average next-event contribution from each region, *IR*, to the detector is the same. By requiring the contribution to be uniform throughout the system, the variance of λ should be reduced. The next-event contribution from a region can be approximated as

$$\lambda_{IR} \sim \sum_{IG} \mathrm{WTAV}(IG,IR) * R(IG) * \exp[-\eta(IG,IR)] \ , \tag{15}$$

where

$R(IG)$ = response function,
$\eta(IG,IR)$ = number of mean-free paths between the midpoint of region *IR* and the detector in the XSDRNPM-S geometry (see Fig. 1).

PROB(*IR*) is then obtained with the following equation:

$$\mathrm{PROB}(IR) = \frac{\lambda_{IR}}{\lambda_{\max}} \ , \tag{16}$$

where λ_{max} is the largest λ_{IR}.

In principle, PROB(*IR*) should increase monotomically with the region number, *IR*, and should be unity for the last region. However, it was found that Eqs. (15) and (16) do not lead to a maximum PROB for the last region for gamma-ray problems. This results in very inefficient calculations. Further examination revealed that WTAV(*IG,IR*) has extremely high values for low-energy gamma rays in the inner regions. The high WTAV values are due to the low ϕ^* of the inner regions [see Eq. (2)]. To overcome this problem, WTAV has been deleted from Eq. (15). The next-event contribution from region *IR* is then reduced to

$$\lambda_{IR} \sim \sum_{IG} R(IG) * \exp[-\eta(IG,IR)] , \quad (17)$$

and PROB*(IR)* is calculated from Eqs. (17) and (16) instead.

Since this procedure is a fair game, any values of PROB between 0 and 1 will, as the number of histories goes to infinity, produce the correct answer. However, from a practical standpoint, if PROB*(IR)* is very small, few or no estimates will be made from region *IR* and could lead to erratic results. Therefore, to allow for the approximate nature of λ_{IR}, PROB*(IR)* is required to be >0.001.

Finally, for situations where azimuthal symmetry exists, point detectors are replaced by ring detectors to improve the efficiency of the calculation. This technique is described in detail in Refs. 12 and 13.

IV. APPLICATIONS AND RESULTS

The automated biasing procedure for an adjoint calculation, biasing parameters generation, and a Monte Carlo calculation of dose rates outside a spent fuel cask has been implemented in the SAS4 module[1] of the SCALE system. A depleted uranium cask had been analyzed, and good agreement with 2-D discrete ordinates was obtained.[14] In this paper, analyses of a series of cast-iron casks of varying complexities were performed using the automated procedure. These casks include a simple geometry cask as defined by the NEACRP[5] working group and a transport cask[6] loaded with 12 PWR spent fuel assemblies. For comparison and verification, multiple solutions were obtained for a variety of computational methods including point and multigroup Monte Carlo, discrete-ordinates, and point-kernel methods.

IV.A NEACRP CAST-IRON CASK ANALYSIS

The first cask analyzed has been used as one of the problems for the international intercomparison of codes for transport cask shielding calculations sponsored by the NEACRP. The geometry of this cask is quite simple and is shown in Fig. 2. The cask is composed of a source region and a cask body. The source region has a radius of 40 cm and a height of 450 cm and is entirely filled with a homogeneous spent fuel material.

The cask body is composed of cast iron, with both the wall and the base having thicknesses of 38 cm. The lid is stainless steel of 42-cm thickness. A modified version of the SCALE 27n-18g cross-section library is used for this problem. The dose response functions used were based on the ANSI/ANS 6.1.1 (1977) standard.[15] The sources are isotropic and uniformly distributed over the entire source region.

Neutron and primary gamma-ray responses were evaluated for radial and axial detector locations. For each response function (neutron or gamma-ray response function), radial and axial doses required separate sets of adjoint XSDRNPM-S and MORSE-SGC/S calculations to carry out the automated biasing procedure. In each Monte Carlo calculation, there are four surface detectors and three point detectors. The point detectors are 1, 2, and 10 m, respectively, from the outer

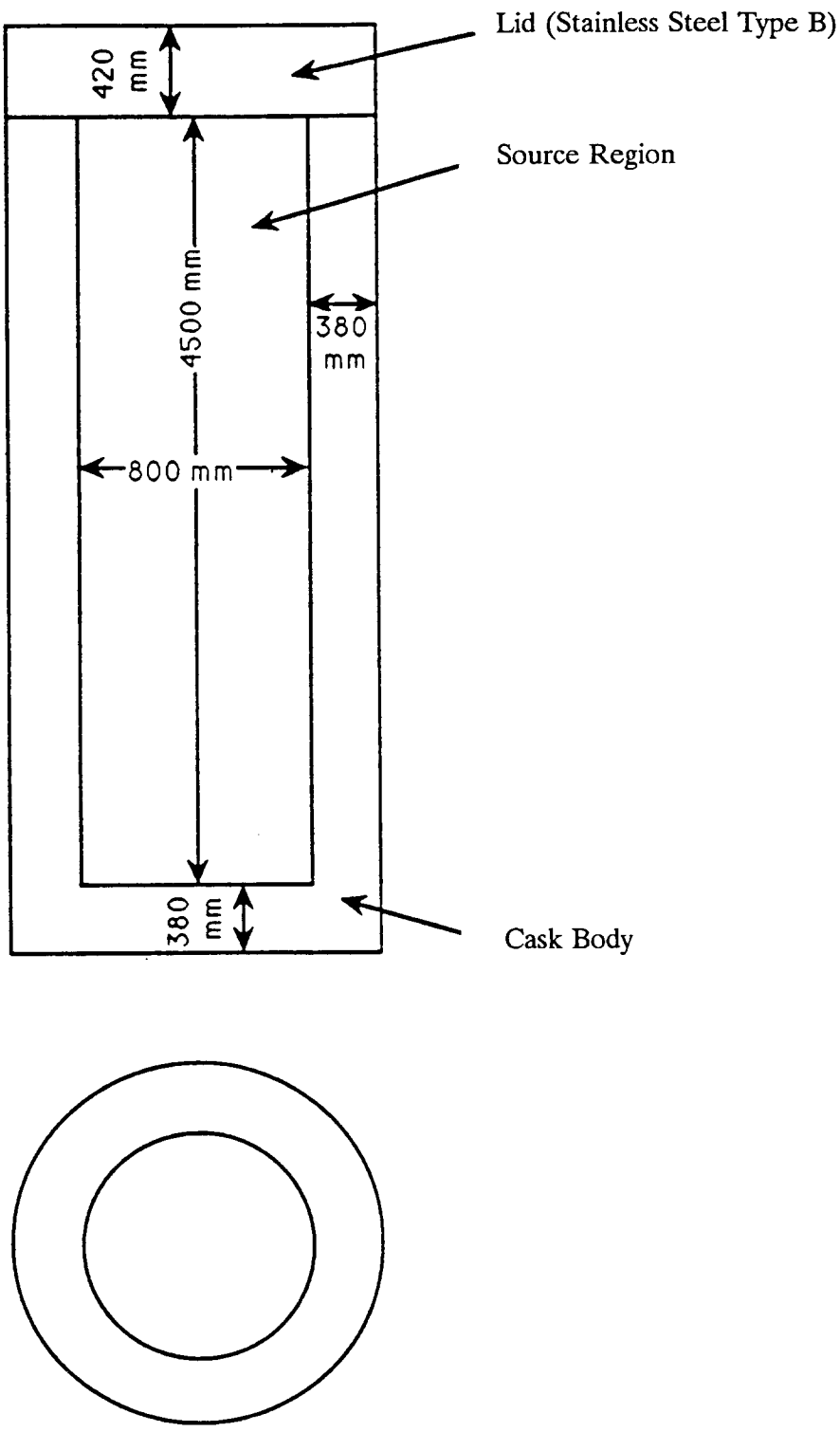

Fig. 2. Geometry of the NEACRP cast-iron cask.

radial or axial surface. The surface detectors are on the cask outer surface and are 1, 2, and 3 m, respectively, from this surface.

Results of calculations for this cask are presented in Table 1. These results are presented only at the cask surface. The results for locations away from the cask surface are given in Ref. 15.

In Table 1, the number of histories processed were 200 per batch for 50 batches for the neutron cases, 3000 per batch for 70 batches for the FP gamma cases, and 150 per batch for 80 batches for the capture gamma cases. The typical running time for a neutron case was 30 min, and less than 60 min for a gamma-ray case on a CRAY computer.

The sidewall surface doses given in Table 1 show excellent agreement between the 1-D SAS1[2] values and the 2-D DORT[17] values. An interesting effect can be observed by comparing these 1-D values (using a 0.5-cm mesh in the shield) with the 2-D values (using a 1.0-cm mesh in the shield). The two neutron cases with a homogeneous shield (1a and 1c) give essentially identical results, but the two-material shield (1b) results are about 15% different. A similar effect is also seen for the fission-product gamma results. When the DORT mesh is refined to 0.5 cm, each of these cases then agrees well with the fine mesh 1-D results. Thus, for fission-product gammas transport through heterogeneous shields the mesh needs to be finer for a given degree of accuracy.

The QAD-CGGP[18] results shown in Table 1 indicate that for this problem the point-kernel technique performs quite well. The QAD-CGGP results are, in general, 15–20% high compared to the discrete-ordinates values. In this instance, the QAD-CGGP result that compares best with the discrete-ordinates results is that for the multiregion shield. This result is most likely fortuitous since the approximations within QAD-CGGP are less accurate for multiregion shields. Previous work[15] has shown that although QAD-CGGP performs well on the cask surface, it tends to be overly conservative 10 m away from the surface.

The DORT, SAS4, and MCNP results for the sidewall surface-averaged doses allow for several different comparisons to be made. First, the results labeled DORT-avg give the 2-D discrete-ordinates solution averaged over the cavity height. The SAS4-avg results use the same multigroup cross sections as the DORT-avg case but employ the Monte Carlo method. Both methods give results that agree to 10% or better. The MCNP fission-product (FP) gamma results similarly agree to within 10%. For the neutrons, the agreement is only about 20%, with the point cross sections giving higher results than the multigroup cross sections. The most likely cause is the better representation of the iron neutron cross-section minima with the point cross-section data. Lack of an appropriate multigroup cross-section library for this problem thus appears to induce a 20% error in the neutron dose with the multigroup codes.

The results for the cask lid and bottom surface doses follow somewhat similar trends as those of the surface sidewall. The FP gamma results are all very consistent, as was seen before. The agreement between the multigroup discrete-ordinates and Monte Carlo results continues to be good. The comparison between the continuous energy (MCNP) and multigroup neutron results is somewhat confusing in that the 20% trend seen at the sidewall surface is not maintained. In fact, the agreement at the bottom is much better (2% between the DORT and MCNP) and much worse at the top (60% difference between DORT and MCNP).

IV.B TN-12 CASK ANALYSIS

To further demonstrate the applicability of the automated biasing procedure, the TN-12 transport cask was analyzed and comparisons made to a series of measured dose rates. This problem was also analyzed by the NEACRP working group on transport cask shielding. A detailed description of the TN-12 cask is given in NEACRP-A-961 (ref. 6). The cask was loaded with 12

Table 1. Summary results of NEACRP problem 1[a]

Surface doses (μSv/h)

	Neutron			FP gamma			Capture gamma		
	a	b	c	a	b	c	a	b	c
Sidewall									
QAD	–	–	–	296	1336	203	–	–	–
SAS1	517	53.7	47.1	268	1300	185	4.1	40.6	0.30
DORT	518	45.8[d]	47.2	240[d]	1168[d]	166[d]	4.1	49.9	0.30
DORT-avg[b]	485	40.1	45.8	233	1134	162	3.81	45.8	0.29
SAS4-avg	476(4)[c]	51.3(2)	48.0(4)	260(3)	1244(5)	193(3)	3.53(4)	38.5(3)	0.30(5)
MCNP-avg	589(2)	–	–	279(6)	–	–	–	–	–
Lid									
QAD	–	–	–	35.6	35.6	22.8	–	–	–
DORT	413	412	47.0	36.7	36.7	25.8	2.8	2.8	0.26
DORT-avg	313	312	36.1	31.4	23.1	16.4	2.19	2.18	0.20
SAS4-avg	304(6)	284(5)	37.0(10)	26.6(7)	24.5(8)	17.7(7)	2.31(16)	2.45(11)	0.19(13)
MCNP-avg	524(6)	–	–	29.0(8)	–	–	–	–	–
Bottom									
QAD	–	–	–	382	382	245	–	–	–
DORT	541	541	61.5	403	403	287	3.9	3.9	0.38
DORT-avg	410	410	47.4	291	267	190	3.11	3.08	0.30
SAS4-avg	352(7)	385(10)	41.3(8)	325(10)	252(7)	183(9)	2.78(8)	2.74(13)	0.28(16)
MCNP-avg	422(7)	–	–	316(10)	–	–	–	–	–

[a]Case a = dry fuel, 38-cm solid cast iron shield.
Case b = dry fuel, 32-cm cast iron with 6 cm polyethylene.
Case c = wet fuel, 38-cm solid cast iron shield.
Calculations with SAS1, DORT, and SAS4 performed using 27n-18g group cross sections (ENDF/B-V).
QAD used built-in attenuation data and log-log interpolation.

[b]"avg" indicates dose is averaged over cavity height for the sidewall doses and over cavity diameter for axial doses. Otherwise, point detectors are used and located at the axial midplane for the sidewall doses and at the radial center for the axial doses.

[c]Number in parentheses indicates percent standard deviation.

[d]Upon rerunning with a finer spatial mesh, agreement with the SAS1 results is obtained.

PWR spent fuel assemblies from Unit 1 of the Fessenheim Nuclear Power Plant. Some assemblies had been irradiated for only one cycle, while others were irradiated for two cycles. The TN-12 cask consists of a cylindrical cavity of diameter 122-cm housing 12 PWR fuel assemblies as shown in Fig. 3. The cask body consists of a 30-cm-thick forged carbon-steel shield clad with stainless steel to provide for attenuation of gamma radiation. The neutron shield is made from resin 10-cm thick surrounding the cask body and traversed by nickel-copper cooling fins. The 3-D model represented the fuel assemblies in a smeared fashion while explicitly modeling the cavity basket and gamma shield. The neutron shield and corresponding fin portions penetrating the neutron shield were smeared such that the explicit geometry was not modeled. All results presented in the following tables are for smeared fins. Estimates performed separately by applying an approximate fin model determined effects of only 3–5% for a smeared vs explicit fin model. Thus, no correction was applied to account for the discrete vs smeared fin models.

The results shown in Tables 2 and 3 give comparisons between the SAS4 predictions and measurements for the neutron and gamma-ray dose rates, respectively. These comparisons are given near the cask surface and in some cases 1 and 2 m from the cask surface for three locations, the axial mid-height, the top peak and the bottom peak along the cask side. The neutron results in Table 2 were calculated from processing 140 batches of 200 histories per batch, and the CPU time was about one hour. The gamma-ray results in Table 3 were obtained from 1200 batches of 2000 histories per batch, and the CPU time was about 5 h. The neutron predictions are somewhat higher than the measured values; however, problems were found in the neutron measurements that could easily account for these differences. The neutron detector responses were initially believed to represent the neutron dose rate. This was later found to be untrue. The calculations given in Table 2 utilized an approximate detector response function that was subsequently issued informally to the working group.

The gamma-ray results produced by SAS4 and an alternate solution by the QAD-CGGP code are given in Tables 3 and 4, respectively. Both sets of calculated results yield acceptable agreement with the measurements. The QAD-CGGP results are uniformly within 20% of the measured values, while, in general, the SAS4 results also fall within this range. Due to the statistical nature of Monte Carlo and, in particular, the point detectors as utilized here, several of the SAS4 results fall outside the 20% range but still lie within 2 σ of the Monte Carlo statistics. The two exceptions to this trend occur at the bottom of the cask where the 0.65 and 0.64 C/E's differ by some 5 to 6 σ's.

These results suffer from the classical pitfall of undersampling of point-detector response whereby the majority of the contribution comes from particles very far away (greater than 10 mean-free paths) from the point detectors. The combination of low responses (C/E of 0.65 and 0.64) and low uncertainties (6% standard deviations) strongly support this observation. In fact, if we examine the top and bottom responses in Table 3, six of seven responses with C/E less than 1.0 have a standard deviation less than 7%. However, all results with C/E greater than one have a standard deviation greater than 14%. The results at the top and bottom locations are the consequences of undersampling due to the source axial burnup profile which started very few particles near the ends of the cask.

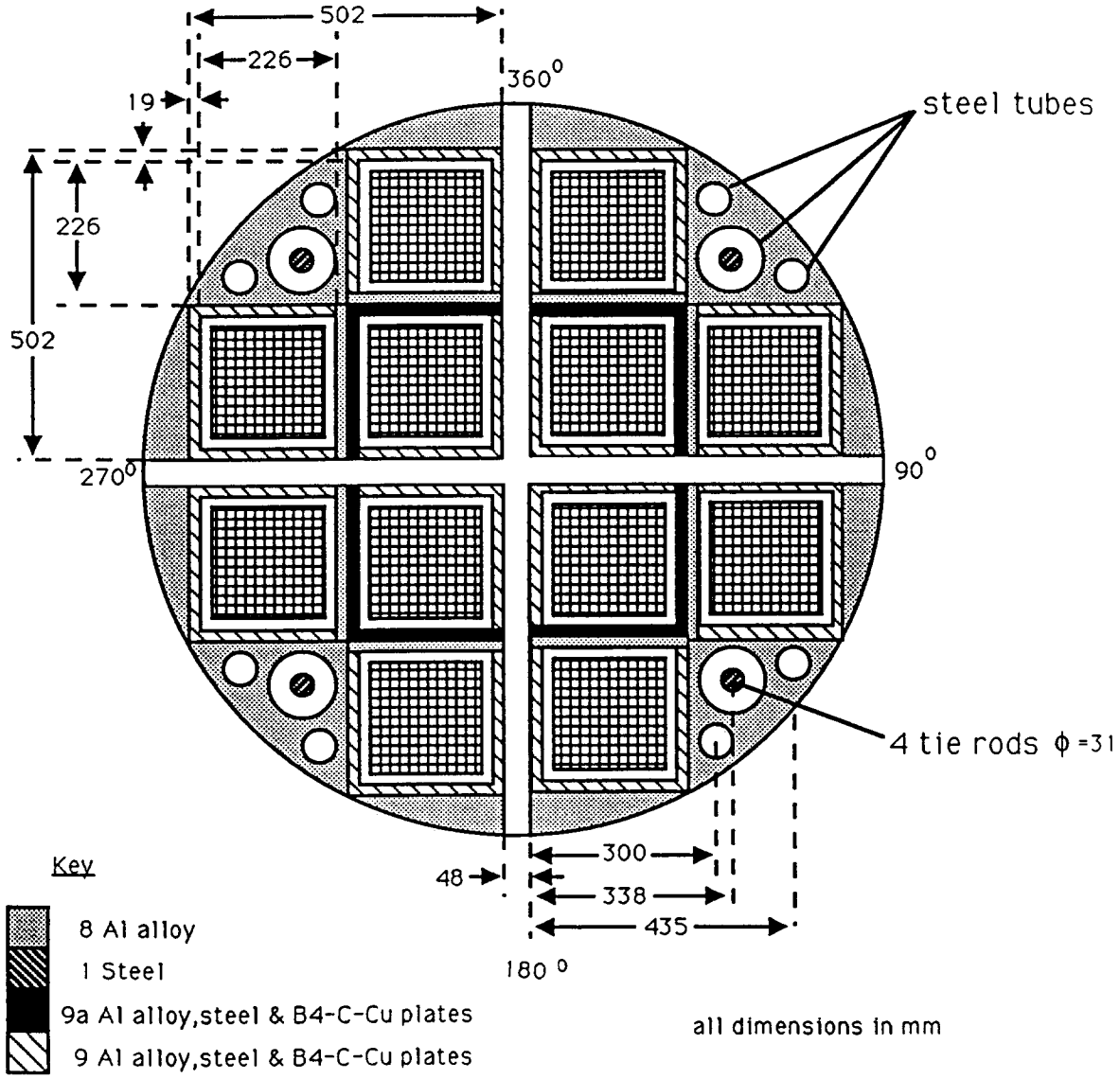

Fig. 3. Cross-sectional view of the TN-12 cask.

Table 2. TN-12 Neutron dose rates at $\theta = 90°$ (SAS4)

Dose point	Distance from fin tips (cm)	Experiment		Calculation	
		Dose rate (μ Sv/h)	Z[a] (cm)	Dose rate (μ Sv/h)	C/E
Peak at bottom of flask	15.5	35.0	47.5	48.6 ± 60%	1.39
Peak of top of flask	15.5	59.3	467.0	62.2 ± 17%	1.05
At mid-height of active fuel	15.5	52.9	271.9	79.3 ± 7%	1.50
	100	28.6	271.9	36.9 ± 4%	1.29
	181.5	19.0	271.9	21.6 ± 3%	1.14

[a]Z = height above bottom of flask.

Table 3. TN-12 gamma-ray dose rates (SAS4)

			Experiment		Calculation	
Dose point	θ	Distance from fin tips (cm)	Dose rate (μ Sv/h)	Z (cm)	Dose rate (μ Sv/h)	C/E
Peak at bottom of flask	135°	7	150	118.0	97.5 ± 6%	0.65
	153°	7	162	118.0	176.2 ± 36%	1.09
		100	54	108.0	50.2 ± 18%	0.93
	180°	7	145	112.0	92.4 ± 6%	0.64
Peak of top of flask	135°	7	210	420.0	274.1 ± 20%	1.31
		200	39	402.0	48.1 ± 22%	1.23
	153°	7	248	416.0	237.9 ± 7%	0.96
		100	80	402.0	72.2 ± 5%	0.90
		200	42	405.0	37.7 ± 5%	0.90
	180°	7	210	417.0	221.6 ± 14%	1.06
		200	38	396.0	35.8 ± 6%	0.94
At mid-height of active fuel	135°	7	80	271.9	92.6 ± 9%	1.16
		200	31	271.9	32.4 ± 3%	1.05
	153°	7	97	271.9	102.1 ± 5%	1.05
		100	49	271.9	58.4 ± 11%	1.19
		200	33	271.9	38.0 ± 10%	1.15
	180°	7	79	271.9	108.1 ± 20%	1.37
		200	31	271.9	34.1 ± 4%	1.10

Table 4. TN-12 gamma-ray dose rates (QADS)

			Experiment		Calculation	
Dose point	θ	Distance from fin tips (cm)	Dose rate (μ Sv/h)	Z (cm)	Dose rate (μ Sv/h)	C/E
Peak at bottom of flask	135°	7	150	118.0	136	0.91
	153°	7	162	118.0	172	1.06
		100	54	108.0	63	1.17
	180°	7	145	112.0	140	0.93
Peak of top of flask	135°	7	210	420.0	190	0.90
		200	39	402.0	41	1.05
	153°	7	248	416.0	219	0.88
		100	80	402.0	86	1.08
		200	42	405.0	43	1.02
	180°	7	210	417.0	186	0.89
		200	38	396.0	39	1.03
At mid-height of active fuel	135°	7	80	271.9	87	1.09
		200	31	271.9	37	1.19
	153°	7	97	271.9	104	1.07
		100	49	271.9	58	1.18
		200	33	271.9	39	1.18
	180°	7	79	271.9	84	1.06
		200	31	271.9	36	1.16

V. CONCLUSIONS

The results obtained for neutron and gamma-ray responses of numerous spent fuel casks indicate that with the automated biasing procedure, Monte Carlo shielding analyses of spent fuel casks can be performed with minimum effort and that accurate and reliable results can be obtained. The major task of setting up biasing parameters in a Monte Carlo deep-penetration calculation has been eliminated. With the automated procedure, the difficulty of carrying out a 3-D analysis of spent fuel casks has been greatly reduced.

However, further study is still needed to improve calculation of the corner doses. One possible solution is to allow source axial biasing in the radial calculation so that more source particles start from the ends of the cask. Another approach may be to develop 2-D importance functions for the corner detectors. Finally, the systematic biasing approach described in this paper can be applied to other Monte Carlo shielding problems.

VI. REFERENCES

1. J. S. TANG, "SAS4: A Monte Carlo Cask Shielding Analysis Module with Automated Biasing Procedure," see Sect. S4 of *SCALE: A Modular Code System for Performing Standardized Computer Analyses for Licensing Evaluation*, NUREG/CR-0200, Rev. 4 (ORNL/NUREG/CSD-2/R4), Vols. I, II, and III (draft February 1990). Available from Radiation Shielding Information Center at Oak Ridge National Laboratory as CCC-545.

2. *SCALE: A Modular Code System for Performing Standardized Computer Analyses for Licensing Evaluation*, NUREG/CR-0200, Rev. 4 (ORNL/NUREG/CSD-2/R4), Vols. I, II, and III (draft February 1990). Available from Radiation Shielding Information Center at Oak Ridge National Laboratory as CCC-545.

3. G. GOERTZEL and M. H. KALOS, *Progress in Nuclear Energy*, Vol. 2, p. 315, Pergamon Press, Inc., New York (1958).

4. J. E. HOOGENBOOM, *Nucl. Sci. Eng.* **70**, 210 (1979).

5. A. F. AVERY and H. F. LOCKE, *NEACRP Intercomparison of Codes for the Radiation Protection Assessment of Transportation Packages. Solutions to Problems 1-4*, NEACRP-L-331 (March 1992).

6. C. M. DIOP, J. C. NIMAL, P. BLUM, and R. CAGNON, *TN12 Shipping Cask Calculations Benchmark*, NEACRP-A-961 (January 1989).

7. J. S. TANG, T. J. HOFFMAN, and P. N. STEVENS, *Nucl. Sci. Eng.* **62**, 617 (1977).

8. J. S. TANG, T. J. HOFFMAN, and P. N. STEVENS, *Nucl. Sci. Eng.* **64**, 837 (1977).

9. R. R. COVEYOU, V. R. CAIN, and K. J. YOST, *Nucl. Sci. Eng.* **27**, 219 (1967).

10. J. C. NIMAL et al., *Programme de Monte Carlo polycinetique á trois dimensions TRIPOLI*, CEA.N.1919, Commissariat á l'Energie Atomique, Saclay (1976).

11. *MCNP - A Generalized Monte Carlo Code for Neutron and Photon Transport*, LA-7396-M, Los Alamos National Laboratory (1981).

12. J. E. STEWART, *Trans. Am. Nucl. Soc.* 28, 643 (1978).

13. T. J. HOFFMAN and J. S. TANG, *XSDRNPM-S Biasing of MORSE-SGC/S Shipping Cask Calculations*, ORNL/CSD/TM-175, Union Carbide Corp., Nucl. Div., Oak Ridge Natl. Lab. (1982).

14. J. S. TANG and T. J. HOFFMAN, *Nucl. Sci. Eng.* 99, 329 (1988).

15. B. L. BROADHEAD, M. C. BRADY, and C. V. PARKS, *Benchmark Shielding Calculations for the NEACRP Working Group on Shielding Assessment of Transportation Packages*, ORNL/CSD/TM-272, Martin Marietta Energy Systems, Inc., Oak Ridge Natl. Lab. (November 1990).

16. *ANSI/ANS-6.1.1-1977, Neutron and Gamma-Ray Flux-to-Dose-Rate Factors*, American Nuclear Society, LaGrange Park, Illinois (1977).

17. W. A. RHOADES and R. L. CHILDS, *Two- and Three-Dimensional Discrete Ordinates Transport*, January 1992. Available from Radiation Shielding Information Center at Oak Ridge National Laboratory as CCC-543/TORT-DORT.

18. *QAD-CGGP. A Combinatorial Geometry Version of QAD-P5A. A Point Kernel Code System for Neutron and Gamma-Ray Shielding Calculations Using the GP Build-up Factor.* Available from Radiation Shielding Information Center at Oak Ridge National Laboratory as CCC/493/QAD-CGGP.

The Advanced Features of the Monte Carlo Code MCBEND

S J Chucas, I J Curl & P C Miller
AEA Technology, UK

Summary

Monte Carlo codes for radiation shielding applications have been continually developed for more than 30 years. The geometric modelling capabilities and detailed cross-section representations afforded by Monte Carlo initially gave the method the status of a reference against which to test more approximate solutions. This has changed with the development of efficient acceleration procedures and the modern computer workstation. As a consequence the Monte Carlo method, as implemented in codes such as MCBEND, is now firmly established as a standard design tool for a wide range of practical problems and it is no longer necessary to develop the basic method algorithms. As part of the on-going developments of MCBEND it has become appropriate, therefore, to incorporate features aimed at simplifying applications for new Monte Carlo users and to improve the ease of specification and efficiency of calculation for new and more complex problems.

Features of the MCBEND code aimed towards the new user include an easily assimilated user-guide with associated documentation, a comprehensive geometry checking and visualisation package, and a fully automated, robust, acceleration procedure. Applications guides for specific design problems are also being developed. Advanced features of the code aimed towards extending its range of application include a new geometry package (based upon pre-defined sub-parts, with hole tracking options), charged particle tracking, angular biasing of scatter, a forced flight option and the ability to interface to other shielding codes. Parallel versions of MCBEND have been available for several years for use on a Meiko Parallel Surface. The latest version of the code has been adapted to operate in parallel on a network of Sun workstations.

The report reviews the functionality of the current version of MCBEND. The advanced features of the code are described together with an outline of the on-going development programme. A number of applications are briefly described in order to quantify the performance of MCBEND in terms of the man days needed to prepare data and the required computing resource.

1 INTRODUCTION

The Monte Carlo method has been developed in the UK as a corner stone to the calculational procedures for shielding design and assessment. It has been used both as a reference to validate simpler design procedures or approximate datasets and as a design method in its own right. Increasingly it has become the first choice method for the majority of design assessment studies. This has been brought about mainly as a result of two separate factors. Firstly the development of improved, automated, acceleration techniques now greatly simplifies the preparation of the case data and removes much of the mysticism previously associated with the method. Within a few days the newcomer to Monte Carlo can, with confidence, set up a practical case and, owing to the automatic acceleration, obtain a reliable design estimate. Secondly the advent of the modern workstation has provided the user with a massive, yet inexpensive, computer resource for individual use. The cpu times for Monte Carlo calculations are comparable with the elapsed times previously associated with job submissions to main frames. With the Monte Carlo method the shield designer now has a method capable of solving most practical problems associated with radiation transport. Furthermore the method is rigorous and, within constraints imposed by material tolerances and subjective modelling approximations, its accuracy is limited only by the knowledge of the basic cross-section data.

The Monte Carlo code MCBEND has now been developed to the extent that cost efficiency improvements made available through purchase of new computer hardware are likely to exceed the possible gains available through the development of new calculational algorithms. For this reason the on-going development programme for MCBEND is aimed towards simplifying applications of the method for new users and improving the ease of specification and efficiency of calculation for new and more complex problems

This paper summarises the current status of MCBEND with particular reference to the advanced features now incorporated for efficient solution of a diverse range of practical problems. Brief comments on the on-going development programme are included.

2 BASIC SPECIFICATION

The functionalities of the current generation of major Monte Carlo codes used in the analysis of radiation transport are very similar. A basic description of MCBEND is provided for completeness and by way of introduction to the following sections.

MCBEND (1) is a general geometry Monte Carlo code for shielding calculations. It may be used for neutron, gamma-ray, electron/positron and coupled calculations. The neutron data are presented in 8000 groups and are derived from the UK Nuclear Data Library and JEF compilations. The gamma-ray data are described in a continuous energy scheme and based upon the UKNDL compilations, which are derived from the work of Hubbel (2). Coupled n-γ calculations are performed by running the neutron calculation and writing details of the neutron collisions to a dump file. This is then combined with a gamma-ray production library to produce the source for the gamma-ray calculation. Multi-group data input options are also available for neutron, gamma-ray or coupled calculations.

The material regions in the system are described using Combinatorial Geometry (CG) techniques, which construct the material zones by the combination or subtraction of simple geometric bodies. This allows a very accurate model of the system to be created. An orthogonal mesh is usually mapped onto the CG model for specifying importances, these varying in space, energy and (if appropriate) time. The importance values are usually generated by adjoint diffusion calculations (3) but can be user defined. The basic acceleration method is based upon the combined techniques of splitting and roulette

The source regions are defined with respect to either an orthogonal geometry mesh or by a CG representation. The former allows sophisticated weighting algorithms to be applied; eg, angular weighting, and the direct use of space/energy importances for source weighting. Built-

in fission spectra are available. The latter source type has more geometric flexibility, being based on the same body types as used in CG.

Several quantities may be scored in a MCBEND calculation. The basic tally is of volume-averaged flux or response, but facilities exist to score sensitivity, angular currents, heat or charge deposition and pulse height distribution. A simple point estimator is also available.

3 SOFTWARE QUALITY MANAGEMENT

The development of MCBEND is now the responsibility of the Nuclear Code Development, NCD, collaboration, which was set up by AEA Technology and BNFL (British Nuclear Fuels plc). This provides a stable framework, with substantial financial backing and long term commitment, for the on-going support of the Monte Carlo expertise associated with MCBEND and the criticality code MONK (4). The background of NCD is reviewed in reference 5. One outcome of the collaboration has been the development of a modular scheme, MCANO, to be used for the development of the codes within an organised system environment. The features of MCANO are described in a companion paper (6).

MCBEND development is carried out using the QA Standards established by the ANSWERS Service of AEA Technology. ANSWERS is responsible for on-going maintenance of the production versions of the code and for the release of code versions to users. It also provides full user support by way of training, documentation and a hot-line service. The ANSWERS Service and the associated software development departments have been awarded certification under the TickIT Scheme, sponsored by the UK Department of Trade and Industry, confirming full compliance with the BS5750 (ISO 9001) software quality standards.

4 ADVANCED FEATURES

In this presentation the advanced features of MCBEND are considered under three categories. Firstly, and possibly most importantly, there are those concerned with improvements to the user image and ease of use. Secondly there are those features concerned with improvements to the efficiency of the calculation. Finally we review those features which have been incorporated into the code to improve its range of application and utility. A number of features result in benefits within more than one category.

4.1 USER IMAGE

i) Documentation.

The first stage of the on-going programme of work to improve the user image of the code has been the modernisation of the user guides. An input syntax has been developed, based upon a flow diagram format, which permits a quick and easy user assimilation of the input requirements with adequate provision for detailed notes to clarify specific items. It is intended, shortly, to make the flow diagrams available to the user via an interactive display within the windows operating system. The user guide is supported by an expanding range of introductory texts and applications guides.

ii) Error Trapping.

The input routines perform extensive checking to identify and trap input errors. Errors arising due to inconsistency of data or to omissions are flagged and an informative error message output.

iii) Geometry Preparation Macros

Data preparation macros have been written to simplify the preparation of the input data for selected standard problems. An example is PUFFIN, which takes the user, step by step,

through the preparation of the input data for the analysis of a steady state neutron porosity tool as used for bore hole logging in oil exploration. PUFFIN is primarily intended to help the new user to get started and has been simplified by restricting the available options. Nevertheless, mud lining of the bore holes and stratified rock beds, with intrusions, can be analysed. The simple PUFFIN models can also form the basis of more specific cases by using an editor to modify the general model.

iv) Geometry Visualisation.

A user-friendly, mouse-driven, visualisation package, VISAGE, has been developed for geometry display and error diagnosis. To ensure portability it has been developed using the C language and the X Windows system/OSF Motif tool-kits. VISAGE overlays the geometry with a fine orthogonal mesh and employs the tracking routines of MCBEND to output an identifier (representing the material or geometry zone) for each mesh. A resolution of up to 5000 meshes across the display can be employed. VISAGE displays a two-dimensional cross-section of the model in either colour or monochrome. The user can interactively confirm the location of the geometry bodies, change the colour of individual regions, zoom in on regions of particular interest and output the display to a printer. The high resolution provides for accurate checking of geometry models.

With the adoption of international graphics standards (i.e. X11, OSF Motif and PHIGS) by the major hardware manufacturers it has become possible to develop graphics codes giving full 3 dimensional displays of geometry models, etc, whilst retaining full portability of the software. The new VISTA suite, now undergoing pre-release testing, comprises two graphics codes. The first, VISTA-WIRE, creates wire frame displays of the geometry models using PHIGS and allows user manipulation of the display through a Motif based interface. The companion code, VISTA-RAY, outputs a rendering of the 3-dimensional geometry model using simulated optical ray tracing techniques. The image is produced by analysing the propagation of rays through transparent or semi-transparent media and interacting with opaque surfaces. The contrast of the picture is enhanced through the simulation of the diffuse reflection resulting from a single light source.

v) Output Display.

The full output of the MCBEND calculation is contained within a dump file. Exploratory studies have been carried out, using widely available commercial software packages, to display the importance function, particle flows, fluxes and reaction rates as contour maps and 3-dimensional plots. For the production version of the code it is intended that these data should be displayed as an overlay on top of a geometric section produced by VISAGE. A commonly requested user option concerns the display of individual particle trajectories rather than the averaged population behaviour, as represented by the particle inflows between the importance mesh. The required information to produce these plots is not readily obtained from MCBEND owing to the use of splitting/roulette for the acceleration. Nevertheless studies have shown that representative trajectories can be constructed for display and this option will be provided in a future release of the code.

vi) User Support.

An integral part of the code image is the support available to the user. No matter how good the documentation, diagnostics and visualisation the user is always likely to require some access to a code expert. This may be for no more than the identification of the most appropriate code facilities or acceleration techniques for a particular application. Dialogue between the user and the code developer can lead to the identification of new code features to improve the efficiency of the code for a specific type of problem. The dialogue between the users and MCBEND developers is facilitated through the formal arrangements provided by the ANSWERS Service. This provides for 'hot-line' telephone support for general queries, seminars to provide updates on code developments and to review applications, workshops and more specific user training.

4.2 EFFICIENCY OF CALCULATION

In this section we review the improvements in the efficiency of calculation made available either through the development of new calculational algorithms or as a consequence of the new computer hardware.

4.2.1 Acceleration Methods

i) Automatic generation of space/energy importance function.

A central feature of any Monte Carlo code for penetration studies is the provision of an efficient suite of acceleration techniques. For most calculations MCBEND employs the well-established method of splitting and roulette to direct particles from remote regions of low importance to those of higher importance close to the dose point. A multigroup importance function is used to represent fully the energy variation, and data are derived from an adjoint solution of the ADC diffusion equation (3). This approximates the single energy group transport equation by a two-component diffusion model and may be considered at least the equivalent of a P4 representation.

The importance function is specified with respect to an orthogonal material mesh superimposed upon the material geometry. The user may specify the mesh and use auxiliary codes, such as the finite element code FENDER (7) or the finite difference code SNAPSH (8) to derive the importance function. However most users now prefer to make use of the automatic generator built into MCBEND (9). This functions by converting the general geometry material description to an orthogonal XYZ or RθZ mesh for a diffusion solution performed using the ADC diffusion method.

The automatic importance generator of MCBEND requires only the specification of the 3 dimensional mesh boundaries and the adjoint source spectrum as defined by the selected response function. Output of a trial run can provide data to optimise the importance, but the method is not over sensitive to the choice of mesh, and revisions are not usually required. The method, being based upon splitting/roulette, is commendably free from the introduction of bias in the solution. It has been demonstrated to be robust in the hands of even the novice user.

ii) Angular biasing

Monte Carlo calculations of void streaming are notoriously difficult to accelerate. In order to improve the efficiency of MCBEND for these applications, an option has been provided to bias the angle of scatter at chosen collision sites according to a super-imposed angular importance function aimed at directing particles along the streaming path. These importances may be estimated from the angular fluxes at the sides of the void determined using an adjoint MCBEND calculation. It has been generally found that the introduction of angular biasing results in efficiency improvements of factors two to three compared with comparable cases employing space/energy biasing only.

The use of the MCBEND adjoint is an effective technique to determine angular importances provided there are no multi-legged streaming paths between the duct edge and the detector. A possible option in these cases is to produce angular importances by combining diffusion theory with kernel methods. A kernel module has been written to provide the coupling between the mesh surfaces forming the boundary of a void region for use with the finite difference diffusion code SNAPSH (8). Surface currents entering the void are estimated from the diffusion solution for the solid material, and are then combined with the transmission kernels to provide the surface currents entering the wall. Any number of void regions can be included and, unlike albedo methods, the coupling due to transmission between voids is correctly treated. Initial comparisons with Monte Carlo suggest the method accurately predicts

the forward flux. The module has been written for XYZ geometries. SNAPSH can, however, solve for different 3-dimensional geometries, including cylindrical, spherical, hexZ and triZ.

iii) The Forced Flight Method.

Another area where the acceleration of Monte Carlo is difficult to achieve because of streaming effects is the transport of gamma-rays in collimated systems. For example, a typical logging tool, as illustrated in Figure 1, contains a gamma-ray source and a detector which measures gamma-rays scattered back from the rock formation surrounding the borehole. The detector housing, made of tungsten, has only a narrow opening through which a collimated beam of gamma-rays can reach the detector.

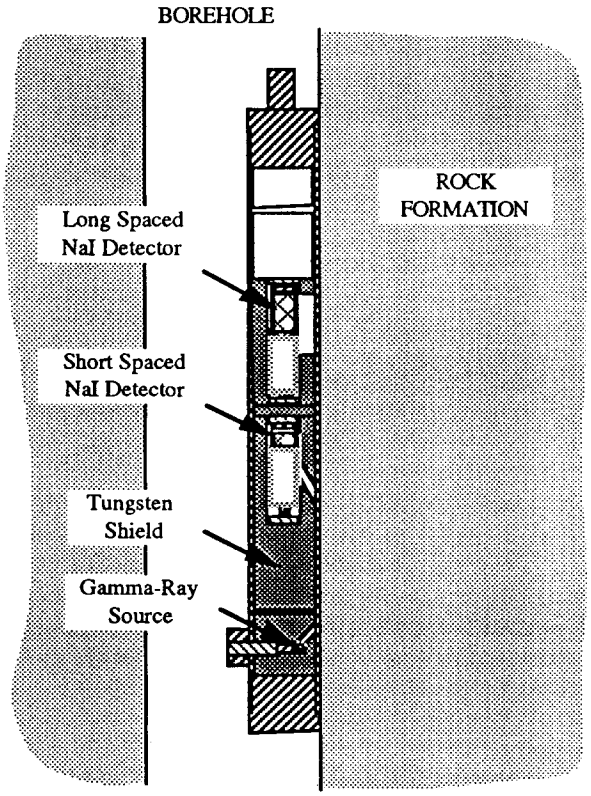

Figure 1 - A Gamma-Ray Density Sonde

It is very difficult, using conventional splitting/roulette, to persuade the gamma-rays to travel down the collimator to the detector. Angular biasing, as described above, has been shown to give a useful improvement in efficiency, but the calculations still require a very long time to achieve the required statistical accuracy. An alternative approach has been developed, known as the "forced-flight" technique, which has similarities to the established point flux estimator. An interface is introduced into the collimator, and at each collision outboard of this interface (ie away from the detector) the current crossing the interface is calculated deterministically by ray-tracing from the collision site to the interface, with an allowance for the probability of scatter through the appropriate angle. The interface may be circular, elliptical, rectangular or spherical, and there may be more than one. To reduce inefficiencies due to processing unimportant events the user specifies the domain over which forced flight is permitted and the probability of a forced flight event is biased by reference to the importance at the collision site. The value of the current at the interface is used to generate new particles which travel to the detector. The weight of the gamma-ray at the collision site is not altered, and it proceeds as normal; but to avoid double-counting, it is killed if it naturally crosses the interface. The procedure is

illustrated in Figure 2, where the interface is shown extending into the tungsten for a short distance so that those particles which just clip the walls of the collimator are included. The use of this method has led to an increase in the efficiency of calculation by about a factor 30. The technique has recently been developed to include the determination of sensitivity.

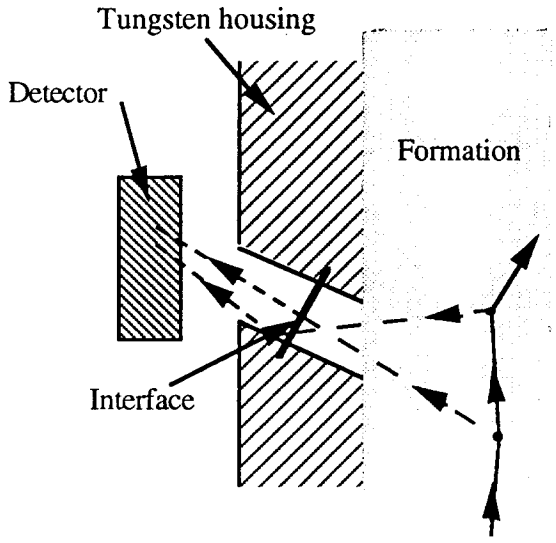

Figure 2 - Illustration of forced Flight Method

4.2.2 Adaptation to New Hardware

i) Parallel processing.

The first exploratory studies of parallelism were begun in 1986 using a Meiko parallel computer surface, which is a MIMD (Multiple Instruction Multiple Data) architecture machine, and T414 transputers. The transputer is unique in that it embodies in its logic a complete parallel language called OCCAM and the early studies were conducted in this language. The initial studies were restricted by the limited memory and fixed point arithmetic of the early transputers. It was nevertheless clear that Monte Carlo represented a simple example of event-farming. This is a natural parallelism that is scaleable and robust against changing inter-processor communication speeds and changing processor computation speed. These are highly desirable characteristics in the rapidly changing world of computer hardware.

The criticality code MONK6 (4) was the first to be converted successfully to the parallel environment (10) and by 1988 the parallel version was being used extensively for routine studies within AEA Technology. The experience gained with the development of MONK6 was applied to MCBEND. A single version of the code has been developed for use on either serial or parallel machines. An almost linear speed-up with the number of processors has been found, holding out the promise for limitless performance improvements. The code in parallel mode is used for routine applications where stochastic uncertainties of better than 1% are required.

By the middle of 1990 the Meiko Computing Surface was transformed to be a completely transparent UNIX work-station operating against Fortran 77 with a CSTOOLS supplement for parallel execution. By the end of that year our Monte Carlo codes had been transferred to this new standard.

Our Meiko surface now comprises a SPARC workstation board which hosts the surface transparently and provides a standard SUNOS UNIX environment. The range of processors used with the surface are currently either T800 transputers or i860 vector processors. The i860 boards each comprise two i860 processors and an associated pair of T800 transputers, which are used to handle the inter-processor communication. They are supplied with their own memory of up to 32MB. For Monte Carlo studies we find 16MB per processor is adequate for complex energy-dependent shielding problems.

The development version of MCBEND can be run in parallel on the distributed processors of a Sun network. This makes parallel processing available to all users with access to a suitable network and ensures efficient utilisation of surplus cpu capacity.

ii) Random Number Generation.

The demands to decrease to near insignificance the stochastic uncertainty on the Monte Carlo predictions combined with the advent of the parallel processor, which has helped to make this possible, have drawn attention to the inadequacies of the commonly used random number generation packages. It was found that the large number of samples that could be analysed economically on the new, cheap, high performance hardware would rapidly exhaust the available random number sequence. The situation was made worse by many of the new acceleration procedures placing extra demands on the random number generation. We have changed over to UNI the lagged Fibonacci series of Marsaglia and Zaman (11) with certain refinements which we have found necessary. The new package generates 2^{79} ($\sim 6 \times 10^{23}$) numbers before the cycle repeats, and is faster and more portable than the package used in earlier versions of MCBEND.

4.3 NEW FACILITIES

i) Fractal Geometry.

A rational rethink of the geometry modelling of the material space for Monte Carlo calculations has been carried out. The perceived geometry modelling problems related to the need to maintain a user-friendly and numerically robust code whilst permitting an efficient method of tracking the particles during the random walk. The former requirements suggested that the construction of the model should be based upon a set of body primitives; the latter favoured the definition by mathematical surfaces. An alternative option attractive for regions with detailed fine structure or high order surfaces was the hole tracking technique due to Woodcock which eliminates the need to determine boundary crossings. An analysis of the problem and the development of the so-called 'Fractal' Geometry (FG) which combines the best features of the various techniques is described in a companion paper (12). For the present it will suffice to note that FG allows for the separate specification of the individual geometry components, or parts, and for the testing of these prior to their inclusion within the full geometry model. The parts are defined with respect to their own co-ordinate system and can be combined with other parts to form new parts to any level of complexity. Thus it is possible to assemble unique user libraries of tested models of fuel elements, instruments, logging tools, etc., which can be combined with other parts to create the complete geometric model.

A secure geometry option has also been built into FG. This provides a facility whereby a model of a commercially sensitive item, such as a neutron spectrometer or oil well logging tool, can be made available to the user, in an encrypted form, as a fractional part for incorporation within the overall calculational model without its structure being revealed.

ii) Source.

The source in MCBEND may be defined either with respect to an XYZ or RθZ orthogonal mesh or using a general source module. The latter is derived from that of the point-kernel code RANKERN (13) and retains a common user image. It is based upon CG techniques. Sources, defined relative to the CG body primitives, are superimposed to create the desired spatial distribution. Recent developments have included the provision of several new source body types to allow the source to be described with the same degree of geometric flexibility as the material regions. The new bodies include hemispheres, truncated cones, toroids and ellipsoids. They are defined by both an inner and an outer surface; the source region being either one of the surfaces or the volume enclosed between the surfaces. Additional flexibility in the definition of complicated sources is provided by a new option allowing linear variation of source over a body. The variation is defined with respect to the body axes and can apply along more than one axis.

For an efficient calculation it is necessary to adjust the source sampling according to the energy and spatial variations of the importance function. Using the XYZ and RθZ mesh options this can be carried out automatically. At present the user is required to input sampling importances for the CG source bodies; an automatic option is proposed for a future release of the code.

The MCBEND source routines have also been extended for the specification of an angular variation, both polar and azimuthal, of source strength. This option was provided for use as part of a linked calculational sequence as discussed below but can be used independently.

A new module is being written to interface MCBEND with the UK Core Performance Package for the accession of core source data for LWR radial shield calculations. The UK Core Performance Package is based upon the established WIMS lattice codes (14) and the whole core code PANTHER (15) developed by Nuclear Electric. PANTHER employs nodal diffusion methods for steady state performance, fuel management, safety transient analysis and on-line operational support. It is accessed via Nuclear Electric's Reactor Physics Workbench, or RPW, which provides a graphical user interface combined with a relational data base for storage of data and for a QA audit trail. The module will greatly speed up the acquisition of core source data in the form required by MCBEND for all periods of reactor operation.

iii) Pulse height scoring.

For the bore hole logging tool, described above, and other gamma-ray systems containing detectors such as NaI, MCBEND has the capability to score a pulse height distribution (PHD). The technique has recently been developed so that it can be requested in a calculation in which splitting/roulette is used for variance reduction. Up to this point, PHD scoring and splitting/roulette were incompatible because the contributions from each split particle could not be determined individually. The problem was overcome by switching splitting/roulette off near the detector; ie. combining the beam of split particles. The particle then undergoes analogue transport until its death, when splitting/roulette is switched back on. In this way, particles can be accelerated efficiently towards a detector, using the forced-flight technique as appropriate, and the correct PHD score can be obtained.

iv) Linked calculational sequences.

In many instances the efficient utilisation of the Monte Carlo method for reactor shield design in the UK has been achieved by linking MCBEND with other codes to form calculational sequences (16). Modules have been developed to interface between MCBEND and the generalised geometry, point kernel and scatter code, RANKERN (13), the ADC (Adjusted Diffusion Coefficient) codes SNAPSH (8) and FENDER (7) and the kernel-albedo code MULTISORD (17). The determination of the containment dose-rates on a PWR serves to illustrate the procedure. The penetration from the reactor source, through the radial shield, to

the reactor pressure vessel (RPV) cavity is determined by MCBEND using an exact geometry model. The dispersion of the radiation within the cavity is estimated using MULTISORD, which generates a wall leakage source term for the RANKERN code. Streaming currents at the nozzle and flange regions, predicted by RANKERN, are input to MCBEND, which predicts the dispersion over these complicated geometry regions. The migration within the containment is also determined using MCBEND and it is usual to represent wall regions by albedo surfaces. The linked sequence of calculations is shown schematically in Figure 3.

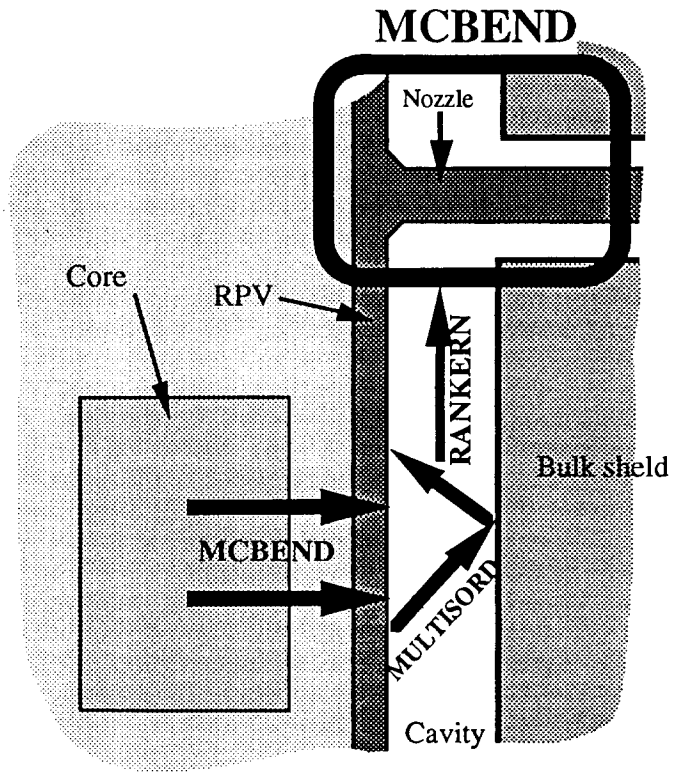

Figure 3 - Calculational Route for LWR Cavity Streaming

In some calculational routes, SNAPSH is used to calculate the bulk penetration through the system. To improve the accuracy of this stage of the calculation it was decided to provide an option to employ the Sn method as an alternative to the ADC method. A module has, therefore, been written to link MCBEND and the Sn code BISTRO (18), which has been developed at CEA, Cadarache. The angular fluxes at a geometric boundary are written onto a dump file by BISTRO for use as source by MCBEND. The form of the BISTRO output file is similar to that produced by DOT (19) and the same link can therefore be used with DOT.

Modifications have been made to the source and scoring routines of MCBEND to allow for the linking of separate MCBEND runs. The code will now output a file containing the angular current at a surface of a CG body which can be accessed by the source routines for use in a subsequent calculation. This technique is very powerful and three examples are given to illustrate its usage;

- for a complicated calculation it may be beneficial to use different importances for the different penetration stages. For an LWR RPV calculation a switch can be made from the use of XYZ splitting geometry in the core to RθZ splitting geometry for the radial shield penetration.

- for calculation of the reaction rates within small samples the penetration calculation can be carried out in the conventional forward mode and linked to an adjoint calculation for the detector position.
- for a gas cooled reactor charge face the leakage from an individual channel can be obtained and used to construct the total leakage over the entire charge face for the subsequent penetration calculation. This technique, referred to as the 'black albedo technique', is described more fully within Section 5.1 i.

v) New Data Libraries.

The original cross-section libraries used by MCBEND were based upon the UK Nuclear Data Library. The UK has participated in the setting up of the European JEF Library and MCBEND has been used extensively for benchmarking this library. The new JEF 2.2 Library is being processed for use with MCBEND and preliminary benchmarking for a range of typical LWR applications is being carried out. Similar studies are being performed for the ENDF/B-VI Library. It is expected that new releases of MCBEND will allow users the choice of either JEF 2.2 or ENDF/B-VI Libraries.

Now that statistical uncertainties in calculation can be removed it has become appropriate to consider more fully the uncertainties due to the nuclear data. A new $S(\alpha,\beta)$ treatment for the scattering of thermal neutrons has been developed which employs a continuous sampling algorithm. For gamma-rays, work is about to start on the provision of a new data library which will include fluorescence and coherent scatter, which have been neglected up to now. This will use the same collision package as that used for neutrons, but with some modification for the new laws required.

vi) Point Data Adjoints

The existing adjoint capability in MCBEND is based upon the use of multi-group data-sets. This is often acceptable but for general use the uncertainties associated with the use of multi-group files do not allow the full potential of the Monte Carlo method to be realised. Work is now in hand to provide the capability through the production of an adjoint version of the DICE data library used by the collision processing routines in MCBEND. This library will contain transformed scattering laws but will have the same basic structure as the normal library so that no major structural changes will be needed in the MCBEND code itself to provide the adjoint option. The prototype code is now being tested.

5 EXAMPLES OF RECENT APPLICATIONS

As noted in the introduction to this paper, the MCBEND code is the cornerstone of the UK calculational methods for radiation transport analysis. It is used in almost all areas of application, either as a design method in its own right or to validate more approximate design procedures. The shield design of all the major UK nuclear facilities, including the THORP plant of BNFL at Sellafield and the Sizewell B PWR have been substantiated using the code. It has been used within the European fast reactor collaboration for the design of the EFR and in the fusion field for the analysis of the experiments at JET. Outside the reactor field it has been widely used in the analysis of nuclear techniques used in process control and in borehole logging. A few examples from recent studies are presented to illustrate the range of problems which are routinely examined using MCBEND.

5.1 RPV DOSIMETRY

The determination of the neutron fluence on a reactor pressure vessel for damage predictions is one of the most demanding of radiation transport problems. It is necessary to model in detail the outer core, shield and structural regions between the core and RPV in order to satisfy the

accuracy requirements. Multi-group methods impose an unacceptable bias unless compensated using correction factors derived from an extensive range of validation studies. It is the UK view that the only method capable of handling the geometry and material data with sufficient precision to meet the target accuracies is the point-energy Monte Carlo method. Studies have recently been carried out for both Magnox and LWR's.

i) Magnox

The re-evaluation of the safety of the UK Magnox reactors, which has been carried out over recent years, has involved the reassessment of the dosimetry of the reactor pressure vessels. Accurate predictions are required at all positions on the vessels of these reactors and account must be taken of local fine structure due to source variations, core restraints, structural steel work and the vessel internals. The problem is illustrated in Figure 4, which is a section through a typical Magnox reactor with a spherical vessel. The geometry is accurately modelled using CG with all significant features included. The detail in the lower corner region is illustrated by the VISAGE section shown in Figure 5. Separate calculations are performed for the radial and axial penetration paths using the appropriate importance functions. Other calculations are performed to estimate the damage at particular vessel welds or in surveillance samples. In the latter case, coupled n-γ calculations are also performed to predict the energy deposition in cylindrical samples only 6cm long and 2cm radius, so that their temperatures may be estimated.

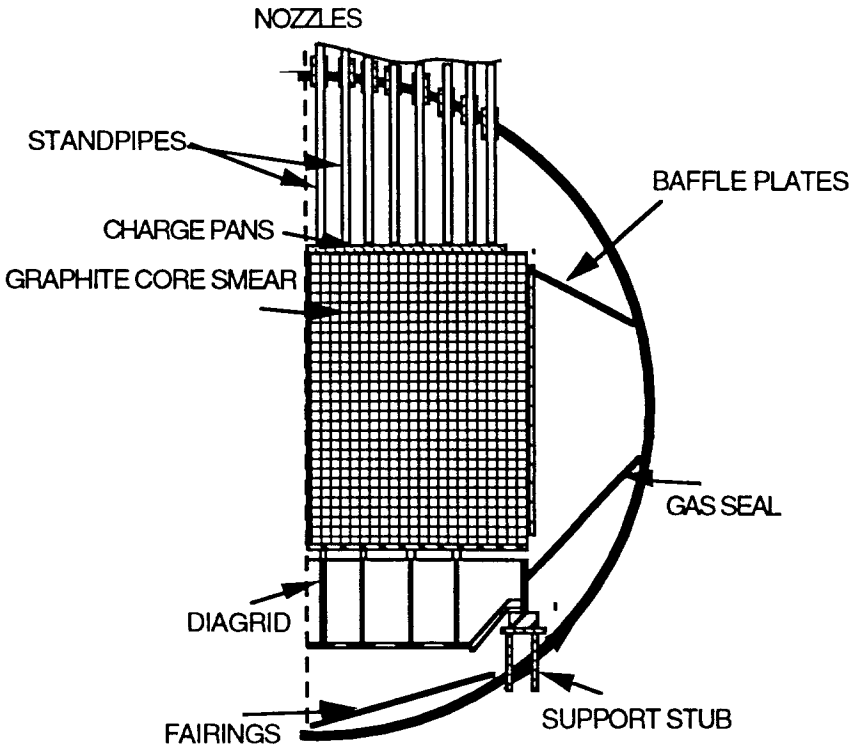

Figure 4 Geometry Model of Typical Magnox Reactor

The principles of the method for the above core region are described in reference 20). The neutron doses are dominated by neutrons leaking from the core and streaming along the open reflector channels to the charge pan regions before migrating to the RPV. Because streaming is a significant feature of the neutron leakage from the core, it is not acceptable to approximate the

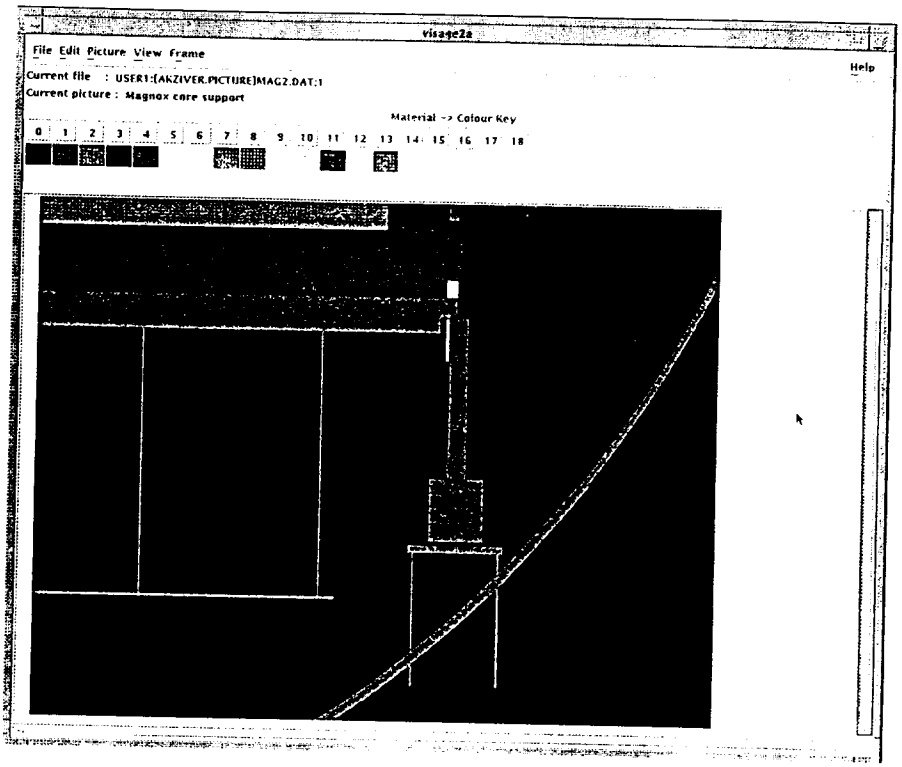

Figure 5 - VISAGE Display of Part of a MAGNOX Reactor

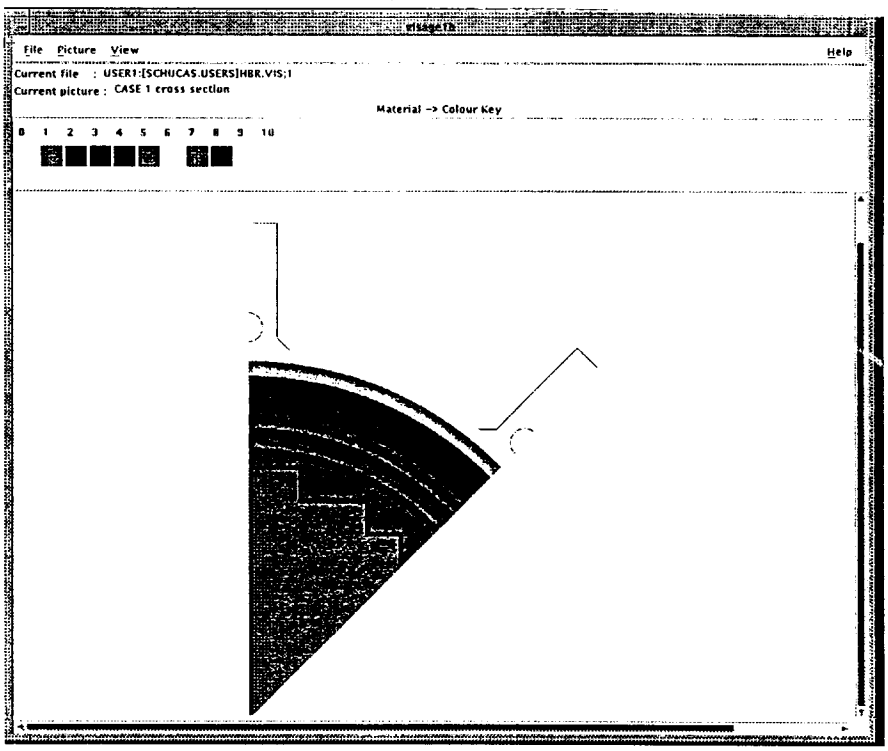

Figure 6 - Section Through the Geometry Model of the H B Robinson PWR

modelling of the upper core region. The calculation is, therefore, split into two stages. In the first stage, a detailed model of the top of the core, reflector and charge pan regions is created for either a single fuel channel cell, or a super cell comprising the smallest symmetrical zone of fuel and absorbers. The top of the charge pans is represented by a "black albedo" surface and neutrons crossing into this region are recorded on a collision file before the trajectory is terminated. The file provides a spatially invariant leakage which is folded with the core radial power profile to generate a surface source for the second stage of the calculation. The above-core steelwork and vessel penetrations are modelled explicitly whilst the core, reflector and charge pans are approximated by smeared zones to adequately treat the back scatter of neutrons. For the calculations described in reference 20) the interfacing between the two stages of the calculation was performed manually. Recent calculations, in which the link is automated, required approximately 15 days to set up the calculational models once the data had been extracted from the engineering drawings and 30 hours cpu on a Vaxstation 4000.

ii) LWRs

The application of MCBEND for LWR pressure vessel damage predictions is illustrated in reference 21), which describes the calculations performed for the H B Robinson Unit 2 PWR of the Carolina Power & Light Company. The calculational model was based upon the eight-fold symmetry element illustrated by the radial section shown in figure 6. The initial round of calculations required approximately 60 days of effort. Most of this time was expended in the acquisition and processing of the engineering information for the plant, the processing of the detailed fuel pin sources to allow for variations with time and for assessment of the uncertainties. Further studies suggest that only three days are required to set up a basic MCBEND model given the engineering and source data. Separate calculations are performed for predictions at the surveillance capsules and for the determination of the RPV damage and cavity fluxes. The running times for the in-vessel surveillance position calculation was ~50 hours to achieve an accuracy of better than 2% on all detectors in a 700cc volume using a Vaxstation 4000.

The studies for the H B Robinson plant have identified requirements for a number of minor developments to MCBEND and associated codes to improve the user convenience and to simplify the uncertainty analysis. The main requirement concerns the accession of the core pin powers during the reactor operation which will be proved by the new module, described in Section 4.3 ii, interfacing the UK Core Performance Package to MCBEND. The other requirements all form part of the development programme.

5.2 BORE HOLE LOGGING

Gamma-Ray Density Sondes are commonly used in petrophysical logging for the in-situ measurement of the bulk density of the formation immediately surrounding the borehole. The formation is irradiated with gamma-rays which interact with the atomic electrons of the formation. If the gamma-rays arriving back at the sodium iodide detectors in the density tool are counted above an energy threshold (~200keV), then the gamma-rays detected will have undergone only Compton scattering interactions in the formation. Hence irrespective of the number of collisions the gamma-rays have undergone it is only the electron density (which is directly related to the bulk density) of the formation which determines the detector response.

MCBEND's ability to model gamma-ray transport can be applied to the interpretation of the performance of such density tools (22). It has major advantages over other calculational methods in that it can accurately model the complex geometry of the tool and formation; it can calculate the measured quantity (the pulse height distribution from gamma-ray interactions in the sodium iodide detector) directly; it can automatically generate a comprehensive, energy dependent importance map to accelerate the calculation; and it incorporates the 'Forced Flight Method', described in Section 4.2.1, to improve the efficiency of Monte Carlo calculations for configurations with detector collimators.

A full range of studies have been carried out to validate MCBEND for use with gamma-ray density tools by comparisons with a new series of experimental benchmarks. The validation programme started with a simple bare NaI detector and mono-energetic gamma-ray source in air and ranged progressively through more complicated configurations. Simple transmission benchmark studies were followed by backscatter studies with a simplified slab geometry mock up of a density tool. The final studies were against measurements using a complete, well-characterised, reference gamma-ray density tool in a series of calibrated test formations. Perturbations in response of the reference tool caused by a variety of mudcakes on the borehole wall completed the programme.

For the bare detector benchmark studies and the simple transmission benchmark studies the calculated absolute detector responses - integrated count-rates above an energy threshold - were in good agreement with the corresponding measured values, with typical calculated/measured ratios of between 0.96 to 1.05.

For the backscatter benchmark studies in the gamma density rig the calculated absolute detector responses were generally in good agreement with the corresponding measured values - with typical C/M ratios of between 0.91 and 1.01 for both clean hole and mudcake conditions.

The final benchmark studies included the treatment of complicated borehole and tool geometries through a series of realistic measurements in full size test formations using a reference tool which closely resembled the geometry and characteristics of a commercial tool. Initially the agreement for these studies was not so good - with typical C/M ratios of between 0.76 and 0.91 in both the clean hole and mudcake conditions. However it was demonstrated that the *relative* changes in the detector responses, caused by changes in the borehole environment, were predicted well in most cases.

An investigation into the cause of this discrepancy in the absolute detector responses concentrated on the identification and specification of key dimensions in the reference tool geometry within the MCBEND model. The investigation showed that the detector responses are very sensitive to small changes (of the order of fractions of mm) in key tool parameters eg. source and detector location . The investigation concluded that although no single cause was found to explain totally the C/M discrepancy, a combination of carefully chosen adjustments to a number of key dimensions (within their uncertainties) within the MCBEND model went a long way to eliminate the C/M discrepancy and gave C/M ratios of between 0.94 and 0.99 for clean hole conditions. The investigation demonstrated conclusively the ability of MCBEND to accurately calculate the sensitivity of the tool response to small changes of tool design thus confirming MCBENDS use as a valuable diagnostic tool.

5.3 PIPELINE ASSAY

Linked calculation methods provide an efficient route for the analysis of design variations or to determine sensitivity of results to parametric changes.

It is sometimes required to determine the effects of changing the material compositions of parts of a system. A particular case is that of nuclear logging devices which are passed through sea floor pipelines to detect whether they are supported by sediment or whether the sediment has been eroded leaving the pipeline unsupported and possibly stressed. In such cases it is laborious to perform complete calculations for each tool/pipeline/sediment configuration, especially as only small changes in response might be expected. The "black albedo" technique is therefore used. An interface is specified at the outer surface of the pipe. The particles crossing the interface are used as the source terms for a series of second-stage calculations which model the external systems and, in this example, the subsequent transport of radiation back to the tool detector. This method isolates those particles which will be affected by changes in the material surrounding the pipe. The particles which reach the detector without passing through the pipe wall are not modelled so the method is also free from any uncertainties in the background signal. Because the tracking of particles to the interface is

performed only once, the overall efficiency of the calculations is increased. Furthermore, as the first stage of each calculation is common, the statistical uncertainties in the interface source for the second stages are fully correlated and can be cancelled from the analysis. Thus the differences in the results of the second stage may be directly related to differences in the configurations. It is a straightforward task to analyse the changes in detector signal to better than 2%. A typical cpu time to achieve this accuracy for a two stage calculation is about 30 hours on a Vaxstation 4000.

6 SUMMARY

The Monte Carlo method, and in particular the MCBEND code, is firmly established as the preferred method of calculation in the UK for most radiation physics and shielding studies. The applications extend from reactor design, through radiation transport and the fuel cycle, to process industries and oil exploration studies. An on-going development programme ensures that MCBEND is adapted to meet user requirements and is able to exploit new calculational algorithms or improvements in computer hardware.

MCBEND is used both as a design method in its own right and as a component of a linked calculational sequence. This situation is likely to be maintained into the foreseeable future, despite the rapid developments in the Monte Carlo method and in computer hardware, as the linked sequence provides a good understanding of the penetration mechanism for design analyses and optimisation. However, we expect that increasingly the more approximate stages will be replaced by rigorous Monte Carlo stages.

The Monte Carlo method, as implemented in the MCBEND code, can be considered fully to have come of age for radiation shielding applications. In MCBEND we already have a code able to handle the most complex problems in a precise and efficient manner. The developments to the user image, particularly in the graphics area, should further enhance user satisfaction with the code.

7 ACKNOWLEDGEMENTS

The authors are indebted to their many colleagues in AEA Technology for assistance in the preparation of this paper.

8 REFERENCES

1 Current Status of the ANSWERS version of MCBEND
ANSWERS/MCBEND, The ANSWERS Service, AEA Technology, UK

2 HUBBEL J H
Photon Cross Sections, Attenuation Coefficients and Energy Absorption Coefficients from 10KeV to 100GeV
NSRDS-NBS 29

3 SHUTTLEWORTH E and CHUCAS S J
Linked Monte Carlo and Finite Element Diffusion Methods for Reactor Shield design
Page 180, Proceedings of the Sixth International Conference on Radiation Shielding,
May 1983, Tokyo, Japan

4 Current Status of the ANSWERS version of MONK
ANSWERS/MONK, The ANSWERS Service, AEA Technology, UK

5 BRISSENDEN R J
The Next Generation of the MONK7 Criticality Code
Paper II.1.5, Proceedings of the International Conference on Nuclear Criticality Safety,
September 1991, Oxford, UK

6 SMITH N R, BRISSENDEN R J AND WATMOUGH M H
The Development of the MONK and MCBEND Codes Within the New Monte Carlo Modular Code Scheme MCANO
Seminar on Advanced Monte Carlo Computer Programs for Radiation Transport,
April 1993, Saclay, france

7 Current Status of the ANSWERS version of FENDER
ANSWERS/FENDER, The ANSWERS Service, AEA Technology, UK

8 Current Status of the ANSWERS version of SNAPSH
ANSWERS/SNAPSH, The ANSWERS Service, AEA Technology, UK

9 Miller P C, Wright G A, Boyle C B, Power S W
The Use of an Inbuilt Importance Generator for acceleration of the Monte Carlo code McBEND.
International Conference on the Physics of Fast Reactors: Operation, Design and
Computation, Marseille, April 1990, France

10 SMITH N R
Parallel Processing of Monte Carlo Methods
ANS Winter Meeting, San Fransisco, 1989

11 MARSAGLIA G and ZAMAN A
Toward a Universal random Number Generator
Supercomputer Computations Research Institute and Department of Statistics,
The Florida State University

12 SMITH N R, SHUTTLEWORTH E AND WATMOUGH M H
A New Approach to Geometry Modelling and Visualisation for MONK and MCBEND
Seminar on Advanced Monte Carlo Computer Programs for Radiation Transport,
April 1993, Saclay, France

13 Current Status of the ANSWERS version of RANKERN
ANSWERS/RANKERN, The ANSWERS Service, AEA Technology, UK

14a Current Status of the ANSWERS version of LWRWIMS
ANSWERS/LWRWIMS, The ANSWERS Service, AEA Technology, UK

14b Current Status of the ANSWERS version of WIMSE
ANSWERS/WIMSE, The ANSWERS Service, AEA Technology, UK

15 HUTT P K
Overview Functional specification of PANTHER: A comprehensive Thermal Reactor Code for use in
Design, Assessment and Operation.
PANTHER/FSPEC/OVERVIEW 2.0, The ANSWERS Service, AEA Technology, UK

16 Kinniburgh C G, Smith PN
Neutron scaterring through the main loop penetration of the Sizewell 'B' PWR
7th International Conference on Radiation Shielding,
September 1988, Bournemouth, UK

17 Current Status of the ANSWERS version of MULTISORD
ANSWERS/MULTISORD, The ANSWERS Service, AEA Technology, UK

18 PALMIOTTI P et al
Optimised Two Dimensional Sn Transport (BISTRO)
International Topical Meeting on Advances in Reactor Physics, Mathematics
and Computation, April 1987, Paris, France

19 RHODES W A
DOT IV, Version 4.2:Two Dimensional Discrete Ordinates Radiation Transport Code System
RSIC Code Package CCC-320

20 HEFFER P J H et al
Magnox Reactor Pressure Vessel Dosimetry - A New Assessment
Proceedings of the Seventh ASTM-EURATOM Symposium on Reactor Dosimetry,
August 1990, Strasbourg, France

21 POWER S W
An Analysis of the H B Robinson Unit 2 PWR Using the Monte Carlo Code MCBEND
Proceedings of the Seventh ASTM-EURATOM Symposium on Reactor Dosimetry,
August 1990, Strasbourg, France

22 BUTLER J, Curl I J, Locke J
Advances in Modelling Nuclear Logging Tools.
SPE 25652, Society of Petroleum Engineers Meeting, April 1993, Bahrain.

Some results concerning the effect of variance reduction techniques on the figure of merit of Monte Carlo calculations

C. Oliveira and J. Salgado
Physics Department, ICEN-INETI, Est. Nac.10, 2685 Sacavém Portugal

Abstract

The MCNP-4.2 code is being used with a microcomputer model IBM-PS 486 SX with mathprocessor to study the neutron transport in several media, such as quartz, limestone, coal and shale.

Isotropic point neutron sources (14 MeV, ^{241}Am-Be and ^{252}Cf) were simulated in the centre of a sphere of radius 100 cm. The average scalar thermal, epithermal and fast fluxes in 5 cm thick layers were calculated in the interval 0 to 100 cm.

Calculations performed with and without variance reduction techniques, show that the differences in the values of those quantities are within the standard deviations. The relative errors, computer time, figure of merit (FOM) and relative efficiency (ratio of the FOM using the variance reduction technique to the analogue FOM) are discussed. Relative efficiencies up to 20 were achieved for coal and shale when using ^{241}Am-Be and ^{252}Cf sources.

1. Introduction

The increased performance of computers and the evolution of Monte Carlo codes made it possible to use these codes on many applications by teams equiped with supercomputers and mainframes.

The MCNP version 4 [1] was released internationally in 1991, giving, for the first time, the possibility to run it on a desktop computer.

This version was run on a microcomputer, model PS-486 SX from IBM, with mathprocessor.

The goal of this work was to study the efficiency of different geometry splittings on the neutron transport problems.

2. Simulated configuration

The geometrical configuration which was adopted is an approximation of a point source in an "infinite medium". The isotropic point neutron source was located in the centre of a sphere of radius 100 cm surrounded by vacuum.

Three different neutron sources were considered: monoenergetic 14 MeV, ^{241}Am-Be and ^{252}Cf.

Four different materials were simulated: quartz, limestone, coal, shale and shale with 7 ppm of gadolinium.

The thermal, epithermal and fast neutron fluxes having energies below 0.1 eV, 1 to 10 eV and higher than 0.1 MeV, respectively, were calculated in cells 5 cm thick in the interval 0 to 100 cm. The corresponding standard deviations were also calculated.

3. Geometry splitting

The variance reduction techniques used are the geometry splitting with russian roulette and the implicit capture. The weight cutoffs of the russian roulette are fixed in 0.25 and 0.50 in all cells. The source cell importance is always equal to unit.

Problems involving particles transport are very sensitive to the importances assigned to the different depths. The splitting ratio, $\upsilon = I_{i+1}/I_i$, where I_i is the importance of the cell i, should control the number of tracks reaching the boundary of the sphere.

Three different splittings were used. They are shown schematically in Fig. 1.

In standard splitting or without splitting the importances and the splitting ratios of all cells are equal to 1.

In splitting 1 the splitting ratio, υ, is <1 for the first cells (up to 35 cm radius, for quartz) and $\upsilon>1$ for the outer cells (greater than 50 cm, for quartz); between these radii there is a region where $\upsilon=1$. These limits depend on the material and the source, undergoing small translations when one or both of these parameters change.

In splitting 2 the cells importance and the ratio υ are equal to 1 in the first cells around the source, and >1 for the outer cells.

Consequently:

a) in standard splitting there is an initial increase in the track population entering the cells, reaching a maximum value, followed by a decrease in that quantity;

b) in splitting 1 the track population is roughly constant in all cells, including the one where the source is located;

c) in splitting 2 the track population is growing up to a maximum, (corresponding to those cells in which the importance is equal to 1), reaching a saturation in cells with importance >1.

The number of tracks entering the last cell is very much different in the three splittings, as shown in Table 1, for quartz with the 14 MeV source.

4. Results and discussion

4.1. Relative standard deviation

For each material, neutron source and geometry splitting, the fast, epithermal and thermal neutron fluxes and their relative standard errors were calculated.

The differences between the fluxes calculated with the different geometry splittings are equal or lower than their standard deviations.

An example of this is shown in Fig. 2, concerning coal, where the ratio of the flux with splitting 2 to the flux without splitting for the fast, epithermal and thermal fluxes, and three neutron sources is plotted against the radius.

The relative standard deviations for each simulation arrangement are shown in Figs. 3 to 7.

In the region near the centre of the sphere the relative standard deviation (r.s.d.) is the same using splitting 2 or without splitting, because in this region the importances and the splitting ratios are equal to 1 in both simulations.

In the outer regions the r.s.d. calculated without splitting increases significantly up to the boundary of the sphere, while the r.s.d., using splitting 2 increases very slowly.

The increase observed in r.s.d. without splitting is a consequence of the exponential decrease of the track population with increasing the distance to the source.

The r.s.d. of the flux using splitting 1 are higher than those corresponding to splitting 2. This fact is due to a large number of tracks entering the cells in splitting 2.

4.2. Computer time

Fig. 8 shows the computer time, expressed in minute, of each run. Splitting 2 appears as the more time consuming due to higher track population.

For coal and shale (for 14 MeV neutron source), quartz and limestone (for all the sources), splitting 1 is less time consuming than without splitting. In effect, the run time depends on the tracks entering cells. Splitting ratios $\nu < 1$ in the first cells reduce this value, although $\nu > 1$ in the others cells increases it. The degree of influence of these opposite effects is dependent on material and source.

A new set of inputs were run using others weight cutoffs, 0.05 and 0.1; the computer time has duplicated for all the cases, without appreciable improvement in the relative standard deviations.

4.3. Figure of merit

The measure of efficiency for MCNP calculations is the figure of merit, FOM, defined as:

$$FOM = 1/\sigma^2 t$$

σ being the maximum r.s.d. associated with each flux, which corresponds to the outer cells, and t the computer time.

Fig. 9 shows the FOM for fast, epithermal and thermal fluxes with the three different splittings.

i) for fast fluxes, splitting 2 appears to be the best choice. It has higher values in 9 cases and in other 7 cases its values are very close to the values for other splittings.

For quartz, using the 14 MeV neutron source and for limestone using any of the three neutron sources the higher computer time with splitting 2 is compensated by the standard deviation reduction. For quartz with the ^{241}Am-Be and ^{252}Cf sources, splitting 1 improves the results.

For coal and shale (for 14 MeV), due to low density and higher carbon content the fast flux decreases quicker than in the other materials, and therefore the splitting of the tracks becomes important. The increase in time is compensated by the reduction in the r.s.d. due to the rise in the track population.

ii) for epithermal fluxes in quartz and limestone, splitting 1 originates higher FOM for 14 MeV and ^{241}Am-Be sources, although for ^{252}Cf source splitting 2 is preferable.

For coal (14 MeV and ^{241}Am-Be), splitting 1 has the highest FOM. Splitting 2 is the best choice for ^{252}Cf source due to the quicker decrease in the flux.

For shale, splitting 1 is recommended for the 14 MeV source, whilst splitting 2 is more convenient for ^{241}Am-Be and ^{252}Cf sources.

iii) for thermal fluxes, splittings 1 and 2 do not improve the results in materials with poorer moderating properties and more energetic sources, whilst they have remarkable effects for the other materials and sources.

4.4. Relative efficiency

In order to estimate the efficiency of splittings 1 and 2 as compared with standard splitting, it is convenient to define the relative efficiency, ε, as:

$$\varepsilon_i = FOM_{(i)}/FOM_{(st)}$$

where i refers to splitting 1 or 2 and st to standard splitting. This quantity is independent of the speed of the particular computer used.

The results are shown on Fig. 10.

For fast flux a gain from 1 to 20 is observed (the latter corresponds to the case of shale, with and without gadolinium, for ^{252}Cf source).

For epithermal flux the gain ranges from 1 to 23 for shale with gadolinium and ^{252}Cf source.

Finally, the relative efficiency for thermal flux is smaller than 1 in several cases, but reaches a maximum value of 23 for shale with and without gadolinium.

5. Conclusions

The use of variation reduction techniques in Monte-Carlo computations should be carefully tested to improve the final results (standard deviations or CPU run time).The results show that the differences in the fluxes calculated by using different splittings are within the standard deviations. The large effects of geometry splitting are upon the CPU run time and the standard deviation. However, the best splitting depends on the particular case studied. The relative efficiency is a quantity which reflects the performance of the splitting used.

6. References

[1] J.S. Hendricks and J.F. Briesmeister (1992), Recent MCNP developments. IEEE Transactions on Nuclear Science, Vol 39, n° 4, 1035-1040.

Table 1. Number of tracks entering the last cell. Quartz, 14 MeV.

	number of tracks
without splitting	2669
splitting 1	26370
splitting 2	86973

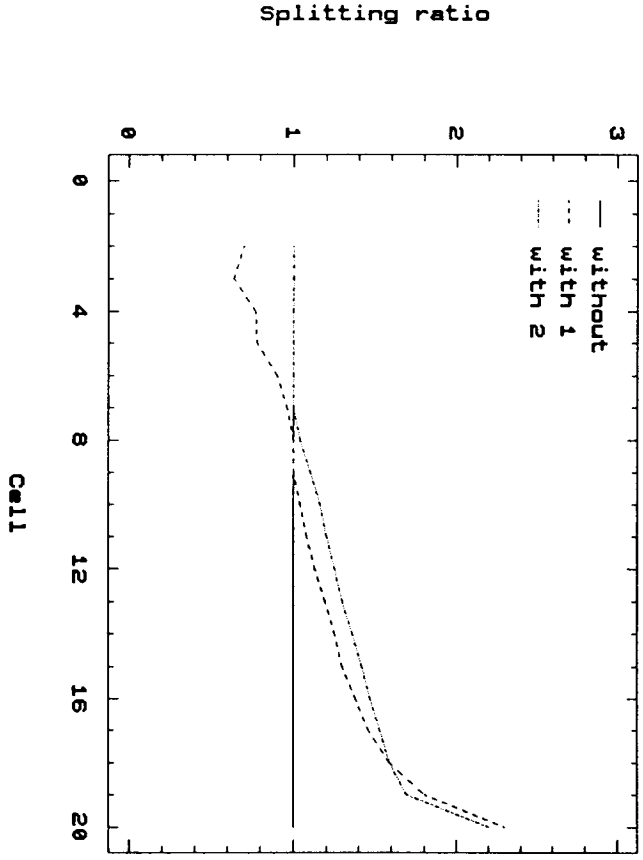

Fig. 1: Spliting ratios for the three geometry splittings as a function of cell number

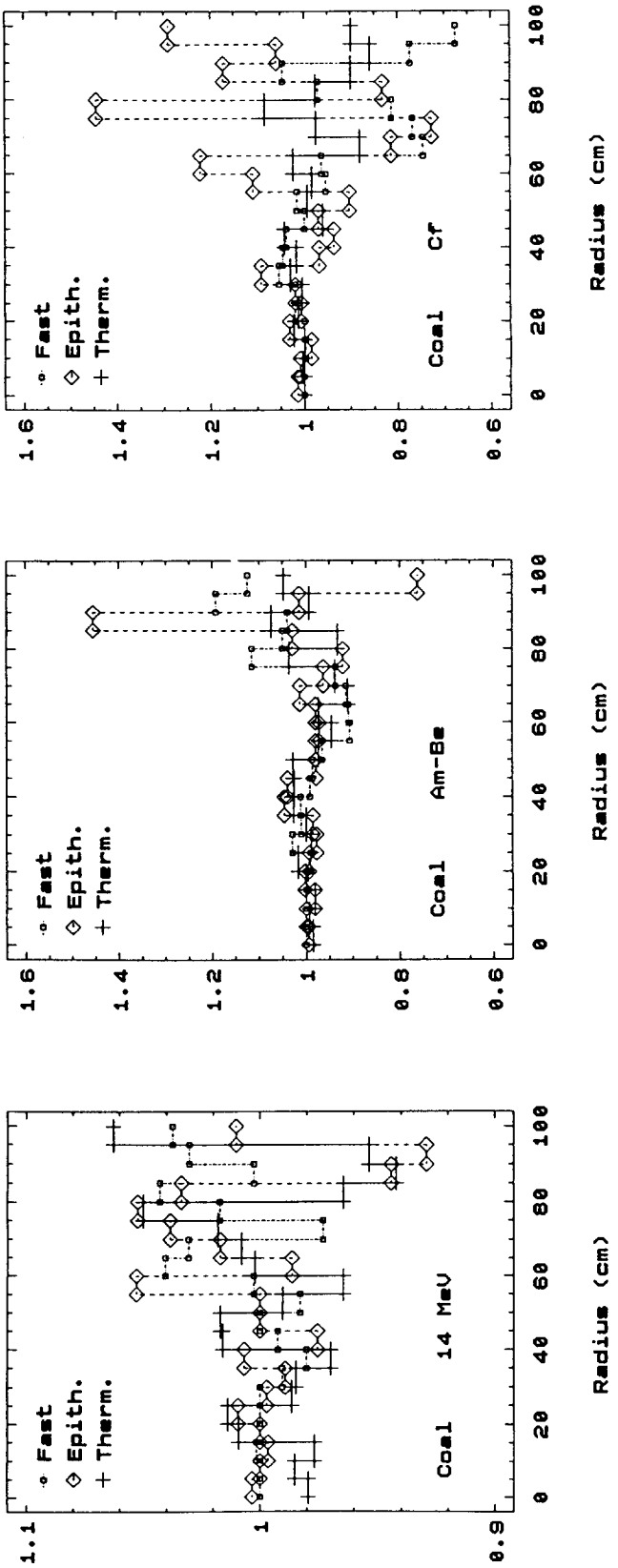

Fig. 2: Ration of the flux with splitting 2 to flux without splitting as a function of the radius

Fig. 3: Relative standard deviation of the flux calculated for quartz with and without splitting as a function of the radius

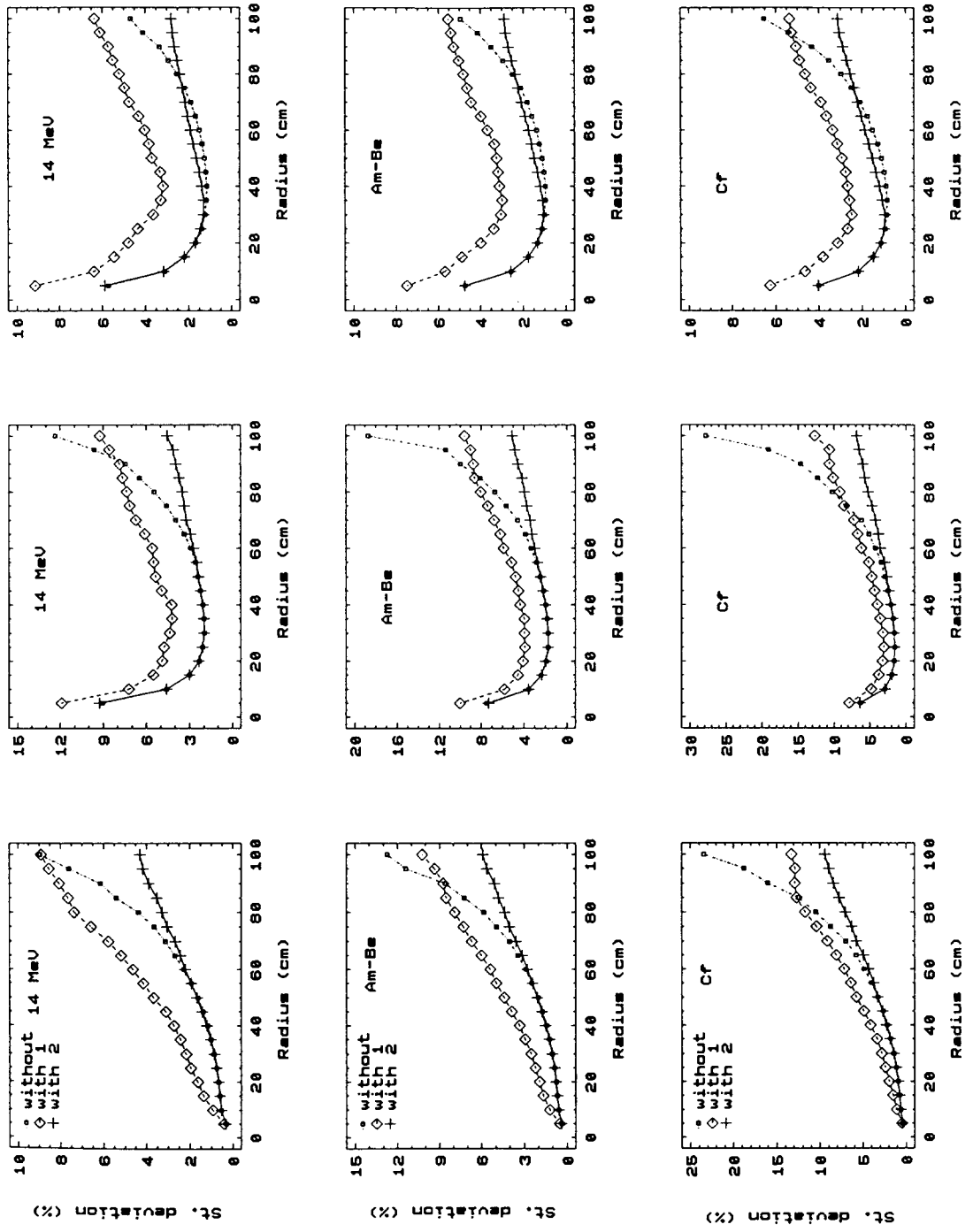

Fig. 4: Relative standard deviation of the flux calculated for limestone with and without splitting as a function of the radius

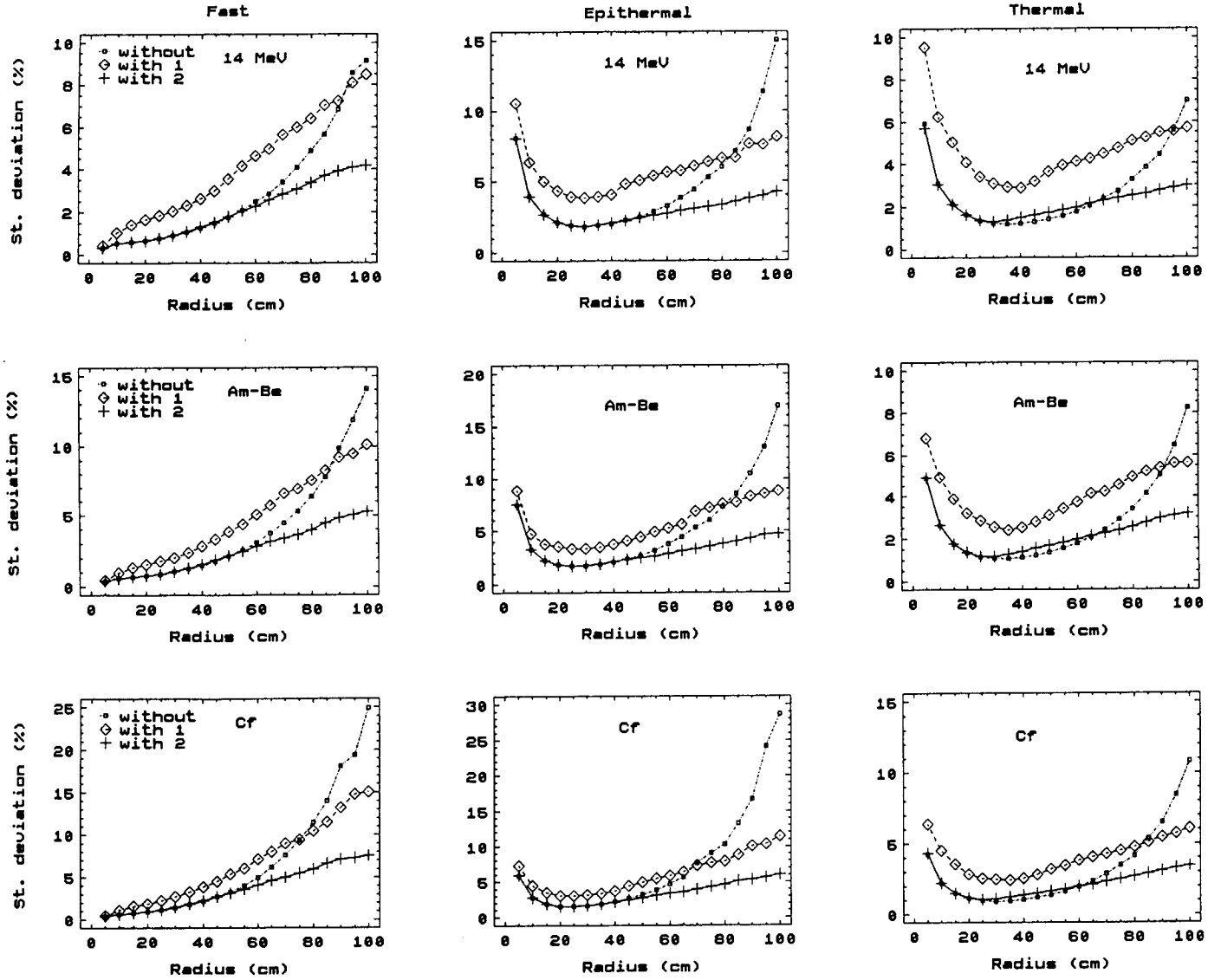

Fig. 5: Relative standard deviation of the flux calculated for coal with and without splitting as a function of the radius

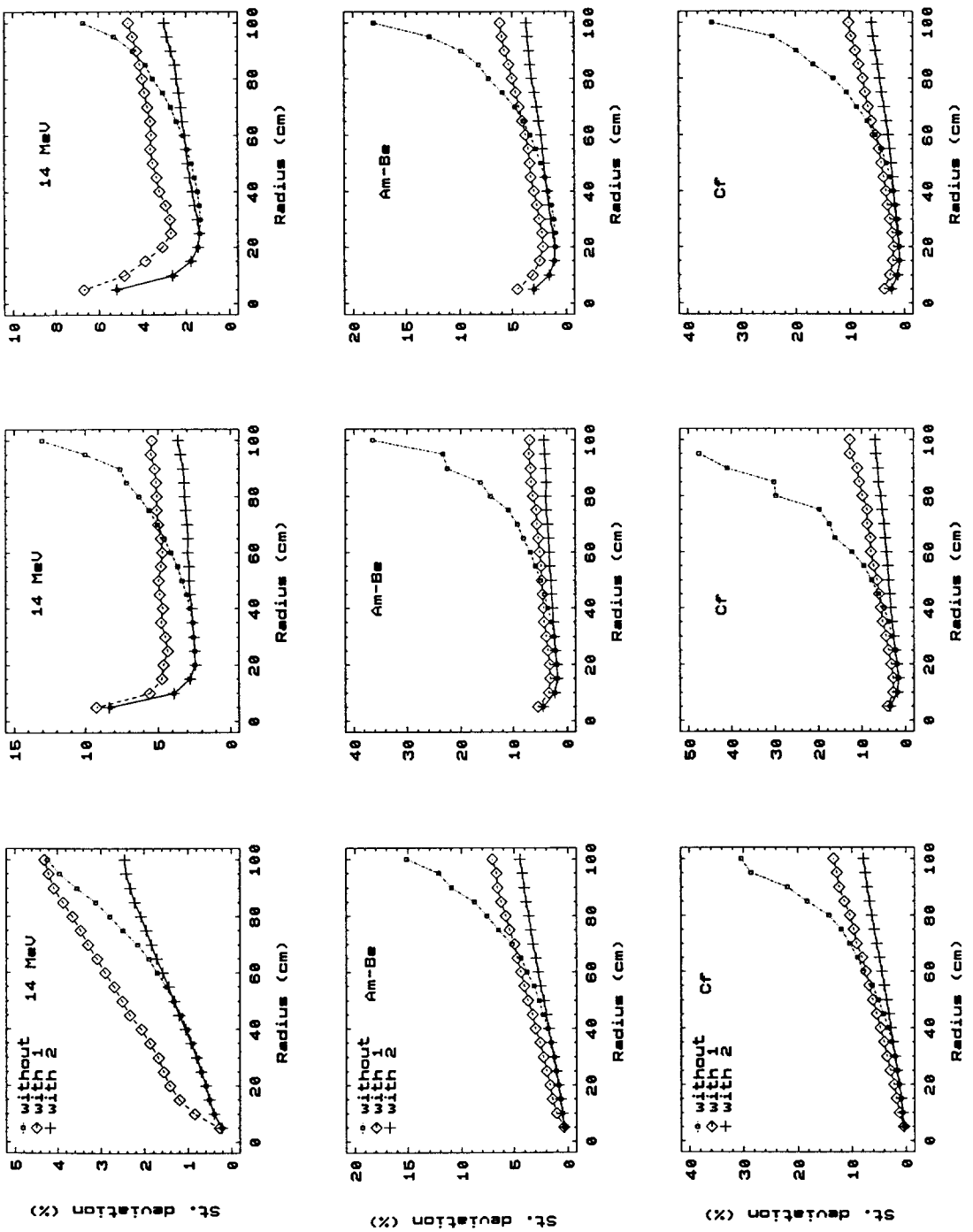

Fig. 6: Relative standard deviation of the flux calculated for shale with and without splitting as a function of the radius

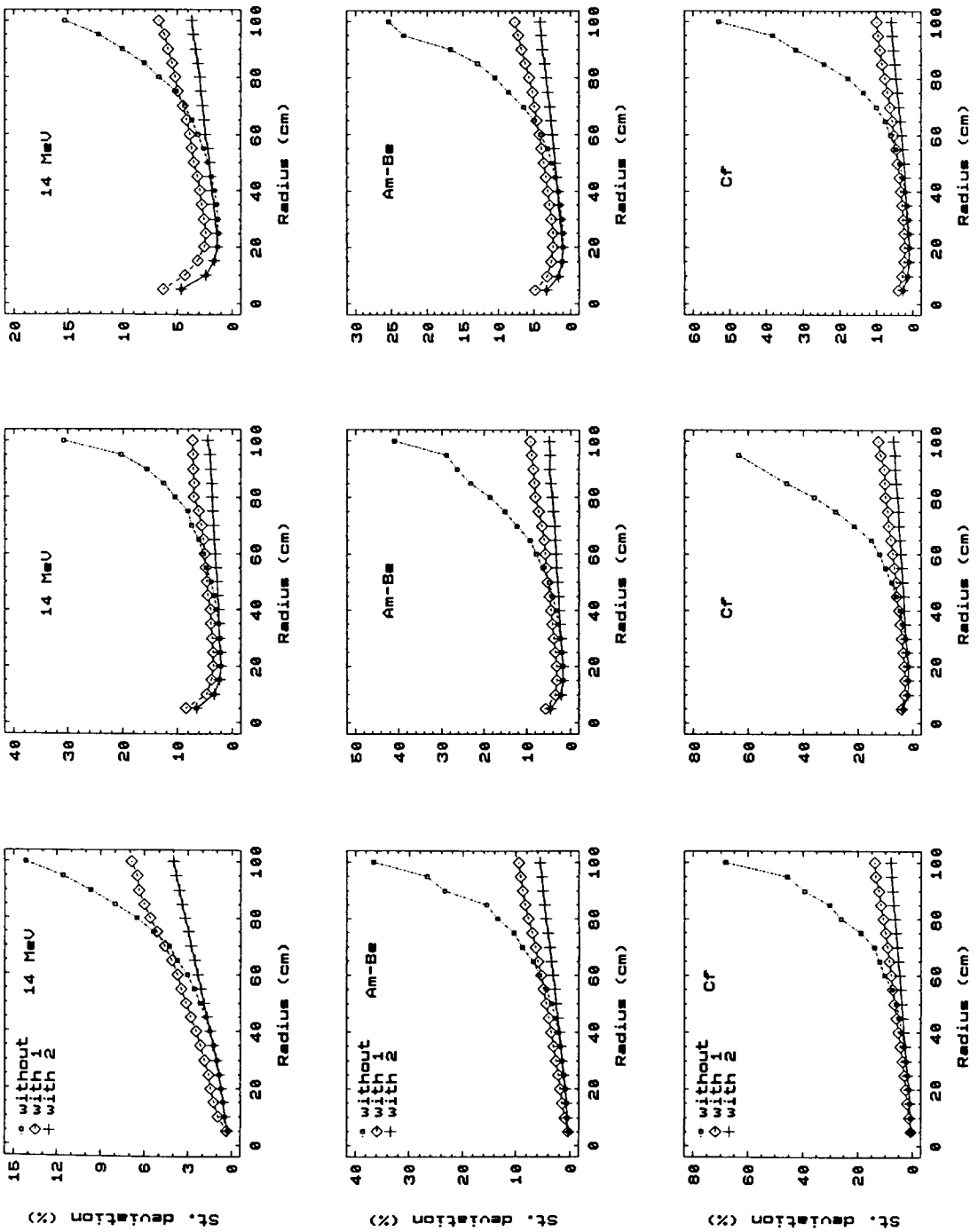

Fig.7: Relative standard deviation of the flux calculated for shale with Gd with and without splitting as a function of the radius

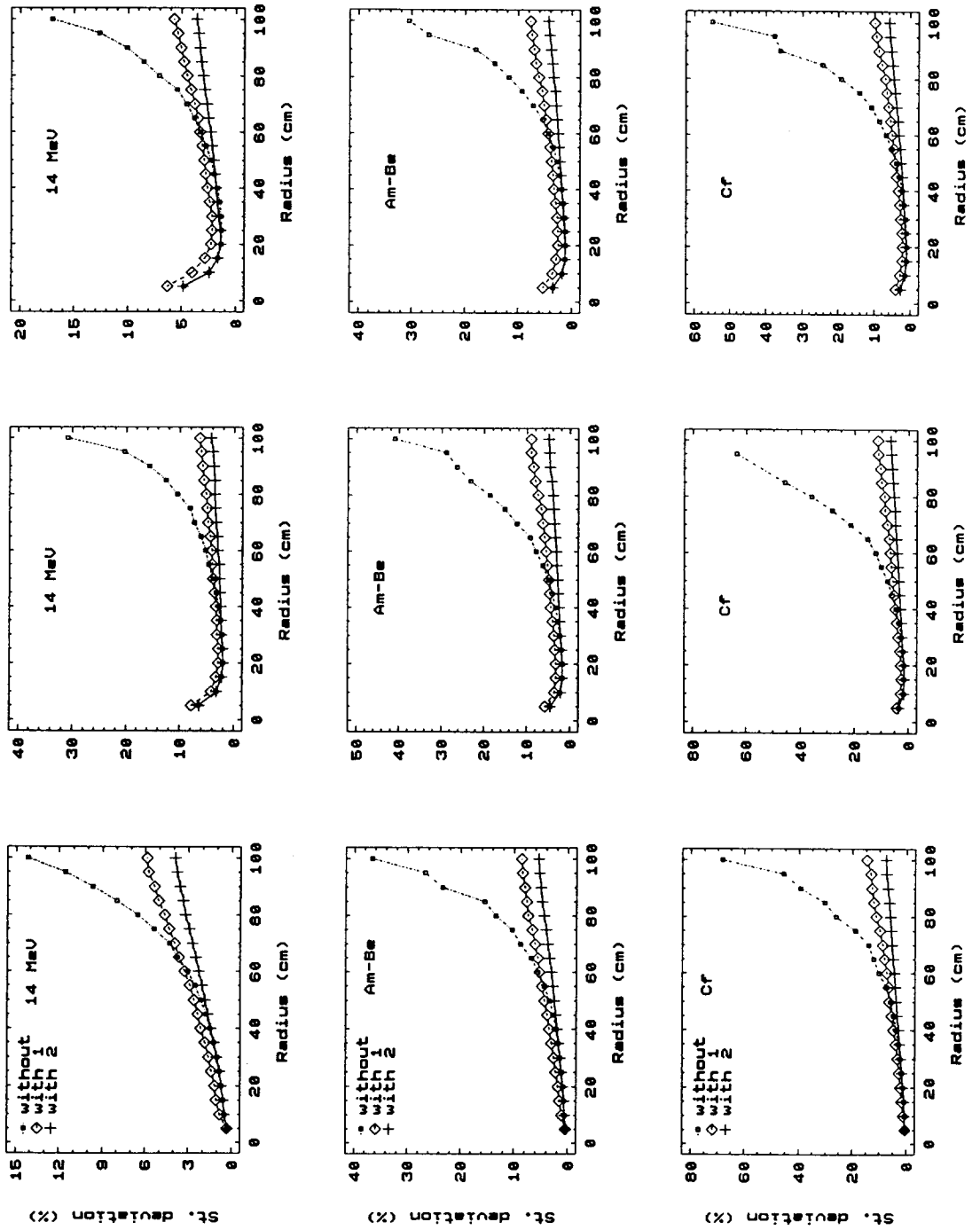

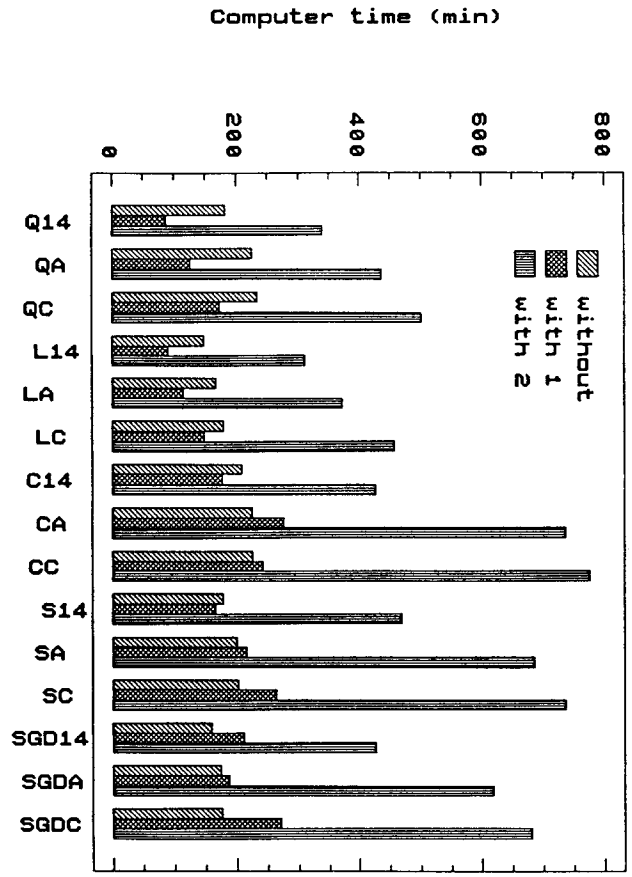

Fig. 8: Computer time for different material and sources
Material: Q - quartz; L - limestone; C - coal; S - shale;
SGD - shale with gadolinium
Neutron source: 14 - 14 MeV, A - ^{241}Am -Be, C - ^{252}Cf

Fig. 9: Fifure of merit for the different computations (a.u. arbitrary unit)

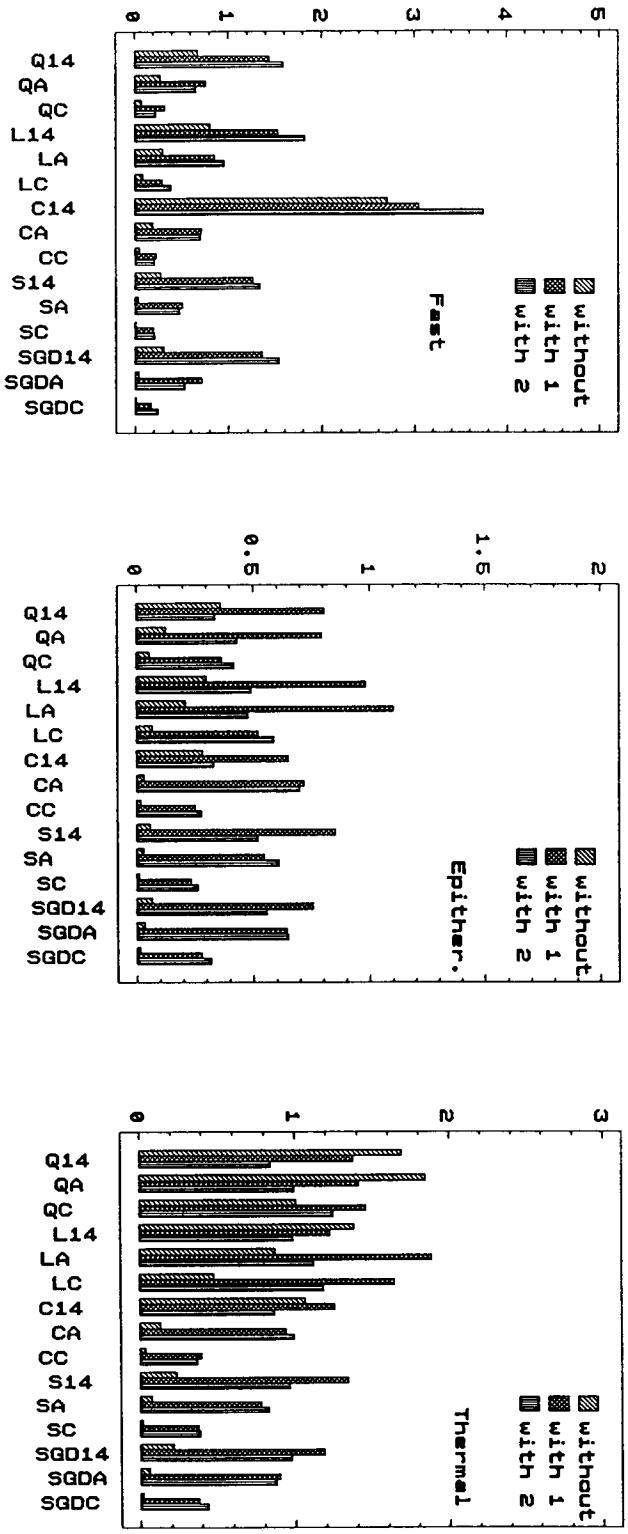

Material: Q - quartz; L - limestone; C - coal; S - shale; SGD - shale with gadolinium

Neutron source: 14 - 14 MeV, A - ^{241}Am -Be, C - ^{252}Cf

Fig. 10: Relative efficiency for different computations

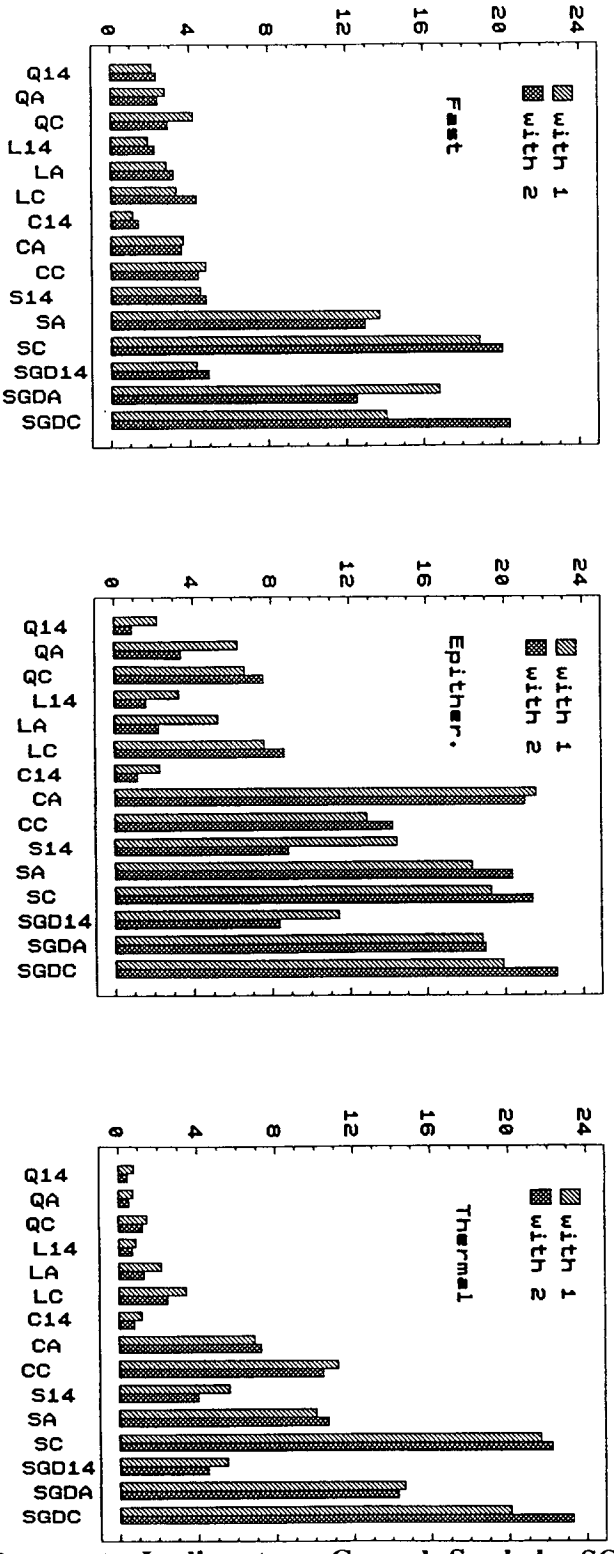

Material: Q - quartz; L - limestone; C - coal; S - shale; SGD - shale with gadolinium
Neutron source: 14 - 14 MeV, A - ^{241}Am -Be, C - ^{252}Cf

Automatic Generation of Biasing Parameters for MORSE Shielding Problems

J. Eduard Hoogenboom

Delft University of Technology, Interfaculty Reactor Institute Delft, The netherlands

Jan Lee Kloosterman

Netherlands Energy Research Foundation

Abstract

To enhance the efficiency of Monte Carlo calculations, several variance and CPU time reduction techniques have to be applied, among which importance biasing, splitting, path length stretching and Russian roulette. One of the major problems in application of these methods is to determine the optimum biasing functions or parameters.
Optimum importance sampling requires the knowledge of the event value, which is the expected detector response of a particle entering a collision, and the point value, which is the expected detector response of a particle emerging from a collision or the source. The calculation of these optimum biasing functions is, in general, as least as demanding as the calculation of the desired detector response. Sometimes the optimum biasing functions are calculated with a one- or two-dimensional discrete ordinates code with simplified geometry.
A derivation will be given how the point value for a certain geometrical zone and energy range is obtained from the space and energy dependent adjoint function, weighted by the firstly emitted particle density for that zone and energy range. These quantities can be obtained from the Monte Carlo calculation itself in a multigroup Monte Carlo code as MORSE. The calculation starts with a number of batches of particles without importance sampling and using "reasonable" parameters of the weight window for splitting and Russian roulette. From these batches an estimate of the point value per region and energy group can be obtained by registration of specific quantities. This needs considerable programming in the MORSE code. The calculated point values of each zone of the geometry can be used to bias the pdf for selection of the energy group of the particles at collision sites (energy biasing at collision sites) or from the source zone for the source energy group (source energy biasing). Moreover, the particle weight after surviving the Russian roulette for each zone and energy range can be taken inversely proportional to the point value of that zone and energy range. To determine the input parameter for exponential biasing of path lengths, the point values as a function of the optical thickness from the source region to the detector are fitted to an exponential function.
The method will be illustrated by application to a shielding problem involving a 1 m thick block of concrete with a 5 cm diameter cylindrical duct, irradiated from one side by reactor neutrons and with a detector positioned at the other end of the duct. Several combinations of variance reduction techniques were studied.
Although this procedure can be fully automated, one should be careful with using estimated point values for certain zones or energy groups from too few particles. In such cases it will be useful to combine zones or energy groups.

1. Introduction

Although the power of present day computers, including workstations and PCs increased dramatically over the last decade, Monte Carlo calculations still suffer from long calculational times to get a sufficiently small statistical error in the calculated quantities. Variance and CPU-time reduction techniques are applied from the early introduction of Monte Carlo, but determination of appropriate biasing parameters or density function still remains a problem, especially to obtain them automatically from calculations, without manual intervention.

Importance functions for biasing distribution functions in the Monte Carlo game can appreciably reduce the variance of a calculation and thereby increase its efficiency. In theory zero-variance schemes can be deviced [1]. This requires the knowledge of the so-called event value, which is the expected detector response of a particle entering a collision, and the so-called point value, which is the expected detector response due to a particle emerging from a collision or the source. Approximate calculation of these functions, e.g. using lower-dimensional deterministic codes in adjoint mode can be of use, but the approximation necessary for describing the geometry may seriously limit their application. Therefore, it would be better if the biasing functions can be obtained from the Monte Carlo calculation itself. This is discussed in this paper as well as the way to obtain biasing parameters from it for splitting, Russian roulette and path length stretching. The method will be demonstrated for a shielding problem solved with the MORSE-SGC/S Monte Carlo code of the SCALE-system.

2. Calculation of biasing parameters from point values

The point value is the expected contribution to a detector response of a particle emerging from the source or from a collision. It can be shown [2] that for source energy biasing and energy biasing at collision sites the point value is an optimum choice, at least if we consider only the reduction in variance. For optimum performance one also has to take into account the computing time. Hence, we use the point value for all energy groups, averaged over a geometrical zone, to bias the energy distribution at a collision or the source as follows. If p_g is the probability that a particle emerging from a collision or the source is emitted in energy group g and $\chi^*_{r,g}$ is the point value for region r and group g, then the energy group is actually selected with probability

$$\hat{p}_g = \frac{p_g \chi^*_{r,g}}{\sum_{g'} p_{g'} \chi^*_{r,g'}} \qquad (1)$$

and the weight of the particle is multiplied by $p_g/\hat{p}_g$.

For application of splitting and Russian roulette a weight window (WTHI, WTLO) must be defined for each region and energy group above which a particle is split in two with both half the weight of the original particle and below which a particle is subject to Russian roulette. In the MORSE-SGC/S code [3] Russian roulette is played as follows. If the particle survives the Russian roulette it gets a weight WTAV. If it does not survive, the history is ended or, equivalently, the particle gets a zero weight. Hence, the probability for surviving the Russian roulette for a particle with stastistical weight WT is WT/WTAV. Following Tang and Hofman [4] the weight after surviving the Russian roulette is chosen as

$$WTAV_{r,g} = \frac{S_g \chi^*_{s,g}}{\hat{S}_g \chi^*_{r,g}} \qquad (2)$$

with $\hat{S}_g$ the biased source energy group distribution according to Eq.(1) and $\chi^*_{s,g}$ the point value for the source region and energy group g. The values of WTHI and WTLO are set a certain factor higher and lower than WTAV, e.g. WTHI=10*WTAV and WTLO=0.1*WTAV.

A path length for determining a new collision site is selected from the probability function

$$p(\eta) = e^{-\eta} \qquad (3)$$

with η the mean free path length. For path length stretching MORSE-SCG/S uses a parameter PATH to bias this distribution as follows

$$\hat{p}(\eta) = (1 - PATH)\, e^{-(1-PATH)\eta} \qquad (4)$$

Here a possible directional dependence of the biasing is disregarded. If PATH=0 the unbiased distribution is retained. Again following Tang and Hoffman [4] the parameter PATH for every region and energy group can be determined from the spatial dependence of the point value function (in fact the event value should be used) in the direction of the detector by fitting it to an exponential function

$$\chi^*_{r,g}(z) = a\, e^{cz} \qquad (5)$$

with z the distance to the detector in mean free path and a and c fit parameters dependent on the radial region and energy group considered. Then PATH is set equal to the fit parameter c.

For path length biasing the event value, being the expected response of a particle entering a collision instead of emerging from a collision is the appropriate biasing function [5]. Although the energy and directional dependence of these function differ because of the sacattering that takes place, a main factor of difference is the non-absorption probability at the collision site. Even for shielding materials like concrete this factor is close to unity for all energies. Therefore, the approximation is made to substitute the point value function for the event value function wherever applicable.

3. Calculation of averaged point values

In this section we will derive an expression for the point value, propriately averaged over an importance region. As shown above, this function will be used, amongst others, to set the parameters for splitting and Russian roulette. In a shielding calculation the particle weight will change at a collision with the non-absorption probability, if no importance biasing is applied. As stated above the non-absorption probability is close to unity and the particle weight will not change much within a region. Therefore, one can expect that the first collision after entering a new region is the most important with regard to splitting or Russian roulette, as the weight window may be very different compared to the previous region where the particle was tested for splitting or Russian roulette. So it makes sense to weight the point value for a certain zone (and group) by the firstly emitted particle density when averaging over a region.

The point value function $\chi^*(r)$ as a function of the phase space variable r is given by

the equation

$$\chi^*(\tau) = h(\tau) + \int_\Gamma \chi^*(\tau')\, L(\tau \rightarrow \tau')\, d\tau' \qquad (6)$$

with $h(\tau)$ the detector response function for the emerging particle density and $L(\tau \rightarrow \tau')$ the transport kernel for transport of the particle from τ to τ'. Integration is over the whole phase space Γ. This equation is adjoint to the equation for the emerging particle density χ

$$\chi(\tau) = S(\tau) + \int_\Gamma \chi(\tau')\, L(\tau' \rightarrow \tau)\, d\tau' \qquad (7)$$

with S the particle source density. The detector response is given by

$$R = \int_\Gamma h(\tau)\chi(\tau)\, d\tau = \int_\Gamma S(\tau)\chi^*(\tau)\, d\tau \qquad (8)$$

We now define a subspace Γ_d which involves the spatial volume of a geometric region r, the energy range of a group g and the whole angular space 4π. Multiplying Eq.(6) by $\chi(\tau)$ and integrating over Γ_d yields

$$\int_{\Gamma_d} \chi(\tau)\chi^*(\tau)d\tau = \int_{\Gamma_d} \chi(\tau)h(\tau)d\tau + \int_\Gamma \left[\int_{\Gamma_d} \chi(\tau) L(\tau \rightarrow \tau')d\tau \right] \chi^*(\tau')\, d\tau' \qquad (9)$$

where the integration order in the last term has been reversed. The term between the square brackets is the number of particles emerging from a collision at τ' per unit phase space, which were emitted previously in Γ_d. This will be referred to by $[\chi(\tau')]_{\Gamma d}$. The second term on the RHS of Eq.(9) is now split into an integration over Γ_d and over the remaining space Γ_n. Then Eq.(9) can be rewritten as

$$\int_{\Gamma_d} \{ \chi(\tau) - [\chi(\tau)]_{\Gamma_d} \}\, \chi^*(\tau)d\tau = \int_{\Gamma_d} \chi(\tau)h(\tau)d\tau + \int_{\Gamma_n} [\chi(\tau)]_{\Gamma_d} \chi^*(\tau)\, d\tau \qquad (10)$$

We can now define the average point value $\chi^*_{r,g}(\tau)$ for region r and energy group g as

$$\chi^*_{r,g} = \frac{\int_{\Gamma_d} \{ \chi(\tau) - [\chi(\tau)]_{\Gamma_d} \}\, \chi^*(\tau)d\tau}{\int_{\Gamma_d} \{ \chi(\tau) - [\chi(\tau)]_{\Gamma_d} \}\, d\tau} \qquad (11)$$

In this definition the average point value is weighted by the density of particles emitted in that region and group minus the density of particles emitted previously in that region and group. We call this the density of particles firstly emitted in that region and group. Particles contributing to this density may have emerged from a collision in region r and group g before, but not directly befor their last emission in that region and group. In words Eq.(11) can be read as

$$\chi^*_{r,g} = \frac{\text{Total detector score of firstly emitted particles in (r,g)}}{\text{Total weight of firstly emitted particles in (r,g)}} \qquad (12)$$

where the score of a particle includes the contribution of its progeny.

To implement Eq.(12) in the MORSE-SCG/S code requires additional bookkeeping. This prevents the use of the supergrouping facility. The weight of each firstly emitted particle is added to an array WEIGHT, which finally contains the sum of weights of such particles per region and group. Particles which emerge from the source or a collision in region r and group g, enter another region and/or group, scatter to region r and group g again and emerge from a collision there, must be counted twice. However, its detector contribution must also be counted twice. Therefore, an array NUMBER is introduced which registers the number of times a particle contributes this way. Each time a particle or one of its progenies scores in the detector, its score is multiplied by the contents of the NUMBER array and added to the SCORE array, which contains the sum of all scores per region and group. Dividing the elements of the SCORE array by the corresponding elements of the WEIGHT array gives the estimated point value of each region and group. If the score for a certain region and group is zero or obtained from very few particles, energy groups can be combined to get a better estimate of the point value, which results in biasing parameters being equal for all the energy groups taken together.

4. Practical application

The method is illustrated by application to a shielding problem with geometry shown in Fig. 1. It consists of a cylindrical duct in a large concrete block of 100 cm length. The duct of 5 cm inner radius has a 1 cm thick iron liner. The geometry is irradiated from one side by neutrons from a reactor. This is a simplified representation of a shielding experiment performed at the Technical University of Budapest [6,7]. As this paper concerns the effect of the method of variance reduction no attempt has been made here to reproduce the measured quantities as good as possible. The detector at the end of the duct registers the neutron flux in three energy ranges, for fast neutrons (E> 1 MeV), for intermediate neutrons (0.4 eV <E< 1 MeV) and for thermal neutrons (E< 0.4 eV) and the total flux. A boundary crossing estimator was used. The calculation was actually done using 25 energy groups,

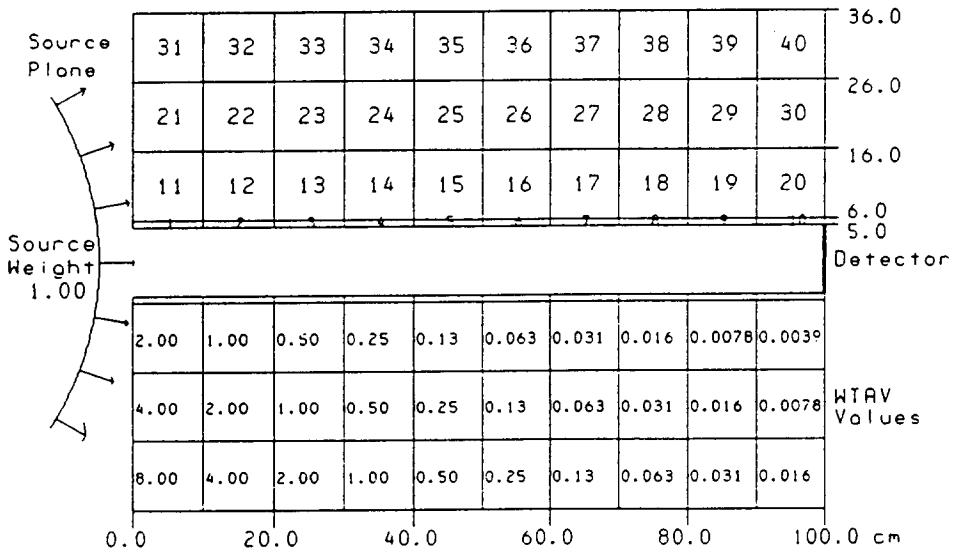

Fig. 1. Cross section of the geometry of the shielding problem with indication of region numbers and standard WTAV parameters

3 in the fast range, 16 in the intermediate range and 6 in the thermal range. The source energy and directional distribution were obtained from a DOT3.5 [8] calculation of the reactor core and converted to the format required by MORSE-SCG/S using the DOMINO code [9].

The importance regions, each having a set of biasing parameters for energy biasing, path length stretching, splitting and Russian roulette, are chosen as concentric annuli. One in the iron liner and three in the concrete. In axial directions 10 equidistant intervals have been chosen. A first calculation was done without energy biasing at collision sites or source energy biasing. The weight WTAV after surviving Russian roulette was set at values increasing a factor 2 for each region in radial direction and decreasing a factor 2 for each region in axial direction as shown in Fig. 1. The values of WTHI and WTLO were chosen a factor 10 larger and smaller than WTAV, respectively. Other weight windows were also tried.

Table I. Flux calculations with different types of biasing

WTAV	PATH	Typification	Fast flux	Interm. flux	Therm. flux	Total flux
input	no	no EB	2.9 (35)	4.3 (17)	2.3 (26)	9.5 (15)
	0.5	no EB	3.6 (30)	4.4 (17)	2.2 (26)	10.3 (13)
	0.5	6x CPU	2.6 (12)	5.0 (8)	2.5 (10)	10.2 (6)
autom	no	no EB	2.1 (14)	5.7 (16)	3.4 (30)	11.2 (13)
autom	autom	autom EB	2.3 (15)	5.3 (14)	1.7 (19)	9.3 (10)

A selection of results is shown in Table I. In the first calculation no path length stretching was applied. In the second calculation path length stretching was applied with the parameter PATH set rather arbitrary to 0.5 for all regions. For comparison the same calculation was done with a six times larger CPU time (1200 min CPU time on a VAX 3100 M76 workstation) to see the convergence of the results. All other calculations were set at 200 min CPU time, so that calculational efficiencies can be compared and not only reduction of variances. From the second calculation the point values were determined as described in Sect. 3 and were used in the next calculations to see their effect when used for setting the weight window, the path length stretching parameter and the effect of biasing the energy distributions.

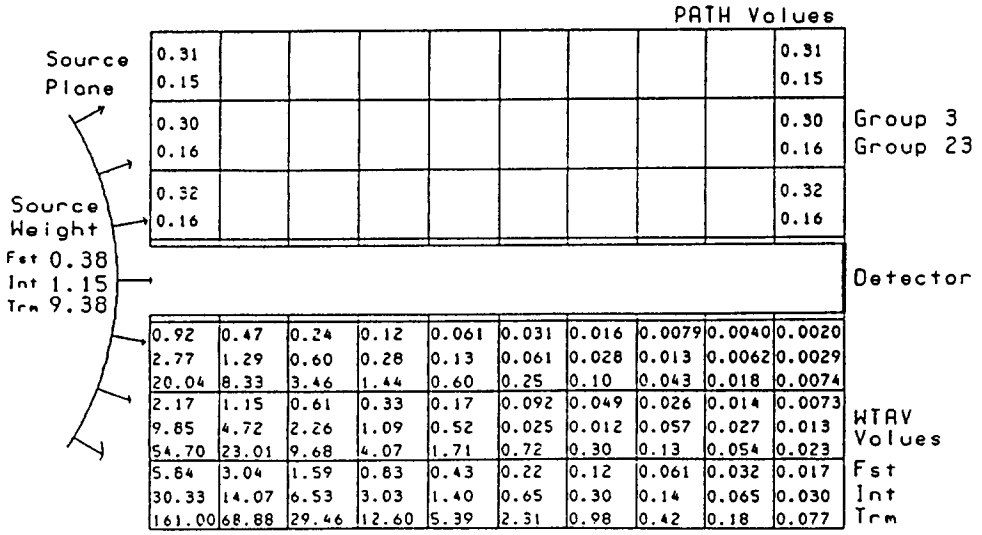

Fig. 2. Indication of biasing parameters obtained from importance functions

Fig. 2 shows the WTAV parameters according to Eq.(2) for the various regions and the three energy ranges defined above. When applied to each of the 25 energy groups the statistical accuracy may introduce undesired behaviour of the weight window going from one group to another. Therefore, only a distinction between the fast, intermediate and thermal energy range was made for the determination of WTAV. The results show a considerable difference with the original, rather arbitrary, input settings. This is especially true for the regions far away from the detector. There is also a considerable difference with regard to the different energy ranges. These weight windows were applied in the last calculations mentioned in Table I. Using only the new weight windows an appreciable improvement in efficiency of the calculation was gained, except for the thermal flux.

In the last calculation also the energy biasing at collision sites and source energy biasing was applied as well as automatic determination of the path length stretching parameter PATH. To determine the latter the point values obtained from the second calculation were fitted to an exponential as a function of the distance in mean free path from the axial centre of a region to the axial plane of the detector. This was done for each energy group and each annulus of importance regions. An example is shown in Fig. 3 for energy group 3 (1.0-2.23 MeV) for the three radial importance annuli in the concrete. This results in one value of PATH for each annulus and each energy group. The values of PATH for energy groups 3 and 23 (0.025-0.05 eV) are indicated in the upper half of Fig. 2. Also shown in this figure are the statistical weights assigned to source particles for the three broad energy ranges. The high thermal value indicates that thermal neutrons are about 10 times less frequently sampled than in a calculation without source energy biasing. The last calculation of Table I shows that energy biasing and path length stretching are particularly effective for the calculation of the thermal flux.

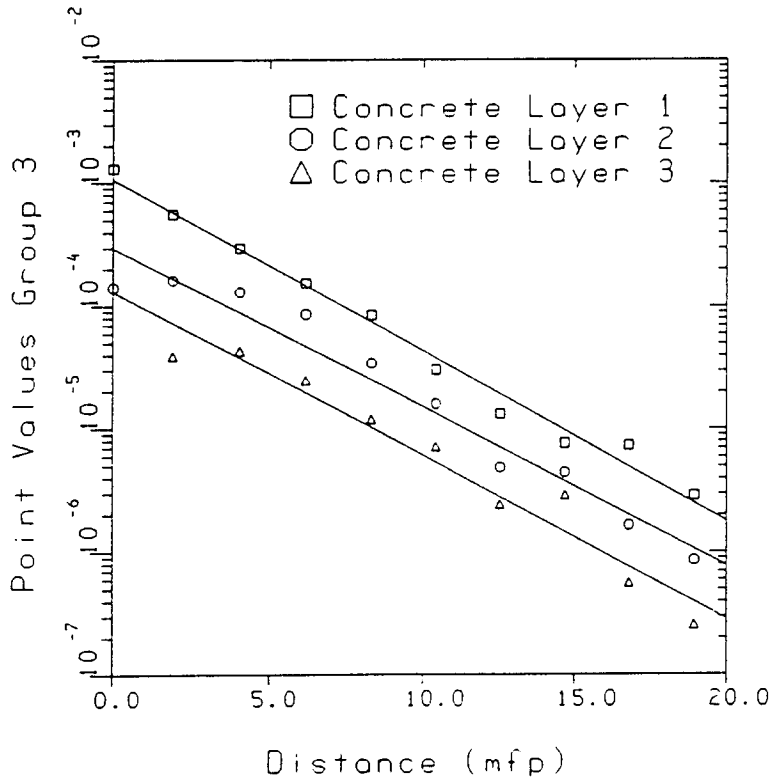

Fig. 3. Point values for energy group 3 (1-2.23 MeV) as a function of the axial optical shield thickness to the detector plane

5. Discussion and conclusion

This paper shows the possibility of deriving importance functions for biasing energy distributions and determination of parameters for path length stretching, splitting and Russian Roulette from the Monte Carlo calculation itself. Then no further approximations to the geometry of the system under consideration are necessary. From a numerical example it turns out that the efficiency of the use of splitting and Russian roulette can be improved considerably. This also applies to energy biasing if the thermal energy range is considered. However, as some of the standard deviations are rather large, one should be careful in interpreting the reliability of these standard deviations.

Considerable programming had to be added to a number of subroutines of the MORSE-SCG/S code. This allows an automatic generation of biasing parameters after processing a limited number of particle batches. These biasing parameters can be used in the batches to follow for improved efficiency of the Monte Carlo calculation. It seems possible that during the whole calculation the estimated biasing parameters can be regularly updated when more accurate estimations of the point value functions become available. This may also allow to differentiate more with respect to energy, whereas in the example above a number of energy groups were taken together to broader energy ranges for which weight window parameters were obtained in order to have reliable estimates of these parameters. It also seems feasible to estimate both the point value and the event value from the Monte Carlo calculation. Then the parameters for splitting, Russian roulette and path length stretching can be obtained from the event values, which are more appropriate for this case.

It should be noted that it seems hard to extend the programming of this method to any arbitrary geometry problem. Therefore some adaptions will have to be made by a user when applying to basically different geometrical problems. Nonetheless this effort seems to be worthwile. Although the particular programming is specific for the MORSE-SCG/S code, the method can, of course, be applied to other general purpose Monte Carlo codes.

References

[1] J.E. Hoogenboom, *Nucl. Sci. Eng.*, **70**, 210 (1979).

[2] R.R. Coveyou et al., *Nucl. Sci. Eng.*, **27**, 219-234 (1967).

[3] J.T. West et al., MORSE-SCG/S for the SCALE System. Oak Ridge National Laboratory, Oak Ridge Tennessee, USA. Report NUREG/CR-0200 (1981).

[4] J.S. Tang and T.J. Hoffman, *Nucl. Sci. Eng.*, **99**, 329-342 (1988).

[5] J.S. Tang et al., *Nucl. Sci. Eng.*, **64**, 837-842 (1977).

[6] J.L. Kloosterman, On Gamma Ray Shielding and Neutron Streaming Through Ducts. PhD Thesis, Delft University of Technology, Delft, The Netherlands. ISBN 90-73861-07-1 (1992).

[7] J.L. Kloosterman, J.E. Hoogenboom and E.M. Zsolnay, Experiments and Calculations on Neutron Streaming Through Bent Ducts, *J. Nucl. Sci. Techn.* (1993, in press).

[8] F.R. Mynatt et al.,The DOT III Two-Dimensional Discrete Ordinates Transport Code. Oak Ridge National Laboratory, Oak Ridge, Tennessee, USA. Report ORNL-TM-4280 (1973).

[9] M.B. Emmet et al., DOMINO, a General Purpose Code for Coupling Discrete Ordinates and Monte Carlo Radiation Transport Calculations. Oak Ridge National Laboratory, Oak Ridge, Tennessee, USA. Report ORNL-TM-4853 (1973).

VARIANCE REDUCTION UNIQUE TO COUPLED ELECTRON/PHOTON MONTE CARLO TRANSPORT*

J. A. Halbleib, R. P. Kensek & G. D. Valdez
Sandia National Laboratories

ABSTRACT

The disparity between the mean free paths of electrons and photons leads to unique variance-reduction procedures for the coupled transport at intermediate energies. It is electrons that ultimately deposit charge and energy and yet electron transport is much more expensive than photon transport. The objective, then, is to control the variance of the energy, angular, and spatially dependent populations of the two species within the generation and transport of the cascade in such a way that all contributions to electron flux in the vicinity of the detector are represented to a degree commensurate with their importance. However, in β/γ transport, biasing techniques are often unique to one or the other of the species.

* This work was supported by the U.S. Department of Energy under Contract No. DE-AC04-76DP00789

1. Introduction

There are certain assumptions that define the approach to variance reduction in time-independent coupled electron (positron)/photon Monte Carlo transport at intermediate energies. It is first assumed that electron transport is important to the application. Otherwise, there are many photon-only or neutral particle codes that could solve the problem more efficiently. The second assumption of this work is that it is the electron transport, not the photon transport, that is expensive. The rare exceptions to this assumption will not be considered here. Photon histories are usually terminated by absorption, leakage, or falling below cutoff after no more than a few interactions. Electrons, on the other hand, will often undergo many orders of magnitude, more interactions before suffering the same fate. Even when non-absorption transport is used for electrons, transport of the latter usually dominates the run time.

The guiding principle of variance reduction in electron/photon transport becomes the maximization of electron transport that can contribute to the effect of interest - either directly or through radiation production, and the simultaneous minimization of all other electron transport. Even though electron/photon codes put less emphasis on explicit estimation of particle fluxes than neutral particle codes, our goal is to implicitly maximize the accuracy and precision of the electron flux where it counts the most, while minimizing it elsewhere.

Two quite different situations present themselves. First there are the simulations dominated by the direct effects of electron sources. If primary electrons (source elctrons) dominate the response, there are not a lot of options. However, for photon sources and for effects beyond the range of primary electrons, there are a number of variance reduction procedures that can be brought to bear.

Moreover, because cross sections are so much larger for charged particles than for photons, and because the former lose their energy almost continuously, biasing techniques are often unique to one or the other of the species. A method based on particle mean free path, such as forcing, stretching, or last-flight estimation may be fine for photons, but is useless in the condensed-history simulation of electron transport. On the other hand, testing for trapping can be very useful for charged particles, with their well-defined ranges, but entirely inappropriate for neutrals. Finally, uncorrelated secondary production (a form of event splitting) can be quite useful for their species, but cannot be used when simulating a highly correlated quantity such as a pulse-height distribution.

Because we are primarily users and not Monte Carlo theorists, we do not carry out much formal research in variance reduction. Moreover, because the important function is never really known, and because overbiasing can lead to misleading results, we generally take the approach that *less is better* when it comes to variance reduction. We tend to confine ourselves to the simplest techniques until the application demands something more sophisticated. We often wait until we cannot solve the problem any other way before invoking complex modifications to reduce variance. Consequently, we do not or cannot always quantify the increased efficiency.

In the following Section, we will discuss a variety of variance reduction features employed in the ITS (Integrated TIGER Series) code system, [2] - [4]. Most are available in the currently released version (Version 3.0). In Section 3, we will discuss how these and more sophisticated procedures can be employed in combination to address a particularly difficult generic application. Finally, in Section 4, results obtained from a version of ITS that has been extensively modified to reduce the variance in a complex three-dimensional application will be verified against linac experiments.

2. Individual Features

For the purposes of this work, variance reduction refers to the attainment of the same statistical uncertainty in a lesser amount of run time. As such, it includes more efficient coding, as well as successful biasing. From a practical, if not theoretically rigorous, point of view, biasing in Monte Carlo can generally be described as the distortion of the natural analog to achieve variance reduction in certain desired output quantities. Except where absolutely necessary, biasing should be used sparingly. In any case, it should be used with great care. Reckless use of biasing can lead to results that are erratic and/or easily subject to misinterpretation. Except where stated otherwise, the following biasing features are easily accessed in ITS via the standard execution input described in Reference [2], where the features are described in more detail. Other electron/photon codes are likely to have similar features.

2.1. Trapped electrons

In problems where only electrons that cross certain boundaries are important, histories of electrons that cannot reach those boundaries can be terminated by a procedure referred to as electron trapping. In ITS the option becomes effective when an electron with an energy below a specified trapping energy is trapped, that is, does not have enough energy to escape from a zone. When this occurs, its history is immediately terminated via local deposition of its charge and energy. This option is commonly used when one is primarily interested in the accurate transport of those electrons escaping from all or some portion of the problem geometry. Great care should be taken in employing this option where production of secondaries (e.g., bremsstrahlung) may be important because histories are terminated in this fashion. It is important to note that the contribution to leakage from the zone of any untrapped electrons with energies above the zone-dependent cutoff is much more rigorous than that of untrapped electrons with energies below the zone-dependent cutoff because a much cruder form of transport is employed for the latter.

2.2. Scaling of bremsstrahlung production

In ITS the user can artificially increase the bremsstrahlung production to improve that statistical accuracy of bremsstrahlung flux without increasing the number of primary electron histories, which would be much more time consuming. The number of primary electron histories needs only to be large enough to ensure an implicitly accurate electron flux. This is accomplished by scaling up the production cross sections by a specified amount. Simultaneous scaling of the cross section for electron impact ionization probability is also desirable, in order that any subsequent fluorescent photons will have comparable weights. This option is used primarily for the prediction of thick-target bremsstrahlung production (e.g., prediction of the X-ray environment produced by an electron source). Consequently, a Russian Roulette (RR) procedure is employed by default to reduce the number of secondary electrons generated from the interaction of this artificially high bremsstrahlung population to the naturally occurring number. Although this default feature is very effective for predicting **external bremsstrahlung**, it can lead to statistically poor results for energy and charge deposition and electron flux in regions of the problem where these quantities are determined by the transport and secondary electron production of the bremsstrahlung radiation. In such cases, ITS has a feature for overriding the default to ensure that a sufficiently large fraction of the secondary electrons survive RR.

2.3. Forced photon collisions or path length stretching

In the TIGER and CYLTRAN codes of the ITS system, a feature is avalilable for forcing a selected fraction of photons either entering a given zone or leaving a collision site within the zone to interact in that zone. The feature is useful for forcing photons to interact in certain regions where their natural interaction probability is so small as to make it difficult to obtain statistically significant results, or for preventing excessive removal of photons in regions where their natural interaction probability is high. In the ACCEPT codes, the user has the ability to decrease (or increase) the photon interaction probability in a given zone relative to its natural value by a different method from that used in the TIGER and CYLTRAN codes. The interaction cross section is scaled so as to stretch (or shorten) the mean free path. With either the stretching or forcing features, care must again be taken not to overbias.

2.4. Zone-dependent electron cutoff energies

The user has the option in ITS of varying the electron cutoff energy from zone to zone. When the energy of an electron in a given zone falls below the cutoff for that zone, a check is first made to see if it is trapped in the sense of Section 2.1. If so, the history is terminated via on-the-spot deposition of charge and energy. Otherwise, a final calculation of non-local energy and charge deposition is made (see Reference [2] for M-Codes exception), based on the residual range of electron. It is important to remember that there is no production of secondary particles (e.g., bremsstrahlung) by electrons with energies below the zone-dependent cutoff, nor is there any contribution to electron flux and electron escape by such electrons. This option has proven useful in problems that invlove the generation of bremsstrahlung in some zones and deposition caused by that bremsstrahlung in other zones. A relatively high cutoff may be used in the converter zones, since low-energy electrons are relatively inefficient for producing bremsstrahlung. On the other hand, in the zones where deposition is dominated by bremsstrahlung transport, the user may be interested in the details of the deposition from the low-energy bremsstrahlung-produced secondaries (e.g., interface effects), or he/she may not want electron transport in those zones at all (bulk deposition).

2.5. Last flight estimator for photon escape

For a geometry that is highly absorbent to secondary photons generated in the transport process, scoring as leakage photons only those secondary photons that actually escape the geometry while being tracked can be quite inefficient. This problem is remedied in ITS by using instead a last-flight estimator for photon leakage. With this estimator, a score is obtained **ech time a phton emerges from a collision**. The score is simply the emergent photon weight times the probability of escape without further interaction. This feature is automatically activated whenever the user requests photon escape distributions as output.

2.6. Scaling of secondary electron production

Just as scaled bremsstrahlung production can be invoked once there is an implicitly accurate electron flux (see Section 2.2.), scaled production of electrons by photons may be invoked in a region where there is an implicitly accurate photon flux. In this way, an arbitrarily high density of secondary electrons can be generated in some region of interest without increasing the number of photon histories generating them. This feature has been employed as a modification of ITS, [5], but is not available in the publicly released system.

2.7. Angle biasing of photon production and scattering

The angular distributions of photons emerging from collisions can be biased to preferred directions. This is a common feature of neutral particle codes and provides a powerful method of estimating point fluxes when properly combined with features such as the last-flight estimator (often considered an intrinsic component of such estimators). This feature has been employed as a modification of ITS, [6], but is not avalaible in the publicly released system because explicit flux estimation is used much less frequently in electron/photon than in neutral particle Monte Carlo.

2.8. Automatic subzoning

Automatic subzoning refers to that feature whereby a user may specify that a given input zone is to be automatically susdivided into specified subzones for the purpose of obtaining the spatial variation of energy and charge deposition, electron flux, and photon flux within the given input zone. This powerful feature has the potential for substantially reducing:

a) user time for generating the input file,

b) machine memory requirements,

c) and machine CPU time.

Without this feature, the user would have to describe each subzone as a separate input zone. For example, a 10x10x10 subzoning of a rectangular parallepiped with the ACCEPT codes would require at least 1000 lines of input without automatic subzoning. Moreover, because the subzones are defined in terms of equal increments of the intrinsic co-ordinates of the input zone, there is no need for explicit storage of the boundaries of subzones, and very little memory is required to locate the subzone containing an arbitrary point within the input zone. Finally and perhaps most important, because the internal subzone boundaries are not material discontinuities, they can be ignored by the CPU-intensive tracking logic. Automatic subzoning was always an input feature of the TIGER codes. In Version 3.0 of ITS, full automatic subzoning has been implemented in the CYLTRAN codes, extending it to three dimensions with the addition of azimuthal subzoning. Moreover, the ACCEPT codes now feature the full three-dimensional automatic subzoning of input zones consisting of a single body of type RCC, RPP, BOX, or SPH. There are, however, certain limitations on the effectiveness of automatic subzoning, as currently implemented in ITS. These limitations are discussed in Appendix L of Reference [2].

2.9. Efficient termination of electron histories

When appropriate, the two most efficient methods of terminating electron histories are RR and trapping. Efficient coding will then give priority to testing for these features. The primary motivation for the Version 3.0 upgrade of ITS was to reduce the algorithms for the production and transport of electrons in a way that would reflect this priority. RR of secondary electrons produced by photons are given top priority, and the RR decision based on a single sampling is enforced for the entire photon history. Next, all electrons are immediately tested for trapping; if trapped, they are terminated via local charge and energy deposition. Only after survival of RR and trapping are computations relevant to that survival initiated. Carefull and systematic incorporation of this logic resulted in run-time reductions of up to 40% in test problems.

2.10. Improved Combinatorial Geometry (CG) logic

The three dimensional CG logic of the ACCEPT codes was originally taken from an older version of the MORSE code, [7]. Over the years since the original implementation, inaccuracies, inconsistencies and inefficiencies have been identified. Diagnoses of these problems were hampered by the fact that there was vitually no commenting of the algorithms. In Version 3.0, the CG routines have been extensively revised and heavily commented. In particular, the core analytic geometry routine (Subroutine CG) was completely rewritten. Not only is the software now much more robust (e.g., fewer particles lost and allowance for coicident body boundaries) and accessible to the user, but we routinely achived 10-15% reductions in run time during testing.

2.11. Photon-only transport

Ordinarily, if electron transport effects are unimportant, neutral particle Monte Carlo codes should be more efficient than electron/photon Monte Carlo. Nevertheless, the convenience of using familiar software may outweigh the higher efficiency of unfamiliar software. With the addition of an option for photon-only transport, the ITS system now includes a very fast and sophisticated set of photon transport codes. This option is much faster than coupled transport (up to an order of magnitude for test problems). It can be used in applications involving source photons for which:

1. the finite ranges of the secondary electrons are unimportant;

2. radiation by those electrons is unimportant.

Photon-only transport should also be useful for parameter studies where approximate results are acceptable and the above conditions are not rigorously satisfied, or for low-energy photon sources where the ITS codes, because they are continuous-energy codes, have the advantage of highly accurate simulation of line radiation.

3. The Combined X-Ray Effects Problem

There are many examples of scientific and industrial applications involving responses to space, nuclear and accelerator radiations that have benefited from the variance reduction methods described in Section 2. However, an important class of problems cannot be adequately solved with these methods as currently implemented in ITS.

The combined X-ray effects problem is illustrated schematically in Figure 1. On the left is the X-ray source (converter) region and on the right is the X-ray response (detector) region. An electron source has a fraction of its energy converted into X-ray energy in the X-ray source region. In the response region, some object responds to the portion of that X-ray energy to which it is exposed.

It is assumed that none of the primary electrons can escape from the source region to reach the response region. Otherwise, the respose would almost always be dominated by those primaries. It is also assumed that higher order bremsstrahlung produced in the response region is negligible, thus excluding electron-initiated radiation showers and effectively limiting the maximum energy of the electron source. One can still think of many examples of this problem. Exposures to X-ray machines are the most obvious, but any electron source will produce wanted or unwanted radiation effects well beyond the ranges of the primary electrons that must be considered.

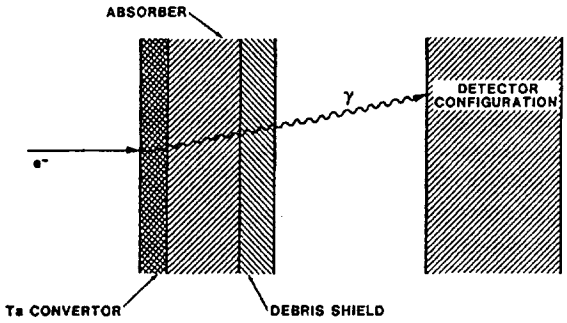

Figure 1. Schematic of the combined X-ray effects problem

How do we solve the combined radiation problem in general?

In order to accurately model such experiments, in general, full Monte Carlo transport of electrons and photons must be carried out in **both** the source and response regions. However, such calculations are very expensive, and, in some cases, may not be possible, even using the variance reduction techniques of Section 2.

Under suitable conditions, an acceptable equilibrium dose in the resonse region can be approximated by the integral over photon energy of the product of the local X-ray flux and a mass energy absorption coefficient of some sort. For such applications, a very powerful and efficient method has been developed, [8] - [9], and implemented in ITS (not publicly released system) that makes use of the scaled bremsstrahlung production and last-flight estimator of Section 2. The full Monte Carlo transport is only carried out for the production and transport of X-rays in the source region. Each time a photon emerges from a collision in the source region travelling in the direction of the response region, the last-flight estimator is employed as usual to adjust its weight by the probability of escaping the source region without further interaction. It is then projected across the separation distance between source and response regions, if any, and its contribution to the uncollided equilibrium response is calculated. This is all accomplished within the Monte Carlo code itself, so that any coupling between the spatial, energy and angular distributions of the X-rays emitted from the source region are rigorously accounted for.

The speed, simplicity, and flexibility of the method make it a powerful tool for predicting the uncollided response, which can be quite accurate under the appropriate circumstances. However, the approximation breaks down when:

a) elements of the response region are so thin that electron equilibrium cannot be established;

b) photon build-up within the response region itself cannot be neglected;

c) radiation loss of secondary electrons cannot be neglected;

d) an appropriate definition of the energy absorption is not possible;

e) or, photoemission from the source region cannot be neglected.

However useful the method may be, clearly it does not represent a very general solution to the combined X-ray effect problem.

When this uncollided response method fails, one has no choice but to carry out Monte Carlo transport in the response region as well. However, it is difficult to include within a single Monte Carlo simulation the generation, transport, and subsequent response to the X-rays without employing more advanced variance reduction than is routinely available from the techniques of Section 2.

The problem with many of the features in Section 2. is that they are global in their effect. They operate in the same way throughout the problem geometry, whereas we are faced with opposing requirements in the source and response regions. While it is very efficient to enhance X-ray production in the source region, it is inefficient to do so in the response region where the response is dominated by transport of lower energy secondary electrons. While it is efficient to RR kill the artificially high population of secondary electrons produced by the enhanced X-ray population in the source region, it is precisely those electrons that we must transport in the response region. Conversely, while it is efficient to terminate the transport of trapped electrons in the response region, doing so for the primary electrons in the source region would preclude their production of X-rays.

A relatively general scheme, called the full transport (FT) method, [8] - [9], was developed for the ITS system, which has been successfully applied to the simulation of a variety of combined X-ray effects problems. It involves a combination of code modifications with careful selection of certain standard input parameters. The major components of the FT method are:

a) modifications of the bremsstrahlung scaling, electron trapping, and electron RR features to make them spatially dependent, and choices of appropriate values for the source and response regions;

b) further mofifications of the coding so as to exclude from RR those electrons generated in the source region that have sufficient energy to be photoemitted from the source region into the response region;

c) choices of spatially dependent photon forcing or stretching parameters to optimize photon attenuation and interaction;

d) choices of spatially dependent electron cutoff energies appropriate to the source (high) and response (low) regions.

4. Linac Verification

In this Section the FT of Section 3 and an extended version of that method required for highly attenuated absorption measurements are verified against linac experiments.

Figure 2 shows the experimental arrangement employed for the linac measurements, [10] - [13]. It consists of the source region, Figure 2.(A), and three different experiments (response regions), Figures 2.(B), 2.(E) and 2.(C), which are referred to as the arc, equilibrator, and absorption experiments, respectively. In all of the experiments, the energy deposition was measured in TLD (thermoluminescent dosimeter) detectors, the active elements of which were CaF_2: Mn chips. The chips were encapsulated in 0.23 cm of Al, which was not sufficient to isolate the chip from the external electron flux over the 5-25-MeV range of accelerator energies employed in the experiments.

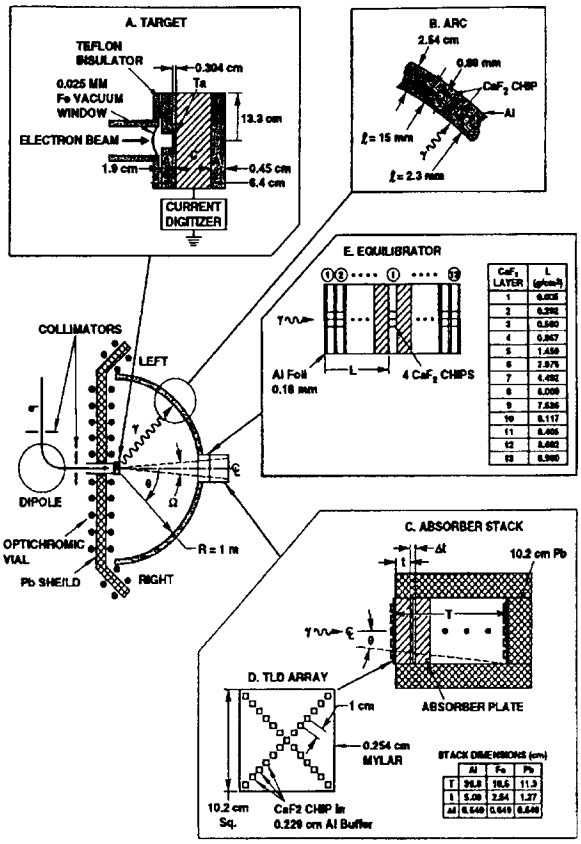

Figure 2. Schematic of experimental arrangement for linac measurements showing details of
(A) X-ray source region, (B) arc experiment
(C) absorption experiment, (D) TLD array in absorption experiment
(E) equilibrator experiment

The FT method of Section 3 was employed to simulate the arc and equilibrator experiments. The purpose of the equilibrator experiment was to measure the dependence of the TLD deposition on equilibrator (encapsulation) thickness. Results at a source electron energy of 15.5 MeV, [11], are shown in Figure 3.

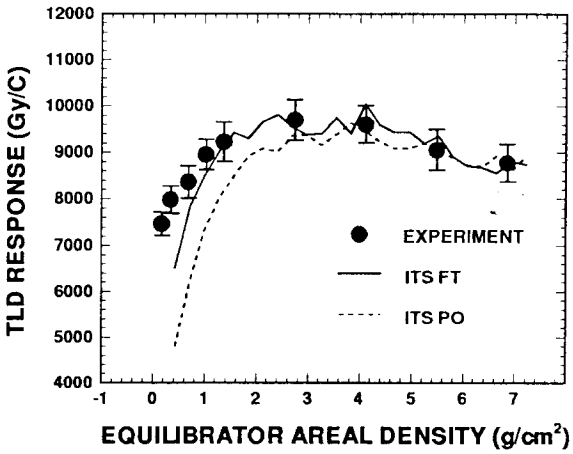

Figure 3. Results of equilibrator experiment at 15.5 MeV

The FT predictions are in good agreement with experiment, underpredicting slightly at small thicknesses. The PO results show the effect of modifying the Monte Carlo simulation to exclude the contribution to the deposition of electrons photoemitted from the source region. The purpose of the arc experiments was to measure the angular distribution of the X-ray deposition. Results are shown in Figures 4 and 5, respectively, for unequilibrated and equilibrated chips at a source electron energy of 10.6 MeV, [13]. Agreement is excellent, except at large angles where the discrepancy is due to experimental background not simulated in the Monte Carlo. It should be emphasized that Figures 3, 4 and 5 are absolute comparisons.

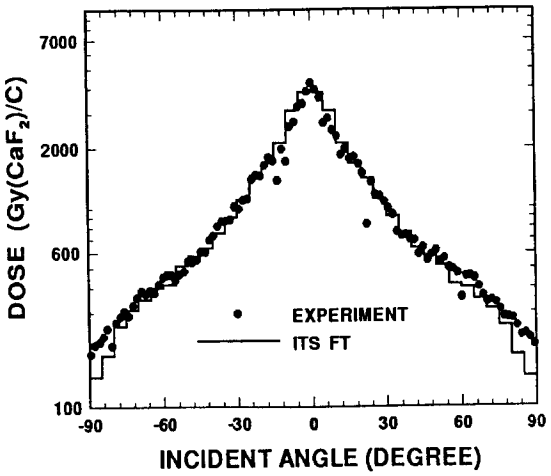

Figure 4. Results of unequilibrated arc experiment at 106 MeV

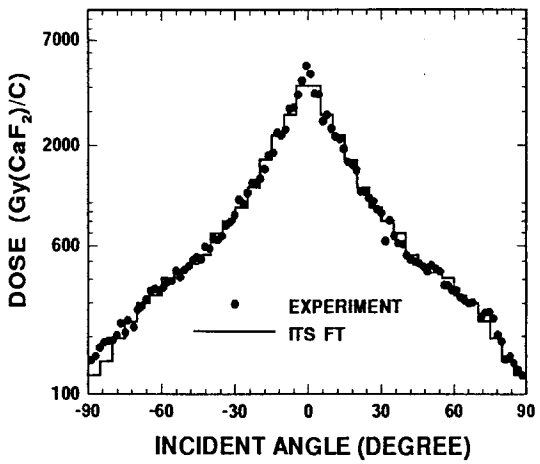

Figure 5. Results for equilibrated arc experiment at 10.6 MeV

Motivation for linac absorber experiments came from our desire to resolve a discrepancy between similar experiments and ITS simulations on a high-intensity, single-pulse, electron accelerator. The absorption data was obtained from that accelerator in support of an investigation of photoneutron production by such high-power machines. A modified version of ITS was also employed to simulate the photoneutron production, [14]. Simulations seriously underpredicted the measured absorption data for Pb and U absorbers.

The absorber simulations are among the most difficult ever attempted using the ITS system. First, there is the inefficient bremsstrahlung production in the converter by the primary electrons. Next, it is only those photons emitted from the source region in a small forward solid angle that significantly contribute to the deposition in the absorber configuration. Once the radiation reaches the absorber layers (the uncollided attenuations of the full absorber configurations for 1.5-MeV photons are about two orders of magnitude for the Al, Fe and Pb absorbers) to reach most of the detector assemblies. Assuming that a photon finally reaches a detector assembly, it must now interact with this highly-transparent multiple-layer region. Finally, only a small number of the electrons generated in these interactions will eventually reach the active element of the detector assembly (TLD chip).

Simulation of all of these inefficient processes within a single Monte Carlo calculation is a formidable task. Our only recourse was to implement a complex set of biasing or variance-reduction procedures that were tailored specifically to the simulation of the absorber experiments, [12]. We did this by building upon the concepts of the FT method.

However, by far the most novel and important feature of the modification is the almost continuous and detailed examination of all electrons to determine the likelihood that their continued transport will contribute to the energy deposition in a selected CaF_2: Mn chip. In the pursuit of variance reduction, there is no concern for energy conservation. As soon as it is concluded that a particular electron can no longer make a significant contribution, it is summarily discarded.

As an aid in the development of the biasing scheme, we employed a diagnostic algorithm to assist in determining the relative importance of the various spatial regions surrounding the active chip, [15]. The algorithm resolves the deposition in the chip according to where the electrons contributing to that deposition were generated.

The trapping efficiency for photon-generated secondary electrons in zones within or near a particular TLD assembly was improved. Instead of simply testing to see if the electron residual range was sufficient for it to escape from the zone, a more complex range-energy interpolation was employed to see if it had sufficient energy to pass through any intermediate zones and reach the CaF_2: Mn chip.

The linac analysis resulted in the identification of two primary causes for the underpredictions of the earlier simulations. First of all, it was found for both Pb and Fe absorbers that the build-up in photon flux due to bremsstrahlung production by photon generated secondary electrons in the absorber configuration itself, especially just upstream of a given TLD plane, cannot be neglected. Secondly, the geometric modelling employed in the earlier experiments caused excessive attenuation by all TLD assemblies upstream of the assembly for which a given calculation was being performed.

When these differencies were corrected in the linac simulations, good agreement was obtained for the absorption in all three materials over the entire experimental energy range. Results for Al and Pb absorber experiments at an accelerator energy of 15.5 MeV, [12], are shown in Figures 6 and 7. Again, these are absolute comparisons.

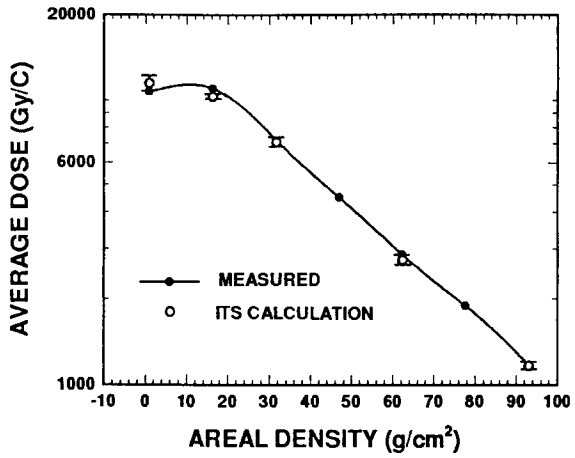

Figure 6. Results of Al absorption experiment at 15.5 MeV

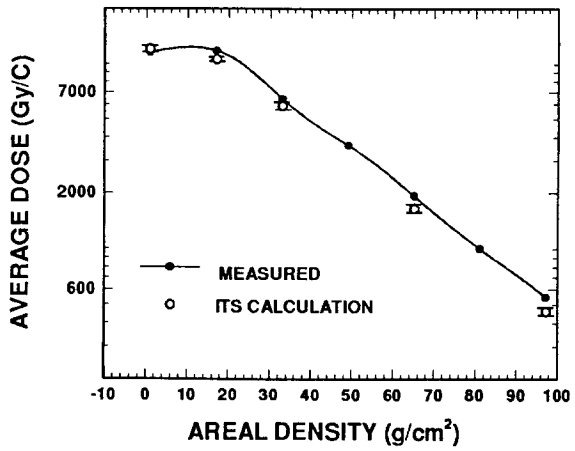

Figure 7. Results of Pb absorption experiment at 15.5 MeV

5. Conclusions

Differences in the methods employed in the Monte Carlo transport of charged and neutral particles lead to different techniques for obtaining variance reduction for the two species. Electron/ photon transport is somewhat unique in that the transport of the two species is strongly coupled. Existing production codes already contain a variety of individual variance reduction features. These features can be integrated into elaborate modifications that are customized to specific problems in order to make possible the simulation of highly complex applications.

References

[1] This work was supported by the U.S. Department of Energy under Contract No. DE-AC04-76DP00789

[2] J. A. Halbleib, R. P. Kensek, T. A. Mehlhorn, G. D. Valdez, S. M. Seltzer & M. J. Berger "ITS Version 3.0: The Integrated TIGER Series of Coupled Electron/Photon Monte Carlo Transport Codes", Sandia National Laboratories Report No. SAND91-1634, March 1992

[3] J. A. Halbleib, R. P. Kensek, T. A. Mehlhorn, G. D. Valdez, S. M. Seltzer & M. J. Berger "ITS: The Integrated TIGER Series of Electron/Photon Transport Codes - Version 3.0", IEEE Trans. Nucl. Sci 39, (1992) 1025

[4] M. J. Berger, S. M. Seltzer, J. A. Halbleib & R. Wang, "Monte Carlo Transport of Electrons and Photons", edited by T. M. Jenkins, W. R. Nelson & A. Rindi, (Plenum Publishing Corporation, 1988) Chapter 2-4 and 7-11

[5] Y. S. Horowitz, M. Moscovitch, J. M. Mack, H. Hsu & E. Kearsley, "Incorporation of Monte Carlo Electron Interface Studies into Photon General Cavity Theory", Nucl. Sci. Eng. 94 (1986) 233

[6] W. A. Stygar, D. L. Fehl, H. C. Ives, R. P. Kensek, V. Harper-Slaboszewicz, J. A. Halbleib, M. A. Hedemann, B. Peyton & P. Reyes, "The Saturn X-Ray Framing Camera", DASIAC-89-77-V2 Vol. II, p. 3-129, March 1990

[7] S. A. Dupree & R. E. Lighthill, "Sandia National Laboratories CDC 7600 Version of MORSE-SGC", Sandia National Laboratories Report No. SAND80-1337, 1982

[8] A. L. Pregenzer & J. A. Halbleib, "Accuracy of Coupled Monte Carlo/Next-Event-Estimator for Bremsstrahlung Dose Predictions", IEEE Trans. Nucl. Sci. Vol. NS-32, No. 6, December 1985, p. 1025

[9] J. A. Halbleib & J. R. Lee, "Predicted Radiation Environment of the Saturn Baseline Diode", Sandia National Laboratories Report No. SAND87-1650, September 1987

[10] D. E. Beutler, J. A. Halbleib, T. W. L. Sanford, D. L. Fehl & D. P. Knott, "Dosimetry Considerations for the High-Energy Photon/Electron Environment of HERMES III: Implications for Experiments and Modeling", IEEE Trans. Nucl. Sci. 38, No. 6, December 1991, 1736

[11] T. W. L. Sanford, D. E. Beutler, J. A. Halbleib & D. P. Knott, "Experimental Verification of Bremsstrahlung Production and Dosimetry Predictions for 15.5 MeV Electrons", IEEE Trans. Nucl. Sci. 38, No. 6, December 1991, 1160

[12] T. W. L. Sanford, J. A. Halbleib, D. E. Beutler & D. P. Knott, "Experimental Verification of Dosimetry Predictions of Bremsstrahlung Attenuation as a Function of Material and Electron Energy", to be published, IEEE Trans. Nucl. Sci., December 1993

[13] D. E. Beutler, J. A. Halbleib, T. W. L. Sanford & D. P. Knott, "Experimental Verification of Bremsstrahlung Production and Dosimetry Predictions as a Function of Energy and Angle", to be published, IEEE Trans. Nucl. Sci., December 1993

[14] T. W. L. Sanford, L. J. Lorence, J. A. Halbleib, J. G. Kelly, P. J. Griffin, J. W. Poukey, W. H. McAtee & R. C. Mock, "Photoneutron Production Using Bremsstrahlung from the 14-TW Pulsed-Power HERMES III Electron Accelerator", Nucl. Sci. Eng., to be published, July 1993

[15] T. W. L. Sanford, J. A. Halbleib, D. E. Beutler, W. H. McAtee, R. C. Mock & D. P. Knott "Production and Measurement of Flash X-Ray Dose Rates in Excess of 10^{13} RAD(CaF_2)/s", IEEE Trans. Nucl. Sci. 38, No. 6, December 1991, 1195.

Some Preliminary Remarks concerning the Proposal of an International Benchmark on Variance Reduction Schemes employed in Monte Carlo Neutron and Photon Transport Codes.

K.W.Burn, ENEA-DRI,Via Martiri di Monte Sole, 4, 40129 Bologna, Italy

1. Circumscription of the exercise

It is apposite to firstly enquire whether the exercise should be limited to automatic (in some sense) variance reduction methods, or not. The former case should severely restrict the number of participants.

2. Problems to be treated

It would seem reasonable to start with three problems, two of which deal with the transport of neutrons and one which deals with the transport of photons. One of the neutron problems should involve spatial streaming (for example in an air duct with at least one corner). The other neutron problem should deal with bulk shielding (with some materials containing cross-section minima giving rise to energy streaming effects). One of the three problems should contain at least two distinct contributing channels (probably spatial channels as this is easier to design and envisage). All three problems should be reasonably deep penetration - for example involving an analogue (i.e. not including any variance reduction) probability of 10^{-5} that a source particle give on the average at least one score (see next section). The problems in their analogue form should not necessarily be binomial (each source particle giving a score of 1 or 0 - for example a detector involving the neutron current); on the contrary, inclusion of a response function that strongly varies with energy is more desirable than just using a flat response function.

3. Calibration of the results

To allow intercomparison of the efficiencies of the calculations carried out by the participants on different computers and with different operating systems, it is necessary to somehow eliminate the variable of the speed of the particular computer used. One way to do this is to execute an analogue calculation on each problem as well as the calculation involving the variance reduction scheme. The quantity of interest is then the gain of efficiency when using the variance reduction scheme compared with the analogue efficiency. More precisely defining the figure of merit (fom) of a calculation as the inverse of the product of the square of the fractional standard deviation (fsd) and the CPU time employed, the quantity of interest is the ratio of the fom using the variance reduction scheme to the analogue fom. It is open to discussion whether instead of the square of the fsd, the estimate of the sample variance should be used. This may be derived from the response, its fsd and the number of source histories, N (which appears as the factor (N-1)/N and as N is large is usually ignored). To be able to run the analogue calculation, the attenuation should not be too high - viz. the value of about 10^{-5} suggested in section 2 (which may actually be rather too high if a response function that strongly varies with energy is used).

4. Cross-Sections

If participants were to use their codes exactly as they are, with the particular cross-sections read by the codes, then the following situation might arise:

For one of the problems which is non-binomial, a result with a small fsd obtained by one participant is many fsd's below the results of the other participants (which are reasonably well grouped together). This situation occurs both for the analogue calculation and for the calculation with the variance reduction scheme. There are then two possible causes for the seemingly anomalous result: 1) cross-section differences; 2) non-sampling of one or more important contributory paths - i.e. not sampling the correct population - in both the analogue and the variance reduction calculations. It is not possible to distinguish between these two causes, but in the former case the calculation with the variance reduction scheme that produces the anomalous result is probably efficient whilst in the latter case this is definitely not the case.

This problem of lack of sampling is a common one and is precisely one of the phenomena that will be under investigation in the benchmark. Therefore I believe that all participants should use exactly the same cross-sections. In this way the expected values of the results from all participants will be the same, so long as no errors are present in the codes that give rise to biased results.

The common cross-sections would probably have to be group ones so as to minimize the work required by each participant to modify his code to accept them. However as each of the participants should know his own code quite well, this should be a feasible undertaking.

5. Results

In each problem a single response will be requested. Thus for each problem six results will be required: the response, fsd and CPU time for the analogue and for the variance reduction calculations. It is probably interesting to add the number of source histories in each calculation.

As well as the bare results, the participants should give a full account of all the steps they took to arrive at their final variance reduction scheme. If the method they use is a semi-automatic one, then any interventions should be clearly stated and justified. This complete reporting of all the steps taken is very important. In this way the use of each method with its advantages and disadvantages can be clearly understood, both by the other participants and by any interested third parties.

SUMMARY OF DISCUSSION ON VARIANCE REDUCTION BENCHMARK PROPOSAL

K. W. BURN, ENEA-DRI, Italy

1. Session "Presentation of Proposals", 27th April 1993

1.1. Responses from participants received prior to the seminar

A summary was given of the responses received from the form that was circulated to the users before the seminar. The following points emerged:

- the kind of sample problem: should it be a real problem for which experimental results exist, or an idealization of a real problem, or a completely artificial problem? One participant has suggested a benchmark streaming problem for which experimental results exist;
- one participant suggested that a common, simple group-wise cross-section library should be used.
- one participant underlined the importance of including sample problems for which variance reduction techniques may be easily abused, causing some response contributions to be ignored. This may occur through a kind of positive feedback effect in which, in the preliminary calculation of the variance reduction parameters, the calculation is led in a direction in which the probability of some response contributions to appear gets progressively lower, so that the generated variance reduction parameters mask these contributions out in the final calculation. The outcome is that a too low response is obtained with a fractional standard deviation (fsd) which does not show this.

Comment: such sample problems may include multi-space or energy contributing channels and/or a strongly varying response function.

1.2. Presentation of the principal questions to be resolved

A presentation was made of the main questions to be resolved in the definition of such a variance reduction benchmark. The questions were divided as follows:

1. calibration;
2. cross-sections;
3. choice of the sample problems;
4. presentation of the results.

1. **Calibration**: It was suggested, rather than give as a result the ratio of the FOM (figure of merit = $(fsd^2 * CPU\ time)^{-1}$ (fsd = fractional standard deviation)) with the variance reduction parameters to the analogue fom, instead the CPU time per source history in an analogue calculation for each sample problem could be an easier means of calibration. One problem that immediately arises is that some codes might not be able to make a purely analogue calculation.

2. **Cross-sections**: A choice exists between adopting a single common set of cross-sections to be used by all participants (advantage: all participants should have the same expected value for the response; disadvantages: work required to modify codes to accept these cross-sections, problem with some codes using point-wise cross-sections and some codes using group-wise cross-sections), and participants using their own cross-sections (advantage: easy; disadvantage: different expected values of the response -- we will not know if a response is low because some contributions are not being picked up, or because of the cross-sections used).
   If a common cross-section set is adopted, a second choice exists between using real or at least realistic cross-sections and using artificial cross-sections. If artificial cross-sections are adopted then isotropic scattering should probably be used as it is not believed that the angular distribution of scattering should play any role in such an exercise.

3. **Choice of the sample problems**: Should they be real problems for which experimental results exist, or idealized models of real problems, or purely artificial problems? If real problems, then of course cross-sections should also be real.

   The various sample problems should include the following characteristics:

   - bulk shielding;
   - streaming;
   - cross-section windows?
   - multi-contributing channel.

   Anyway we should start off with simple problems!

   Responses:

   - in some sample problems current or flux;
   - in some sample problems a strongly varying response function;
   - probably a boundary-crossing estimater could always be used.

4. **Presentation of the results**:

   At least:

   - the response;
   - the fractional standard deviation;
   - CPU time - unnormalized
     - normalized - see calibration
   - figure of merit ($(fsd^2 * CPU\ time)^{-1}$) - unnormalized
     - normalized

   Plus probably:

   - all the variance reduction parameters and how they were used;
   - what the participant did (not too long!)

1.3. Public discussion following the presentation

Concerning the question of calibration, W.R. Martin suggested that instead of using an analogue run, the measure: number of "tracks" should be logged by each participant in the calculation that uses his variance reduction parameters. Here "tracks" is defined as the number of collisions plus the number of boundary crossings. This parameter is a reasonable measure of the amount of work done in the calculation, and together with the CPU time can be used to calibrate.

J. S. Tang brought up the question of what kind of estimators would be used, and in particular that it is important in a given sample problem not to have some participants using point or ring detectors, and others using real event detectors. This is because the different kinds of estimation might have very different intrinsic efficiencies. If we ask the participants to use exactly the same kind of estimators, we might run into problems in that codes do not usually contain all the estimators, e.g. for volume estimation, some codes only have the track length estimator whilst other codes might only have the collision density estimator. So without detracting in any way from the exercise it is thought maybe to use surface-crossing estimators, which all codes should contain. It is open whether to include a sample problem which imposes the use of a point detector.

Hoogenboom made some general remarks:
Such a benchmark exercise is in his opinion useful and starting with a fictitious problem seems best.
Measuring the effectiveness of a variance reduction scheme (i.e. the question of calibration) seems problematic as some codes cannot run a full analogue calculation.
Concerning cross-sections, there will always be a difference between continuous and multigroup treatment. The best you can do is to specify the continuous energy cross-sections as groupwise constant.

2. Session "Discussion of Proposals and Decisions", 29th April 1993, 15:25

It was firstly underlined that the benchmark is directed at neutron and photon transport and not at charged particle transport, there having been a number of contributions on electron transport at the seminar. Then it was mentioned that an updated version of the paper: "Some preliminary remarks concerning the proposal of an international benchmark on variance reduction schemes employed in Monte Carlo neutron and photon transport codes" was included as paper no. 60. The main difference compared to the original version which was circulated to the participants prior to the meeting was the inclusion of the question of whether the exercise should be restricted to variance reduction schemes that have some built-in automatism or whether it should be widened to include also participants who find their variance reduction parameters using intuition and experience. In the discussion that followed there was a complete consensus in favour of the latter.

2.1. Summary of points brought up in informal discussion since the previous session

We conveniently divide these points into specific and general:

Specific:

- one of the sample problems could be based on a well logging problem which show interesting variance reduction schemes and have relatively simple geometries.

- the problem of using different cross-section libraries might be resolved by employing gamma transport only as all gamma transport libraries should be similar.

- rather than simply comparing the result, fsd, CPU time and fom, more information could be generated from each calculation and compared. Such information could include the variance of the variance and the probability density function of the detector scores. Generating suchinformation could allow a richer comparison.

- some sample problems could be very simple artificial ones for which analytic results exist (monoenergetic, 1-dimensional). Such problems could allow a clean comparison between the various techniques.

General:

- a number of potential participants agreed on the desirability of employing cross-sections that are the same for all participants and that should be artificial. It was agreed that the work required to change the codes would be compensated by the advantage that all participants should have the same expected value of the response.

- if using common artificial cross-sections then obviously simple idealized geometries should be employed.

- although no one spoke against using common artificial cross-sections, some potential participants expressed an interest in running at least one real problem with their own cross-sections, probably after theother problems.

- as far as calibration/normalization of the results is concerned, a consensus does not seem to have been reached. Two general suggestions have already been reported: the time per source history in an analogue calculation and counting the number of tracks in the calculation with the variance reduction parameters. Other informal suggestions were:
  ⇒ for each participant to implement each code on his own machine so as to directly compare the running times on each machine.
  ⇒ to use the running speeds of each machine according to the machine specifications. This is probably more approximate compared with the other suggestions as it is well known that relative running times between machines are very problem-dependent.

The question of calibration depends on what the object of the benchmark is. If it is to provide as good a comparison as possible between theacceleration provided by each variance reduction scheme, then clearly a large effort should be spent on assuring as good a calibration as possible. If on the other hand the object is to see the way in which each variance reduction scheme is used on particular types of sample problem, with just a general idea of the relative accelerations of the schemes, then not much effort needs to be spent on the calibration. Perhaps any participants using intuition/experience will be interested in as precise a calibration as possible.

Comment: the suggestion of Dr. Martin seems a good one even if some codes might need to be modified to count collisions and boundary crossings.

2.2. Creation of a "Steering Committee"

As there has been a favourable response to the benchmark proposal, it was proposed to widen the organizational burden by setting up a steering committee. It was suggested that firstly a representative of each code employed should be co-opted, and informal soundings were made before and during the meeting for the well-known general purpose codes. So far the list is, in alphabetical order of code:

• M. Caillaud	CEA CELV	(KAISSA)
• T. E. Booth	LANL	(MCNP)
• J.S. Tang	ORNL	(MORSE)
• G. Ledanois	CEA CELV	(SICOMORE)
• T. Vergnaud	CEA Saclay	(TRIPOLI)

This list is open (underlined). Apologies to those who have not been sounded out (due to time problems) but please come forward if you would like to participate with another code and wish to be involved in the organization. Also please come forward even if you are using a code already represented if you wish to contribute to the organization.

2.3. Public Discussion

The subject was then opened to the floor. Here there were a number of interventions which unfortunately have not been recorded. Those recorded are reported in a summary form as follows:

- J.C. Nimal was of the opinion that there should be a mixture of problems using common artificial cross-sections and problems using real but different ones. He proposed 3 sample problems:
  ⇒ Top Hat (artificial geometry, artificial cross-sections which were originally concrete)
  ⇒ A streaming problem in a bent duct with 1 or 2 corners and quite high attenuation (artificial geometry, artificial cross-sections)
  ⇒ A real benchmark problem for which experimental results exist. (real geometry, real cross-sections) CEA Saclay is willing to provide the geometrical specifications of all three problems.

- J.S. Hendricks asked if it was the intention to present results of the exercise at the conference at Arlington (April 1994). K.W. Burn replied that it was the intention to present something at Arlingtonalthough he had his doubts as to whether any results would be ready by then. Others thought that it was desirable to present results atArlington and would be possible if the exercise got underway quickly.

- J.E. Hoogenboom disagreed with the proposal of a purely analytical problem, but agreed with the use of idealized geometries relevant to real problems.

At this point as there had been time overrunning the session was closed without any conclusions on next actions having been made. Closing the meeting the conference secretary, E. Sartori, stated the interest and availability of the NEA in coordinating the benchmark exercise.

2.4. Proposal of immediate actions

Everyone wishing to participate should write to E. Sartori at his e-mail address:

sartori @ frneab51 (Bitnet)
sartori @ nea.oecd.circe.fr (Internet)

stating:

- the code they will use
- the method they will use if automatic/ semi-automatic or
- user experience
- comment/criticism on what has been reported or proposed here

Anyone wishing to join the steering committee either because they are using a different code or because they wish to contribute should state this

The question of the format and nature of the artificial cross-sections was not discussed. Therefore anyone with concrete and specific proposals (and also any offers to do this work!) please come forward.

Any further specific proposal associated with offers to do the work are welcome.

As far as the organization of the exercise through the steering committee is concerned, some means of communication among the members needs to be established so that meetings can be held and decisions taken "at a distance". Hopefully the NEA can play a role here as well.

Session III

IMPACT OF NEW COMPUTER ARCHITECTURES SPECIAL MONTE CARLO GAMES

CHAIRS:

***W. R. MARTIN**, UNIVERSITY OF MICHIGAN - USA*
***H. RIEF**, COMMISSION OF EUROPEAN COMMUNITIES*

MONTE-4 for Monte Carlo Simulations with High Performance

K. HIGUCHI

Computing and Information Systems Center, Tokai Research Establishment,
Japan Atomic Energy Research Institute
Tokai-mura, Naka-gun, Ibaraki-ken 319-11, Japan

ABSTRACT

Along with the power increase of current vector processors such as the computational speed and capacity of fast memory, there has been growing interest in numerical simulation by particle models such as those by Monte Carlo methods and so on. The current vector processors have attained good performance in many calculations with long vector lengths and high vectorization ratios. However, the calculation of particle transport problem with particles having varying attributes by Monte Carlo method in unstructured or complex spaces is not suitable to the current vector processor because the calculation contains many nests of conditional branches, short and diminishing vector lengths. The Monte Carlo machine, MONTE-4, has been developed based on the architecture of existing supercomputer with a design philosophy to realize high performance in vector-parallel processing of Monte Carlo codes for particle transport problems. In this paper we present the effective performance of our Monte Carlo machine through practical applications of multi-group criticality safety code KENO-IV and continuous-energy neutron/photon transport code MCNP. We have obtained ten times speedup on MONTE-4 compared with the execution time in the scalar processing.

INTRODUCTION

Along with the power increase of current vector processors such as the computational speed and capacity of fast memory, there has been growing interest in numerical simulation by particle models such as those by Monte Carlo methods and so on.

The current vector processors have attained good performance in many calculations with long vector lengths and high vectorization ratios. The computational schemes which correspond to the cases are, for example, finite-difference method(FDM), finite element method(FEM), Monte Carlo method(MCM) on lattice structured objects. As a result the current vector processors show more than ten times speedup ratios in the most of these cases.

On the otherhand, the calculation of particle transport problem with particles having varying attributes by MCM in unstructured or complex spaces does not correspond to the above cases. In this case the calculation contains many nests of conditional branches due to categorizations of particles, short and diminishing vector lengths due to decrease of number of particles by leakage, absorption and so on. We can generally consider two approaches to resolve this difficulty in vector processing of Monte Carlo codes for particle transport problems. One is to

rewrite the program to make it have pseudo-lattice structures. [1] Another is to develop a Monte Carlo machine, of which concept has been proposed in elsewhere, [2] so as to meet the algorithms used in the existing particle codes.

As for the former, Brown and Nakagawa have developed new Monte Carlo codes and achieved sufficient gains in computational efficiency on CYBER-205 and VP-2600, respectively. Brown has shown the results in the analyses of deep-penetration of fission neutrons in concrete and two-dimensional light water reactor lattice regions. [3] The algorithm has been coded so as to derive the peak performance from the current vector processor. The concept of reconstruction of the code for the current vector processors has been firstly done by his group. Nakagawa has obtained the significant performance [4] through the neutron transport problems of pressurized water reactor fuel subassembly, a slab of iron or iron and concrete and so on. The algorithms has made use of lattice structure arisen from periodic geometry in the problem and has been coded suitable to the current vector processor as well as Brown's.

Through our experience with vectorizations of existing Monte Carlo codes such as KENO-IV, [5] MORSE, [6] VIM [7] and MCNP, [8] we have chosen the latter approach because it is very expensive to develop new Monte Carlo codes which are equivalent to the four codes, and it takes long time to establish a reliability equal to those of codes widely used in the nuclear field in a construction of new Monte carlo codes.

In this paper we present the effective performance of our Monte Carlo machine through practical applications of multi-group criticality safety code KENO-IV and continuous-energy neutron/photon transport code MCNP. We have obtained ten times speedup ratio on MONTE-4 with the hardware system described above, compared with the execution time in scalar processing. It seems to indicate that significant gains in computational efficiency have been obtained on MONTE-4, taking account of about 1.5 times speedup obtained on the current vector processor with respect to KENO-IV and MCNP codes.

DESIGN PHILOSOPHY AND ARCHITECTURE OF MONTE-4

The JAERI Monte Carlo machine, MONTE-4 has been designed under the philosophy that i) since existing Monte Carlo codes have been widely used on large-scale computers or vector processors, the machine should have a similar architecture to those of existing computers such as high speed machine cycle, vector and parallel processing capability and large memory size, ii) since there remains a scalar computation part in Monte Carlo calculation, the machine should have a high speed cycle, and iii) the machine should be well balanced between data transfer rate and vector processing capability. As the basis of our Monte Carlo machine, we have chosen SX-3/11 because it was the supercomputer with vector processing capability and the world highest machine cycle when we started the design.

From the point of view mentioned above, Monte Carlo machine, MONTE-4 has been developed based on the architecture of existing supercomputer with a design philosophy to realize high performance in vector-parallel processing of Monte Carlo codes for particle transport problems. Accordingly, MONTE-4 should also overcome the difficulties in vector processing of Monte Carlo codes for achieving highly computational performance. Such difficulties are caused by the following characteristic operations.

(1) Short and diminishing vector length
Although large number of particles are simultaneously tracked at the beginning of the calculation, the number of particles decrease whenever one of them is killed by absorption or escape. In an extreme case, we are forced to a vector processing with one particle at the end of the calculation.

(2) Nests of conditional branches
Production level Monte Carlo codes have complicated structure with a large number of conditional branches in order to treat many kinds of physical phenomena or to find a particle position in boundary crossing through the tracking of the particle. We sometimes find the nests of conditional branches impossible to vectorize such as computed GO TO statements or backward GO TO statements.

(3) Indirect addressing
It is convenient to use indirect addressing in vector processing of Monte Carlo codes because of tracking of plural particles whose numbers change in the processes of calculation. Regardless to say, we can use direct addressing by replacing the values in order before and after the calculations for particle storages. However, the time reduction by using direct addressing was lower than the overhead of the operation for replacing values, with our experience.

All causes described above give rise to low performance of vector processing and low vectorization ratio. In order to overcome these difficulties, MONTE-4, of which configuration is shown in Fig. 1, has been equipped with special hardwares as follows.

(1) Geometric pipelines
Categorization of the particles according to the geometry is made by using multi-way conditional branches. It is impossible on conventional vector processor to vectorize a DO loop with such a multi-way conditional branch. MONTE-4 has been equipped with special pipelines called geometric pipelines to accelerate such DO loops.

(2) Event pipelines
In vectorized Monte Carlo simulation, particles in the same events are gathered and processed. These pipelines accelerate categorizations of the particles by the events, such as collisions, boundary crossings and so on.

(3) Region check pipelines
This pipelines accelerate the region-check procedures, which are necessary to judge whether particles' locations are in correct regions using logical expressions and the procedures are impossible to vectorize because of nests of conditional branches.

(4) Enhanced load/store pipelines
Data transfer in regard to indirect addressing has been improved by enhancement of the load/store pipelines, so that the data transfer ratio by indirect addressing has been multiplied by factor of eight.

(5) Parallel processing with four processors
Parallel processing with four processors multiplies the performance of vector processing. Each processor has lightly-equipped vector pipelines to cope with vector processing with short and

diminishing vector lengths. The method used in the parallel processing is discussed in next section.

For all such reconstruction, both 15% of total LSI circuits for processor and 32% for memory controller of the base processor have been newly developed. As for multi-chip package, both 67% of for processor and 100% for memory controller have been newly developed.

VECTORIZATION AND PARALLELIZATION METHOD

An algorithmic change of the code is required for vector-parallel processing so as to completely derive the performance of MONTE-4. In this section a methodology used in the modification of the codes is described.

Vectorization and parallelization of production level Monte Carlo codes

(1) Vectorization method
As for the vectorization of the Monte Carlo codes for particle transport problem, an algorithmic change of original codes from tracking single particle to tracking plural particles simultaneously is necessary to make computational granularities for vector processing. After the modification of the codes, particle number assigned to identify particles are stacked in storages corresponding to the major events such as collision, boundary crossing and so on. Physical attributes of a particle such as position, energy, scattering angle, etc. are obtained through the particle number.

(2) Parallelization method
Since the history of each particle is independently simulated in the Monte Carlo codes for particle transport problem, sharing and tracking of the particles in four processors can be performed. Equal number of particles has been allocated to each processor. Input/output procedures have been sequentially processed. Local common areas are prepared as temporary storages for quantities to accumulate statistics which are referred to during parallel processing. The quantities obtained by the calculation on each processor was summed up after the parallel processing on main processor.

Experience with vectorization and parallelization of KENO-IV code

After the modification for vector and parallel processing described above, histories of a few of hundreds of neutrons are started in each processor. Various efforts have been made to attain higher vectorization ratio. The important modifications among them are as follows. i) Vectorization of random numbers : The random number generator of the original KENO-IV, which is written in assembly language, has been replaced by a vectorized library routine to make random numbers by congruent multiple method. ii) Vectorization of selecting operation of an energy group after collision : The computation time for selection of a new energy group is a rather time-consuming task and the original algorithm is hard to vectorize. The binary search method by Walker [9] is used in our version. iii) Isolations of rare events : Although most neutrons in a storage follow the same computational algorithms in an event, one or a few neutrons occasionally require a special treatment. In spite of low cost required for such an operation, it leads low performance of vector processing because preferable vector processing is prevented by conditional branches. Thus it is very important for a vectorized Monte Carlo code to separate rarely used statements from a DO loop and isolate them so they will not be used in main stream of computations.

Experience with vectorization and parallelization of MCNP code

In addition to the same efforts as ones of KENO-IV code following efforts have been made. i) Selection of vector or scalar processing : In the case that the vector length is extremely short, the performance of vector processing become lower than one of scalar processing. Thus, the calculations with very short vector length have been dynamically detected and processed in scalar. ii) Inline expansion of the routines : Routines, which have low cost and are predicted to cause low performance in vector processing because of overhead of routine calls, have been expanded into routines which call these routines or not modified at all by making interface routines. iii) Interface routines : When a code is vectorized the most of routines need to be modified because all variables indicating particle attributes need to be in array structure. However, some routines with low cost have been used without modifications. Alternately interface routines have been introduced for connections of vectorized and unvectorized routines.

As for the parallelization, a few of thousands of particles have been allocated to each processor. Synchronization for tallying has not produced so much decrease of efficiency by load imbalance, differently from the case of KENO-IV code because MCNP code has been tested for a shielding calculation.

EFFECTIVE PERFORMANCE BY KENO-IV AND MCNP CODE ON MONTE-4

Input data used for the estimation

As for the calculation model for KENO-IV code, one of a series of experiments of a tank-type critical assembly(TCA) at JAERI has been chosen. Fuel rods of low-enriched UO2(2.3% U-235)are arranged as a manner of 19 X 19 array in the tank type core. The criticality calculation has been made with a model of 1200 neutrons per generation and 53 generations.

As for the calculation model for MCNP code, a dose evaluation [10] by anthropomorphic phantom, i.e., Cristy phantom [11] developed at ORNL has been chosen. The phantom is constructed by 200 surfaces and 110 regions. The photon exposures in energy range from 10 KeV to 10 MeV of 15 energy groups and 1,000,000 histories for each monoenergy parallel source have been calculated.

Effective performance of MONTE-4

(1) Effective performance of enhanced load/store pipelines
Since the architecture of MONTE-4 is based on the one of SX-3/11, we can estimate the effective performance of enhanced load/store pipelines in regard to a code by comparison between execution time in two cases as follows.

- Execution time of the code on SX-3/11.
- Execution time of the code on MONTE-4 with only load/store pipelines .

Table 1 shows the results of KENO-IV and MCNP codes. Taking into account of the difference of machine cycles, we can estimate that the enhanced load/store pipeline reduce nearly 13% of the whole execution time for each code. These data indicate that one of reasons for decrease of the efficiency of the vector processor in the case of KENO-IV and MCNP codes on the conventional vector processor has been improved.

(2) Effective performance of geometric, event and region check pipelines
The effective performance of three Monte Carlo pipelines, geometric, event and region check pipelines in regard to a code has been estimated by comparison between execution time in two cases as follows.

- Execution time of the code on MONTE-4 with only load/store pipeline.
- Execution time of the code on MONTE-4 with load/store, geometric, event and region check pipelines.

Table 2 shows the results of KENO-IV and MCNP codes. As for the KENO-IV code, 20% of the whole execution time has been reduced by three Monte Carlo pipelines. As for the MCNP code, nearly 50% of the whole execution time has been reduced. It mainly depends on the effectiveness of region check pipelines.

(3) Effective performance by KENO-IV code
The measured speedup ratios are shown in Table 3. The ratios are defined as CPU time ratios of the scalar calculation of original version to vector calculations of vectorized versions. The reduction of execution time on the single processor has been mainly achieved by the indirect addressing hardware feature and geometric pipelines. The region check pipeline is not used in our KENO-IV version. It is required to elaborate the Fortran compiler to get a good performance by the event pipeline designed for high-speed two-way branches and the revision of the compiler is planed.

The speedup ratio of parallel processing is lower than four, namely the number of processors. This is due to two reasons. First is load imbalances among processors. We can estimate the decrease of efficiency by load imbalance in parallel processing by the comparison between following values.

- Execution time on single processor divided by the number of processors.
- The longest execution time among four processors in parallel processing simulated on single processor so as to remove the decrease of efficiency by memory conflicts.

The decrease of efficiency estimated by this way was 15% in this calculation. Second, memory conflicts decrease effect of data transfer performance. We can roughly estimate the decrease of efficiency of parallel processing by memory conflicts using M/M/1 queueing model. [12] The percentage of utilization of memory controller in the calculation was 20% by our analysis. We can estimate that the decrease of efficiency is 15% by the relation between efficiency of performance of four processors and the percentage of utilization of memory controller. We can estimate the performance of parallel processing as follows.
$0.85 \times 0.85 \times 4 = 2.89$
This value is close to the measured speedup ratio by parallel processing.

(4) Effective Performance by MCNP Code
The measured speedup ratios are shown in Table 3. The reduction of execution time on single processor has been mainly achieved by the region check pipeline.

The performance of parallel processing is higher than that of KENO-IV code. This is due to two reasons. First, the decrease of efficiency by the load imbalance was 10% in this calculation. The reason why the decrease of efficiency is less than that of KENO-IV code is that the synchronization for tallying does not produced so much load imbalance, different from the case of KENO-IV code as described above. Second, the decrease of efficiency by memory conflicts is

7%, which has been estimated using 15% of utilization of memory controller by the same way as one of KENO-IV code. Thus, we can estimate the performance of parallel processing as follows.
0.90 X 0.93 X 4 = 3.35
This value is close to the measured speedup ratio by parallel processing.

CONCLUDING REMARKS

We have obtained significant gains in vector processing on MONTE-4 compared with the low performance ratios of 1.5 time, according to our experience, on the conventional vector processor in cases of KENO-IV, MCNP, MORSE and VIM codes. We can expect better performance also in parallel processing by the elaboration of the load sharing algorithm to improve the load imbalance and the coding to avoid the memory conflicts as possible.

We are modifying other production level Monte Carlo codes such as MORSE and VIM codes widely used in nuclear field and expect the good performance with respect to these codes as well as KENO-IV and MCNP codes.

Vector-parallel processing with high performance will be expected in regard not only to Monte Carlo codes for particle transport problem but also to other codes for particle simulation by coding suitable to the hardware features of MONTE-4.

Acknowledgement

The authors express their sincere thanks to H. Matsumoto and Y. Seo at NEC Corporation, S. Shingu at NEC Software Kansai, Ltd., N.Watari at NEC Scientific Information System Development, Ltd.and M. SASAKI at The Japan Research Institute, Ltd·for their variable discussion and comments and Mr. Y. Hasegawa on leave from Nuclear Data Center for his help in the evaluation calculations.

References

1 Nakagawa, M. et al., Development of Monte Carlo Code for Particle Transport Calculations on Vector Processors, Proc. Supercomputing in Nuclear Applications, P.160, Mito, March(1990).

2 Asai, K. et al., Monte Carlo Calculations on High Speed Machines, Prog. Nucl. Energy, 24, 175(1990).

3 Brown, F. B. and Martin, W. R., Monte Carlo Methods for Radiation Transport Analysis on Vector Computers, Prog. Nucl. Energy, 14, 269(1984).

4 Nakagawa, M. et al., Monte Carlo Calculations on Vector Supercomputers Using GMVP, Prog. Nucl. Energy, 24, 183(1990).

5 Asai, K. et al., Vectorization of the KENO IV Code, Nucl. Sci. & Eng., 92, 298(1986).

[6] Higuchi, K. et al., Vectorization of MORSE-DD Code: *JAERI-M* **87**-032 (1987), in Japanese.

[7] Suganuma, M. et al., Vectorization of Continuous Energy Monte Carlo Code VIM: *JAERI-M* **86**-190 (1987), in Japanese.

[8] Kurita, Y. et al., Vectorization of Monte Carlo Code MCNP, *JAERI-M* **87**-022 (1987), in Japanese.

[9] Walker A. J., An Efficient Method for Generating Discrete Random Variables with General Distributions, ACM Trans. Math. Soft., 3, 3, 253(1977).

[10] Higuchi, K. and Yamaguchi, Y., Application of MCNP Code of External Dose Evaluation with Human Phantom, Proc. 1991 Fall Meeting of the Atomic Energy Society of Japan (1991), in Japanese.

[11] Cristy, M., Specific Absorbed Fractions of Energy at Various Ages from Internal Photon Sources, ORNL-TM-8381(1981).

[12] Kleinrock, L., Queueing Systems, Vol. I, John Wiley & Sons, Inc., New York. London(1975).

Table 1 Comparison of Execution Time Using Only Load/Store Enhancement Feature on MONTE-4 with SX-3/11

	Execution time on SX-3/11	Execution time on MONTE-4 (one processor)
KENO-IV	62.8 (sec.)	54.8 (sec.)
MCNP	1020.3 (sec.)	889.9 (sec.)

In the table, execution time on SX-3/11 is converted by 2.5 ns of machine cycle since machine cycle of SX-3/11 and MONTE-4 are 2.9 ns and 2.5ns, respectively.

Table 2 Execution Time Using Enhanced Load/Store and Three Monte Carlo Pipelines

	Execution time without Monte Carlo pipelines (one processor)	Execution time with Monte Carlo pipelines (one processor)
KENO-IV	54.8 (sec.)	44.9 (sec.)
MCNP	889.9(sec.)	463.4 (sec.)

Table 3 Speedup Ratios of the KENO-IV Code on MONTE-4

	1 processor		4 processors
Scalar/Vector	Scalar	Vector	Vector
Execution time	167.1 sec.	44.9 sec.	16.7 sec.
Speedup ratio(A)	1.0	3.7	10.0
Speedup ratio(B)		1.0	2.7

i) In the table, execution time of 167.1 indicates one of original version in scalar calculation with single processor. The others indicate ones of vector version in vector processing.

ii) Speedup ratio(A) means one of execution time of original veision in scalar calculation. The other means one of execution time of vector version in vector calculation with single processor.

Table 4 Speedup Ratios of the MCNP Code on MONTE-4

	1 processor		4 processors
Scalar/Vector	Scalar	Vector	Vector
Execution time	1284.2 sec.	463.4 sec.	137.8 sec.
Speedup ratio(A)	1.0	2.8	9.3
Speedup ratio(B)		1.0	3.4

Figure 1. Configuration of MONTE-4.

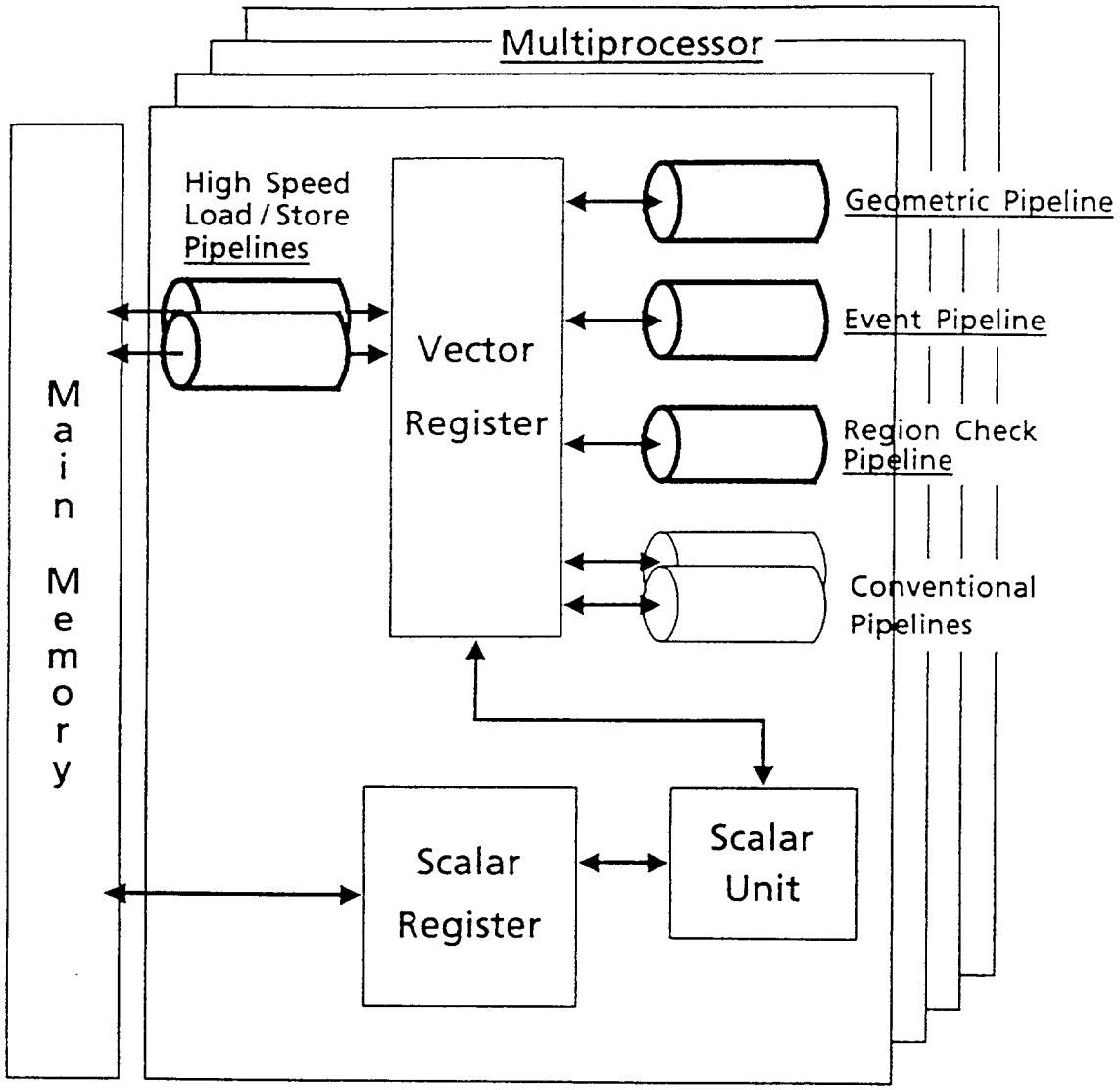

DISTRIBUTED PROCESSOR MONTE CARLO: MCNP RESULTS ON A 16-NODE IBM CLUSTER

G. W. McKinney
Los Alamos National Laboratory
Los Alamos, NM 87545 USA

ABSTRACT

MCNP is a general 3-D Monte Carlo neutron, photon, and electron transport code developed by LANL (Los Alamos National Laboratory, X–6 Group). With the widespread use of high-performance workstations, an increased interest for multiprocessing MCNP on distributed memory systems has emerged. Such systems, connected by high-speed communication networks, provide the capability for codes like MCNP to achieve order-of-magnitude higher performance over current common memory systems. The software communication package chosen for use within MCNP is Parallel Virtual Machine (PVM), available as public domain software. This package supports a variety of communication networks and computer systems. The PVM version of MCNP on a 16 processor IBM RS/6000 cluster produced speedups that approach the number of processors.

I. INTRODUCTION

The advent of high-performance computer systems has brought to maturity programming concepts like vectorization, multiprocessing, and multitasking. Although there are many schools of thought as to the most significant factor in obtaining order-of-magnitude increases in performance, such speedup can only be achieved by integrating the computer system and application code.

Vectorization leads to faster manipulation of arrays by overlapping instruction CPU cycles. Discrete ordinates codes, which require the solving of large matrices, have proved to be major benefactors of vectorization. Monte Carlo transport, on the other hand, typically contains numerous logic statements and requires extensive redevelopment to benefit from vectorization.

Multiprocessing and multitasking provide additional CPU cycles via multiple processors. Such systems are generally designed with either common memory access (multitasking) or distributed memory access. In both cases, theoretical speedup, as a function of the number of processors (P) and the fraction of task time that multiprocesses (f), can be formulated using Amdahl's Law

$$S(f,P) = 1/(1 - f + f/P)$$

However, for most applications this theoretical limit cannot be achieved, due to additional terms (e.g., multitasking overhead, memory overlap, etc.) not included in Amdahl's Law.[1] Monte Carlo transport is a natural candidate for multiprocessing, since the particle tracks are generally independent and the precision of the result increases as the square root of the number of particles tracked.

II. MCNP MULTIPROCESSING WITH PVM

The Monte Carlo neutron, photon, and electron transport code MCNP,[2] developed by LANL (Los Alamos National Laboratory, X-6 Group), has an extensive list of attractive features, including continuous energy cross sections, generalized 3-D geometry, time dependent transport, and comprehensive source and tally capabilities. It is widely used for nuclear criticality analysis, nuclear reactor shielding, oil well logging, and medical dosimetry calculations (to mention a few) in many research laboratories within the United States, Canada, Europe, and Japan, in addition to over 100 universities and private companies throughout the world. MCNP geometry is described by the union and intersection of general quadratic surfaces and includes such features as repeated structures and nested lattices. The source capability allows for particles to be started from arbitrary user defined distributions with general hierarchical dependencies. Numerous variance reduction techniques provide the user with powerful statistical tools to optimize complex radiation transport problems. Several different tally options allow the user to obtain the flux or current (or virtually any flux-weighted quantity) across a surface, averaged over a volume, or at a point.

Since the inception of multitasking software, MCNP developers have made it a high priority to support multitasking on a variety of common memory systems. With the widespread use of high-performance workstations, interest in multiprocessing MCNP on distributed memory systems has increased. Such systems, connected by high-speed communication networks, make it possible for codes like MCNP to achieve order-of-magnitude higher performance over current common memory systems. Ideally, MCNP communication on such a system could be limited to a few seconds at the beginning of a calculation (to initialize the tasks) and at the end (to collect the results). However, software QA standards imposed on MCNP require that multiprocessing versions track exactly with that of sequential versions, increasing communication between tasks to sum results at established rendezvous points.

The software communication package currently supported within MCNP is Parallel Virtual Machine, PVM[3] (version 2.4.2), developed by ORNL (Oak Ridge National Laboratory). This package enables concurrent computing on loosely coupled networks of processing elements. PVM may be implemented on a hardware base consisting of different machine architectures, including single CPU systems, vector machines, and multiprocessors (see Table I). These computing elements may be interconnected by one or more networks, which may themselves be different (e.g., Ethernet, Internet, and fiber optic networks). These computing elements are accessed by applications via a library of standard interface routines. These routines allow the initiation and termination of processes across the network as well as communication and synchronization between processes.[3]

III. MCNP SPEEDUP ON AN IBM RS/6000 CLUSTER

The PVM version of MCNP was evaluated on a 16 processor IBM RISC (Reduced Instruction Set Computer) System/6000 Model 560 workstation cluster at LANL. Determining true speedup in a multi-user environment can be difficult due to a lack of appropriate timing routines. On a dedicated system, simple wall-clock time can be used to calculate speedup. The IBM RS/6000 operating system (AIX) provides user, system, and wall-clock timing routines; however, the user and system routines do not include "sleep" time. Thus, CPU time "wasted" during communication lag (e.g., the PVM master task waiting for replies from spawned subtasks) is not included in these timing routines. (The term "wasted" here is used in the strict sense – on a multi-user system, these CPU cycles will most likely be used by other applications). The wall-clock time on a nondedicated system is a function of the system load and cannot be used to estimate speedup.

In previous versions of MCNP, results were summed every 1000 particles to update certain tally tables. (e.g., Tally Fluctuation Chart, detector/DXTRAN Russian roulette criteria). The value of 1000 changes with the number of particles tracked and was chosen somewhat arbitrarily. However, in the current version of MCNP this parameter can be altered by the user and determines the amount of inter-task communication. Thus, this parameter has a significant impact on speedup. The sleep time of the master task, associated with this communication, is a result of the random nature of Monte Carlo tracking (i.e., processors tracking the same number of particles

will not finish at the same time). Wall-clock timing on a virtually dedicated system indicates that this sleep time can be substantial, especially if communication is required every 1000 particles.

Speedup estimates were made using the following equation

$$S(P) = T_s/T_m(P)$$

where T_s is the CPU time for a single processor to complete execution and $T_m(P)$ is the CPU time for the PVM master task to complete execution with P subtasks. In MCNP, the master task initializes the problem, spawns the subtasks, collects the results, and writes the output files. Communication sleep time was accounted for in $T_m(P)$ by using the wall-clock time (AIX TIME utility) on a virtually dedicated system. Multiple off-hour runs and system-load monitoring were used to ensure that the system was dedicated. While this approach provided estimates of speedup to within about $\pm 2\%$, it most likely underestimates the speedup since system applications also compete for CPU cycles.

Table II presents MCNP speedup for the 16 processor IBM RS/6000 cluster (based on MCNP version 4xe with PVM version 2.4.1). Ten test problems, representing a wide range in geometry and complexity, were chosen from the MCNP 25 problem test set for inclusion in this analysis. Execution times were made sufficient ($\sim$ 120 minutes) to eliminate any effect of the sequential problem initialization time (1-20 seconds). Figure 1 is a plot of the average speedup (of all ten problems) for saturated and standard communication (saturated being every 1000 particles and standard being the current MCNP default of 10 rendezvous during execution). The curve for saturated communication does indeed show that above 8 processors communication saturates the performance. On the other hand, the average speedup for standard communication increases linearly with the number of processors. Longer execution times result in a curve that approaches that of the theoretical limit.

IV. CONCLUSIONS

The PVM version of MCNP on a 16 processor IBM RS/6000 cluster produced speedups that approach the number of processors. Such speedup, in units of a single processor Cray Y-MP (see figure 1, right ordinate), leaves little doubt that MCNP performance on a workstation cluster can greatly surpass that of most supercomputers. Reliability and speed of the communication network are critical factors in exploiting such distributed memory systems. Of the links available on the LANL IBM cluster, the Ethernet and FDDI links proved most reliable (>95%).

REFERENCES:

1. Gregg W. McKinney, "Multiprocessing Monte Carlo Codes on Distributed and Common Memory Computer Systems," Ph.D. Thesis, University of Washington, May 1987.

2. Judi F. Briesmeister, Editor, "MCNP - A General Monte Carlo Code for Neutron and Photon Transport, Version 3A," LA–7396–M, Rev. 2, 1986, Los Alamos National Laboratory.

3. Adam Beguelin et al., "A Users' Guide to Parallel Virtual Machine," Oak Ridge National Laboratory, ORNL/TM-11826, July 1991."

TABLE I

COMPUTER SYSTEMS SUPPORTED BY PVM*

Architecture Mnemonic	Description	
AFXS	Alliant FX/S	
ALPHA	DEC Alpha	(OSF-1)
BAL	Sequent Balance	(DYNIX)
BFLY	BBN Butterfly TC2000	
BSD386	80386/486 Unix box	(BSDI)
CM2	Thinking Machines CM2	
CM5	Thinking Machines CM5	
CNVX	Convex C-series	
DGAV	Data General Aviion	
CRAY	C-90, YMP, Cray-2	(UNICOS)
CRAYSMP	Cray S-MP	
HP300	HP-9000 model 300	(HPUX)
HPPA	HP-9000 PA-RISC	
I860	Intel iPSC/860	
IPSC2	Intel iPSC/2 386 host	(SysV)
KSR1	Kendall Square KSR-1	(OSF-1)
NEXT	NeXT	
PGON	Intel Paragon	
PMAX	DECstation 3100, 5100	(Ultrix)
RS6K	IBM/RS6000	(AIX)
RT	IBM RT	
SGI	Silicon Graphics IRIS	
SUN3	Sun3	(SunOS)
SUN4	Sun 4, SPARCstation	
SYMM	Sequent Symmetry	
TITN	Stardent Titan	
UVAX	DEC MicroVAX	

*Listed in a preliminary release of PVM version 3.0.

TABLE II

MCNP SPEEDUP ON THE LANL 16 PROCESSOR IBM RS/6000 CLUSTER

Number of Processors	MCNP Test Problem										
	3	5	10	11	12	14	15	16	20	23	Average
	SATURATED COMMUNICATION										
2	2.0	1.9	1.9	1.9	1.8	1.9	1.9	1.9	2.0	1.9	1.9
4	3.7	3.5	3.5	3.3	2.9	3.6	3.7	3.5	3.7	3.6	3.5
8	6.5	6.1	5.7	5.3	4.0	6.6	6.8	6.3	6.6	6.1	6.0
12	9.0	7.8	7.3	6.7	4.3	8.7	9.0	8.2	9.1	7.8	7.8
16	10.2	9.5	7.7	7.0	3.6	7.6	9.3	8.4	9.9	7.5	8.1
	STANDARD COMMUNICATION										
2	2.0	2.0	2.0	2.0	2.0	2.0	2.0	2.0	2.0	2.0	2.0
4	3.9	3.9	3.8	3.8	3.7	3.9	3.9	3.9	3.9	3.9	3.9
8	7.7	7.5	7.2	7.2	6.5	7.7	7.7	7.6	7.5	7.4	7.4
12	11.2	10.6	10.1	10.1	8.9	11.2	11.3	11.0	10.9	10.7	10.6
16	14.3	13.4	12.6	12.4	10.8	14.3	14.5	13.8	13.6	13.5	13.3

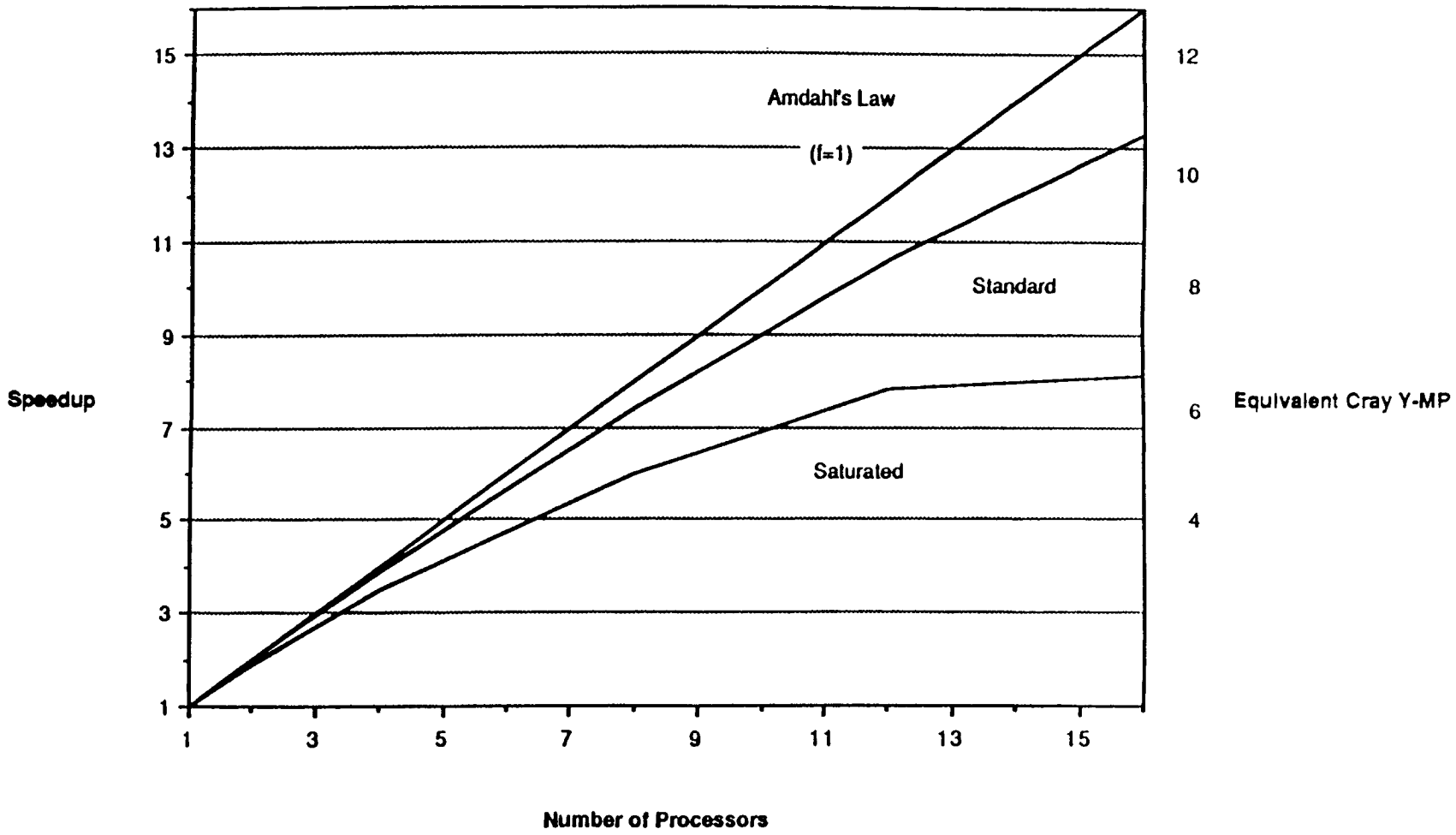

Fig. 1. MCNP Speedup on the LANL 16 Processor IBM RS/6000 Cluster.

Capability and Performance of Vectorized Monte Carlo Codes for Neutron and Photon Transport Calculations

Masayuki Nakagawa and Takamasa Mori
Japan Atomic Energy Research Institute,
Tokai Research Establishment
Tokai-mura, Naka-gun, Ibaraki-ken, 319-11, Japan

Abstract

Multigroup and continuous energy vectorized Monte Carlo codes have been developed for general purpose use in neutron and photon transport calculations. The vectorization algorithm is based on a stack-driven zone selection method. These can treat repeated rectangular and hexagonal lattices together with combinatorial geometry which are very useful to achieve a high gain by vectorization. The performance of the codes was evaluated by solving various type of problems with external and fission sources. The multigroup code was installed on other different vector supercomputers to investigate portability and computer dependence of performance. It was also tested on a computer with scalar massive parallel processors. The algorithm developed for a vector processor is efficient enough on a parallel computer.

1. Introduction

The recent supercomputers with vector processors save much computation cost by vectorization of conventional scalar codes. In the case of Monte Carlo codes, the conventional scalar codes use the history based algorithm, so they are impossible to be vectorized. We have to completely rewrite a program to achieve a high computational gain by vectorization. All the vectorized Monte Carlo codes adopted the event based algorithm, however, there are important differences in individual approach to the vectorization procedures that significantly affect the performance of the vectorized codes. In addition, a vectorization efficiency depends on the nature of the problem to be solved, such as geometry, batch size, importance and tally, and also on computer architecture. Furthermore, the point detector estimator and, neutron and photon coupled computation bring complexity in algorithm.

We have developed vectorized codes, GMVP and MVP, for multigroup and continuous energy calculations on the FACOM VP series computers. Those are general purpose codes used in calculations of neutron , photon and their coupling. The portability between different type computers are important to be used widely. We have demonstrated that the potability is good for those codes between different supercomputers.[1] Those codes are involved in the PRESTO Monte Carlo code system.

Vectorized codes can also run on scalar machine such as a large scalar machine, a workstation and a parallel machine. We are testing performance on a massive parallel computer AP-1000 which installs 512 processors at the most. The performance is satisfactory in some cases but there are some problems to be resolved in order to optimize various calculations.

2. Vectorization Algorithm

In order to vectorize a Monte Carlo simulation, we adopted the stack-driven zone selection method[2] which ia a variation of the event-based stack-driven algorithm. In this method, the simulation process consists of a source particle generation task and six other basic tasks as shown in Fig.1. Spatial tracking algorithm is similar for the multigroup and the continuous energy group models, however, the collision analysis and cross section handling routines are quite different.[3]The details of algorithms are described elsewhere.

One of the time consuming problems in the Monte Carlo calculations is a point detector estimator. If the number of detectors increase, the computation time roughly proportionally increases. This estimator is often used in calculations of shielding and some experimental analyses. To speedup computation of this estimator, we have developed a new vectorization algorithm.[4] It should note that many particles are traced simultaneously in the vectorized code, so many pseudo particles are generated in the collision task. Management of such particles is complex. An example of point detectors is shown in Fig.2 and Table 1. This example is an analysis of spectrum measurement leaked from a slab sample and five point estimators are used. The results by GMVP and MORSE-DD(a modified version of MORSE-CG) are compared. Both results show close variances while the number of particles are different due to the difference of algorithm. The total computation time by GMVP shown in the table is less by a factor of 57 compared with that by MORSE-DD. Hence, the present vectorization method is very efficient.

3. Main Capability of Codes

Most of functions for production use are implemented in the codes. The current capabilities of the GMVP and MVP codes are summarized as follows:

(1) Problem to be solved: external and eigenvalue problems of neutron and photon transport. GMVP can solve an adjoint problem.

(2) Description of geometry: combinatorial geometry with multiple rectangular and hexagonal lattices. Even reactor cores with complex geometry can be easily modeled by this lattice geometry. As boundary conditions, vacuum, perfect and white reflections can be treated.

(3) Variance reduction techniques: Russian roulette kill and splitting based on cell importance and weight window.

(4) Estimator: track length, collision, point and neutron balance(k_{eff} problem)

(5) CGVIEW: a color display code of input geometry, which is interactively used on a workstation. It can show input data errors such as lost particles.

(6) LICEM: a library generation code for MVP from ENDF/B and JENDL.

4. Validation Tests

(1) Fuel Assembly of Fast Reactor[5]

A model fuel is composed of fuel, cladding, calandria, tube and sodium as shown in Fig.3. A reflective boundary condition is imposed. This geometry is simply presented by using hexagonal lattice geometry. The results are shown in Table 2 for the lattices which include 19 pins or 91 pins. The values of k_{eff} are different between the two problems because the relative compositions of a calandria tube and sodium to fuel are different. To confirm the accuracy, the values obtained by the collision probability method code are also shown. In

these calculations, an isotropic or a reflective boundary condition was imposed. The results by GMVP agree well with those by the C.P. method. The vectorization efficiency is 24 and 21.5 with lattice and non-lattice geometries, respectively. The computation time of the former is smaller by a factor of 2 than the latter. It should be noted that the lattice geometry can reduce computation time.

(2) Deep Penetration through 3 m Thick Iron Slab[6]

A benchmark calculation for a deep penetration problem of 14 MeV neutrons through a 3 m thick iron slab was carried out by using MVP with JENDL-3 and ENDF/B-IV cross sections. To validate MVP and its cross section library, comparison was made with MCNP. Excellent agreement is obtained between both results. Beyond 1 m depth, the statistical error of the MCNP results are very large compared with the MVP ones though the former consumed 5 times longer computation time than the latter. Computation speed of MVP is higher by a factor of 20 compared with that by MCNP. The high speed calculation due to vectorization is essential to obtain a reliable solution of such a deep penetration problem. It should be noted that the multigroup calculations with 295- and 125-group libraries underestimate the streaming effect through the cross section windows, which results in the underestimation of fluxes above 24 keV by more than two decades at 3 m penetration as shown in Fig.4. When we take into account the spatial dependence of effective cross sections, the underestimation was reduced to about one decade.

(3) Dose Equivalent of Human Phantom

Dose equivalent of human phantom was calculated using a point photon source to validate photon transport and geometry capability. This model as shown in Fig.5 which is drawn by the CGVIEW code is rather complex and weak for a vectorized code because the vector length is generally short. However, the computation speed is higher more than a factor of 20 compared with MORSE-CG.

(4) Whole Core Calculation of a Commercial Size PWR[7]

Reactor cores consist of nearly identical fuel assemblies and fuel pin cells. It makes possible to describe a whole core by defining only once the cells that appears repeatedly appeared in geometry. The capability to treat multiple lattice geometry (lattice-in-lattice geometry) can significantly reduce an amount of work required in geometry data preparation. To demonstrate this capability, we calculated neutronics parameters (criticality, control rod worth, assembly and pin powers) of a commercial size PWR (1160 MWe). The core involves more than 50,000 fuel pins and control rod channels. It was precisely represented using a pin-by-pin model as shown in Fig.6. We used both multigroup and the continuous energy codes. Computation of one million histories takes 14 min on the FACOM VP-2600 computer and the vectorization efficiency (ratio of cpu times by scalar and vector) is 12 - 14. The achieved variances are 0.03% for criticality, 4% for 12 control rods worth, a few % for assembly power and 10% for pin power. To satisfy a few percent accuracy for pin power which is a design target accuracy, a few tens million neutrons should be tracked. From this calculations, we can conclude that some neutronics parameters can be practically calculated within required design accuracy while further speedup is desired to obtain pin power within a few percent accuracy. The Monte Carlo method would provide a powerful tool in a detailed design stage of a reactor core in near future.

5. Parallel Computation on Massive Parallel Computer

Other way to speedup the Monte Carlo calculations is to use parallel processing. A vector-parallel supercomputer is progressively used around the world. The present vectorized codes are easily installed on such a computer and will show speedup proportional to the number of processors when the number is not so large. We are installing the codes on the JAERI MONTE4 vector-parallel machine.

In the case of massive parallel computers, further investigation would be necessary to increase the parallel efficiency. We are investigating the parallel algorithm using a massive parallel computer AP-1000 which is a MIMD type machine. This computer has 512 processors and three types of networks. Each processor cell has 16 MB memories.

We have developed the Monte Carlo codes for vector processors based on the event-based algorithm as described above, and those codes can run on scalar processors, of course. Furthermore, those often show better performance than conventional scalar codes even on scalar machines. It is easy to implement these codes on AP-1000. Minor modifications are necessary to transfer data from host to each cell and vice versa, and random number generator, time account to measure the parallel efficiency. Our method is slightly different between an external source and an eigenvalue problems.

The efficiency of a sample problem is shown in Fig.7. This is the problem 2(a fast critical assembly) used in the NEACRP 3-D transport code benchmarks[8]. Speedup factors vs. the number of processors obtained by the parallel GMVP is plotted in the figure. The speedup factors are proportional to the number of processors up to 128 processors and gradually decrease with increase of the number of processors. When 512 processors are used, the speedup factor is 360, so the efficiency is about 70 % in this case. The difference between total and random walk corresponds to the time consumed in data transfer. When the number of processors increases beyond several hundreds, the batch size becomes too small and hence the efficiency drops. It is necessary to evaluate the procedure to determine a batch size and the number of batch. It is interesting that the total cpu time with 512 processors is about 70% compared with that by the FACOM VP-2600. A drawback of the present AP-1000 is lack of core memory for the continuous energy calculation. If a problem need many nuclide, the required core memory is beyond the present total one, so practical problems could not be solved on this machine.

References

(1) M. Nakagawa T. Mori, M. Sasaki: Prog. Nucl. Energy, 24, 183(1990)
(2) *idem*: Nucl. Sci. Eng., 107, 58(1991)
(3) T. Mori, M. Nakagawa, M. Sasaki: J. Nucl. Sci. Technol., 29, 325(1992)
(4) *idem*: *ibid*, 29, 1224(1992)
(5) M. Nakagawa, T. Mori, M. Sasaki: Ann. Nuclear Energy, 18, 467(1991)
(6) T. Mori, M. Nakagawa: J. Nucl. Sci. Technol., 29, 1061(1992)
(7) M. Nakagawa, T. Mori: to appear in J. Nucl. Sci. Technol. 30(1993)
(8) T. Takeda, H. Ikeda: "3-D Neutron Transport Benchmarks", NEACRP-L-330(1991)

Table 1 Comparison of performance between GMVP and MORSE-DD (case of five point detectors corresponding to results in Fig. 2)

	GMVP	MORSE-DD
Particle/batch	10,000	10,000
Batches	100	39
CPU time (min)	1	57
Vectorization (%)	98.8	—
CPU ratio (scalar/vector)	25.4	—

On FACOM VP-2600 vector supercomputer

Table 2. Hexagonal Lattice Problems'

Number of fuel pins	19 (3 layers)		91 (6 layers)
	Lattice	Non lattice	
Monte Carlo method			
k_{eff}	1.2815	1.2817	1.3493
FSD(%)[b]	±0.048	±0.052	±0.042
Scalar/vector	23.9	20.5	24.1
CPU time(s)[c]	245	469	216
Collision probability method			
k_{eff}	1.2814		1.3489
CPU time(s)	264		503

[a] batch size = 10 000 particle/batch.
total number of batches = 17.
The calculations were carried out on the FACOM VP-2600 supercomputer.
[b] fractional standard deviation(%).
[c] computation time (in second) for 170 000 particles.

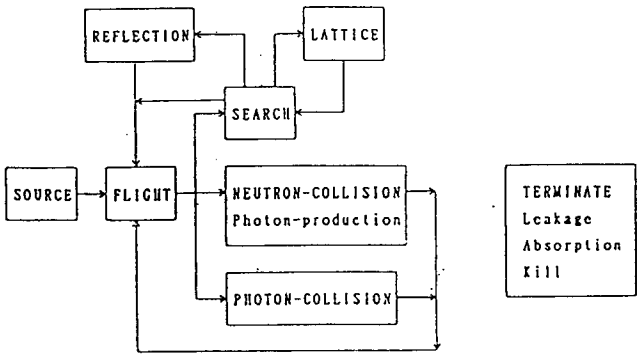

Fig.1 Tasks of vectorized Monte Carlo code

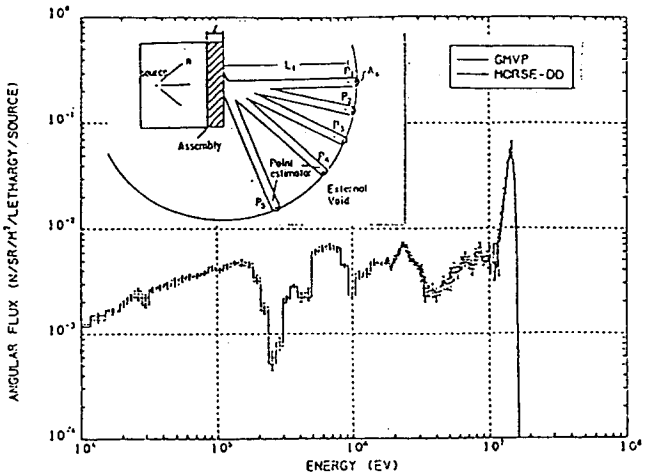

Fig.2 Neutron spectrum calculation
by using 5 point detector estimators

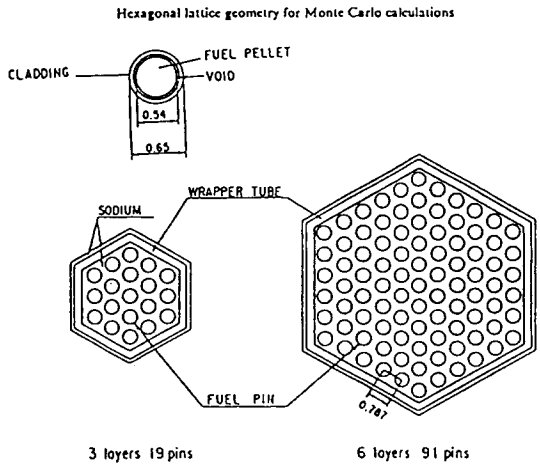

Fig.3 Calculation models of hexagonal
fuel assemblies

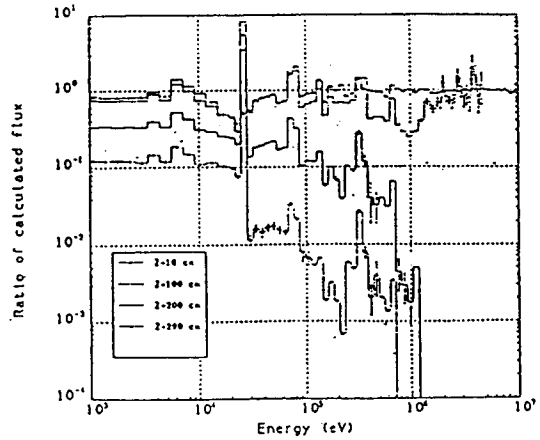

Fig.4 Ratios of neutron spectra calculated by MVP and multigroup method with 125-group library(multigroup/continuous energy)

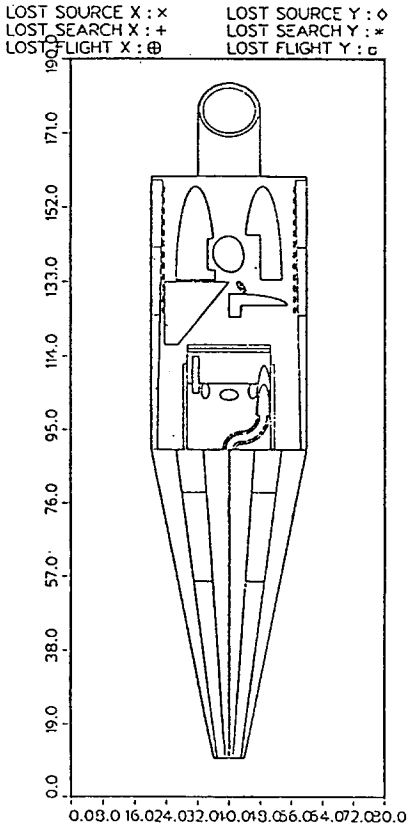

Fig.5 Calculation model of human phantom

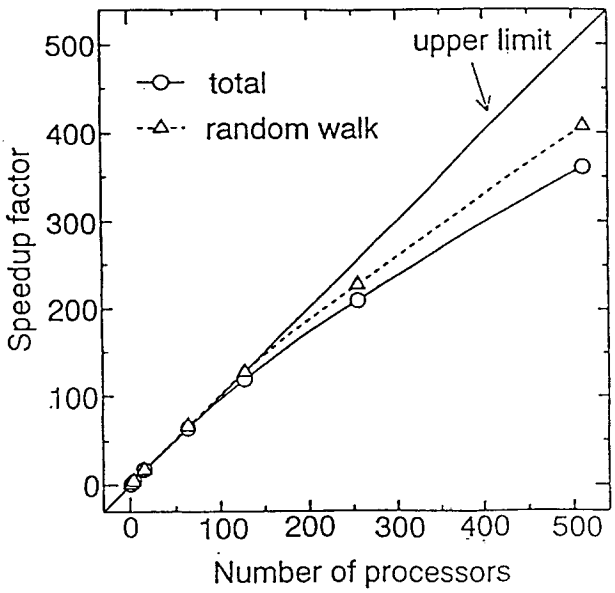

Fig.7 Speedup vs. the number of processors on a massive parallel computer

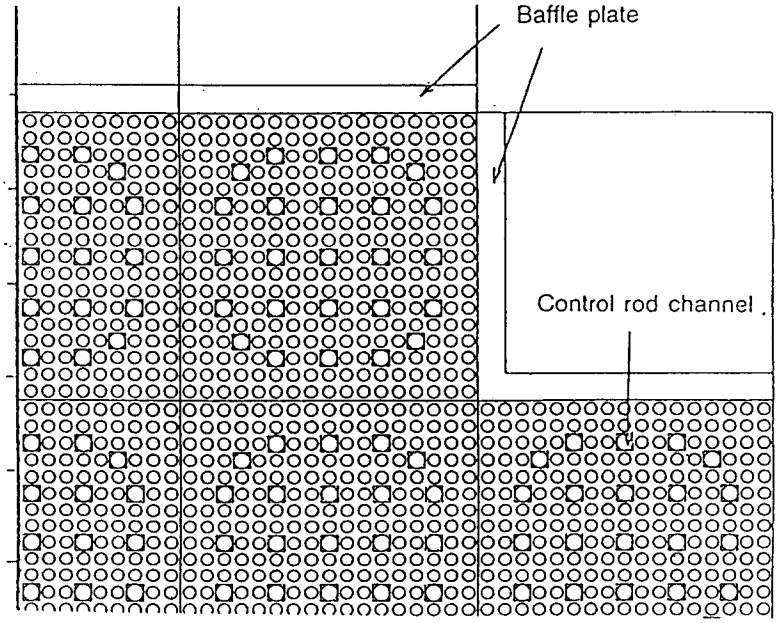

Fig.6 Calculation model of whole core of PWR

A Communication Library for TRIPOLI-4

J.P.Both
Commissariat à l'Énergie Atomique
C.E.N Saclay, DRN/DMT/SERMA

April 26, 1993

Abstract

In writing a new version of the TRIPOLI code we considered the need of taking advantage of new parallel computers. Monte-Carlo code is naturally event-driven so we choose a message-passing scheme. This paper describes a message-passing library, its interface, its implementation on a workstation network and on a shared memory model. We present small tests with 2 , 5 and 8 tasks.

1 Description of the message-passing library

The langage used for this library is C++, so the basic entities of the library are classes. One major requirement for the library was that the user's interface should be independant of the underlying architecture. To achieve this goal, we heavily relied on the inheritance mechanism of the language. We first implemented a small kernel defining a user interface and containing the code which is independant of any particular implementation (for example message definition can be done at this level). For classes dependant of a particular implementation (such as the class defining what is a task in the application), we redefined a new class inheriting from the lower level class. The inheritance mechanism of the language then dispatches a user call done at lower level to the correct level in the class hierarchy corresponding to a given implementation.

1.1 Classes

The classes of the library accessible to the user are the following :

- IPC_message
  This class is the basic unit of transmission between tasks. It is common to all implementations.
- IPC_mailbox
  This class is also implementation-independant. It provides a way of buffering messages on emission and after reception.

The following classes are implementation-dependant :

- IPC_process
  This class corresponds to the basic unit of processing. It contains all user level communication primitives. This class is inherited by classes specializing the notion of unit of computation in each implementation.

- IPC_monitor
  This class is derived from class IPC_process. It implements the task which initialize the graph of communication between slave tasks and maintains traffic statistics.

1.1.1 class IPC_message

From the user's point of view, a message is composed from an arbitrary list of all basic types (long , float , char ...) or array of values of basic types. All methods to compose a message are overloaded , that is they have the same name. For example we can write successively : `msg.put(3.14)`, `msg.put("Hello")` and `msg.put(tab,len)`, to compose a message containing 3.14, the string Hello and an array len values, whatever the common type of these values is.
In the same way to decode such a method we would code: `msg.get(int_val)`, `msg.get(string_val,length)` and `msg.get(tab,length)`.
Space to hold the strings and array are allocated by the library and the user is given their length in the last argument of `get` method. In fact the library encodes in the message the format at emission so that the receiver cannot decode a value of a given type into another type.

Messages can be given a key which can be a string , an integer or a character so that messages can be retreived in a mailbox from a given value of a key and not from their arrival order.

1.1.2 class IPC_mailbox

Methods accessible by users are just methods to get and store messages. Users can ask for the first message, the first message with a given key and the last message. We add a message by writing `mailbox.add(message)`. We can also ask the number of messages present in the mailbox. This is quite simple but very useful to avoid deadlock in sending messages. In fact library uses it internally to implement non-blocking send.

1.1.3 class IPC_process

From the user's point of view a process is identified by a name, and a command name if the process correspond to a unix process as in the cluster of workstation case. This is a stub class giving users access to communication primitives. Each class IPC_process posseses a class IPC_mailbox, the utility of which will be seen later. User's methods are:

- `get_nb_msg_in_mailbox`
- `IPC_msg* get_first_msg_in_mailbox()`
- `IPC_msg* get_first_msg_by_key(const IPC_msg_key &key)`

- `sendmsg(char *dest, IPC_msg &message)`
  This method is non blocking. In fact the library stores the message in a mailbox associated to the communication channel the message will go through. Depending on user's application the message will be automatically sent by the library or the user can take all the responsability to control when a message is really sent by using the following method.

- `flush_msg()`
  This method really sends all messages waiting to be sent in emission mailbox.

- `recvmsg(char *from, IPC_msg &message)`
  This is a blocking method to wait for a message from a given task.

- `poll(int timeout)`
  This method is used to implement asynchronous reception of message and multiplexing. It waits during timeout seconds for a message and returns. User can then scan the mailbox attached to the process.

In fact default initialization of the library is to install a polling class (highly implementation-dependant) in each class inheriting from class IPC_process. Calls to the polling method of class IPC_process are forwarded to the polling class of the correct implementation. Upon reception of a message, a service associated to the communication channel by which the message arrived is automatically called by the library. The default service installed is to store the message in the process mailbox. It must be noted that an intermediate level accessible to users allows them to install the service of their choice on each communication channel.

1.1.4 class IPC_monitor

This process is the manager of the tasks launched. It reads a file describing the collection of tasks to be launched, the graph of communications to be setup, installs tasks and performs all functions ensuring that the network of tasks is well initialized. It collects statistics such as number of messages going from and to tasks as well as idle time of each tasks. It also detects the end of global computation and tells tasks when to exit.

It offers some methods to users.

2 Implementation

Two implementations of the library are now available. The first, on a network of workstation. This implementation correspond to distributed memory paradigm with explicit message-passing such as in CM5, Ncube ... In this case we used TLI (Transport Level Interface).

The second implementation is on top of the multithreading primitives defined by POSIX 1003.4 drafts, an implementation of which was given to us in a beta-version by SUN Microsystems. This implementation corresponds to shared-

memory machines such as Kendall Square Research machines [6] or SUN multiprocessors.

2.1 workstation network case

Details are too technical to be reported here. Let us just mention that we chose the TCP protocol because of its message delivery reliabiblity. The counterpart of this choice is that when sending a message, we must check if transport is ready to accept bytes to be sent in order to avoid deadlock. If not, emission of message is delayed. Besides this problem, TLI just offers us the necessary sending, receiving and polling primitives.

2.2 multithreading case

There is no difference in the user's interface except if the user wants fine tuning on the polling stategy which requires to go into the intermediate level of the library. The main multithreading primitives provide the following functionalities : acquire (and release) a lock, signalling an event, waiting an event. The basic idea is that when a process A wants to send a message to a process B it must acquire a lock granting him exclusive access to the mailbox of process B and signal the event to wake up B in case B was waiting for an event.

3 Application

We used the library on a tiny Monte-Carlo program to evaluate some domain partitioning strategy. The problem is one-dimensional and monokinetic. It just consists in simulating a random walk with exponential flight on a slab with a reflection condition on the left and leakage condition on the right. The slab is 40 cm wide. Source particles start at left of the slab with direction towards the right. In all these tests, source particles were sent by the monitor. We made variations on the following parameters:

- the number of processes used to partition the slab and the overlap between the domain covered by each process.
- probabilities of going to the right or to the left.
- the number of calls to the logarithm function made at each collision. Variation of this number gives this test a cpu consumption nearer a real Monte-Carlo game. Its variation corresponds also to a modification of the ratio *cpu performance / communication performance.*

The comparison of performance were made with a monoprocessor version of the test. We did tests with 2 , 5 and 8 slave tasks.

3.1 tests with 2 slave tasks

3.1.1 test 1

Collision was isotropic. The mean free path of particles is chosen to 1. The time of the serial program was 453 s for 5000 particles.

process	domain	cpu time	idle time	nb msg sent	nb msg received
slab1	[0-25]	179	53	11000	11000
slab2	[15-40]	144	134	6000	11000

Total time (including system time) for this configuration was 5mn 20s giving a speedup of 1.43.

3.1.2 test 2

We have now a probability 0.55 of going to the right (and so 0.45 to the left). The time of the serial program was 255 s.

process	domain	cpu time	idle time	nb msg sent	nb msg received
slab1	[0-25]	66	51	5800	5800
slab2	[15-40]	80	74	1800	5800

Total time (including system time) for this configuration was 2mn 50s giving a speedup of 1.5.

3.1.3 test 3

This test is the same test as the preceding but with a loop of 100 logarithms at each collision. The time of the serial program was 35 mn.

process	domain	cpu time	idle time	nb msg sent	nb msg received
slab1	[0-25]	634	358	5800	5800
slab2	[15-40]	865	170	1800	5800

Total time (including system time) for this configuration was 17mn 50s giving a speedup of nearly 2.

3.2 tests with 5 slave tasks

In all these tests, the probability of going to the right was 0.55. The mean free path of particles was set to 0.5.

3.2.1 test 1

The first test was made with a loop of 100 logarithms at each collision and 8000 particles. The time of the serial test program was 526 s for 1000 particles.

process	domain	cpu time	idle time	nb msg sent	nb msg received
slab1	[0-6]	527	459	17890	9890
slab2	[4-8]	654	398	27616	27616
slab3	[10-22]	991	54	27311	27616
slab4	[20-32]	970	67	25526	25526
slab5	[30-40]	517	562	7941	15941

Total time (including system time) for this configuration was 18 mn, thus giving a speedup of nearly 3.9. About 105.000 messages have been sent (or received).

3.2.2 test 2

This test was made with a loop of 1000 logarithms at each collision and 2000 particles. The time of the serial test program was 530 s for 100 particles.

process	domain	cpu time	idle time	nb msg sent	nb msg received
slab1	[0-6]	1155	981	4541	2541
slab2	[4-8]	1366	887	7058	7058
slab3	[10-22]	2185	69	7057	7057
slab4	[20-32]	2079	184	6523	6523
slab5	[30-40]	1105	1177	1983	3983

Total time (including system time) for this configuration was 38 mn thus giving a speedup of about 4.6 and so despite the bad balance of work between tasks. About 27.000 messages have been sent (or received).

3.3 tests with 8 tasks

In all these tests we kept the probability to go to the right to 0.55. The mean free flight of particles was set to 0.5.

3.3.1 test 1

The first test was made with a loop of 100 logarithms at each collision and 8000 particles. The time of the serial test program was 526 s for 1000 particles.

process	domain	cpu time	idle time	nb msg sent	nb msg received
slab1	[0-5]	486	252	24531	16531
slab2	[4-9]	542	156	40956	40956
slab3	[8-13]		214	40923	40923
slab4	[12-18]	621	152	40626	40626
slab5	[17-24]	650	99	33450	33450
slab6	[22-28]	454	340	26243	26243
slab7	[26-34]	583	206	23775	23775
slab8	[32-40]	362	479	6854	14854

Total time (including system time) for this configuration was 14 mn thus giving a speedup of 5. About 240.000 messages have been sent (or received).

3.3.2 test 2

This test was made with a loop of 1000 logarithms at each collision and 2000 particles. The time of the serial test program was 530 s for 100 particles.

process	domain	cpu time	idle time	nb msg sent	nb msg received
slab1	[0-5]	1031	383	6242	4242
slab2	[4-9]	955	563	10337	10337
slab3	[8-13]	957	573	10233	10233
slab4	[12-18]	1147	380	10093	10093
slab5	[17-24]	1238	284	8348	8348
slab6	[22-28]	881	633	6678	6678
slab7	[26-34]	1188	334	6054	6054
slab8	[32-40]	769	772	1769	3769

Total time (including system time) for this configuration was 25 mn 30s thus giving a speedup of nearly 6.9. About 60.000 messages have been sent (or received).

3.4 Commentary

In all these tests a satisfactoy speed up is obtained only if we launch a sufficiently large number of particles. This is necessary to minimize the influence of the time at the beginning of the simulation where particles are only near the source, and the time at the end of the simulation when only a few particles are wandering from one process to another before leaving. The tests with 2 tasks show the dramatic impact of biasing on communication. Tests with 5 or 8 tasks show that a good efficiency is maintained so long as the number of messages per unit of cpu time is below 10. It must be emphasized that this depend on the relative performance of the processor versus the communication efficiency. The challenge of such an approach is to have a code such that its behaviour does not depend too much on the characteristics of the machine on which it runs. So the code should have a special run to sample the characteristics of the underlying machine on which it runs and adapt to it.

4 impact on tripoli-4 conception

4.1 data locality versus parallelization efficiency

We want Tripoli to run with both ponctual cross sections and multigroup cross sections associated with probability tables. Zhong showed [1] that about 4000 groups are necessary to achieve a reference calculation. On the other hand we have spatial ponderation data associated to a mesh. Moreover we are considering [2] the possibility to have energetic ponderation data associated to this mesh. This can get us well above 20 Mega-words.

Despite statistical traps to avoid [4], it is clear that the best efficiency in parallelization should be obtained in following particles independantly on each processor. This leads each processor to access data (cross section and ponderation data) corresponding to all phase space in a way difficult to foresee. On a distributed memory machine, this would generate a lot of traffic or lead to storing in memory of each processor the totality of data. On a machine with not so much memory, this is a potential problem. On a virtual shared memory machine [6] there seems to be no more problem, because all processors can access the data. But looking closer, particles going down in energy in a random fashion

the same page of data would migrate between processors or get duplicated. So it seems difficult to completely overlook the problem of locality of data.

4.2 development prospects for TRIPOLI4

The solution we are considering in TRIPOLI4 is a hybrid solution. Each task will receive the phase space part it will treat, thus partitioning data between processors. When it is possible each task will receive the totality of the problem. Due to ovelapping all intermediate situations between partition and replication are possible. The partitioning will be primarily spatial for many reasons:

- A slight variation of the probability collision method used to initialize the ponderation data [2] could give us valuable information on how to partition space between tasks to get a good load balance. In fact the load balance problem and the ponderation problem are quite similar.
- The use of overlap between energetic zones is less useful than between spatial zones. In fact, during the life of a particle, it rarely goes up in energy except for fission events and thermal diffusion.
- Our collision biasing scheme requires to have in memory all total cross sections of nuclides present a given space point thus leading naturally to a space partitioning.
- Our main storage requirements could come from ponderation data, and in this respect spatial partitioning is efficient even in a one group ponderation mesh.

A dispatcher of particles, corresponding to the source of the problem, should route particles according to their birth position. In the case where each process receives the totality of the problem to treat the dispatcher should be able to do distribute fairly particles among tasks. Statistics will be maintained locally and merged at the end of the calculation.

5 Conclusion

We have described a message passing library implemented over both paradigms, distributed memory and shared memory. Small tests showed that partitioning of space is worth of consideration. A good efficiency and relative scalability have been achieved provided the number of messages per unit of cpu time remains bounded. Prospects of developments in TRIPOLI4 have been given.

References

[1] S. Hui. *In this conference.*

[2] B. Morillon. *Thesis to appear and in this conference.*

[3] G.R Andrews. *Paradigms for process interaction in distributed programs.* ACM Computing Surveys, Vol. 23,No 1,March 1991

[4] P. Heidelberger. *Discrete event simulations and parallel processing: satistical properties.* SIAM J. Stat. Comput. Vol. 9, No 6, Nov 1988

[5] H.E Bal, J.G. Steiner and A.S. Tanenbaum. *Programming languages for distributed computing systems.* ACM Computing Surveys, Vol. 21,No 3,March 1991

[6] Kendall Square Research *Technical summary.*

MONTE CARLO CALCULATIONS ON A PARALLEL COMPUTER USING MORSE-C.G.

J Wood
Queen Mary and Westfield College,
University of London
London E1 4NS
UK

ABSTRACT

The general purpose particle transport Monte Carlo code, MORSE-C.G., is implemented on a parallel computing transputer-based system having MIMD architecture. Example problems are solved which are representative of the 3-principal types of problem that can be solved by the original serial code, namely, fixed source, eigenvalue (k-eff) and time-dependent. The results from the parallelised version of the code are compared in tables with the serial code run on a mainframe serial computer, and with an independent, deterministic transport code. The performance of the parallel computer as the number of processors is varied is shown graphically. For the parallel strategy used, the loss of efficiency as the number of processors is increased, is investigated.

INTRODUCTION

The Monte Carlo method is an important computational tool in the field of radiation transport. In essence, it consists of following the particles from 'birth' to 'death', in a simulated random walk through the problem geometry, and by random sampling from the probability distribution functions that are considered to represent the collision physics of the particles' interactions with the media. In many practical applications, the Monte Carlo technique is the only feasible means of solving problems characterised by complicated geometry and/or complicated interaction probabilities. It is also of value in providing an independent validation of results obtained from transport codes based on deterministic methods. Due to the stochastic nature of Monte Carlo, there is an inherent degree of statistical uncertainty associated with the results, and in serious applications a large number of particles (many thousands) must be followed in order to obtain statistically meaningful results. Therefore, the main disadvantage of Monte Carlo is the large amount of computing time required, even on the most powerful serial computers, to follow the large number of particles necessary to obtain acceptable statistical uncertainties on the computed averages, even when variance reduction techniques are in operation [1].

With the computer execution time as the principal disadvantage of Monte Carlo, it is natural to consider using the multi-processing capabilities of parallel computers to speedup Monte Carlo calculations. Cursory consideration of particle transport Monte Carlo indicates it has a substantial parallel content, since the life-history of each particle can be followed independently, and it is therefore, on the face of it, a numerical technique particularly well-suited to parallel implementation. Thus parallel computers, such as the transputer-based Meiko Computing surface, would appear, in principle, to have enormous potential for such computations, since each of the many processors can be employed simultaneously to run an independent sequence of events.

A review of the status in developing and implementing particle transport Monte Carlo methods on advanced computer architectures can be found in [2,3]. In this paper we consider the implementation of the general purpose Monte Carlo code, MORSE-C.G., on a parallel computer having MIMD architecture. In order to validate the parallel strategies employed, a number of example problems are solved, and the results from the parallelised code are compared with the original serial code, and from an independent, deterministic code using the identical nuclear cross-section data. The CPU times on the parallel and two serial computers for equivalent computations are compared. The performances obtained from running the parallelised code when the number of transputers is varied are shown graphically. A modification to Amdahl's law for highly parallel computations is suggested. Finally, conclusions are made regarding the potential of the Meiko Computing Surface for radiation transport computations by the Monte Carlo method.

PARALLEL COMPUTER ARCHITECTURES

Computer systems may be classified according to how the machine conveys its instructions to the data being processed. Three practical classes can be identified, according to whether the instruction or data streams are single or multiple [4,5]. These are:

(i) SISD: Single Instruction, Single Data
(ii) SIMD: Single Instruction, Multiple Data
(iii) MIMD: Multiple Instruction, Multiple Data

Conventional (i.e. serial) computers have SISD architecture. Examples of machines with SIMD architectures are the CONNECTION machine [6] and the AMT-DAP [7,8]. These are usually referred to as massively parallel machines (greater than 1000 processors) and are classified as SIMD because all the processors operate synchroneously, obeying an identical instruction with different data stored locally. An important class of computer is the vector processor. There is some ambiguity as to where to place it in the above simple classification, but it is usually referred to as SIMD-vector or MIMD-vector depending on whether it has single or multiple processors. Examples are the CRAY X-MP and the CONVEX-C3840. Vector computers exploit "pipelining" to achieve speedup over corresponding scalar operation. An example of a machine which has MIMD architecture is the transputer based Meiko Computing Surface [9]. It is classified as MIMD because the processors can operate independently, obeying different instructions with different data stored locally. In this paper, it is with this machine that we are concerned.

BRIEF DESCRIPTION OF THE MEIKO COMPUTING SURFACE

The Meiko Computing Surface is a multiprocessor system based on transputers. The transputer [5] is a generic name used to describe a family of programmable VLSI devices of essentially similar design. Each is a complete computing unit consisting of processor, memory and communication links, all on a single chip. The member of the family most commonly used at present is the T800 transputer which was the first to include hardware support for floating-point arithmetic [10]. The T800 transputer is a single chip containing a 32 bit integer arithmetic processor unit, a 64 bit floating-point co-processor unit, with up to 32 Mbytes of memory, and four serial communication links with a performance of up to 20 Mbit/s. The T800 processor we utilise has a clock speed of 20 MHz. It has an integer arithmetic performance of 5 VAX MIPS and a floating-point arithmetic performance of 1 MFLOP (double precision) and 1.5 MFLOP (single precision).

To run on transputers, application programs can be written in OCCAM, FORTRAN and C. Initially, the Meiko Computing Surface necessitated the use of OCCAM and the OCCAM programming system (OPS). However, an advanced parallel programming system, called Meiko CSTools [11], based on the use of standard FORTRAN and C, which does not require the user to have a knowledge of OCCAM, has been developed. We use the parallel programming environment Meiko CSTools to effect parallel computation.

The Communicating Sequential Tools (CSTools) is a program development toolset for multiprocessor computer systems. It supports the programming of single and multiprocessor applications using familiar development environments and standard languages, namely, C and FORTRAN. In CSTools the communication between different processors is provided by system library calls (a set of message-passing library routines) which are included in and called from application programs written in FORTRAN or C. Interprocessor communication and synchronisation takes place through system-global message ports. Several program configuration systems are available within the CSTools package. The most straightforward is the parfile loader. This utility program reads a simple test file (filename.par), prepared by the programmer, which states which processes are involved in the computation, and on which particular processor they are to be executed.

PARALLEL ALGORITHMS

The main objective of implementing a program on a parallel machine is, of course, to speedup the calculations. Cost considerations may also be important, but these will not be discussed here. The basic idea behind parallel processing is that if an algorithm can be divided among m independent processes running on n processors, it should run n times as fast as the same algorithm running on a single processor of similar type. For many reasons, the actual speedup achieved is often smaller than this ideal. The speedup depends on the particular machine used, and also on the amount of concurrency that can be extracted from the particular application: it significantly depends on the data transfer rate between the processors and the amount of communication between the processors. Thus, for an efficient algorithm on a distributed memory multiprocessor parallel machine, a number of guidelines must be observed, of which the two most important are: (i) the processors must be kept as busy as possible doing useful work, and (ii) the amount of data transfer between processors must be minimised.

THE TRANSPUTER VERSION OF THE MONTE CARLO CODE

Three common broad strategies of parallelism may be considered in modelling physical systems on MIMD computers, namely, processor farm, geometric parallelism, and algorithmic parallelism [5]. The form of parallelism we use in porting the code to run efficiently on the transputers is the processor farm strategy, which may be considered as the simplest form of parallelism, in which each processor executes the same program independently from all the other processors, each operating on a different part of the total data.

The processor farm strategy employs one control processor - the master, and various worker processors - the slaves. The particular configuration in which the slaves are connected to the master is not important to the particular application in the sense of determining the feasibility of the algorithm, since every slave can provide the same services, i.e. render the same jobs, to the master; this is the principal reason why the processor farm strategy is so simple and effective to use. However, the system configuration chosen may have a significant effect on the efficiency of the system, if a large amount of data transfer is required between the processors and/or the system contains a large number of processors, due to the increase in communication path-length. The CSTools environment readily allows the user to choose a variety of connecting arrangements, for example, binary-tree, ternary-tree or pipeline. We use the binary-tree configuration.

In our implementation of MORSE-C.G. on the transputers, the relationship between the master and the slaves (or farmer and workers) can be summarised as follows:-

(i) The master reads in the basic data for the problem, processors it, and passes it down to the slaves.

(ii) The slaves independently carry out their share of the particle tracking calculations, and the results are passed back up to the master from the slaves.

(iii) In the master, the results from the slaves are combined, processed, and then printed out.

There are two principal components of the parallel code: the master code and the slave code. In particular, the identical code is loaded onto and executed by all the slaves. Only the master communicates with the outside world.
In our implementation we observe the maxim, that whatever the code can do in serial, it can do in parallel.
It is obvious from the above description that the master processor, after sending the data to the slaves, would be idle while waiting until they completed their calculations. To avoid this, we execute the same program on the master as on the slaves, in order to use it as an additional processor after it has sent the data to the other processors; for this reason, it is called the master/slave processor. An equal number of particles are followed on the master and each of the slaves. We therefore rely on the natural load-balancing property of Monte Carlo, that is the fluctuations in the path-lengths of individual particles will average out if a large number of particles is processed on each processor.

RANDOM NUMBERS

A significant amount of CPU time in particle transport Monte Carlo is spent computing the pseudorandom numbers that are essential to the method. Moreover, the quality of the random numbers used has an important influence on the accuracy of the results obtained. On the serial computers to which we refer later, the NAG library random number routine GO5CAF [12] is used. On the transputer system, the algorithm briefly described in the following section is used.

LEAPFROG METHOD

The linear congruential method is almost universally used for generating random number sequences on serial computers. It may be summarised as follows [13]:

$$x_i = (a\, x_{i-1} + c) \bmod m \qquad (1)$$

where

m,	the modulus ;	$m > 0$
a,	the multiplier ;	$0 < a < m$
c,	the increment ;	$0 < c < m$
x_o,	the starting value or 'seed'	$x_o > 0$

The pseudorandom numbers themselves (normalised to lie between 0 and 1) are generating by forming the squence ($\xi_i = x_i/m$). When suitable choices are made for the integer parameters, a, c, x_o, and m, an adequate sequence of random numbers is produced which has many of the desired statistical properties of truly random numbers.
The implementation of Monte Carlo methods on the Meiko Computing Surface requires a method for supplying appropriate portions of sequences such as (1) to each of the parallel processes in a timely and efficient manner. In addition to having suitable statistical properties within themselves, the individual parallel sequences must be independent of one another.
In this work, the leapfrog method suggested by Bowman and Robinson [14] is used to tackle the problem of random number generation in a parallel environment. This method, which is easily implemented, produces disjoint subsequences of the original pseudorandom number sequence in each of the parallel processors.
In the leapfrog method, for n parallel processors, the first n values from the sequence (1) are delivered as initial seeds to each of the processors, along with the 'jump' multiplier a_n and the jump increment c_n, defined by:

$$a_n = a^n \bmod m \qquad (2)$$

$$c_n = c\,(a^{n-1} + a^{n-2} + \ldots\ldots + 1) \bmod m \qquad (3)$$

Then each processor generates its own subsequence according to:

$$x_{i+n} = (a_n\, x_{i+n-1} + c_n) \bmod m \qquad (4)$$

Each subsequence consists of every nth member of the original sequence, starting in each processor at a different point. Only the starting information need by passed by the master to the slave processors.

SPEEDUP AND EFFICIENCY

In measuring the performance of a multiple processor system employing parallel algorithms, one often requires some measure of how fully the parallel algorithms utilise the potential of the parallel system and how much advantage, for example in CPU time, is gained over sequential algorithms. Hence, a relative factor relating the increase in

performance in a parallel system over a uniprocessor system is required. This factor is called speedup factor, S, and it is defined as the time required to solve a problem by a given sequential algorithm on a sequential machine (t_s), divided by the time required to solve the same problem by a parallel algorithm on a parallel machine (t_p). Thus, the parallelisation speedup factor is given by

$$S = t_s/t_p \quad . \qquad (5)$$

On an MIMD machine, another parameter of interest is the parallelisation efficiency, E, which is defined as

$$E = S/n \qquad (6)$$

where now $S = t_1/t_n$ (7)

and t_i is the time required to solve the same problem on i processors.

THE MONTE CARLO CODE, MORSE-C.G.

This is a multipurpose neutron and gamma-ray transport Monte Carlo code, written in FORTRAN, and intended for running on conventional computers. It was developed at Oak Ridge National Laboratory [15] and is in world-wide use. It has a number of notable features, such as a three-dimensional combinatorial geometry package (C.G.) to assist the user in defining the problem geometry, and the nuclear cross-section data input is in the multigroup format that has become standard for deterministic transport codes.

The code uses three parameters that have particular significance for us:

NSTRT - number of particles per batch
NITS - number of batches
NQUIT - number of 'outer' or 'time' iterations in time-dependent problems.

In multiplying systems, NITS has an important physical interpretation - it is the number of generations of neutrons coming from fissions, that are processed in the calculations.

DESCRIPTION OF EXAMPLE PROBLEMS

Four problems are solved:

1. Fixed Source
   The fast neutron flux at several radial distances is calculated for a point,isotropic, fission source in an infinite medium of air. This is the example problem 1 distributed with the serial source code from ORNL. 22 neutron groups/P_5 data.

2a. k-eff Calculation of the Critical 235 U Godiva Sphere (radius = 8.7407 cm)
   11 neutron groups/P_3 data, derived from the Jef1 Library [16,17].

2b. k-eff Calculation of the Critical 239 Pu Jezebel Sphere (radius = 6.66 cm)
   20 neutron groups/P_3 data, derived from the Jef1 Library.

3. Time-Dependent: Sub-critical 239 Pu Jezebel Sphere (radius = 5.71 cm).
   20 neutron groups/P_3 data, derived from the Jef1 Library.

NUMERICAL RESULTS AND DISCUSSION

The results from the serial and parallelised forms of MORSE-C.G. are compared (where possible) with those from the finite elements code, TRIPAC [18], using the identical nuclear cross-section data. The TRIPAC results are P_{11}/P_5 or P_{11}/P_3 and are taken as benchmarks.

Strictly speaking, the Convex-C3840, referred to later, is not a serial computer - it has vector capability. It ran the serial form of MORSE-C.G., but with the vector-switch on during compilation.

In the results tables (Tables 1 to 3), the estimated errors shown are the fractional standard deviations from MORSE-C.G., expressed as percentages. The actual errors are the fractional errors relative to the exact (TRIPAC) values shown in the tables, expressed as percentages.

RESULTS

Problem 1. Fixed Source

The total and uncollided neutron fluxes ($cm^{-2}s^{-1}$) at various distances from the point source are compared in Table 1. The source strength is 10^{10} particles per second. For 1- transputer, NSTRT = 100, NITS = 100, NQUIT = 1. Since the total number of particles processed is 25 times greater, we would expect the estimated errors for the 25-transputers to be approximately 1/5 that for 1-transputer.

Problems 2a and 2b. k-eff Calculations

The eigenvalues and reaction rates are compared in Tables 2a and 2b. The eigenfluxes are normalised to the sum of absorption and leakage rates equal to unity.

In Table 2a, for 1-transputer, NSTRT = 200, NITS = 100, NQUIT = 1. Again, we would expect the estimated errors for 25-transputers to be approximately 1/5 that for 1-transputer.

In Table 2b, for both the Convex and 10-transputers, NSTRT = 200, NITS = 1000, NQUIT = 1. Because in this example the same total number of particles are processed in both machines, we would expect the estimated errors from both forms of the code to be approximately the same.

Problem 3. Time-Dependent Fission Problem

The various time-dependent reaction rates from the parallelised code are shown in Figure 1.

In time-dependent mode, MORSE-C.G. also gives an estimate of the k-eff for the system. The serial and parallelised code values are compared in Table 3. For both the Convex and the 10-transputers, NSTRT = 200, NITS = 80, NQUIT = 30. Again, we would expect the estimated errors from both forms of the code to be approximately the same.

PERFORMANCE OF THE PARALLEL COMPUTER

The speedups and efficiencies for the 3-principal types of problem solved by MORSE-C.G. are shown in Figures 2, 3 and 4. For a given problem, the total number of particles processed is the same, irrespective of the number of transputers. A comparison of CPU times for equivalent computation, for two serial computers and the transputers, is given in Table 4. Based on the data in this table, approximately 13-T800 transputers in parallel are equivalent to the computing power of the Convex-C3840 and approximately 3-T800 transputers equivalent to the DRS6000 ; that is for MORSE-C.G. computations.

LOSS OF EFFICIENCY WITH INCREASE IN NUMBER OF PROCESSORS

It is clear from Figures 2, 3 and 4 that if the number of processors, i.e. transputers is increased beyond, say, 20 or 30, the efficiency of the system, for the problems we have considered, falls below 90% (which might be considered an acceptable level). In the simple strategy which we employ, there are two obvious areas of the computation that require detailed timing investigation:

(i) The time taken by the master to broadcast the processed initial data to the slaves.

(ii) The time the master "waits", after it has finished its share of the particle processing until it finishes receiving the results back from each of the slaves.

These times are shown in Table 5 as a percentage of the total CPU time, when different numbers of transputers are used (for the same total amount of particles processed in each problem). This table shows clearly that, as the communication path-lengths increase, and the individual processor's share of the total number of particles processed continues to decrease, the time "wasted" in steps (i) and (ii) above, becomes a greater proportion of the total computing time.

AMDAHL'S LAW

An early attempt to predict, theoretically, the behaviour of the speed-up curve, such as those shown in Figures 2, 3 and 4, is commonly referred to as Amdahl's Law [19]. It takes the form

$$S^A = \frac{1}{\alpha + (1-\alpha)/n} \qquad (8)$$

where α is the sequential fraction of the computations and n is the number of processors.

For the parallelised form of Monte Carlo which we are considering here, the sequential component is virtually zero and a more appropriate expression is

$$S = \frac{1}{a_1/n + (1-a_1)n^{a2}} \qquad (9)$$

where a_1 is the parallel fraction of the computations, and as before, n is the number of processors. The terr containing n^{a2} is included to allow for the interprocessor communication time, which will of course increase with th increase in n.

The data points shown in Figure 4 plus some additional data are least-squared fitted to the expression (9), and giv the values $a_1 = 0.9997$ and $a_2 = 0.97$. Using these values, the theoretical curve for large n is shown in Figure Clearly, the theoretical curve is a good fit to the measured values. The broad maximum in the curve can b explained as due to the dominance of the interprocessor communication time as the number of processors become very large. We remind the reader that Figure 5 shows the behaviour for a fixed total number of particles processed.

CONCLUSIONS

We have shown that a sophisticated, general purpose, Monte Carlo particle transport code, written in FORTRAN for conventional computers, can readily be adapted to run efficiently on a transputer based parallel computer, using a parallel programming environment such as Meiko CSTools.

For the principal types of problem solved by the code, a parallelisation efficiency of greater than 90% can be achieved with up to 15 to 20 transputers, and an impressive gain in performance achieved over expensive mainframe serial computers.

For large transputer systems, say, greater than about 25 transputers, a load-balancing scheme should be incorporated into the parallel strategy to delay the fall-off in efficiency as the number of transputers increases.

ACKNOWLEDGEMENT

The author would like to express his gratitude to the Edinburgh University Parallel Computing Centre (EPCC) for permission to access their transputer based Meiko Computing Surface.

REFERENCES

1. Carter, L.L. and Cashwell, E.D. (1975) "Particle Transport Simulation with the Monte Carlo Method", USAEC Report, TID-26607.
2. Al-Bahadili, H. (1991) "The Implementation of Particle Transport Monte Carlo on Parallel Computer Architectures", Ph.D. Thesis, Queen Mary and Westfield College (University of London).
3. Martin, W.R. (1992) "Monte Carlo Methods on Advanced Computer Architectures". Adv. Nuc. Sci. Techy, 22, 105-164.
4. Flynn, M.J. (1972) "Some Computer Organisations and their Effectiveness", *IEEE Transactions on Computers*, C-21, 948-960.
5. Hockney, R.W. and Josshope, C.R. (1988) "Parallel Computers", Adam Higler Ltd.
6. McBryan, O.A. (1988/1989) Parallel Computing 9, 1, 24.
7. AMT Ltd. (1989) "Technical Review", Reading, U.K.
8. AMT Ltd. (1990) "Introduction to New DAP/CP8", Reading, U.K.
9. Meiko Ltd. (1987) "The Computing Surface Reference Manual", Bristol, U.K.
10. INMOS Ltd. (1988) "IMS T800 Product Review", Prentice-Hall, London, U.K.
11. Meiko Ltd. (1990) "CSTools for SUNOS", Vols. 1 and 2, Bristol, U.K.
12. NAG Ltd. (1981) "NAG FORTRAN Library Manual", Vol. 6, Oxford, U.K.
13. Knuth, D.E. (1981) "The Art of Computer Programming", Vol. 2, Addison-Wesley.
14. Bowman, K.O. and Robinson, M. (1987) "Studies of Random Generators for Parallel Processing", Proc. of the 2nd Inter. Conf. on Hypercube Multiprocessors (ed. Heath M.T.), 445-453 Philadelphia.
15. Emmett, M.B. (1984) "The Morse Monte Carlo Radiation Transport Code System", ORNL-4972/R2.
16. Gruppelaar, H. (1986) "Europe Sets Up Its Own Fusion File", Nuclear Europe, Vol. 6, p.40.
17. Vontobel, P. and Pelloni, S. (1987) "JEF/EFF Based Nuclear Data Libraries", Paul Scherrer Inst. EIR-Bericht, Nr. 636.
18. Wood, J. and de Oliveira, C.R.E.(1990) "A Finite Element Study of Gamma Ray Transport", Ann. Nucl. Energy, Vol. 17, No. 4, 195-205.
19. Amdahl, G. (1967) "Validity of the Single Processor Approach to Achieving Large Scale Computing Capabilities". Proc. Spring Joint Conf. AFIPS 30, 483-485.

Table 1 Comparison of 1 and 25 Transputers
Fixed Source Problem : (Point Fission Source in Air)

RESPONSE VALUES : TOTAL FLUX AT POINT R

R cms	TRIPAC 'exact'	1-Trans Est Err (%)	1-Trans Act Err (%)	25-Trans Est Err (%)	25-Trans Act Err (%)
10000.0	1.535E+01	3.340	0.218	0.676	0.236
20000.0	4.132E+00	3.899	2.930	0.866	0.087
30000.0	1.578E+00	3.319	0.742	0.779	0.509
60000.0	1.465E-01	4.583	4.381	1.275	1.104
70000.0	7.068E-02	5.927	1.668	1.452	3.956
90000.0	1.717E-02	6.464	2.254	1.633	0.408
120000.0	2.176E-03	10.462	0.250	2.247	0.731

RESPONSE VALUES : UNCOLLIDED FLUX AT POINT R

R cms	Exact	1-Trans Est Err (%)	1-Trans Act Err (%)	25-Trans Est Err (%)	25-Trans Act Err (%)
10000.0	2.687E+00	0.304	0.685	0.060	0.073
20000.	2.508E-01	0.536	1.296	0.109	0.163
30000.0	4.426E-02	0.748	1.850	0.153	0.261
60000.0	8.863E-04	1.353	3.252	0.274	0.553
70000.0	2.974E-04	1.534	3.642	0.309	0.636
90000.0	3.974E-05	1.861	4.325	0.373	0.774
120000.0	2.555E-06	2.280	5.169	0.459	0.923

Table 2.a Comparison of 1 and 25 Transputers
K-eff Problem : Godiva Sphere (critical)

K - EFF VALUES

TRIPAC K-eff	K-eff	1-Trans Est Err (%)	Act Err (%)	K-eff	25-Trans Est Err (%)	Act Err (%)
1.00427	1.00244	0.522	0.183	1.00563	0.102	0.136

RESPONSE VALUES : 11-GROUP ABSORPTION RATES

TRIPAC 'exact'	1-Trans Act Err (%)	25-Trans Act Err (%)
8.947E-05	13.099	2.802
1.077E-02	5.772	0.244
5.201E-02	3.340	0.587
4.933E-02	0.820	0.036
7.558E-02	0.702	0.284
7.399E-02	0.069	0.278
6.720E-02	0.462	0.731
6.611E-02	2.230	0.015
2.967E-02	0.334	0.693
2.888E-03	25.478	1.778
5.578E-05	44.287	26.431

RESPONSE VALUES : 11-GROUP LEAKAGE RATES

TRIPAC 'exact'	1-Trans Act Err (%)	25-Trans Act Err (%)
1.499E-04	61.014	18.458
2.063E-02	1.924	0.906
8.840E-02	4.549	0.247
7.303E-02	3.571	0.205
1.114E-01	0.284	0.703
1.090E-01	0.736	0.148
8.877E-02	0.778	0.149
6.400E-02	2.488	0.032
1.638E-02	1.680	0.510
5.797E-04	36.187	4.394
6.324E-08	-	-

Table 2.b Comparison of Convex with 10 Transputers
K-eff Problem : Jezebel Sphere (critical)

K - EFF VALUES

TRIPAC K-eff	Convex K-eff	Convex Est Err (%)	Convex Act Err (%)	10-Trans K-eff	10-Trans Est Err (%)	10-Trans Act Err (%)
0.99646	0.996	0.193	0.004	0.9976	0.200	0.122

RESPONSE VALUES : 20-GROUP ABSORPTION RATES

TRIPAC 'exact'	Convex Act Err (%)	10-Trans Act Err (%)
2.181E-05	128.104	25.519
5.256E-05	20.792	32.551
1.353E-04	3.934	2.091
5.931E-04	6.815	1.208
2.724E-03	5.309	2.555
6.286E-03	4.918	1.036
2.905E-02	1.513	0.218
2.507E-02	1.058	0.883
3.051E-02	1.595	0.476
3.369E-02	0.893	0.757
3.377E-02	1.081	0.233
5.961E-02	0.597	0.085
4.369E-02	0.795	0.470
2.835E-02	2.173	1.032
1.654E-02	0.583	0.421
1.514E-02	3.008	0.844
4.311E-03	1.023	0.859
1.078E-03	5.115	15.376
2.743E-04	25.713	8.802
8.971E-05	44.098	5.563

RESPONSE VALUES : 20-GROUP LEAKAGE RATES

TRIPAC 'exact'	Convex Act Err (%)	10-Trans Act Err (%)
3.697E-05	22.584	1.977
9.312E-05	134.926	6.471
2.585E-04	15.470	8.699
1.156E-03	15.282	10.267
5.064E-03	4.807	1.000
1.294E-02	3.164	0.493
6.297E-02	1.937	1.073
5.032E-02	0.646	0.504
5.859E-02	0.811	1.758
6.298E-02	2.214	0.072
6.407E-02	0.288	0.378
1.201E-01	0.214	0.509
9.568E-02	0.114	0.914
6.403E-02	0.817	0.408
3.594E-02	0.843	0.104
2.746E-02	0.003	1.780
6.044E-03	5.284	3.560
1.084E-03	8.249	2.608
1.659E-04	40.357	18.271
2.449E-05	0.890	22.502

Table 3 Comparison of Convex with 10 Transputers
Time-dependent Problem : Jezebel Sphere (Sub-critical)

		K - EFF VALUES				
TRIPAC K-eff	K-eff	Convex Est Err (%)	Act Err (%)	K-eff	10-Tran Est Err (%)	Act Err (%)
0.87118	0.87056	0.142	0.071	0.87326	0.144	0.239

Table 4 Computing Time Comparisons
Total time in CPU seconds

Problem	Transputers Number	Transputers Time	Convex Time	DRS6000 Time
Fixed	25	114.3	243.3	1381
K-eff	10	123.2	106.9	574
Time	12	466.0	435.7	2470

Table 5 Master Transputer Non-Productive Time as a
Percentage of the Total CPU Time

Fixed Source Problem

Transputers	Stage (i) (data to slaves)	Stage (ii) ("waiting")	Total (seconds)
10	1.02 (0.46 %)	0.89 (0.40 %)	219.8
25	2.82 (3.02 %)	2.50 (2.68 %)	93.43
50	6.91 (12.34 %)	5.13 (9.16 %)	56.0

K-eff Problem (Godiva Critical)

Transputers	Stage (i) (data to slaves)	Stage (ii) ("waiting")	Total (seconds)
10	1.18 (0.96 %)	2.28 (1.85 %)	123.18
25	3.90 (6.48 %)	9.49 (15.8 %)	60.14

Time-Dependent Problem (Jezebel Sub-Critical)

Transputers	Stage (i) (data to slaves)	Stage (ii) ("waiting")	Total (seconds)
12	1.97 (1.03 %)	2.34 (1.23 %)	190.8
24	5.50 (5.18 %)	5.79 (5.45 %)	106.2

Fig. 1 Time - Dependent Reaction Rates ; 16 Transputers
MORSE-C.G. Time - dependent JEZEBEL , K-eff = 0.8718

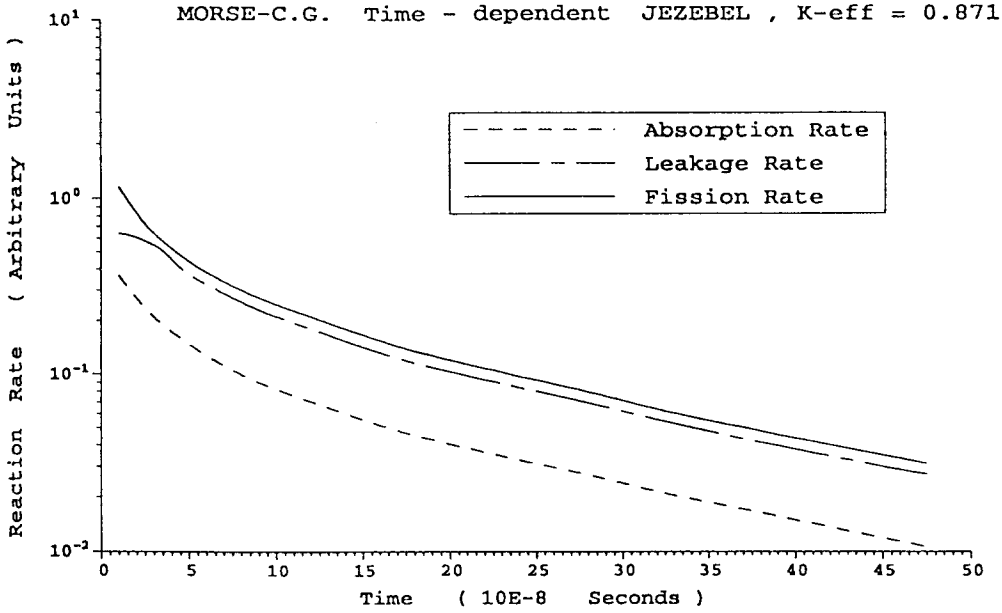

Fig. 2 Point Fission Source in Air Fixed Source Problem
Total Number of Particles Started = 90,000

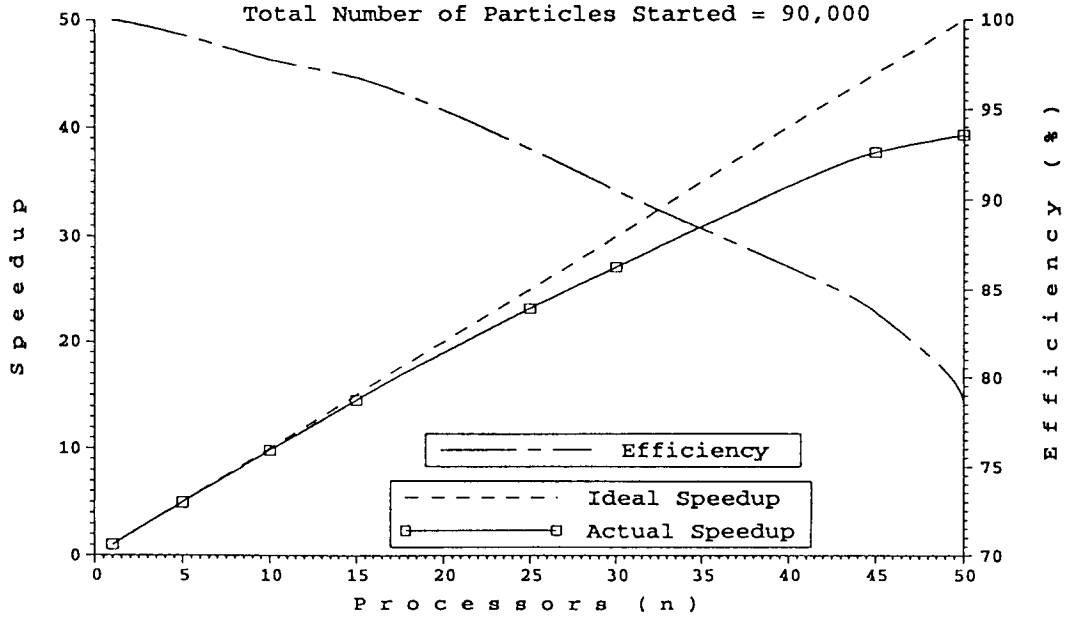

Fig. 3 GODIVA K-eff Problem ; MATXS87 11 Grp Data

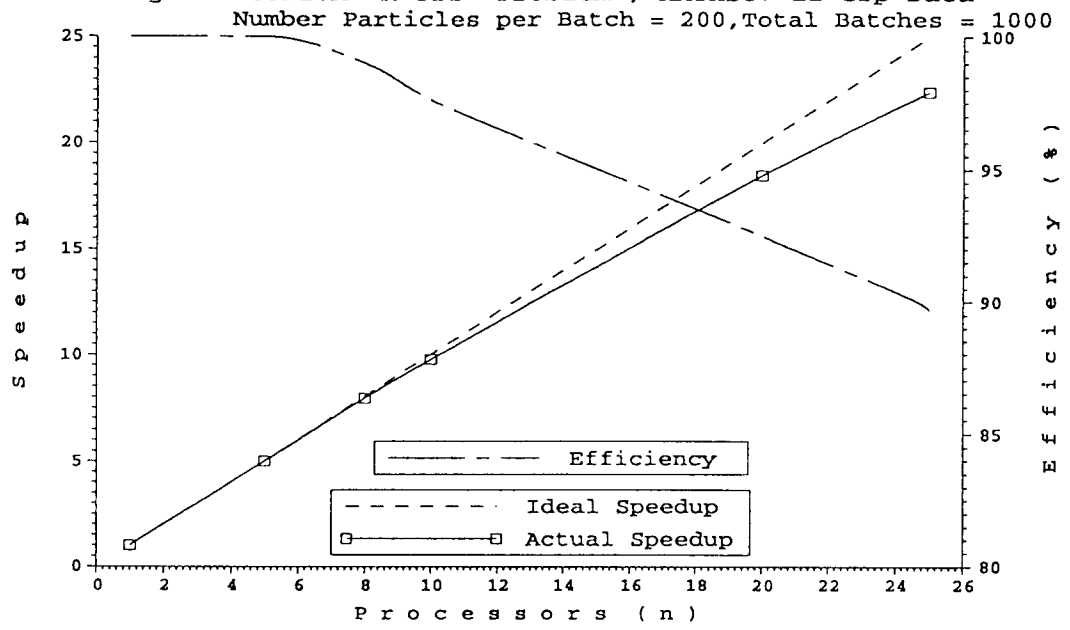

Fig. 4 JEZEBEL Time - dependent K-eff Problem ; MATXS87 20 Group Data

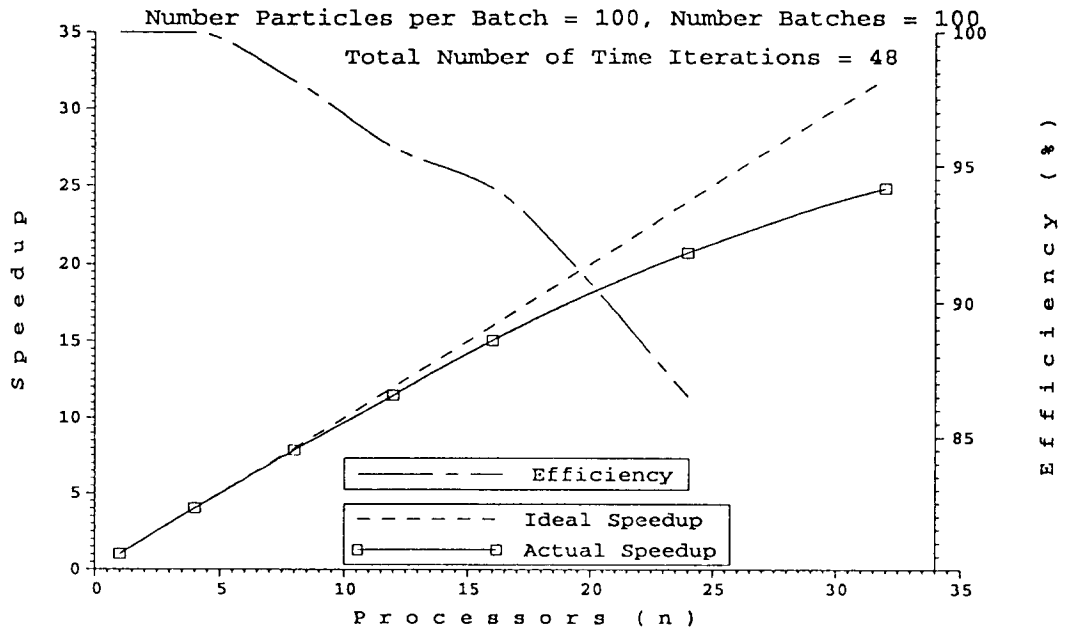

Fig. 5 Speedup Curves for Problem 3

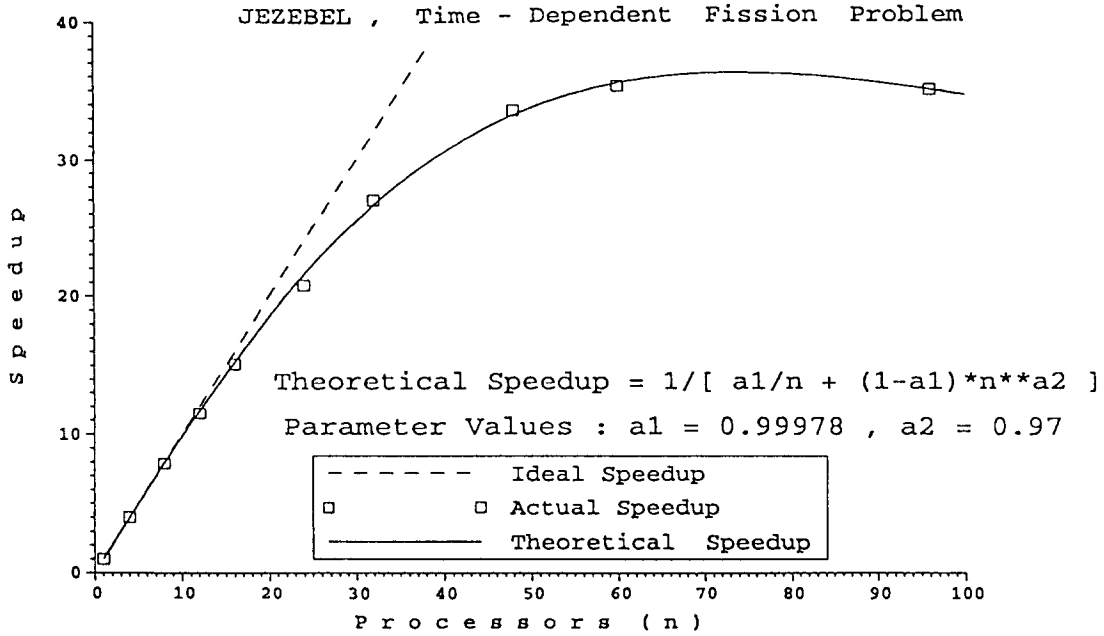

PARALLELISM IN CONTINUOUS ENERGY MONTE CARLO METHOD FOR NEUTRON TRANSPORT

Yuji UENOHARA
Nuclear Engineering Lab., TOSHIBA Corp.
PHONE:+81-(0)-44-288-8130, e-mail:rae@rcg.nel.rdc.toshiba.co.jp

ABSTRACT

The continuous energy Monte Carlo code VIM was implemented on a prototype highly parallel computer called PRODIGY developed by TOSHIBA Corporation. The author tried to distribute nuclear data to the processing elements(PEs) for the purpose of studying domain decomposition for the velocity space. Eigenvalue problems for a 1-D plate-cell infinite lattice mockup of ZPR-6-7 was examined. For the geometrical space, the PEs were assigned to domains corresponding to nuclear fuel bundles in a typical boiling water reactor. The author estimated the parallelization efficiencies for both highly parallel and a massively parallel computer. Negligible communication overhead derived from neutron transports resulted from the heavy computing loads of Monte Carlo simulations. In the case of highly parallel computers, the communication overheads scarcely contributed to the parallelization efficiency. In the case of massively parallel computers, the control of PEs resulted in considerable communication overheads.

INTRODUCTION

Monte Carlo simulations of neutron transport will give accurate solutions if large computing resources are available. Current supercomputing is entirely based on vector processors. It is difficult to vectorize Monte Carlo codes and vector processors cannot be improved any further. Massively parallel computers, which are now under development, are about 1,000 times faster than current vector computers. Monte Carlo simulations are ideally suited to parallel computing, so massively parallel computers will make highly accurate Monte Carlo simulations of neutron transport feasible.

Since the Monte Carlo method can be parallelized in a natural way, several investigations[1,2,3] have been made. They have been done on simple problems, such as photon transport in spherical balls. Geometrical data and nuclear data are minimized in these problems. These data, therefore, can be distributed to all processing elements (PEs) in a parallel computer.

Recently, full-core models of power reactors have been examined using super computers[4]. A large amount of memory is required if detailed and accurate simulations are desired for complicated systems; the memory is used for statistical tallies and nuclear data. The databases for this type of calculation exceed several hundred megabytes, and tally data are necessarily expanding. Detailed geometrical and energy space configurations add to the memory requirement for statistical tallies. This data will be able to be stored in full memories of massively parallel computers. This memory, however, is distributed among about ten thousand PEs. A PE, therefore, cannot contain both tally and nuclear data. A PE of the conventionally largest parallel computer, CM-5, cannot do it.

Parallelization in other fields, such as fluid dynamics, has been based on the concept of data parallelism. Massively parallel computers are generally designed according to this philosophy. Data parallelism is a parallelization strategy based on data structure which enables massive amounts of data to be handled. Data parallelism needs to be introduced into the parallel computing of Monte Carlo simulations. Ones can find such data parallelism of the Monte Carlo method from the domain decomposition strategy.

In the present work, the parallelization of VIM[5] is demonstrated. VIM is a continuous-energy Monte Carlo code developed at the Argonne National Laboratory. The VIM code is being implemented on a prototype highly parallel computer called PRODIGY developed by TOSHIBA Corporation. This machine is a MIMD parallel computer of the distributed memory type. It is comprised of 128 PEs connected with an extended hypercube network, Base-8 3-cube. Each PE is a 16-bit processor, SCC68070, with 2 megabytes memory. The computing resource of the PEs is similar to that of computer used in the development of the VIM code except for computing speed. Slight modifications to the VIM code were required for the present implementation.

The author formulated the parallelization efficiency derived from stochastic fluctuations. This becomes the basis for more detailed estimations. The domain decomposition for velocity space is discussed. In this chapter, the author shows the distribution of nuclear data to PEs. The speed-up of parallelized VIM is presented. Finally, the domain decomposition for geometrical space is discussed. The PEs are assigned to domains which correspond to the bundles of nuclear fuels in a typical boiling water reactor. Communications among the PEs describe the transports of neutrons through the fuel bundles. A fuel bundle takes neutrons from surrounding bundles. Communication collisions then occur. The author extrapolated the parallelization efficiency measured with PRODIGY to both highly parallel and massively parallel computers. The control of PEs of massively parallel computers resulted in considerable communication overheads.

STOCHASTIC BEHAVIOR OF EXECUTION TIME

A Monte Carlo simulation for neutron transport is an event driven type of problem. When all PEs execute the same problem, these execution times are different. However, the expected value of these execution times can be predicted. The actual computation time is the maximum among them. The ideal parallelization efficiency, therefore, cannot become unity, even though no communication between PEs occur. This problem should be discussed seriously related to eigenvalue problems. Eigenvalues are calculated through the outer iterations, which is usually called a batch. A batch is repeated sequentially until the neutron flux converges.

The execution time is distributed stochasticaly. The total execution time is the sum of simulation time from the generation to the disappearance of one neutron. The simulation time for one neutron varies. The probability distribution function is given as an exponential distribution. From the central limit theorem, the probability density function of the simulation time for n neutrons is given by

$$p_n(t) = \frac{1}{\sqrt{2\pi}\,\sigma} \exp\left(-\frac{1}{2}\left\{\frac{(t - \langle t_n \rangle)}{\sigma}\right\}^2\right). \qquad (1)$$

The mean time and standard deviation are related to the number of simulated neutrons as

$$\langle t_n \rangle \propto n \qquad (2)$$

and

$$\sigma_n \propto \sqrt{n}, \qquad (3)$$

respectively. A fractional standard deviation is given by

$$\rho = \frac{\sigma_n}{\langle t_n \rangle} \qquad (4)$$

$$\propto 1/\sqrt{n} \qquad (5)$$

The total execution time is more sharply distributed with the number of simulated neutrons. Therefore, the efficiency increases with the number of simulated neutrons.

Some PEs in parallel computer simulate for a very long time with a given probability. The probability density function of the maximum simulation time in N PEs is given by

$$f_N(\mathrm{Tmax}) = N\, p_n(\mathrm{Tmax})\, \mathrm{erf}(\mathrm{Tmax})^{N-1}, \qquad (6)$$

where erf(t) is an error function which is an integrated normal distribu-

tion. The expected value is given by

$$\langle T_{max} \rangle = \langle T_n \rangle + Z(N)\,\sigma\,(n). \tag{7}$$

The factor Z(N) is calculated by solving the following equation.

$$\mathrm{erf}(\langle T_{max} \rangle) = \frac{N}{N+1}. \tag{8}$$

The parallelization efficiency derived from a stochastic process is given by

$$\eta = \frac{1}{1 + Z(N)\,\rho_n}. \tag{9}$$

The dependence of the factor Z on N is shown in Fig.1. The factor Z is proportional to the logarithm of N. Eq.(9) shows the ideal efficiency on parallelized Monte Carlo method. Although about ten thousand PEs are used, there are very few chances for the execution time to become much longer than the mean execution time.

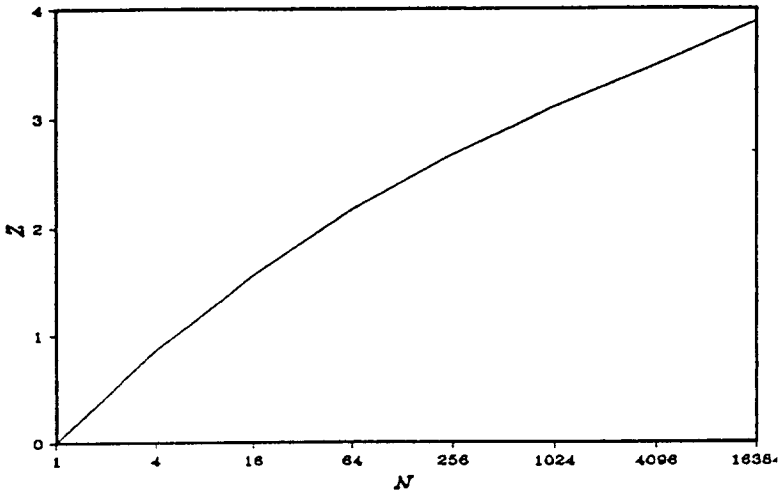

Fig. 1 Dependence of Z on N

DOMAIN DECOMPOSITION: VELOCITY SPACE

Neutron energy is distributed from the cold to fast regions in nuclear facilities. The excitation curves for neutron cross sections have very complex structures such as resonances. The energy and angular distribution of secondary neutrons are also complex. The accuracy of nuclear data dominates over that of Monte Carlo simulations. A huge memory is required for an accurate description of nuclear data. Since many PEs access nuclear data frequently and at random, it is difficult for PEs to share them. Only few investigations have referred to these problems. In the past, such large amounts of data were processed by a file-processing technique based on bulky external media. These conventional file management methods are inadequate for massively parallel computing because of the increasing file access overheads.

The author parallelized the VIM code with respect to nuclear data. The nuclear data file was divided into high and low energy portions, and some PEs were assigned to high energy and others to low energy. The nuclear data are banded with respect to neutron energy in the original VIM code.

Thus, this implementation was a slight modification of the VIM code. The PEs have little memory, so a continuous Monte Carlo code cannot be implemented without this modification. The memory required for nuclear data grows with the scale of the problem, but the present modification is usable even if much larger memories are installed in the PEs.

The author tested eigenvalue problems for a 1-D plate-cell infinite lattice mockup of ZPR-6-7[6]. Fig.2 shows the dependence of computing speed on the number of PEs. These tests are classified according to the number of simulated neutrons. No communication collisions occur in the present implementation, so the computing speed increases linearly. The maximum efficiency was 50%. This can be improved in several ways, but modifying the VIM code requires a large amount of work. Such work would result in only doubling the computing speed and thus would not be worthwhile. More detailed modifications to the VIM code are not needed unless the nuclear data are banded into at least ten energy regions. Massively parallel computing is completely different from conventional computing techniques, and it is very difficult to trace ten thousand PEs at the same time. The debugging of programs, therefore, becomes very difficult. Sophisticated procedures cannot be used because of the complicated operation. Simple procedures are desired even though they decrease the efficiency to some degree.

DOMAIN DECOMPOSITION: GEOMETRICAL SPACE

Data parallelism for the geometrical space is necessary for Monte Carlo simulations of full-core models of power reactors. The PEs, then, are assigned to a domain, which corresponds to a bundle of nuclear fuels in a boiling water reactor. Communications among the PEs describe the transport of neutrons through the fuel bundles. A fuel bundle takes neutrons from surrounding bundles. Communication then occurs. The parallelization efficiency, therefore, is smaller than that estimated by Eq.(9). Let us estimate the parallelization efficiency. The communication schemes are described based on the VIM algorithms in Fig.3.

In the present scheme, the information on transported neutrons is stored in the buffer memories. When all neutrons in their domains disappear by absorption reactions and transportation, the PEs send the stored information to the PEs corresponding to neighboring domains and wait to receive the information from other PEs. This procedure is repeated until all neutrons are absorbed: the end of a batch. It, however, is difficult to detect the end of a batch. Neutrons are traveling through many PEs and are absorbed by the medium. In the final stage of the simulations, a few PEs simulate one or two neutrons and others are waiting. If all neutrons disappear, all the PEs will be waiting. Every PE, however, can never detect the end of a batch by themselves. If no PEs count up neutron absorption, all PEs must wait forever. It is necessary for some PEs to count the number of total disappearances in order to avoid a deadlock. The present monitoring scheme is shown in Figs.4 and 5. Three types of PEs, which are General-PE, Head-PE, and Soldier-PE, are shown. General-PE controls Head-PEs. Head-PEs controls Soldier-PEs. Soldier-PEs perform only simulations. When all neutrons in the Soldier-PEs disappear by

absorption reactions and transportations, they send the counts of absorption reactions to their Head-PE. Head-PEs gather counts from all Soldier-PEs and count up the number of total absorption reactions in their domains. Head-PEs send them to the General-PE. The General-PE tests the equality of the received total number of absorption reactions and the number of initially generated neutrons. If they are equal, the general PE confirms the end of a batch. The General-PE then broadcasts the end-signal to the Head-PEs and the Head-PEs broadcast it to their Soldier-PEs. The present implementation do not always give maximum efficiency, since all PEs must synchronize. The parallelization efficiency, however, can be formulated because the algorithm is simple.

In order to extrapolate the communication overhead, the author simplified the problem so that the same number of PEs, Npe, are assigned to each domain and the macroscopic cross sections and geometrical configurations of the Nrgn domains are the same. The communication time for one batch is estimated approximately by

$$\begin{aligned} Tc = 10\ \tau_c \sum_{i=0}^{Nstep} \left(\mathrm{Max}_{j=1}^{Mpe} Nout_{ij}\right) \\ + Nstep((Npe + Nrgn)\ t_{off}) \\ + ((Npe - 1) + (Nrgn - 1))(t_{off} + \tau_c), \end{aligned} \tag{10}$$

where Nstep is the number of synchronizations occurring in one batch and $Nout_{ij}$ is the number of transported neutrons from the j-th PE in the i-th synchronization.

The author assumed the communication time required to process m bytes of data as

$$T(m) = t_{off} + m\tau_c, \tag{11}$$

where t_{off} and τ_c correspond to the offset time and the baud-rate, respectively. It takes t_{off} to initialize the communication systems for PEs. The architecture of the PE gives the value of the offset-time. The baud-rate depends on the system clock. The offset-time dominates in the transportation of a small size of data. The baud-rate dominates over the offset-time for a large size of data.

The first term of Eq.(10) means the communication time for sending information on transported neutrons. The author assumed that ten words of memory were required for information on one neutron. The second term means the communication time required to gather the number of absorptions. It is very difficult to precisely evaluate the gathering time. This strongly depends on the communication architecture. The author, therefore, estimated this term roughly. The third term means the communication time for broadcasting the end signal.

The author estimated the parallelization efficiency of Monte Carlo simulations for BWRs. Massively parallel computers are still now unavailable.

The author estimated them by using data measured from small sample problems. Since the computing and communication time fluctuates, it is worth while to discuss their expected values.

The actual computing time of parallel computers is given by

$$<Tp> = t_c \sum_{i=0}^{Nstep} <(\mathrm{Max}_{j=1}^{Mpe} Nevnt_{ij})>. \quad (12)$$

The total execution time is the sum of Eqs.(10) and (12) and becomes

$$<Tpl> = <Tp> + <Tc>, \quad (13)$$

where t_c is the CPU time required to simulate one event, and $Nevnt_{ij}$ is the number of events occurring in the i-th synchronization and in the j-th PE. The total CPU time is calculated by

$$<Ts> = t_c \sum_{i=0}^{Nstep} \sum_{j=1}^{Mpe} <Nevnt_{ij}>, \quad (14)$$

where the number of events, $<Nevnt_{ij}>$, is assumed to be

$$<Nevnt_{ij}> \propto <N_{ij}>. \quad (15)$$

It is now assumed that macro cross sections and geometrical configurations are the same for all domains. Therefore, the expected number of simulated neutrons are given by

$$<N_{ij}> = N_0 \exp(-\alpha i) \quad (16)$$

and

$$<N_{i0}> = <N_{i1}> = \ldots = <N_{iMpe}>. \quad (17)$$

Applying Eq.(7), the expected maximum number of events and transported neutrons are given by

$$<(\mathrm{Max}_{j=1}^{Mpe} Nevnt_{ij})> = <Nevnt_{ij}> + Z(Mpe)\,\sigma(<Nevnt_{ij}>) \quad (18)$$

and

$$<(\mathrm{Max}_{j=1}^{Mpe} Nout_{ij})> = <Nout_{ij}> + Z(Mpe)\,\sigma(<Nout_{ij}>), \quad (19)$$

respectively. Their standard deviations are proportional to their square roots. The author applied

$$\eta' = <Ts> / (Mpe\ <Tpl>) \quad (20)$$

to estimate the parallelization efficiency. Nstep, t_c, and α were measured from small sample examples. The third term of Eq.(10) takes a minimum when Nrgn is equal to Npe. The parallelization efficiency, then, takes its maximum. In the present work, the maximum efficiency was estimated for highly parallel and massively parallel computers. The specifications for the assumed machine PEs were 100[MIPS] computing speed, 25[MW/sec.] baud-rate, and 10[μsec.] offset-time. The degree of parallelization of the assumed machines were 1,024 PEs and 65,536 PEs, respectively. The estimated parallelization efficiencies are shown in Figs.6-9. These figures show their dependence on the number of neutrons. The efficiency grows with the number of neutrons. In the case of highly parallel computers, the communication overheads scarcely contributed to the parallelization efficiency. In the case of massively parallel computers, the second and third terms of Eq.(10) dominated over the communication overhead. The negligible contributions of the first term resulted from the heavy computing loads of the Monte Carlo simulations. If a very powerful CPU and a special algorithm for the Monte Carlo method were supplied, the first term would dominate over the communication overhead. It is very difficult to develop such a CPU and algorithm. Even when vectorized Monte Carlo codes are applied, this will not become a severe problem. The present results, therefore, can be applied to vector-parallel machines.

SUMMARY

A continuous energy Monte Carlo code VIM was implemented on a prototype highly parallel computer called PRODIGY developed by TOSHIBA Corporation.

The author tried to distribute nuclear data to PEs. Thus, this implementation was a slight modification of the VIM code. Eigenvalue problems for a 1-D plate-cell infinite lattice mockup of ZPR-6-7 was examined. The maximum efficiency was 50%. This can be improved in several ways, but modifying the VIM code requires a large amount of works. Such work would result in only doubling the computing speed and thus would not be worthwhile. More detailed modifications to the VIM code are not needed unless the nuclear data are banded into at least ten energy regions.

The PEs were assigned to domains corresponding to nuclear fuel bundles in a typical boiling water reactor. The author estimated the parallelization efficiencies for highly parallel and massively parallel computers. In the case of highly parallel computers, the communication overheads scarcely contributed to the parallelization efficiency. In the case of massively parallel computers, controlling the PEs resulted in considerable communication overheads. Negligible communication overhead derived from neutron transports through domains resulted from the relatively heavy computing loads of the Monte Carlo simulations. The present results can be applied to vector-parallel machines.

Massively parallel computing is completely different from conventional computing techniques, and it is very difficult to trace ten thousand PEs at the same time. The debugging of programs, therefore, becomes very

difficult. Sophisticated procedures cannot be used because of their complicated operation. Simple procedures are desired even though they decrease the efficiency to some degree.

ACKNOWLEDGMENT

The author wishes to thank Dr. S. Oyanagi, Mr. Y. Kawakura and other staffs of TOSHIBA RDC for providing the parallel computing environment and valuable suggestions.

REFERENCES

/1/ D.Ugolini et al., TRANS. AM. Nucl. Soc. (USA) 55 326 1987
/2/ C.Zhao and J.Wood, Ann. Nucl. Energy 16 649 1989
/3/ J.Wood et al., ibid. 18 155 1991
/4/ K.C.Okafor and J.F.Zino, "Eigen Value Analysis Using a Full Core Monte Carlo Method," Proc. on Topical Meeting on Advances in Reactor Physics, Vol. 2 277-287, Charleston 1992.
/5/ R.N.Blomquist et al., "VIM A Continuous Energy Monte Carlo Code at ANL, "ORNL/RSIC-44, April 21-23, 1980
/6/ L.G.LeSage et al.,"Initial Experimental Results from ZPR-6 Assembly-7," Trans. Am. Nucl. Soc., 14 1971 pp.17-18

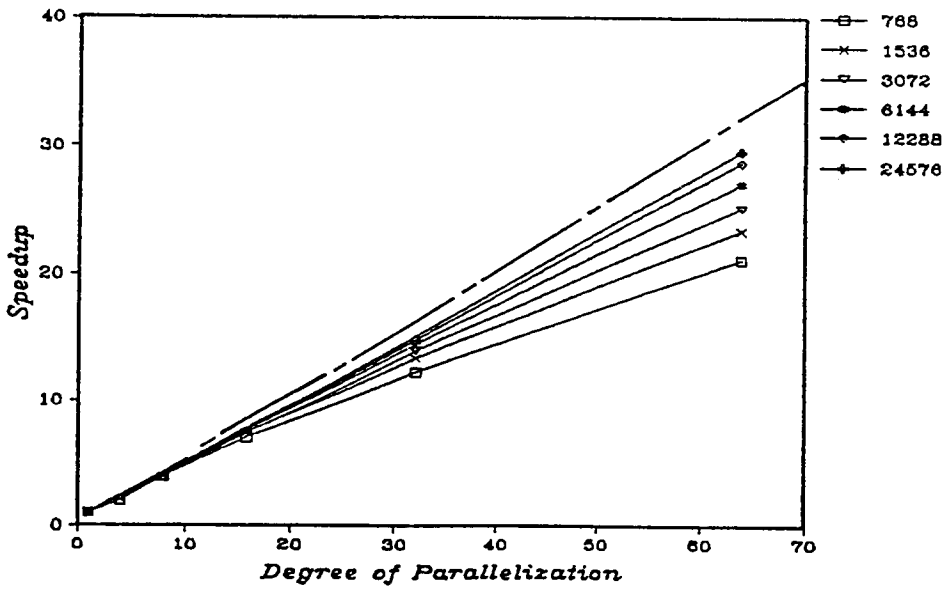

Fig. 2 Speedups of Parallelized VIM. The eigenvalue problems for 1-D plate infinite lattice mockup of ZPR-6-7 was examined. The symbols, —□—, —×—, —▽—, —●—, —◆—, and —+— indicate the case of 768, 3,072, 6,144, 12,288, and 24,575 neutron simulations. The dash-dotted line denotes the maximum speedup in the present implementation.

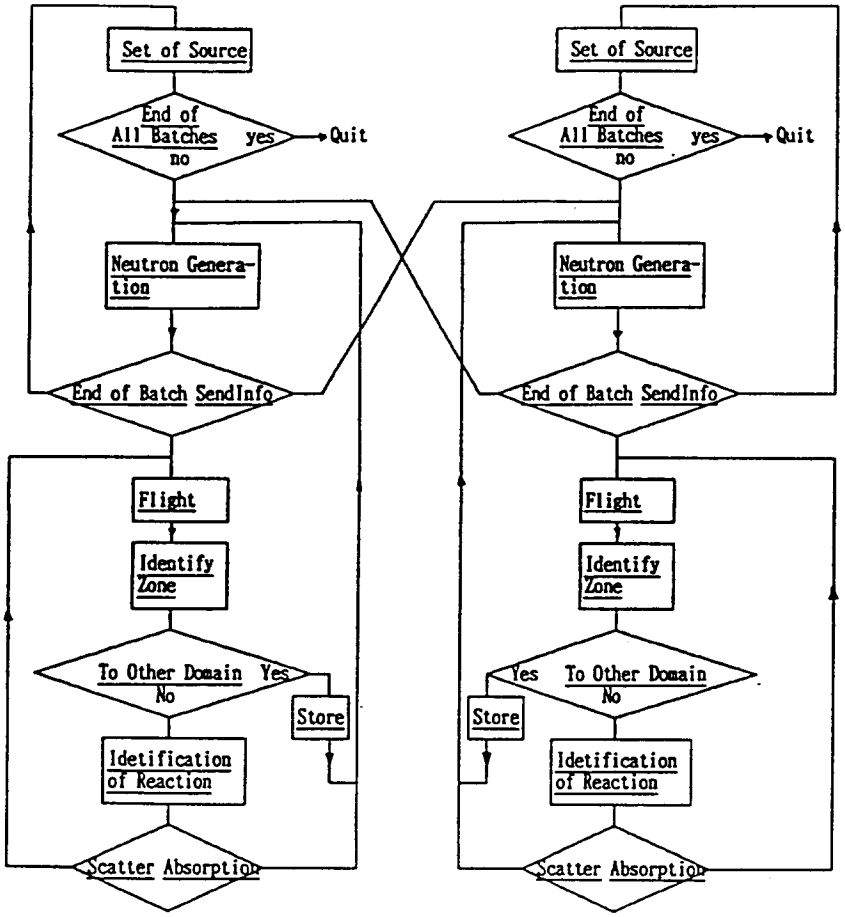

Fig. 3 Communication Procedure for Transportations of Neutrons to Other Domains

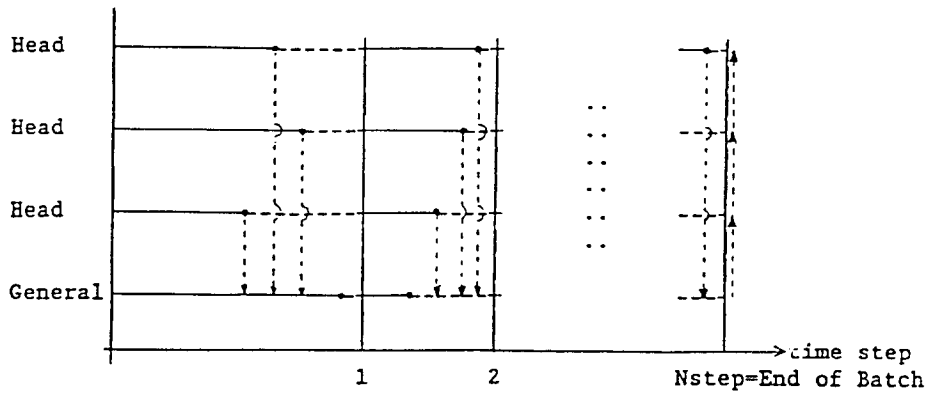

Fig. 4 Synchronization for Monitoring PEs. Soldier-PEs are not shown to simplify the display. The horizontal solid lines show the time intervals for the simulations. The horizontal dashed lines are those for waiting. The arrows directed downward indicate the gathering of the counts of absorption. The arrows directed upward indicate the broadcasting of the end signal.

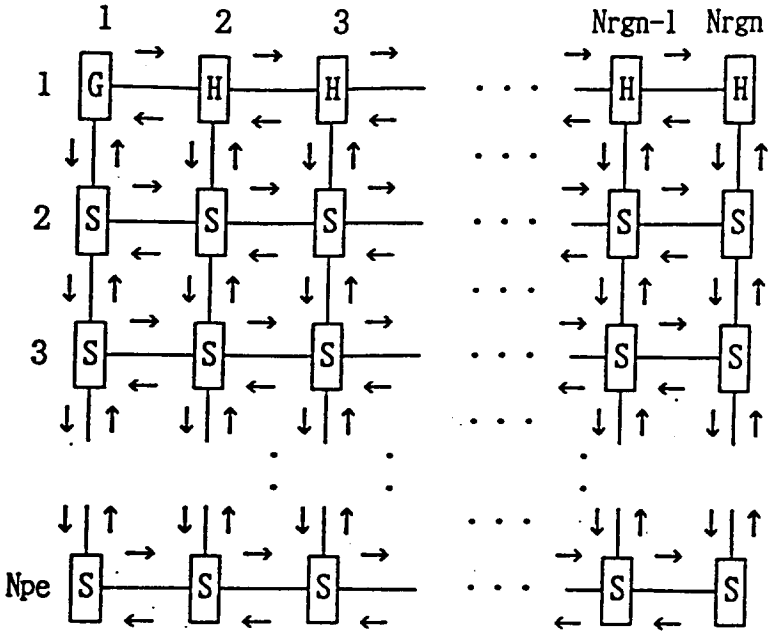

Fig. 5 Communication Scheme for Broadcast of End Signal and Gathering of Counts of Absorption. The characters G, H, and S in the squares denote General-PE, Head-PE, and Soldier-PE, respectively. The arrows indicate the direction of broadcasting and gathering.

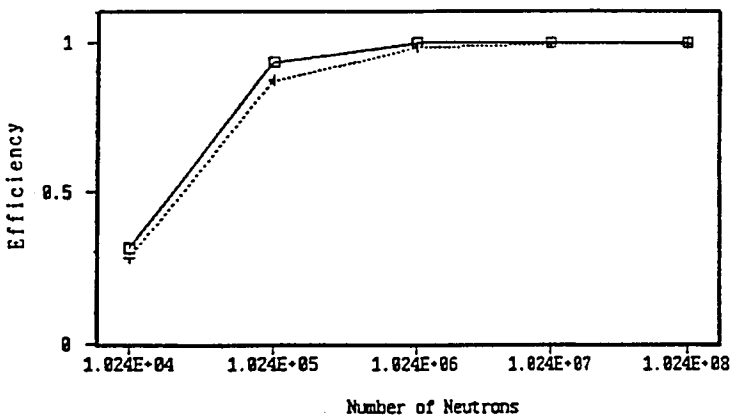

Fig. 6 Parallelization Efficiency of Assumed Highly Parallel Computer. It is assumed to be comprised of 1,024 PEs. The symbols indicate the efficiency derived from only stochastic fluctuations. The symbols + indicate the efficiency derived from stochastic fluctuations and communication overheads.

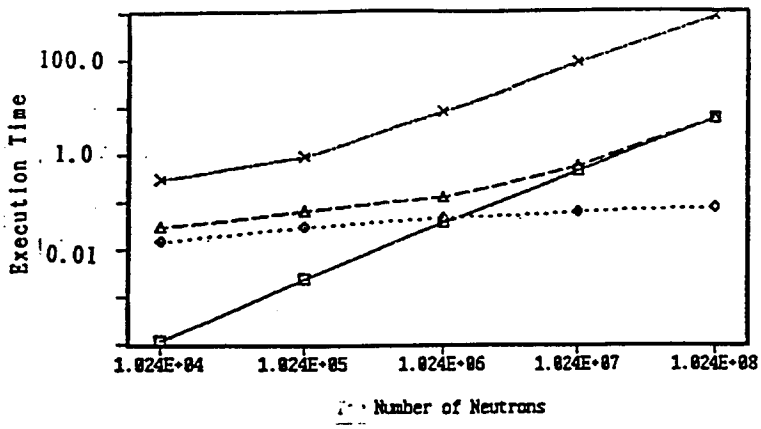

Fig. 7 Components of Execution Time for Assumed Highly Parallel Computer. It is assumed to be comprised of 1,024 PEs. The symbols and indicate the first and third term of Eq.(10), respectively. The symbols Δ and × indicate the total communication the total execution time, respectively.

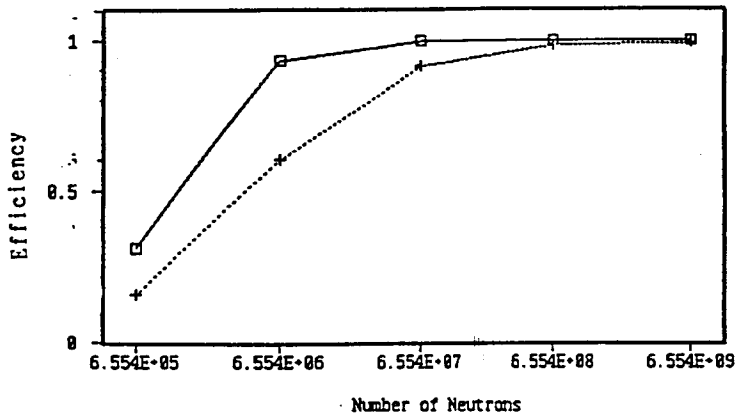

Fig. 8 Parallelization Efficiency of Assumed Massively Parallel Computer. It is assumed to be comprised of 65,536 PEs.

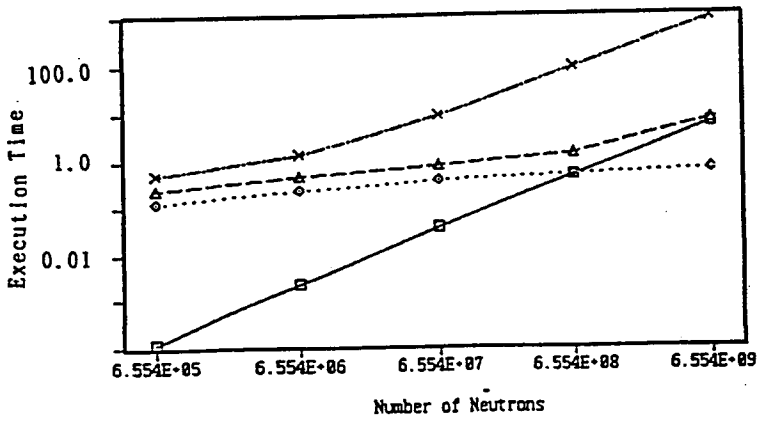

Fig. 9 Components of Execution Time for Assumed Massively Parallel Computer. It is assumed to be comprised of 65,536 PEs.

Session IV

MONTE CARLO PERTUBATIONS, HYBRID METHODS, GEOMETRY MODELLING - ANY NEW MONTE CARLO DEVELOPMENT -

CHAIRS:

***H. U. BARZ**, FORSCHUNGSZENTRUM ROSSENDORF - GERMANY*
***E. HOOGENBOOM**, DELFT UNIVERSITY - THE NETHERLANDS*

Monte Carlo Perturbation Algorithms Exploit New Computer Architectures

Herbert RIEF

Commission of the European Communities
Ispra Establishment
I-21020 ISPRA (Va), Italy

ABSTRACT

Fundamental aspects of correlated sampling and differential operator procedures applied to systems of linear equations modelling Markov processes are investigated. Algorithms providing sensitivities (gradients, Jacobians) and perturbation estimates obtained by a single simulation experiment are described in detail. In this context it becomes evident that the algorithm for calculating the Jacobians may benefit considerably from the use of vector processors. Mathematical proofs are provided which show that under most conditions a finite relative variance can be obtained for arbitrarily small parameter variations.

INTRODUCTION

In science and technology the demand for the analysis of complex, multidimensional systems is continuously increasing. Compared to deterministic methods Monte Carlo allows a less demanding modelling of such problems, provided the underlying elementary processes are of a stochastic nature or can be formulated in such terms.

Until quite recently most Monte Carlo programs had to be run on expensive mainframe computers. The advent of inexpensive workstations based on mass produced CPUs, including Transputers or acceleration boards, is going to change this situation dramatically.

Despite this advantage the probabilistic nature of the method imposes certain limitations if it is applied in a straightforward manner. Parameter studies which constitute a great fraction of any complex system analysis prove, for example, impossible if the differences of the sampled responses are of the same size or smaller than their uncertainties. Actually, more often than not, the perturbation of a response as a consequence of small parameter changes, turns out to be of greater interest than the response itself.

To overcome this shortcoming, two methods allowing for the calculation of small parameter variations will be described here in a systematic manner. One is based on *correlation techniques* and and the other deals with *differential operator sampling*. The author tries to prove that for most conditions the perturbation estimates determined by these sampling schemes have a finite relative variance.

While *correlation techniques* provide straight-forward perturbation estimates, *differential operator sampling* allows for the determination of gradients and higher order derivatives. The latter method offers the possibility to perform perturbation calculations by the use of a multivariate Taylor expansion and to analyze the stochastic simulation process in terms of additional criteria.

Fundamental aspects of correlated sampling and differential operator procedures applied to systems of linear equations modelling Markov processes are investigated. Algorithms providing sensitivities (gradients, Jacobians) and perturbation estimates obtained by a single simulation experiment are described and a mathematical prove is provided which shows that for most conditions a finite relative variance can be obtained for arbitrarily small parameter variations.

Right from the beginning it was realized that the Monte Carlo method was one of the most promising candidates specifically suited for parallel computers. But in the case of multiple

correlation and differential operator sampling the execution time can also substantially be shortened if the score of the Jacobian is calculated by a vector processor.

1. Solution of Linear Matrix Equations by Random Walk Techniques

A set of linear equations

$$r = Pr + a \tag{1}$$

of order m can be interpreted as a random walk process if the matrix P describes transition probabilities in a system which can assume a set of states from 1 to m. If the probability for transition from state i to the next state j does not depend on the past, i.e.: on the path by which j was reached, the system is said to be Markovian. A typical Markov chain will start in some state l_0 with subsequent transitions through a sequence of states $l_1, l_2, \ldots$ and finally a termination in state l_k yielding a series of integers $\gamma_k = (l_0, l_1, l_2, \ldots l_k)$ where $l_n \in \{1, 2, \ldots m\}$. In Monte Carlo terminology such a chain is often called a *history*.

After a start with probability

$$P(l_0 = i) = a_i ;$$

the successive states are connected by the transition probabilities

$$P(l_{n+1} = i \mid l_n = j, n < k) = p_{ij} ,$$

and the termination probability

$$P(k = n \mid l_n = i) = p_i .$$

The $p_{i \leftarrow j}$-s being elements of the matrix P (dimension $m \times m$) are the transition probabilities from state j to i, for which the following conditions must be satisfied:

$$p_{ij} \geq 0 , \quad \max_j \left(\sum_i p_{ij} \right) \leq 1 , \quad \sum_i a_i = 1 \quad \text{and} \quad p_j = 1 - \sum_i p_{ij} \leq 1 . \tag{2}$$

The last condition is the terminating criterion for a chain of events. There must be at least one p_j for which $p_j < 1$ is met. Furthermore, only matrices P with spectral radius $\rho(P) < 1$ are allowed. (The *spectral radius* of the matrix P is the largest modulus of all eigenvalues of P. Thus it is the radius of the smallest circel in the complex plane which contains all eigenvalues of P.)

For each state i we define a variable r_i which is the average number of entries into state i. The state i can be reached either by an event starting in i with probability a_i or by a transition to i from state j with probability $p_{i \leftarrow j}$. The mean number of transitions from j to i corresponds to the product $p_{i \leftarrow j} r_j$.

It is worth noting: the solution of this system of linear equations by the random walk algorithm

described here requires that the p_{ij} are interpreted as transfer probabilities from j to i leading to the "backward" notation $p_{i \leftarrow j}$.

All events in state i are the sum

$$r_i = p_{i \leftarrow 1}\, r_1 + p_{i \leftarrow 2}\, r_2 + \ldots + p_{i \leftarrow m}\, r_m + a_i .$$

The expected number of transitions from all states to all other states are then taken into account by the matrix equation (1). The solution of this system of m linear equations by a random walk procedure requires the following additional considerations. If $P_i^{(n)}$denotes the probability that the n-th transition (in the sequence) occurs to state i

$$P_i^{(n)} = P(l_n = i \mid n\text{-}1 < k) ,$$

a recursion expression for $P_i^{(n)}$ can be formulated

$$P_i^{(n)} = \sum_j p_{ij}\, P_j^{(n-1)} \qquad \text{for } n \geq 1 \text{ and } P_i^{(0)} = P(l_0 = i) = a_i .$$

It stands for the probability that transition n enters state i provided $P_j^{(n-1)}$ is the probability that the $(n\text{-}1)$-th transition occurs in j summed over all intermediate states j. If x_i denotes the number of entries into state i then r_i can be interpreted as being the expectation of $\langle x_i \rangle$, which is

$$\langle x_i \rangle = a_i + \sum_{l_1=1}^{m} p_{il_1} a_{l_1} + \sum_{l_2=1}^{m} \sum_{l_1=1}^{m} p_{il_2} p_{l_2 l_1} a_{l_1} + \ldots \tag{3}$$

$$= a_i + \sum_{k=1}^{\infty} \sum_{l_k} \cdots \sum_{l_1} p_{il_k} \cdots p_{l_2 l_1} a_{l_1} \tag{4}$$

$$= a_i + (Pa)_i + (P^2 a)_i + \ldots\ldots \quad \text{(corresponds to the Neumann Series !)}$$

$$= a_i + P[a_i + (Pa)_i + (P^2 a)_i \ldots\ldots]$$

$$= a_i + P\,\langle x_i \rangle . \tag{5}$$

Written in matrix notation

$$\langle \boldsymbol{x} \rangle = \boldsymbol{P}\,\langle \boldsymbol{x} \rangle + \boldsymbol{a} \tag{6}$$

is equivalent to equation (1).

The *sample mean* $\hat{x}_i$ of all chains of events (histories) $\gamma_k = (l_0, l_1, l_2, \ldots\ldots l_k)$ is the normalized sum of all entries into state i:

$$\hat{x}_i = \frac{1}{H} \sum_{h=1}^{H} \sum_{n=0}^{k(h)} \delta_{il_n} , \tag{7}$$

with Kronecker's symbol $\delta_{ij} = 0$ for $i \neq j$ and $\delta_{ij} = 1$ for $i = j$. H is the total number of histories and $k(h) < \infty$ the length of the transition chain γ in the h-*th* history.
The estimates of $\hat{x}_i$ converge to the exact solution of the matrix equation as the number of histories increases (see Fig. 1).

2. Perturbation Algorithms solving Linear Matrix Equations by Random Walk Techniques

It has been shown [1 p. 85] that a matrix equation

$$x = Qx + b , \tag{8}$$

satisfying less stringent conditions than those required by (2) may be solved by "*mapping*" it onto a random walk as described above. A correlation technique which makes this possible, is also the base for the perturbation analysis of *Linear Matrix Equations* discussed in this chapter.
Using the same notation as previously, we define two likelihood ratios

$$\alpha_i = b_i/a_i \text{ and } \pi_{ij} = q_{ij}/p_{ij} \text{ requiring } \begin{cases} \neq 0 & \text{for } p_{ij} \neq \\ = 0 & \text{for } p_{ij} = 0 , \end{cases}$$

and

$$\|Q\| = \max_j \left(\sum_i |q_{ij}| \right) < 1 .$$

To solve equation (8) we again follow random walks $\gamma_k = (l_0, l_1, l_2, \ldots l_n, \ldots, l_k)$ connected by the transition probabilities p_{ij}. But in this case the random walk is accompanied by a weight factor w_n being the product of all π_{ij} associated with the states it passed through before entering state n.

$$w_n = w_{n-1}\pi_{l_n l_{n-1}} = \pi_{l_n l_{n-1}} \ldots \pi_{l_3 l_2}\pi_{l_2 l_1}\alpha_{l_1} \qquad (w_0 = \alpha_{l_1}) .$$

Instead of just counting the transition events as in (7) the score of x_i up to the k-th transition is the sum of thoose weight factors which refere to transitions into state i. It leads to the sample mean

$$\hat{x}_i = \frac{1}{H} \sum_{h=1}^{H} \sum_{n=0}^{k(h)} w_n \delta_{il_n} .$$

To calculate the second moment, the score of x_i must be summed up and squared for each history separately:

$$\hat{x}_i^2 = \frac{1}{H}\sum_{h=1}^{H}\left(\sum_{n=0}^{k(h)} w_{l_n}\delta_{il_n}\right)^2 , \tag{9}$$

rendering the sample variance

$$var(\hat{x}_i) = \hat{x}_i^2 - \hat{x}_i^2 , \tag{10}$$

To facilitate the reading of the formulae we adopted the convention of indicating p.d.f.s from which samples are taken by Roman letters (*italic*) and likelihood ratios (determining weight factors) by Greek letters.

The frequency with which these weight factors are chosen corresponds to the random walk distribution governed by the matrix $\boldsymbol{P}$ and the start distribution $\boldsymbol{a}$. In analogy to expression 3 the expectation of x_i for all chains of events starting with the distribution $a_1, a_2, \ldots a_m$ and reaching the final state k is:

$$\langle x_i \rangle = \alpha_i a_i + \sum_{l_1=1}^{m} \pi_{il_1}\alpha_{l_1} p_{il_1} a_{l_1} + \sum_{l_2=1}^{m}\sum_{l_1=1}^{m} \pi_{il_2}\pi_{l_2 l_1}\alpha_{l_1} p_{il_2} p_{l_2 l_1} a_{l_1} + \ldots .$$

$$= \alpha_i a_i + \sum_{k=1}^{\infty} \sum_{l_k} \ldots \sum_{l_1} \pi_{il_k} \ldots \pi_{l_2 l_1}\alpha_{l_1} p_{il_k} \ldots p_{l_2 l_1} a_{l_1} . \tag{11}$$

In perturbation analysis the interest is focused on the difference of two (or more) estimates $\hat{x}_i^*$ and $\hat{x}_i$ being solutions of the two matrix equations

$$\hat{\boldsymbol{x}}^* = \boldsymbol{Q}\hat{\boldsymbol{x}}^* + \boldsymbol{b}^* \quad \text{and} \quad \hat{\boldsymbol{x}} = \boldsymbol{Q}\hat{\boldsymbol{x}} + \boldsymbol{b} , \tag{12}$$

which are of the same dimension and may differ only slightly from each other.

A straightforward approach would be to perform two independent calculations with $\boldsymbol{Q}^*$, $\boldsymbol{b}^*$ and $\boldsymbol{Q}$, $\boldsymbol{b}$ where $\boldsymbol{Q}^* = \boldsymbol{Q} + \Delta\boldsymbol{Q}$ and $\boldsymbol{b}^* = \boldsymbol{b} + \Delta\boldsymbol{b}$. In the case of two independent and uncorrelated computer runs the variance for the difference becomes

$$V(\Delta x) = V(x^*) + V(x) .$$

As $V(x^*)$ and $V(x)$ are always positive quantities, the relative variance $V(\Delta x)/|\Delta Q|$ is unbounded as $|\Delta Q| \to 0$.

Applying a correlation technique it is possible to avoid this shortcoming and to obtain a finite variance even for very small changes of the matrix $\boldsymbol{Q}$ and/or the start distribution $\boldsymbol{b}$. Correlation is achieved by mapping both systems $\boldsymbol{Q}^*$, $\boldsymbol{b}^*$ and $\boldsymbol{Q}$, $\boldsymbol{b}$ onto the same random walk process which we call the *reference system*. It is governed by a transition matrix $\boldsymbol{P}$ and a vector $\boldsymbol{a}$.

The *reference system* can be chosen arbitrarily, provided it satisfies the condition (2). If all $q_{ij}^* \geq 0$ and $q_{ij} \geq 0$ it can be constructed as the arithmetic mean of two (or more) systems $\boldsymbol{Q}^*$, $\boldsymbol{b}^*$ and $\boldsymbol{Q}$, $\boldsymbol{b}$.

$$p_{ij} = (q_{ij}^* + q_{ij})/2 , \tag{13}$$

or

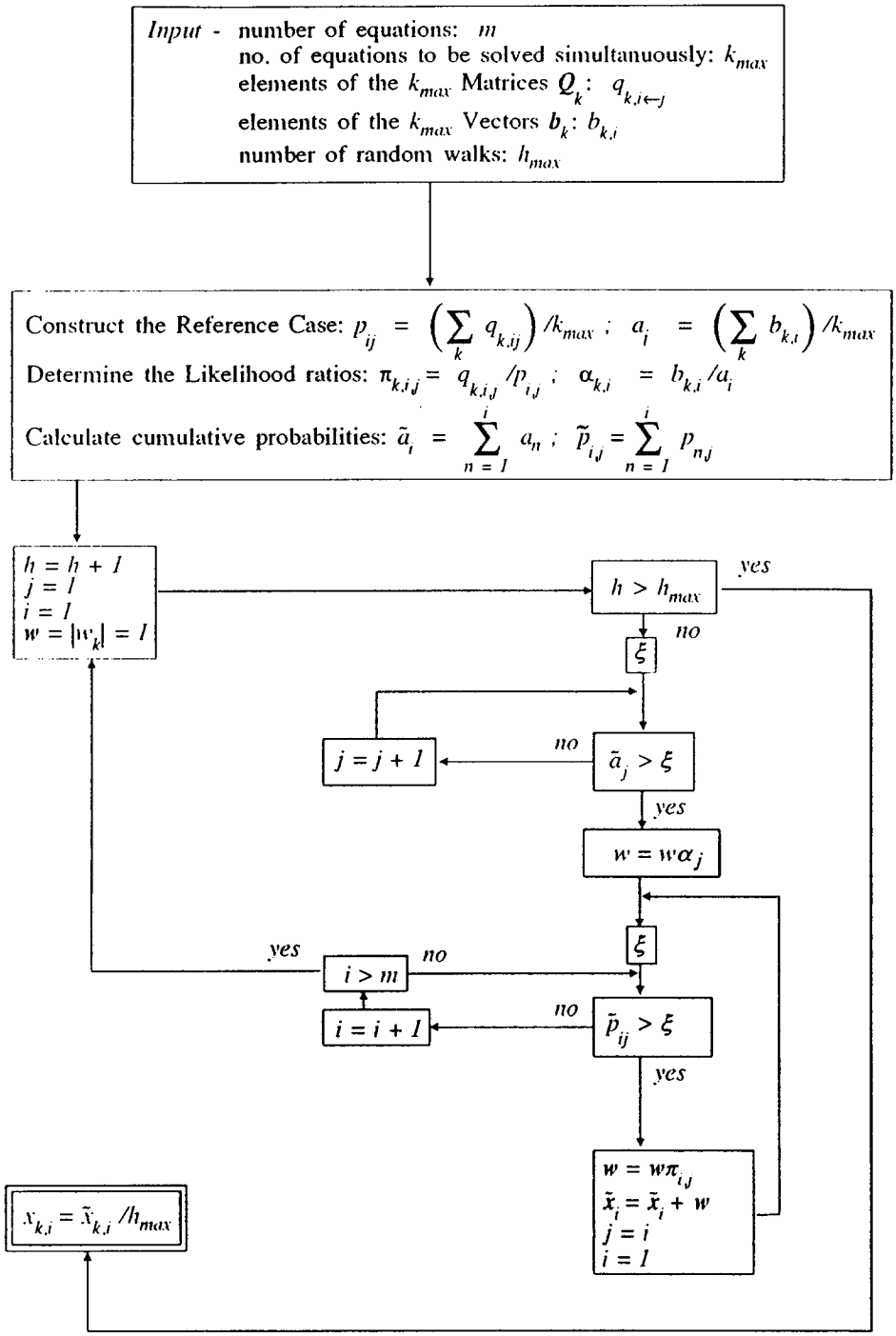

Figure 1: Flow-chart for the simultanuous solution of systems of Linear Matrix Equations by the *Multiple Correlation* algorithm. In constructing the reference case it is assumed that all $q_{k,i,j}$ are positive. For a large number of correlations the calculation of the vector sum $\tilde{x}=\tilde{x}+w$ benefits considerably from the use of a vector processor.

$$p_{ij} = \frac{max(|q_{ij}^*|,|q_{ij}|)}{\sum_i max(|q_{ij}^*|,|q_{ij}|)} \sum_i \frac{1}{2}\,(|q_{ij}^*|+|q_{ij}|)\ , \tag{14}$$

The *reference system* can also be identical with one of the systems Q^*, b^* or Q, b.

The *likelihood ratios* determining the solution of equations (11) are

$$\pi_{ij}^* = q_{ij}^*/p_{ij} \quad \text{and} \quad \alpha_i^* = b_i^*/a_i$$

$$\pi_{ij} = q_{ij}/p_{ij} \quad \text{and} \quad \alpha_i = b_i/a_i$$

These ratios should be as close to unity as possible.
With this assumption both systems follow the same random walk, one with the product of weights

$$w_n^* = w_{n-1}^*\,\pi_{l_n l_{n-1}}^* = \pi_{l_n l_{n-1}}^* \pi_{l_{n-1} l_{n-2}}^* \cdots \pi_{l_2 l_1}^* \alpha_{l_1}^* = \prod_{i=1}^{n} \pi_{l_i l_{i-1}}^*\ , \tag{15a}$$

and the other with

$$w_n = w_{n-1}\pi_{l_n l_{n-1}} = \pi_{l_n l_{n-1}} \pi_{l_{n-1} l_{n-2}} \cdots \pi_{l_2 l_1}\alpha_{l_1} = \prod_{i=1}^{n} \pi_{l_i l_{i-1}}\ , \tag{15b}$$

where $\pi_{l_1 l_0} = \alpha_{l_1}$ and $\pi_{l_1 l_0}^* = \alpha_{l_1}^*$.

To simplify the further considerations we assume that in Q^* only one element $\iota\eta$

$$q_{\iota\eta}^* = q_{\iota\eta} + \Delta q_{\iota\eta}\ ,$$

is different from Q and that Q, b serves as the reference system. With these assumptions all matrix elements of P are $p_{ij} = q_{ij}$ and all likelihood ratios π_{ij} and a_j are 1 except:

$$\pi_{\iota\eta}^* = \frac{q_{\iota\eta}+\Delta q_{\iota\eta}}{p_{\iota\eta}} = 1+\frac{\Delta q_{\iota\eta}}{q_{\iota\eta}} = 1+\Delta\rho_{\iota\eta}\ , \tag{16}$$

where $\Delta\rho_{\iota\eta}$ is the relative change of the element $q_{\iota\eta}$.
The score of the difference Δx_i in a *single* history (chain of events γ_k) is:

$$\Delta\hat{x}_i(\gamma_k) = \sum_{n=1}^{k} \left[\prod_{\nu=1}^{n} \left(1+\Delta\rho_{\iota\eta}\,\delta_{\iota l_\nu}\delta_{\eta l_{\nu-1}}\right)\pi_{l_\nu l_{\nu-1}} - \prod_{\nu=1}^{n} \pi_{l_\nu l_{\nu-1}}\right]\delta_{il_n}\ ,$$

$$= \sum_{n=1}^{k} \left\{\left[\prod_{\nu=1}^{n} \left(1+\Delta\rho_{\iota\eta}\,\delta_{\iota l_\nu}\delta_{\eta l_{\nu-1}}\right) - 1\right]\prod_{\nu=1}^{n} \pi_{l_\nu l_{\nu-1}}\right\}\delta_{il_n}\ . \tag{17}$$

If $\Delta\rho_{\iota\eta} \ll 1$ the following approximation is possible:

$$\prod_{\nu}\left(1+\Delta\rho_{\iota\eta}\,\delta_{\iota l_\nu}\delta_{\eta l_{\nu-1}}\right) \cong 1+\sum_{\nu}\Delta\rho_{\iota\eta}\,\delta_{\iota l_\nu}\delta_{\eta l_{\nu-1}} \,. \tag{18}$$

Introduced into equation (1.17) one has:

$$\Delta\hat{x}_i(\gamma_k) = \Delta\rho_{\iota\eta}\sum_{n=1}^{k}\left[\left(\sum_{\nu=1}^{n}\delta_{\iota l_\nu}\delta_{\eta l_{\nu-1}}\right)\prod_{\nu=1}^{n}\pi_{l_\nu l_{\nu-1}}\right]\delta_{il_n} \,. \tag{19}$$

After moving $\Delta\rho_{\iota\eta}$ to the left hand side and summing over all histories H (where $k(h)$ is the total number of transitions in the h-th history) the sample mean (Monte Carlo estimate) of $\Delta x_i/\Delta\rho_{\iota\eta}$ becomes

$$\lim_{\Delta\rho\to 0}\frac{\hat{\Delta x}_i}{\Delta\rho_{\iota\eta}} = \frac{1}{H}\sum_{h=1}^{H}\sum_{n=1}^{k(h)}\left[\left(\sum_{\nu=1}^{n}\delta_{\iota l_\nu}\delta_{\eta l_{\nu-1}}\right)\prod_{\nu=1}^{n}\pi_{l_\nu l_{\nu-1}}\right]\delta_{il_n} \,, \tag{20}$$

and in analogy to (9) its second moment is

$$\hat{\Delta x_i^2} = \frac{1}{H}\sum_{h=1}^{H}\left\{\Delta\rho_{\iota\eta}\sum_{n=1}^{k(h)}\left[\left(\sum_{\nu=1}^{n}\delta_{\iota l_\nu}\delta_{\eta l_{\nu-1}}\right)\prod_{\nu=1}^{n}\pi_{l_\nu l_{\nu-1}}\right]\delta_{il_n}\right\}^2 \,. \tag{21}$$

With the assumption that in Equation (20) all $\pi_{ij}=1$ and all $\alpha_j=1$ the variance of the relative perturbation is:

$$\lim_{\Delta\rho\to 0}\frac{var(\Delta\hat{x}_i)}{\Delta\rho_{\iota\eta}^2} = \frac{1}{H}\sum_{h=1}^{H}\left(\sum_{n=1}^{k(h)}\sum_{\nu=1}^{n}\delta_{\iota l_\nu}\delta_{\eta l_{\nu-1}}\right)^2 - \left(\frac{1}{H}\sum_{h=1}^{H}\sum_{n=1}^{k(h)}\sum_{\nu=1}^{n}\delta_{\iota l_\nu}\delta_{\eta l_{\nu-1}}\right)^2 \,. \tag{22}$$

As this expression is finite for all terminating random walk procedures, it proves that the *multiple correlation technique* proposed here, renders a bounded relative variance for arbitrarily small perturbations.

3. Differential Operator Sampling: Gradients (Sensitivities) and Higher Order Derivatives

Equation 20 yields another important result. The fact that

$$\frac{\partial\hat{x}_k}{\partial\rho_{ij}} = \lim_{\Delta\rho\to 0}\left(\frac{\Delta\hat{x}_k}{\Delta\rho_{ij}}\right) \qquad \text{where } i,j,k \in \{1,\ldots,m\}$$

allows the calculation of the *Jacobian* of the $\hat{x}_i$-s with respect to all transition probabilities q_{ij}-s by the unbiased random walk algorithm described above. A different and more general method of calculating simultaneously the $\hat{x}_i$-s and the derivatives of the $\hat{x}_i$-s is, however, shown in this paragraph. To this end we express the expectation of the x_i-s of Equation (8) by

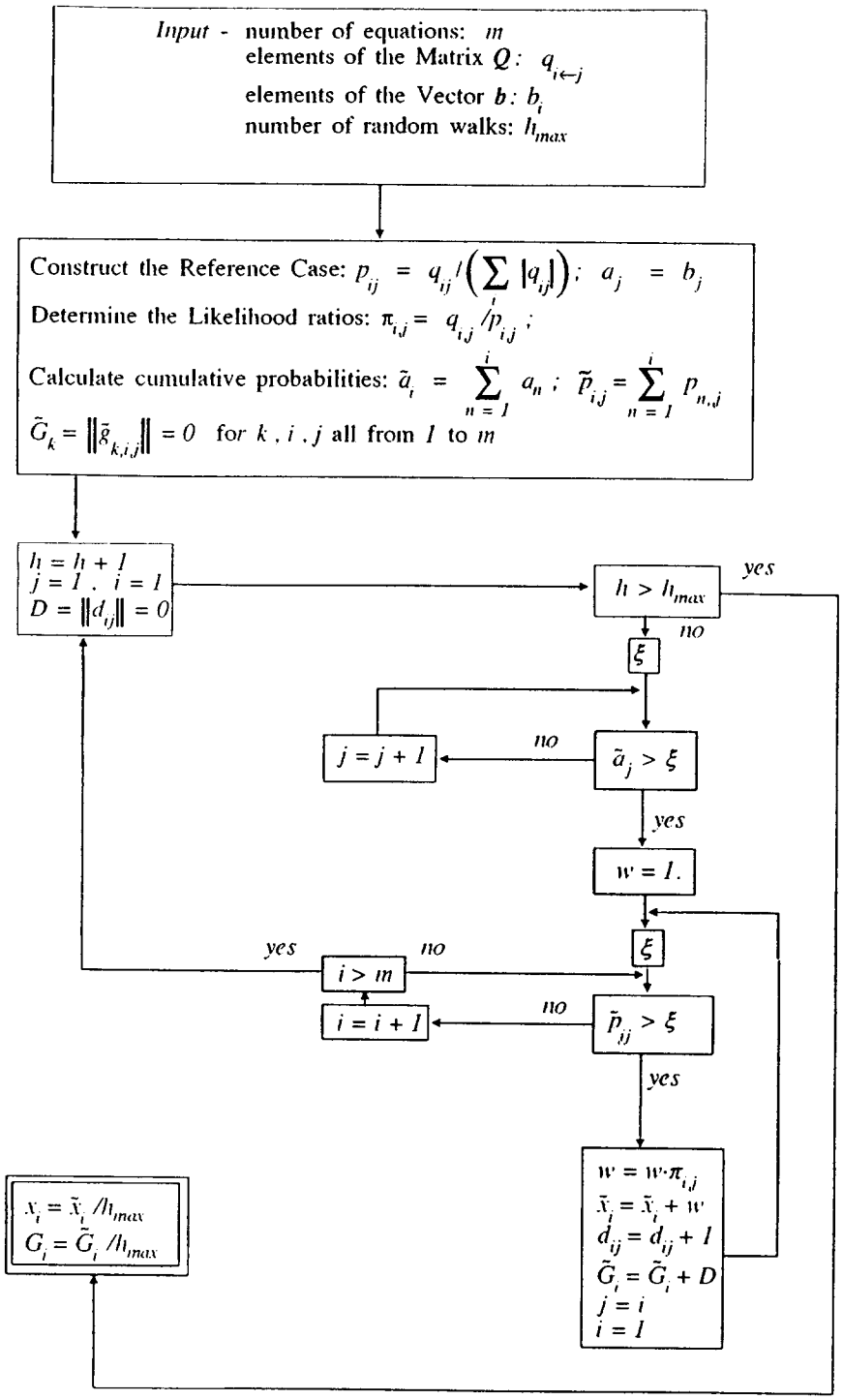

Figure 2: Flow-chart for calculating a system of linear equations including the first order derivatives (sensitivities) with respect to the elements q_{ij} of the matrix $\boldsymbol{Q}$. The matrix operation $\tilde{G}_i = \tilde{G}_i + D$ dominates the calculation effort for large *m-s* ($m > 10$). The use of a vector processor may therefor result in a considerable time saving.

their Neumann Series which describes the random walk procedure rendering the solution of the problem.

$$\langle x_i \rangle = b_i + \sum_{k=1}^{\infty} \sum_{l_k=1}^{m} \cdots \sum_{l_1=1}^{m} q_{il_k} \cdots q_{l_2 l_1} b_{l_1} . \tag{23a}$$

To simplify the further considerations this equation is rewritten in the following form:

$$\langle x_i \rangle = b_i + \sum_{k=1}^{\infty} \sum_{l_k} \cdots \sum_{l_1} \prod_{n=1}^{k+1} q_{l_n l_{n-1}} . \tag{23b}$$

where $q_{l_1 l_0} \equiv b_{l_1}$ and $q_{l_{k+1} l_k} \equiv q_{il_k}$

Now we assume that μ_k transitions $\iota \leftarrow \eta$ were encountered in the chain $\gamma_k = (l_1, \ldots l_k)$, where $\mu_k \in 0, 1, 2, 3, \ldots$ The procedure of differentiating $\langle x_i \rangle$ with respect to the element $q_{\iota\eta}$ becomes more transparen if we take the $q_{\iota\eta}$-s out of the product term so that only thus q-s remain for which $l_n \leftarrow l_{n-1} \neq \iota \leftarrow \eta$. This is formally expressed by the modified upper product boundary $k^* + 1 = k - \mu_k + 1$

$$\langle x_i \rangle = b_i + \sum_{k=1}^{\infty} \sum_{l_k} \cdots \sum_{l_1} q_{\iota\eta}^{\mu_k} \prod_{n=1}^{k^*+1} q_{l_n l_{n-1}} .$$

Differentiation with respect to the element $q_{\iota\eta}$ leads to

$$\left\langle \frac{\partial x_i}{\partial q_{\iota\eta}} \right\rangle = \sum_{k=1}^{\infty} \sum_{l_k} \cdots \sum_{l_1} \mu_k q_{\iota\eta}^{\mu_k - 1} \prod_{n=1}^{k^*+1} q_{l_n l_{n-1}} . \tag{24}$$

Putting $q^{\mu}{}_{\iota\eta}$ back into the product Π this Equation can be rewritten as

$$\left\langle \frac{\partial x_i}{\partial q_{\iota\eta}} \right\rangle = \sum_{k=1}^{\infty} \sum_{l_k} \cdots \sum_{l_1} \frac{\mu_k}{q_{\iota\eta}} \prod_{n=1}^{k+1} q_{l_n l_{n-1}} . \tag{25}$$

Again, as in 2, we generalize the Markovian chain process by mapping it onto a random walk system governed by the matrix $\| p_{ij} \|$. Finally, with $\partial q/q = \partial \rho$ one obtains:

$$\left\langle \frac{\partial x_i}{\partial \rho_{\iota\eta}} \right\rangle = \sum_{k=1}^{\infty} \sum_{l_k} \cdots \sum_{l_1} \mu_k \prod_{n=1}^{k+1} \pi_{l_n l_{n-1}} \prod_{n=1}^{k+1} p_{l_n l_{n-1}} . \tag{26}$$

where $p_{l_1 l_0} \equiv a_{l_1}$ $\pi_{l_1 l_0} \equiv \alpha_{l_1}$ $p_{l_{k+1} l_k} \equiv p_{il_k}$ and $\pi_{l_{k+1} l_k} \equiv \pi_{il_k}$

This equation can be interpreted in terms of the same random walk process by which the

expectation $\langle x_i \rangle$ is obtained. In the chain γ_k a counter μ_k must be increased by 1 each time a transition from η to ι occurs . Simultaneously the value of the counter is multiplied with the weight w_{k+1} (see 15) and added to the score from which the sample mean of the derivative of x_i with respect to $q_{\iota\eta}$ is calculated.

$$\widehat{\frac{\partial x_i}{\partial \rho_{\iota\eta}}} = \frac{1}{H}\sum_{h=1}^{H}\sum_{n=1}^{k(h)}\left[\left(\sum_{\nu=1}^{n}\delta_{\iota l_\nu}\delta_{\eta l_{\nu-1}}\right)\prod_{\nu=1}^{n}\pi_{l_\nu l_{\nu-1}}\right]\delta_{i l_n} . \tag{27}$$

It says: - if the first transition occurs from the source state $l_0 = \eta$ into $l_1 = \iota$ or from a later transition state $l_{\nu-1} = \eta$, $l_\nu = \iota$ and if at the same time $i = \iota$ then $1w_1$ is added to the score of $\partial\hat{x}_i/\partial q_{\iota\eta}$; - if later on in the chain of events γ_k a second transition from $l_{\nu-1} = \eta$ to $l_\nu = \iota$ occurs and if at the same time $i = \iota$ then $2w_\nu$ is added to the score of $\partial\hat{x}_i/\partial q_{\iota\eta}$ and so on. The expression is identical to (20).

Figure 2 shows a flow-chart for a Monte Carlo procedure by which the derivatives of all x_k-s with respect to all π_{ij} (or p_{ij}) can be estimated. The results are listed in m two- dimensional matrices $\boldsymbol{G}_k = \|g_{ij}\|_k$, where $i, j, k = \{1, 2, \ldots, m\}$

$$\frac{\partial \hat{x}_k}{\partial \rho_{ij}} = g_{kij} . \tag{28}$$

To obtain the *second-order derivative* expression (24) is again differentiated with respect to $q_{\iota\eta}$ leading to the expectation

$$\left\langle \frac{\partial^2 x_i}{\partial q^2_{\iota\eta}} \right\rangle = \sum_{k=1}^{\infty}\sum_{l_k}\cdots\sum_{l_1}\mu_k(\mu_k - 1)q_{\iota\eta}^{\mu_k - 2}\prod_{n=1}^{k^*+1} q_{l_n l_{n-1}} .$$

Replacing $\partial q^2/q^2$ by $\partial\rho^2$ and following the procedure described above we obtain

$$\left\langle \frac{\partial^2 x_i}{\partial \rho^2_{\iota\eta}} \right\rangle = \sum_{k=1}^{\infty}\sum_{l_k}\cdots\sum_{l_1}\left(\mu_k^2 - \mu_k\right)\prod_{n=1}^{k+1}\pi_{l_n l_{n-1}}\prod_{n=1}^{k+1} p_{l_n l_{n-1}} . \tag{29}$$

and the corresponding sample mean

$$\widehat{\frac{\partial^2 x_i}{\partial \rho^2_{\iota\eta}}} = \frac{1}{H}\sum_{h=1}^{H}\sum_{n=1}^{k(h)}\left\{\left[\left(\sum_{\nu=1}^{n}\delta_{\iota l_\nu}\delta_{\eta l_{\nu-1}}\right)^2 - \sum_{\nu=1}^{n}\delta_{\iota l_\nu}\delta_{\eta l_{\nu-1}}\right]\prod_{\nu=1}^{n}\pi_{l_\nu l_{\nu-1}}\right\}\delta_{i l_n} . \tag{30}$$

In a similar fashion the cross-terms can be determined if derivatives for two (or more) terms $q_{\iota\eta}$ and $q_{\kappa\lambda}$ are required:

$$\left\langle \frac{\partial^2 x_i}{\partial \rho_{i\eta} \partial \rho_{\kappa\lambda}} \right\rangle = \sum_{k=1}^{\infty} \sum_{l_k} \cdots \sum_{l_1} (\mu_k \nu_k) \prod_{n=1}^{k} \pi_{l_n l_{n-1}} \prod_{n=1}^{k} p_{l_n l_{n-1}} \tag{31}$$

In this case the sample mean is

$$\widehat{\frac{\partial^2 x_i}{\partial \rho_{i\eta} \partial \rho_{\kappa\lambda}}} = \frac{1}{H} \sum_{h=1}^{H} \sum_{n=1}^{k(h)} \left\{ \left[\left(\sum_{\nu=1}^{n} \delta_{il_\nu} \delta_{\eta l_{\nu-1}} \right) \left(\sum_{\nu=1}^{n} \delta_{\kappa l_\nu} \delta_{\lambda l_{\nu-1}} \right) \right] \prod_{\nu=1}^{n} \pi_{l_\nu l_{\nu-1}} \right\} \delta_{il_n} . \tag{32}$$

4. Examples

To demonstrate the functioning of multiple correlation and differential operator sampling described in 2 and 3, the author wrote two *Fortran 77* programs following the schemes developed in Figure 1 and 2. The programs use dynamic storage allocation so that the number of equations is only limited by the available memory space. Experience has shown that scores must be collected in double precision (64 bit) arrays. In the case of differential operator sampling the execution time can be substantially shortened if the score of the Jacobian is calculated by a vector processor.

Example 1 consists of a system of 3 linear equations. The random walk solution can easily be verified by a deterministic method such as *Cramer's Rule*.

$$\begin{pmatrix} x_{1,1} \\ x_{1,2} \\ x_{1,3} \end{pmatrix} = \begin{pmatrix} .25, .50, .08 \\ .30, .30, .10 \\ .20, .20, .20 \end{pmatrix} \begin{pmatrix} x_{1,1} \\ x_{1,2} \\ x_{1,3} \end{pmatrix} + \begin{pmatrix} .30 \\ .30 \\ .40 \end{pmatrix}$$

In the following perturbation analysis carried out either by *multiple correlation (a)* or a *first-order Taylor approximation (b)* two small parameter changes in q_{ij} are considered. In one case q_{11} is increased by *1%* leading to the system

$$\begin{pmatrix} x_{2,1} \\ x_{2,2} \\ x_{2,3} \end{pmatrix} = \begin{pmatrix} .2525, .50, .08 \\ .30, .30, .10 \\ .20, .20, .20 \end{pmatrix} \begin{pmatrix} x_{2,1} \\ x_{2,2} \\ x_{2,3} \end{pmatrix} + \begin{pmatrix} .30 \\ .30 \\ .40 \end{pmatrix}$$

and in the other case q_{32} is decreased by *1%* leading to

$$\begin{pmatrix} x_{3,1} \\ x_{3,2} \\ x_{3,3} \end{pmatrix} = \begin{pmatrix} .25, .50, .08 \\ .30, .30, .10 \\ .20, .198, .20 \end{pmatrix} \begin{pmatrix} x_{3,1} \\ x_{3,2} \\ x_{3,3} \end{pmatrix} + \begin{pmatrix} .30 \\ .30 \\ .40 \end{pmatrix}$$

a) Multiple Correlation: The samples of 50.000 random walks provided for the three

equations (k = 1 to 3) the results shown in *Table 1*.

b) Differential Operator Sampling: In this example simultaneously with the unknowns x_1, x_2, x_3 also their derivatives (Jacobians) with respect to the parameters q_{ij} are calculated. The perturbation of *1%* is so small that a linear Taylor expansion using the sensitivity coefficients $\partial x_k / \partial q_{ij}$ provide good perturbation estimates. Applying the scheme of *Figure 2* the results listed in *Table* 2 were obtained.

Discussion of results: In the second and third column of *Table 3* the results from *multiple correlation* ($\Delta x_{ki} = x_{ki} - x_{1i}$) and a linear Taylor approximation ($\Delta\rho = 0.01$) based on *differential operator sampling* are listed. Comparing these values with each other and a deterministic solution listed in column four shows excellent agreement of the perturbation effect. On the other hand it can be seen that the results from two independent Monte Carlo runs listed in the last column have a standard deviation which is much larger than the differental effect and up to two orders of magnitude greater than that of the correlated calculation.

```
*** LISTING OF OUTPUT ***

NO. OF RAND.WALKS:    50000
EXEC. TIME= 8.39600E+01 [sec]

 THE UNKNOWNS X(K,I) ARE :
              X(K, 1)     X(K, 2)     X(K, 3)
    K= 1   1.2715E+00  1.1360E+00  1.1062E+00
    S.D.   6.9057E-03  7.3807E-03  4.2029E-03
    K= 2   1.2782E+00  1.1392E+00  1.1086E+00
    K= 3   1.2706E+00  1.1351E+00  1.1029E+00

 THE DIFFERENCES DX(K,I)=X(K,I)-X(1,I) ARE :
              DX(K, 1)    DX(K, 2)    DX(K, 3)
    K= 2   6.7040E-03  3.2691E-03  2.4344E-03
    S.D.   1.1089E-04  7.4829E-05  4.4329E-05
    K= 3  -9.0042E-04 -8.0541E-04 -3.2822E-03
    S.D.   2.6821E-05  2.9303E-05  3.7437E-05
```

Table 1: Perturbation analysis of 3 linear equations carried out by *Multiple Correlation.*

```
EXEC. TIME= 7.31000E+01 [sec]
NO. OF RAND.WALKS:    50000

 X( 1)= 1.272  X( 2)= 1.137  X( 3)= 1.106

JACOBIAN OF X( 1) WITH RESPECT TO:
              RHO(I, 1)   RHO(I, 2)   RHO(I, 3)
    I= 1   6.6790E-01  1.1941E+00  1.0040E-01
    I= 2   6.1000E-01  5.4006E-01  1.0042E-01
    I= 3   1.1176E-01  9.0000E-02  8.7500E-02

JACOBIAN OF X( 2) WITH RESPECT TO:
              RHO(I, 1)   RHO(I, 2)   RHO(I, 3)
    I= 1   3.2602E-01  5.0052E-01  9.2300E-02
    I= 2   8.6000E-01  7.7624E-01  2.5632E-01
    I= 3   1.0516E-01  0.0660E-02  0.2900E-02

JACOBIAN OF X( 3) WITH RESPECT TO:
              RHO(I, 1)   RHO(I, 2)   RHO(I, 3)
    I= 1   2.4232E-01  4.3694E-01  7.0400E-02
    I= 2   3.6390E-01  3.3066E-01  1.0954E-01
    I= 3   3.7564E-01  3.2856E-01  3.1990E-01
```

Table 2: Differental Operator Sampling in a system of 3 linear equations.

i	Δx_{2i} *mult. corr.*	$(\partial x_i/\partial \rho_{11})\,\Delta\rho$	Δx_{2i} *analytical*	Δx^*_{2i} *2 indep. M.C. runs*
1	*6.70E–3*	*6.68E–3*	*6.66E–3*	*0.9E–3*
	± 0.11E–3			*± 9.9E–3*
2	*3.27E–3*	*3.27E–3*	*3.20E–3*	*– 2.1E–3*
	± 0.07E–3			*± 10.4E–3*
3	*2.43E–3*	*2.42E–3*	*2.46E–3*	*0.6E–3*
	± 0.04E–3			*± 5.9E–3*
i	Δx_{3i}	$(\partial x_i/\partial \rho_{32})(-\Delta\rho)$		Δx^*_{3i}
1	*– 9.08E–4*	*– 9.08E–4*	*– 9.25E–4*	*2.3E–3*
	± 0.26E–4			*± 9.9E–3*
2	*– 8.85E–4*	*– 8.87E–4*	*– 8.64E–4*	*5.6E–3*
	± 0.29E–4			*± 10.5E–3*
3	*– 3.28E–3*	*– 3.29E–3*	*– 3.28E–3*	*– 9.1E–3*
	± 0.04E–3			*± 5.9E–3*

Table 3: Comparison of Perturbation Estimates

Example 2 deals with multiple correlation estimates using *reference equations* constructed in two different manners. The first is based on the *arithmetic mean* as in expression *3.11* and the other on the slightly modified procedure *5.13*. (Note the difference in the *likelihood ratios* in *Table 1.4* and *Table 1.5.)* In both cases we solve the first equation of the previous example assuming that in the perturbed case *q(1,3)* changes from *0.08* to *0.0*.

With the *reference equation* based on the arithmetic mean *50.000* random walks render the results listed in *Table 1.4*. The same problem calculated with a *reference equation* based on the procedure 5.14 leads to the results of *Table 1.5*.

```
*** INPUT DATA ***

CUMULATIVE PROBABILITIES OF P(I,J):
          P(I, 1)       P(I, 2)       P(I, 3)
  I= 1  2.5000E-01 5.0000E-01 4.0000E-02
  I= 2  5.5000E-01 8.0000E-01 1.4000E-01
  I= 3  7.5000E-01 1.0000E+00 3.4000E-01

LIKELIHOOD RATIOS PI( 1,I,J) :
          PI( 1,I, 1)   PI( 1,I, 2)   PI( 1,I, 3)
  I= 1  1.0000E+00 1.0000E+00 2.0000E+00
  I= 2  1.0000E+00 1.0000E+00 1.0000E+00
  I= 3  1.0000E+00 1.0000E+00 1.0000E+00

LIKELIHOOD RATIOS PI( 2,I,J) :
          PI( 2,I, 1)   PI( 2,I, 2)   PI( 2,I, 3)
  I= 1  1.0000E+00 1.0000E+00 0.0000E+00
  I= 2  1.0000E+00 1.0000E+00 1.0000E+00
  I= 3  1.0000E+00 1.0000E+00 1.0000E+00


*** LISTING OF OUTPUT ***

NO. OF RAND.WALKS:   50000
EXEC. TIME= 4.47600E+01 [sec]

 THE UNKNOWNS X(K,I) ARE :
          X(K, 1)       X(K, 2)       X(K, 3)
 K= 1  1.2699E+00 1.1364E+00 1.1087E+00
 S.D.  ±7.8462E-03 ±7.8264E-03 ±4.5533E-03
 K= 2  1.0972E+00 1.0550E+00 1.0451E+00

 THE DIFFERENCES DX(K,I)=X(K,I)-X(1,I) ARE :
          DX(K, 1)      DX(K, 2)      DX(K, 3)
 K= 2 -1.7268E-01 -8.1400E-02 -6.3560E-02
 S.D.  ±4.8356E-03 ±3.5014E-03 ±2.2833E-03
```

Table 1.4: Perturbation analysis of 3 linear equations carried out by *Multiple Correlation* and a *reference case* based on the *arithmetic mean.*

```
*** INPUT DATA ***

CUMULATIVE PROBABILITIES OF P(I,J):
          P(I, 1)       P(I, 2)       P(I, 3)
  I= 1  2.5000E-01 5.0000E-01 7.1579E-02
  I= 2  5.5000E-01 8.0000E-01 1.6105E-01
  I= 3  7.5000E-01 1.0000E+00 3.4000E-01

LIKELIHOOD RATIOS PI( 1,I,J) :
          PI( 1,I, 1)   PI( 1,I, 2)   PI( 1,I, 3)
  I= 1  1.0000E+00 1.0000E+00 1.1176E+00
  I= 2  1.0000E+00 1.0000E+00 1.1176E+00
  I= 3  1.0000E+00 1.0000E+00 1.1176E+00

LIKELIHOOD RATIOS PI( 2,I,J) :
          PI( 2,I, 1)   PI( 2,I, 2)   PI( 2,I, 3)
  I= 1  1.0000E+00 1.0000E+00 0.0000E+00
  I= 2  1.0000E+00 1.0000E+00 1.1176E+00
  I= 3  1.0000E+00 1.0000E+00 1.1176E+00


*** LISTING OF OUTPUT ***

NO. OF RAND.WALKS:   50000
EXEC. TIME= 4.46700E+01 [sec]

 THE UNKNOWNS X(K,I) ARE :
          X(K, 1)       X(K, 2)       X(K, 3)
   K= 1  1.2720E+00 1.1369E+00 1.1108E+00
   S.D.  ±7.2779E-03 ±7.6264E-03 ±4.5107E-03
   K= 2  1.0955E+00 1.0498E+00 1.0450E+00

 THE DIFFERENCES DX(K,I) = X(K,I) - X(1,I) ARE :
          DX(K, 1)      DX(K, 2)      DX(K, 3)
   K= 2 -1.7644E-01 -8.7145E-02 -6.5822E-02
   S.D.  ±3.6295E-03 ±2.7564E-03 ±1.7438E-03
```

Table 1.5: Perturbation analysis of 3 linear equations carried out by *Multiple Correlation* and a *reference case* based on the *procedure 3.12.*

It is interesting to note, that the second type of *reference equation* improves the efficiency of calculating the perturbation effects [DX(K,I)] almost by a factor of two.
(e.g.: $2.28^2 / 1.74^2 = 1.7$)
For completeness the same perturbation effects are also calculated by a linear Taylor expansion using $\Delta\rho = -1$ and the corresponding elements of the Jacobian calculated in *example 1:*

$$(\partial x_1 / \partial \rho_{1,1,3})\,\Delta\rho = -1.885E{-}1, \quad (\partial x_2 / \partial \rho_{2,1,3})\,\Delta\rho = -9.23E{-}2, \quad (\partial x_3 / \partial \rho_{3,1,3})\,\Delta\rho = -7.04E{-}2$$

These approximations show a small, but systematic deviation from the "exact" solution

obtained by the correlation technique.
The examples shown above were calculated on an *Archimedes 440 (ACORN Computers Ltd., UK)* home computer with an ARM2 processor and a FP Co-processor.

REFERENCES

1. Hammersley J.M., Handscomb D.C., *Monte Carlo Methods*, (Methuen & Co. Ltd, London, 1964)
2. Rief H., *A Synopsis of Monte Carlo Perturbation Algorithms*, J. of Computational Physics, to be published (1993)

HYBRID S_N/MONTE CARLO RESEARCH AND RESULTS

R. S. Baker
Radiation Transport Group, MS B226
Los Alamos National Laboratory
Los Alamos, New Mexico 87545 USA

ABSTRACT

The neutral particle transport equation is solved by a hybrid method that iteratively couples regions where deterministic (S_N) and stochastic (Monte Carlo) methods are applied. The Monte Carlo and S_N regions are fully coupled in the sense that no assumption is made about geometrical separation or decoupling. The hybrid Monte Carlo/S_N method provides a new means of solving problems involving both optically thick and optically thin regions that neither Monte Carlo nor S_N is well suited for by themselves. The hybrid method has been successfully applied to realistic shielding problems.

The vectorized Monte Carlo algorithm in the hybrid method has been ported to the massively parallel architecture of the Connection Machine. Comparisons of performance on a vector machine (Cray Y-MP) and the Connection Machine (CM-2) show that significant speedups are obtainable for vectorized Monte Carlo algorithms on massively parallel machines, even when realistic problems requiring variance reduction are considered. However, the architecture of the Connection Machine does place some limitations on the regime in which the Monte Carlo algorithm may be expected to perform well.

INTRODUCTION

TWODANT/MC[1-3] is an extension to the existing S_N code TWODANT. TWODANT/MC solves the neutral particle transport equation by a hybrid method that iteratively couples regions where deterministic (S_N) and stochastic (Monte Carlo) methods are applied. Unlike previous hybrid methods,[4] the Monte Carlo and S_N regions are fully coupled in the sense that no assumption is made about geometrical separation or decoupling. TWODANT/MC provides a new means of solving problems involving both optically thick and optically thin regions that neither Monte Carlo nor S_N is well suited for by themselves. TWODANT/MC is capable of solving forward, inhomogeneous source problems in $X-Y$ and $R-Z$ geometries. This capability includes multigroup problems involving upscatter and fission.

The fully coupled Monte Carlo/S_N technique used in TWODANT/MC consists of defining spatial and/or energy regions of a problem in which either a Monte Carlo calculation or an S_N calculation is to be performed. The Monte Carlo region may comprise the entire spatial region for selected energy groups, or may consist of a rectangular area that is either completely or partially embedded in an arbitrary S_N region. The Monte Carlo and S_N regions are then connected through the common angular boundary fluxes and scattering/fission sources, which are determined iteratively using the response matrix technique.

The hybrid method has been implemented in TWODANT/MC by adding special-purpose vectorized Monte Carlo subroutines, and linkage subroutines to carry out the interface flux iterations. The common angular boundary fluxes are included in TWODANT as interior boundary sources, leaving the logic for the S_N solution of the transport flux unchanged, while the diffusion synthetic accelerator remains effective in accelerating the S_N calculations. The physical description of the Monte Carlo region is derived from the standard TWODANT input file, reducing the required user input at some expense in generality, since this limits the Monte Carlo region to two-dimensional $X-Y$ and $R-Z$ grids. The S_N cross sections are used to form multigroup cross sections for the Monte Carlo region.

THEORY

Let ${}^{*}\vec{\psi}^{in}$ represent the flux entering the Monte Carlo region from the S_N region, and ${}^{+}\vec{\psi}^{out}$ the flux entering the S_N region from the Monte Carlo region. Then, the outgoing flux from the Monte Carlo region is related to the incoming flux from the S_N region by

$$ {}^{+}\vec{\psi}^{out} = {}^{+}\mathbf{R}^{*}_{mc}\, {}^{*}\vec{\psi}^{in} + {}^{+}\vec{S}^{out}, \tag{1} $$

where ${}^{+}\vec{S}^{out}$ is the exiting flux from the Monte Carlo region under vacuum boundary conditions (${}^{*}\vec{\psi}^{in} = 0$), and ${}^{+}\mathbf{R}^{*}_{mc}$ is the Monte Carlo response matrix.

The fluxes entering (${}^{*}\vec{\psi}^{in}$) and leaving (${}^{+}\vec{\psi}^{out}$) the Monte Carlo region are represented numerically as N_{in} and N_{out} length vectors, respectively. Since the Monte Carlo/S_N boundary may consist of both spatial and energy interfaces, N_{in} does not necessarily equal N_{out}. That is, although the number of discretized states along the spatial boundary (energy x spatial x discrete direction) are the same for ${}^{*}\vec{\psi}^{in}$ and ${}^{+}\vec{\psi}^{out}$, the number of discretized states along the energy boundary (energy x spatial x angular moment) are not, since a different number of Monte Carlo energy groups may be reachable from collisions in the S_N groups than vice versa (see Figure 1 for an example). Here, we

use an asterisk (*) to indicate a dimension of length N_{in} and a plus ($^+$) for a dimension of length N_{out}.

Equation (1) is solved iteratively by

$$ {}^+\vec{\psi}^{out(p+1)} = {}^+\mathbf{R}^*_{mc} \, {}^*\vec{\psi}^{in(p)} + {}^+\vec{S}^{out}, \tag{2} $$

where we set ${}^+\vec{\psi}^{out(1)} = {}^+\vec{S}^{out}$, and ${}^*\vec{\psi}^{in(p)}$ is obtained by using an S_N solver (TWODANT) with the prescribed boundary flux ${}^+\vec{\psi}^{out(p)}$. Note that for problems involving upscatter/fission, the S_N calculation includes multiple outer iterations, as usual.

Since ${}^+\mathbf{R}^*_{mc}$ is an $N_{out} \times N_{in}$ sized matrix and, for multigroup problems in two dimensions, N_{out} and N_{in} are typically on the order of 10^5 to 10^6, the direct calculation/storage of the Monte Carlo response matrix is not feasible. Instead, the response matrix is represented by P orthogonal interface basis vectors,[5] where P typically ranges from 4 to 8. This reduces the size of the Monte Carlo response matrix to $N_{out} \times P$. Furthermore, after $P+1$ iterations, a $P \times P$ representation of the overall S_N/Monte Carlo response matrix can be obtained. Then, since P is small, the converged interface boundary fluxes can be predicted using direct inversion.

IMPLEMENTATION

Each interface state on the Monte Carlo/S_N boundary corresponds to a unique spatial cell, energy group, and angular direction, for spatial interfaces, or angular moment, for energy interfaces. An angular bin $\Delta\vec{\Omega}^m$ is used to assign a range of continuous Monte Carlo directions to the discrete S_N direction $\vec{\Omega}^m$. Since S_N quadrature sets specify the angular weight (the area subtended on the unit sphere by $\Delta\vec{\Omega}^m$) for each S_N direction, but not its shape, there is considerable freedom in defining the $\Delta\vec{\Omega}^m$. The system we use is depicted in Fig. 2. Note that as a particle streams in $R-Z$ geometry, $\vec{\Omega}_z$ remains constant. The bin configuration we have chosen preserves this property, since streaming particles can only flow into bins whose quadrature directions have the same $\vec{\Omega}_z$.

As explained in Ref. 1, the Monte Carlo region ideally comprises a zone of low scattering material, surrounded by a boundary layer ($\sim$ 1 mfp thick) of highly scattering material. Although eliminating the boundary layer from the Monte Carlo region would speed up the Monte Carlo calculations, it would also require using a higher quadrature order in the S_N calculation for accurate results, since the angular flux near a low-scattering region can be a rapidly varying function of angle and position. By including a boundary layer with the Monte Carlo region, a lower S_N quadrature order can be used. Note that for multigroup problems, the mean free path may vary from group to group, resulting in a Monte Carlo region of varying size (see Fig. 1).

The Monte Carlo routines in TWODANT/MC use the macroscopic multigroup S_N cross sections, so that no additional cross section input is required. The treatment of angular scattering is somewhat complicated, however, because the direct sampling of the group-to-group transfer moments is usually not possible since they may be negative. Instead, TWODANT/MC generates $L-1$ equiprobable bins, with L bin boundaries, such that the L Legendre moments of the angular scattering cross sections are (approximately) conserved. That is, in a P_4 approximation, the code will generate three equiprobable bins, with boundaries between $\mu = -1$ and $\mu = +1$, for sampling angular scattering directions. This approach is the same one currently used in the multigroup version of MCNP, and is further described in Ref. 6.

The special-purpose Monte Carlo routines implemented with TWODANT are basically analog routines since, ideally, the Monte Carlo region is low-scattering, and should not require extensive variance reduction methods. However, several basic variance reduction techniques have been incorporated. These include implicit capture, weight cutoffs, geometry splitting/Russian roulette, energy splitting/Russian roulette, and source direction biasing.

To increase the efficiency of the Monte Carlo calculations, the Monte Carlo routines have been vectorized through the formation of event-based stacks,[7] where each stack ideally consists of a group of 64 particles undergoing an identical event, such as a collision. On the Cray, assembly language routines are used to encode particle destination tag words, and to move particles between stacks. Vectorization resulted in a factor of four to five increase in speed of the vectorized Monte Carlo routines over the non-vectorized Monte Carlo routines on a Cray Y-MP.

RESULTS

The hybrid Monte Carlo/S_N method has been successfully applied to a realistic cylindrical duct shielding problem. The problem consists of a duct (void) with an isotropic ($\vec{\Omega}_z > 0$) neutron source incident at $z = 0$. The duct is surrounded by an iron liner, and an iron and water shield (see Fig. 3). Thirty energy groups are used in the problem, where the source neutrons are located in group 2 (13.5–15.0 MeV).

For the TWODANT/MC calculations, the Monte Carlo option was used only for the source energy group (Group 2), while pure S_N was used in all remaining energy groups. The void region along the centerline was designated as the Monte Carlo region, along with an additional 1 mfp boundary layer, which, for Group 2, was equivalent to 6 cm. Thus, the actual Monte Carlo region consisted of the void region, the iron liner (2 cm), and 4 cm of the shield (see Fig. 3). S_N was used in the remainder of the shield region for Group 2. The S_N calculation used an S_{12} quadrature order, with a P_4 Legendre expansion.

The neutron fluxes from the TWODANT/MC calculations, as well as the results from a multigroup MCNP calculation, are shown at Table 1, for selected regions of interest. The relative error in the MCNP results is shown in parentheses, while the difference (in terms of standard deviations) from the MCNP results is shown for the TWODANT/MC results. Note that the S_N/Monte Carlo results are all within three standard deviations of the multigroup MCNP results, and that most fall within two standard deviations.

MASSIVELY PARALLEL SIMD IMPLEMENTATION

The Monte Carlo algorithm in TWODANT/MC has been ported to the massively parallel SIMD architecture of Thinking Machines Corporation's CM-2/CM-200.[8] Although the coding was rewritten in CM FORTRAN, the Monte Carlo algorithm itself, which had already been vectorized as described above, was essentially unchanged. The most significant problem encountered in porting the algorithm to the CM was the expense of communications. With the event-stack method of vectorization, we have found that the time spent in moving particles between different event stacks typically averages around 10% for most problems on a Cray Y-MP with shared memory. Due to the distributed memory architecture of the CM, however, particle movement between stacks usually requires general ("router") communication, since a particle located in a particular position in Stack A may need to be moved to a different position in Stack B, and the particle movement

pattern is essentially random. Timing tests revealed that the problem time on the CM was entirely dominated by the time spent in moving particles between stacks, with an adverse affect on performance.

To remedy this, a two-step process was used to move particles between stacks. If in moving a particle from Stack A to Stack B, the corresponding location in Stack B (i.e., the element in Stack B located on the same VP (Virtual Processor) as Stack A's particle) is empty, the particle is moved directly into Stack B without any required communications. This is possible since all event-stack arrays are allocated as conformable arrays. If the corresponding location in Stack B is already filled, only then are general communications used to move the particle to an empty location in Stack B. Typically, 80% of the particle movement occurs "in place" for most problems, and only 20% requires general communications. However, even with these changes, communications still consumes over 50% of the total time for most problems.

To compare the performance of the vectorized Y-MP version of the algorithm against the parallelized CM version, we selected a sample two-dimensional well logging problem in $R - Z$ geometry (see Fig. 4), which we solved entirely by the Monte Carlo method. Given an (α,n) neutron source (AmBe) located in a tool positioned in the center of a borehole, the problem is to transport particles from the source out into the surrounding formation, then back into one of two ^{3}He detectors located in the tool. The detectors are protected by shields to prevent any direct contribution from the source. From the relative response of the two detectors, an analyst can then determine the porosity of the surrounding formation. The problem was run with geometry splitting/Russian roulette, implicit capture, source direction biasing, a .4 eV energy cutoff (for epithermal neutron porosity tools, the detectors are surrounded by cadmium foil), and thirty energy groups. At Figure 5, we present the speed (Source Particles/Minute (SPM)) for various VP ratios and number of source histories/batch on the CM-2, normalized to the speed of the Y-MP version (single processor). The abscissa gives the VP ratio, where a VP ratio of 2 corresponds to a stack size of 4096 particle events, since all CM-2 calculations were performed on a 2048 Processing Element (PE) machine. The ordinate is the ratio of the speed on the CM-2 to that of the Y-MP. The lines represent varying numbers of source histories/batch, from 80,000 to 2,560,000. We see that at low VP ratios (< 16), the performance of the CM-2 suffers. As the VP ratio increases for a fixed number of source histories/batch, the performance of the CM-2 increases, passes through a maximum, and then decreases. Also, although the performance at low VP ratios is relatively unaffected by the number of source histories/batch, that at higher VP ratios varies dramatically. In general, however, the performance of the massively parallel algorithm on the CM-2 is comparable to that of the vectorized version on a single processor Y-MP.

The performance of the CM-2 on the left-hand side of the graph is due to the nature of the CM-2 hardware, since each Floating Point Accelerator associated with a PE has a vector length of 4. Thus, efficient use of the CM-2 requires a minimum VP ratio of 4. To amortize the overhead associated with code execution, actual peak efficiency for the CM-2 is not usually achieved until VP ratios of 32 or 64. This is evident from the top (solid) line in Figure 5.

However, as the VP ratio goes up, the stack length also increases, and thus more particles are necessary to fill a stack. At some point, one runs out of source particles, and is forced to execute a less than full stack. This results in a degradation in stack efficiency. Obviously, the fewer the amount of source particles, and the more the last remaining particles "straggle", the lower the overall stack efficiency. As an example, the average collision stack efficiency for 80,000 source particles/batch ranged from 79%, at a VP ratio of 2, to just 6% at a VP ratio of 128. In contrast,

the collision stack_efficiency for 2,560,000 source particles/batch only varied from $\sim$ 100%, at a VP ratio of 2, to 72%, at a VP ratio of 128. Stack efficiency accounts for the drop-off in performance on the right-hand side of the graph.

Currently, for actual hybrid Monte Carlo/S_N calculations, the Monte Carlo calculation runs on the Connection Machine, while the S_N runs on the SUN front–end. Thus, the total calculation time on the CM for hybrid problems is greater than that on a Cray, due to the much slower processing of the S_N calculation by the SUN. However, we have recently developed a version of the code where the S_N calculation is performed on a Cray, the Monte Carlo calculation on a CM, and PVM (Parallel Virtual Machine) is used to link the calculations. This version is operational and undergoing testing, and we hope to report results in the near future.

CONCLUSIONS

TWODANT/MC provides a new means of solving inhomogeneous source problems in $X-Y$ or $R-Z$ geometry that neither Monte Carlo nor S_N is well suited for by themselves. These problems typically consist of those with a singular type source, such as a point or beam source, and/or large amounts of streaming through voids, which pose difficulties for S_N calculations, and also contain regions with large amounts of scattering, which increase the expense of Monte Carlo calculations. For these types of problems, the hybrid Monte Carlo/S_N method can perform more efficiently than either the S_N or Monte Carlo methods can alone. Since the Monte Carlo and S_N regions are fully coupled through the response matrix technique, the hybrid Monte Carlo/S_N method can be used even in situations where the Monte Carlo and S_N regions are closely coupled.

ACKNOWLEDGEMENTS

The hybrid Monte Carlo/S_N method was developed in conjunction with Raymond E. Alcouffe, Los Alamos National Laboratory, and William L. Filippone, University of Arizona. The cylindrical duct test problem and MCNP results were provided by William T. Urban, Los Alamos National Laboratory.

REFERENCES

1. "The S_N/Monte Carlo Response Matrix Hybrid Method", W. L. Filippone, and R. E. Alcouffe, *Nucl. Sci. & Eng.*, **100**, p. 209 (1988).

2. "The Multigroup and Radial Geometry Formulation of the Monte Carlo/S_N Response Matrix Method", R. S. Baker, W. L. Filippone, and R. E. Alcouffe, *Nucl. Sci. & Eng.*, **105**, p. 184 (1990).

3. "Extension of the Fully Coupled Monte Carlo/S_N Response Matrix Method to Problems Including Upscatter and Fission", R. S. Baker, W. L. Filippone, and R. E. Alcouffe, Int. Topical Meeting on Advances in Math., Comp., and Reactor Phy., **5**, p. 21.2 3–1, Pittsburgh, PA (1991).

4. "Domino, A General Purpose Code for Coupling Discrete Ordinates and Monte Carlo Radiation Transport Calculations", M. B. Emmett, C. W. Burgart, and T. J. Hoffman, ORNL–4853 (1973).

5. "The Monte Carlo/S_N Hybrid Method With Orthogonal Interface Basis Vectors", W. L. Filip-

pone, R. S. Baker, and R. E. Alcouffe, to be published, Joint Intl. Conf. on Math. Methods and Supercomputing in Nuclear Applications, Karlsruhe, Germany (1993).

6. "Transfer Matrix Treatments for Multigroup Monte Carlo Calculations – The Elimination of Ray Effects", L. L. Carter and C. A. Forest, *Nucl. Sci. & Eng.*, **59**, p. 27 (1976).

7. "Vectorized Monte Carlo Photon Transport", F. W. Bobrowicz, J. E. Lynch, K. J. Fisher, and J. E. Tabor, LANL Report LA-9752-MS (1983).

8. "Implementation of a Monte Carlo Algorithm for Neutron Transport on a Massively Parallel SIMD Machine", R. S. Baker, to be published, Joint Intl. Conf. on Math. Methods and Supercomputing in Nuclear Applications, Karlsruhe, Germany (1993).

Table 1

Neutron Fluxes for Cylindrical Duct Problem

Region	Flux	MCNP/MG	TWODANT/MC
I	Group 2	2.06-3 (.003)	2.05-3 (-1.6σ)
	Total	5.14-3 (.006)	5.15-3 (0.3σ)
II	Group 2	3.31-7 (.022)	3.35-7 (0.5σ)
	Total	9.46e-6 (.015)	9.04-6 (-3.0σ)
III	Group 2	4.42-5 (.019)	4.28-5 (-1.7σ)
	Total	2.28-4 (.021)	2.20-4 (-1.7σ)
IV	Group 2	1.11-8 (.042)	1.03-8 (-1.7σ)
	Total	4.07-7 (.038)	3.92-7 (-1.0σ)
V	Group 2	7.18-6 (.041)	6.92-6 (-0.9σ)
	Total	2.20-5 (.059)	1.91-5 (-2.2σ)
VI	Group 2	3.98-5 (.028)	3.82-5 (-1.4σ)
	Total	5.01-5 (.052)	4.63-5 (-1.5σ)

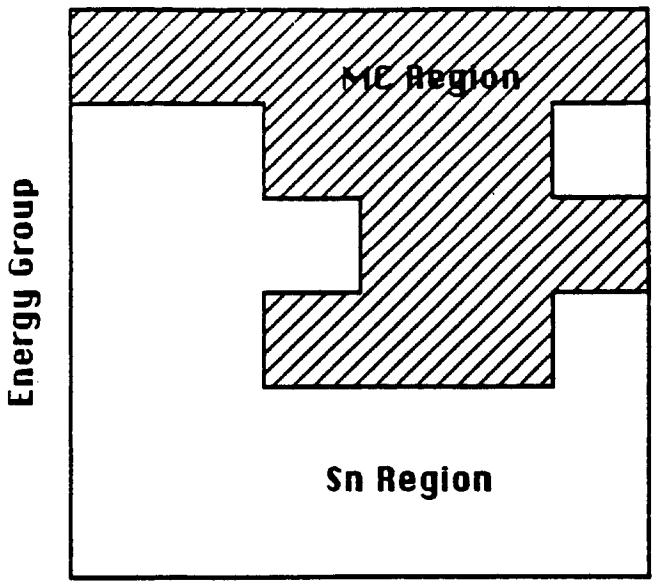

Fig. 1. Monte Carlo Region Size as a Function of Energy Group.

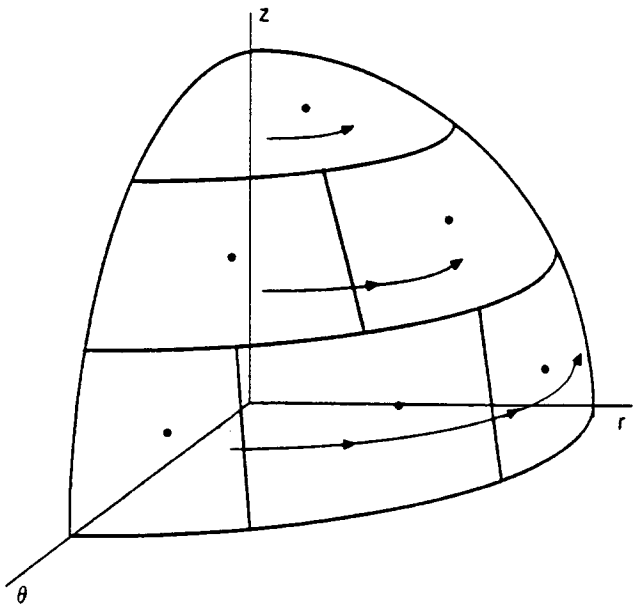

Fig. 2. The S_N Angular Bin Arrangement for N = 6.

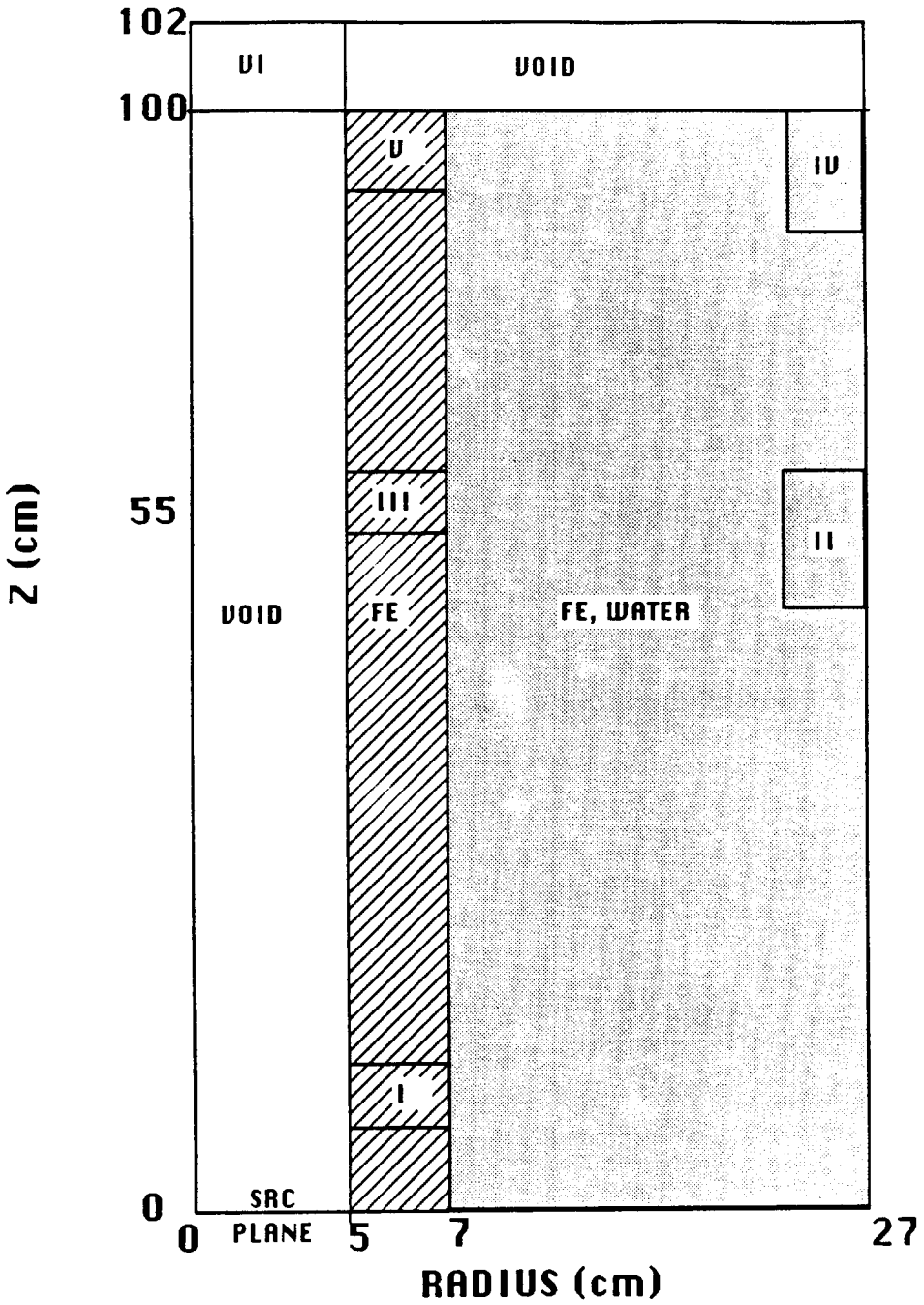

Fig. 3. Cylindrical Duct Shielding problem.

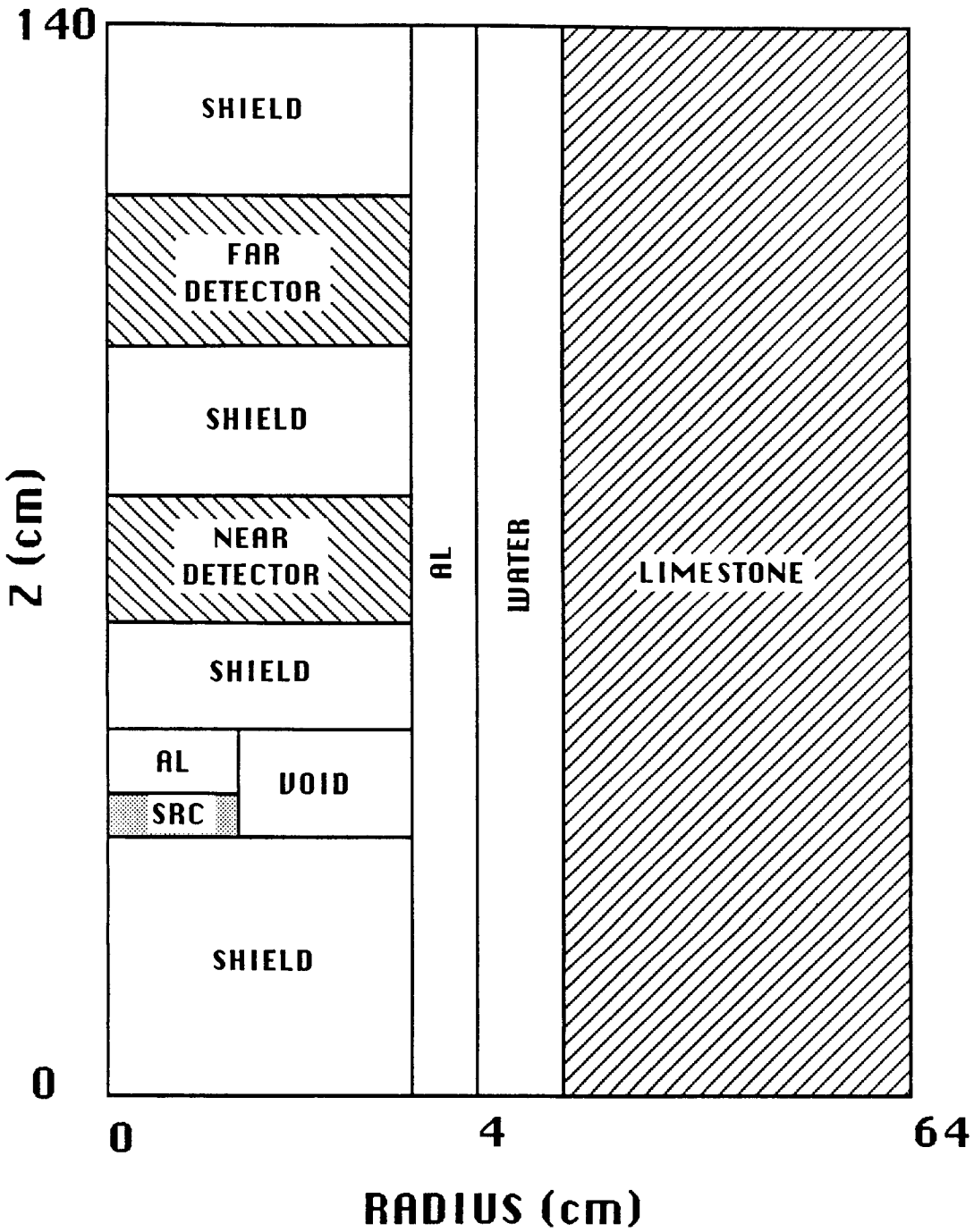

Fig. 4. Sample Two-Dimensional Well Logging Problem.

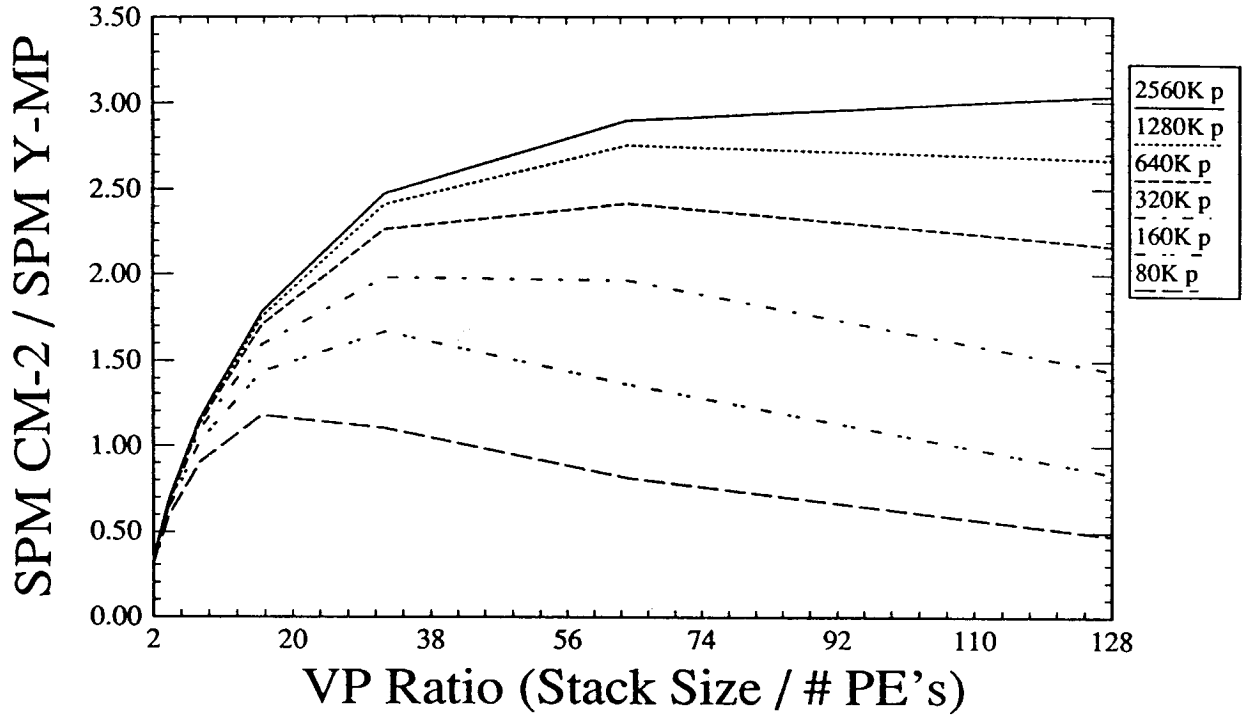

Fig. 5. CM-2 Performance, Well Logging Problem.

Recent Developments and Applications of the MORSE Code*

S. N. Cramer
Oak Ridge National Laboratory
Radiation Shielding Information Center
P.O. Box 2008
Oak Ridge, TN 37831-6362 USA

ABSTRACT

Several recent analyses using the multigroup MORSE Monte Carlo code are presented. (1) In the calculation of a highly directional-dependent neutron streaming experiment it is shown that P_7 cross section representation produces results virtually identical with those from an analog code. Use has been made here of a recently released ENDF/B-VI data set. (2) In the analysis of neutron distributions inside the water-cooled ORELA accelerator target and positron source, an analytic hydrogen scattering model is incorporated into the otherwise multigroup treatment. (3) The radiation from a nuclear weapon is analyzed in a large concrete building in Nagasaki by coupling MORSE and the DOT discrete ordinates code. The spatial variation of the DOT-generated free-field radiation is utilized, and the building is modeled with the array feature of the MORSE geometry package. (4) An analytic directional biasing, applicable to the discrete scattering angle procedure in MORSE, is combined with the exponential transform. As in more general studies, it is shown that the combined biasing is more efficient than either biasing used separately. Other tracking improvements are included in a difficult streaming and penetration radiation analysis through a concrete structure. Proposals are given for the code generation of the required biasing parameters.

"The submitted manuscript has been authored by a contractor of the U.S. Government under contract DE-AC05-84OR21400. Accordingly, the U.S. Government retains a nonexclusive, royalty-free license to publish or reproduce the published form of this contribution, or allow others to do so, for U.S. Government purposes."

---

*Research sponsored by the U.S. Department of Energy Office of Nuclear Energy, under contract No. DE-AC05-84OR21400 with Martin Marietta Energy Systems, Inc.

The MORSE multigroup Monte Carlo[1,2] code has been in general use worldwide for almost twenty-five years. Although various improvements have been added over the years, the basic framework of the code has remained unchanged. Because of the multigroup cross-section structure no code changes are necessary when new data and formats are released, the necessary changes being made in the cross-section processing codes. The ability to adapt MORSE to almost any type of radiation transport problem, through the use of the user-written routine interface, has enabled many installations to customize the code according to local needs.

One of the potentially serious problem areas in the use of MORSE is low-order P_N expansion for directionally-dependent systems. This is illustrated in the analysis of a neutron streaming experiment shown in Fig. 1.[3] Neutrons are created in the target by the deuteron beam. Small detectors (simulated as points in the analysis) are located at 40 cm off the axis at 3 and 4 meters from the target. A differential analysis has shown that the high-energy neutrons scattered to these detectors are dominated by first collisions near the exit of the duct. In Fig. 2 the flux at the 3 meter detector for a P_3 MORSE calculation is compared to the experimental results and also to an MCNP[4] calculation. The difference in calculational results (both using ENDF/B-V data) virtually disappears when the MORSE cross-section expansion is extended to P_7 (see Fig. 3). Similar results for the 4 meter detector are shown in Figs. 4 and 5. Due to the positions of the two detectors relative to the first collision sites, the P_3 results are too high in one case and too low in the other. The analysis of this experimental system was initially involved with attempting to resolve the experimental-calculational discrepancies in the high-energy peak, and not as a companion of calculational methods and codes. The discrepancies remain unresolved, but the results illustrate the proper utilization of the P_N expansion. MORSE calculations have also been made for the two detectors using ENDF/B-VI data (collapsed from the VITAMIN-J group structure for comparison with the VITAMIN-E structure),[5] but no improvement in the high-energy comparisons from Fig. 3 and 5 were found. There was some change in the low, intermediate-energy fluxes, where the uncertainty in all results is the greatest and where the difference in the two Monte Carlo code scattering models and data can be seen.

The use of a few energy groups to cover wide energy ranges has also been a source of error for any multigroup cross-section method of analysis. However, with large sets such as the 174-38 group neutron-photon VITAMIN-E library now in general use, this source of error has greatly diminished. This library has been used in MORSE, with a P_5 expansion, in the neutron analysis of the Oak Ridge Electron Linear Accelerator (ORELA) target and positron source system,[6] both water-cooled and shown schematically in Figs. 6 and 7. The energy range covered was 20 MeV to 10 eV. The electron beam produces a bremsstrahlung photon source in the tantalum plates, which then produces neutrons via photoneutron reactions and positrons via pair production in aluminum-clad tungsten plates. The neutrons are collected into beam tubes of various lengths for time-of-flight cross-section measurements. Of particular interest was the calculation of the delay time distributions (resolution function) of the neutrons inside the target between birth (electron pulse) and escape into the flight tube. This resolution function was computed in MORSE by redefining the time

variable as a distance equal to the elapsed time in the target multiplied by the neutron mid-group velocity at escape. A second change introduced into the code was an analytic hydrogen scattering model to more properly account for neutron collisions with hydrogen in the cooling water of both the target and positron source. An extra cross-section mixture for hydrogen, with an atomic density of that for the nuclide in water, was made available in the standard mixing procedure. For each collision in water a random determination was made of the struck nuclide using this extra data. An oxygen collision proceeded in the normal multigroup mode, but for hydrogen the outgoing direction and energy were determined analytically and then re-coupled with the standard method. A third non-standard feature of the ORELA target analysis consisted of a next-event type coupling calculation from the target to the positron source, then following neutron collisions there, a second coupling back into the target. In this manner the effect of neutron backscatter from the positron source on the target resolution function could be determined. The positron extraction tube, located further from the target, was ignored. A typical set of calculated data is shown in Fig. 8 in the form of the probability of an effective neutron distance in the target at escape. The two components of this data were not analyzed experimentally. The calculated leakage spectra from the target is shown in Fig. 9 and compared with an earlier, less detailed model analysis using a continuous-energy code.[7] Here a shadow bar, blocking the neutron escape from the tantalum plate area, was simulated in both calculations. In Fig. 10 the MORSE-calculated effective distance spectrum is shown. The slight maximum and then high-energy decline of the distributions, for escape from the tantalum plate area only, has been observed experimentally.

In another analysis using MORSE, several code features and applications of multigroup Monte Carlo are presented: (1) general discrete ordinate-Monte Carlo coupling, (2) adjoint mode of operation, (3) forward flux spectra from adjoint calculations, and (4) array geometry capability. The calculations are for radiation doses and neutron activation at various locations in Hiroshima and Nagasaki due to the nuclear weapon detonations over these cities in World War II.[8] The coupling geometry is shown in Fig. 11, and the source point is on the central cylindrical axis (not shown). The forward discrete ordinate free-field, air-over-ground angular flux is made available at the indicated node points in the cylindrical volume element by a calculational sweep through the angle $\Delta\psi$. When an adjoint Monte Carlo particle escapes the interior geometry, the appropriate discrete ordinate forward flux is determined by interpolations in space, closest polar angle cosine and azimuthal angle, and one-to-one correspondence in energy group. The result is given for general phase space coordinate ρ

$$\lambda = \int_{\bar{n}\cdot\bar{\Omega}>0} \phi(\rho)\phi^*(\rho)(\bar{n}\cdot\bar{\Omega})d\rho \qquad (1)$$

where $\phi(\rho)$ is $\phi_{g'}$, the discrete ordinate flux in group g', and $\phi^*(\rho)(\bar{n}\cdot\bar{\Omega})$ is the adjoint leakage current $J^*_{gg''}$. This coupling procedure represents an increased capability over the much-used DOMINO code,[9] in which the MORSE geometry must be exterior to the entire cylinder of the discrete ordinates calculation ($\Delta\psi$ must be 2π). The forward flux in group g at the adjoint source point (detector location) is determined by

$$\phi_g = 4\pi N \sum_{g'} \int_{\substack{\text{coupling} \\ \text{surface}}} \int_{\bar{n}\cdot\Omega>0} J^*_{gg''}\ \phi_{g'}\ d\bar{\Omega}d\bar{r} \qquad (2)$$

where the adjoint group number at escape is $g''=N-g'+1$, N is the total number of groups, and $4\pi N$ is the adjoint source normalization.[2] The adjoint source group g is selected uniformly within the N groups and this value is retained by the particle history and used to score in the above integral at escape. In the evaluation of an energy-integrated quantity the adjoint source g is selected from an energy-dependent response function, and no further reference is made to this group number. In the application of this coupling procedure, a large concrete building in Nagasaki was modeled as shown in Fig. 12. It was placed inside the coupling system replacing the geometry in Fig. 11 at the proper orientation as indicated in Fig. 12, approximately 500 meters ground range from and 500 meters below the detonation point. The vertical and horizontal lines on the exterior of the building represent the array matrix, into which individually modeled segments of the building were placed by appropriate input instructions. The results of the calculation were given as radiation reduction factors at locations interior to the building relative to the free field radiation at those locations with no building present. For the weapon neutron output only, the reduction factors at the center of the building on the first floor were calculated by the coupling method to be $14\pm8\%$ for neutron dose and $27\pm12\%$ for secondary photon dose. The three-dimensional code TORT[10] computed these values to be 13 and 26, respectively.

All the above analyses were made with an ORNL in-house version of MORSE which uses combined directional and path length biasing.[11] The advantages of this combined biasing scheme are (1) the outgoing direction after collision is preferentially biased toward (or away from) the same point toward which path lengths are preferentially stretched (or shortened), (2) undesirable weigh correction fluctuations that occur when either biasing is used separately are reduced, (3) the method is problem independent, (4) the general method is a direct consequence of manipulations with the Boltzmann transport equation, (5) the importance region geometry of a complicated calculational system can be simplified from that with other forms of biasing, although the user-written DIREC routine defining the preferential direction for each importance region is still required, (6) only one empirical parameter is required for both biasings, and (7) for a code with discrete scattering angles such as MORSE, the biasing application is analytic in contrast to a numerical integration at each collision required for general application.

In MORSE the biased collision kernel is

$$\tilde{C} = \frac{C}{N(1-p\mu)} \tag{3}$$

where

C	=	the unbiased kernel
p	=	the empirical biasing parameter, $0<p<1$
μ	=	the cosine of the angle between the preferential direction $\bar{\Omega}_0$ and the outgoing direction $\bar{\Omega}$ to be selected (see Fig. 13; $\bar{\Omega}'$ is the incident direction)
N	=	normalization constant

The biased transport kernel for the selection of the mean free path η is

$$\tilde{T} = (1-p\mu)e^{-(1-p\mu)\eta} , \tag{4}$$

and the combined weight correction is (applied separately in different parts of the code)

$$WT = (C/\tilde{C})\ (T/\tilde{T}) = Ne^{-p\mu\eta} . \tag{5}$$

The biased distribution for the discrete scattering angle selection is

$$f_n' = \frac{\int_{-\pi}^{\pi} \frac{f_n d\phi}{(1-p\mu)}}{\sum_{i=1}^{L} \int_{-\pi}^{\pi} \frac{f_i d\phi}{(1-p\mu)}} , \tag{6}$$

where f_i is the unbiased probability for scattering angle cosine μ_i and L is the expansion order. From Fig. 13

$$\mu = \mu_i\mu_0 + \sqrt{1-\mu_i^2}\ \sqrt{1-\mu_0^2}\ \cos\phi , \tag{7}$$

the distribution for the azimuthal angle is,

$$P_n' = \frac{\frac{1}{1-p\mu_n}}{\int_{-\pi}^{\pi} \frac{dp}{(1-p\mu_n)}} , \tag{8}$$

and

$$\tan\frac{\phi}{2} = \sqrt{\frac{1-p\mu_{nx}}{1-p\mu_{nm}}} \tan\left[\pi\left[RN-\frac{1}{2}\right]\right] , \tag{9}$$

where μ_{nx} and μ_{nm} are the values of μ_n for ϕ=0 and π, respectively in Eq. (7), and *RN* is a uniform random number on the unit interval. The ϕ from Eq. (9) must be given a final adjustment, $\psi = \phi+\phi'$, where using the cosine components of $\bar{\Omega}'$ and $\bar{\Omega}_0$

$$\cos\phi' = \frac{\mu_0 W' - W_0}{\sqrt{1-\mu_0^2}\sqrt{1-W'^2}} , \tag{10}$$

and

$$\sin\phi' = \frac{U'V_0 - U_0V'}{\sqrt{1-\mu_0^2}\sqrt{1-W'^2}} . \tag{11}$$

The normalization constant in Eq. (5) is

$$N = \sum_{i=1}^{L} \frac{f_i}{\sqrt{1-p\mu_{ix}}\sqrt{1-p\mu_{im}}} . \tag{12}$$

In order to capitalize on the combined biasing scheme, two other changes should be made in MORSE: (1) the transport process should be interrupted at importance region boundaries so that changes in $\bar{\Omega}_0$ and p can be made [even without collision and path length biasing this should be done in order to permit boundary splitting and Russian roulette; i.e., call TESTW from BANKR(7)[12]], and (2) apply collision splitting and Russian roulette after both the collision and transport processes are completed, not between them. The

programming changes necessary to implement the combined biasing into MORSE are given in Appendix F of Ref. 13 with corrections for P_N, $N>3$, in Ref. 14 (page 11).

The original analysis using the combined biasing in MORSE consisted of an experimental system simulating a concrete building shown in Fig. 14. The entire system is shown schematically in Fig. 15. Neutrons and photons from the Oak Ridge Tower Shielding Reactor and spectrum modifier impinge on the front face of the structure. The source for the MORSE calculation at the exit of the spectrum modifier was adjusted to agree in magnitude with experimental values. TLD energy deposition is computed at the indicated detector locations and compared with experimental results, as *C/E* ratios, in Table. I.

In the combined biasing study, proposals are given for the possible code generation of the $\bar{\Omega}_0$ and p as adjoint flux-weighted values for an importance volume V_l of the form, for a general parameter ω_l[11]

$$\omega_l = \frac{\int_{V_l} \omega(\rho)\phi^*(\rho)d\rho}{\int_{V_l} \phi^*(\rho)d\rho}, \tag{13}$$

where the value of ω for each history created in or passing through V_l is carried with it until a contribution to the desired result by that history is made at the detector. The adjoint flux is accumulated in the forward calculation in the same general manner as for the forward flux in the adjoint application for Eq. (2). This parameter generation method has not been completely successful in reduced variance and increased efficiency in general applications and is still under development. However, it is recommended that the combined biasing scheme, with empirical parameters p, be included in any MORSE code system, as well as boundary splitting and Russian roulette and the analytic hydrogen scattering model. Several features of the next-event estimation routines should also be considered: (1) for photon calculations use of the Klein-Nashina equation for Compton scattering[15] significantly reduces the statistical uncertainty from the standard routine (this routine also accounts for pair production and the photoelectric effect), (2) estimation to all energy groups,[2] (3) ring detectors for azimuthally symmetric detectors,[16] and (4) estimation to finite detectors.[2,6,15,17,18]

Table I. Detector response comparisons inside the concrete building.

Detector in Fig. 15	Experimental Response[a]	C/E	Calculated uncertainty[b] (%)	Fractional response and uncertainty from source segmentation					
				Uncollided		Front face		Other	
					(%)		(%)		(%)
1	1.33	0.96	2.7	0.128	0.4	0.702	2.6	0.170	11.7
2	6.73	0.99	0.4	0.802	0.3	0.122	2.3	0.076	2.0
3	1.36	1.00	3.6	0.129	0.4	0.732	2.9	0.139	20.9
4	5.41	0.99	0.4	0.816	0.3	0.128	1.4	0.056	4.7
5	1.11	0.92	4.4	0.136	0.4	0.629	1.9	0.235	18.0
6	3.84	1.01	0.4	0.837	0.3	0.120	1.6	0.043	5.7
7	0.24	0.98	9.1	0.001	0.8	0.756	6.0	0.243	32.5
8	1.23	1.12	1.6	0.578	0.6	0.354	4.0	0.068	9.7
9	2.80	1.07	0.7	0.762	0.3	0.206	3.1	0.032	5.4
10	0.28	1.14	6.0	0.001	0.8	0.722	3.6	0.267	20.3

[a]TLD energy deposition in MeV · g^{-1} · min^{-1} · kW^{-1} × 10^{-4} from *Nucl. Sci. Eng.*, 98, 279–98 (1988), with experimental uncertainty ~5%.
[b]One standard deviation as a percent of the calculated response.

REFERENCES

1. M. B. Emmett, *MORSE-CGA, A Monte Carlo Radiation Transport Code with Array Geometry Capability*, ORNL-6174 (1985).

2. S. N. Cramer, *Applications Guide to the MORSE Monte Carlo Code*, ORNL/TM-9355 (1985).

3. S. N. Cramer and T. Y. Lee, "Monte Carlo Analysis of a Neutron Streaming Experiment," *Nucl. Sci. Eng.*, 107, 180–87 (1991).

4. J. F. Briesmeister, Ed., *MCNP — A General Monte Carlo Code for Neutron and Photon Transport, Version 3A*, LA-7396-M, Rev. 2, Los Alamos National Laboratory (1986).

5. J. E. White, private communications, Oak Ridge National Laboratory (1992).

6. S. N. Cramer and F. G. Perey, "Time-Dependent Monte Carlo Calculations of the Oak Ridge Electron Linear Accelerator Target Neutron Spectrum," *Nucl. Sci. Eng.*, 111, 102–11 (1992).

7. C. Coceva *et al*, "Calculation of the ORELA Neutron Moderator Spectrum and Resolution Function," *Nucl. Instrum. Meth.*, 211, 459 (1983).

8. S. N. Cramer and C. O. Slater, *Investigation of Radiation Effects in Hiroshima and Nagasaki Using a General Monte Carlo-Discrete Ordinates Coupling Scheme*, ORNL/TM-11532 (1990).

9. M. B. Emmett, *DOMINO-II, A General Purpose Code for Coupling DOT-IV Discrete Ordinates and Monte Carlo Radiation Transport Calculations*, ORNL/TM-7771 (1981).

10. W. A. Rhoades *et al*, *Radiation Exposure Inside Reinforced Concrete Buildings at Nagasaki*, ORNL/TM-10589 (1989).

11. S. N. Cramer, "Angle Biasing in Monte Carlo Radiation Transport," *Nucl. Sci. Eng.*, 98, 279-98 (1988).

12. S. N. Cramer, unpublished notes, RSIC Workshop on the MORSE Code (1985).

13. S. N. Cramer, *Discrete Angle Biasing in Monte Carlo Radiation Transport*, ORNL/RSIC-50 (1988).

14. T. Y. Lee and S. N. Cramer, *Neutron Streaming Benchmark Calculations*, ORNL/RSIC-52 (1989).

15. S. N. Cramer, "Adjoint Gamma-Ray Estimation to the Surface of a Cylinder — Analysis of a Remote Reprocessing Facility," *Nucl. Sci. Eng.*, 79, 417-25 (1981).

16. T. J. Hoffman and J. S. Tang, *XSDRNPM-S Biasing of MORSE-SGC/S Shipping Cask Calculations*, ORNL/SSD/TM-175;NUREG/CR-2342 (1982).

17. S. N. Cramer and J. S. Tang, *Variance Reduction Methods Applied to Deep-Penetration Monte Carlo Problems*, ORNL/TM-9643 (1986).

18. S. N. Cramer, "Analytic Estimation of Radiation Effects in Space Using Solid Angles," in *Nuclear Technologies for Space Exploration*, ANS NTSE-92, Vol. III, Jackson, Wyoming (1992).

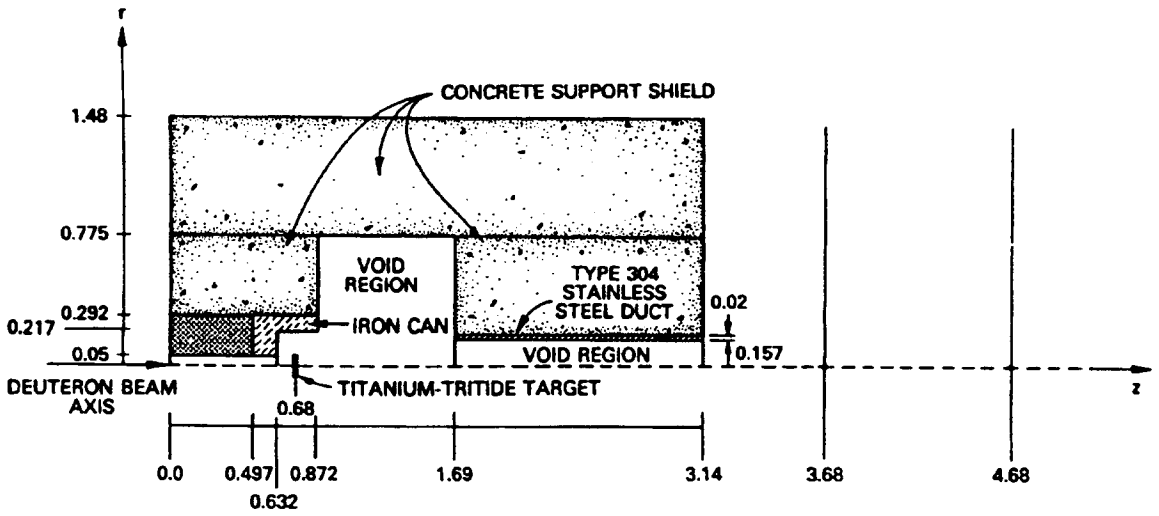

Figure 1 Two-dimensional calculational model of the experimental geometry. All dimensions are in meters.

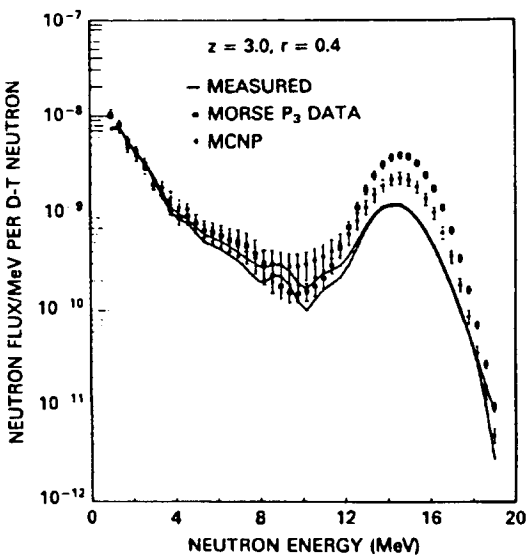

Figure 2 Neutron flux per unit energy versus neutron energy for the detector at $z = 3$ m and $r = 0.4$ m. The order of scattering of the MORSE calculation is P_3.

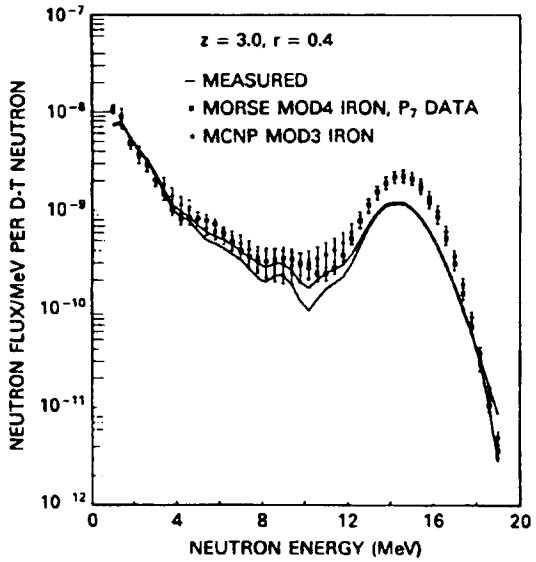

Figure 3 Neutron flux per unit energy versus neutron energy for the detector at $z = 3$ m and $r = 0.4$ m. The order of scattering of the MORSE calculation is P_7.

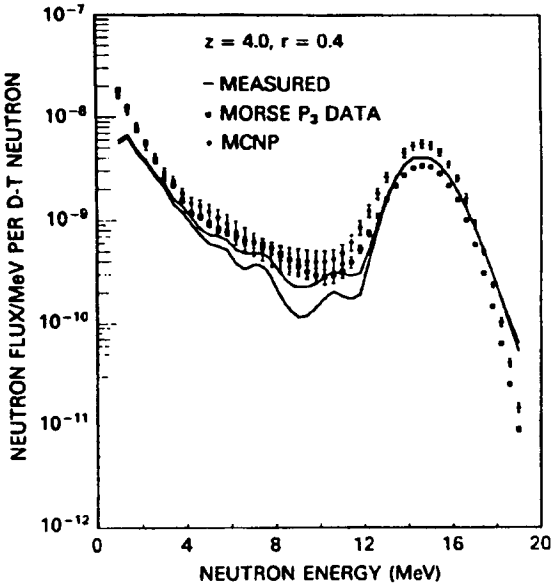

Figure 4 Neutron flux per unit energy versus neutron energy for the detector at $z = 4$ m and $r = 0.4$ m. The order of scattering of the MORSE calculation is P_3.

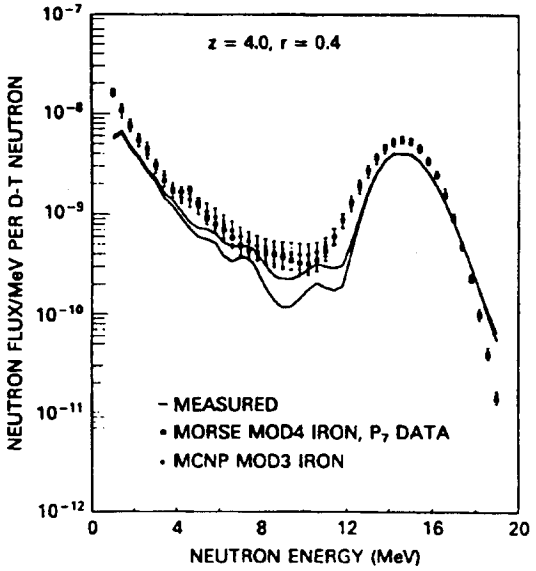

Figure 5 Neutron flux per unit energy versus neutron energy for the detector at $z = 4$ m and $r = 0.4$ m. The order of scattering of the MORSE calculation is P_7.

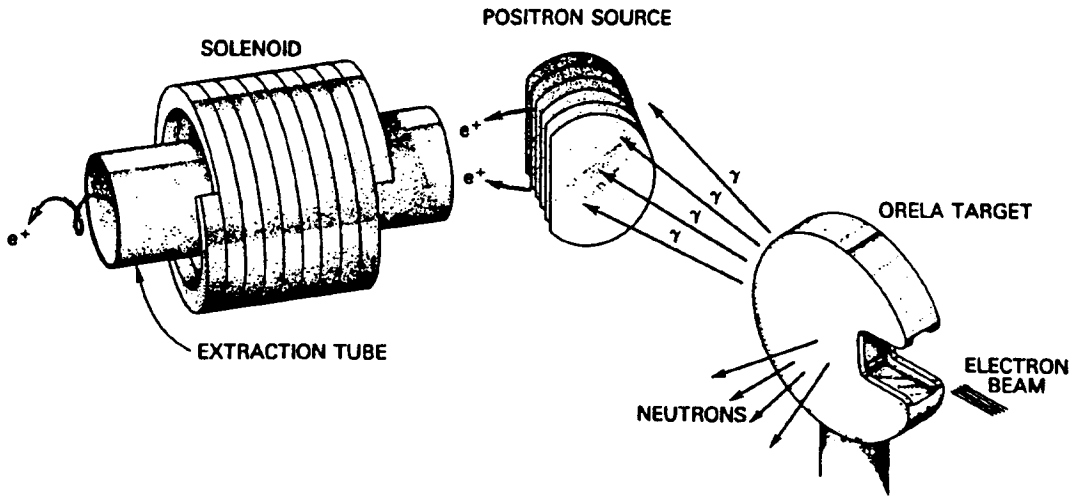

Figure 6 ORELA positron source facility.

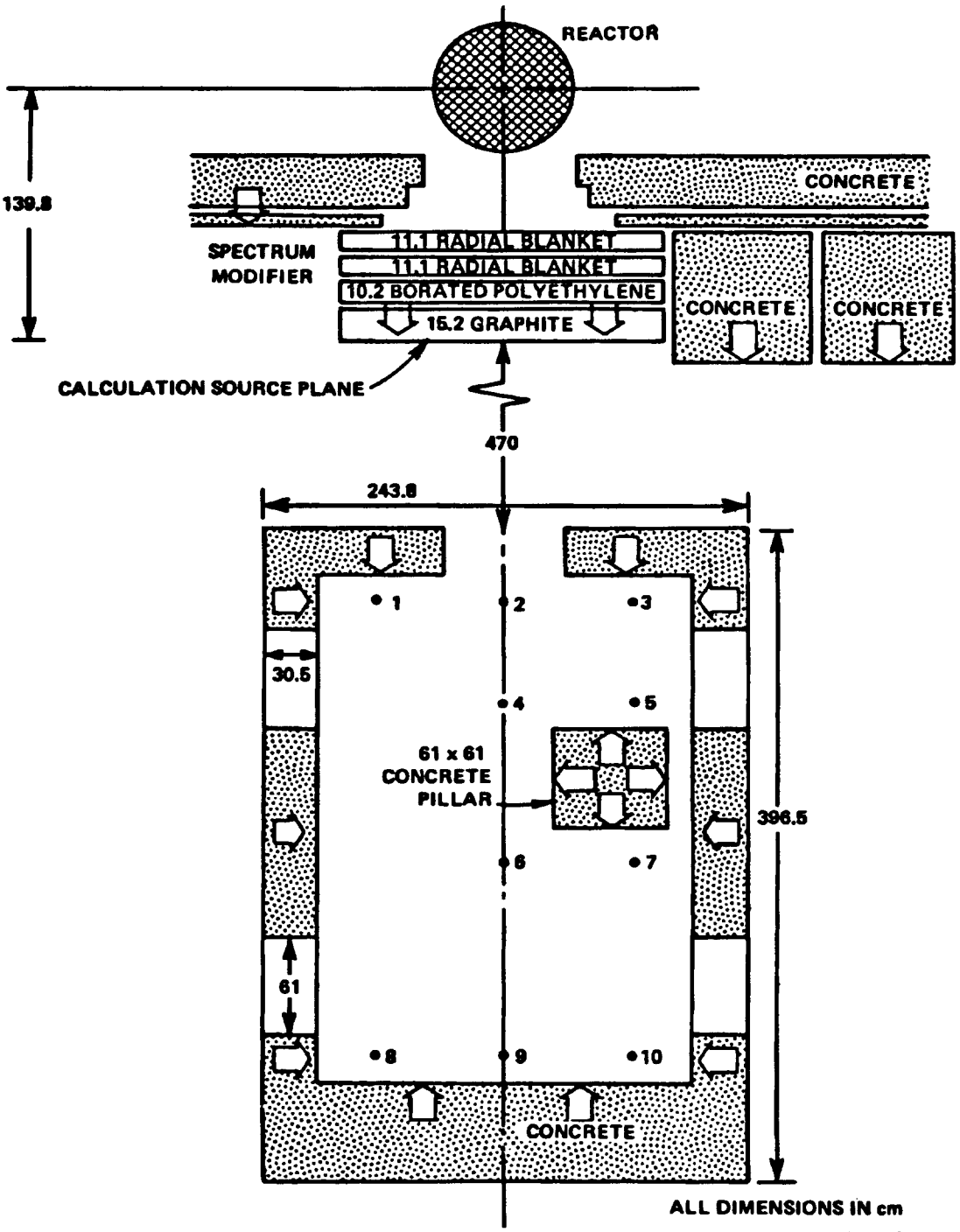

Figure 15 Schematic of spectrum modifier and concrete block house with detector locations and preferential directions ω_0 (large arrows) used in calculations. All dimensions are in centimeters.

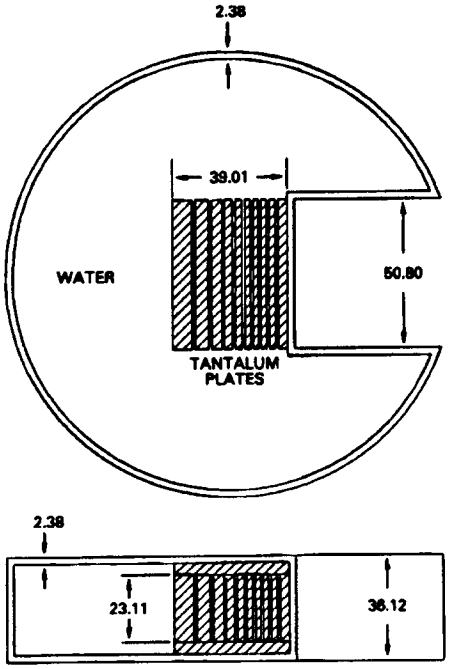

Figure 7. Model of the 15.24-cm-diam ORELA target (dimensions are given in millimeters).

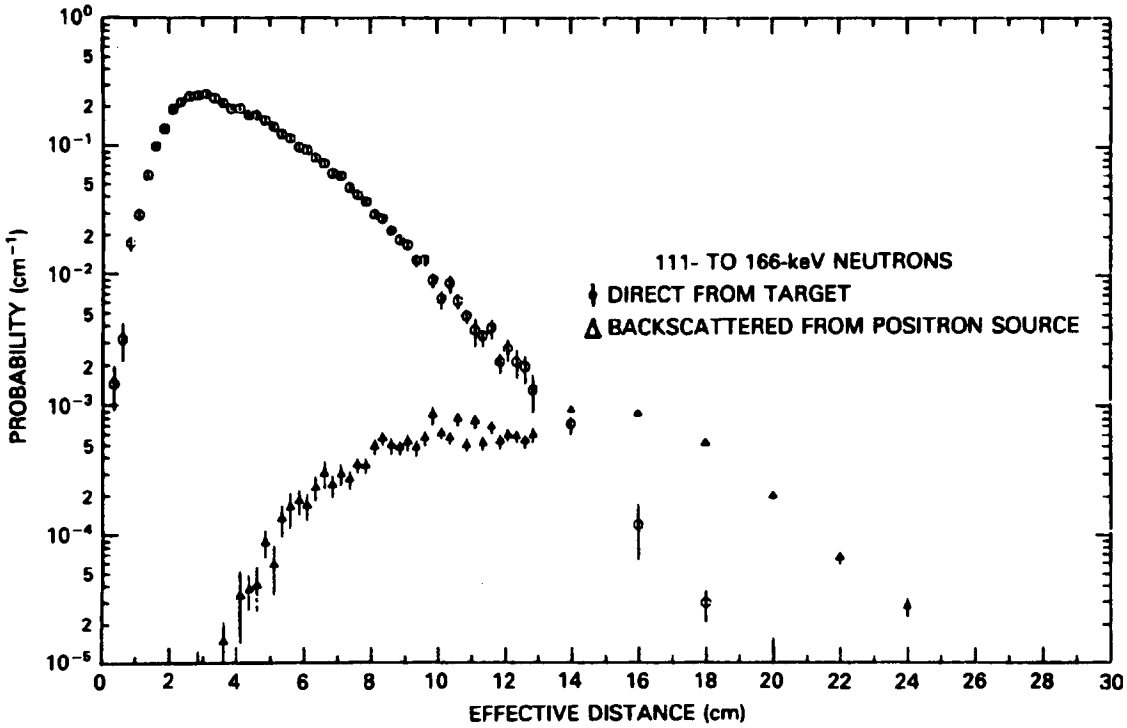

Figure 8 Direct and backscattered effective distance distribution from the ORELA target.

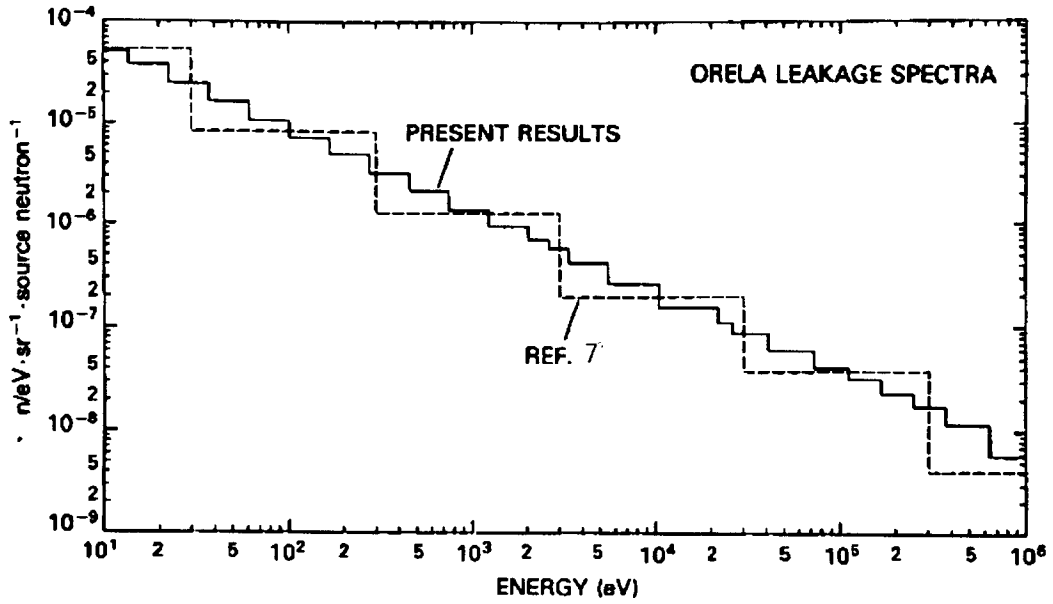

Figure 9 Comparison of the ORELA target neutron leakage spectrum with the tantalum plates blocked out.

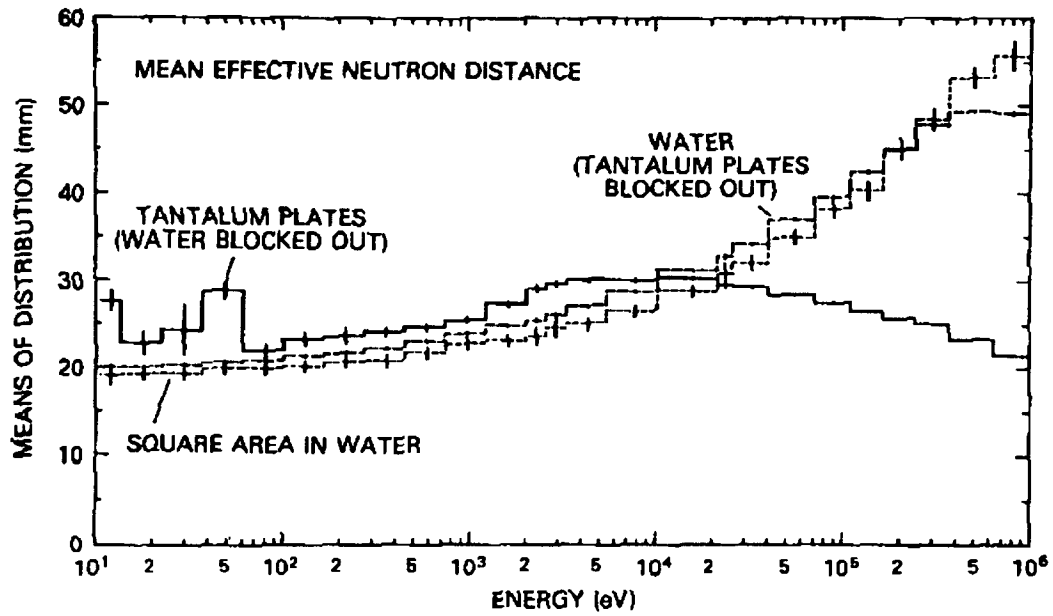

Figure 10 Mean effective neutron distances for the three ORELA target leakage configurations.

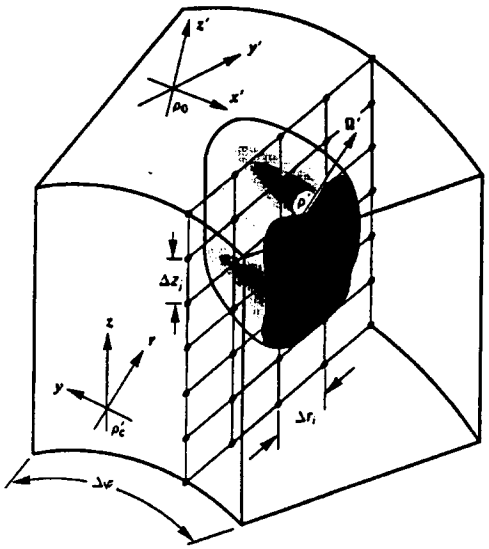

Figure 11. Monte Carlo geometry and discrete ordinates flux grid.

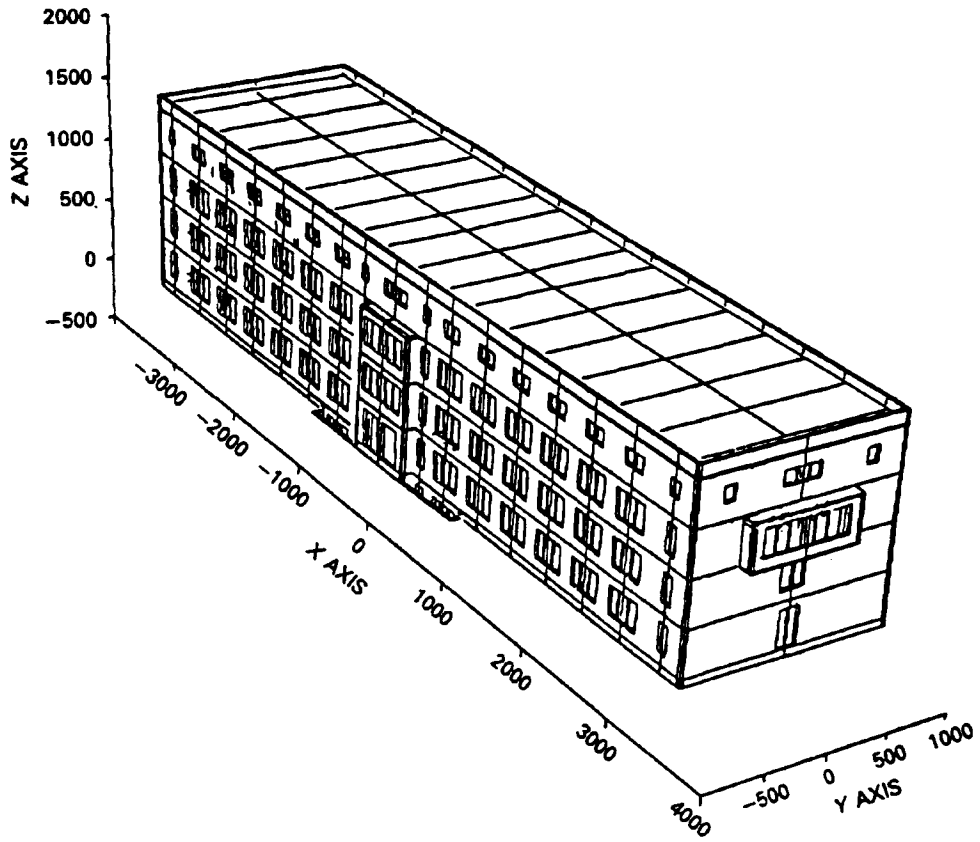

Figure 12 Computer mockup of a reinforced concrete building in Nagasaki.

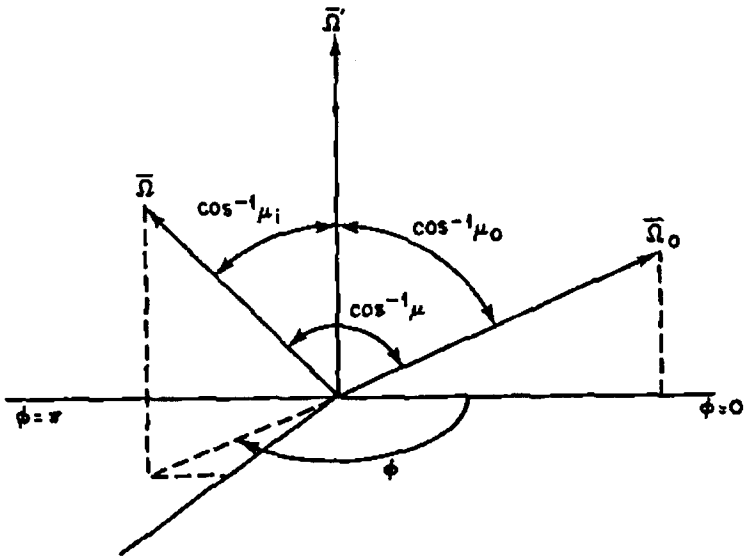

Figure 13 Angular biasing geometry.

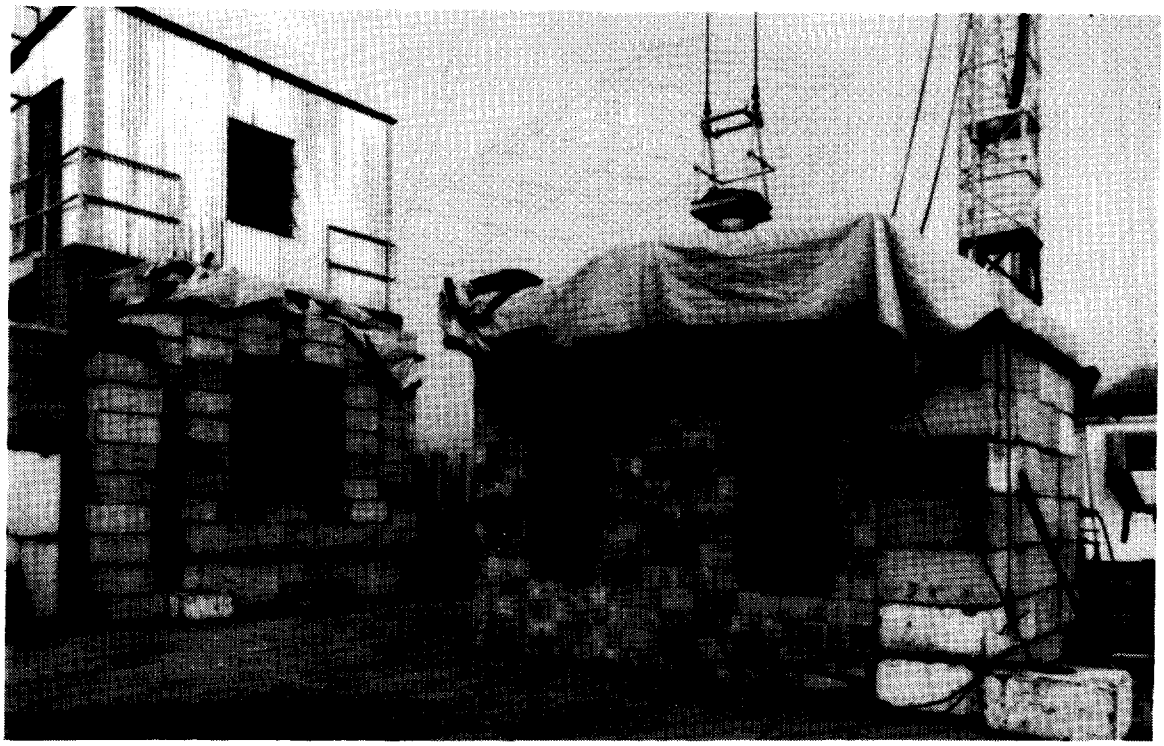

Figure 14 Experimental configuration showing the spectrum modifier on the left and the concrete block house on the right.

THE MASH 1.0 CODE SYSTEM: UTILIZATION OF MORSE IN THE ADJOINT MODE*

J. O. Johnson and R. T. Santoro
Oak Ridge National Laboratory
Oak Ridge, Tennessee 37831-6363**

ABSTRACT

The Monte Carlo Adjoint Shielding Code System - MASH 1.0, principally developed at Oak Ridge National Laboratory (ORNL), represents an advanced method of calculating neutron and gamma-ray environments and radiation protection factors for complex shielding configurations by coupling a forward discrete ordinates radiation environment (i.e. air-over-ground) transport calculation with an adjoint Monte Carlo treatment of the shielding geometry. The primary application to date has been to determine the radiation shielding characteristics of armored vehicles exposed to prompt radiation from a nuclear weapon detonation. Other potential applications include analyses of the mission equipment associated with space exploration, the civilian airline industry, and other problems associated with an external neutron and gamma-ray radiation environment. This paper will provide an overview of the MASH 1.0 code system, including the verification, validation, and application to "benchmark" experimental data. Attention will be given to the adjoint Monte Carlo calculation, the use of "in-group" biasing to control the weights of the adjoint particles, and the coupling of a new graphics package for the diagnosis of combinatorial geometry descriptions and visualization of radiation transport results.

---

*Research sponsored by the Defense Nuclear Agency
**Managed by Martin Marietta Energy Systems, Inc. under Contract No. DE-AC05-84OR21400 for the U. S. Department of Energy

I. INTRODUCTION

An armored vehicle can provide important protection against the effects of a nuclear weapon. In the case of a tactical weapon, prompt radiation may be the dominant effect over a considerable area surrounding the detonation. To facilitate the calculation of radiation protection factors for armored vehicles, the Vehicle Code System (VCS)[1,2] was developed by Oak Ridge National Laboratory (ORNL). For over a decade, the U. S. Department of Defense (DoD) and the North Atlantic Treaty Organization (NATO) relied almost exclusively on VCS for calculating neutron and gamma-ray radiation fields and shielding protection factors for tactical armored vehicles, buildings, and other shielded configurations from nuclear weapon radiation. While the title implies the code system was to be used only for vehicles, VCS could also be used to study other shielded structures.

Over the course of time, VCS was modified by installations using the code to suit their particular purposes. The result of these independent modifications was a proliferation of different versions of VCS, most of which were not compatible and yielded different results. The Defense Nuclear Agency (DNA) expressed concern over the potential for disagreement between independent VCS analyses of the same armored vehicle. As a result, Ballistic Research Laboratory (BRL), ORNL, and Science Applications International Corporation (SAIC) were tasked to identify the problems associated with the "current" version(s) of VCS, incorporate the various modifications (which would improve the code), and create a singular referenced version of VCS. This final version of VCS was renamed MASH - the Monte Carlo Adjoint Shielding Code System[3] and assigned a version number, i.e., MASH 1.0, for referencing purposes.

MASH 1.0 (referred to as MASH through the remainder of this paper) was used to analyze a series of nuclear radiation shielding experiments performed in the Fall of 1989, Spring of 1990, and Spring of 1991 at the Army Pulse Radiation Facility (APRF) in Aberdeen Proving Ground, Maryland. The objective of these efforts was to "benchmark" MASH against the experiments performed at the APRF and determine the capability of MASH in reproducing the measured neutron and gamma-ray integral and spectral data. The results of these analyses[4-6] and additional studies involving armored vehicles were used in recommendations to the U. S. Army Nuclear and Chemical Agency (USANCA) to make MASH 1.0 the reference code for future U. S. armored vehicle nuclear vulnerability calculations. As a result of these recommendations, MASH 1.0 is the code of choice as stated in the recent update to the U. S. Army's Qualified Research Requirements (QRR). Furthermore, the results of these analyses were used in recommendations to the NATO Panel VII Ad Hoc Group of Shielding Experts for replacing VCS with MASH 1.0 for all future armored vehicle nuclear vulnerability calculations.

This paper will provide an overview of the MASH code system, including the verification, validation, and application to "benchmark" experimental data. Attention will be given to the adjoint Monte Carlo calculation, the use of "in-group" biasing to control the weights of the adjoint particles, and the coupling of a new graphics package for the diagnosis of combinatorial geometry descriptions and visualization of radiation transport results.

II. OVERVIEW OF MASH 1.0

A typical MASH problem involving an armored vehicle is shown in Figure 1. MASH employs a GRTUNCL-DORT[7] forward discrete ordinates calculation to determine the neutron and gamma-ray fluence on a coupling surface surrounding the armored vehicle or shielded structure and a MORSE[8] adjoint Monte Carlo calculation to determine the dose importance of the surface fluence. MASH then utilizes the Detector Response Code (DRC)[3] to fold the fluence together with the dose importance to yield the desired detector response(s). The data flow diagram of the MASH code system is shown in Figure 2.

The GIP code is used to create and mix the materials required to run the air-over-ground transport analysis. The compositions and source data for the air-over-ground transport calculation are input into both the GRTUNCL and DORT codes. In order to maintain particle balance and reduce ray effects, GRTUNCL calculates the uncollided fluence and first-collision source throughout the problem space. This information is input to DORT which calculates the resulting collided fluence, and merges the two results. All scalar and directional fluence information is passed to the Variable Input Source Transformation and Assembly (VISTA) code[3], where it is condensed and reordered for convenient processing. Typically, only a few ground ranges from the radiation source are processed at this step. Additional ground ranges may be obtained by rerunning the VISTA code at a minimal cost.

The complex three-dimensional target (vehicle) geometry description and material compositions are input into a modified version of the MORSE code. In MASH, the combinatorial geometry description is modeled in GIFT format.[9,10] The GIFT combinatorial geometry (CG) package is similar to the MORSE CG package in that specified geometric shapes may be combined to describe complex geometry configurations. However, GIFT contains more solid "body" types and is compatible with the armored vehicle geometry descriptions generated by BRL. MORSE records the required information for each adjoint track leaving the coupling surface on a leakage data set which is input to DRC. DRC folds the adjoint leakage data together with the reformatted DORT fluence at the coupling surface, i.e., the VISTA code output fluence file, for the selected orientation, range, and detector response(s). DRC bins the contributions to the dose in several arrays (called detectors in the code) for calculation of radiation protection factors and reduction factors.

The radiation transport coupling method employed in DRC allows for any complicated Monte Carlo geometry inside the coupling surface to be modeled in three dimensional detail. The two-dimensional GRTUNCL/DORT discrete ordinates air-over-ground environment is defined by an r-z coordinate system, where the radial axis **r** coincides with the MORSE **x** axis and is perpendicular to the **y** axis. The three dimensional Monte Carlo geometry system is completely contained within a cylindrical volume element defined by the maximum and minimum values chosen from the radial and axial mesh in VISTA. The coupling between the two systems occurs at the outer leakage surface of the Monte Carlo geometry within the cylindrical volume element.

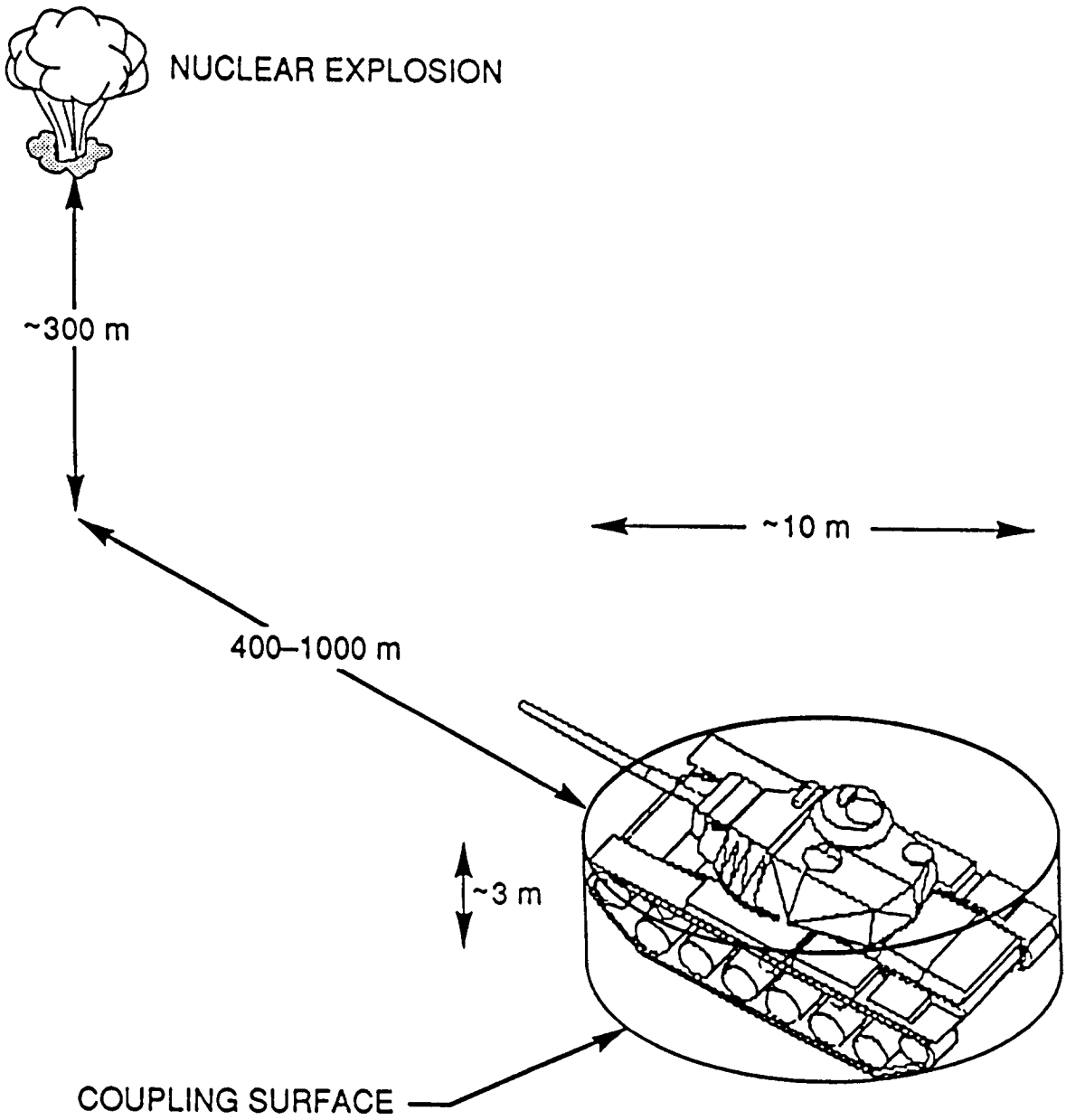

Figure 1. Typical MASH Problem Involving an Armored Vehicle.

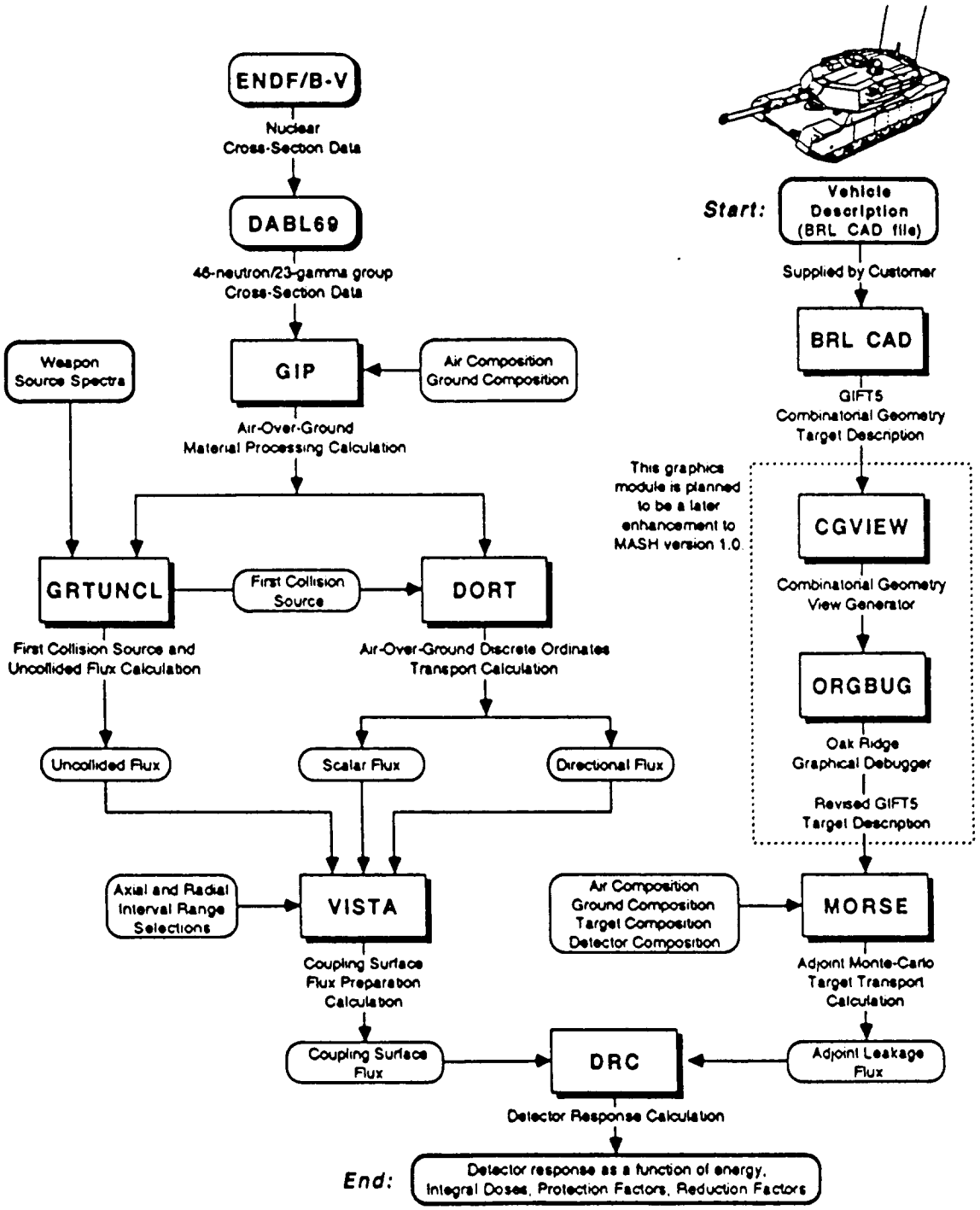

Figure 2. Data Flow Diagram of the MASH 1.0 Code System.

This coupling requires the Monte Carlo coordinate system to be rotated to align the x,y,z axes parallel to and in the same sense of the x,y,z axes (r, z where $r=\sqrt{x^2+y^2}$) of the GRTUNCL/DORT discrete ordinates system. When the adjoint Monte Carlo particle escapes its geometry system at a given point and in a given direction defined by its coordinate system, the coordinates, direction, and energy group are converted to the discrete ordinates system so that the appropriate forward fluence can be determined. A full Eulerian rotation matrix is incorporated in DRC to allow for the alignment/rotation of the Monte Carlo geometry system within the discrete ordinates system. As presently configured, MASH only allows for the rotation of the Monte Carlo geometry system in the x-y plane, i.e., rotation about the z axis.

In order to calculate the radiation protection and reduction factors, the MORSE adjoint leakage tape includes a parameter which identifies the detector type in DRC in which a leaking particle is scored. Table 1 identifies the seven detector types utilized in DRC. The first four are utilized on the MORSE adjoint leakage tape for scoring purposes. The last three detector types, along with the free-field neutron, gamma-ray, and total fluences and/or doses, are used to calculate the neutron, gamma-ray, and total protection factors (PFs) and reduction factors (RFs) defined in Table 1. These factors are indicative of the ability of a vehicle or shielded structure to protect occupants or sensitive electronic equipment from penetrating nuclear radiation.

The neutron and gamma-ray protection factors are a measure of how much the vehicle shielding reduces the dose from free-field neutrons and gamma-rays, respectively, and is a useful parameter in engagement analysis. The reductions factors, however, are a measure of how much the vehicle shielding alters the neutron or gamma-ray dose as measured by a neutron or gamma-ray sensitive detector. While the protection factors are most useful for engagement analyses, the reduction factors are most useful for comparing calculated results with experimental measurements.

In MASH, special advantage is taken of the fact that the target (vehicle) is small compared to the separation distance between the source (weapon) and target. This means that the fluence in a given direction and at a given elevation and energy is essentially independent of the azimuthal variation about the target. This reduces the volume of data processed by DRC, minimizes the cost of both VISTA and DRC, and simplifies the construction of both codes. It should be noted that this assumption could lead to error for structures such as house clusters, large buildings, etc., where the distance from the detector location to the coupling surface may be significant relative to the gradient in the external fluence field.

Most of the computer cost of performing a MASH analyses is incurred in the DORT and MORSE codes. Therefore, it is advantageous to save the VISTA output for use with many MORSE runs. Likewise, it is practical to use a single MORSE leakage tape for a target (vehicle) to examine a number of target orientations, source ranges and types, and detector response functions.

III. IN-GROUP BIASING IN THE MORSE COMPONENT OF MASH 1.0

Several types of optional importance sampling and variance reduction techniques are available to the user in standard MORSE. In particular, these include splitting, Russian roulette exponential transform, and source energy biasing to name a few. In the version of MORSE used in MASH, there is an additional variance reduction technique referred to as in-group energy

Table 1. Detector Response Definitions in DRC and Definitions of Parameters and Protection Factors used to Characterize the Effectiveness of Shields.

Detector	Response Definition
1	Direct neutron - a neutron entering the vehicle and contributing a neutron dose.
2	Capture gamma rays from vehicle - a gamma ray resulting from a neutron entering the vehicle and contributing a secondary gamma-ray dose.
3	Capture gamma rays from ground - a gamma ray resulting from a neutron entering the ground without passing through the vehicle and generating a secondary gamma-ray dose from a ground interaction. (This dose is already included in the upward-directed gamma rays that enter the vehicle. This generally is negligible.
4	Direct gamma rays - a gamma ray entering the vehicle and contributing a gamma-ray dose. This source of gamma rays includes both gamma rays originating from the source, and capture gamma rays from the air.
5	Total gamma-ray dose - Sum of detectors 2, 3, and 4.
6	Gamma-ray dose from gamma rays entering the vehicle (usually dominated by directed gamma rays) - Sum of detectors 3 and 4.
7	Neutron and gamma-ray dose from neutrons incident on the vehicle - Sum of detectors 1 and 2.

Parameter	Response Definition
FFN	Free-Field Neutron Response
FFG	Free-Field Gamma-Ray Response
NPF	Neutron Protection Factor [NPF = FFN / Det. 7]
GPF	Gamma-Ray Protection Factor [GPF = FFG / Det. 6]
TPF	Total Protection Factor [TPF = (FFN+FFG)/(Det. 7 + Det. 6)]
NRF	Neutron Reduction Factor [NRF = FFN / Det. 1]
GRF	Gamma-Ray Reduction Factor [GRF = FFG / Det. 5]
TPF	Total Reduction Factor [TRF = (FFN+FFG)/(Det. 1 + Det. 5)]

biasing. In-group energy biasing was developed by W. Scott of SAIC[11-13] to adjust for irregularities observed in adjoint Monte Carlo analyses in thick media where the weights of adjoint particles can, in undergoing multiple scattering events, become very large, i.e., "the fat particle" problem. Such particles may be scored with a wide variety of weight values, which results in a very inefficient calculation with poor statistical precision, and is not improved by longer run times. The major objective of the in-group biasing scheme is to eliminate the instability in the variance for the adjoint random walks. This is equivalent to eliminating the problem in which the weight of an adjoint particle can grow unbounded by many repeated in-group scatterings. The procedure was first implemented in the MIFT2[14] version of the VCS MORSE code. After extensive testing by both ORNL and SAIC, the procedure was installed into MASH. A detailed description of the theoretical basis for in-group biasing is presented in Appendix B of Reference 3. The user should examine this section to understand the physics of the biasing technique. Here only a cursory explanation of in-group biasing is given.

The defining feature of in-group energy biasing is that for all but the last energy group, a particle's weight only changes when it scatters to a new group. If the particle stays in the same group, its weight remains the same. Thus, when an adjoint particle has a probability of non-absorption (PNAB) greater than 1.0, its weight will not increase so long as it scatters in the same group. When it finally upscatters to a new group, its weight will be increased by a fixed amount that is a function only of the cross sections and not of how many times the particle scattered in the same group. With standard adjoint MORSE, such a particle would have its weight increased by PNAB each time that it scattered so that its final weight upon upscatter would depend upon how many in-group scatterings that it had.

MORSE is easily modified to incorporate in-group energy biasing. Scattering in MORSE is handled in Subroutine COLISN using data in the form of the non-absorption factor $PNAB_i$ and the normalized scattering probabilities, P_{ij}, which give the probability of scattering to group j provided that a scattering has occurred in group i. The original coding is very simple in that the particle weight WATE is multiplied by $PNAB_i$, where i is the energy group of the particle coming into the collision, and then a random number is compared with the probabilities P_{ij} to select the outgoing energy group. This sampling scheme is easily modified to treat in-group scattering. Define a bias factor F_j as follows:

$$\text{if} \quad i = j = 1, \text{ then} \quad F_j = 1.0$$

$$\text{if} \quad i = j \neq 1, \text{ then} \quad F_j = PNAB_i$$

$$\text{if} \quad i \neq j, \text{ then} \quad F_j = \frac{1 - P_{ii}PNAB_i}{1 - P_{ii}}$$

The same sampling coding in Subroutine COLISN is used except that the random number is compared to $F_j \cdot P_{ij}$ instead of simply P_{ij} as before. After the outgoing energy group has been sampled, the weight is corrected by:

$$WATE = WATE \cdot PNAB_i/F_j$$

These modifications have been implemented into the MORSE component of the MASH code system. The implementation correctly treats in-group biasing with or without energy biasing, and includes logic for splitting whenever WATE exceeds WTMAX. Splitting in standard MORSE is normally performed in Subroutine TESTW when a particle's weight is above an importance region- and energy-dependent maximum weight. The particle's weight is halved and an identical particle is stored in the secondary bank. When the weight increase occurs at upscatter, the excessive weight is not identified until entering Subroutine TESTW. Thus, all the splitting secondaries will be in the same energy group and have the same direction cosines. They will be essentially the same particle. This has been significantly improved by playing the splitting game in Subroutine COLISN and actually resampling the upscatter distribution for each splitting secondary particle. In this manner each secondary is independent of the others so that this important probability transition is much more completely represented. It should also be noted that the definition of GWLO depends on whether or not in-group biasing is specified. If in-group biasing is invoked, GWLO is the fraction of the natural production probability specified by the cross sections and may be assigned values greater than, equal to, or less than one. If in-group biasing is not invoked, GWLO is the probability of generating a gamma ray (adjoint neutron).

Based on test results obtained with the MIFT2 and MASH (MORSE) codes, in-group biasing generally improves both the answer and the statistics of the calculation. Based on theory, it may be expected that the largest gains from the use of in-group biasing occur for fairly thick shielding problems. However, improvements for thinner problems have been seen as well. Based on both the theory and the results of test cases, it is suggested that in-group biasing always be used for adjoint Monte Carlo. However, recognizing that users may at times prefer not to use in-group biasing or may wish to compare results obtained with and without the use of in-group biasing, the methodology has been implemented in MASH with a switch so that its use is optional.

In-group energy biasing is easy to use. Unlike other Monte Carlo biasing methods, in-group biasing does not require that the user set up and input, based on his judgment, arrays of data to improve the efficiency of the Monte Carlo calculation. This means that a person less skilled in adjoint Monte Carlo can successfully use MASH, since use of in-group biasing requires only the setting of a switch in MORSE. Success in the use of the other biasing methods generally requires considerable adjoint Monte Carlo experience.

IV. VALIDATION AND APPLICATION OF THE MASH 1.0 CODE SYSTEM

MASH has been extensively benchmarked through comprehensive comparisons with measured data obtained at the Army Pulse Radiation Facility (APRF) at Aberdeen Proving Ground, MD. Several experimental configurations have been studied including, the Soviet Armored Infantry Fighting Vehicle (BMP-1), the U.S. Abrams Tank (Version XM-1 and M1A1), and two steel-shielded assemblies: the Radiological Test Configuration (RTK) and the Two-Meter Box Test-Bed Assembly.[4-6] For the BMP, XM-1, and M1A1 armored vehicles, the purpose of the measurements was to determine the neutron and gamma-ray reduction factors for the vehicle armor. For the steel-shield assemblies, particularly the two-meter box, the objective was to compile an extensive data base of measured neutron and gamma-ray differential energy spectra and dose data for evaluating the full range of capabilities of the MASH code system in reproducing the measurements. For this paper, comparisons of measured and calculated results for the two-meter box experiments are reviewed to demonstrate the performance of MASH.

The two-meter box experiments consisted of measurements of differential (spectra) and integral radiation environments in the free-field and inside the box at a distance of 400 meters from the APRF. The 400 meter site has been accepted as the NATO Standard Reference for measurements made at the reactor and the two-meter box is the NATO Standard Test Bed Configuration for intercomparisons of measured and calculated spectra and dose data. The box has steel wall thicknesses of 10.16 cm (80 gm/cm^2) on all sides and an interior air space with dimensions of 200 cm x 200 cm x 200 cm. The in-box measurements were made with and without a 5.08-cm-thick (4.8 gm/cm^2) 5% borated polyethylene liner on the interior walls. Measurements and calculations of the neutron and gamma-ray dose distributions were also made as a function of dosimeter locations on and inside a humanoid phantom (tissue equivalent construction) positioned either standing in the box or standing in the free-field environment outside the box.

Table 2 presents measured and calculated tissue doses for different two-meter box configurations. The uncertainties on the measured results are of the order of ± 10-15% depending on the experimental configuration and detector location in the assembly or in the phantom. The fractional standard deviations of the calculated doses are ± 3-5%. The calculated-to-experimental (C/E) ratios of the free-field and in-box doses at the 400 meter location are in excellent agreement for most of the neutron and gamma-ray doses except for the neutron dose at the mid-gut location in the phantom for both the unlined and lined box configurations. The C/E ratios generally agree within 10%. However, where the C/E values are larger than 10%, the cause of the disparity can be attributed to the measured data. In these cases, the data acquisition times were not sufficient to acquire adequate statistical accuracy in the measured doses even though the run times were as long as eight hours. The C/E ratios for the neutron (NRF) and gamma-ray (GRF) reduction factors (the ratio of the free-field dose to the in-box dose) also agree within 10% for both the unlined and lined box configurations. The liner reduces the neutron dose by a factor of seven but has no effect on the reduction of the gamma-ray dose due to n,γ reactions in the liner. Typical results for the measured and calculated differential spectra, given in Figure 3a-3b, also demonstrate favorable agreement between the calculations and measurements and support the caliber of the integral data comparisons.

MASH results were also compared with those calculated previously using VCS for prompt nuclear weapon radiation shielding characteristics of both the U. S. XM-1 and M60A1 tanks. Calculation of the dose to the tank crew members and the shielding protection afforded the crew by the tank armor were performed as a function of vehicle ground range and orientation relative to the weapon detonation. The XM-1 calculation was performed for exposure to tactical fission weapon radiation while a boosted fission weapon source was used in the M60A1 study. Both weapons were assumed detonated at a height of 100 meters above ground. Radiation effects were characterized at ground ranges from 340 to 1700 meters.

The neutron and gamma-ray doses and protection factors for the XM-1 and M60A1 calculated using MASH were in excellent agreement with the VCS results. The MASH and VCS protection factor results, averaged over all source/vehicle ground ranges and vehicle orientations, agreed within 10% except at the driver location where the agreement between the two calculations was 19%. This agreement is within the statistical error quoted in the original VCS results. The vehicle protection factors, averaged over the four crewmen, agreed within 6% for both the XM-1 and M60A1. The principal contributors to differences in the MASH and VCS results were cross sections, angular quadrature, and mesh spacing in the air-over-ground calculations.

Table 2. Comparison of Measured and Calculated Neutron and Gamma-Ray Free-In-Air Tissue Kerma and Reduction Factors for the 170 and 400 Meter Free-Field and In-Box Environments at the Two-Meter Box Test Bed Experiments Performed at the Army Pulse Radiation Facility (APRF).

Radiation Type	Detector Location	Experimental Measurement	MASH Calculation	C/E
170m Free-Field Free-In-Air Tissue Dose (cGy/kWh)				
n	Free-Field	80.8	78.7	0.97
γ	Free-Field	18.5	13.7	0.74
400m Free-Field Free-In-Air Tissue Dose (cGy/kWh)				
n	Free-Field	4.78	4.97	1.04
γ	Free-Field	1.33	1.36	1.02
n	Phantom Mid-Head	1.16	1.23	1.06
γ	Phantom Mid-Head	2.03	1.96	0.97
n	Phantom Mid-Gut	0.65	0.72	1.11
γ	Phantom Mid-Gut	2.04	1.95	0.96
400m In-Box (Unlined) Free-In-Air Tissue Dose (cGy/kWh)				
n	Center-of-Box	2.80	2.76	0.99
γ	Center-of-Box	0.36	0.34	0.94
n	Phantom Mid-Head	0.32	0.36	1.13
γ	Phantom-Mid-Head	0.91	0.93	1.02
n	Phantom Mid-Gut	0.25	0.19	0.76
γ	Phantom Mid-Gut	0.79	0.85	1.08
400m In-Box (Lined) Free-In-Air Tissue Dose (cGy/kWh)				
n	Center-of-Box	0.36	0.38	1.06
γ	Center-of-Box	0.40	0.39	0.98
n	Phantom Mid-Head	0.12	0.08	0.67
γ	Phantom Mid-Head	0.41	0.39	0.98
n	Phantom Mid-Gut	0.06	0.05	0.83
γ	Phantom Mid-Gut	0.34	0.35	1.03
400m In-Box (Unlined) Neutron and Gamma-Ray Reduction Factors (NRF & GRF)				
n	Center-of-Box	1.71	1.80	1.05
γ	Center-of-Box	3.69	4.00	1.08
400m In-Box (Lined) Neutron and Gamma-Ray Reduction Factors (NRF & GRF)				
n	Center-of-Box	13.3	13.1	0.98
γ	Center-of-Box	3.33	3.49	1.05

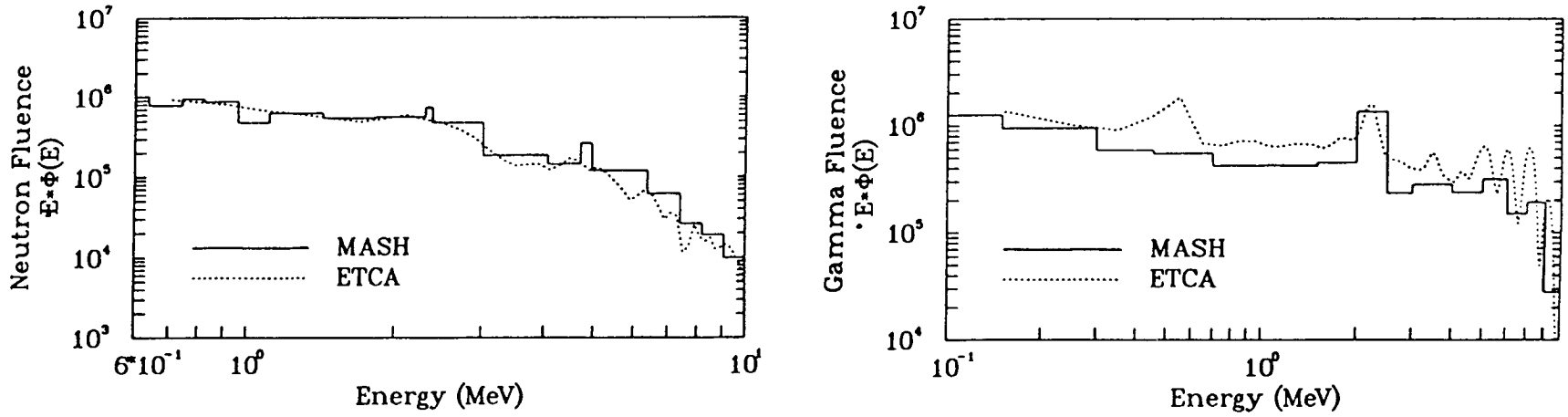

Figure 3a Comparison of ETCA Measured and MASH Calculated Neutron and Gamma-Ray Free-Field Fluence Spectra at 400 Meters.

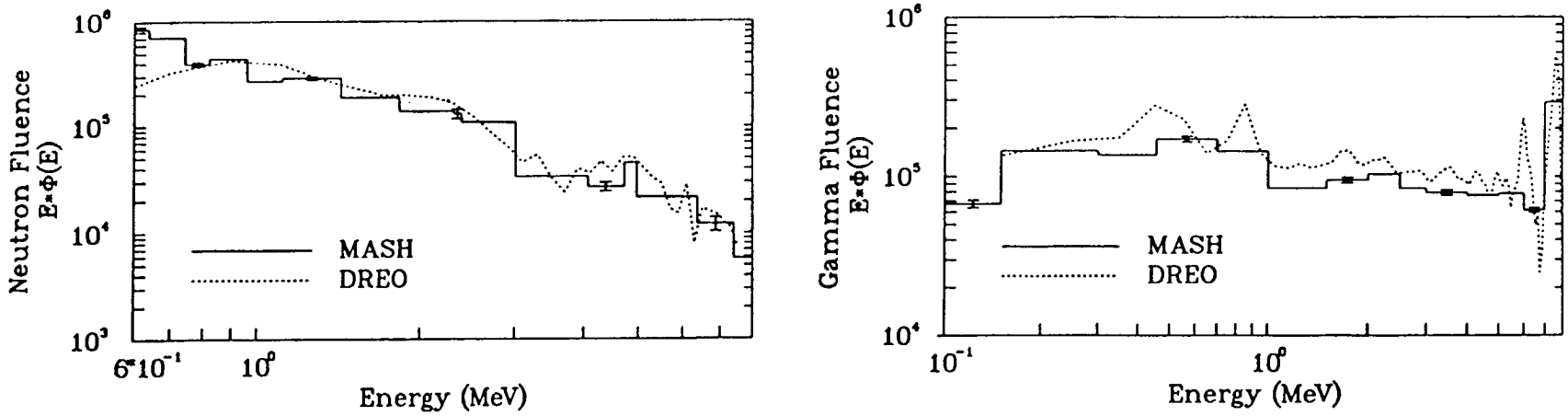

Figure 3b Comparison of DREO Measured and MASH Calculated Neutron and Gamma-Ray In-Box Fluence Spectra at 400 Meters.

MASH has also been used to estimate the dose to sensitive electronic components and personnel in the M1A1 and M1A2 Abrams tanks, the dose inside buildings at Hiroshima and Nagasaki, and to soldiers in fox-holes at the Nevada Test Site. For a considerably different problem, MASH has been applied to estimate the dose to astronauts in a regolith-shielded habitat module located on the surface of Mars from radiation emanating from a power reactor.

V. GRAPHICAL CONSTRUCTION OF COMBINATORIAL GEOMETRIES FOR RADIATION TRANSPORT AND SHIELDING APPLICATIONS

One recurring difficulty in radiation shielding and transport analyses is the construction and verification of the geometric model (together with the associated material assignments) that represents the actual physical configuration to be analyzed. Current armored vehicle models generated by BRL and analyzed in MASH utilize 8,000 to 12,000 solids, 6,000 to 8,000 zones, and up to 75 different materials. In many cases, the resources expended in "setting up" the problem far outweigh the resources expended in executing the various shielding and transport codes. Currently, the geometric models required by the shielding and transport codes such as MORSE, MASH, and TORT[15] are laboriously translated from blueprints or other descriptions into combinatorial geometries by specifying both the fundamental objects (spheres, cylinders, cones, etc.) as well as the Boolean operations required (AND, OR, and NOT) to combine the objects into meaningful assemblies. For even simplified models, the number of fundamental objects and the number of Boolean specifications can easily number in the hundreds or thousands. Both the number of objects and the complexity of the combinations tends to mitigate against the successful construction and verification of the geometric models based on the data as formatted for the input stream of the radiation transport codes.

Two principal improvements would greatly facilitate the model construction process. First, it would be very useful to import the geometry and material parameters for assemblies or components directly from the CAD/CAM applications used to describe the objects. Second, it would be advantageous for the analyst to be able to "see" the geometric model as the algorithms inherent in the transport codes do, during the construction and verification process. Additionally, the potential for graphically positioning of the assemblies relative to each other, as well as the capability of specifying interstitial materials (i.e. void, air, etc.) as appropriate would also be of value.

ORNL has developed a graphics-based code system to manipulate combinatorial geometries for radiation transport and shielding applications. As shown in Figure 2, the current version consists of two parts, CGVIEW[16] and ORGBUG.[17] The system is being developed to accept geometric data from IGES (Interim Graphics Exchange Specification)[18] files, a format compatible with a number of CAD/CAM applications. Additionally, the system utilizes files formatted for the MORSE, MASH (GIFT format), and TORT radiation transport codes. A principal criterion for the design of the system was that it "see" the model exactly as the transport codes do. To this end, the prototype incorporates the same ray-tracing routines utilized in the Monte Carlo codes, MORSE, and MASH. While the prototype currently implements only a few of the functions of the ultimate system envisioned by ORNL, it has already proved to be extremely useful. In its current form, the prototype can be used as a graphically-based debugger for combinatorial geometries. It permits a level of verification and debugging for complex combinatorial geometry models, which was not previously available.

To facilitate initial development and investigation, the prototype has been written as two modules, exchanging data via a metafile. The first half of the prototype system is the "view" generator, CGVIEW, designed to be executed on the same computer used to run the transport code. User-specified options permit the selection of an arbitrary viewpoint in space and the generation of either an isometric or perspective view. The code also permits the user to select the degree of aggregation to be displayed in a particular view. The code permits selective invisibility, i.e. any combination of zones, materials, or regions can be flagged as invisible or transparent to the view generator. Alternatively, an arbitrary body, i.e., any body which can be described using MORSE or MASH (GIFT) geometry, can be "cut away" from the geometry to facilitate debugging internal details. Both of these options can be employed simultaneously. Additional options to the view generator permit the selection of an appropriate aspect ratio for the view, as well as the specification of the desired resolution for the final output. The view generator is designed to produce a metafile, which consists of a compressed version of the "view" itself, which serves as input into the second half of the system.

The second part of the combinatorial geometry debugging system consists of a Microsoft Windows application, ORGBUG, that executes on an IBM compatible personal computer. ORGBUG accepts the metafiles produced by CGVIEW and displays the particular viewpoint represented by each file. Display options range from monochrome wireframe representations to color surface representations. If a color representation is selected, "colorization" can be done on a zone, material, or region basis using either a default palette or user-assigned colors. As a consequence of the decision to split the system into two modules, the image displayed is a fixed one, i.e. no rotation or zoom functions are implemented. An added bonus of being linked to the metafile which contains the zone, body, and surface identifiers for each pixel, is that ORGBUG can utilize an identification option. Using a pointing device, the user can request the identifiers for any visible pixel. This feature has proved to be invaluable for debugging complicated geometries.

Illustrations of the utility of the graphics codes are given in Figures 4 and 5. Figures 4a and 4b illustrate the use of the selective invisibility feature. Figure 4a depicts an isometric view of a Soviet BMP-1 (armored personnel carrier). The model is described in GIFT geometry for use with the MASH code system. By using the selective invisibility feature on the zones, regions, and materials comprising the gun turret and top armor of the model, the view depicted in Figure 4a can be converted to that of Figure 4b. It should be emphasized that the geometry model used for both Figure 4a and 4b is identical - selective invisibility does not require any changes to the input data stream.

Although the primary purpose of the code system being developed is to permit the analyst to validate and correct the *input* for the radiation transport codes, the images produced have also proved useful in displaying the *output* of these codes. Both discrete ordinates codes such as TORT, and stochastic codes such as MORSE and MASH can produce significant quantities of output data. A parallel effort is also being pursued at ORNL to use the graphics system as a visualization tool for displaying the results of the transport calculations.

One visualization option currently being developed using the combinatorial geometry graphics codes is a "vulnerability" map. An adjoint Monte Carlo (MASH) calculation is run for a given response function. The adjoint particles are scored when they exit the particular surface(s) of interest. For example, for the vehicle illustrated in Figure 4a, the surface of interest consist of the vehicle itself as well as the pad representing the ground. These particles are the

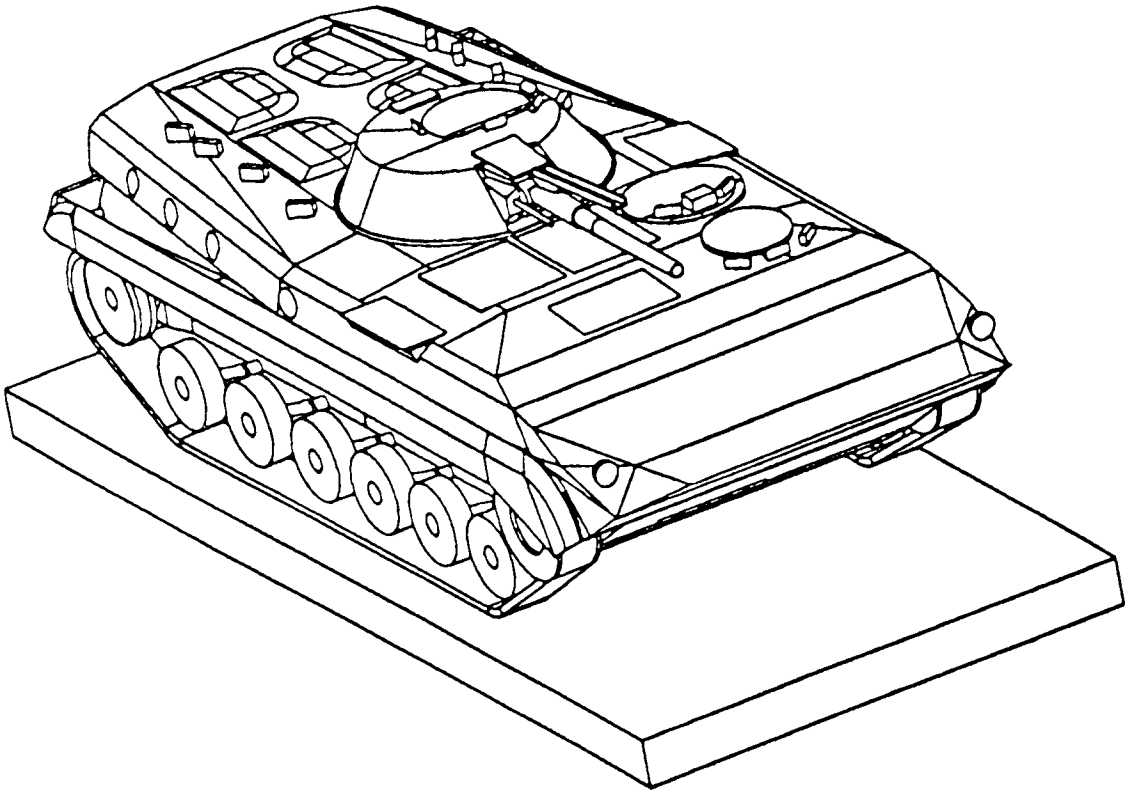

Figure 4a. Isometric View of the Soviet BMP-1 Infantry Fighting Vehicle.

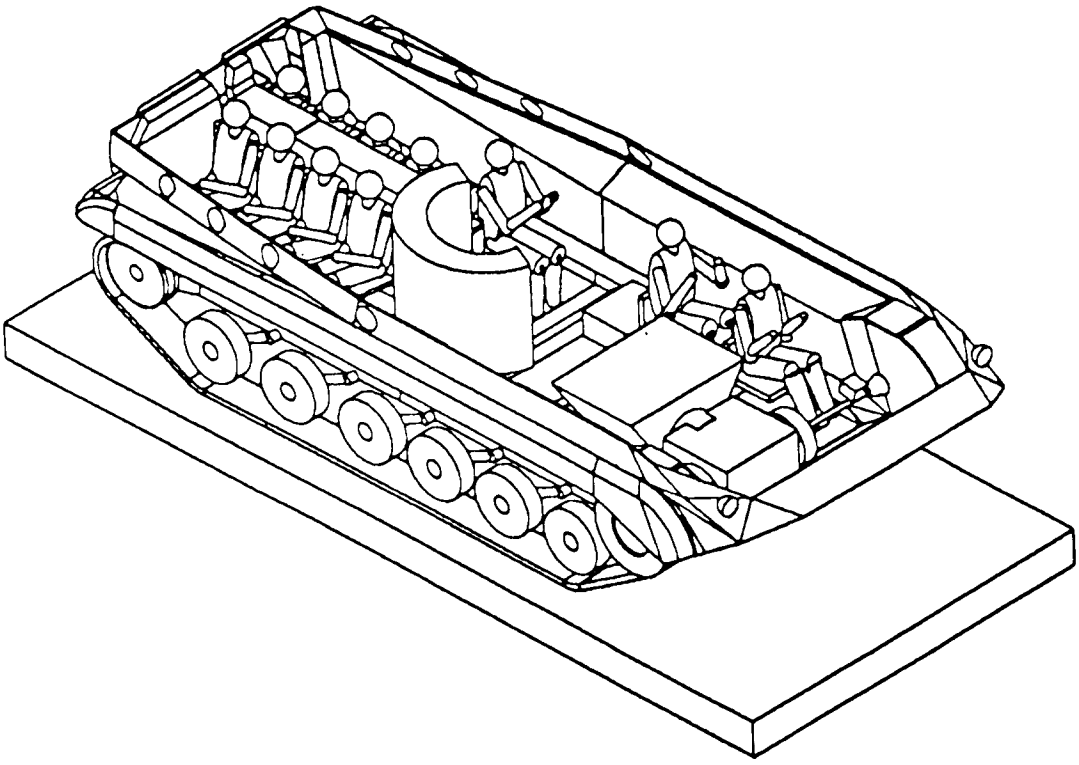

Figure 4b. Isometric View of the Soviet BMP-1 Infantry Fighting Vehicle with the Turret and Top Armor Removed.

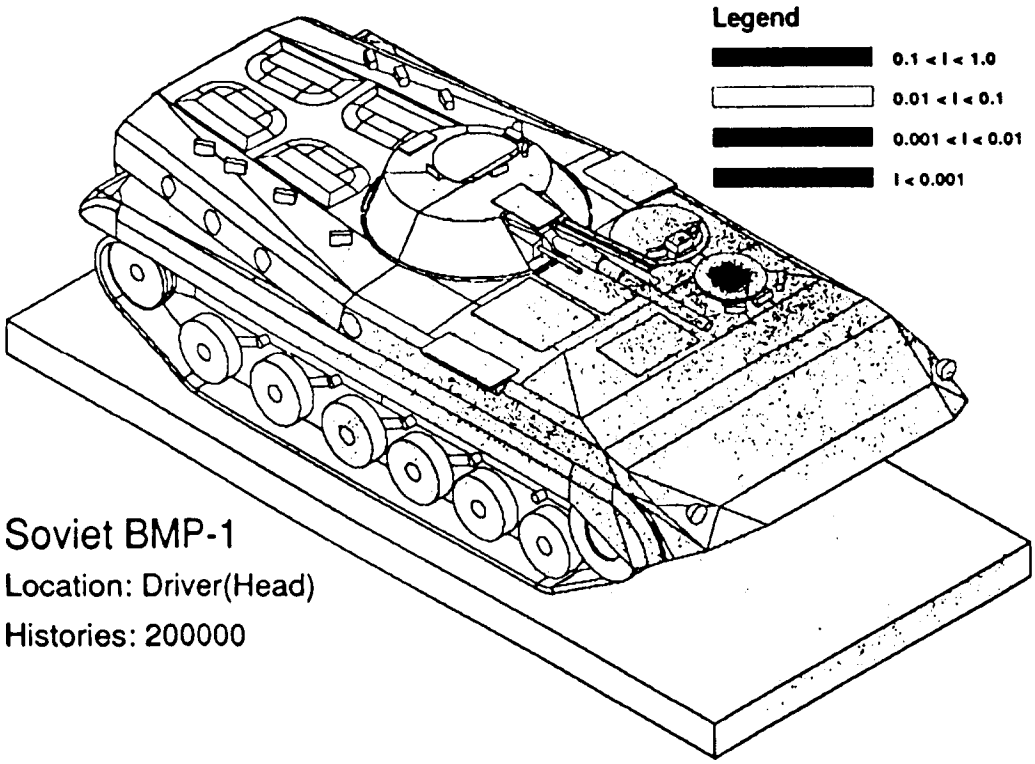

Figure 5a. Vulnerability Map for the Soviet BMP-1 Driver's Mid-Head Dose.

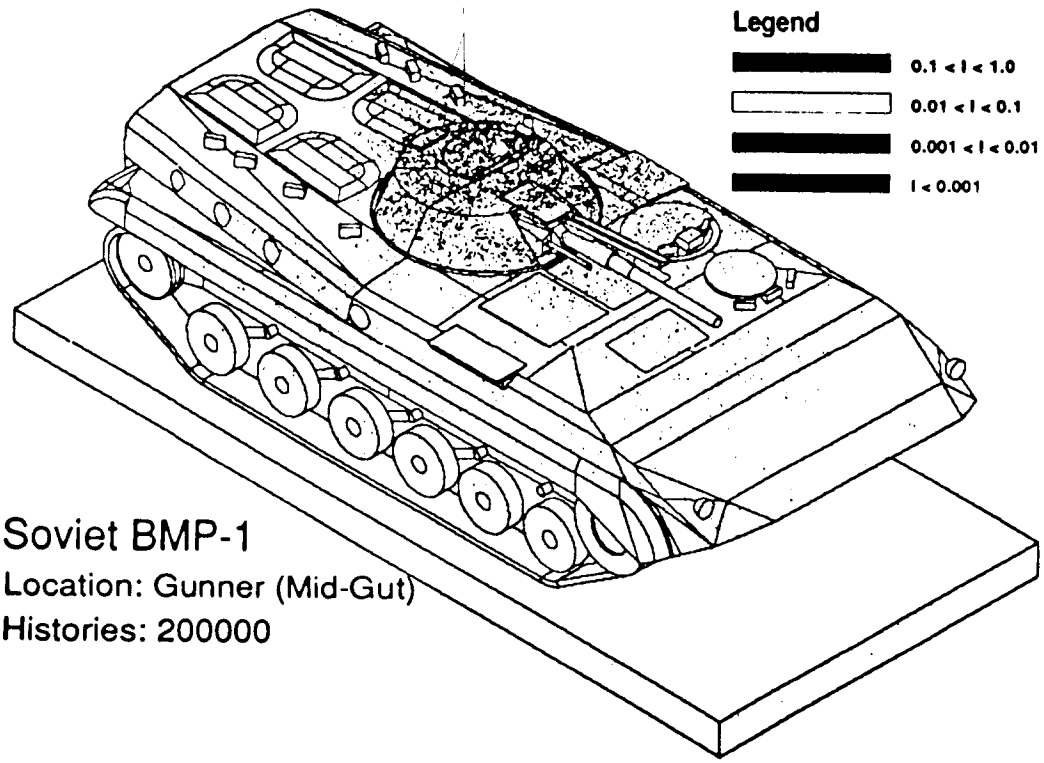

Figure 5b. Vulnerability Map for the Soviet BMP-1 Gunner's Mid-Gut Dose.

folded with the results of a forward discrete ordinates calculation for the source of interest. The resulting values can then be literally plotted on a wireframe representation of the geometry to emphasize the particular "vulnerabilities" of particular regions of the model for the response in question. A set of example "vulnerability" maps are shown in Figure 5 for the Soviet BMP-1. Figure 5a depicts the contributions to the drivers mid-head dose, and Figure 5b indicates the contributions to the gunners mid-gut dose. These "vulnerability" maps are logarithmic intensity plots and do not indicate any information as to the magnitude of the dose. The primary purpose of this type of graphical output is to determine where the radiation source is penetrating the shield and possible determine how to mitigate the high intensity areas. On the computer, these plots are shown in color with colors ranging from red (largest contributors to the dose) to green (smallest contributors to the dose).

VI. CONCLUSIONS

The principal purpose for developing the MASH code system was to provide the U. S. Army, and in particular, the U. S. Army Nuclear and Chemical Agency (USANCA) with the capability to calculate radiation protection factors and reduction factors of armored vehicle shielding materials against neutrons and gamma rays produced in nuclear weapon explosions. The results of the benchmark validation comparisons and the subsequent applications of MASH to armored vehicles have indicated this goal has been achieved. The additional incorporation of the graphics-based combinatorial geometry analysis/visualization tools have made MASH a sophisticated code package capable of accurate, state-of-the-art radiation transport analyses and display in complex, three-dimensional geometries. However, extending MASH to a full three-dimensional code system, enhancing the radiation environment calculation to include delayed radiation, fallout, multiple burst scenarios, and fully integrated time dependence, and enhancing the capabilities of the graphics design/analysis/visualization tools remain to be accomplished.

VII. REFERENCES

1. W. A. Rhoades et al., "Vehicle Code System (VCS) User's Manual," ORNL/TM-4648, Oak Ridge National Laboratory, (August 1974).

2. W. A. Rhoades et al., "Development of a Code System for Determining Radiation Protection of Armored Vehicles (The VCS Code)," ORNL/TM-4664, Oak Ridge National Laboratory, (October 1974).

3. J. O. Johnson, ed., "A User's Manual for MASH 1.0 - A Monte Carlo Adjoint Shielding Code System," ORNL/TM-11778, Oak Ridge National Laboratory, (March 1992).

4. J. O. Johnson, J. D. Drischler, and J. M. Barnes, "Analysis of the Fall-1989 Two-Meter Box Test Bed Experiments Performed at the Army Pulse Radiation Facility (APRF)," ORNL/TM-11777, Oak Ridge National Laboratory, (May 1991).

5. J. O. Johnson, J. D. Drischler, and J. M. Barnes, "Analysis of the Spring-1990 Two-Meter Box Test Bed Experiments Performed at the Army Pulse Radiation Facility (APRF)," ORNL/TM-11917, Oak Ridge National Laboratory, (August 1992).

6. J. O. Johnson, J. D. Drischler, and J. M. Barnes, "Analysis of the Spring-1991 Two-Meter Box Test Bed Experiments Performed at the Army Pulse Radiation Facility (APRF)," ORNL/TM-11918, Oak Ridge National Laboratory, (September 1992).

7. W. A. Rhoades and R. L. Childs, "The DORT Two-Dimensional Discrete Ordinates Transport Code," Nuclear Science & Engineering 99, 1, 88-89 (May 1988).

8. M. B. Emmett, "The MORSE Monte Carlo Radiation Transport Code System," ORNL-4972 (1975), ORNL-4972/R1 (1983), ORNL-4972/R2 (1984), Oak Ridge National Laboratory.

9. Lawrence W. Bain, Jr. and Mathew J. Reisinger, "The GIFT Code User Manual; Volume I. Introduction and Input Requirements," BRL 1802, Ballistic Research Laboratory, (July 1975).

10. Gary G. Kuehl, Lawrence W. Bain, Jr. and Mathew J. Reisinger, "The GIFT Code User Manual; Volume II. The Output Options," ARBRL-TR-02189, Ballistic Research Laboratory, (September 1979).

11. W. H. Scott, Jr., "Vehicle Code System (VCS) Documentation and Uncertainty Analysis," SAI Report SAI-133-79-977-LJ, Science Applications International Corporation, (December 1979).

12. W. H. Scott, Jr., and V. E. Staggs, "Adjoint Energy Biasing and Thermal Neutron Diffusion in the MORSE and VCS Codes," SAI-133-81-384-LJ Science Applications International Corporation, (November 1981).

13. W. H. Scott, Jr., et al., "Predictive Algorithm for Radiation Protection," Volume 1, "VCS In-Group Energy Bias, The DACM Code and DOT Calculations," SAIC-85/1710, Science Applications International Corporation, (May 1985).

14. J. A. Stoddard, S. D. Egbert, and W. H. Scott, Jr., "The Vehicle Code System with In-Group Energy Bias and GIFT5 Geometry," DNA-TR-87-23, Science Applications International Corporation, (January 1987).

15. W. A. Rhoades and R. L. Childs, "TORT A Three Dimensional Discrete Ordinates Neutron/Photon Transport Code," Nuclear Science & Engineering 107, 4, 397-398 (April 1991).

16. T. J. Burns, "CGVIEW - A Program to Generate Isometric and Perspective View of Combinatorial Geometries", ORNL/TM-12019, Oak Ridge National Laboratory, (July 1992).

17. T. J. Burns, "ORGBUG - A Windows-based Combinatorial Geometry Debugger", ORNL/TM-12020, Oak Ridge National Laboratory, (to be published).

18. B. Smith et al., "Initial Graphics Exchange Specification (IGES), Version 4.0", SP-767, Society of Automotive Engineers,(June 1988).

A NEW METHOD TO ASSESS MONTE CARLO CONVERGENCE

R. A. Forster, T. E. Booth, And S. P. Pederson
Los Alamos National Laboratory
Los Alamos, NM 87545

ABSTRACT

A new method is presented to assess the convergence of Monte Carlo solutions by analyzing the shape of the empirical probability density function of history scores, $f(x)$, where the random variable x is the score from one particle history. Unless there is a largest possible history score, the empirical $f(x)$ must eventually decrease more steeply than $1/x^3$ for the second moment ($\int_{-\infty}^{\infty} x^2 f(x)dx$) to exist as required by the central limit theorem. It is postulated that if such decreasing behavior in the empirical $f(x)$ has not been observed, then N is not large enough to satisfy the central limit theorem because $f(x)$ has not been completely sampled.

The largest x's for an unbounded $f(x)$ have been fit to a generalized Pareto function to find the n in $1/x^n_{large}$. A slope value greater than 3 should be observed in the empirical unbounded $f(x)$ to satisfy the $1/x^3$ convergence criterion.

Several test problems were run with the latest version of MCNP that calculates $f(x)$ and the Pareto estimate of the slope. One result for a point detector appeared to be converged, but was a factor of 4 below the correct result. The empirical $f(x)$ clearly shows that a confidence interval should not be formed for this result because the estimated slope was only 1.4.

I. INTRODUCTION

Accurate confidence intervals can only be created when the number of Monte Carlo histories N becomes large enough such that the conditions of the central limit theorem (CLT) are met. The Monte Carlo user has a limited number of marginal methods to assess the fulfillment of this condition, such as statistical error reduction proportional to the $1/\sqrt{N}$ and error magnitude rules of thumb,[1] third moment estimators,[2] and fourth moment estimators such as the variance of the variance.[3,4] A new method is described in this paper that examines the empirical probability density function (PDF) distribution of history scores.

Little work appears to have been done in this area. Score distribution histograms have been generated[4] with an emphasis on determining if a small number of histories account for a large fraction of the total result. Score distribution histograms can also be used to create and study both analytic[5,6] and empirical[7] PDFs for history scores. These are useful in determining if the distribution has been sampled well enough to expect a well converged solution. This paper focuses on initial studies of Monte Carlo history score distributions from particle transport problems. The test calculations have been performed using a the latest version of MCNP[1] that contains this new method.

II. THE HISTORY PROBABILITY DENSITY FUNCTION $f(x)$

A history score posted to a tally bin by MCNP can be thought of as having been sampled from an underlying and generally unknown history score PDF $f(x)$, where the random variable x is the score from one complete particle history to a tally bin. The history score can be either positive or negative. The quantity $f(x)dx$ is the probability of selecting a history score between x and $x+dx$ for the tally bin. Each tally bin will have its own $f(x)$.

The most general form for expressing $f(x)$ mathematically is

$$f(x) = f_c(x) + \sum_i p_i \delta(x - x_i) \quad , \tag{1}$$

where $f_c(x)$ is the continuous part and $\sum p_i \delta(x-x_i)$ represents the different discrete components occurring at x_i with probability p_i. An $f(x)$ could be composed of either or both parts of the distribution. A history score of zero is included in $f(x)$ as the discrete component $\delta(x-0)$. By the definition of a PDF,

$$\int_{-\infty}^{\infty} f(x)dx \equiv 1 \quad . \tag{2}$$

The mean or expected value $< x >$ of the history scores is the first moment of the history scores distribution; namely,

$$< x >= \int_{-\infty}^{\infty} x f(x)dx \quad . \tag{3}$$

The n^{th} central moment of x is defined to be

$$n^{th} \ central \ moment = \int_{-\infty}^{\infty} f(x)(x- < x >)^n dx \quad . \tag{4}$$

The variance σ^2 of the population of x's is defined to be the second central moment of x, which is equal to

$$\sigma^2 = < x^2 > - < x >^2 \quad , \tag{5}$$

where the expected value of the second moment $< x^2 >= \int_{-\infty}^{\infty} x^2 f(x) dx$. The square root of the variance is called the standard deviation σ and is a measure of the dispersion in the values of x.

Since $f(x)$ is seldom explicitly known, Monte Carlo samples the history score PDF implicitly using particle random walks. The true mean $< x >$ is estimated by

$$\overline{X} = \sum_{i=1}^{N} x_i / N \quad , \tag{6}$$

where x_i is the i^{th} history score to a tally bin. The estimated mean $\overline{X}$ is the sum of all of the history scores normed by the number of histories run; i.e., $\overline{X}$ is the average score per history for each tally bin.

The standard deviation σ is estimated by S where S is given by (and dropping the i subscript from the $\sum$ and assuming N is much greater than one)

$$S = \sqrt{\sum x_i^2 / N - (\sum x_i)^2 / N^2} \quad . \tag{7}$$

The estimated standard deviation of the mean is

$$S_{\overline{X}} = S / \sqrt{N} \quad . \tag{8}$$

This implies that $S_{\overline{X}}$ should decrease as the inverse of the square root of N as long as the estimate of σ, S, does not change markedly during the calculation.

For each tally bin, MCNP prints the estimated mean (Eqn. (6)) and the estimated relative error RE, where the RE is

$$RE = S_{\overline{X}} / \overline{X} \tag{9}$$

$$= \sqrt{\sum x_i^2 / (\sum x_i)^2 - 1/N} \quad . \tag{10}$$

This quantity is convenient because the estimated statistical uncertainty in the result is given as a fraction of the result.

III. THE CENTRAL LIMIT THEOREM AND $f(x)$

The CLT states that the estimated mean will appear to be sampled from a normal distribution with a KNOWN standard deviation $\sigma / \sqrt{N}$ when N approaches infinity. In practice, σ is NOT known and must be approximated by the estimated standard deviation S. The major difficulty in applying the CLT correctly to a Monte Carlo result to form a confidence interval is knowing when N is large enough.

How can this be assessed? Several marginally quantifiable methods were mentioned in the introduction. A new method described in this paper involves examining the behavior of $f(x)$ for large history scores to attempt to assess if $f(x)$ appears to have been "completely" sampled. If "complete" sampling has occurred, the largest values of the sampled x's should have either nearly reached

the upper limit (if such a limit exists) or should decrease faster than $1/x^3$ so that $< x^2 >= \int_{-\infty}^{\infty} x^2 f(x)dx$ exists (σ is assumed to be known in the CLT). Otherwise, N is assumed not to have approached infinity in the sense of the CLT. This is the basis of the proposed use of the empirical $f(x)$ to assess Monte Carlo tally convergence.

The argument should be made that since S must be a good estimate of σ, the expected value of the fourth history score moment $< x^4 >= \int_{-\infty}^{\infty} x^4 f(x)dx$ should exist. In the paper, we will assume that only the second moment needs to exist so that the $f(x)$ convergence criterion will be relaxed somewhat. Nevertheless, this assumption should not be forgotten.

IV. ANALYTIC STUDY OF $f(x)$ FOR TWO-STATE PROBLEMS

This work was divided into two parts: 1) derive and examine analytic Monte Carlo score distributions both to assess their general nature and to use for statistical confidence interval studies; and 2) create and examine empirical history score PDFs for real transport problems to assess their usefulness in predicting Monte Carlo convergence. For the first part, the tally distribution of history scores has been examined analytically[5,6] for both an analog two-state splitting and exponential transform problem. This work provides the theoretical foundation for statistical studies on relevant analytic functions to increase understanding of confidence interval coverage rates for Monte Carlo calculations.

It was found that the splitting problem history score PDF decreases geometrically as the score increases by a constant increment (this is equivalent to a negative exponential behavior for a continuous score PDF). The history score PDF for the exponential transform problem decreases geometrically with geometrically increasing x. Therefore, the splitting problem produces a linearly decreasing PDF for the history score on a linear-log plot of the score probability versus score. The exponential transform problem generates a linearly decreasing score behavior (with high score negative exponential roll off) on a log-log plot of the score probability versus score plot. In general, the exponential transform problem is the more difficult to sample because of the larger impact of the low probability high scores.

The analytic shapes were compared with comparable problems calculated with the latest version of MCNP. These shapes of the analytic and empirical $f(x)$s were in excellent agreement.[6]

V. PROPOSED USE FOR THE EMPIRICAL $f(x)$

In general, there has been very little discussion about the empirical $f(x)$ for Monte Carlo transport problems.[7] A new capability has been added to MCNP to allow inspection and analysis of the empirical $f(x)$ for the tally fluctuation chart bin of each tally. This should be important for assessing if there are any unexpected unsampled regions in the empirical history score PDF $f(x)$.

The most important proposed use for the empirical $f(x)$ is to attempt to determine if N has approached infinity in the sense of the CLT so that valid confidence intervals may be formed. The application of the CLT to Monte Carlo results to form a valid confidence interval requires the existence of the first two moments of $f(x)$. The history score PDF is assumed to have these properties for all of our current estimators and variance reduction techniques. (Point detectors with no constant flux neighborhoods in scattering materials and the exponential transform with a

"large" [problem dependent] stretching parameter and no weight window are two known exceptions.)

It is assumed that the underlying $f(x)$ satisfies the CLT requirements. Therefore, so should the empirical $f(x)$. Unless there is a largest possible history score, the empirical $f(x)$ must eventually decrease more steeply than x^{-3} for the second moment ($\int_{-\infty}^{\infty} x^2 f(x)dx$) to exist. It is postulated[7,8] that if such decreasing behavior in the empirical $f(x)$ with no upper bound has not been observed, then N is not large enough to satisfy the CLT because $f(x)$ has not been completely sampled. Therefore, a larger N is required before a confidence interval can be formed. It is important to note that this convergence criterion is NOT affected by any correlations that may exist between the estimated mean and the estimated RE. In principle, this should make this $f(x)$ diagnostic robust in assessing "complete" sampling.

As mentioned in Section III, the argument could be made that the fourth moment of $f(x)$ should exist so that the estimate of $S_{\overline{X}}$ in Eqn. (8) is valid for use in the CLT in the place if $\sigma/\sqrt{N}$. This would increase the decreasing behavior requirement to x^{-5} so that $\int_{-\infty}^{\infty} x^4 f(x)dx$ exists. We have elected to use the x^{-3} requirement because it is less stringent, but will still detect the many important cases of incomplete sampling. This loosened $f(x)$ criterion for convergence could be modified in the future as experience with the method increases.

Both the analytic and empirical history score distributions suggest that large score fill-in and one or more extrapolation schemes for the high score tail of the history score PDF could provide a meaningful estimate of scores not yet sampled to help assess the impact of unsampled history scores on the mean and confidence interval. This has not yet been considered.

VI. CREATION OF $f(x)$ IN MCNP

We wanted the creation of empirical $f(x)$s in MCNP to automatically cover nearly all tally fluctuation chart bin tallies that a user might reasonably be expected to make. We finally settled on using a logarithmically spaced history score grid for $f(x)$ because the tail behavior is assumed to be of the form $1/x^n, n > 3$ (unless an upper bound for the history scores exists). This would produce an equal bin width histogram of a straight line for $f(x)$ on a log-log plot that decreases n decades in $f(x)$ per decade increase in x.

We used 10 bins per x decade and covered the unnormalized tally range from 10^{-30} to 10^{30}. The term "unnormalized" indicates that MCNP normalizations that are not performed until the end of the problem, such as cell volume or surface area, are not included in $f(x)$. The user can multiply this range using MCNP input when the range is not sufficient. We keep track of both history score number and history score in the x grid to examine the cumulative number and score distributions. We use a linear fit to the logarithmically spaced x grid of the form $a + b \cdot ln(x)$ to find the grid location without a time-consuming search.

With this x grid in place, the average empirical $f(\overline{x_i})$ between x_i and x_{i+1} is defined to be

$$f(\overline{x_i}) = (number\ of\ history\ scores\ in\ i^{th}\ score\ bin)/(N(x^{i+1} - x^i)) \quad , \qquad (11)$$

where $x^{i+1} = 1.2589x^i$. The quantity 1.2589 is $10^{0.1}$ and comes from 10 equally spaced log bins per decade. The calculated $f(\overline{x_i})$s are available in MCNP on printed plots in the output or using the new tally graphics commands. Any history scores

that are outside the x grid are counted as either above or below to provide this information to the user.

Negative history scores are a possibility for some charge deposition tallies. The default procedure lumps any negative history score into the one bin below the lowest history score in the built-in grid. If desired, a $f(-x)$ can be created for negative scores. Positive history scores will then be lumped into the highest bin in this case.

VII. PARETO FIT TO THE LARGEST HISTORY SCORES

We estimate the slope n in $1/x^n$ of the largest history tallies x to determine if and when they decrease faster than $1/x^3$. This requires saving and sorting the largest history tallies at various points during the calculation. We use the "heapsort" sorting algorithm because it is reasonably fast and robust.[9]

We used the generalized Pareto function[10]

$$Pareto\ \ f(x) = a^{-1}(1 + kx/a)^{-1-1/k} \tag{12}$$

to fit the largest x's. This function fits a number of extreme value distributions including $1/x^n$, negative exponential ($k = 0$), and constant (k=−1). We developed a large history tally tail fitting technique using the "simplex" algorithm,[9] which finds the values of a and k that best fit the largest history scores by maximum likelihood estimation. Other algorithms, such as those using the derivative of the Pareto, could be used for increased speed, but the simplex method appears to be more robust and not that time consuming for this MCNP application.

The number of largest history score values to use for the fit is a variable that was investigated. We settled on a maximum of 201 points because this would provide about 10% precision[10] on the slope estimator at $n = 3$. The precision increases for smaller values of n and vice versa. The number of values actually used in the fit is the lesser of 5% of the nonzero history scores or 201. The minimum number of values used for a Pareto fit is 25 with at least two "different" values, which requires at least 500 nonzero history scores with the 5% criterion. We were careful about the implementation to be sure the technique would multitask and be reasonably efficient.

From the Pareto fit, we defined the slope of $f(x_{large})$ to be

$$slope \equiv 1 + 1/k \quad . \tag{13}$$

A slope value of zero is defined to indicate that not enough $f(x_{large})$ tail information exists for a slope estimate. The slope is not allowed to exceed a value of 10 (defined to be a "perfect score"), which would indicate an essentially negative exponential decrease. If the 100 largest history scores all have values with a spread of less than 1%, an upper limit is assumed to have been reached and the slope is set to 10. The slope should be greater than 3 to satisfy the second moment existence requirement. Then, $f(x)$ will appear to be "completely" sampled and hence N will appear to be large enough to satisfy the CLT.

VIII. MCNP TEST PROBLEM RESULTS AND ANALYSIS

Several test problems were run with the latest version of MCNP that calculates the empirical $f(x)$ and the Pareto estimate of the slope for the user-defined tally fluctuation chart bin of each tally. One test problem[3,7,8] was to calculate the surface neutron leakage flux above 12 MeV from an isotropic 14 MeV neutron point source

of unit strength at the center of a 30 cm thick concrete shell with an outer radius of 390 cm. Point and ring detectors[1] were deliberately used to estimate the surface neutron leakage flux with highly inefficient, long tailed $f(x)$s.

The variance reduction methods employed[1] were implicit capture with weight cutoff, low-score point detector Russian roulette, and a 0.5 mean free path (4 cm) neighborhood around the detectors to produce large, but finite, higher moments. Other tallies or variance reduction methods could be used to make this calculation much more efficient, but that was not the object of this calculation.

One point detector result at 14,000 histories was 1.41×10^{-8} n/cm^2/sec with an estimated relative error of 0.041. The estimated $S_{\overline{X}}$ was decreasing as approximately $1/\sqrt{N}$ for the last half of the problem. Using the currently accepted rules-of-thumb for a valid Monte Carlo result, the confidence interval formed from this tally could easily be accepted by even a careful Monte Carlo practitioner.

The correct detector result, obtained from a 50 million history ring detector tally, is 5.68×10^{-8} n/cm^2/sec with an estimated relative error of 0.0054 and a slope of 4.9. (The ring detector result for 14,000 histories was 4.60×10^{-8} n/cm^2/sec with an estimated relative error of 0.17 and a slope of 2.1.) The apparently converged 14,000 history point detector result is a factor of four below the correct result!

The new convergence criterion proposed here provides compelling evidence that an N of 14,000 is not large enough and a confidence interval should NOT be formed. The large x slope is a very shallow 1.4 (i.e., $1/x^{1.4}$), which could not continue indefinitely because the mean would not exist. This is a clear indicator that the unbounded $f(x)$ has not yet been completely sampled.

Figure 1 compares the empirical point detector $f(x)$s for 14,000 and 200 million histories. The 14,000 history $f(x)$ clearly has unsampled regions in the tail, which

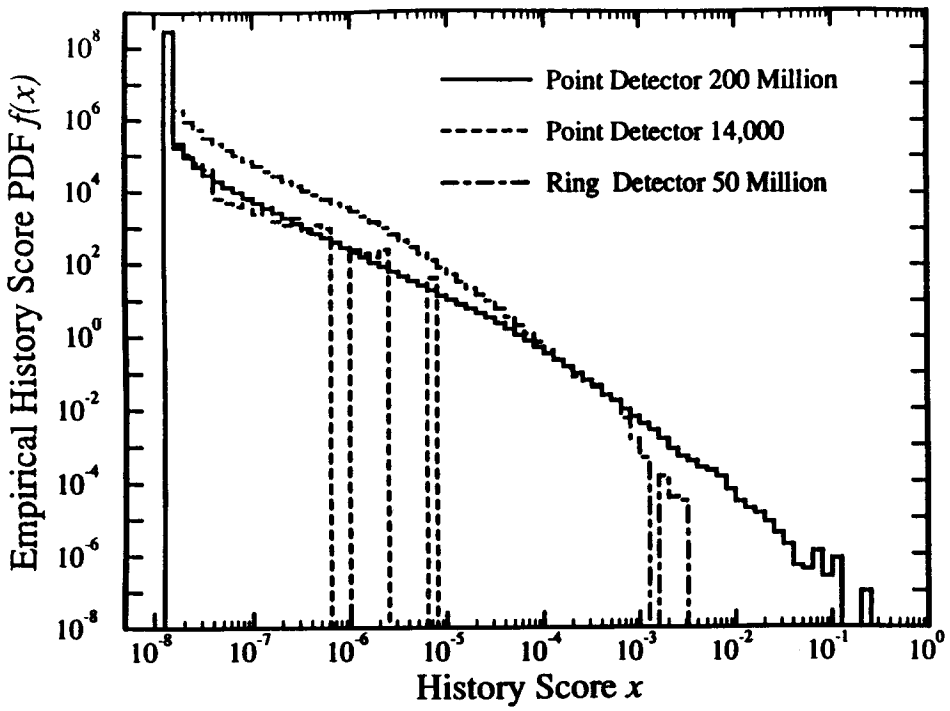

Fig. 1. Empirical point detector $f(x)s$ for 14,000 and 200 million neutron histories and the empirical ring detector $f(x)$ for 50 million neutron histories versus the history score x.

indicate incomplete $f(x)$ sampling. For the point detector, over seven decades of x have been sampled by 200 million histories compared to only three decades for 14,000 histories. The largest x's occur from the extremely difficult to sample histories that have multiple small energy loss collisions close to the detector. The 200 million history point detector result is 5.44×10^{-8} n/cm^2/sec with an estimated relative error of 0.036 and an estimated slope of 2.4. The point detector $f(x)$ slope is increasing, but still does not yet appear completely sampled. The more compact empirical ring $f(x)$ for 50 million histories, shown in Fig. 1, appears to be completely sampled because of the large slope.

IX. CONCLUDING REMARKS

The proposed empirical $f(x)$ convergence criteria should provide new insight into the quality of a Monte Carlo result. The empirical $f(x)$ is available for the first time for user to examine in MCNP. The Pareto fit for the slope is hoped to be a useful new diagnostic for predicting the importance of large scores that have not yet been sampled. The pathological example discussed above was easily identified as a result for which a confidence interval should NOT be formed.

This new capability has been incorporated into the latest version of MCNP. Additional experience with this diagnostic is required to determine its effectiveness in assessing the fulfillment of the central limit theorem requirements for Monte Carlo solutions. It is emphasized that even an apparently well-sampled $f(x)$ may have an important, but improbable, portion that has not yet produced a large history score. *CAVEAT EMPTOR.*

REFERENCES

1. J. F. Briesmeister, Ed., "MCNP – A General Monte Carlo Code for Neutron and Photon Transport," LA–7396–M, Rev. 2, Los Alamos National Laboratory (1986).

2. M. H. Kalos, P. A. Whitlock, *Monte Carlo Methods, Volume I: Basics*, John Wiley & Sons, p. 27 (1986).

3. G. P. Estes, E. D. Cashwell, "MCNP1B Variance Error Estimator," Los Alamos National Laboratory memo TD–6–27–78 (1978).

4. W. J. Vieira, "A General Study of Undersampling Problems in Monte Carlo Calculations," Doctoral Dissertation, University of Tennessee (1989).

5. T. E. Booth, "Analytic Comparison of Monte Carlo Geometry Splitting and Exponential Transform," *Trans. Am. Nucl. Soc.*, **64**, 303 (1991).

6. T. E. Booth, "Analytic Monte Carlo Score Distributions for Future Statistical Confidence Interval Studies," *Nucl. Sci. Eng.*, **112**, 159 (1992).

7. R. A. Forster, "A New Method of Assessing the Statistical Convergence of Monte Carlo Solutions," *Trans. Am. Nucl. Soc.*, **64**, 305 (1991).

8. R. A. Forster, S. P. Pederson, and T. E. Booth, "Two Proposed Convergence Criteria for Monte Carlo Solutions," *Trans. Am. Nucl. Soc.*, **66**, 277 (1992).

9. W. H. Press, B. P. Flannery, S. A. Teukolsky, and W. T. Vetterling, *Numerical Recipes (FORTRAN Version): The Art of Scientific Computing*, p. 229 and 289, Cambridge University Press (1990).

10. J. R. M. Hosking and J. R. Wallis, "Parameter and Quantile Estimation for the Generalized Pareto Distribution," *Technometrics*, **29**, 339 (1987).

A New Approach to Geometry Modelling and Visualisation for MONK and MCBEND

N R Smith & E Shuttleworth
AEA Technology, UK

M H Watmough
British Nuclear Fuels plc, UK

Summary

There are a number of user groups who make regular use of both the MONK and MCBEND Monte Carlo particle transport codes. However each code has traditionally had a radically different approach to the process of geometry modelling, which forms a significant component of the input data preparation time. This has meant that familiarisation with two different geometry modelling schemes has been required with the resulting overheads in training and maintenance of expertise. As part of the major review of Monte Carlo particle tracking codes that has been going on in the UK, a decision was taken to solve this problem by creating a new geometry modelling scheme called Fractal Geometry that integrated the key capabilities of the two independent schemes within a single modelling environment. To accompany the new modelling package, interactive geometric visualisation software packages have been developed called VISAGE and VISTA which between them offer two- and three-dimensional solid body and wire frame components. This paper describes the creation of the Fractal Geometry package and the associated visualisation software that is now available.

1. INTRODUCTION

One of the principal strengths of the Monte Carlo method for solving particle transport problems is the accuracy with which the geometry of the system can be modelled. This is exploited by Monte Carlo computer codes in various ways but what is achieved by all is the sub-division of the problem space into volumes (or zones) of constant composition. The surface shapes available in major Monte Carlo codes are capable of following the boundaries of most common engineering structures with acceptable precision. Indeed there is no real theoretical limit to the flexibility which such a code could provide with the practical limitations being set by the range of facilities provided by the code developer and the ingenuity of the code user.

When simulating the movement of a particle in a Monte Carlo calculation, its position may be monitored with reference to the surfaces describing the geometry. The code may determine which side of a given surface the particle is, or it may evaluate the point(s) of intersection between the particle track and a given surface. This in turn allows the code to identify the defined volume of space in which the particle is travelling and hence, the composition of that volume.

These principles, used in all major Monte Carlo codes, may be implemented in a variety of ways. The ideal form would be efficient on computer time and storage, robust in long calculations for complicated cases, and user-friendly at the input stage. The advantages and

disadvantages of various options are discussed in this paper leading up to the description of a new system that will be employed in future versions of the criticality code MONK[1] and the general particle transport code MCBEND [2]. This new system is called Fractal Geometry and it has been designed to achieve a reasonable balance between the conflicting requirements.

In addition to a powerful and versatile geometric modelling capability, it is essential that a Monte Carlo particle transport code has a visual means of checking the specified geometry. Traditionally this has been performed by examining low-resolution two-dimensional slices through the problem geometry. However to accompany the Fractal Geometry package, interactive geometry visualisation software packages have been produced which provide a quicker and more accurate means of verifying the geometry model. These packages provide interactive high-resolution facilities within a modern portable environment and enable two- and three-dimensional images of the geometry model to be displayed and manipulated. This paper also describes the development of these packages.

2. BASIC METHODS

This section describes the various basic methods of geometry modelling that are used in major Monte Carlo particle tracking codes.

2.1 Surface Systems

In surface systems the zone boundaries are specified as mathematical surfaces and the requirements of efficient processing usually limits the surface repertoire to those defined by first or second order equations. Among the more useful surfaces are planes, cylinders, spheres, cones and paraboloids. The surfaces may be numbered and a sign convention is often used to indicate the volumes of space on either side of a given surface.

A zone is defined by a list of signed boundary surfaces. By introducing operators, the system may include the unions, intersections and complements of the spaces on given sides of the surfaces. This is the basis of the geometry modelling system used in MCNP [3]. The sketch on the right shows a simple application of this system in two dimensions. The shaded zone is defined by the intersection of infinite half-spaces each defined by a plane surface.

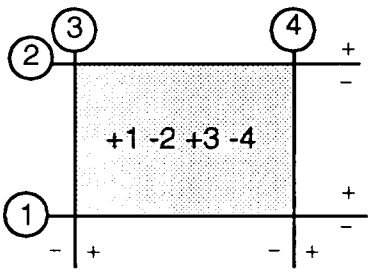

2.2 Body Systems

In body systems the zone boundaries are specified by the surfaces of simple, solid bodies such as cuboids, cylinders, spheres, truncated cones and arbitrary polyhedra. The bodies are usually numbered and a sign convention is employed to indicate the volumes of space inside and outside of the bodies. A zone is defined by the intersections and differences of the defined bodies. This is the basis of the geometry modelling system used in MCBEND and MORSE [4]. The sketches below show (in two dimensions) ways in which two bodies may be combined.

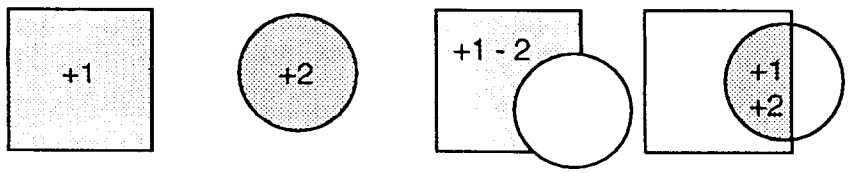

Inside body 1 Inside body 2 Difference Intersection

2.3 Part Systems

The criticality code MONK uses a variation on the body system in which the model is subdivided into *parts*. Each part is a self-contained sub-system with its own local co-ordinates. The outer surface of a part is referred to as the part *container* body. Any body, in any part, may contain a *subsidiary* part provided that the container of the subsidiary part matches the shape and size of the *parent* body. This system is specifically tailored to the repeated structures common in criticality applications. Consider the example of a simplified flask model (see below). A fuel pin (with cladding, fuel pellets and end caps) may be defined as a part. A fuel element is a part which includes the fuel pins and an absorber pin as subsidiary parts.

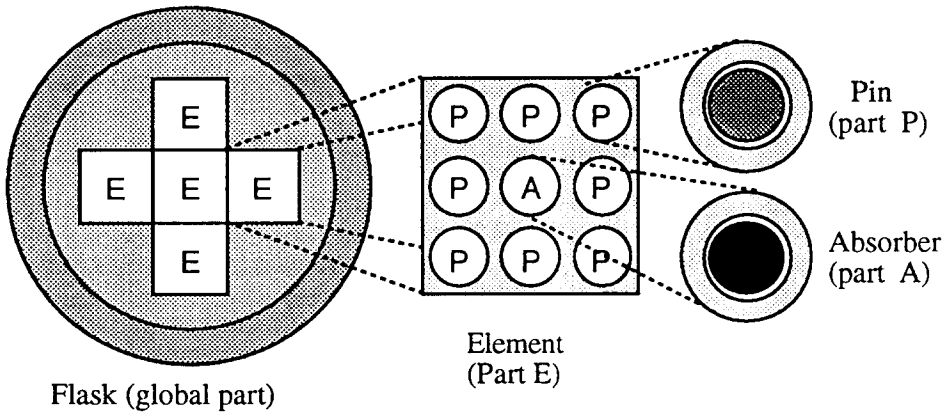

In this simple example, each part (E, P and A) is defined just once but included in parent parts as often as required. Common requirements are met by simple structured parts and a one-to-one correspondence between bodies and zones is maintained; this serves to simplify the user image. The structure and the local co-ordinate systems are retained into the execution stage of the calculation.

2.4 Woodcock tracking

The movement of a particle in the geometric model is usually monitored by calculating the intersection points of the particle track with the surfaces or bodies of the defined system. This in turn involves finding the roots of an equation involving the boundary surface parameters and those of the particle track. For efficient tracking this limits the equations to be solved to first or second order - though most codes include a torus body with its associated quartic equation.

An alternative form of tracking (called Woodcock tracking) is available in MONK. A uniform, total cross-section is used within each special region of geometry. Its value, Σ_t, is the maximum (at the current particle energy) of all the materials in the region. When a collision occurs, the material at the collision site and its total cross-section, Σ_m, are identified. If a random number R ($0<R<1$) is less than the ratio Σ_m/Σ_t then the collision is considered to be a real collision. Otherwise it is a null collision and the track continues undisturbed. By this means the distribution of real collisions is unbiased.

Locating a zone containing a particular point generally involves testing the signs of a series of functions evaluated at the current particle position. This is far faster than finding the roots of an equation and there is no limit to the order of the function as the code simply has to evaluate the function not solve the equation for when it equals zero. In this method of tracking it is possible to model such structures as a screw feeder (see below) or a pump impeller with spiral blades. It is also efficient when modelling fine detail such as large arrays of fuel pins.

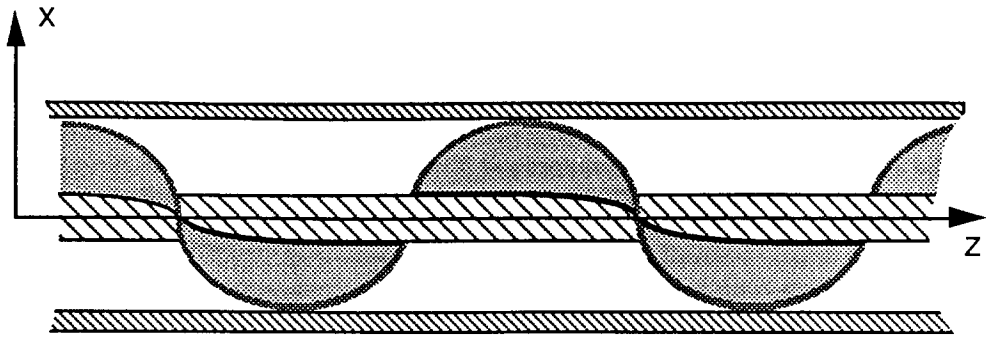

3. ADVANTAGES AND DISADVANTAGES

3.1 Bodies versus Surfaces

From the user's point of view the body system is generally easier to employ since most physical zones to be modelled are solid engineering objects. The quantity of real data necessary to define co-ordinates and dimensions are similar in both systems but the zone descriptions are much shorter in the body system.

Take, for example, the containing material of a closed rectangular tank.

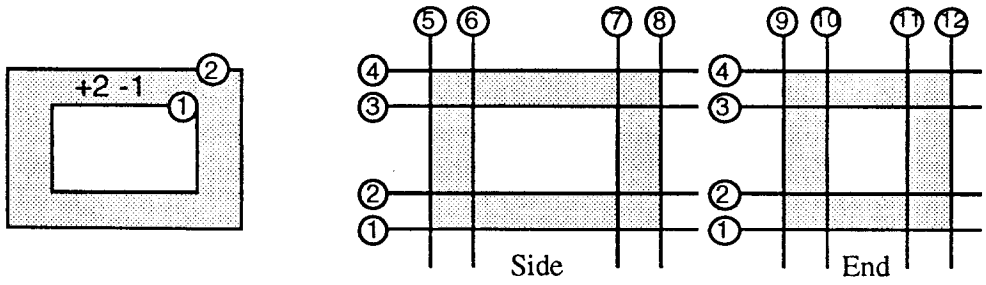

The left hand sketch shows a representation using the difference of two cuboidal bodies. The right hand pair of sketches show a representation using plane surfaces. It is necessary to refer to twelve of these in order to define the required zone. If the zone is to be defined as a single entity then elaborate input conventions are required to handle both unions and intersections within the single zone.

The body system may lead to difficulties when two bodies meet at a common plane surface. During execution, rounding errors (however small) may cause the intersection of a particle track with the body surfaces to evaluate to different results at the common surface. Elaborate checks are then required to prevent the moving particle thinking that it has left one body but not yet entered the other. It is also inefficient to repeat the calculation of the intersection point more than once where common planes exist.

The net effect is that the surface system is better for the tracking activities of the code but the body system presents a more user-friendly image. This conflict may be reconciled by introducing a stage during which a model defined using bodies is converted by the code into one based on surfaces. This principle has been used in the code MCBEND.

A problem common to both methods is that of finding the next zone to be entered after a moving particle has left the previous zone, P. In a completely general system there is no simple way of establishing which zones are neighbours of P. One solution is to test all other zones during the early stages of tracking and remember which trials were successful. The list of successes for a given zone may be scanned first when a subsequent particle leaves zone P. Gradually, the code learns a list of neighbours for each zone and tracking becomes more efficient. In principle, the surface system could allow a short list to be drawn up of possible neighbours for each zone. This could be prepared before tracking commences in order to speed up the learning process. This is not possible in a pure body system since neighbouring zones could be defined without having any bodies in common.

The problem is alleviated in MONK for many practical situations by the provision of structured parts, each limited in geometric complexity. This means that potential neighbours of each zone are identified by the part structure itself. On its own this tends to restrict the power of the modelling package, but as one component of a larger package, as in MONK, it has much to recommend it as an aid to both code and user efficiency.

3.2 Global versus Local Systems

The code MONK retains the part structure and its associated sets of local co-ordinate systems from the input to the execution stage. This is very economical on storage but, during tracking, the parameters defining the particle trajectory are constantly being revised to the local co-ordinates of the parts being entered. If rotations are involved in addition to translations then there could be an execution time penalty. A potential solution would be to include a processing stage which expands the part structure into a global model before tracking begins.

If a model contains extensive replication of parts such as fuel elements it is inefficient to expand the zone definitions into a global form. This consumes unnecessary storage and, more significantly, makes the tracking less efficient. The map of neighbouring zones within one fuel element is equally valid in all identical elements and should not have to be re-learned as particles move through a global system. By creating a representation of the part structure and introducing simple offsets it is possible to interface the local zone descriptions with the global set of body data.

3.3 Boundary crossings versus Woodcock tracking

Woodcock tracking is a versatile and widely-applicable algorithm but it cannot be regarded on its own as a complete alternative to the evaluation of boundary crossings. This is due to a loss of calculational efficiency that arises when the total cross-sections of the materials in the special geometry region vary by orders of magnitude. The frequency of collisions in a Woodcock tracking region is governed by the maximum cross-section of all the materials present in the region. In the presence of heavy absorbers (e.g. boron at thermal energies) the number of null events to be processed can become excessive in specific situations, although by a judicious mix of Woodcock tracking and boundary crossing this potential problem can be avoided in many practical situations. Irrespective of any such problems though, the power and ease of specification mean that Woodcock tracking is an important component in any new system.

3.4 User Image Issues

Even in the absence of extensive repetition there are advantages to be gained from dividing the total geometry into sub-sets. It is not uncommon for a major geometry model to include hundreds of bodies/surfaces and zones. It is a severe test of the user's memory to grasp the entirety of such a model. Communicating the model to another user or attempting modifications after the passage of time are difficult and error prone operations. The use of small, self-contained parts, as in MONK, alleviate such problems.

This modelling structure is analogous to the engineering drawing practice of detailing components and then combining them in drawings of larger assemblies. Advantages include the simplification of exercises involving a series of related calculations (such as the evaluation of a transport flask with different loadings) and the ability to create and use libraries of standard parts. The use of local co-ordinate systems and component numbering means that there are few problems associated with the assembly of a complex model from a kit of relatively simple parts.

4. FRACTAL GEOMETRY

Having considered the major options of existing methods, the new Fractal Geometry (FG) system has been developed which satisfies the requirements for an efficient, powerful and user-friendly geometry package. The FG systems is now included in the MCANO modular code scheme [5] from which future versions of the codes MONK and MCBEND will be created. The FG system can be summarised as follows:

The input stage

- The geometry uses solid bodies for its basic construction units.
- The geometric model is constructed as a set of parts which may be hierarchic to any level. Any zone in the system which is defined as the 'inside' of a single body may contain a part. A part is bounded by a body which corresponds in size and shape to the body in its parent part.
- The bodies in each part are defined using a co-ordinate system local to that part.
- The zones in a part are the insides of single bodies or the differences and intersections of two or more bodies.
- Woodcock tracking geometries can be included in any zone.

Intermediate processing

- The code expands the input geometric data to form a global model in which each body definition is translated and rotated to an absolute location.
- The bodies are converted to a surface system for robust and efficient tracking. Coincident surfaces are identified and discarded during this process.
- The zone definitions are retained in the part structured form.
- A zone relationship map is prepared to allow the code to follow the logic of the input part structure.

Tracking

- The final model is based on zones bounded by surfaces.
- The map of neighbours will be learned as the tracking process continues.
- Woodcock tracking may be used in any zone.

An advantage of Fractal Geometry is its ability to absorb the user image of established systems. A conventional MCBEND model is achieved by having a global part with no daughter parts. Additional bodies corresponding to single surfaces may be introduced to simulate a surface geometry input. The standard structures of the MONK geometry exist as a sub-set of permitted FG structures. By this means acceptable back-compatibility with existing models can be provided while at the same time providing a common way forward across different application areas. This will provide increased flexibility to user groups as well as reduced overheads associated with training, maintenance of expertise and software development.

5. GEOMETRY VISUALISATION

Geometry models for use with MONK and MCBEND have traditionally been verified by the calculation and display of two-dimensional slices through the geometry specification. These slices were generated by utility programs and took the form of low-resolution, text-based pictures enabling hard copy to be produced on a conventional line printer. In order to provide a modern day equivalent to this, the interactive graphics tool VISAGE has been produced.

VISAGE is a high-resolution mouse/menu driven graphics tool for the generation, display and manipulation of two-dimensional slices through the geometry specification. VISAGE has been implemented in C and uses the X-Windows and OSF/Motif tool-kits and hence is as portable as possible. To date VISAGE has been implemented on a range of systems including Sun, DEC (VMS and ULTRIX) and HP, as well as IBM-compatible PC's running SCO UNIX. VISAGE images are produced using the geometry tracking routines of MONK and MCBEND and so are a genuine indication of the geometry seen by the modelling codes themselves.

Following the success of VISAGE work has commenced on an advanced verification graphics tool called VISTA. VISTA will perform the generation, display and manipulation of three-dimensional images by two independent means. Firstly an option will exploit the portability of X-Windows, OSF/Motif and PHIGS, and the power of modern workstations, to give three-dimensional wire-frame based displays of the geometry specification. PHIGS is an international standard for three-dimensional computer graphics which has been implemented on many of the major computers currently in use.

The user image for VISTA will employ the same mouse/menu environment as VISAGE. VISTA will enable materials, source bodies, dose points and splitting boundaries to be displayed and will have a range of viewing and manipulation options. The use of PHIGS means that the images produced from this part of VISTA will not be produced using the geometry tracking routines of MONK and MCBEND. However the power and versatility of PHIGS enables a comprehensive interactive display package to be produced compatible with the power of today's computers.

The second component of the VISTA package will be the generation, display and manipulation of three-dimensional images using particle tracking techniques. Here the images will be produced using the geometry tracking routines of MONK and MCBEND so the images produced are a genuine indication of the geometry seen by the modelling codes themselves. X-Windows and OSF/Motif have again been employed to provide a similar user image to that of VISAGE. The images will be produced using a simulated optical ray tracing algorithm which requires the tracking of rays from a viewing plane into the geometry model until a visible zone boundary is reached.

Although this component of the VISTA package will be slow in execution compared with the wire-frame generation component, it will provide a valuable additional verification function due to its direct link with the geometry tracking routines of the modelling codes. In combination, VISAGE and VISTA provide a comprehensive set of geometry verification tools to accompany the Fractal Geometry package of MONK and MCBEND.

6. CONCLUSIONS

This paper has described the creation of a new geometry modelling scheme for the Monte Carlo particle tracking computer codes MONK and MCBEND. The scheme, called Fractal Geometry, is a pragmatic integration of the earlier schemes of the two codes and maintains the major benefits of each. At the same time judicious rationalisation has improved the overall efficiency of the Fractal Geometry package with respect to both of the earlier schemes. Significant benefits from the new scheme will be gained by the code user community, in the form of greater flexibility and reduced overheads in related application areas. In addition code maintenance and development costs are reduced. To accompany the Fractal Geometry package, the modern geometry visualisation software packages VISAGE and VISTA have been produced to improve the efficiency and accuracy of the geometry model verification process. These packages provide two- and three-dimensional image generation, display and manipulation facilities in a portable mouse/menu environment and in combination with the Fractal Geometry package provide a powerful and user-friendly geometry modelling and verification capability.

7. REFERENCES

[1] N R Smith
A Summary of the Current Status of the MONK6 Code and its Validation for Criticality Applications (International Conference on Nuclear Criticality Safety ICNC'91, Oxford, UK 1991)

[2] S J Chucas, I J Curl & P C Miller,
The Advanced Features of the Monte Carlo Code MCBEND (Seminar on Advanced Monte Carlo Computer Programs for Radiation Transport, Saclay, France 1993)

[3] Judith F Briesmeister (Editor)
MCNP - A General Monte Carlo Code for Neutron and Photon Transport (LA-7396-M,Rev. 2)

[4] M B Emmett
The MORSE Monte Carlo Radiation Transport Code System (ORNL-4972/R2)

[5] N R Smith, R J Brissenden & M H Watmough
The Development of the MONK and MCBEND Codes within the New Monte Carlo Modular Code Scheme MCANO (Seminar on Advanced Monte Carlo Computer Programs for Radiation Transport, Saclay, France 1993)

MONTE CARLO CALCULATION OF A "QUADRATIC AVERAGE" $\int q(x)\, W^2(x)\, dx$

W. K. MATTHES
JRC Euratom, ISPRA

1. General Comments

In the Monte Carlo simulation of neutron coincidence experiments we have to deal with integrals of the type:

$$W = \int q(x)\, W^l(x)\, dx \qquad (l = 1,2)$$

where:

q(x) is the normalized spatial fission distribution and,
W(x) is the mean number of counts due to one fission neutron.

To evaluate an integral of the general type:

$$\mathbf{I} = \int q(x)\, F(x)\, dx$$

by Monte Carlo, we have to observe that:

1. the function value **F(x)** at each spatial point **x** has to be estimated by MC, and;
2. the space-integral itself has to be estimated by MC.

So we proceed in two steps:

1. according to the source distribution **q(x)** we choose NS source points $\boldsymbol{X}_i$(i = 1,2...NS)
2. from each source point $\boldsymbol{X}_i$ we run NH histories to estimate **F(x)** by an unbiased estimator **G** of **F**, where **G** is a function of all $w_\lambda(\boldsymbol{X}_i)$.

$$\varepsilon\,(x_i) = G\,[w_\lambda\,(x_i)]$$

$w_\lambda(x_i)$ is the (random) contribution to $\varepsilon\,(\boldsymbol{X}_i)$ from history λ $\quad(\lambda = 1,2..NH)$.

Eventually we estimate the spatial integral **I** by:

$$\varepsilon = \quad (NS)^{-1} \sum_{i=1}^{NS} \varepsilon(x_i)$$

Taking the expactation value of $\varepsilon(\boldsymbol{X}_i)$ and ε first with respect to λ we obtain:

$$E_\lambda\,[\varepsilon(x_i)] = F(x_i) \qquad \text{by definition}$$

$$E_\lambda\,(\varepsilon) = (NS)^{-1} \sum_{i=1}^{NS} F(x_i)$$

We still have to average over different source point distributions $\{\ \boldsymbol{X}_i\ \}$ (at fixed NS). For this reason we think the source region divided in (very) small space-cells $\Delta\mathbf{x}_\sigma$. such that $\Delta\mathbf{N}_\sigma$ points fall in $\Delta\mathbf{x}_\sigma$. If $p_\sigma = q(x_\sigma)\,\Delta x_\sigma$ is the probability for a source point to fall in $\Delta\mathbf{x}_\sigma$, we have:

$$\langle \Delta N_\sigma \rangle = NS \bullet p_\sigma$$

$$\langle \Delta N_\sigma^2 \rangle = NS \bullet p_\sigma\,(p_\sigma - 1)$$

$$\langle \Delta N_\sigma \Delta N_\rho \rangle = NS\; p_\sigma\; p_\rho$$

multinomial distribution of the source points

Then we can write:

$$E_\lambda(\varepsilon) = (NS)^{-1} \sum_\sigma \Delta_\sigma F(x_\sigma)$$

and further averaging over the $\{\ \mathbf{X}_i\ \}$ distributions gives:

$$E_i\; E_\lambda(\varepsilon) = \sum_\sigma p_\sigma\, F(x_\sigma) \qquad \Rightarrow \int q(x)\, F(x)\, dx$$

ε is therefore an unbiased estimator for the integral **I**.

For variance of ε we find similarly:

$$\sigma^2_\varepsilon = E_i\; E_\lambda(\varepsilon^2) - [E_i\; E_\lambda(\varepsilon)]^2$$

$$= (NS)^{-1} \sum_\sigma p_\sigma \{\sigma^2_{\varepsilon(x\sigma)} + (F(x_\sigma) - I)^2\}$$

A straightforward calculation shows that

$$S^2 = [NS(NS-1)]^{-1} \sum_i (\varepsilon(x_i) - \varepsilon)^2$$

is an unbiased estimator for σ^2_ε in the sense that

$$E_i E_\lambda(S^2) = \sigma^2_\varepsilon$$

and the relative error (σ_ε/I) will be estimated by (S/ε).

It turns out, that σ_ε becomes a minimum for well defined values of NS and NH for a fixed total number NTOT (=NS*NH) of histories. This minimum itselfs of course decreases for increasing NTOT.

2. Application to the coincidence counting rate ("REALS")

To evaluate the "statistical uncertainty" of the "REALS" we have to evaluate integrals of the type I with:

$$F(x) = W^2(x)$$

We play the "two-step" game mentioned above and use as $\varepsilon_\lambda(\boldsymbol{x}_i)$ the mean number of counts produced in the **λ.th** history starting at $\boldsymbol{x}_i$ and evaluate at each $\boldsymbol{x}_i$:

$$\varepsilon(x_i) = [NH(NH-1)]^{-1} \{ [\sum_\lambda W_\lambda (x_i)]^2 - \sum_\lambda W_\lambda^2 (x_i) \}$$

(note that ε **(x)** is an unbiased estimator for $\mathbf{W^2(x)}$)

Eventually we evaluate by summing over all $\boldsymbol{x}_i$

$$\varepsilon = (NS)^{-1} \sum_{i=1}^{NS} \varepsilon(x_i)$$

$$S^2 = [NS(NS-1)]^{-1} \sum_i \{ \varepsilon(x_i) - \varepsilon \}^2$$

and take:

$$W^2 \approx \varepsilon \qquad\qquad \sigma_{W^2} / W^2 \approx S/\varepsilon$$

Session V

PRESENTATION OF USER EXPERIENCE, APPLICATIONS, PERFORMANCE
WITH EMPHASIS ON NEW ASPECTS

CHAIRS:

***J. HALBLEIB**, SANDIA NATIONAL LABORATORIES - USA*
***R. A. FORSTER**, LOS ALAMOS NATIONAL LABORATORY - USA*
***CH. M. DIOP**, CEA - FRANCE*
***J. S. HENDRICKS**, LOS ALAMOS NATIONAL LABORATORY - USA*
***K. W. BURN**, ENEA - ITALY*

VARIOUS APPLICATIONS

CROSS SECTIONS AND DETECTORS

A Comparison between the ITS-3 and EGS-4 Monte Carlo Codes in Radiation Physics

Pedro Andreo

Department of Radiation Physics, Karolinska Institute and University of Stockholm
Box 60211, 104 01 Stockholm, Sweden

ABSTRACT

The Monte Carlo systems EGS and ITS are today standard tools for the simulation of the transport of electron and photon beams in Radiation Physics, mainly in the area of dosimetry at radiotherapeutic energies, and to a lesser extent at lower incident energies. ITS and EGS differ in the way in which electron interactions are grouped (Class I versus Class II), and in their treatment of energy-loss and scattering. Cross-section data is generated by their accompanying programs, PEGS and XGEN, that now include ICRU-37 stopping-powers and updates in the physics of bremsstrahlung interactions. Results obtained with the two systems for a number of configurations will be presented in this comparison. Cases chosen correspond to configurations where either the physics in each code is the main reason to explain differences in the results, or specific algorithms governing electron step-sizes or boundary crossing might play an important role.

INTRODUCTION

The two Monte Carlo codes EGS [1] and ITS [2] have become standard tools for the simulation of the transport of electron and photon beams in Radiation Physics, mainly in the area of dosimetry at radiotherapeutic energies (5-50 MeV), and to a lesser extent at lower incident energies. ITS and EGS differ in the way in which electron interactions are grouped (Class I versus Class II), and in the cross-section data generated by their accompanying data preparation programs, PEGS and XGEN, that now include ICRU-37 stopping-powers. Although updates in the treatment of the physics of bremsstrahlung interactions have been implemented, the two codes still differ in their treatment of electron energy-loss and multiple-scattering. Details on the insides of the two Monte Carlo systems fall outside the scope of this presentation; a general overview has been published elsewhere [3].

Results obtained with the two systems for a number of configurations will be presented in this comparison. Cases chosen correspond to configurations where either the physics in each code is the main argument to explain differences in the results, or specific algorithms governing electron step-sizes or the crossing of boundaries might play an important role. Most calculations have been performed under cylindrical geometry, using the codes CYLTRAN, of the ITS system, and DOSRZ, distributed in the EGS package. Both codes have been run using practically identical parameters, with special emphasis on electron step-sizes for different materials.

RESULTS

Electron energy-deposition distributions

Monte Carlo calculated electron pencil beams are used in different applications of electron beam dosimetry and radiotherapy treatment planning [3, 4]. Calculations of electron pencil beams in the form of 1-D and 3-D dose distributions provide a valuable method for comparing different Monte Carlo codes, as different aspects of electron beam penetration regarding energy-loss and scattering can be obtained from a single distribution.

When a point–monodirectional beam impinges on a homogeneous medium and the distribution of absorbed dose determined, properties of the penetration of electron beams into matter can be observed. Figure 1 shows dose distributions of 50 MeV electron and positron pencil beams incident on water calculated with the Monte Carlo system EGS4 using half-million histories (see reference [3] for the treatment of positron transport in EGS and ITS). Levels shown correspond to a dose range between about 10^{-10} and 10^{-18} Gy per incident electron. The widening of the isodose levels with

increasing depth due to multiple scattering can be clearly observed, as also the rapid decrease of absorbed dose on the central axis, as in such narrow beam the loss of electrons scattered out from the axis is not compensated by in-scattering as it happens in broad beams. Bremsstrahlung photons produced in water are predominant in the forward direction showing that they are produced at the beginning of the electron trajectories, before the initial direction is modified by scattering. For positrons, in-flight annihilation is thought to be responsible for the slightly smoother iso-contours at low dose levels.

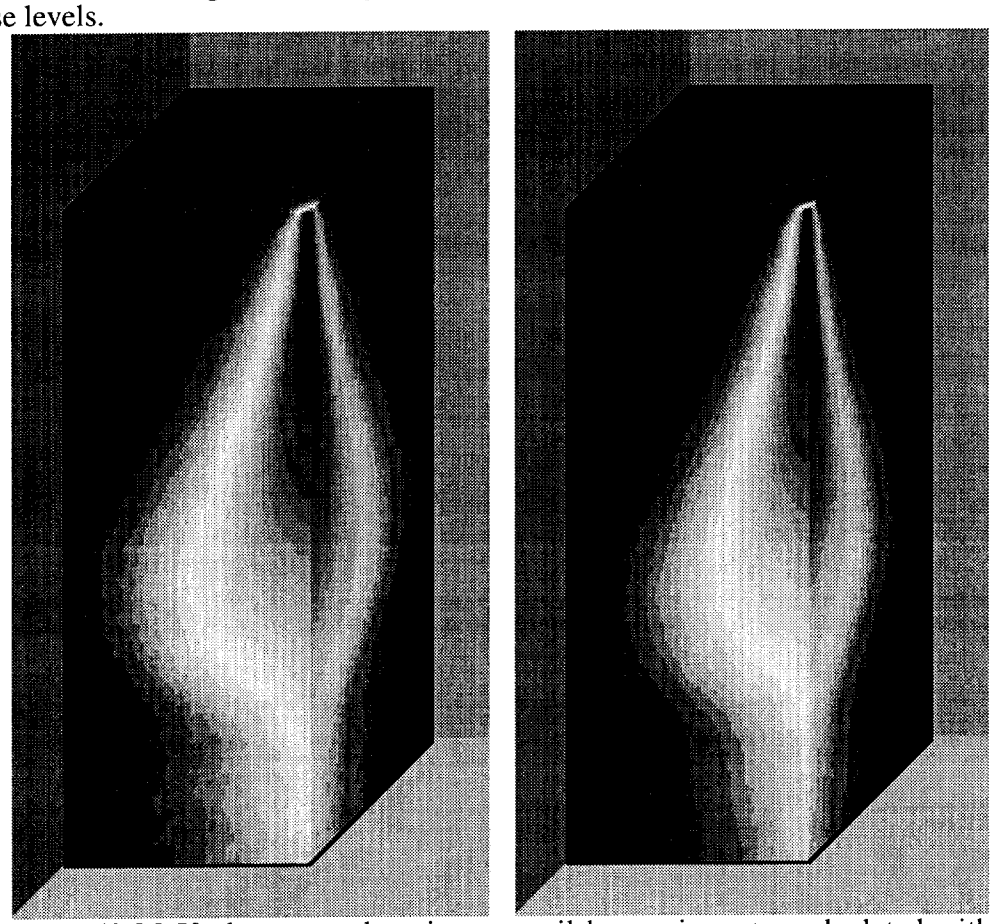

Figure 1. 50 MeV electron and positron pencil beams in water calculated with the EGS4 Monte Carlo system. Levels shown correspond to a dose range between about 10^{-10} and 10^{-18} Gy per incident electron.

Integrating the pencil beam distribution radially up to a given R yields plane-parallel broad-beam dose distributions, which constitute the simplest calculation of energy deposition in a semi-infinite medium. Except for scoring purposes no special algorithms are required for this kind of calculations. Differences in the results will then be mainly caused by the intrinsic physics in the codes to account for energy straggling and multiple scattering.

Electron pencil beams and broad-beam distributions have been computed with

the two Monte Carlo systems in different media and for a wide range of energies. A database between 0.1 and 100 MeV and Z=4-92 has been built using ITS [5]. Figure 2 shows a comparison of broad-beam depth-distributions for Be, Al, Ag and U. Although good agreement is obtained between the two codes at intermediate energies and atomic numbers, there are large differences outside this domain, mainly at low energies. They raise incognites on the different approaches used in the two Monte Carlo systems. In figure 3 a comparison between pencil beam radial profiles in Au is shown at the depths indicated in the inset. Not only multiple scattering is very critical in this example, but also the treatment of bremsstrahlung produced by electrons which have already been scattered through large angles. At this stage it is interesting to point out that electron radiative stopping-powers are today practically the same in both codes (those from ICRU-37), and the sampling of the angular distribution of bremsstrahlung-produced photons is also quite similar, although slightly simplified in the EGS implementation. However, cross-sections for the production of bremsstrahlung are still quite different in the two systems, and their influence cannot be neglected when comparisons are made. Similar comparisons for low Z's show smaller, but non-negligible, discrepancies between the two codes.

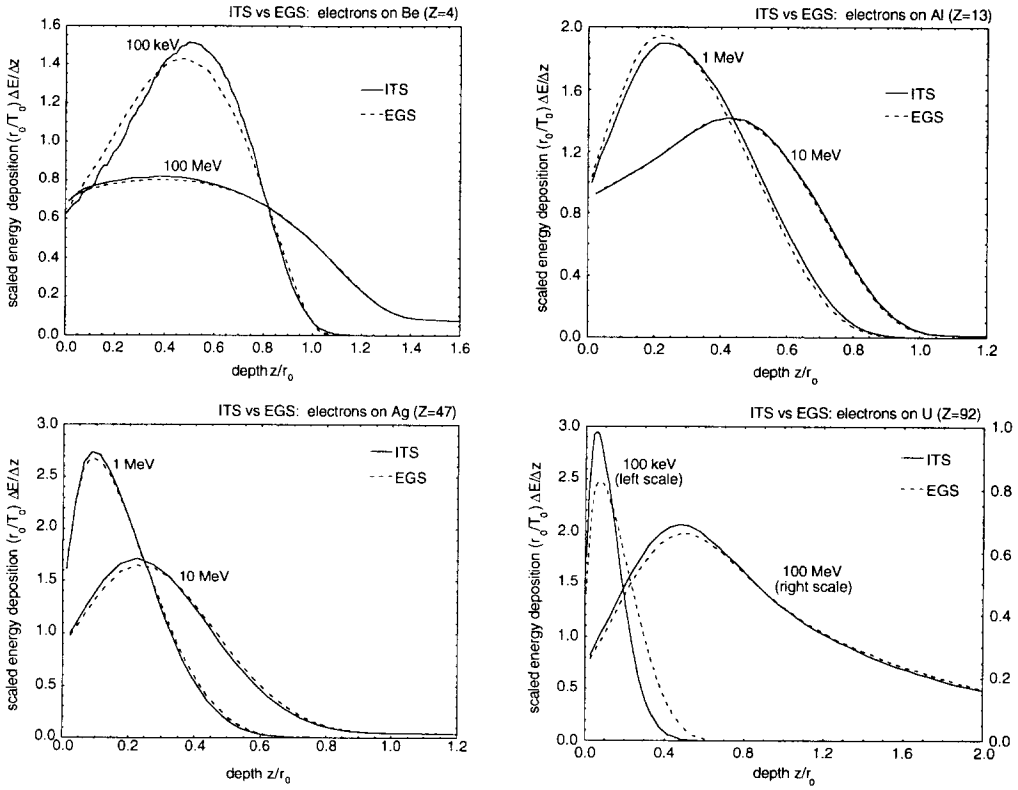

Figure 2. Depth-dose distributions for plane-parallel electron broad beams incident on semi-infinite slabs of different materials. Monte Carlo calculations using ITS3/CYLTRAN (solid lines) and EGS4/DOSRZ (dashed lines). From [5].

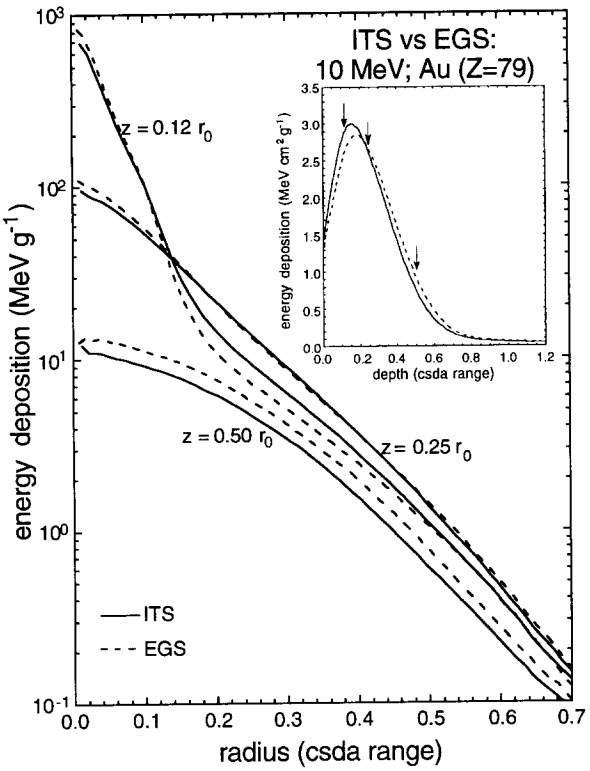

Figure 3. Radial profiles of energy deposition by a pencil beam of 10 MeV electrons in Au (Z=79) at different depths (shown in the inset by arrows). Distances are given in units of the csda range. Solid lines, ITS; dashed EGS. From [5].

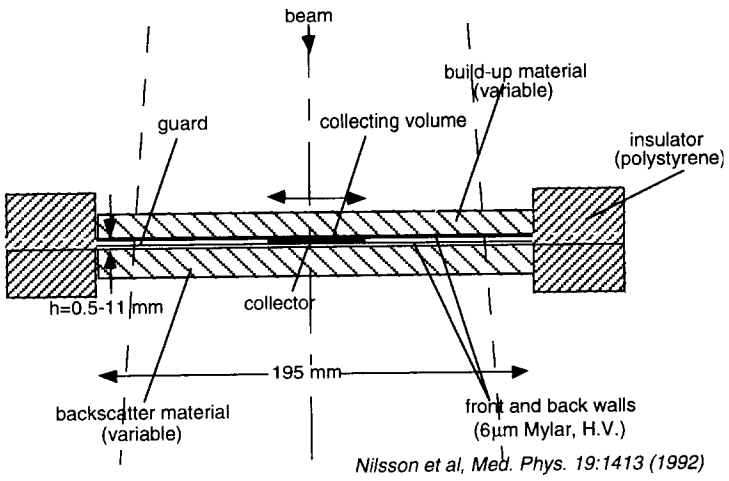

Figure 4. Plane-parallel ionization chamber used for benchmarking Monte Carlo calculations. From [6].

It becomes obvious that at energies and materials of interest in therapy the two Monte Carlo codes yield approximately the same results for broad-beam depth-dose distributions. Outside this range the two codes yield very different results for all kind of distributions (broad- or pencil-beams) in high Z elements. This might be of importance when the two codes are used for instance to simulate accelerator treatment heads, especially targets and filters, and the effect of collimators. Possible reasons to explain the discrepancies are the well-known different multiple-scattering formalisms (Goudsmidt-Saunderson vs Moliere) and rather different cross-sections for electron bremsstrahlung. Influence of electron-positron differences in the codes are not considered to be of importance for these calculations, as EGS still does not take into account specific interactions of positrons for multiple-scattering, bremsstrahlung cross-sections and radiative energy losses.

Backscattering calculations in ^{60}Co γ-ray beams

Backscattering calculations are one of the most demanding exercises of any Monte Carlo code, especially when interfaces of different materials are involved. Electron multiple-scattering processes are treated differently in the two codes and the respective theories are very often pushed down below their limits during simulations. Backscattering calculations will also be affected by the algorithms used for the transport of particles close to boundaries. Gamma ray beams of ^{60}Co including the transport of all generations of photons and electrons down to low energies (1 keV) are an interesting calculation as the effects mentioned play an important role for both photons and electrons.

A special ionization chamber, figure 4, has been built at our department whose simple design provides the ideal configuration for benchmarking Monte Carlo simulations [6]. Most parameters can be varied in the chamber, such as the height of the sensitive cavity and the materials for both front and back walls. The large size of the guard prevents the detection of particles coming from the sides, and therefore the measured signal is practically produced by interactions in the front and back walls. This simple geometry allows a detailed Monte Carlo simulation of different front/back wall configuration without the need for introducing approximations often justified in terms of the complexity of the problem.

Figure 5 shows a comparison of experimental results and those obtained with the two codes. Results have been normalised to a configuration with Al in the two walls, and the data shown correspond to different materials in the back wall. The two Monte Carlo systems yield good agreement with experiments for low- and medium-Z (main interest in dosimetry and radiotherapy), but very large discrepancies can be observed for high-Z materials. All differences are outside the limits of the uncertainty of the calculations. The discrepancy with opposite sign at high-Z seems fortuitous; any systematic error in the experimental procedure would favour the agreement with one of the two codes. It has been customary to normalise these type of results to a configuration having polystyrene in the two walls, due to its similarity with water. Our results with ITS shown in the inset, however, show a large discrepancy both with experiments and with EGS for polystyrene and graphite; no explanation has been found for this behaviour.

Of special interest for this comparison is the amount of energy deposited in each region as given by the two codes. Figure 6 shows that only the energy deposition

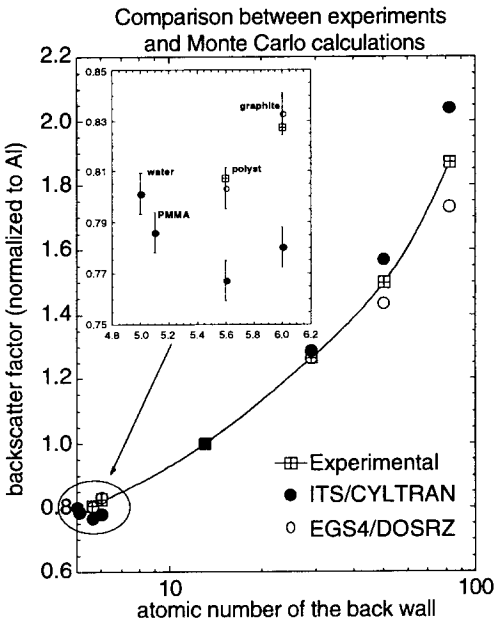

Figure 5. A benchmark of ITS and EGS simulating experiments with ^{60}Co γ-rays that involve interface effects (based the ionization chamber shown in figure 4). Experiments correspond to a fixed Al front wall and varying Z's in the back wall, cavity height 1mm. Adapted from [3].

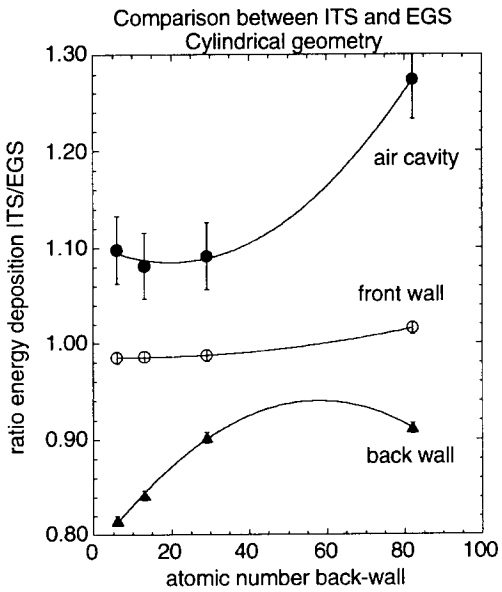

Figure 6. Ratio of Monte Carlo calculated energy deposition in each region for the same configuration as in figure 5.

in the front wall is similar in the two codes, but discrepancies in the back wall and in the air cavity reach up to 20%. Even for low Z materials discrepancies are much larger than the uncertainty of the calculations. All results correspond to a front wall of Al.

It is not obvious to find an explanation for the discrepancy between the two codes, although boundary crossing algorithms might be responsible for a part of it. Recent findings [7] have demonstrated that when EGS forces the validity of the Moliere theory for multiple scattering down to *e* collisions for short path-lengths, the angular distribution used by the code becomes significantly distorted, see figure 7. The relation between this distortion with the above discrepancies remains to be investigated.

Low-energy photons

Most correction and conversion factors used today in ionising dosimetry have been determined using Monte Carlo methods. This gives great importance to the role of the technique at the time of comparing international procedures and standards. The two systems discussed in this work are actually being involved in a comparison among the Monte Carlo codes used at Primary Standard Dosimetry Laboratories of different countries under the auspices of the BIPM[8]. Different configurations for photon beams have been suggested by a working group of the CCEMRI(I), which starting from simple simulations will compare quantities scored under different geometries. No results are formally available yet from this comparison.

Results presented here correspond to calculations performed by this author using EGS and ITS for two of the CCEMRI(I) configurations, see figure 8. The aim is to compare the codes regarding algorithms for photon scattering (geometry A) and fluorescent x-rays effects and cross-sections near absorption edges (geometry B). No electron transport is simulated, as opposed to the comparisons in the preceding section, and therefore all discrepancies are exclusively due to the photon part of the codes. Table 1 shows that the relatively simple photon algorithms yield good agreement in most of the cases, especially at high energies where agreements within 2% or even better are obtained. Differences are slightly larger for low photon energies in geometry A. However it is at 90 keV in configuration B, close to the K-edge of Pb, where results differ by about two orders of magnitude.

It has to be pointed out that the two systems have large differences in the physics of low-energy photons which play an important role in the behaviour of scattered radiation, especially for high atomic numbers. ITS includes cross-sections for bound electrons, effect which is ignored in the EGS basic data. The two codes include Rayleigh scattering and fluorescent effects, but it is clear that an updated database at low-energies is needed in the EGS system.

CONCLUSIONS

The results presented here show that the two most widely distributed Monte Carlo codes for electron and photon transport yield results in good agreement for medium energies and atomic numbers only, and whenever the geometrical configuration does not require a sophisticated algorithm. In these cases the use of one code or another should depend on personal preferences.

However, the discrepancies shown for many other conditions demonstrate the

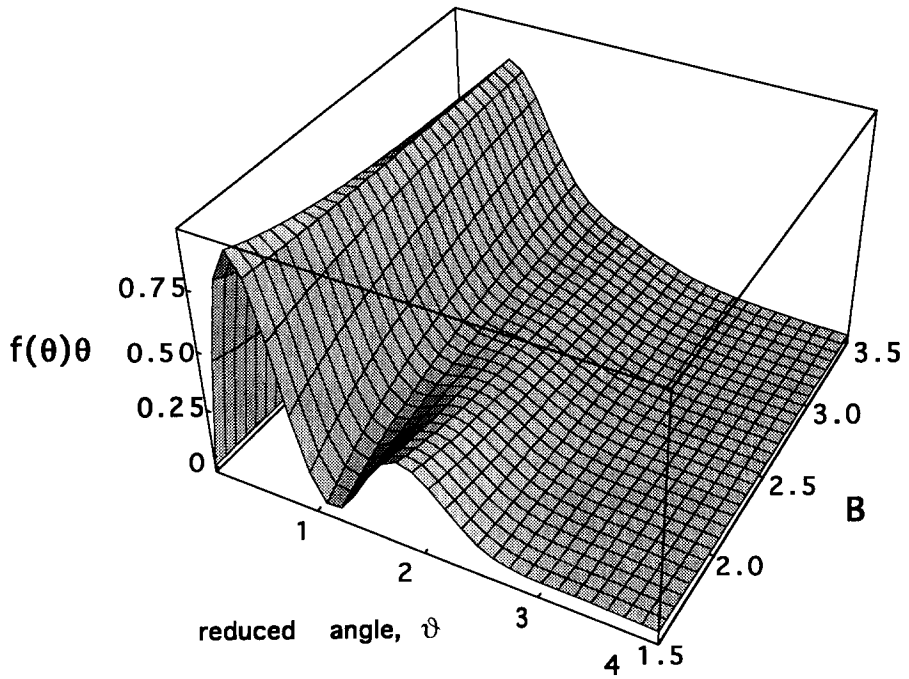

Figure 7. Break down of the universal Molière's expansion series for multiple scattering including 3 terms (as a function of the parameters B and reduced angle ϑ), below about Ω_0= 10 collisions. From [7].

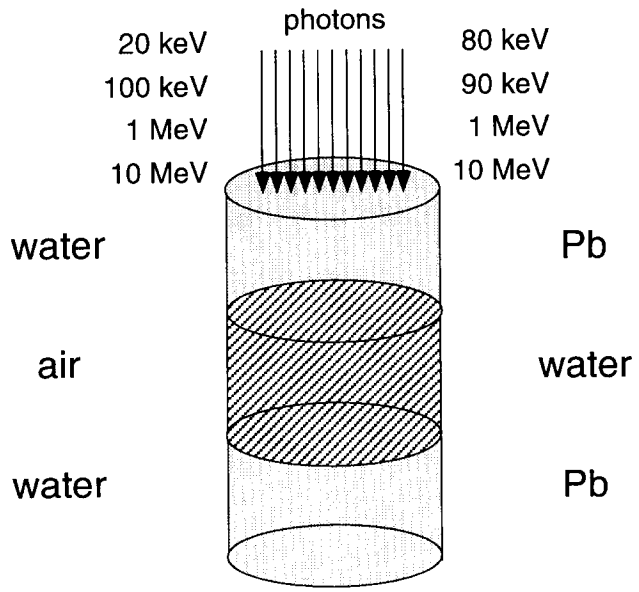

Figure 8. Configurations A (water/air/water) and B (lead/water/lead) proposed by a working group of the CCEMRI(I) to compare Monte Carlo codes used at Primary Standard Dosimetry Laboratories [8]. The diameter and height of each sub-cylinder is 1 g cm-2.

need for being aware of the limitations of the two codes. No code is perfect, and depending on the problem at hand it is important to know if a weak aspect of a particular code might be relevant to the simulation being performed.

REFERENCES

1. Nelson, W.R., Hirayama H., and Rogers D.W.O., *The EGS4 Code System*. Report SLAC-265. 1985, SLAC, Stanford, CA.
2. Halbleib, J. A., Kensek, R. P., Mehlhorn, T. A., Valdez, G. D., Seltzer, S. M., & Berger, M. J., *ITS Version 3.0: The Integrated TIGER Series of coupled Electron/Photon Monte Carlo Transport Codes*. Report SAND91-1634. 1992, Sandia National Laboratories, Albuquerque, NM.
3. Andreo, P., *Monte-Carlo techniques in Medical Radiation Physics*. Phys. Med. Biol., 1991. **36**: 861-920.
4. Andreo, P., *Electron Pencil Beam calculations,* in *Monte Carlo Transport of Electrons and Photons,* T.M. Jenkins, W.R. Nelson, and A. Rindi, Editors. 1988, Plenum Press: New York. p. 437-452.
5. Andreo, P., Ito R., and Tabata T., *Tables of charge- and energy-deposition distributions in elemental materials irradiated by plane-parallel electron beams with energies between 0.1 and 100 MeV*. Report RIAST-UOP-TR 1. 1992, Research Institute for Advanced Science and Technology, University of Osaka Prefecture, Japan.
6. Nilsson, B., Montelius A., and Andreo P., *A study of interface effects in Co-60 beams using a thin-walled parallel plate ionization chamber*. Med. Phys., 1992. **19**: 1413-1421.
7. Andreo, P., Medin J., and Bielajew A., *Constraints of the multiple scattering theory of Molière in Monte Carlo simulations of the transport of charged particles*. Medical Physics, 1993. (submitted).
8. CCEMRI(I) Comite Consultatif pour les Etalons de Mesure des Rayonnements Ionisants (Section I), *Report to the Comite International des Poids et Mesures (N J Hargrave, Rapporteur)*. 1991, BIPM, Pavillon de Breteuil, F-92312 Sevres Cedex, France.

Table 1. Comparison of results with the EGS4 and ITS3 Monte Carlo codes for the geometries A and B (figure 8) proposed by CCEMRI(I) [8]. Photon transport only. Results shown correspond to absorbed dose per incident fluence (10^{13} Gy cm^2) ± SEOM (%)]

PHOTONS		A			B			PHOTONS	
REGIONS ->		**1** (water)	**2** (air)	**3** (water)	**1** (lead)	**2** (water)	**3** (lead)	<- REGIONS	
20 keV	**ITS**	13.39±0.0	8.234±0.2	6.081±0.0	110.7±0.0	0.287±0.2	8.260±0.0	**ITS**	**80 keV**
	EGS	13.05±0.0	7.460±2.0	6.107±0.1	108.8±0.0	0.293±0.5	8.371±0.2	**EGS**	
	ratio	**1.026**	**1.104**	**0.996**	**1.017**	**0.980**	**0.987**	**ratio**	
100 keV	**ITS**	3.996±0.0	3.254±0.2	3.389±0.1	96.92±0.0	0.0046±1.5	0.063±0.4	**ITS**	**90 keV**
	EGS	3.990±0.0	3.165±3.1	3.381±0.0	95.61±0.0	0.0351±1.4	0.741±0.4	**EGS**	
	ratio	**1.002**	**1.028**	**1.002**	**1.014**	**0.131**	**0.085**	**ratio**	
1 MeV	**ITS**	48.96±0.1	42.33±0.5	45.98±0.2	63.46±0.6	45.22±1.0	55.45±0.6	**ITS**	**1 MeV**
	EGS	48.88±0.0	41.55±1.6	45.75±0.0	63.58±0.1	45.01±0.1	55.39±0.0	**EGS**	
	ratio	**1.002**	**1.019**	**1.005**	**0.998**	**1.005**	**1.001**	**ratio**	
10 MeV	**ITS**	258.5±0.1	236.1±0.5	253.8±0.1	660.4±0.1	248.9±0.5	613.4±0.1	**ITS**	**10 MeV**
	EGS	257.5±0.0	234.4±1.7	252.5±0.0	643.8±0.0	244.8±0.1	600.1±0.1	**EGS**	
	ratio	**1.004**	**1.007**	**1.005**	**1.026**	**1.017**	**1.022**	**ratio**	

Options: 10^7 histories. Rayleigh scattering.
PHOTON CUTOFFS: 1 keV for $E_o \leq 100$ keV; 10 keV for $E_o > 100$ keV.
EGS4 v2.0 (NRCC code **DOSRZ** v.17 incl. fluor., no bound x-sctns)
ITS 3.0 (code **CYLTRAN**; P-code for $E_o \leq 100$ keV)

ELECTRON TRANSPORT OFF
$T_{c,electrons} = T_{o,photons}$
PHOTRAN switch

MONTE CARLO ACTIVITIES AT THE DEPARTMENT OF REACTOR PHYSICS, CHALMERS UNIVERSITY OF TECHNOLOGY

Berit Dahl
Department of Reactor Physics
Chalmers University of Technology
S-412 96 Göteborg, Sweden

During the last years a Monte Carlo subroutine package, McSUB, has been developed at our Department. These subroutines treat the transport of neutrons and protons in some organic materials. Further, the Monte Carlo code MORSE has been used for calculations on a) a boron neutron capture therapy method and b) transport of fusion neutrons in vacuum ducts. We are just installing MCNP on our own SUN SPARC server. We will continue our medical studies and studies on vacuum ducts using MCNP. There are also new problems to be solved using MCNP. Hopefully we will be able to include Monte Carlo calculations in our education, e.g. as a support to laboratory exercises. These latter will concern only simple cases.

The Monte Carlo Library McSUB

The problem treated by McSUB is scattering of neutrons and protons in different media, e.g. scintillators and plastic foils. The material can be any mixture of H and C atoms. The density and the H/C relation can be varied. The neutron energy range covered is 0.1 - 20 MeV and both elastic and inelastic scattering of the neutrons is simulated. For inelastic scattering the four first excited states of ^{12}C are taken into account. The γ sent out by the de-excitation of the C-atoms is not considered. When the neutron is scattered against an H atom there will be a proton recoil. The range is calculated and the energy deposited in the media may be considered. In the case of a scintillator the released energy is transformed into light pulses, and hence a light signal can be simulated. The result from the calculations is the light pulses, summed in energy bins, the total time for the neutrons, summed in time bins, and the paths of the neutrons. The subroutine package only simulates the particle transport. The geometry is specified by the user, and the summing of the result also has to be taken care of. Thus, the main routine has to be user written. For further details on the package, see Hök (1990) and Hök (1991). We have found this package to be a very helpful and flexible tool in our development of new detector types. The response function of a detector for monochromatic neutrons can be calculated, thus helping the assessment of the resolution of the detector. Examples of how we have used the package can be found in Hök (1992) and Hök et al. (1992).

Medical calculations using MORSE

Neutron capture cancer therapy is based on the possibility of accumulating ^{10}B compounds in the tumour cells. The large thermal capture cross section for ^{10}B coupled with the damage efficient reaction $^{10}B(n,\alpha)^{7}Li$ gives a large and localised dose. Tissue, with its high water content, acts as a good moderator of neutrons. The requested performance of the neutron source was initially that the main part of the neutrons on the surface of the body should have an energy between 1 and 100 keV and the fluence should be of the order 10^{13} neutrons/cm^2 delivered during approximately 3 hours. Higher energy neutrons, at least from 0.5 MeV and up, cause undesirable damage to the healthy cells, and have to be screened away. The problem is thus to construct a source, so that one achieves a well specified energy spectrum in a certain position inside a human being. This is merely done with a "trial and error" method, and then Monte Carlo calculations are very helpful. This particular project was run by a group at the University of Uppsala led by professor Börje Larsson. We were merely supplying initial calculational support. The experimental tests were performed at PSI, Würenlingen, using a spallation source. The geometry of one of the calculations is shown in Fig. 1. Protons of 72 MeV were stopped in a small copper cylinder. Neutrons from 0.8 to 72 MeV were produced by spallation in the copper cylinder. The characteristics of such a neutron source was measured by Broome et al. (1983), and these values were our input to MORSE. The neutrons were then moderated in a water tank before emerging to the detector. One difficulty was the high energies involved. Very few cross section libraries cover anything above 20 MeV. We used the library DLC-58/HELLO, which covers energies from 10^{-4} eV to 60 MeV. Unfortunately very few isotopes are included, and that limited our choice of moderator and shielding to get rid of neutrons with unwanted energies. Some Monte Carlo calculations were compared with experimental results, see e.g. Condé et al. (1987). Later on the Uppsala group made their own calculations using MCNP. The drawback with that is that they have not found any library for MCNP that covers the energy ranges above 20 MeV. Later investigations showed that the use of a tungsten target instead of copper increases the neutron intensity per proton by almost a factor two, and is thus preferred. A further improvement is to first slow down the spallation neutrons in a bulk of iron and after that use heavy water or graphite as moderator. This significantly decreases the number of unwanted, high energy neutrons.

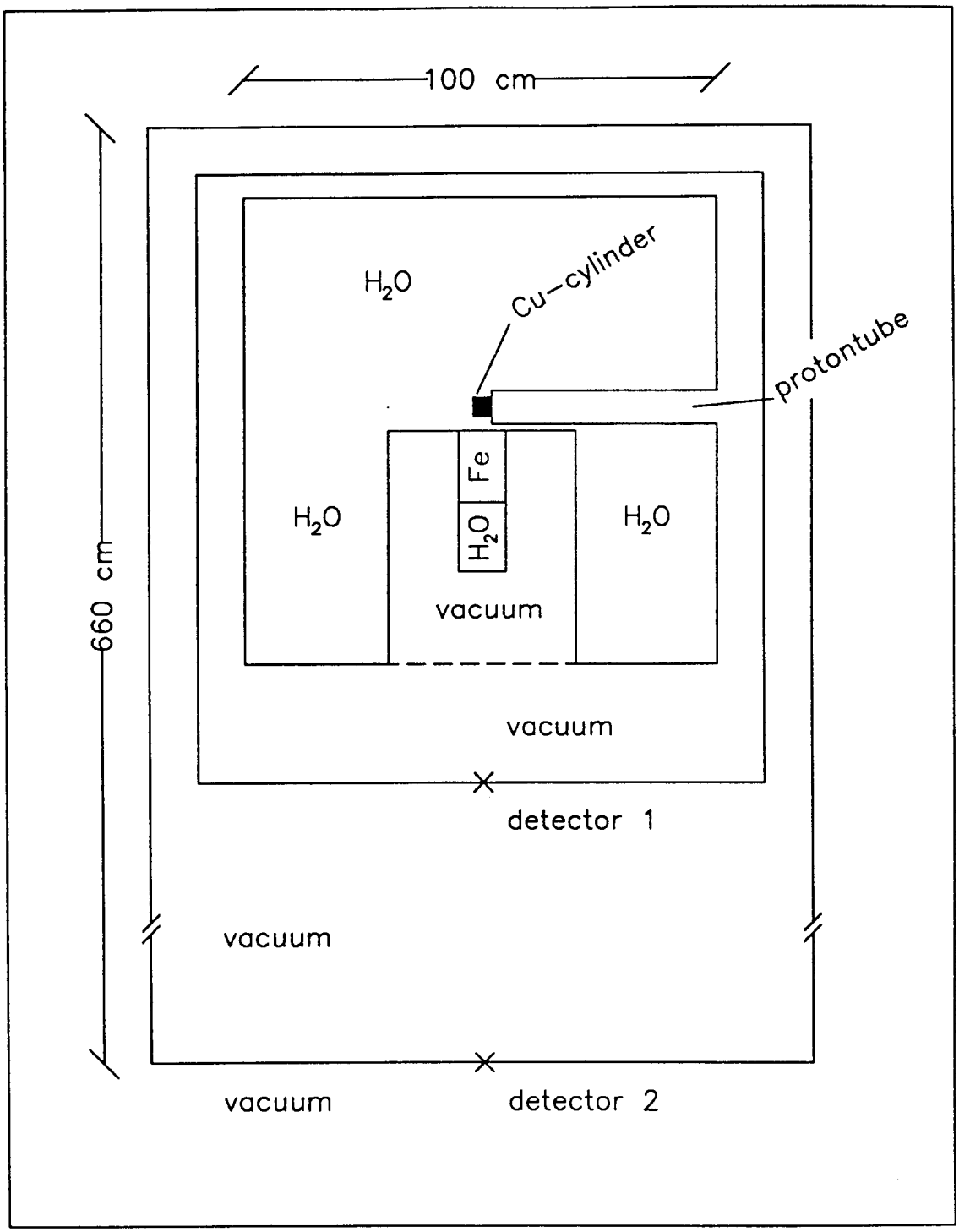

Fig. 1. An example of a geometry for calculations on a boron therapy method.

Calculations on vacuum ducts using MORSE

We are considering the problem how to make corrections for a new detector at the planned fusion energy research facility, ITER. The detector is supposed to measure the neutrons in the plasma just in front of the collimator. However, both direct and scattered neutrons will be detected, and also neutrons from other parts of the plasma. One geometry for the calculations is shown in Fig. 2. We want to decide the response in the detector from sources at different positions in the centre of the plasma. The calculations aim at constructing a shield for neutrons coming from those parts of the torus on which we are not measuring, and to find the optimal shape of collimator. Then the percentage of scattered neutrons and neutrons from other parts of the plasma will become correction values for the detector. We make runs for a ^{252}Cf source, as such a source probably will be used for calibration purposes. Then calculations are also made for a 14 MeV source, which simulates the neutrons from the D-T plasma. So far only preliminary calculations have been performed.

Future plans

We are installing MCNP on our own SUN SPARC server and will probably mainly use this code in the future. Our version of MORSE is for an IBM-360/370 computer, which is costly for us to run. Also, the latter code was made for FORTRAN IV, which is now obsolete on the available IBM computer. At recompilation of the code, FORTRAN-77 gives many warnings and also has real difficulties with some part of the code.

We are planning to proceed with other medical studies, e.g. evaluation of protein contents of a human being. This is important in deciding doses for tumour therapy. The aim is to construct a source, so that we get thermal neutrons in the bone and muscles of the patient. The source used gives 2.35 MeV neutrons on an average. The energy spectrum in the patient with the existing equipment should be decided, and then a better suited collimator should be constructed.

The calculations for the detector at ITER will continue using MCNP.

For measuring the flux in a reactor, one often uses a rabbit system with uranium rabbits. Then it is desirable to know the self shielding in the rabbits and also the shielding effects of the whole test system. For this purpose, Monte Carlo calculations are suitable, and we have some plans to look at this problem.

We are also planning some measurements using neutrons or γ, where damping is used to measure density, e.g. two phase flow. Then it is necessary to use two correlated beams. Monte Carlo calculations can be used to get an idea of the number of backscattered particles.

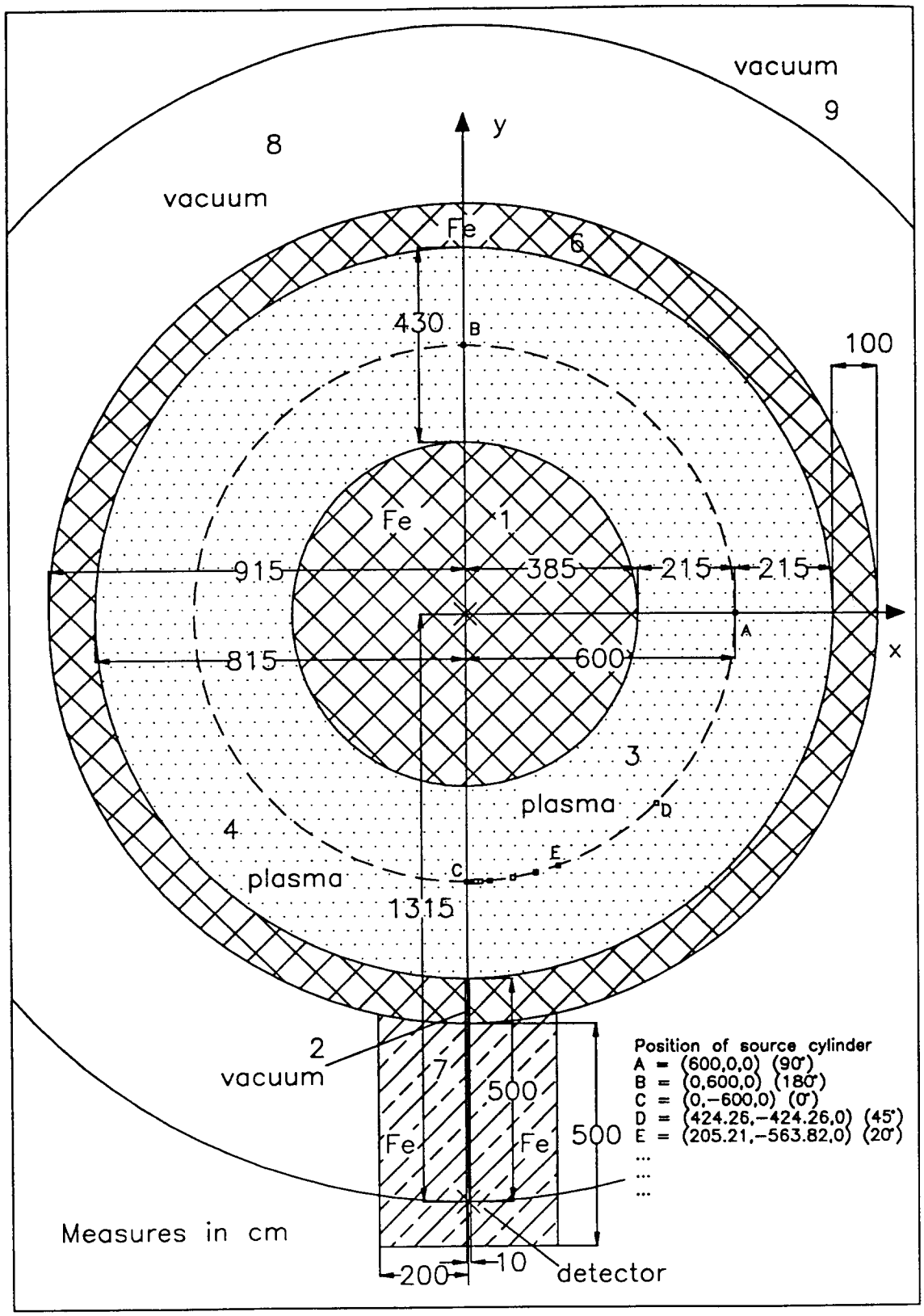

Fig. 2. An example of geometry for the fusion neutron detector, including the whole torus.

References

Broome T.A. (1983) *Health Physics* 44, 487

H. Condé et al. (1987) *Nucl. Instr. Meth.* 261, 587.

Hök M. (1990) McSUB, a Monte Carlo Library for Neutron Transport in Two Different Media for the Neutron Energy Range 0.1 - 20 MeV. CTH-RF-71

Hök M. (1991) McSUB V2.0, an Upgraded Version of the Monte Carlo Library McSUB with Inclusion of Weight Factors. CTH-RF-77

Hök M. (1992) *Nucl. Instr. Meth.* A323, 656

Hök M. et al. (1992) *Nucl. Instr. Meth.* A322, 248

USER EXPERIENCE OF THE MCNP CODE IN NUCLEAR POWER PLANT RADIATION SAFETY ANALYSES AND DESIGN

Tapani EURAJOKI
IVO International Ltd

1. Introduction

IVO International Ltd belongs to the Finnish IVO Group that operates two nuclear power plants of the VVER-440 type (Loviisa 1&2).

At IVO International Ltd the MCNP Monte Carlo code is used mainly in radiation safety analyses and design. In this paper two applications with user experience of the MCNP code as well as a proposition for a weight window generator are shortly presented.

The computers in which the code is run are VAX 9000 mainframe computer and VAXStation 3200 workstation. In the nearest future the code will be transferred into a DECStation 5000/200 workstation.

2. Application 1: Skyshine

One of the main reasons to start Monte Carlo calculations for radiation analyses was the skyshine radiation at the Loviisa NPP if a severe reactor accident occurs. If the core is damaged, noble gases and other fission products as well are released into the containment. Since the shielding thickness of the containment roof is remarkably thin compared with the walls, the radiation transported through the roof and scattered in air may cause high dose rates in the NPP area.

The dose rates in the NPP area have been calculated both outside the buildings and the auxiliary building, turbine hall and others after being attenuated in the roofs.

The main remarks in this application in the point of view of user-friendliness are related to the form of data input to the programme.

- The first remark is the modelling of the geometry, which is probably the part of a Monte Carlo analysis that requires most purely mechanical human work. That work should be reduced as much as possible. One solution to the problem, especially when new projects are considered, may be an interface between a CAD programme package and a Monte Carlo programme. Most new NPP projects are designed by CAD model, and since all the structures including geometry and materials are with a high accuracy contained in a CAD model, they could also be utilised as input data for a Monte Carlo programme.

• The second remark that has arisen in the skyshine analysis as well as in other analyses with sources typical of a NPP is the need of a nuclide library directly read by MCNP. Instead of transforming the nuclide inventory into a spectrum by other means, the possibility to directly input the inventory or even to read it e.g. from some simulator process model, would also save mechanical human work and reduce the possibility of errors.

3. Application 2: Neutron Streaming

As another application of the MCNP code a neutron streaming problem is referred to. The neutron fluxes and dose rates have been calculated outside the reactor pressure vessel where the main contribution is due to neutrons streamed through the vertical annulus around the pressure vessel and also attenuated in radiation shields. The geometry is presented in Figure 1. The neutron flux in the pressure vessel wall was defined as the source for the calculation. The results obtained in the Monte Carlo calculation are in a very good agreement with the measured dose rates.

In addition to the remark on the geometry modelling, this problem showed the need of more freedom to specify three-dimensionally the biasing of directions of the source particle in the input data (card SDEF). The method in which the azimuth angle is sampled uniformly is not a very efficient way for the direction sampling. Another remark is the need of a space-energy-angle weight window system that is also mentioned in the manual of the MCNP code and that probably will be included in future versions of the code.

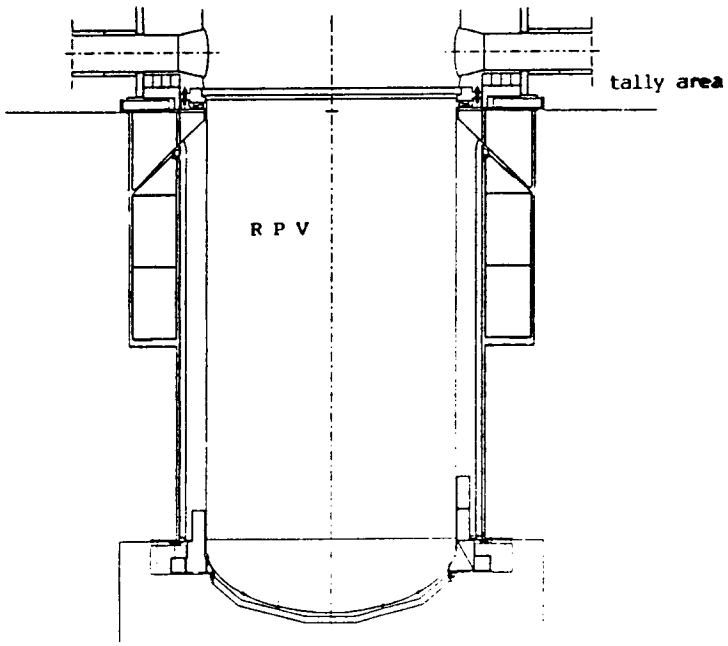

Figure 1. The geometry of the neutron streaming problem

4. Proposition for a Weight Window Generator

The main problem with the type of weight window generator used in the MCNP code is that it is based on the arbitrary particle histories calculated so far. Hence there is a risk that a particle with a low probability but a high contribution has not yet occurred in the calculation and is not taken into account when weight windows are generated. Such weight windows may even reduce the probability of such a particle to occur. The problem can naturally be solved by intelligent user guesses about the most significant tracks or values of other parameters, but, at least in principle, the computer may also be programmed to "guess" in an analytical way. Let us take a most trivial and simplified example. For simple spatial photon problems the most significant track can be defined as the minimum mass through which the photon can reach the detector. If, in addition to that, some angular dependence, maybe albedo effects, is also taken into account, we get a first approximation for the set of most significant tracks expressed as a function to be minimized. In more complex problems the idea remains but the amount of parameters to be included in the minimization problem increases.

It is clear that such a way must be a very complex one and hence it may waste a lot of computer time. However, in principle such a solution may remarkably improve the normal weight window generation and make the Monte Carlo method better usable also for non-specialists.

PETSI, A PACKAGE BASED ON MONTE CARLO TECHNIQUES TO SIMULATE THE POSITRON EMISSION TOMOGRAPHY

N.CERULLO, M.BOGLIARDI
DINE,UNIVERSITY OF GENOA,Via all'Opera Pia 15/A,I-16145,GENOA,ITALY

R.GUZZARDI
CNR,INSTITUTE OF CLINICAL PHYSIOLOGY,Section of LECCE,Via Arnesano ex-collegio Fiorini,I-73100,LECCE,ITALY

P.RISCOSSA
ANSALDO S.p.A.,Divisione Nucleare,Corso Perrone 25,I-16161 GENOA,ITALY

ABSTRACT

The performances of a Monte Carlo Code, (PETSI) able to simulate the emission of the positrons, their annihilation with the electrons,the transport of the produced pair of photons and their interaction with the BGO crystals detectors are briefly described. The ability of Monte Carlo simulation to separate scattered from true events is also evidenced.

1. INTRODUCTION

Positron Emission Tomography is a quantitative imaging technique based on detection of radiative decay events from radiotracers distributed in a human body. His use is very suitable mainly for both heart and brain functional controls

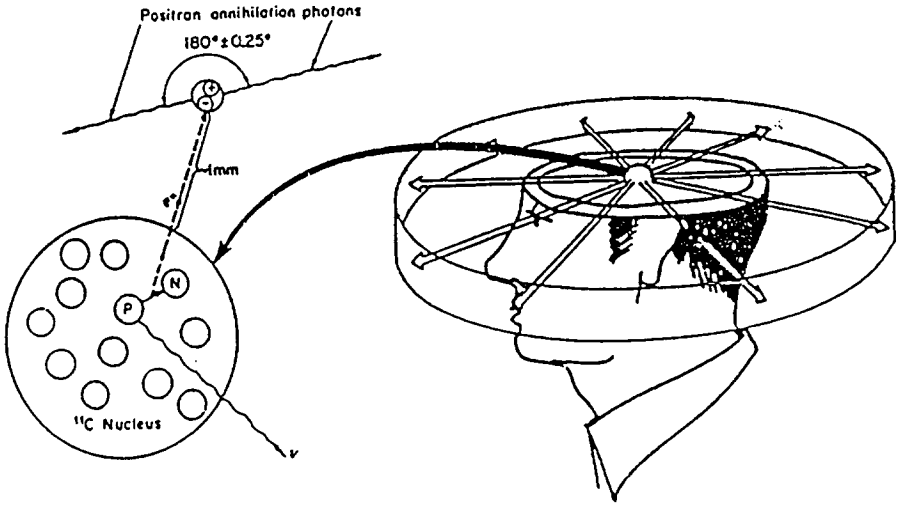

Fig.1- PET localization of radionuclides achieved by coincidence detection of the arrival of the annihilation photons from the positron electron interaction.

The accuracy of a PET scanner, i.e. efficiency, spatial resolution and so on, are not independent functions as they are connected with several parameters of the scanner.

The study of the relationships between the imaging properties of a positron tomograph and the set-up variables is not simple: analytical and semi-empirical treatments, quoted in literature (1) (2), are based on hypotheses and approximations so that , in some cases, the obtained results are rather unreliable (3). On the other hand evaluations based on experimental measurements are often of limited value depending on the experimental set-up characteristics.

It is possible to avoid these limitations applying some correction by a computer simulation of the tomograph behaviour using a Monte Carlo approach. It shows several advantages as the possibility to evaluate new design solutions or predicting and analyze the experimental tests. Therefore, the need to analyze the imaging properties of a Whole Body Tomograph, with specific reference to the properties of the Compton Noise, had lead to implement a Monte Carlo code able to simulate this kind of scanner.

2. PET SIMULATION

The package, named PETSI (PET SImulation), is a Monte Carlo code able to simulate the emission and the annihilation of the positrons, the transport of the pairs of photons, produced in the annihilation, and their detection by the tomograph.

Unlike the previous packages and published results (3) (4) (5), that reproduce only neurological single-slice tomographs or report data concerning single detector performance, PETSI was created with the aim of simulating a Whole Body multiring scanner (6) (7) (8).

The code simulates the transport of radiation :

a) within the source;
b) in one or more scattering media surrounding the source;
c) in the collimators;
d) in a removable septum with a trapezoidal section placed between the detector ring;
e) within the detectors;
f) in the separating septa placed between adjacent detectors in the ring itself.

The simulation code takes into account both the range of the positrons and the misalignment of the two photons produced during the annihilation. Only Compton scattering and photoelectric effects are considered as possible interactions according to the energy of the photons and the characteristics of the simulated materials.

Among the informations supplied by the simulation there are: the energetic spectrum of the detected photons, the sinogram and the axial response function (see Fig. 2).

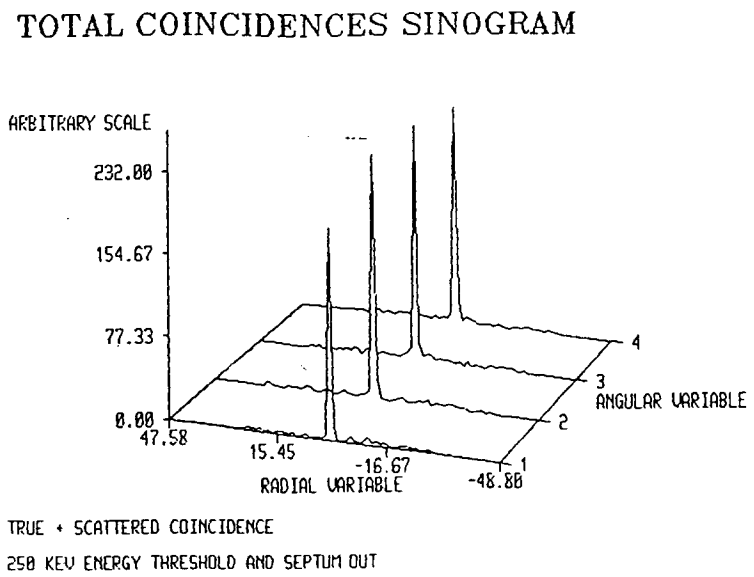

Fig. 2 - 250 KeV energy treshold : a total coincidences sinogram.

PETSI supplies separately these plots for:

a) all single detected photons;
b) the true coincidences;
c) the scattered pairs, in which at least one photon underwent one or more interactions before reaching the detectors (see Fig. 3).

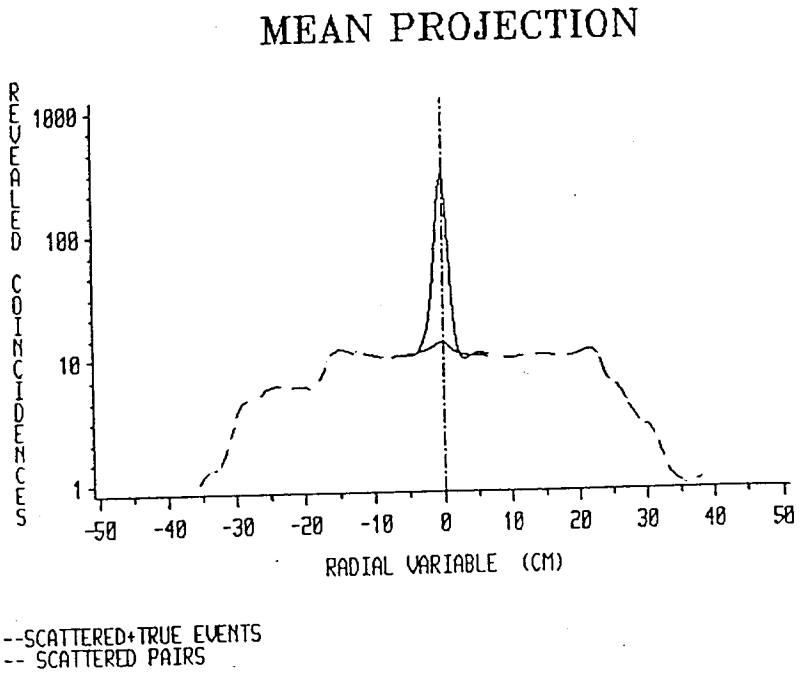

Fig. 3 - 250 KeV energy treshold. Separation between total and scattered pairs.

Furthermore, all data are supplied for the two direct slices and the cross slice. On the basis of data provided by the code is possible, using suitable reconstruction algorithms, to obtain a graphical representation of the distribution of the radiotracer in the investigated anatomical regions.

In comparison with the experimental tests, where the scatter fraction is estimated from the total response (3), the simulation code allows a more precise and analytical prediction of this parameter. As additional output, the axial distribution of both true and scatter coincidences is provided. It is important to notice that the knowledge of the scatter fraction distribution permits to optimize the development of correction procedures to subtract the Compton noise.

PETSI provides the possibility of selecting the configuration of the system. In fact, it is possible to choose among different geometries (pointwise source with sferical media,sferical source with sferical media, cylindrical source with cylindrical media and two rings of detectors), to remove or to change the size of the interplane septum in order to study the sensitivity of the cross section, or to move side collimation changing the detector apertures allowing to reproduce the set-up conditions applied in the clinicals protocols.

3. CONCLUSIONS

The description of the PETSI performance and the preliminary simulation results, the comparison between calculated and experimental data allow to evaluate the code efficiency. Furthermore, the large number of available possibilities permits further analysis: for example, using the computer simulation it is possible to exactly evaluate the effect on the image quality of the scattered coincidences and so on.

The results of the experimental comparison demonstrate the validity of the code and the opportunity of using the obtained information to predict and analyze the experimental data.

The potentiality of PETSI allows also the possibility to simulate more complex geometries, in order to reproduce organs like heart, lungs and brain, and to use positron annihilation, photoelectric effect and Compton scattering cross section of the code MCNP4.

Last but not least, PETSI enables the designer to simulate, at low cost and in short time, the scanner performance allowing to evaluate the various technological solutions during the optimization process of PET Scanner design.

4. ACKNOWLEDGEMENTS

This work was done using the research funding of CNR (National Research Council).

5. REFERENCES

(1) S.E.DERENZO et al.
"Analytical study of a high-resolution positron ring detector system for transaxial reconstruction tomography." J. Nucl. Med. , vol. 16, pp. 1166-1173, (1975)

(2) E.TANAKA
"Analytical study of the performance of a multilayer Positron Computed Tomography Scanner." J. Comput. Assist. Tomogr., vol. 6, pp. 350-364, (1982)

(3) L.R.LUPTON, N.A.KELLER
"Performance Study of Single-Slice Positron Emission Tomography Scanners by Monte Carlo Techniques." IEEE Trans. Medical Imaging, vol. 2, pp. 154-168, (1983)

(4) U.BOTTIGLI et al.
"Monte Carlo Simulation and Experimental Tests on BGO, CsF and NaI (Tl) Cristals for Positron Emission Tomography." J. Nucl. Med. and Allied Sciences, vol. 29, pp. 221-227, (1985)

(5) S.E. DERENZO et al.
"Monte Carlo calculation of the detection efficiency of arrays of NaI, BGO, CsF, Ge and Plastic Detectors for 511 KeV photons." IEEE Trans. Nucl. Sci., vol. 28, pp. 131-136, (1981)

(6) D. ACCHIAPPATI, N. CERULLO and R.GUZZARDI
"Assessment of the scatter fraction evaluation methodology using Monte Carlo simulation techniques." Eur. J. Nucl. Med. (1989) 15; 683-686

(7) D. ACCHIAPPATI, N. CERULLO and R. GUZZARDI
"Analysis of the performance of a PET scanner through Monte Carlo simulation and experimental comparison." Presented at the European Nuclear Medicine Congress, Milano, ITALY, August 29 - September 2,1988

(8) D. ACCHIAPPATI, N. CERULLO and R. GUZZARDI
"Development of a Monte Carlo simulation package for PET and validation through comparison with the experimental performance of a whole body tomograph." Presented at the IEEE 1988 Nuclear Science Symposium, Orlando, FLORIDA, November 9-11.

COMMENTS ON POLARIZATION EFFECTS IN PHOTON TRANSPORT*

J.E. Fernández** and M. Sumini
Laboratorio di Ingegneria Nucleare di Montecuccolino
Università di Bologna
via dei Colli 16 - Bologna - Italy

Up to now, the polarization effects of the radiation field are not included in the most important codes of Monte Carlo photon transport, except for one recent attempt of adapting EGS4 to include linear polarization [Namito *et al.*, 1993] and some dedicated codes which also deal with linear polarization [Felsteiner *et al.*, 1974; Felsteiner and Pattison, 1975; Tanner and Epstein, 1976; Chomilier *et al.*, 1985; Pitkanen *et al.*, 1986; Janssens *et al.*, 1993; Vincze *et al.*, 1993]. This omission precludes the use of MC simulation with synchrotron light sources having an important polarized component, which, in general, must be considered as non-linear. In fact, although the X-ray photons emitted by the synchrotron light in the plane of the orbit of the electrons are linearly polarized, out of this plane the beam always presents an elliptically polarized component. For this case, recent research on analytical photon transport models [Fernández and Molinari 1993; Fernández *et al.* 1993] has proven useful in establishing a sound physical and mathematical basis that suggests some new ideas for MC simulation. Indeed, the non-linear components of polarization cannot be described with the usual scalar approach. It is necessary to recur to a vector model that, in addition, renders complementary information about the other physical magnitudes involved in the description of the polarization state of the photons. In this paper we discuss the formal aspects of the vector approach and its applicability to a MC random walk.

REPRESENTATION OF POLARIZED RADIATION WITH THE STOKES PARAMETERS.

The polarization of X-rays, a net wave effect, needs four parameters to be represented. The *intensity of the beam* clearly constitutes one parameter. It is the only parameter taken into account in scalar representations of radiation transport, the "usual" modeling in Monte Carlo simulations [Cashwell and Everett, 1959; Carter and Cashwell, 1975]. In addition, at each space point and for a given wavelength and direction of propagation, the most general mixture of γ-rays can be regarded as a mixture of an elliptically polarized fraction and an independent fraction of unpolarized γ-rays. The proportion of each of these two components (*the degree of polarization*) constitutes the second parameter. The remaining two parameters are necessary to describe the ellipse associated with the elliptically polarized component. One of these parameters specifies the orientation of the ellipse, i.e., the angle between the major (or minor) axis of the ellipse and a fixed coordinate axis in the space. This is generally referred to as *the orientation of the ellipse of polarization*. The final parameter is *the ellipticity of the ellipse*, i.e., the ratio of the two axes of the ellipse. Because of the diverse nature of these four quantities, it is convenient to use the equivalent set of quantities, introduced by Sir George Stokes (1852), which contains all the physical information about the polarization state of the γ-ray beam. In this way, the photon transport can be described using a four-component parameterization obeying a vector transport equation [e.g., Chandrasekhar, 1950; Spencer and Wolff, 1953; Fano *et al.*, 1959, Pomraning, 1973; Fernández *et al.*, 1993].

* Work performed with partial finantial support from MURST (Italian National Ministry for the University and Scientific and Technological Research).

** On leave of absence from University of Córdoba, Argentina. Member of CONICET. Buenos Aires, Argentina.

In summary, a polarized beam of γ-rays needs four parameters I_I, I_Q, I_U and I_V - the Stokes parameters, having the dimension of an intensity - to specify the intensity, the degree of polarization, the orientation and the ellipticity of the ellipse of polarization, at each point of the space and in any given direction.

Following Pomraning (1973) we can express the Stokes intensities in terms of the angles χ (rotation of the major axis of the polarization ellipse about a direction parallel to the scattering plane) and β (related to the major-to-minor axes ratio or ellipticity). The meanings of these parameters become apparent from the relationships:

$$I_Q = I_I \cos 2\beta \cos 2\chi \tag{1a}$$

$$I_U = I_I \cos 2\beta \sin 2\chi \tag{1b}$$

$$I_V = I_I \sin 2\beta \tag{1c}$$

The Stokes components for an *unpolarized beam* are simply $[I_I,0,0,0]$. For *elliptically polarized* γ-rays we note that

$$\sin 2\beta = \frac{I_V}{I_I}, \tag{2a}$$

$$\tan 2\chi = \frac{I_U}{I_Q}, \tag{2b}$$

and the Stokes parameters verify the relation

$$I_I^2 = I_Q^2 + I_U^2 + I_V^2. \tag{2c}$$

Consequently, only three of these four parameters are independent.

For *partially polarized* γ-rays (i.e. a mixture of unpolarized and elliptically polarized γ-rays), the four parameters are necessary and the following relation holds

$$I_I^2 \geq I_Q^2 + I_U^2 + I_V^2. \tag{3}$$

Clearly the total intensity I_I and the additional parameters I_Q, I_U and I_V , completely determine, from an experimental point of view, the characteristics of an arbitrary beam. That is, two beams with the same Stokes parameters, are optically equivalent since experimentally they cannot be distinguished.

A *general beam* of X-rays - having components $[I_I, I_Q, I_U, I_V]$ - can be decomposed into two independent beams, one of which is unpolarized and the other elliptically polarized, with their states of polarization defined by

$$[I_I^2 - (I_Q^2 + I_U^2 + I_V^2)^{1/2}, 0, 0, 0], \tag{4a}$$

$$[(I_Q^2 + I_U^2 + I_V^2)^{1/2}, I_Q^2, I_U^2, I_V^2], \tag{4b}$$

where β and χ are given by the relationships

$$\sin 2\beta = \frac{I_V}{(I_Q^2 + I_U^2 + I_V^2)^{1/2}}, \tag{4c}$$

$$\tan 2\chi = \frac{I_U}{I_Q}. \tag{4d}$$

It is customary define the *degree of polarization* P as the fraction of polarized (scattered) radiation after the collision, which in terms of the Stokes intensities is given by

$$P = \frac{(I_Q^2 + I_U^2 + I_V^2)^{1/2}}{I_I}. \tag{4e}$$

It can be easily shown that the *general beam* can be written as

$$\begin{pmatrix} I_I \\ I_Q \\ I_U \\ I_V \end{pmatrix} = I_I \left\{ (1-P) \begin{pmatrix} 1 \\ 0 \\ 0 \\ 0 \end{pmatrix} + P \begin{pmatrix} 1 \\ \cos 2\beta \cos 2\chi \\ \cos 2\beta \sin 2\chi \\ \sin 2\beta \end{pmatrix} \right\}. \tag{4f}$$

THE VECTOR TRANSPORT EQUATION FOR POLARIZED PHOTONS.

The flow of γ-rays is completely determined as the solution of a transport equation describing the balance between the number of photons of given energy and direction entering and leaving an infinitesimal volume element. This balance may be formulated for conditions where the γ-ray source is constant in time (steady-state problem) and, therefore, also the photon flow in the medium.

We define the vector flux $\vec{f}(\vec{r},\vec{\omega},\lambda)\,d\lambda\,d\vec{\omega}$ [components $f_I(\vec{r},\vec{\omega},\lambda)$, $f_Q(\vec{r},\vec{\omega},\lambda)$, $f_U(\vec{r},\vec{\omega},\lambda)$, and $f_V(\vec{r},\vec{\omega},\lambda)$] as the number of photons with wavelengths between λ and λ+dλ, and with directions between $\vec{\omega}$ and $\vec{\omega}+d\vec{\omega}$, which cross a unit area per unit time. The use of the wavelength λ in place of the energy E is entirely equivalent, E = hc/λ. The Boltzmann transport equation for photons obeying photon-atom interactions giving only new photons (more details can be found in Fernández *et al.*, 1993) is

$$\vec{\omega}\cdot\vec{\nabla f}(\vec{r},\vec{\omega},\lambda) = -\mu(\vec{r},\lambda)\vec{f}(\vec{r},\vec{\omega},\lambda) + \int_0^\infty d\lambda' \int_{4\pi} d\vec{\omega}'\, H(\vec{r},\vec{\omega},\lambda,\vec{\omega}',\lambda')\,\vec{f}(\vec{r},\vec{\omega}',\lambda') + \vec{S}(\vec{r},\vec{\omega},\lambda) \tag{5a}$$

where

$$H(\vec{r},\vec{\omega},\lambda,\vec{\omega}',\lambda') = L(\pi-\Psi)\,K(\vec{r},\vec{\omega},\lambda,\vec{\omega}',\lambda')\,L(-\Psi') \tag{5b}$$

is the kernel matrix in the meridian plane of reference; $K(\vec{r},\vec{\omega},\lambda,\vec{\omega}',\lambda')$ the scattering matrix in the scattering plane of reference; and L the four-by-four rotation matrix which transforms the description of the scattered flux from the scattering plane to the meridian plane of the reference; $\mu(\vec{r},\lambda)$ is the narrow-beam attenuation coefficient independent of the state of polarization of the photon (assuming the matter is isotropic) and $\vec{S}(\vec{r},\vec{\omega},\lambda)$ is the source vector flux with components $[S_I,S_Q,S_U,S_V]$. The rotation angles Ψ and Ψ′ in Eqn (5b), are defined by the relationships

$$\cos\Psi = \frac{\eta'\sqrt{1-\eta^2} - \eta\sqrt{1-\eta'^2}\cos(\varphi-\varphi')}{[1-(\vec{\omega}\cdot\vec{\omega}')^2]^{1/2}} \tag{5c}$$

and

$$\cos\Psi' = \frac{\eta\sqrt{1-\eta'^2} - \eta'\sqrt{1-\eta^2}\cos(\varphi-\varphi')}{[1-(\vec{\omega}\cdot\vec{\omega}')^2]^{1/2}} \tag{5d}$$

where η and η′ are the cosines of the polar angles in spherical geometry, and φ and φ′ the azimuthal angles. Primed angles denote incidence.

For a rotation of the axes through an angle Φ in the clockwise direction, the matrix L is defined as

$$L(\Phi) = \begin{pmatrix} 1 & 0 & 0 & 0 \\ 0 & \cos 2\Phi & \sin 2\Phi & 0 \\ 0 & -\sin 2\Phi & \cos 2\Phi & 0 \\ 0 & 0 & 0 & 1 \end{pmatrix} \tag{6}$$

Equation (5a) represents a system of four integro-differential equations

$$\vec{\omega}\cdot\nabla f_i(\vec{r},\vec{\omega},\lambda)= -\mu(\vec{r},\lambda)f_i(\vec{r},\vec{\omega},\lambda)+\int_0^{\infty}d\lambda'\int_{4\pi}d\vec{\omega}'\sum_j H_{ij}(\vec{r},\vec{\omega},\lambda,\vec{\omega}',\lambda')\,f_j(\vec{r},\vec{\omega}',\lambda')+S_i(\vec{r},\vec{\omega},\lambda),\quad (i,j=I,Q,U,V); \tag{7}$$

where H_{ij} denotes the corresponding matrix element of H. It is worth noting that the interaction term introduces coupling between the components of the angular flux as long as H is non diagonal.

APPLICATION TO MONTE CARLO SIMULATION.

The solution of the proposed model can be carried out in some simple but significant geometries, like plane geometry (Fernández and Molinari, 1993), through an orders-of-interaction solution, i.e. using the development

$$f_i(\vec{r},\vec{\omega},\lambda)=\sum_{k=0}^{\infty}f_i^{(k)}(\vec{r},\vec{\omega},\lambda). \tag{8}$$

The coupling of all the components of the *n*th-score in every component of the *(n+1)*th-score is apparent in that solution. It suggests that the random walk must be performed with a vector score which is modified in the *n*th-collision point according to the following equation

$$\frac{1}{\mu(\vec{r},\lambda^{(n)})}H(\vec{r},\vec{\omega}^{(n+1)},\lambda^{(n+1)},\vec{\omega}^{(n)},\lambda^{(n)})\left\{\left(1-P^{(n)}\right)\begin{pmatrix}1\\0\\0\\0\end{pmatrix}+P^{(n)}\begin{pmatrix}1\\\cos 2\beta^{(n)}\cos 2\chi^{(n)}\\\cos 2\beta^{(n)}\sin 2\chi^{(n)}\\\sin 2\beta^{(n)}\end{pmatrix}\right\}$$
$$=w^{(n+1)}\left\{\left(1-P^{(n+1)}\right)\begin{pmatrix}1\\0\\0\\0\end{pmatrix}+P^{(n+1)}\begin{pmatrix}1\\\cos 2\beta^{(n+1)}\cos 2\chi^{(n+1)}\\\cos 2\beta^{(n+1)}\sin 2\chi^{(n+1)}\\\sin 2\beta^{(n+1)}\end{pmatrix}\right\}. \tag{9}$$

The left hand side of Eqn (9) gives the probability function for a photon with an arbitrary state of polarization which undergoes an interaction defined by the matrix K (successively transformed as in Eqn (5b) to obtain the matrix H). The right hand side shows that this operation is equivalent to change the state of polarization of the photon and apply a global survival probability $w^{(n+1)}$ to the photon intensity. In Eqn (9), $P^{(n)}$ and $P^{(n+1)}$ are the polarization degrees before and after the interaction, and $\beta^{(n)}$, $\chi^{(n)}$, $\beta^{(n+1)}$ and $\chi^{(n+1)}$ are the angles that enter into the definition of the Stokes parameters. Thus, a photon undergoing a collision characterized by the matrix H will change not only its phase variables $\vec{\omega}$ and λ but also its polarization state characterized by $\beta^{(n)}$, $\chi^{(n)}$ and $P^{(n)}$ (assuming an unitary intensity). The survival probability $w^{(n+1)}$ after the interaction, and the new polarization state characterized by the parameters $\beta^{(n+1)}$, $\chi^{(n+1)}$ and $P^{(n+1)}$ can be completely calculated from the four nonlinear equations in Eqn (9). However, such nonlinearity is innecessary during the random walk. It is enough to represent the elliptically polarized vectors as Stokes components in both sides of Eqn (9) in order to obtain a set of linear equations:

$$\frac{1}{\mu(\vec{r},\lambda^{(n)})}\mathbf{H}(\vec{r},\vec{\omega}^{(n+1)},\lambda^{(n+1)},\vec{\omega}^{(n)},\lambda^{(n)})\begin{pmatrix}1\\ I_Q^{(n)}\\ I_U^{(n)}\\ I_V^{(n)}\end{pmatrix}=\begin{pmatrix}I_I^{(n+1)}\\ I_Q^{(n+1)}\\ I_U^{(n+1)}\\ I_V^{(n+1)}\end{pmatrix}. \tag{10}$$

where $I_I^{(n+1)}$ clearly represents the survival probability $w^{(n+1)}$.

The vector score represented by equations (9) and (10) carries information on the full polarization state of the photon, and reports adequately the changes due to polarization dependent interactions. It is worth mentioning that all of the photon-atom interactions in the X- and γ-ray regimes are, in major or minor degree, polarization dependent. This is specially true for interactions involving emission of electrons, and for interactions sensitive to the presence of magnetic fields.

REFERENCES

Carter L.L. and Cashwell E.D. (1975) *Particle transport simulation with the Monte Carlo method.* ERDA Critical Review Series, TID-26607.

Cashwell E.D. and Everett C.J. (1959) *A Practical Manual on the Monte Carlo Method.* Pergamon Press. London.

Chandrasekhar S. (1950) *Radiative Transfer.* Clarendon Press. Oxford [(1960) Reprinted with corrections by Dover, New York]. Ch.1 (The Equations of Transfer), particularly Sec. 15 (The Representation of Polarized Light).

Chomilier J, Loupias G. and Felsteiner J. (1985) Correction for multiple scattering in Compton profile experiments: Application for synchrotron source photons. *Nucl. Instrum. Methods* **A235**, 603.

Felsteiner J., Pattison P. and Cooper M. (1974) Effect of multiple scattering on experimental Compton profiles. *Phil. Mag.* **30**, 537.

Felsteiner J. and Pattison P. (1975) Monte Carlo study of multiple scattering of photons in Compton profile measurements. *Nucl. Intrum. Methods* **124**, 449.

Fano U., Spencer L.V. and Berger M.J. (1959) Penetration and diffusion of X-rays. In *Encyclopedia of Physics*, Vol 38/2, p. 660. Springer Verlag, Berlin.

Fernández J.E. and Molinari V.G. (1993) Diffusion of polarized photons in the frame of transport theory. *Nucl. Instrum. Methods* **B73**, 341.

Fernández J.E., Hubbell J.H., Hanson A.L. and Spencer L.V. (1993) Polarization effects on multiple scattering gamma transport. *Radiat. Phys. Chem.* (in press).

Janssens K., Vincze L. Van Espen P. and Adams F. (1993) Monte Carlo simulation of conventional and synchrotron energy-dispersive x-ray spectrometers. *X-Ray Spectrom.* (in press).

Namito Y., Ban S. and Hirayama H. (1993) Implementation of Linearly-Polarized Photon Scattering into the EGS4 Code. *Nucl. Instrum. Methods.* (in press).

Pitkanen T., Laundy D., Holt R.S. and Cooper M.J. (1986) The multiple scattering profile in gamma ray Compton studies, *Nucl. Intrum. Methods* **A251**, 536.

Pomraning G.C. (1973) *The equations of radiation hydrodynamics.* Pergamon Press, Oxford.

Spencer L.V. and Wolff C. (1953) Penetration and Diffusion of Hard X-Rays: Polarization Effects. *Phys. Rev.* **90**, 510.

Stokes G.G. (1852) On the Composition and Resolution of Streams of Polarized Light from Different Sources. *Trans. Cambridge Phil. Soc.* **9**, 399.

Tanner A.C. and Epstein I.R. (1976) Multiple scattering in the Compton effect. III. Monte Carlo calculations. *Phys. Rev.* **A14**, 328.

Vincze L., Janssens K. and Adams F. (1993) A general Monte Carlo simulation of ED-XRF spectrometers. Part I: Unpolarized radiation, homogeneous samples. *Spectrochim. Acta* **B** (in press).

COMPARISON OF MCNP SIMULATED AND MEASURED DOSE RATES FROM DEPTH DISTRIBUTED CHERNOBYL CESIUM-134/137 IN RUSSIA AND UKRAINE

Lars-Erik De Geer

National Defence Research Establishment
S-172 90 SUNDBYBERG, SWEDEN

In the autumns of 1990 and 1991 expeditions to Russia and Ukraine were arranged by the Swedish National Defence Research Establishment in cooperation with the Institute of Radiation Hygiene in St.Petersburg and the All Union Scientific Centre for Radiation Medicine in Kiev. The purpose was to carry out field gamma ray measurements with portable high resolution germanium detectors in a grid 1 m above fields heavily contaminated by Chernobyl cesium fallout, to make separate dose rate measurements in the same points and to bring back soil cores taken under these points for subsequent laboratory analysis of the cesium-134/137 depth profiles.

The profiles were measured in a specially constructed automatic scanner with a germanium detector in front of a 5 mm slit in a lead

shield and with the soil cores behind on a revolving turntable (to give an azimutal average) which is moved vertically in 5 mm steps by computer control (Fig.1).

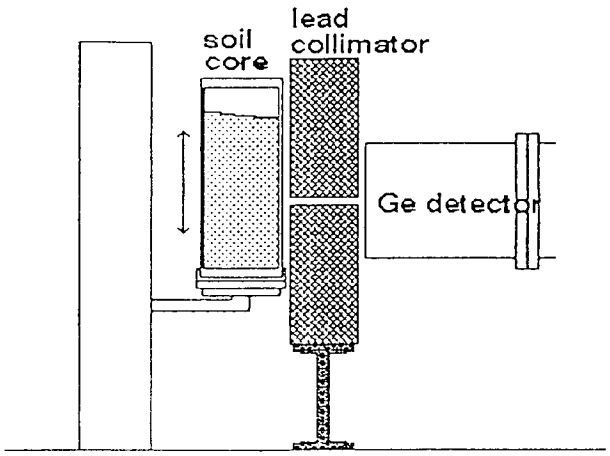

Fig.1: Equipment for automatic scanning of cesium profiles in soil

Suitable testing fields were choosen near the Russian city of Novozybkov some 200 km northeast of the Chernobyl reactors, near Tula some 100 km south of Moscow and within the closed 30 km zone surrounding the Chernobyl Sarcophagus. Reference measurements were also made in the Swedish high deposition area around the city of Gävle. With an improvised new unit, 1 GÄVLE, defined by the deposition density of Chernobyl cesium at Gävle the deposition densities on the test fields in Novozybkov, Tula and within the 30 km zone can be given as approximately 10, 2 and 0.6 - 70 GÄVLE respectively.

With the depth profiles (and the densities of the cores) known, the general Monte Carlo Code MCNP (version 3A) was employed to calculate the fluence rate of primary, uncollided, 661.6 keV photons and the absorbed dose rate in air at a point 1 m above a homogeneous fallout field of unit deposition density. Normalizing the calculated primary 661.6 keV fluence rate to the corresponding value measured by the field spectrometer then yields a MCNP dose rate in air which can be compared with the dose rate actually measured by the dose rate instrument 1 m above ground.

The natural way to formulate the simulation problem would be to define a point detector in air 1 m above origo and have the source

distributed according to the measured profile in soil below the z=0 plane. This will, however, not yield a very efficient calculation; most photons will miss the detector. If instead the profile is used as a vertical line source in the soil below origo and the z=1 m plane is used as a detector there is a much more effective simulation and one can quite easily show that the two problems are equivalent. If the geometry is limited by a ground radius of 1 km, a height in air of 1 km and 1 m of soil, virtually no histories are lost.

If 100000 histories are followed one gets answers with estimated relative errors less than 0.8%, which is good enough. One such simulation performed on a VAX-station 4000 VLC takes less than 36 minutes. On a DEC 3000 Model 500 AXP workstation the corresponding running time is 2 min 25 sec.

At a typical field site gamma spectra and dose rates were measured, and 10 - 20 cm deep core samples were taken in the 9 points of a 3 x 3 square grid with a 10 m spacing. As the actual depth distributions and deposition densities show some variability and the spectrometer collects photons from a rather large area the comparison between measured and simulated dose rates are made between the site means. These are given in the following table together with the standard deviations of the means and the ratio of the simulated to the measured values:

SITE	MCNP (μGy/h)	MEASURED (μGy/h)	RATIO
1	1.08 ± 0.28	1.08 ± 0.23	1.00
2	3.06 ± 0.25	2.69 ± 0.31	1.14
3	1.36 ± 0.09	1.17 ± 0.04	1.16
4	0.48 ± 0.01	0.44 ± 0.03	1.09
5	0.55 ± 0.02	0.49 ± 0.01	1.12
6	0.28 ± 0.06	0.24 ± 0.05	1.17

The simulated values seem to overestimate the doses by about 10 percent. One reason for this is that these simulations were made with the profile taken directly as measured. As the scanner has a nonvanishing slit the profile is somewhat smeared out, resulting in a somewhat too deep distribution. If a deconvolution program is utilized the cesium profile moves a little upwards which reduces the calculated dose a few percent. Another reason is that the dose rate instrument used is somewhat energy dependent while calibrated for 661.6 keV primary radiation. This leads to underestimated doses in a field with a degraded energy spectrum due to many

collisions in the soil. However, as the response curve is known, the simulated spectrum can be used to calculate and apply a correction factor. A preliminary test showed that the measured values should be about about 8 % higher than given in the table.

With these factors taken into account the agreement is almost better than one could possibly expect, given that the test fields are not perfect surfaces with fully homogeneous depth distributions. At all sites a natural background of 0.10 μGy/h has been assumed and subtracted and the uncertainty in this number introduces a noticable error for the sites with the lowest deposition values like SITE 6.

The present comparison validates MCNP simulations as a very useful method to study dose rate factors. As these simulations can be made in more complex geometries than is possible to consider when standard analytical methods are applied, MCNP on a powerful workstation turns out to be a very convenient tool for dose factor research.

Study of Neutron Spectra and Dose Rates Distribution in the VENUS Reactor Building with the Monte Carlo Code TRIPOLI-2

Georges MINSART
Centre d'Etude de l'Energie Nucléaire
Mol, Belgium

Introduction

VENUS is a pool-type critical facility built and operated by the Belgian Research Center at Mol. All parts and auxiliaries of the reactor are located in a room shielded by relatively thick (one meter) concrete walls. The hall around it, (about 22 meter long and 15 meter broad), contains the storage racks, space for measurement devices, a small workshop and the control room (figure 1).

The reactor itself is contained in a stainless steel cylindrical tank whose top is just below a working platform, at about 2.50 m above the ground level of the hall. At the same level a gangway is fixed in front and on the side of the shielded room and gives access to the inner platform through a heavy rolling door (figure 2).

The evolution of the experimental programme during the few last years has led to adopt large core loadings and a reduced water level to reach criticality; furthermore, the available MOX fuel rods are longer than the UO2 rods. As a result, the neutron leakage from the top of the core is markedly increased and induces higher radiation levels in and around the shielded room. In such conditions, during the "power runs", i.e. when the reactor is operated near the maximum allowed flux level, the neutron induced dose rates become larger than the values considered as acceptable according to the ALARA principles.

It has thus been decided :

- to put additional shielding where neutron leakage from the shielded room is most significant,
- to undertake measurement campaigns to localize the zones where the dose rates are larger and to improve the equipment (personal neutron dosimeters) used as monitors for the operation people,
- to run TRIPOLI-2 calculations for obtaining more detailed information on neutron spectra and neutron dose rates at the measurement locations and at a few other positions.

Additional shielding

The weakest part of the original shielding is certainly the junction between the rolling door and the concrete wall. Polyethylene plates have been fixed where gaps are the largest and, to further reduce the streaming of neutrons, the front wall of the shielded room has been reinforced on its inner side by polyethylene plates covering also the opening behind the rolling door.

Additional plates were put at the external border of the gangway and close to the control room, in order to obtain markedly reduced dose rates where operation people is working (figure 3).

Measurement campaigns

Routine measurements have confirmed the good efficiency of the additional shielding around VENUS. The periodic "power runs" give the opportunity to perform more specific measurement campaigns in order to obtain better evaluations of the neutron dose rates at several typical (or critical ?) locations and to check the performance of the dosimeters used up to now or envisaged in the near future for the personal dosimetry. A first series of measurements has taken place mid of last year and a second one is scheduled for July this year; the selected dosimeter is the "PGP-DIN" proposed by the CEA (Fontenay-aux-Roses). The response curve of PGP-DIN worn by a phantom is nearly constant from thermal energy up to about 10 keV ; it decreases rapidly for increasing energies above this value: at 1 MeV, it is roughly 100 times lower. Therefore a significant part of the dose rate due to fast neutrons is not included in the dosimeter response and, as the promotors say: "in all such cases dosemeters must be calibrated at the working post for which they are intended".

Additional data requested

The neutron spectrum emerging from the shielded reactor room covers the whole energy range, from a few MeV (fission neutrons) down to thermal. The PGP-DIN dosimeters have a much lower efficiency above 10 keV; unfortunately, above this energy, the 1990 Recommendations of the ICRP propose much larger weighting dose factors, going from 5 below 10 keV up to 20 between 100 keV and 2 MeV approximately. The maximum weight is in fact attributed to the energy range for which less detection means are available.

In order to calibrate the response of the PGP-DIN dosimeters at the various selected locations, it is thus necessary to obtain sufficient information on the corresponding neutron spectra. This can be provided by detailed multigroup calculations; at the same time, these calculations can produce results for many locations, allowing to optimise the choice of the measurement zones and also to check the correspondence between measured and computed dose rates as a function of position in the reactor hall. Hopefully such an experimental validation of the calculations will allow to have better confidence in computed results which could be produced for different shielding configurations.

Owing to the large dimensions and the complexity of the geometry, calculations are to be performed with a Monte Carlo code and TRIPOLI-2 has been selected.

TRIPOLI-2 calculations

Geometry modelisation

The first step, and probably the most time consuming part of the preparation of the input data, is the detailed modelisation of the geometry. It has been decided to go into a very detailed model of the installation, including all the different pieces of shielding and of structural materials, and also the thin gaps around the rolling door. Most dimensions were remeasured, and particularly the empty spaces remaining between the door and the wall. Sizes and exact locations of

the polyethylene shielding plates were verified; at the time of the first modelling, reported here, the polyethylene door inside the shielded room was not yet installed and a few plates in the hall were not at their present location. The geometry modelisation is being updated now and the final polyethylene configuration will be used both for the calculations and for the measurement campaign of next July.

Great care has been taken for the representation of the gaps between shielding pieces around the rolling door, of the rolling path where concrete thickness is lower, of the control room walls, of the roof above the reactor,... The model is maybe too detailed, but the objective was (and is still) to obtain more information on the "privileged" neutron paths between the core and the control room. As a result, the input data contain 19 compositions, 133 equations and 281 volume elements; the updating of the model will not modify very much these numbers.

Source representation

The fission source distribution is represented by a few cartesian systems. Data are based on fission density measurements performed in the considered core configuration. This part of the data will be updated according to the core loading present when the measurement campaign will take place.

Biasing and steps of calculations

The type of problem (long path for the neutrons, large attenuation,...) requires to apply efficient biasing techniques to improve the statistics and to reduce the computer time required to obtain sufficiently detailed and accurate results. With the help of Mr J-C Nimal, the biasing scheme has been set up: directions of interest, equi-weight surfaces and gradients, coefficients of exponential transform,...; the volumes have been grouped into 12 sets to optimise the biasing parameters. It has been decided also to perform two steps of calculation, both with the available complete geometry modelisation :

- the first one, with the fission neutrons of the core being the source; an additional result, the current around the door, has been requested,

- the second one, with only this neutron current in the gaps around the rolling door acting as the source, in order to identify the fraction of the responses (the dose rates at the selected locations) due to the presence of these gaps.

Preliminary results

The two TRIPOLI runs have been made with a limited number of source neutrons (600) and of generations (50 for the first step and 25 for the second one). The objective was to obtain good orders of magnitude for the few requested results and so to confirm the adequacy of the procedure and of the choice of the biasing parameters. After some updating of the geometrical model and of the source shape (other core loading), these runs will be repeated with larger numbers of source neutrons and of generations.

Presently, only preliminary results produced by the first runs are available. Some results of the first calculation (source in the core) are illustrated on figure 4 ; the neutrons from the gaps around the door (second run) contribute only for a few percents to the total dose rates; it should be recalled that the shielding had already been reinforced at these "critical" locations.

VENUS REACTOR LOCATION

FIG. 1.

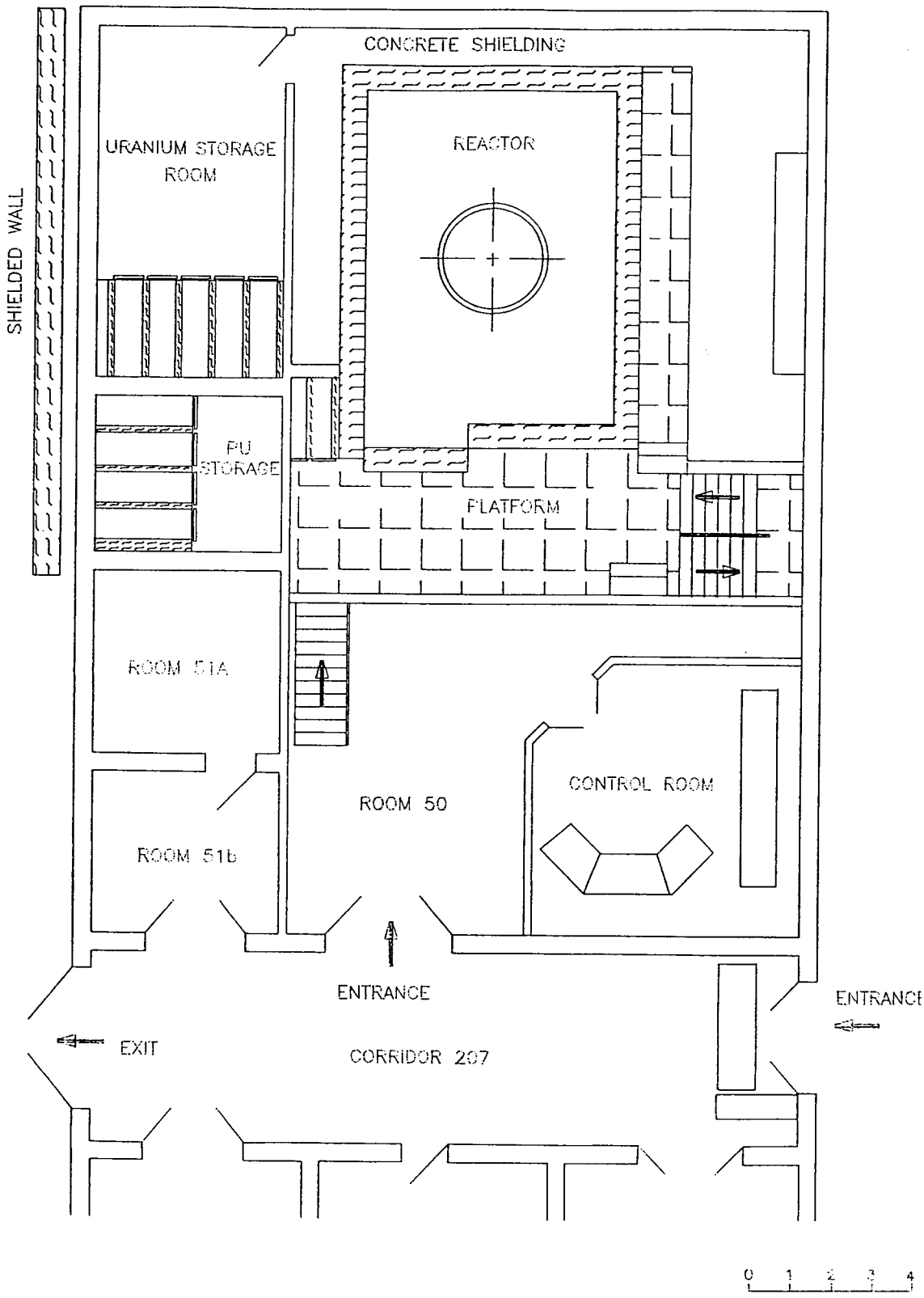

VENUS SHIELDED ROOM

FIG. 2.

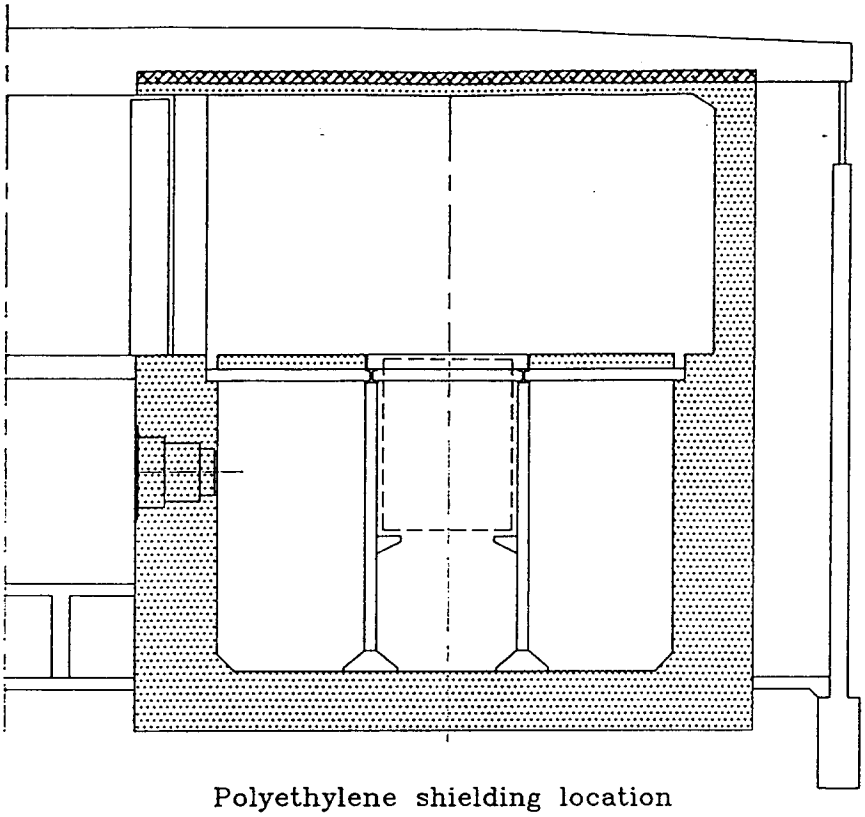

Polyethylene shielding location

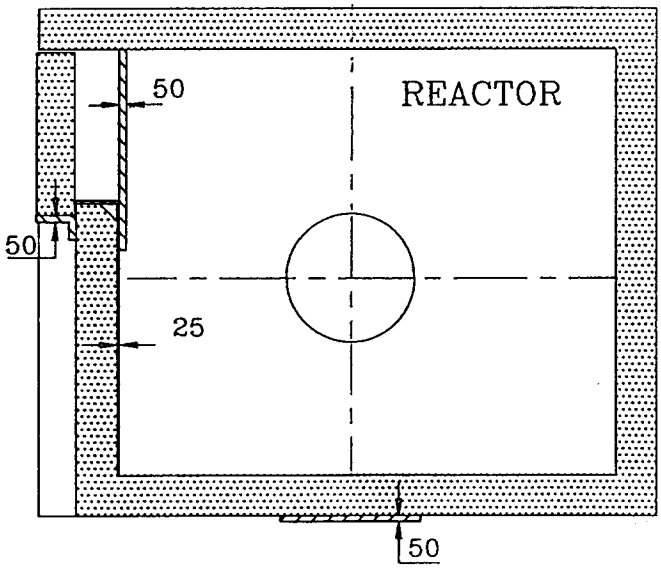

Concrete shielding

Polyethylene (HD500) shielding

0 0,5 1m

(scale 1:50)

April 1993

VENUS REACTOR LOCATION

FIG. 3.

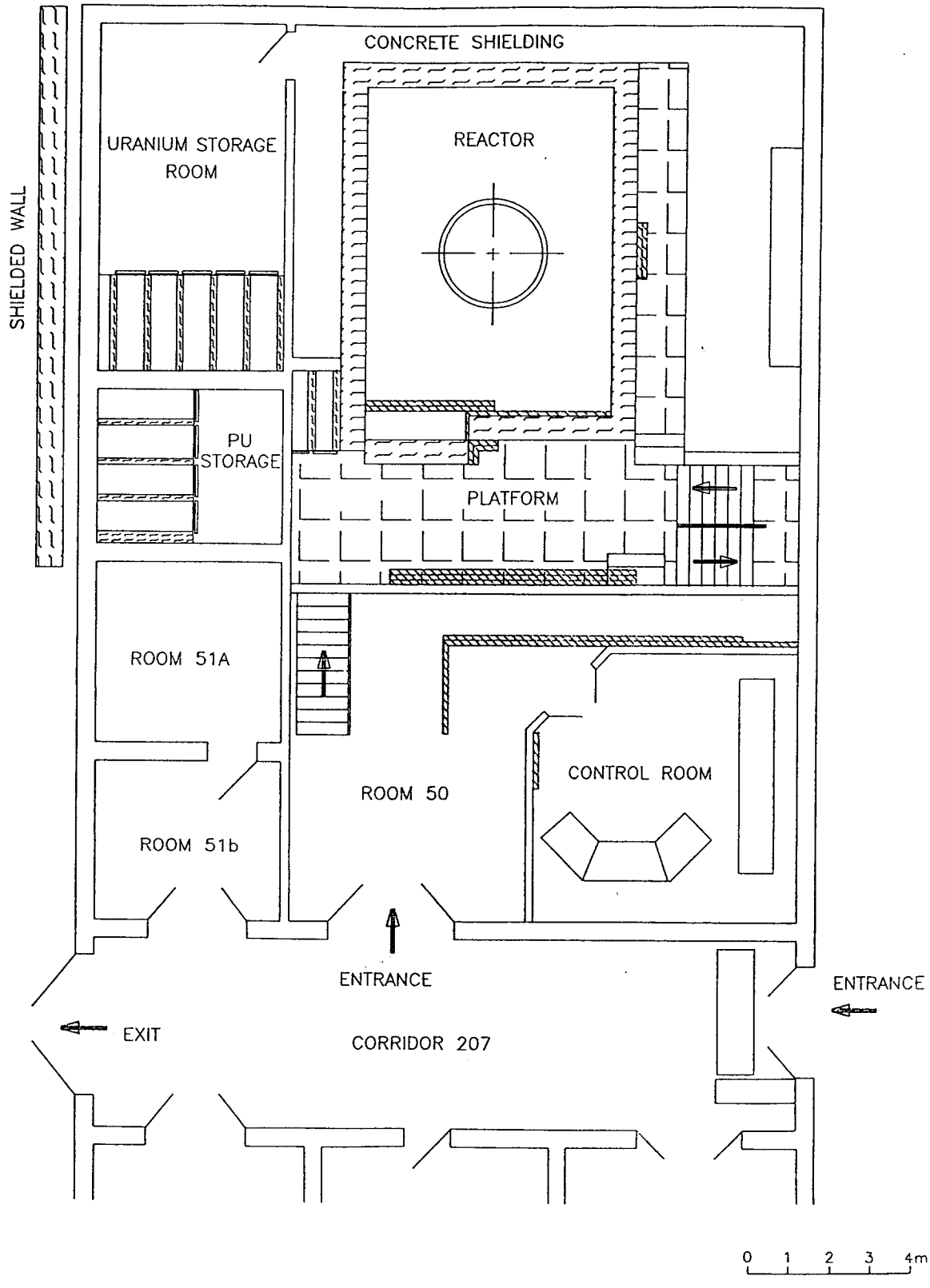

FIG. 4.

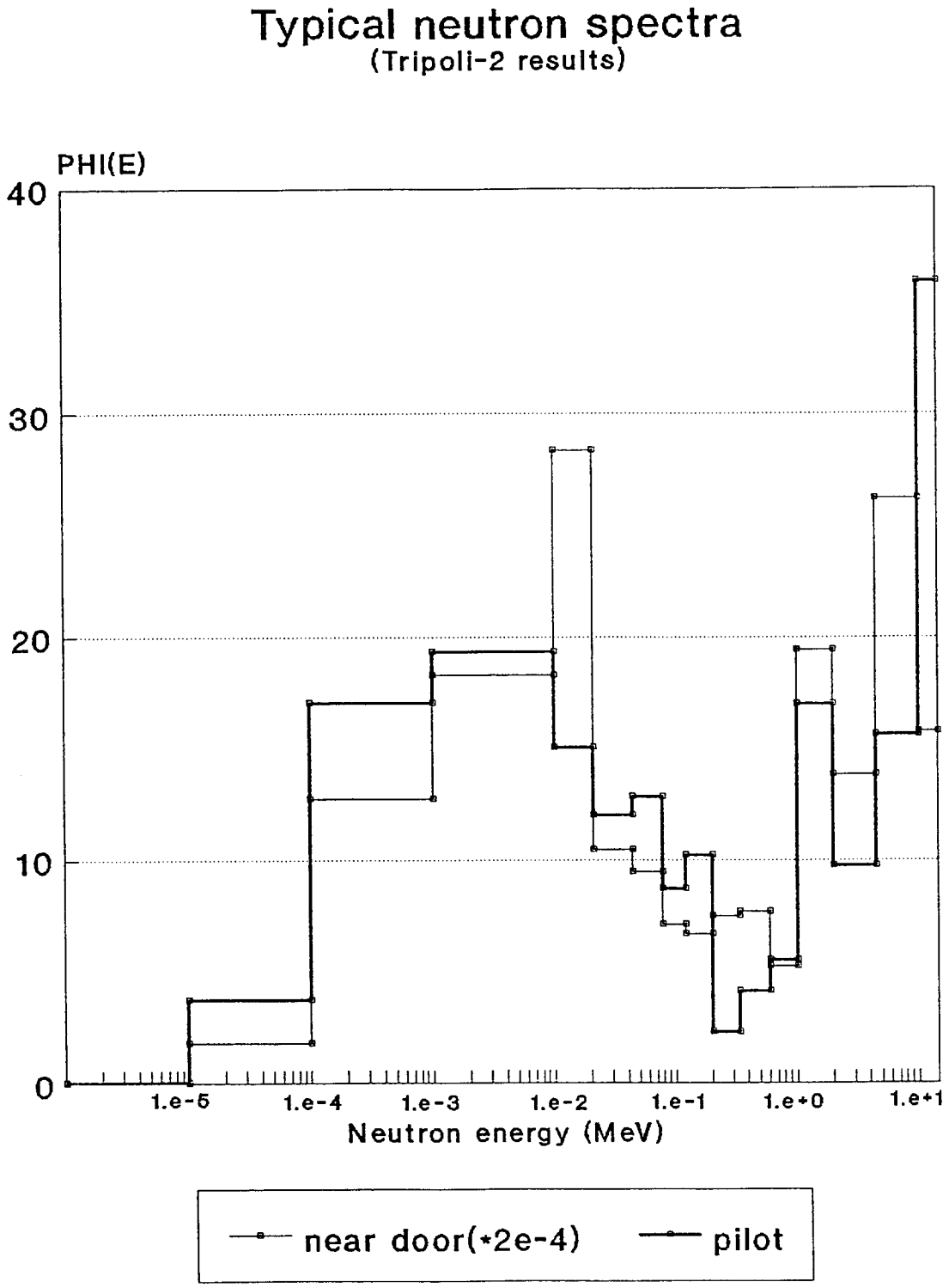

Preliminary

FUSION POWER REACTOR NEUTRONIC ANALYSIS WITH TRIPOLI-3

J-Ch Sublet

AEA Technology, Culham, Abingdon, Oxfordshire, OX14 3DB, UK
(Euratom/UKAEA Fusion Association)

Abstract

The modelling of neutron transport in a conceptual power reactor of the tokamak type presents a number of challenges. The D-T plasma provides a 14 MeV neutron source, from which energy neutrons are slowed to thermal energies in a blanket, which also synthesises tritium through neutron interaction with lithium. The source energy is above the threshold of many reactions not normally significant in fission reactor analysis or shielding, and coupled with the range of unusual materials considered this puts particular requirements on the nuclear data library used.
A further complication is the very complex toroidal geometry, with various penetrations, which must be accurately represented for a proper prediction of the neutron flux distribution, the 14 MeV components of which may fall by ten orders of magnitude between the plasma facing surface and the biological shield.
The 3D capability of the Monte Carlo method is essential for such reactor analyses. A three-step calculational scheme has been developed for application using the TRIPOLI-3 code together with the EFF-1 nuclear data library. This involves firstly a model of the source in 3-D, secondly a "homogeneous" 3-D model of the entire nuclear island and finally a detailed "heterogeneous" model of the blanket in 2-D. The approaches of this scheme are described and plan for its use outlined.

1. STATEMENT OF THE PROBLEM

Fusion power reactor design presents certain challenges in terms of neutron transport calculations. The transport of 14 MeV neutrons, born in the plasma, poses a wide range of problems, each attached to a particular type of calculation. Each of the various methods of solution of the Boltzmann equation have different advantages and disadvantages. However, in view of the following points and recent improvements in efficiency and user friendliness the Monte Carlo method presents major advantages.

Firstly, the general geometry of the nuclear island of a fusion power plant is based around the toroidal, D shape superconducting coils that allow the plasma to be confined within the so-called doughnut centre region. This has an impact on the shape and form of other equipment that needs to be squeezed in between the plasma source and the coils. It is necessary to provide access to the centre region for plasma heating and fuelling equipment by means of radially disposed ports, which run through the radial "thickness" of the reactor. Thus, from every angle, the problem involves non trivial 3D effects that can only be represented with a code capable of modelling in three dimensions.

Secondly, because the neutron source resides in the plasma, where neutronic interaction can be neglected, it is always from the transport point of view a shielding-streaming problem that needs to be resolved. The only exception arises locally, in the blanket region where tritium needs to be synthesised to self-sustain plasma fuelling. In contrast to a fission reactor core, the lattice advantages are nearly non-existent in a fusion power reactor.

Finally, the neutron dose limits imposed by the magnetic confinement technology in the coils and the issue of the overall tritium breeding ratio impose strict requirements on the uncertainties acceptable when analysing these important issues. Factors could be introduced for 1D calculations to take account of 3D effects but they have been found to be as high as 2 to 5 and very dependant on integrated responses after 2 metres of blanket and shield. These factors do not take account of the uncertainty in the cross-section data that are always of great concern in fusion reactor studies, particularly when materials which are not well characterised neutronically are envisaged.

The Monte Carlo techniques employed in the code TRIPOLI-3 combined with its full 3D capabilities allow the needs of fusion power reactor neutronic analysis to be met, minimising the calculational uncertainties. The methodology chosen encompasses a three-step analysis, firstly to deal with the geometrical complexity and secondly to take account of the specific results required in fusion reactor core analysis. These needs are quite different from those of fission core physics since there is no criticality problem but instead many additional neutron reactions occur, including multiplication, whose thresholds are exceeded by the neutron energies encountered.

2. CALCULATIONAL METHODOLOGY

The envisaged methodology includes three different types of calculational models, all represented with TRIPOLI-3 [1], in order to fulfil the analytical requirements. These include detailed analysis of the first wall load distribution, the blanket, neutron shielding and streaming. The scale and size of the problem, either from the geometrical or computational point of view, and the resources that can be allocated to the study, however, unavoidably restrict the possibilities. Nevertheless the following sequential procedure has been devised to allow flexibility and can be adapted as design detail changes during the conceptual analysis.

2.1 The source term model

The fusion reaction D(T-n)^{4}He yields an alpha particle and a neutron with an energy of 14.03 MeV in a very specific environment: a plasma. That plasma is confined by means of electromagnetic fields that gives it its shape and indirectly, through typical plasma parameters, influences the neutron source strength. The neutron source strength is dependent upon the D-T reaction rate which itself is dependent upon the different plasma ion temperatures and density.

The parametric equations for the contour lines of the plasma, following the magnetic field imposed by the TF/PF coils, and the source density distribution and radial shift are combined to obtain a plasma source model for TRIPOLI-3. The D shaped contour equation [2] in radial R and vertical Z geometry is as follows:

$$R = R_p + a.\cos(\alpha + \frac{a}{a_p} C_p.\sin\alpha) + \varepsilon.a_p$$

$$Z = K.a.\sin\alpha \quad \text{where} \quad K = K_o + K_1(\frac{a}{a_p})^2 \qquad (1)$$

$$\varepsilon = \varepsilon_o(1 - [\frac{a}{a_p}]^2)$$

where a represents the radius and Figure 1 describes the geometry

R_p = plasma major radius
a_p = horizontal plasma minor radius
b_p = vertical plasma minor radius
$K = b_p/a_p$ = plasma elongation
C_p = triangularity
ε_0 = plasma radial shift

The thermonuclear neutron source, assumed isotropic and monoenergetic, is proportional to the plasma density and temperature and can be expressed as follows:

$$S = n^2 \langle \sigma v \rangle_{DT} \quad \text{with} \quad n_e = n_i = \frac{n_d}{2} = \frac{n_t}{2}$$

$$\frac{\langle \sigma v \rangle_{DT}}{(KT_i)^q} = cste \quad \text{for} \quad 8KeV \leq T_i \geq 25KeV$$

e = electrons
i = ions

The temperature and density profile obey the following type of law where generally the temperature exponent is higher, the profile is steeper.

$$n = n_o(1 - [\frac{r}{a}]^2)^{\alpha_n} \qquad T = T_o(1 - [\frac{r}{a}]^2)^{\alpha_T}$$

$$\alpha_n \sim \frac{1}{2} \qquad \alpha_T \sim 2$$

If one supposes

$$q = 2 \Rightarrow \langle \sigma v \rangle_{DT} \propto T^2$$

$$\Rightarrow S \propto (1 - [\frac{r}{a}]^2)^{2\alpha_n + 2\alpha_T}$$

The source distribution in the plasma can so be approximated by the following equation

$$S = S_o(1 - [\frac{r}{a}]^2)^{pk} \qquad (2)$$

The combination of equations (1) and (2) allows the spatial distribution of the source to be modelled in the case of plasma-plasma interaction. One needs to remember that the D-T reaction rate could be sensitive to beam-plasma or beam-beam interaction occurring in certain regions of the plasma and so locally influencing the source strength. However, this type of modelling supposes detailed knowledge of the plasma kinematics and is expected to be of less importance. The correct knowledge of the plasma behaviour in the null point region is considered to be of negligible effect when concerned with the neutron source strength.

The source term model is a limited 3D toroidal representation of the reactor first wall and plasma region set up to obtain the distribution in the poloidal direction of the neutron current. The current distribution on the first wall is used, in a fusion reactor conceptual study, as a normalisation factor (wall loading in MW/m^2) for subsequent calculational steps. The effect of the toroidal geometry and the source shape and strength is then considered. Peaking factors in the region of 1.6 are not uncommon

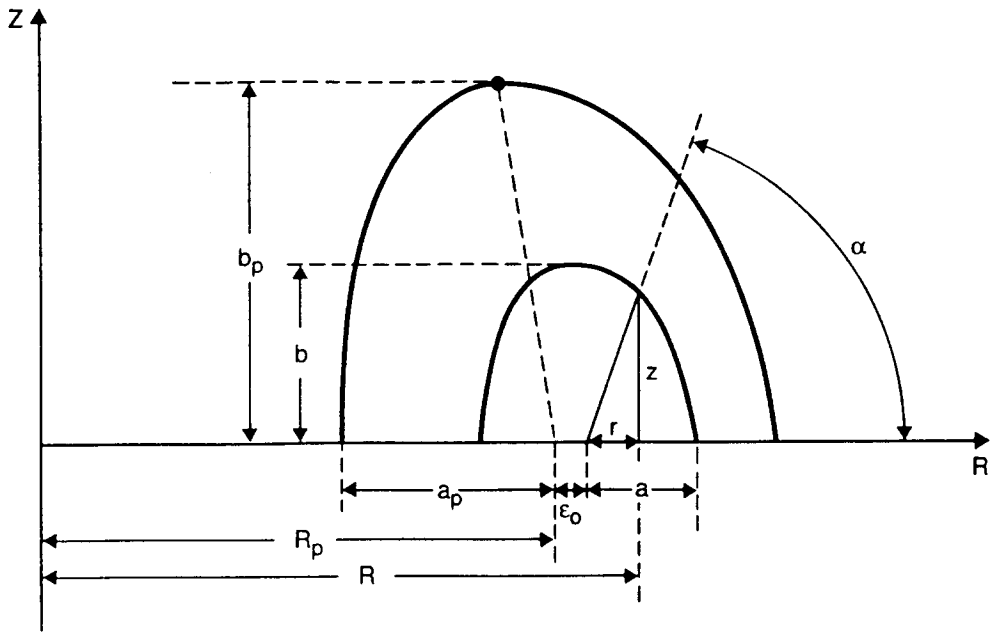

Figure 1 Plasma electromagnetic contour lines

and since they typify the source term in that particular poloidal direction, their impact on the subsequent region is not negligible. Generally the peak load occurs at the outboard central mid-plane of the reactor with this type of source distribution. However, when concerned with a plasma of reactor relevance, which cannot be considered as static, it is likely that other local maxima occur within this source of hundreds of cubic metres. A special program has been written [3] to take account of this complex source spatial distribution and simplify the input data needed for TRIPOLI-3.

2.2 The 3D homogeneous model

The next problem to address is that of neutron streaming and leakage through deep penetration, ports or ducts. It is necessary to extend the first model by means of a set of homogeneous regions, including ports, on a 30° sector of a torus with reflective boundary conditions. The sketch show in Figure 3 illustrates the general layout envisaged in a future fusion power plant. This homogeneous 3D representation of the first wall, blanket, shield and toroidal field coils is used to comprehend the angular and scalar flux distribution through each component-region boundary surface. This allows the determination and selection of a surface of equi-potential and the drawing of a grid at each region boundary. The materials are homogenised by region to simplify the input and the geometry only follows as precisely as permitted the contour lines of the regions external boundaries.

This model gives scope for statistical biasing through the homogeneous layer of material. That is, to favour neutron migration towards the relevant region boundaries where good standard deviations are needed for subsequent analysis. Biasing is

needed where there is strong flux attenuation, greater than 2 or 3 decades, such as in the blanket or magnet shield region of the reactor and should favour the neutron migration towards the chosen area or surface. For more efficiency, the acceleration techniques used by TRIPOLI-3 are based on the exponential transform and the collision biasing processes [4].

If an importance function is selected equal to the solution of the adjoint problem, one can defined a function $\pi(r,E,\Omega)$, the inverse of this importance function [5]. The function $\pi(r,E,\Omega)$, called the particle weight, allocated to each point of the phase space, could be factorised in space r, energy E and angle Ω.

$$\pi(r,E,\Omega) = \pi_1[r]^{F(E)}.\pi_2(\Omega).\pi_3(E)$$

Where

$\pi_3(E)$ is defined by the user
$\pi_2(\Omega)$ is imbedded in the code
$\pi_1(r)$ is either defined by the user or automatically calculated by the subroutine INIPOND

The energy factor F(E) represents the energy component in the function $\pi_1(r)$, where the spatial component varies exponentially, and allows account to be taken of the variation of the cross-sections with the energy. This is important in light materials where the total cross-section increases significantly for low energies.

In TRIPOLI-3 the biasing techniques involving the general notions of surface of equivalent weight and preferred directions, particularly simplify the user workload when dealing with homogeneous regions and a complex layout, without impairing the accuracy of the results. The two combined biasing techniques allowed in TRIPOLI-3 lead clearly to:

- tracking particles of the same importance
- the reduction of the splitting and Russian roulette processes

This is particularly suitable for the typical fusion reactor blanket-shield cases.

2.3 The 2D heterogeneous model.

The design of the blanket and shield regions of a fusion power reactor presents certain technological requirements. Those which have an impact on the neutronics analysis are:

i) The tritium breeding ratio in the blanket region needs to be high enough to self-sustain the plasma fuelling systems.

ii) The bulk of the heat generated comes from the blanket itself and must allow the efficient exploitation of electricity generation by means of a cooling fluid.

iii) The superconducting magnet operates under exacting temperature conditions and their materials physical properties (superconductor, resin) are extremely sensitive to neutron irradiation, so the shield needs to reduce the neutron penetration to an admissible level.

Once the 3D homogeneous model has allowed the equi-potential source grid to be defined, the same penetration calculation is then repeated but in two dimensions for the first wall, blanket and shield regions. This model is limited in space with specific boundary conditions and with detailed geometry through the thickness of each module. Figure 2 represents a typical model of the blanket-shield-TF coils layout of a fusion reactor[6]. The 2D model represents the radial and toroidal dimensions where lattice geometry appears and emphasis is put on calculational accuracy and detailed trend analyses. Such heterogeneous Monte Carlo transport calculations

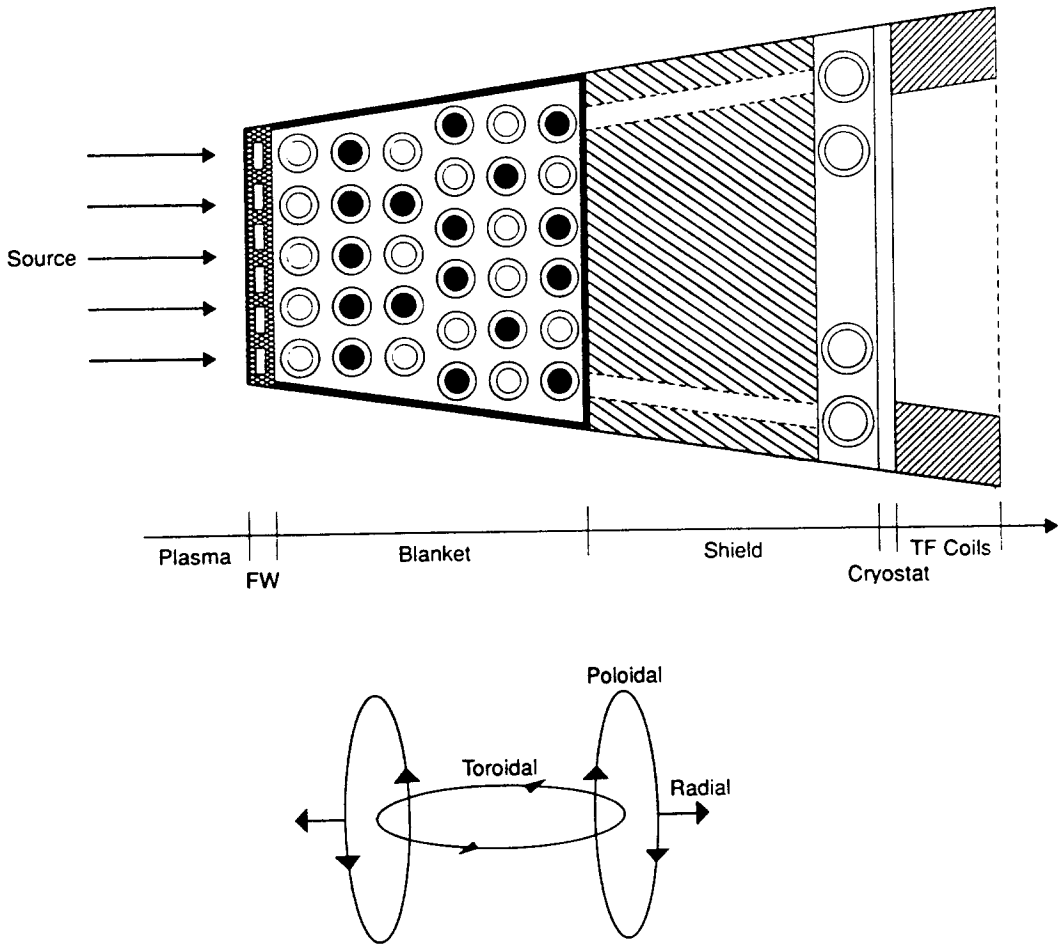

Figure 2 Heterogeneous 2D model of the blanket, shield and TF coils regions of a fusion power reactor

provide the kind of accuracy needed to analyse and optimise the requirements imposed on the blanket and shield regions.

The spatial flux distribution, in heterogeneous media, needs to be known to predict the neutron and gamma responses generated in the different materials encountered in the blanket and shield. The spatial power density distribution can then be obtained for each material and location and used as source data in the subsequent thermohydraulic calculations. The toroidal and radial variations of the Tritium Breeding Ratio (TBR) can be calculated precisely. Various other responses such as Displacement Per Atoms (DPA), gas production or neutron multiplication can be derived and used as part of the materials assessment. The detailed neutron flux distribution is the starting point of the time dependant activation calculation. The activation characteristics of the materials are very sensitive to the spatial distribution of the neutron flux and spectra, and vary according to the duration of the irradiation and the total flux. This variation, involving the resolution of hundreds of differential equations governing the nuclide material inventory through irradiation, is performed after the transport calculation by other means.

The code TRIPOLI-3 is particularly well suited to application to this detailed 2D model. Coupled with the availability of reliable fusion-relevant data libraries, this code has the capabilities required in this type of fusion reactor study.

3. NUCLEAR DATA LIBRARIES

3.1 Neutron cross-section libraries

The neutron transport libraries used in fusion experiment or reactor studies have in the past been based on those used in fission, extended to the energy range relevant to fusion neutrons. However, this type of manipulation, generally obtained by theoretical extrapolation, does not satisfy the accuracy criterion imposed in such studies. Additionally, the materials and isotopes relevant to fusion are very different of those used in fission and the lack of experimental data on particular isotopes is of concern. This has triggered, in Europe, an extensive experimental and theoretical programme to update those particular cross-sections and produce a fusion relevant data base called the European Fusion File (EFF transport library) and European Activation File (EAF activation library). So far the EFF-1 data are available for TRIPOLI-3 as a shielding library in a 318-neutron groups format for 24 elements and isotopes relevant to fusion materials at 300 K [7]. This capability is soon to be updated with level two of this transport library, EFF-2 [8], containing data for 75 isotopes and elements extracted selectively from new evaluations, JEF-2.2 and ENBF/B-V and VI.

The Monte Carlo code TRIPOLI-3 can be linked with pointwise data libraries based on ENDF/B-IV and V, including temperature dependence and thermal treatment that would eventually allow more specific calculations to be performed.

3.2 Response function library

RFL-1 [9], is a library of nuclear response functions in the Vitamin-J group structure and can be used with TRIPOLI-3. Neutron and photon kerma, displacement per atoms cross-sections, gas production and reaction cross-sections have been calculated for 61 isotopes and elements relevant to fusion reactor materials. This library will allow the production of nuclear responses compatible with the EFF-1 neutron transport library since the sources are identical (ENDF/B-VI and JEF 1.1).

REFERENCES

1. Nimal J-C and Vergnaud T,"TRIPOLI-3 Code de Monte Carlo Tridimensionnel Polycinetique", CEA/DRN/DMT/SERMA Saclay, user manual, to be published.

2. D'Ipplitto D.A et al., Finite Beta Theory Workshop, Varenna, Proceedings p.p 75-92, 1977.

3. Diop C, private communication

4. Nimal J-C et al.,"Programme de Monte-Carlo Polycinetique a Trois Dimensions TRIPOLI-2", Tome I, II and III, CEA/DRN/DMT/SERMA Saclay report.

5. Nimal J-C,"Methode de Monte Carlo, Application au Transport des Rayonnements", CEA/DRN/DMT/SERMA Saclay, SERMA/TN 366 report.

6. Kardistas P J,"Fusion Reactor Coolant-Out-of-Tube Blanket concept", AEA Technology report, to be published

7. Diop C et al., Description of a TRIPOLI Neutron Cross-section Library Derived from the European File EFF-1, CEA Saclay, SERMA/LEPP/91/1248, 1991.

8. Kopecky J et al.,"European Fusion File, Version-2, EFF-2", ECN Petten report, ECNC-92-036, 1992.

9. Panini G.C and Peerani P,"RFL-1: A Library of Nuclear Response Functions in Vitamin-J Structure", ENEA Bologna, EFF-DOC-130, 1992.

Acknowledgements

This work is performed as part of the internally-funded research programme of AEA Technology, and is also supported by funding from Euratom. The author acknowledge the CEA-Saclay for making available the Monte Carlo code TRIPOLI-3 with particular thanks to J-C Nimal, T Vergnaud and C Diop for their valuable help in the early days of the program development.

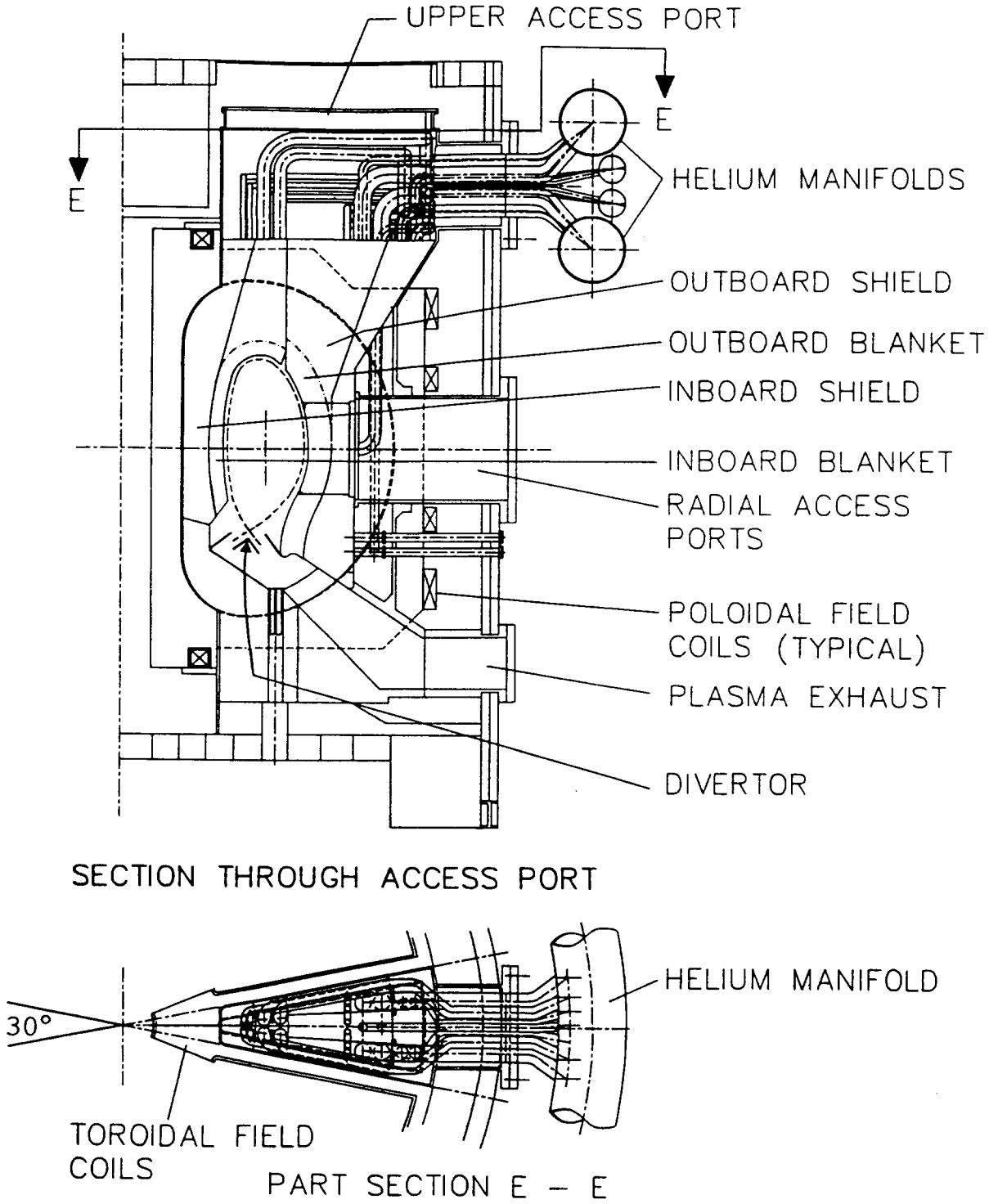

Figure 3 Sketch of a fusion power nuclear island

PROBABILITY TABLES CROSS SECTIONS IN MONTE CARLO CODE TRIPOLI-03

S.H.ZHENG P.RIBON* J.C.NIMAL

COMMISSARIAT A L'ENERGIE ATOMIQUE
CENTRE D'ETUDES NUCLEAIRE DE SACLAY
DMT/SERMA/LEPP
**DMT/SERMA/LENR*
91191 GIF-SUR-YVETTE CEDEX
FRANCE

INTRODUCTION

In the shielding calculation, the neutron cross sections are usually described by multigroup method, a neutron flux was assumed as the weighting function to define the average group cross section. But in many cases (eg. the deep penetration problems) the self-shielding effect is very important and it is difficult to choose the good weighting function to determinate the correct effective cross section.

Another method called probability table method was developed in the 1970's to treat the neutron cross sections in the unresolved resonance energy range, several definitions have been given by NICOLAEV[1], LEVITT[2] and RIBON[3, 4]. This method has been used for Monte Carlo calculation, also for the neutron slowing down calculation even though it is less exact in the resolved resonance energy range. The advantage of this method is to represent properly the neutron cross section fluctuations within an energy group, allowing a correct calculation of the self-shielding, on the other hand, the probability tables are very easily applied in the Monte Carlo calculation and only some small modifications should be done in the Monte Carlo multigroup code. In this paper, the probability table method has been introduced in the general Monte Carlo transport code TRIPOLI3[5]. the simulation of neutron transport by Monte Carlo method with the probability table cross sections will be presented, some examples are given to show the differences between "multigroups" and "probability tables" ; also the comparison between "probability table cross sections" and "pointwise cross sections" will be given in this paper.

PROBABILITY TABLE METHOD

The probability tables of the neutron cross sections used in this study are produced basing on the moments equation[3]. In a given energy group, the total cross sections are showed in Fig.1(a), the total cross section moment is defined as :

$$\mathcal{M}_n = \frac{1}{\Delta E}\int_{\Delta E} \sigma_t^n(E)dE$$

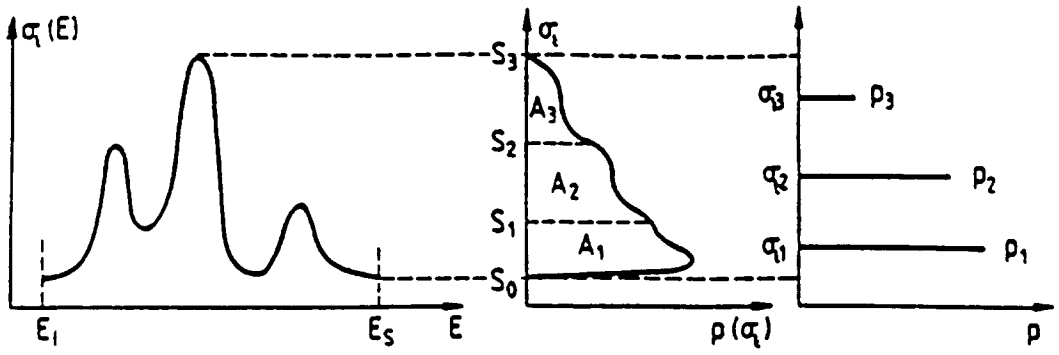

(a) (b) (c)

Fig.1

If one wants to describe the variation of the cross sections, it is interested to transform the RIEMANN integral to the LEBESGUE integral (Fig.1(b) shows the relation between the probability density and the cross sections) :

$$\mathcal{M}_n = \int_{\Delta\sigma_t} \sigma_t^n p(\sigma_t) d\sigma_t$$

where σ_t is the total cross section, $p(\sigma_t)d\sigma_t$ is the probability of total cross section presenting between σ_t and $\sigma_t+d\sigma_t$.

To obtain the discrete cross section values and their probabilities, we can rewrite the moment by the GAUSS quadrature (Fig.1(c)):

$$M_n = \sum_{i=1}^{N} p_i \sigma_{ti}^n$$

For a probability table of N steps, p_i and $\sigma_{t\,i}$ are the probability and the total cross section of step i, they can be calculated by resolving the system $M_n = \mathcal{M}_n$ with 2N values of n (for example n=-N+1, -N+2, ..., N).

Having obtained the probability tables for total cross sections, one will ask whether it is necessary to define a sub-probability table of the partial cross sections for each total cross section step. As we know, partial cross sections are always used linearly in neutronic and this sub-probability table of partial cross sections can be replaced by an average value. It is demonstrated as :

Partial cross section moment, $$\mathcal{P}_{mx} = \frac{1}{\Delta E}\int \sigma_t^m(E)\,\sigma_x(E)\,dE = \iint \sigma_t^m\,\omega(\sigma_t,\sigma_x)\,\sigma_x\,d\sigma_x\,d\sigma_t$$

$$= \int p(\sigma_t)\,\sigma_t^m \left[\int \frac{\omega(\sigma_t,\sigma_x)}{p(\sigma_t)}\,\sigma_x\,d\sigma_x\right] d\sigma_t$$

or

$$P_{mx} = \sum_i p_i\,\sigma_{ti}^m \sum_j \frac{\omega_{ij}}{p_i}\sigma_{xij}$$

where $\sum_j \frac{\omega_{ij}}{p_i}\sigma_{xij}$ can be replaced by an average value σ_{xi}.

We can obtain the partial cross sections σ_{xi} (i=1, 2, ..., N) by resolving the system $P_{mx} = \mathcal{P}_{mx}$ with N values of m.

How many steps we need ?

The number of steps depends on the cross sections structure in the energy group, more the resonances it has and the fluctuation of cross sections is in the group, more steps we need. The number of steps is defined by the precision of the moments, to a small value ε, if $\left|\ln\frac{\mathcal{M}_{-N}}{M_{-N}}\right| < \varepsilon$ and $\left|\ln\frac{\mathcal{M}_{N+1}}{M_{N+1}}\right| < \varepsilon$, the number of steps will be N, if the test is not satisfied, we continues the test for N+1 steps.

Table 1 gives an example of the probability tables calculated by CALENDF code[4] for iron.

Table 1 Probability tables for iron

```
tables de probabilite pour  26-FE- 56 ORNL       DIST-APR90
ZA= 26056. MAT=2631 TEFF= 300.0  315 Groupes de 1.0000E-5 a 1.9640E+7 IPRECI=3
......
IG   15 ENG=1.000000E+7 1.051300E+7 NOR= 2 I= -1 NPAR=3 KP=   2 101   4   0   0
 4.961311E-01 3.066885E+00 1.640399E+00 1.116164E-01 1.314870E+00
 5.038689E-01 3.105799E+00 1.681825E+00 1.043985E-01 1.319575E+00
IG   16 ENG=9.512300E+6 1.000000E+7 NOR= 2 I= -1 NPAR=3 KP=   2 101   4   0   0
 4.942441E-01 3.136579E+00 1.713936E+00 9.960849E-02 1.323035E+00
 5.057559E-01 3.181636E+00 1.760298E+00 9.358172E-02 1.327756E+00
IG   17 ENG=9.048400E+6 9.512300E+6 NOR= 1 I=  0 NPAR=3 KP=   2 101   4   0   0
 1.000000E+00 3.234972E+00 1.813422E+00 8.746376E-02 1.334086E+00
IG   18 ENG=8.607100E+6 9.048400E+6 NOR= 1 I=  0 NPAR=3 KP=   2 101   4   0   0
 1.000000E+00 3.249313E+00 1.825380E+00 7.949171E-02 1.344441E+00
IG   19 ENG=8.187300E+6 8.607100E+6 NOR= 2 I= -1 NPAR=3 KP=   2 101   4   0   0
 4.824680E-01 3.326479E+00 1.900934E+00 7.095761E-02 1.354588E+00
 5.175320E-01 3.441981E+00 2.015535E+00 6.883861E-02 1.357607E+00
IG   20 ENG=7.788000E+6 8.187300E+6 NOR= 2 I= -1 NPAR=3 KP=   2 101   4   0   0
 4.080616E-01 3.382941E+00 1.953477E+00 6.431550E-02 1.365148E+00
 5.919384E-01 3.477480E+00 2.044200E+00 5.955127E-02 1.373728E+00
IG   21 ENG=7.408200E+6 7.788000E+6 NOR= 2 I= -1 NPAR=3 KP=   2 101   4   0   0
 6.550765E-01 3.467907E+00 2.029225E+00 5.381581E-02 1.384866E+00
 3.449235E-01 3.561281E+00 2.120735E+00 5.185770E-02 1.388688E+00
......
      ^            ^            ^            ^            ^
      |            |            |            |            |
probability Pi   total        elastic      capture      inelastic

ENG :  energy limites,
NOR :  number of steps,
I :    order of the first moment,
NPAR : number of partial cross sections,
KP :   reaction type ;
          2-elastic scattering,
        101-capture,
          4-inelastic scattering (n,n'),
         18-fission,
         15-inelastic scattering (n,kn'), k>1.
```

PROBABILITY TABLES IN TRIPOLI3 MONTE CARLO CODE

The neutron transport can be simulated by resolving the integral equation :

$$X(P) = S(P) + \int X(P')K(P' \rightarrow P)dP'$$

where $X(P)$ - collision density at P phase-space ; $S(P)$ - source ; $K(P' \rightarrow P)$ - transfer probability.

In a non sur-critical problem, the solution of this equation can be obtained by summing the Neumann series,

$$X(P) = \sum_{v=0}^{\infty} X_v(P)$$

$X_v(P)$ is the collision density at P with n collisions and we have,

$$X_0(P) = S(P)$$

$$X_v(P) = \int X_{v-1}(P')K(P' \rightarrow P)dP'$$

or

$$X_v(P) = \int S(P_0)K(P_0 \rightarrow P_1)K(P_1 \rightarrow P_2)\cdots K(P_{v-1} \rightarrow P_v)dP_0 dP_1 \cdots dP_{v-1}$$

If the source is known, the only problem is the transfer probability ; in fact, P is represented by the position r, the direction Ω and the energy E. In the multigroup simulation, the energy E will be represented by the group number g and we can rewrite the transfer probability as,

$$K(\mathbf{r}', \Omega', g' \rightarrow \mathbf{r}, \Omega, g)$$

It is clear that only the neutron having the direction $\frac{\mathbf{r}'-\mathbf{r}}{|\mathbf{r}'-\mathbf{r}|}$ can have the next collision at r. With the Monte Carlo method, this transfer probability is simulated by the samplings of the free path and the collision neutron-material. For a neutron at $\mathbf{r}'$, the probability to travel without collision a distance between ρ and $\rho+d\rho$ is :

$$p(\rho)d\rho = \Sigma_T e^{-\Sigma_T \rho} d\rho$$

Σ_T is the total macroscopic cross section of the composition at $\mathbf{r}'$.

This equation allows us to sample the neutron free path by :

$$\rho = -\frac{1}{\Sigma_T}\ln(1-\xi), \quad \xi \text{ is the random number between 0 and 1.}$$

The direction after collision is sampled according to the anisotropic distribution and the energy after collision will be determined either by the well known formula or according to the transfer matrix.

From the above description, we can see that the difference between the simulations with multigroup model and with probability tables model is just the cross sections which are used to simulate the free path and the collision neutron-matter :

Multigroup - Σ_T will be represented by $\Sigma_{T\,g}$ in group g for all free paths and collisions ;

Probability tables - Σ_T will be represented by $\Sigma_{T\,g\,PT}$ in group g for present free path and collision.

In table 2, we will compare the simulation schema with the two models.

Table 2 Monte Carlo neutron transport simulation schema with multigroup cross sections and probability tables cross sections

Multigroup

1) sample the neutron source (r, Ω, E) ;
2) find the energy group g and the total macroscopic cross section $\Sigma_{T\,g}$;
3) sample the free path ρ ;
4) calculate the new position of the neutron r' ;
5) sample the collision isotope, $p_i = \frac{\alpha_i \sigma_{ti\,g}}{\Sigma_{T\,g}}$,

i : isotope number,
α_i : number of atoms of isotope i ;

6) sample the reaction type, $p_x = \frac{\sigma_{xi\,g}}{\sigma_{ti\,g}}$,

x : reaction type ;
7) sample the direction after collision ;
8) calculate or sample the energy after collision ;

repeat from 2) or continue a new neutron if the history of the old neutron is finished.

Probability Tables

1) sample the neutron source (r, Ω, E) ;
2) find the energy group g ;
3) sample the cross section step for each isotope of the composition according to the probability p_i of each step (see table 1) ;
4) calculate the total macroscopic cross section $\Sigma_{T\,g} = \sum_{i=1}^{M} \alpha_i \sigma_{ti\,g\,b_i}$,

M : number of isotopes in the composition,
i : isotope number,
α_i : number of atoms of isotope i,
b_i : step number of the isotope i ;

5) sample the free path ρ ;
6) calculate the new position of the neutron r' ;
7) sample the collision isotope, $p_i = \frac{\alpha_i \sigma_{ti\,g\,b_i}}{\Sigma_{T\,g}}$;
8) sample the reaction type, $p_x = \frac{\sigma_{xi\,g\,b_i}}{\sigma_{ti\,g\,b_i}}$,

x : reaction type ;
9) sample the direction after collision ;
10) calculate or sample the energy after collision ;

repeat from 2) or continue a new neutron if the history of the old neutron is finished.

Example 1 : Study of the influence of energy group structure.

The influence of the number of energy groups in the multigroup-probability table model and in the traditional multigroup model is studied by the calculation of the transmission probability of an iron slab (number of atoms per 10^{-24} cm^3=0.0846) in the two models.

The neutron source is placed on the left side of an iron slab and normalised to unity, the energy distribution of source is uniform between 2.019MeV and 1.653MeV, the results between 2.019MeV and 9.12keV are calculated by using 27, 54, 108, 216, 432, 1296, 2592 groups in the multigroup-probability table model (cross section library ENDF/B6) and 106, 2400 groups in the multigroup model (cross section library UKNDL).

The table 3 gives the multigroup-probability table calculation results and the table 4 gives the multigroup calculation results, the comparison of the results is shown in figure 2.

Table 3.Multigroup-probability table calculation results.

d (cm)	10		50		100	
27grs	0.961	0.34+	0.952	0.75	0.940	0.91
54grs	0.998	0.29	1.005	0.63	1.000	0.98
108grs	0.998	0.29	1.005	0.63	1.009	0.82
216grs	1.002	0.30	0.995	0.53	1.017	0.79
432grs	1.000	0.27	1.000	0.72	1.009	0.90
1296grs	1.004	0.28	1.005	0.59	1.026	0.80
2592grs	1.000*	0.31	1.000	0.61	1.000	0.90

*The calculation of 2592 groups is considered as the reference, the values in the table are the relatif results by comparing with the reference.
+ Statistic error in %.

Table 4. Multigroup calculation results

d (cm)	10		50		100	
106grs	0.93	0.64+	0.74	1.01	0.49	1.04
2400grs	1.00*	0.54	1.00	1.01	1.00	0.73

*The calculation of 2400 groups is considered as the reference, the values in the table are the relatif results by comparing with the reference.
+ Statistic error in %.

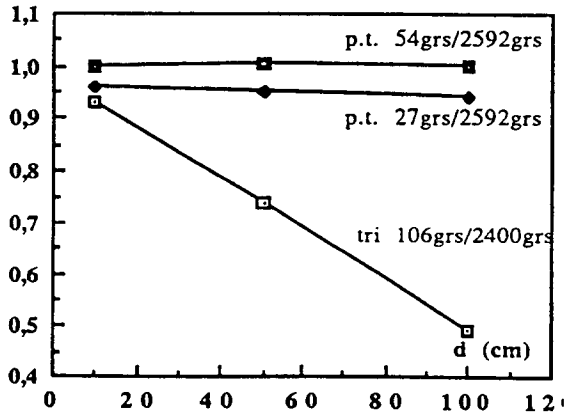

Figure 2. Influence of the number of energy groups in the two models (multigroup and multigroup-probability table)
p.t.---Probability table, tri ---TRIPOLI-3(multigroup)

From the results of this example, it is demonstrated that the influence of the number of energy group is very important in the multigroup model at great distance but not in the multigroup-probability table model because the self-shielding effet has been properly treated by the probability table. In practice, the probability table with a reasonable number of energy group will be very interesting for a calculation at great distance.

Example 2 : ASPIS benchmark.

The second example is a neutron deep penetration in iron benchmark experiment ASPIS[6] which has been carried out at AEA Winfrith to contribute to the OECD (NEA) Collaborative Benchmark Exercise on assessing the nuclear data requirements for radiation shielding.

The figure 3 shows the configuration of the experience. A low power natural uranium converter plate, driven by the source reactor NESTOR, provided a large thin disc source of fission neutrons at the interface of a graphite moderator and a extensive iron shield. The converter plate consisted of a fissile section of 50.8 cm square by 3.18 mm thick; the total power of the converter plate is $7.26 \times 10^{-4} \pm 5\%$ watt per Nestor Watt and the fission rate at the centre of the converter plate was $3.346 \times 10^{3} \pm 5\%$ fission/(sec cm^2 Nestor Watt), the spatial distribution of the fission rate in the converter plate is a cosine function of width 142.9 cm and the equivalent area disc has a radius of 59.3 cm.

$$f(r) = 3.346\,\bar{\nu}_{25}\cos\left(\frac{\pi r}{142.9}\right) \pm 5\% \quad \text{(neutron } s^{-1}\ cm^{-2}\text{/Nestor Watt)}$$

where $\bar{\nu}_{25}$ is the average number of neutrons provided by each fission of U235.

Three detectors are used to measure the neutron reaction rates, Rh103(n,n')Rh103m (threshold 100keV), In115(n,n')In115m (threshold 300keV) and S32(n,p)P32 (threshold 2MeV), all results of the measure are given in 10^{24} d.p.s./Nestor Watt ; the estimated standard deviation of each detector is ±3% for Rh103nn', ±2% for In115nn' and ±4% for S32np.

The calculations have been done with the probability tables and multigroup method. To the first one, only the 315 energy groups structure is used, to the second one, the 315 groups and 3857 groups structures (3592 groups above 9.12keV) are used, the 3857 groups structure gives a negligible error due to the energy collapsing. The comparison of the calculation and the experience is showed in figure 4 and the neutron spectra are showed in figure 5.

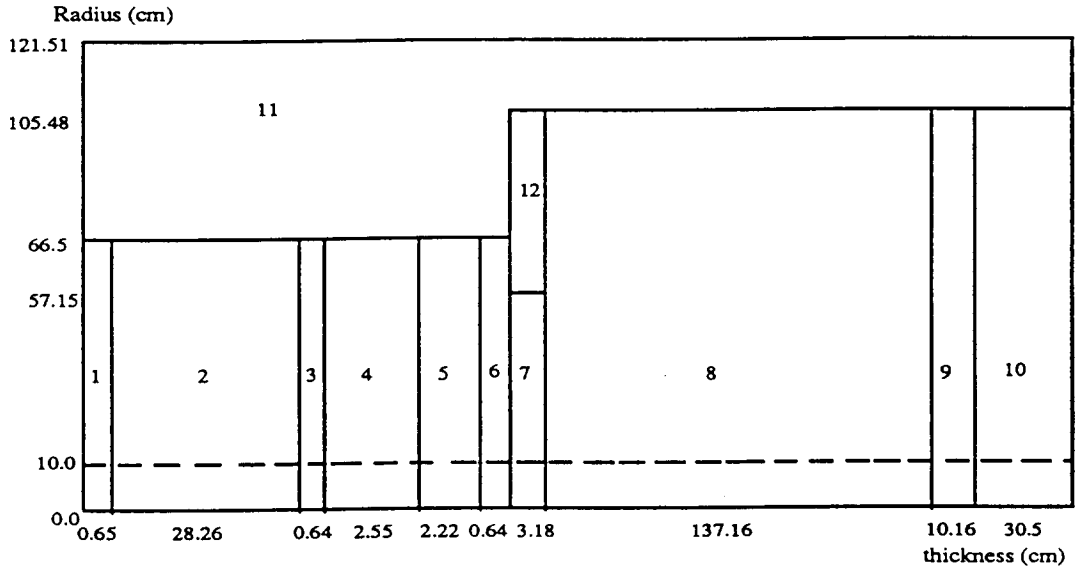

Fig.3 Configuration of the benchmark ASPIS

1, 3, 7: Aluminium 2.Carbon, 4, 6: Air, 5: Converter plate,
8: Iron shield, 9, 12: Mild steel, 10, 11: Concrete.

From the results of the ASPIS benchmark calculations, we can conclude that a 315 group structure is not sufficient to process deep penetration problems for neutrons. The results are improved with probability tables or 3857 group structure which gives a negligible error due to the energy group collapsing.

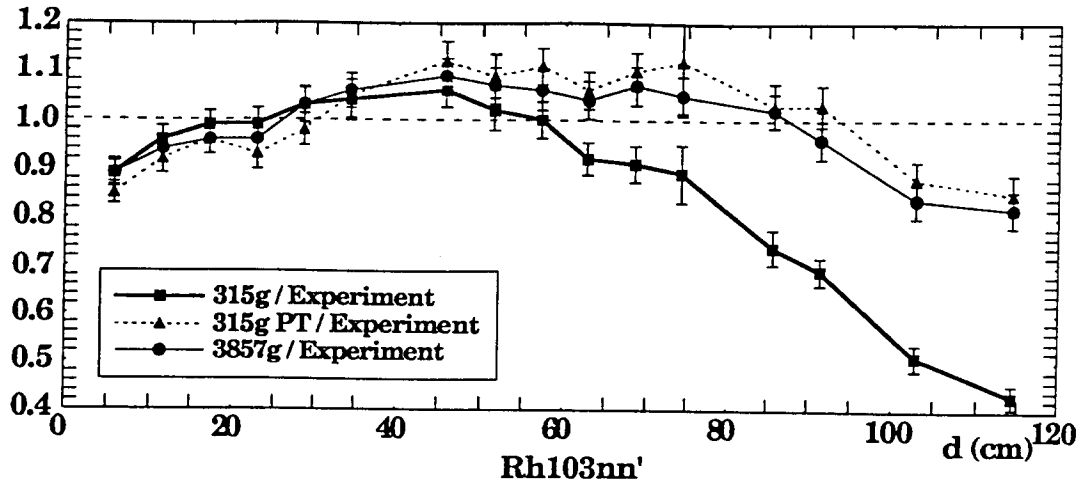

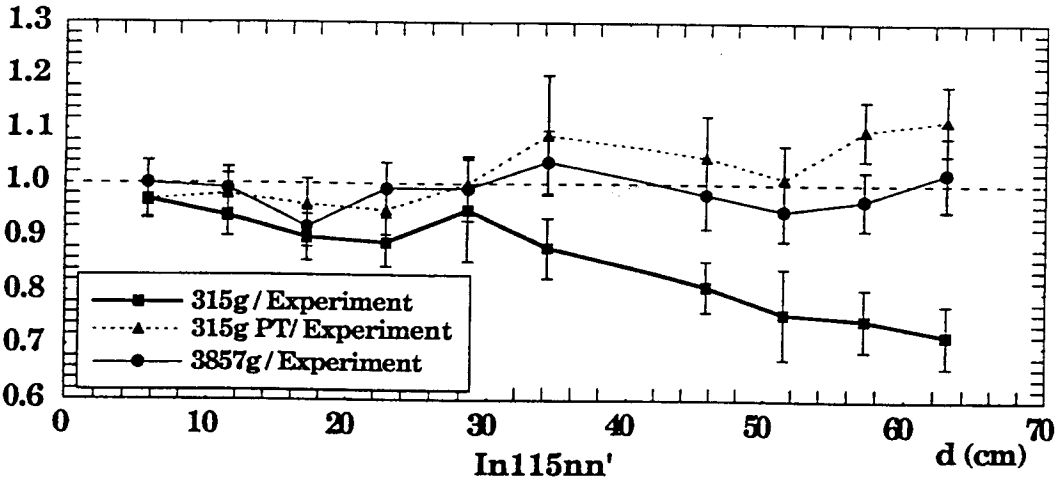

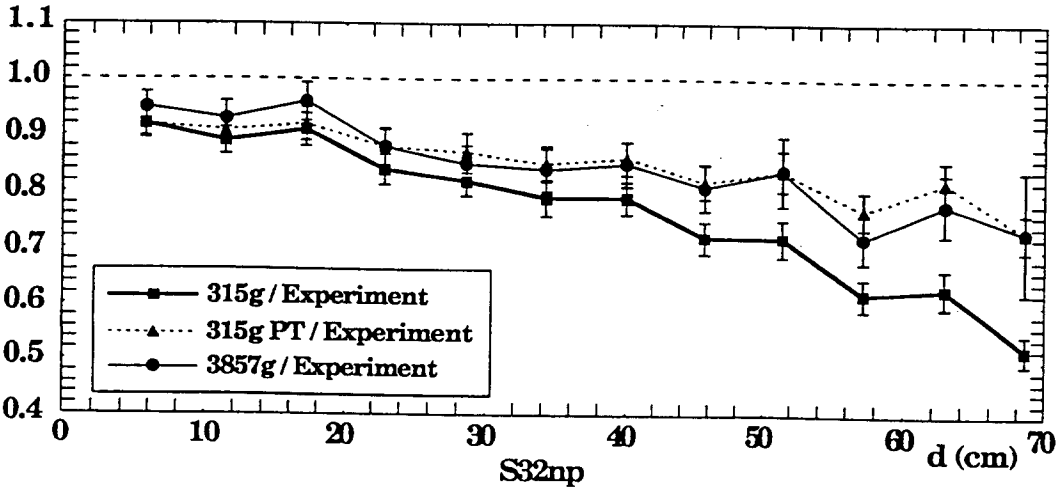

Fig.4 Results of ASPIS benchmark

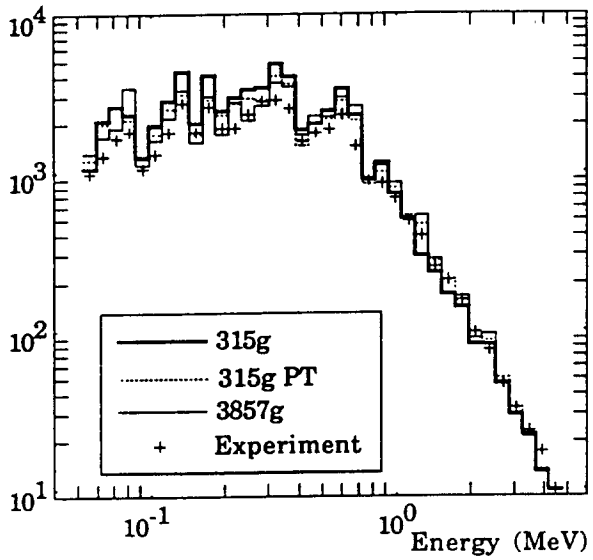

d=22.86cm

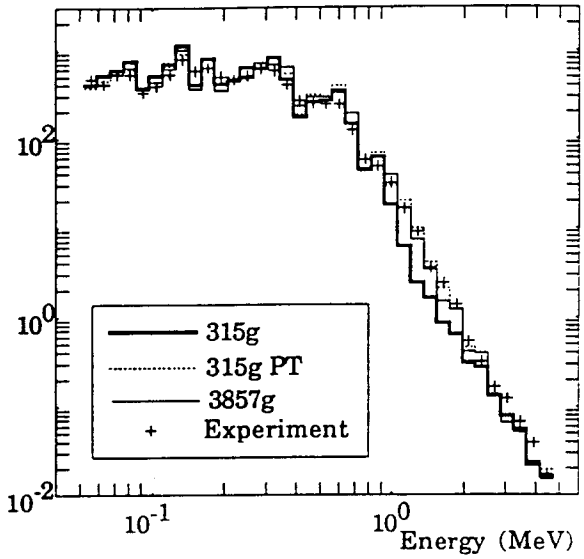

d=57.72cm

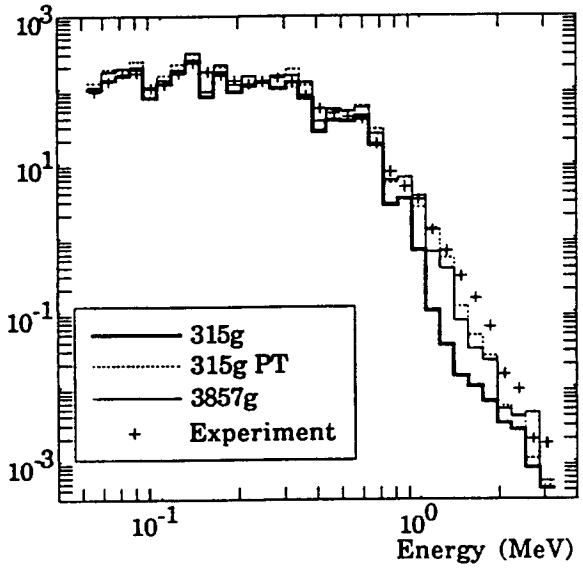

d=85.73cm

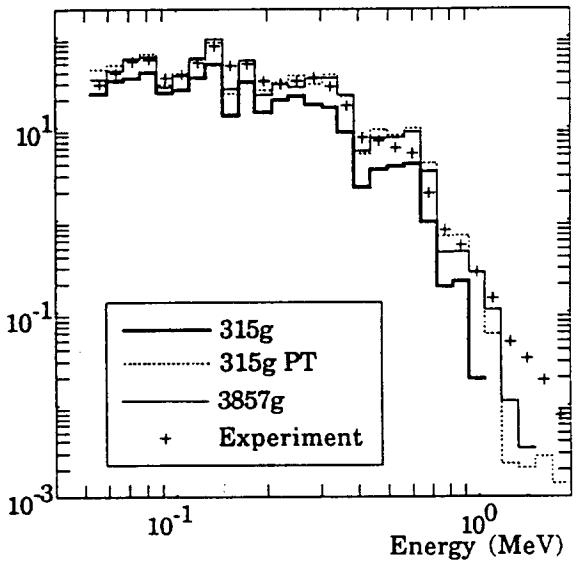

d=114.30cm

Fig.5 Neutron spectra of the ASPIS benchmark

Example 3 : Comparison of "Probability tables" and "Pointwise" cross sections

In the two first examples, we have compared the multigroup method and the probability table method, they have showed the advantages of the probability tables. But which energy groups structure we need with the probability tables ? To answer this question, it is necessary to compare with the "pointwise cross sections" results[7] which can be considered as a reference because there is no error due to the energy group collapsing.

We take the geometry of example 1, but the neutron source is uniform between 4.4933 and 4.0657MeV, the neutron currents between 4.4933MeV and 9.12keV and the neutrons soectra in 41 groups (energy limites are showed in table 5) are obtained. The cross sections are taken from ENDF/B6 FE56.

The probability tables with 315 (122 groups between 4.4933MeV and 9.12 keV, the total number of steps is about 600) and 3857 groups (2928 groups between 4.4933MeV and 9.12 keV, the total number of steps is about 6000) have been used in the calculations. In order to test the effect of the cross sections, two calculations with the pointwise cross sections (about 27000 points between 4.4933 MeV and 9.12 keV) have also been done, one with the anisotropic distribution represented in 315 groups and the other in 3857 groups. The results are given in table 6, the comparison of the neutrons spectra are showed in Fig.6.

Table 5 Energy limites to obtain the neutrons spectra (in MeV)

4.4930E+00	3.3290E+00	2.8650E+00
2.4660E+00	2.3460E+00	2.1220E+00
1.8270E+00	1.5720E+00	1.3530E+00
1.1650E+00	9.6160E-01	8.2090E-01
7.0650E-01	6.0810E-01	5.2340E-01
3.8770E-01	3.0200E-01	2.9450E-01
2.4720E-01	2.1280E-01	1.8320E-01
1.5760E-01	1.3570E-01	1.1680E-01
8.6520E-02	7.9500E-02	6.7380E-02
5.5170E-02	4.6310E-02	3.6980E-02
3.1620E-02	2.9010E-02	2.7380E-02
2.6060E-02	2.4790E-02	2.3580E-02
2.1870E-02	1.9950E-02	1.6620E-02
1.3830E-02	1.1140E-02	9.1200E-03

Table 6 Comparison of the calculational results with probability table cross sections and pointwise cross sections

d (cm)	3857 groups		315 groups	
	PT/Pointwise	σ (%)	PT/Pointwise	σ (%)
10	0.9995	0.07	1.0009	0.07
20	1.0004	0.10	1.0026	0.10
30	1.0000	0.13	1.0043	0.13
40	1.0009	0.16	1.0036	0.16
50	1.0004	0.17	1.0014	0.17
60	1.0004	0.18	0.9979	0.18
70	1.0015	0.19	0.9951	0.20
80	1.0028	0.20	0.9909	0.21
90	1.0020	0.20	0.9873	0.21
100	1.0016	0.20	0.9867	0.19

Fig.6 Neutrons spectra of the "P.T." results (3857 groups) and "Pointwise" results

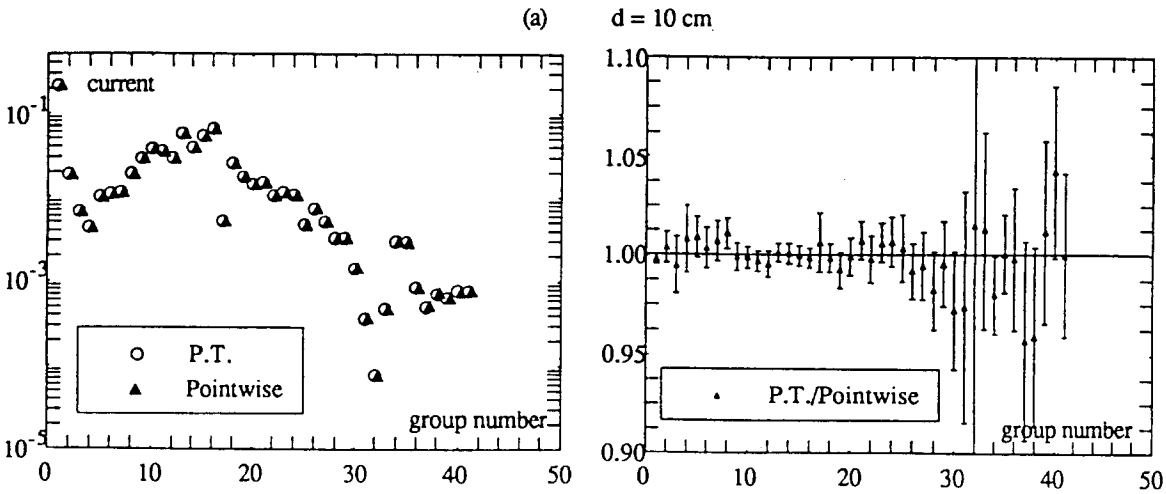

(b) d = 100 cm

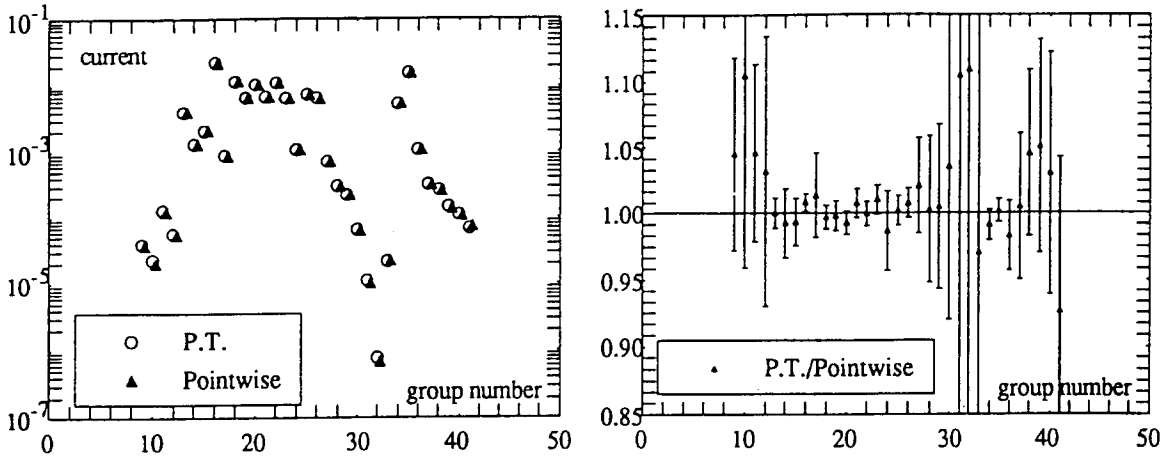

From the table 6 and Fig.6, we can see that the 3857 energy groups structure with probability tables and the pointwise cross sections give almost the same total currents in all distance and the neutrons spectra are very similar if we consider the statistic errors, the two methods have represented correctly the neutron cross sections and they can be used as reference. The 315 groups structure is not so good as 3857 groups structure, specially at great distance, but it is always acceptable for the project calculations.

CONCLUSION

The probability table method has been proved to be very effective to describe the fluctuation of the neutron cross sections, it can be used not only in the unresolved resonance range but also in the resolved range and the non-resonance range. With this method and the general geometry definition and specially the biasing techniques, the Monte Carlo code TRIPOLI-3 will be able to treat the complicate problems, where the self-shielding effect is very important, without using the pointwise cross sections.

REFERENCES

1. M.N.Nicolaev et alii, " Méthode des Sous-groupes pour la prise en compte de la structure résonnante des sections efficaces dans les calculs neutroniques (1ère partie)", Atomnaïa Energïa (1970).
2. L.B.Levitt, "The probability tables method for treating unresolved neutron resonances in Monte Carlo calculations", Nucl. Sci. Eng. 49, 450-457 (1972).
3. P.Ribon, J.M.Maillard, "Les tables de probabilité, application au traitement des sections efficaces pour la neutronique", Note CEA-N-2485, Jun. 1986.
4. P.Ribon, "Les tables de probabilité statistiques: le programme CALENDF", séminaire OCDE/Banque de données, AEN, saclay, 20-21 juin 1989.
5. J.C.Nimal et al., "Le programme de Monte Carlo polycinétique à trois dimensions TRIPOLI3", CEA to be published.
6. A.McCracken, "The establishment of a shielding experimental benchmark at the NEA Data Bank, NEACRP-A-1044, june, 1990.
7. B.Morillon, Private communication.

MONTE CARLO VALIDATION OF SELF SHIELDING AND VOID EFFECT CALCULATIONS

H. TELLIER, M. COSTE, C. RAEPSAET, M. SOLDEVILA and C. VAN DER GUCHT

Service d'Etudes de Réacteurs et de Mathématiques appliquées
Centre d'Etudes de Saclay - 91191 GIF-SUR-YVETTE - France

INTRODUCTION

Because it would be too expensive in computer time and memory, the representation of the cross section behaviour with a fine energy mesh in the resonance energy range is impossible to use for daily reactor core calculations. Thus the physicist must adopt a much broader energy mesh and the effective cross section concept. This is the self shielding formalism. With the new generation of reactor physics codes, it is now possible to compute the space and energy dependence of the heavy nucleus resonant absorption inside the rod of a heterogeneous lattice. Then the problem becomes the validation of the computed results which are obtained with the new self shielding formalism. As it does not exist any experimental result, very detailed and sophisticated calculations which can be used as reference ones are needed. The Monte Carlo method with a continuous energy description of the neutron data is a very efficient tool to generate such reference calculations. A slowing down calculation with a very fine multigroup mesh is also interesting. In the frame of the qualification of the new assembly code APOLLO 2 [1] which solves the Boltzmann equation in the multigroup approximation by the collision probability method, we have made a comparison between the resonant absorption rates which were deduced from a self shielding calculation and the ones given by the reference computations, the slowing down and the Monte Carlo calculations. We were interested in the heavy nuclei which are the most self shielded, uranium 238 and thorium 232 and the ones which have a large resonance in the thermal range, plutonium 240 and plutonium 242.

The cell geometry which is used in this validation is the one of a typical pressurized reactor and corresponds to an infinite array of infinitely long cylindrical cells. The pin is divided into ten concentric areas of equal volume, the clad is constituted by one area and the moderator by two areas [2]. To avoid the interference effects between the resonances of the fuel and the ones of the clad, the latter is made of aluminium and the fuel contents only one resonant nucleus the chimical compound of which is dioxide. All the neutron cross sections come from ENDF/B5 and were processed by NJOY. The temperature is equal to 300 K for all the components. With this geometry and this composition we made a source calculation. The neutron source is a lethargy independent source between 3.35 and 2.25 keV. The neutrons are uniformly and isotropically emitted in the whole moderator. To remove the effects of the transients, the absorption rates are renormalized to one neutron slowed down below 1.507 keV (0.914 keV in the case of plutonium 242 which has a smaller resolved resonance range). The qualification is divided into two parts: the epithermal range where it only exists slowing down effects and the thermal range where thermalization phenomenon and up scattering exist.

There is another case, which is important for safety reason, where we have a lack of experimental results. It is the void effect. That is why we use Monte Carlo results as a "numerical experiment" to assess the void calculation carried out with routine code. We will give an example of such an use of the Monte Carlo method.

SELF-SHIELDING IN THE EPITHERMAL RANGE

In this energy range, we are in a pure slowing down process and we have two different reference calculations at our disposal. The first one is a multigroup slowing down computation with a very fine energy mesh (about 9,000 groups), this computation is performed with the SECOL code [3]. The second one is a continuous energy Monte Carlo calculation carried out with the TRIPOLI code [4]. If t represents the total absorption of the cell above the threshold (generally 1.507 keV in our computation) and R the absorption of the heavy nucleus for a given energy range below the threshold (one group or the entire energy range) the renormalized absorption A of the heavy nucleus is

$$A = \frac{R}{1 - t}$$

For a deterministic calculation (slowing down or self-shielding) t and R are separately known. In a Monte Carlo calculation R and t are known with a standard deviation dR and dt. Although these standard deviations are not independent we have adopted an uncertainty on the renormalized absorption defined by

$$\frac{dA}{A} = \frac{dR}{R} + \frac{dt}{t}\frac{t}{1 - t}$$

As t is small (between 3.10^{-2} and 4.10^{-2}) it is the first component which is predominant.

For each type of computation we have obtained the space and energy dependence of A. The spatial mesh corresponds to the ten concentric areas of the pin and the energy mesh to the group structure of the 172 group European library. The dependences obtained in the slowing down or self shielding calculations are checked against the Monte Carlo results. For this calculation 200,000 neutron histories were concerned. Tables I to IV give the spatial dependence of the heavy isotope absorption, in unit 10^{-5}, and the differences with the SECOL and APOLLO 2 results. It can be seen that in all the cases the slowing down calculation perfectly reproduces the absorption distribution inside the pin. But, if the APOLLO 2 computation gives the right value for the total absorption of the whole pin, it does not always reproduce correctly the gradient and a small shift appears. A detailed study of the energy dependence of the absorption indicates that this effect comes from peculiar resonances, the ones which have a very large reduced neutron width. For such resonances the absorption computed by the self shielding formalism is too high in the peripheral area of the pin and too low in the central area, and it exists more or less a compensation. This effect is well visible in the case of the 36,7 eV resonance of uranium 238. As an example the figures 1 and 2 show the comparison between the absorption rate of SECOL or APOLLO 2 with the Monte Carlo result in the peripheral area. The hatched area represents plus or minus the standard deviation dA. Similar effects exist for the 69.2 eV resonance of thorium 232 and 66.2 eV resonance of plutonium 240 but the magnitudes are smaller because the energy of these resonances is higher than for the uranium 238. Nevertheless this smaller effect is observable as it can be seen on figures 3 and 4.

SELF-SHIELDING IN THE THERMAL ENERGY RANGE

In the thermal energy range, below a few electron-volts, the multigroup library mesh is finer than in the epithermal range. Nevertheless this mesh is not fine enough to avoid the self-shielding effect. In addition this energy domain is sensitive to thermalization and up scattering. Consequently we cannot use as reference a pure slowing down calculation like in the SECOL code and only a continuous energy Monte Carlo code is convenient. As the actual version of TRIPOLI has a multigroup neutron library below 5 eV, we used for reference another Monte Carlo code which has a pointwise library in the thermal range: MCNP [5]. The MCNP library is also deduced from the ENDF/B5 evaluation and it is possible to make comparisons with the other calculations which use the same basic neutron data. In order to assess the influence of the homogeneous-heterogeneous equivalence in a thermal energy range self shielding calculation, we studied with the same source calculation as in the epithermal range a homogeneous mixture prior to the heterogeneous cell. This mixture has a ratio H/Pu equal to 4.65 which corresponds to a 100 barn background cross section. For each nucleus, plutonium 240 and plutonium 242, we performed four

absorption rate computations: a slowing down calculation with SECOL, a self shielding calculation with the most sophisticated option of APOLLO 2 (self shielded removal matrix used in the flux calculation), and two Monte Carlo calculations. The first is a 200,000 neutron history TRIPOLI computation, (Monte Carlo 1) the second a 500,000 neutron history MCNP run (Monte Carlo 2). The heavy nucleus absorption rate is splitted into two components: the epithermal domain above 5 eV and the thermal one below 5 eV. We took advantage of the homogeneous calculation to compare the four results in the epithermal range. In the thermal range only APOLLO 2 and MCNP can be used. The results are given in table V. They are very satisfactory, for both energy ranges. In particular we have a very good agreement between the two Monte Carlo calculations in the epithermal range, for the total absorption as well as for the energy dependence. In the thermal range, the self shielding results are within the 2 σ uncertainty of the Monte Carlo values for the two nuclei. It is a very good qualification of the APOLLO 2 in the thermal range. The figure 5 represents the variation of the Plutonium 240 absorption rate per lethargy unit between 0.3 and 4.0 eV. The agreement between APOLLO 2 and MCNP is good and constitutes a justification of the computation scheme used in APOLLO 2.

As the qualification results are satisfactory in the homogeneous case, the same validation was extended to the heterogeneous case of the PuO_2 rod. This study is underway and the preliminary results are given in table VI. In the energy range where they have both pointwise libraries, above 5 eV, the results of TRIPOLI and MCNP are very similar. This agreement can be seen on figure 6 which displays, in unit 10^{-5}, the difference between the spatial distribution of the absorption rates which are obtained with the two Monte Carlo codes. The figure 7 represents the same kind of comparison for the energy dependence. The hatched area corresponds to

$$\Delta A = (\sigma^{2}_{TRIPOLI} + \sigma^{2}_{MCNP})^{1/2}$$

VOID EFFECT CALCULATION

The importance of the void coefficient was enhanced with the new concept of tight pitch lattices or spectral shift reactors. As these cores content a high amount of plutonium, the stabilizing effect of uranium 238 can be more or less compensated by the opposite effect of the odd isotopes of plutonium, in case of coolant loss. For safety reasons it is important to know the void coefficient value with a very good accuracy. In routine computations the reactor core parameters are obtained with a multigroup transport code, such as APOLLO 2. These transport codes are well qualified for thermal neutron reactor in normal operating conditions. It is not yet the case in accidental conditions in which can appear very hard neutron spectrum or even together the hard and normal spectra in case of local voidage. Up to now, no experimental results exist to assess the validity of a APOLLO 2 calculation in this situation. That is why a numerical simulation can be used to solve the problem and a Monte Carlo computation can give a reference value. In order to obtain this reference, an important set of Monte Carlo calculations was performed with TRIPOLI. The starting point is a standard 17 x 17 light water reactor assembly, the fuel of which contains 5.3 % of first generation plutonium. This assembly is considered as infinite in the axial direction and the albedo is equal to one for the two radial directions. To simulate the partial voidage, calculations were performed with successively 1, 9, 25, 49, 81 and 121 cells without moderator. In each case the infinity multiplication coefficient was obtained with a standard deviation of 0.2 % that corresponds roughly to 300,000 neutron histories. The numerical results are displayed by the figure 8 with a 2 σ uncertainty. The average void coefficient is - $140.10^{-5}/\%$. These results will be compared with APOLLO 2 calculations. But do not forget that the TRIPOLI library is a point wise one only in the resolved resonance energy range. In the unresolved resonance energy domain it is a multigroup library which represents the average cross sections and does not account for the self shielding effects, even if they are small. The introduction of the probability table in this energy range, which is underway, will be a strong improvement in the use of Monte Carlo calculation for void effect reference.

CONCLUSION

The self shielding validation and the void effect study are two examples among others of the importance of the Monte Carlo method for physics reactor code development. In well defined conditions, this computation technics is a very efficient tool to generate reference calculations when experimental results are not available or impossible to obtain. The satisfactory comparison obtained between the APOLLO 2 results of the self shielding effect and the TRIPOLI and MCNP results allows us to be confident in the multigroup transport code. Without Monte Carlo calculation it would not be possible to qualify the APOLLO 2 formalism. As now the Monte Carlo codes can be run on working station, they will become more and more useful in neutron physics. But, in order to become a universal reference calculation some improvements must be done for the unresolved resonance range treatment. The use of the probability table technics seems to be encouraging.

ACKNOWLEDGEMENTS

The authors are indebted to P. YOUNG and R. SEAMON from LOS ALAMOS who provided the Pu 240 and Pu 242 libraries for MCNP calculations. Thanks to this cooperation, the authors had the possibility to use strictly the same neutron data in all the codes, the results of which are thence rigorously comparable.

REFERENCES

1 - R. SANCHEZ, M. COSTE, Z. STANKOVSKY and C. VAN DER GUCHT: "Models for multigroup self-shielded cross section calculations in the code APOLLO 2". Physor, Marseille, Vol III, P II, **149** (1990).

2 - H. TELLIER, M. COSTE, C. RAEPSAET and C. VAN DER GUCHT: "Heavy Nucleus Resonant Absorption Calculation Benchmarks". Nucl. Sci and Eng. **113**, 20 (1993).

3 - M. LIVOLANT and F. JEANPIERRE: "Autoprotection des résonances dans un réacteur nucléaire". Rapport CEA-R-4533 (1974).

4 - J.C. NIMAL, A. BAUR, G. DEJONGHE, J. GONNORD, A. MONNIER and T. VERGNAUD: "TRIPOLI: Energy dependant three dimensional Monte Carlo programm". Report ORNL-OLS-80-110 (1980).

5 - J.F. BRIESMEISTER: "MCNP: A general Monte Carlo code for neutron and photon transport". Report LA-7396-M (1986).

TABLE I
Uranium 238

Area	Monte Carlo	S - T	A2 - T
1	1432 ± 17	- 10 ± 17	- 21 ± 17
2	1460 ± 16	- 5 ± 16	- 19 ± 16
3	1499 ± 15	- 6 ± 15	- 21 ± 15
4	1546 ± 15	- 5 ± 15	- 23 ± 15
5	1597 ± 15	+ 1 ± 15	- 19 ± 15
6	1673 ± 17	0 ± 17	- 23 ± 17
7	1787 ± 17	+ 10 ± 17	- 36 ± 17
8	1944 ± 18	- 2 ± 18	- 30 ± 18
9	2269 ± 22	+ 23 ± 22	+ 17 ± 22
10	4374 ± 44	+ 11 ± 44	+ 66 ± 44
1 to 10	19 582 ± 144	+ 3 ± 144	- 113 ± 144

Spatial dependence of the uranium 238 absorption for neutron energies between 2.7 and 1507 eV obtained in the TRIPOLI calculation and comparison with the SECOL and APOLLO 2 results.

TABLE II
Thorium 232

Area	Monte Carlo	S - T	A2 - T
1	856 ± 11	- 4 ± 11	- 7 ± 11
2	879 ± 10	- 7 ± 10	- 10 ± 10
3	905 ± 10	- 8 ± 10	- 10 ± 10
4	928 ± 10	0 ± 10	- 1 ± 10
5	972 ± 10	- 2 ± 10	- 3 ± 10
6	1031 ± 11	- 5 ± 11	- 6 ± 11
7	1108 ± 11	+ 1 ± 11	0 ± 11
8	1235 ± 13	+ 11 ± 13	+ 9 ± 13
9	1506 ± 16	+ 11 ± 16	+ 10 ± 16
10	2392 ± 26	- 17 ± 26	- 40 ±26
1 to 10	11 812 ± 84	- 22 ± 84	- 61 ± 84

Spatial dependence of thorium 232 absorption between 2.7 and 1507 eV.

TABLE III
Plutonium 240

Area	Monte Carlo	S - T	A2 - T
1	1481 ± 13	+ 2 ± 13	- 2 ± 13
2	1512 ± 12	+ 3 ± 12	- 1 ± 12
3	1544 ± 12	+ 13 ± 12	+ 6 ± 12
4	1601 ± 12	0 ± 12	- 8 ± 12
5	1653 ± 12	+ 7 ± 12	- 4 ± 12
6	1736 ± 12	+ 3 ± 12	- 11 ± 12
7	1850 ± 13	0 ± 13	- 15 ± 13
8	2013 ± 14	+ 14 ± 14	0 ± 14
9	2373 ± 17	+ 8 ± 17	+ 13 ± 17
10	3711 ± 30	+ 18 ± 30	+ 16 ± 30
1 to 10	19 471 ± 108	+ 70 ± 108	- 5 ± 108

Spatial dependence of the plutonium 240 absorption between 5 and 1507 eV

TABLE IV
Plutonium 242

Area	Monte Carlo	S - T	A2 - T
1	736 ± 7	+ 8 ± 7	+ 12 ± 7
2	765 ± 7	- 1 ± 7	+ 4 ± 7
3	790 ± 6	- 2 ± 6	+ 1 ± 6
4	817 ± 7	- 1 ± 7	+ 3 ± 7
5	848 ± 7	+ 3 ± 7	- 7 ± 7
6	887 ± 7	+ 8 ± 7	+ 10 ± 7
7	948 ± 7	+ 6 ± 7	+ 6 ± 7
8	1033 ± 8	+ 5 ± 8	+ 1 ± 8
9	1166 ± 9	+ 9 ± 9	0 ± 9
10	1546 ± 12	+ 14 ± 12	- 1 ± 12
1 to 10	9537 ± 60	+ 48 ± 60	+ 43 ± 60

Spatial dependence of the plutonium 242 absorption between 5 and 914 eV

TABLE V
Homogeneous mixture - H/Pu = 4.65 - σ_e ~ 100 barns

Nucleus	Plutonium 240		Plutonium 242	
Energy range	5 - 1507 eV	0.3 - 5 eV	5 - 914 eV	0.3 - 5 eV
Slowing down	21 332	-	10 313	-
Self shielding	21 255	62 745	10 293	36 385
Monte Carlo 1	21 345 ± 103	-		
Monte Carlo 2	21 276 ± 49	62 887 ± 109	10 300 ± 35	36 302 ± 73

TABLE VI
Ten area PuO_2 rod

Nucleus	Plutonium 240		Plutonium 242	
Energy range	5 - 1507 eV	0.3 - 5 eV	5 - 914 eV	0.3 - 5 eV
Slowing down	19 541	-	9 586	-
Self shielding	19 466		9 580	
Monte Carlo 1	19 471 ± 108	-	9537 ± 60	-
Monte Carlo 2	19 391 ± 48	50 704 ± 107	9437 ± 35	31 878 ± 70

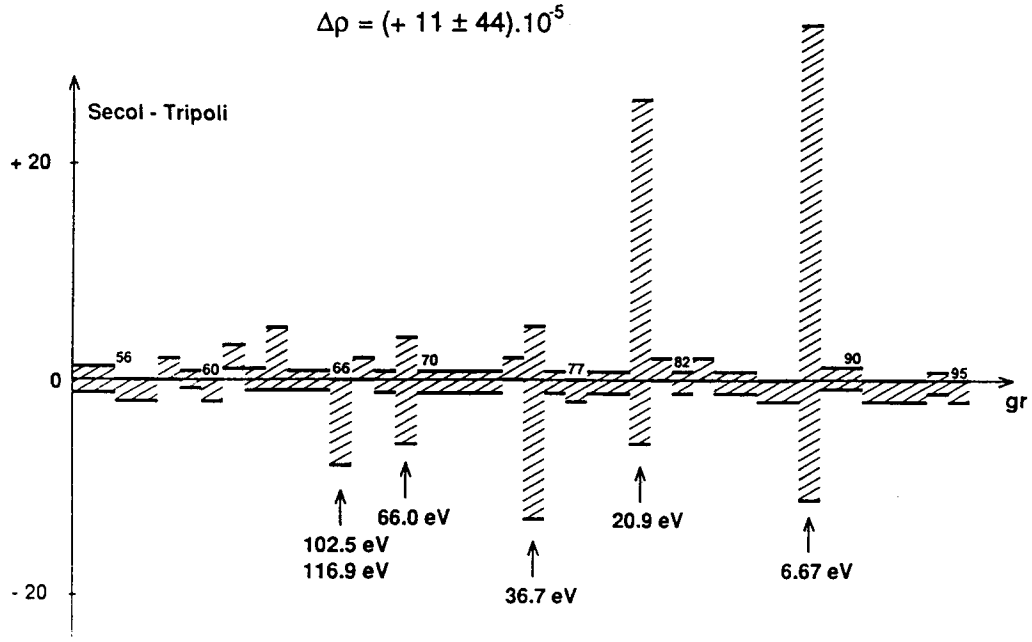

Figure 1

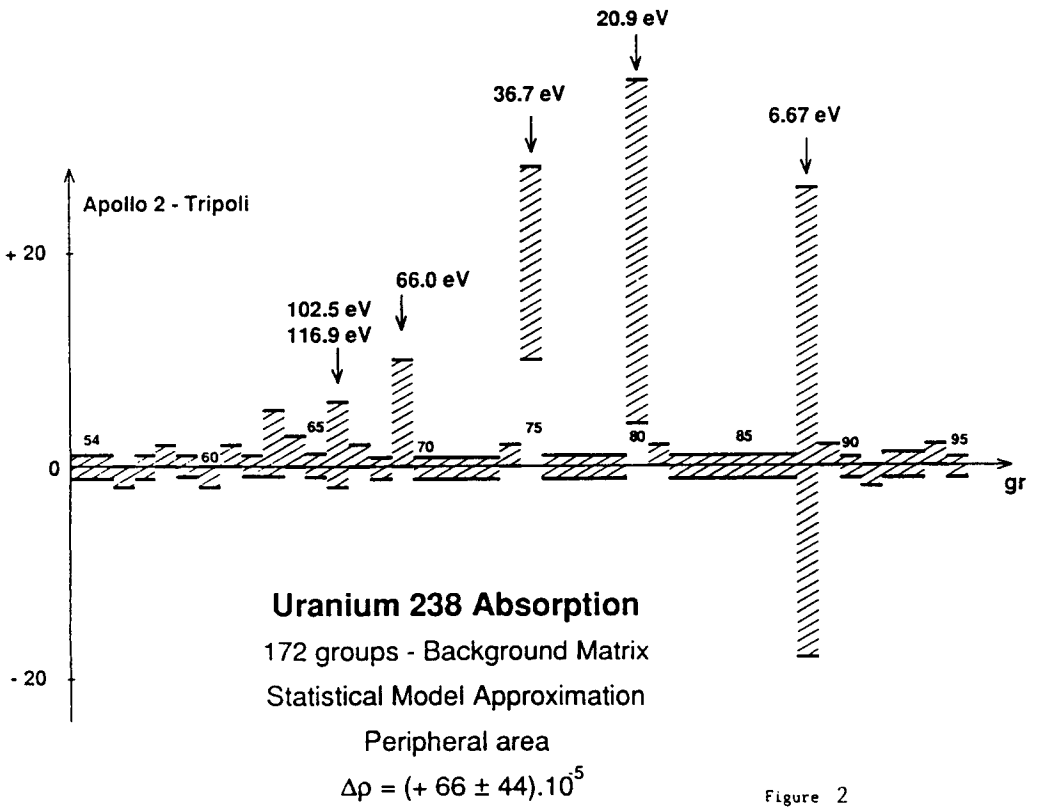

Figure 2

Thorium 232 Absorption

172 groups - Background Matrix

Statistical Model Approximation

Peripheral area

$\Delta\rho = (- 40 \pm 26).10^{-5}$

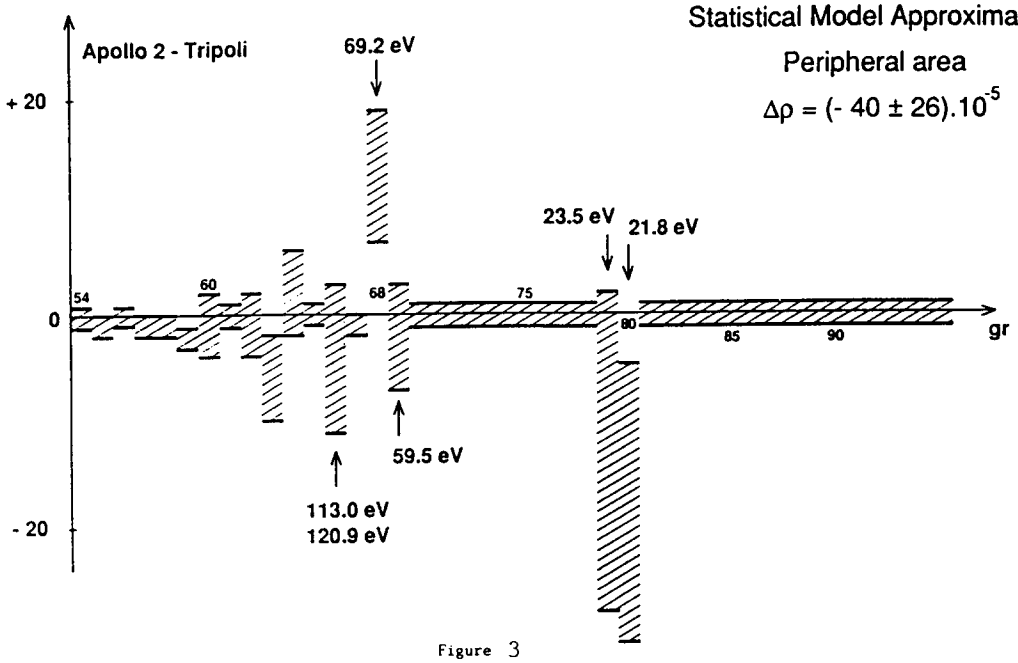

Figure 3

Plutonium 240 Absorption

172 groups - Background Matrix

Statistical Model Approximation

Peripheral area

$\Delta\rho = (+ 16 \pm 30).10^{-5}$

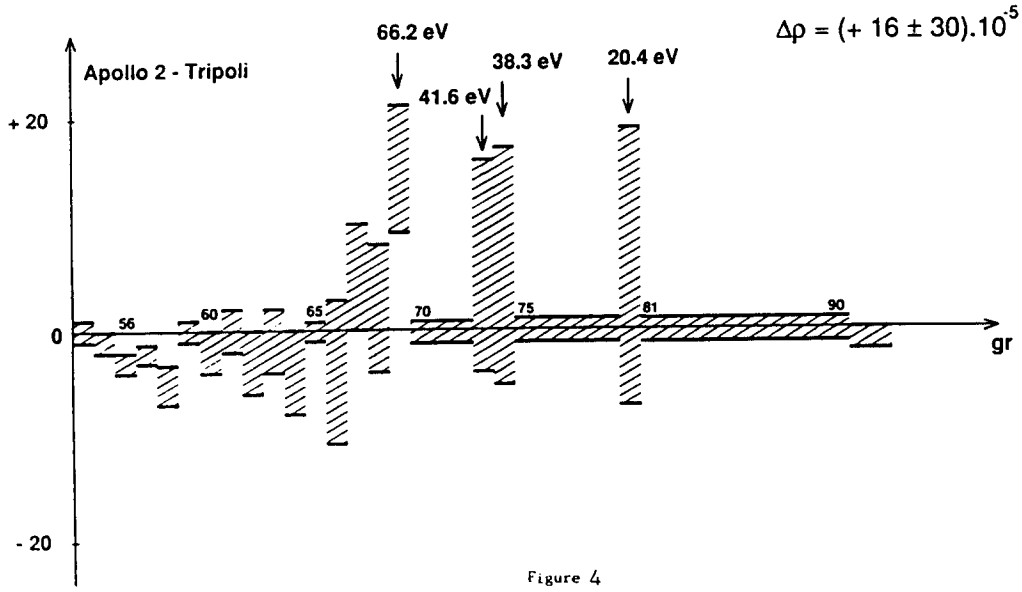

Figure 4

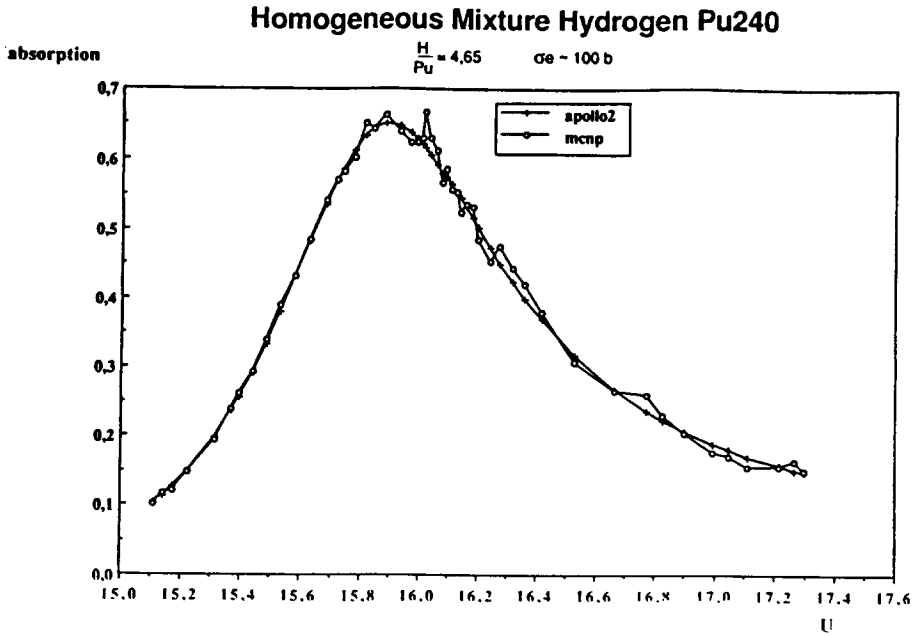

Figure 5

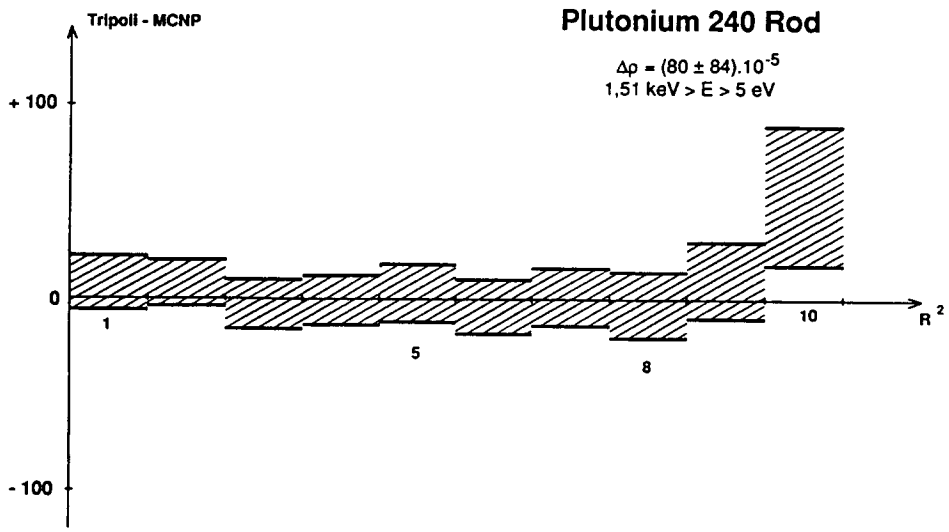

Figure 6

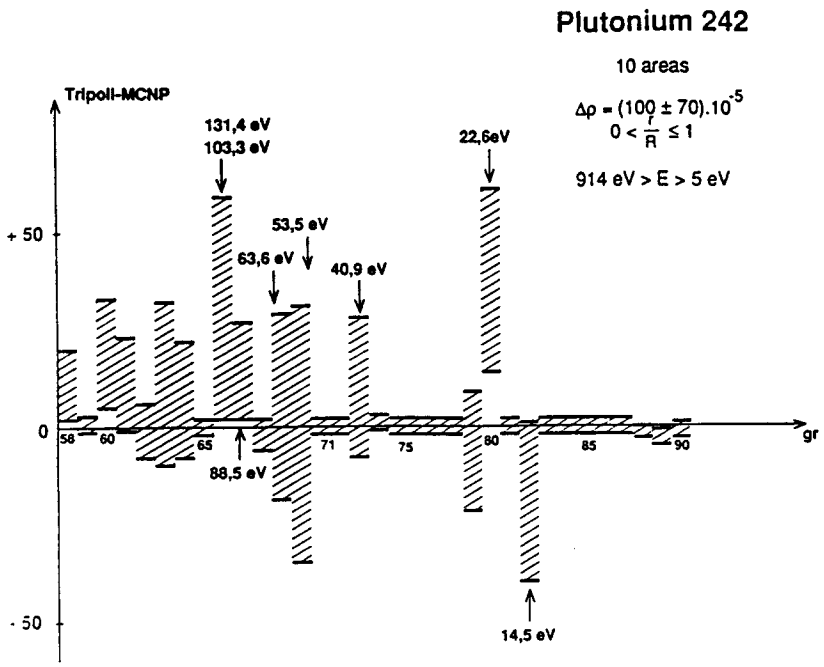

Figure 7

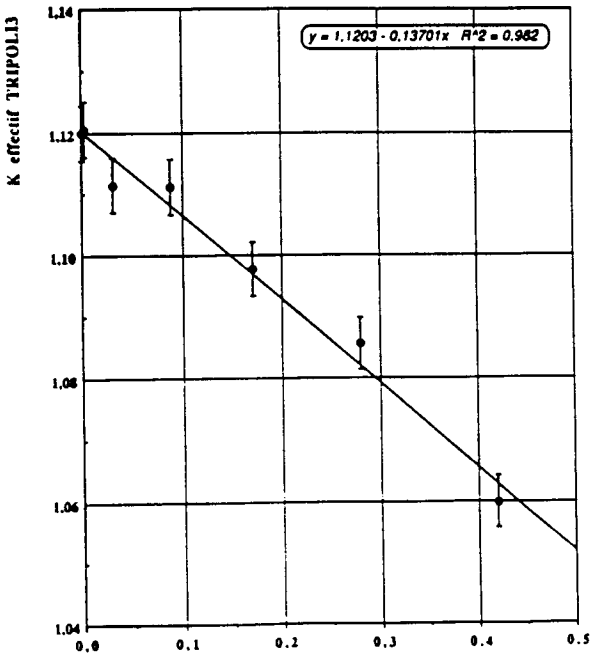

Progressive draining of a 17x17 mixed oxide lattice

Figure 8

STATISTICAL GENERATING THE NEUTRON CROSS SECTIONS IN THE UNRESOLVED RESONANCE ENERGY REGION FOR MONTE CARLO CALCULATIONS.

A.G. Sboev, M.B. Tsitovich

I.V. Kurchatov Institute of Atomic Energy
121182 Moscow

ABSTRACT

A method of statistical generating the neutron cross sections was developed for accuratly Monte Carlo treating neutron transport and self shielding effects in the unresolved resonance energy region. Cross sections are calculated by modelling the set of resonances for different resonance states in a energy point. The level spacing is simulated according to Wigner distributions, each width is distributed according to chi-squared distribution with a desiguated in ENDF/B number of degrees of freedom. In the case of U^{238} the calculations of well known cells NB1,NB2,NB5 were performed by two ways - by the statistical generating cross sections in the unresolved resonance region and by using the subgroup parameters. Obtained results demonstrate a close agreeent of averaged cross sections. Calculations of homogeneous U^{235}-H_2O assemblies with the statistical generating cross sections give the results without systematic increase in Kef values at the low-H/U limit marked in the literature.

INTRODUCTION

In ENDF the initial data to represent cross sections in the unresolved resonance region are the statistical parameters (the average widths, the average level spacing) coupled with their distribution laws. This fact gives the obvious recipe of cross sections representation in the unresolved region by statistical generating the resonance set with the width distributed according Porter-Thomas distributions and the level spacing simulated according to Wigner distributions. The method

was used in [1] for Monte Carlo calculations of the self-shielding factors and the group average cross sections. As a rule, in Monte Carlo neutron transport codes (VIM,SAM-CE and other) the self-shielding effects in the unresolved resonance region are taken into account by using the subgroup parameters or the probability tables, prepeared under the assumptions on neutron flux form and with the limitation of group moment accuracy.

Direct introduction of work [1] method in neutron transport codes is difficult because of the accidental changing of neutron energy in slowing down process and demands of the sufficient ammount of computer memory.

This work presents the more suitable way, which was realised in RSTAT option of MCS code [2]. The procedure can be described as follows.

CALCULATION METHOD

Cross sections are represented on the base of a single level Breit-Wigner formula with ψ and χ temperature broadering.

Total cross sections

$$\sigma_l(E) = \sigma_p(E) + \frac{\pi}{K^2}\sum_J G(J)\sum_{l,r}\frac{\Gamma^J_{n,l,r}}{\Gamma^J_{l,r}}\left[\psi_r\cos 2\varphi_l + \chi_r \sin 2\varphi_l\right] \quad (1)$$

where $\Gamma^J_{n,l,r}$ - neutron width;

$\Gamma^J_{l,r}$ - total width;

φ_l - phase shift.

Radiative capture cross section

$$\sigma_{n\gamma} = \frac{\pi}{K^2} \overline{\sum_{J}} G(J) \overline{\sum_{l,r}} \frac{\Gamma^J_{n,l,r}\,\Gamma^J_{\gamma,l,r}}{\Gamma^2_{l,r}}\,\psi_r, \qquad (2)$$

where $\Gamma^J_{\gamma,l,r}$ - radiative capture width.

Fission cross section

$$\sigma_{nf} = \frac{\pi}{K^2} \overline{\sum_{J}} G(J) \overline{\sum_{l,r}} \frac{\Gamma_{n,l,r}\,\Gamma_{f,l,r}}{\Gamma^{J\,2}_{l,r}}\,\psi_r \qquad (3)$$

where $\Gamma^J_{f,l,r}$ - fission width.

$$\sigma_p = \frac{4\pi}{K^2} \overline{\sum_{e}} (2e+1)\sin 2\varphi_e ,$$

$$G(J) = \frac{(2J+1)}{2(2I+1)}$$ - statistical factor.

Other notations are traditional.

Cross sections are calculated in a energy point E_o by modelling the set of resonances for different resonances states, starting from the resonances neibouring to given energy point and going in the direction of the outlying ones.

The level spacing is simulated according to Wigner distributions, each width is distributed according to chi-squared distribution with a designated in ENDF/B number of degrees of freedom.

$$E_r^{Jl} = E_{r\pm1}^{Jl} \pm Z_r \bar{D}^{Jl}, \quad (4)$$

$$\Gamma_{n,l,r}^{J} = \bar{\Gamma}_{n,l}^{J} \beta_r, \quad (5)$$

$$\Gamma_{f,l,r}^{J} = \bar{\Gamma}_{f,l}^{J} \beta'_r, \quad (6)$$

where $\bar{\Gamma}_{n,l}^{J}, \bar{\Gamma}_{f,l,r}^{J}$ - average neutron and fission width respectively;

$\Gamma_{n,l_r}^{J}, \Gamma_{f,l_r}^{J}$ - neutron and fission width of r resonanse;

Z_r, β_r, β'_r - values distributed according Wigner (Z_r) and chi-squared distributions (β_r);

$\bar{D}^{Jl}$ - average level spacing.

Positions of two resonances neigbouring to given energy point are designed by the distribution, which have been derived under assumption of 1/E neutron flux form between these resonances.

The final expressions for the energy of neigbouring resonances E_1, E_2 are:

$$E_1 = E_0 + \left(\left(1 + \bar{D}/E_0\right)^R - 1 \right) * E_0, \quad (7)$$

$$E_2 = E_1 - \bar{D}, \quad (8)$$

where R is the random number on [0,1].

Total and partial cross sections are obtained by summing up contributions over all resonances of all states.

A study of influence of flux form assumption on averaged cross sections U^{238} was made. As shown in table 1 there is a marked effect of substitution of 1/E form flux assumption by the energy uniform form flux on U^{238} group cross sections.

TEST CALCULATIONS

To test numericaly the presented method the calculations of the infinite diluted U^{238} cross sections σ_t, σ_a and the self shielded factors f_t, f_a for 12 group ABBN (4.65 Kev -10 Kev) were performed and compared with NJOY results. Table 2 shows a good agreement of the statistical calculation with NJOY, the only point is out of 95% confidence intervals from Monte Carlo statistics.

MONTE CARLO CELL CALCULATIONS

The comparative MCS code calculations of well known cells NB1(BAPL1), NB2(UL212), NB5(HICI3), [3] were performed by two ways - by using the statistical generating U^{238} cross sections in unresolved resonance region (RSTAT option) and on the basis of subgroup parameters. The subgroup parameters were prepared by reconstructed version GROUPIE [4] using self shielded cross sections calculated by UNRESR [5]. The table 3 presents the averaged capture group cross sections for 12 group ABBN. As it follows from the table 3 data there are a close agreement of shielded capture cross sections obtained by different ways.

MONTE CARLO CALCULATIONS OF HOMOGENEOUS U^{235}-H_2O ASSEMBLIES

The calculations with statistical generating cross sections of homogeneous U^{235}-H_2O assemblies are of interest because of greate extent of U^{2952} unresolved resonance region (100 eV -25 Kev in ENDF/B-IV,V and 2.25Kev- 25Kev in ENDF/B-VI) The following experiments were chosen for the present study:

-L5,L6,L7 - small Oak Ridge assemblies with low H/U ratios- uranyl fluoride solution in cylindrical and spherical aluminium containers;

-RF1,RF4 - Rocky Flats experiments - uranyl nitrate solutions in cylindrical aluminum containers, which supplement Oak Ridge assemblies.

Values of K_{ef}, δ^{25} (above-thermal U^{235} fission/thermal U^{235} fission), L (total leakage) calculated by MCS-RSTAT and by MCNP codes are compeared in Table 4. MCS calculations and MCNP calculations labelled 'B4.5' were done on the same base of files from ENDF/B library version IV and V. Labelled 'B6' MCNP results were obtained on base of code version adapted to ENDF/B library files, in which the resolved resonance region of U^{235} were extended up to 10 Kev.On the whole MCS values of Kef are more close to unity then others but the part of this effect is due to the resolved resonance energy region. The investigations of the effect will be continued.

CONCLUSION

The suitable method of statistical generating the neutron cross sections was developed for accurate incorporating self shielding effects of the unresolved resonance region into Monte Carlo neutron transport codes. This method was realised in RSTAT option of MCS code. Subroutine RSTAT is compact and can be simply introduced into other Monte Carlo transport codes. RSTAT is recommended to apply in the temperature effect calculations, because of the explicit temperature dependence of the cross sections generated during the neutron slowing down.

REFERENCES

1. V.N. Kocheev et al , The testing of cross sections functional calculations codes in unresolved reconance region. Voprosi Atomnoy Nauki i Tehniki, seria Yadernii Konstanti,vol.4,p. 73.

2. A.G. Sboev et al, MCS - Monte-Carlo code system. Proceeding of the International Topical Meeting Advances in Mathematics, Computations, and Reactor Physics, April 28-May2,1991 Green Tree Marriott,Pittsburgh,PA,USA.vol.5.

3. M.L.Williams, R.Q.Wright, B.A.Worley et al. Analysis of thermal reactor benchmarks with design codes based on ENDF/B-V data. Nuclear Technology,vol.71,Nov.1985,p.386-401.

4. D.E. Cullen. Program GROUPIE (version 79-1) calculation of Bondarenko self-chielded cross sections and multiband parameters from data in ENDF/B format. Lawrence Livermore UCRL-50400, vol.17,part 8,1980.

5.R.E. MacFarlane, D.W.Muir, R.M. Bolcourt. The NJOY Nuclear Data Processing System. LA-9303-M, vol.1,1982.

TABLE 1.INFLUENCE OF FLUX FORM ASSUMPTION ON CROSS SECTIONS U^{238} FOR 12 GROUP ABBN.(4.65 Kev - 10Kev),T=300°K.[a]

Form flux assumption	σ_t	σ_a
1/E	15.808	0.828
Uniform	18.433	1.218

[a]Calculation unsertainties are less 1%

TABLE 2. U^{238} SELF-SHIELDING FACTORS AND DELUTED CROSS SECTIONS FOR 12 GROUP ABBN.[a]

σ_o	10	10	10	10	1	Source
f_a	0.988	0.986	0.910	0.782	0.692	NJOY
f_a	0.988	0.987	0.914	0.758	0.674	RSTAT
f_t	0.998	0.986	0.915	0.814	0.780	NJOY
f_t	0.999	0.986	0.917	0.804	0.747	RSTAT

$\sigma_t^{NJOY} = 16.03$ $\sigma_a^{NJOY} = 0.842$

$\sigma_t^{RSTAT} = 15.82$ $\sigma_a^{RSTAT} = 0.826$

[a] Calculational uusertainties are 1%.

TABLE 3. $\sigma_a^{U^{238}}$ OF 12 GROUP ABBN (4.65 Kev - 10Kev) FOR NB1,NB2,NB5 CELLS.

CELL	MCS-RSTAT	subgroup parameters
NB1	0.723 ± 0.007	0.727 ± 0.006
NB2	0.740 ± 0.009	0.725 ± 0.008
NB5	0.695 ± 0.005	0.682 ± 0.005

TABLE 4. CALCULATION RESULTS OF HOMOGENEOUS U^{235} - H_2O ASSEMBLIES.

ASSEMBLY	CODE	L	σ^{25}	K_{ef}
L5 $\rho_{h/\rho_5} = 27$	MCNP-B4.5	0.444	0.8091(24)	1.0065(13)
	MCS-RSTAT	0.448	0.7917(15)	1.0005(10)
	MCNP-B6	0.444	0.8295(24)	1.0149(11)
L6 $\rho_{h/\rho_5} = 44.3$	MCNP-B4.5	0.455	0.4593(15)	1.0073(15)
	MSC-RSTAT	0.458	0.4571(13)	1.0020(9)
	MCNP-B6	0.458	0.4778(15)	1.0072(13)
L7 $\rho_{h/\rho_5} = 76.1$	MCNP-B4.5	0.471	0.1962(11)	0.9995(21)
	MCS-RSTAT	-	0.1939(10)	1.0010(16)
	MCNP-B6	0.471	0.1977(9)	1.0022(14)
RF1 $\rho_{h/\rho_5} = 68.2$	MCNP-B4.5	0.460	0.2979(16)	0.9983(16)
	MCS-RSTAT	0.463	0.2941(17)	0.9942(17)
	MCNP-B6	0.479	0.3057(15)	1.0018(12)
RF4 $\rho_{h/\rho_5} = 180.2$	MCNP-B4.5	0.448	0.1081(6)	1.0004(18)
	MCS-RSTAT	0.451	0.1069(4)	1.0003(15)
	MCNP-B6	0.453	0.1107(3)	0.9974(12)

Use of MCNP in

fusion blanket design

ITER magnet system shielding analysis

benchmark of the EFF (European Fusion File) neutron data with the FNG (Frascati Neutron Generator) 14 MeV neutron facility

P. BATTISTONI, L. PETRIZZI, M. PILLON, V.RADO

ENEA
Via E. Fermi 27
00044 Frascati (ROMA) ITALY
tel. +39 6 94005741
fax +39 6 94005250

Introduction

Since eight years at our laboratory, MCNP code has been used as a fundamental tool in many fusion directed activities in which we have been or we still are involved. Mainly they are: neutronics analysis of the performances of blanket components, supporting and optimizing their design; the estimation of the nuclear heat and radiation loads on the toroidal superconducting coils to assess the system shielding performances; then, a 14 MeV neutron generator is recently operating in Frascati and an experimental programme started with a benchmark neutron transport in a stainless steel block, MCNP is used to perform calculations.

In our IBM/MVS system we installed gradually from the first MCNP 3A version, all the new updated releases, till the last: MCNP 4.2 . This year, a workstation IBM RISC 6000 has been bought, where the 4.2 version has been installed too. MCNP runs only 1.8 times slower on this machine with respect to the 3090/300 E IBM

machine, allowing, given the total availability of the workstation, practical runtimes much longer than on the mainframe.

Blanket fusion nuclear performances analysis

In fusion nuclear technology, most of the reactor studies have a toroidal shape (NET, ITER, DEMO etc), which gives a great geometrical complexity. Furthermore nuclear component designers (e.g. blanket designer) want to have a detailed map of the nuclear loads on the blanket materials and modules, with a very close to reality description, this more and more as the particular blanket design converges to its final form. Such a detailed nuclear analysis can have a great importance in the optimization of the blanket performances and in the design success. At this scope our experience using MCNP is that it has sastisfied these requests.

Firstly it is a continuous energy code, which means that, compared to multigroup codes, it is easer to use in case of resonances (except in the unresolved regions range) without any proper use of self shielded cross sections.

It is a fully 3-D code, with practically no limit on the complexity of representation. It allows the use of toroidal surfaces, even if simplier surfaces are preferred (truncated cones or similar). Furthermore since version 3B , MCNP has a new very usefull capability: the "repeated structure". It makes possible to describe in the input data only once some cells and surfaces of any structure that appears more than once in a geometry (in MCNP: U, TRCL, FILL, LIKE BUT cards) . This powerfull tool simplifies the number of user "cell" and surfaces inputs and it allows a detailed descriptions of the breeder modules avoiding any homogeization. A detailed representation is requested for a correct estimation of the tritium breeding ratio (TBR), local power densities and to account of streaming effects on shielding performances.
Examples of 3-D models are in figure 1 .

MCNP has a lot of ways to describe every complicated neutron sources, neverthless the user has the capability to write a proper SOURCE subroutine to be linked to the main program MCNP. This has been our case where the neutron source is really too complicated to be described using the input card options.
For example in ITER the neutron source has been sampled according to the following parametric equations

$$R=R_0+a.\cos(a+\delta_0(a/a_0)\sin a)+\varepsilon_0(1-(a/a_0)^2)$$

$$z=(k_0+k_1(a/a_0)^2)a.\sin a$$

where:

$0<a<\pi$

$0<a<a_0$

R_0	major radius	=	5.996 m
a_0	minor radius	=	2.082 m
δ_0	triangularity constant	=	0.3
ε_0	radius shift constant	=	0.0925 m
k_0		=	1.632
k_1		=	0.364

fusion density:

$$S=S_0(1-(a/a_0)^2)^p \quad \text{with} \quad p = 6.35$$

The space coordinates are sampled by means of the external subroutine wich can run in a more general way just entering the proper D-shape constants.
The plasma region is subdivided in D-shaped intensity zones by selecting a set of 2^n values for the parameter a_i ($0< a_i <a_0$; $1< i <2^n$; n=8 in this case).
The source point is sampled first from a uniform space distribution,the proper intensity zone is searched and finally a rejection game is played on the S function with positive probability = $S(a_i)/S_0$.

ITER magnet shielding analysis

Within the frame of the European Task NSN-1 on shielding performances of ITER blanket candidates, a detailed 3-D neutronic analysis has been performed. The scope is to provide sufficiently information on the Toroidal Field Coil (TFC) system respect to given irradiation limits:

Local dose on electrical insulator	5×10^9 rad	
Displacement damage on Cu stabilizer	6×10^{-3}	dpa
Fast neutron fluence(>.1 Mev) in Nb_3Sn S.C.	10^{19}	n/cm^2
Heating density in winding pack	5	mW/cm^3
Total nuclear heating in toroidal field coils	55	kW

The selection of a blanket for ITER is still an open choice between a breeding or a purely shielding blanket.Both the cases have been analysed separately,on the base of

the specifications given by the European Community (EC) designs for the two different options. The overall specifications for the system have been settled during the ITER meetings. In figure 2 is a view of the shielding blanket model as in MCNP.

The 3B version of the MCNP code has been used at the time.A cross section library originated from EFF1 (European Fusion File), by NJOY processing code, has been used. The library includes DPA data for copper and stainless steel.Cross sections for some lacking elements (Mg,Ca,Sn) have been taken from ENDL85.
A space-energy importance sampling, based on self-generated "weight windows", has been adopted to treat the deep penetration problem. The first guess importance values have been calculated by a 1-D adjoint ANISN solution.
Distinct runs have been performed to score on the inboard and on the outboard parts of the magnet. In the outboard side the bulk attenuation is much higher and the penetration is mainly contributed by the streaming through the radial gaps. In this condition is quite impractical to overlap the generation of importance parameters wich are suitable to score on both the sides.
For a comment of the results,summarized in the tables 1,2 , it is better to refer to the related works.

Benchmark experiments with Frascati Neutron Generator

At the end of 1992 the Frascati 14 MeV neutron generator became operating and the experimental programme started with a benchmark experiment of neutron transport in a stainless steel block (1x1x0,7 m). In figure 3 is a schematic view of the assembly. Major characteristics of FNG are in table 3.
The work is performed in cooperation with a CEA (Cadarache) team, in the frame of an European Technology programme to validate the nuclear data for shielding materials in the European Fusion File (EFF).
Integral measurements of neutron flux inside the block are performed by using fission chambers (U35, Np37, U38) and activation foils (Al27, Fe56, Ni58, In115, Mn55, Au197, Rh103). The absolute calibration is mainly based on an alpha particle recoil counter.
The neutron transport inside the block and the contribution of the external background have been calculated by means of MCNP4. Preliminary results are in figure 4 and 5. Further analysis and calculations are required to give a full answer to the discrepances.
Multigroup Sn methods will be used to perform sensitivity analysis(BISTRO) and to compare the obtained reults(DOT) with the 3-D MCNP calculations.

RELATED REFERENCES

/1/ Simbolotti G., Petrizzi L. et al. European Community (EC) design for the ITER driver blanket. Fusion Technology (1990) vol 1 934-938

/2/ Anzidei L., Petrizzi L. et al. First adaptation of the European Ceramic BIT blanket design to the updated DEMO specifications. Fusion Eng. and Design 17 (1991) 117-122

/3/ Petrizzi L., Giancarli L. et al. Further Neutronic analyses of the European Ceramic B.I.T Blanket for DEMO, presented at XVII SOFT in Rome, Sept. 1992.

/4/ Petrizzi L. EFF: A conitnuous energy library for MCNP from the European Fusion File (EFF1), Final Report on task NSN-1.2 EFF/Doc/168

/5/ Rado V., Petrizzi L. 3-D shielding analysis of the magnet in the ITER system, final report on the NET contract /90-240.

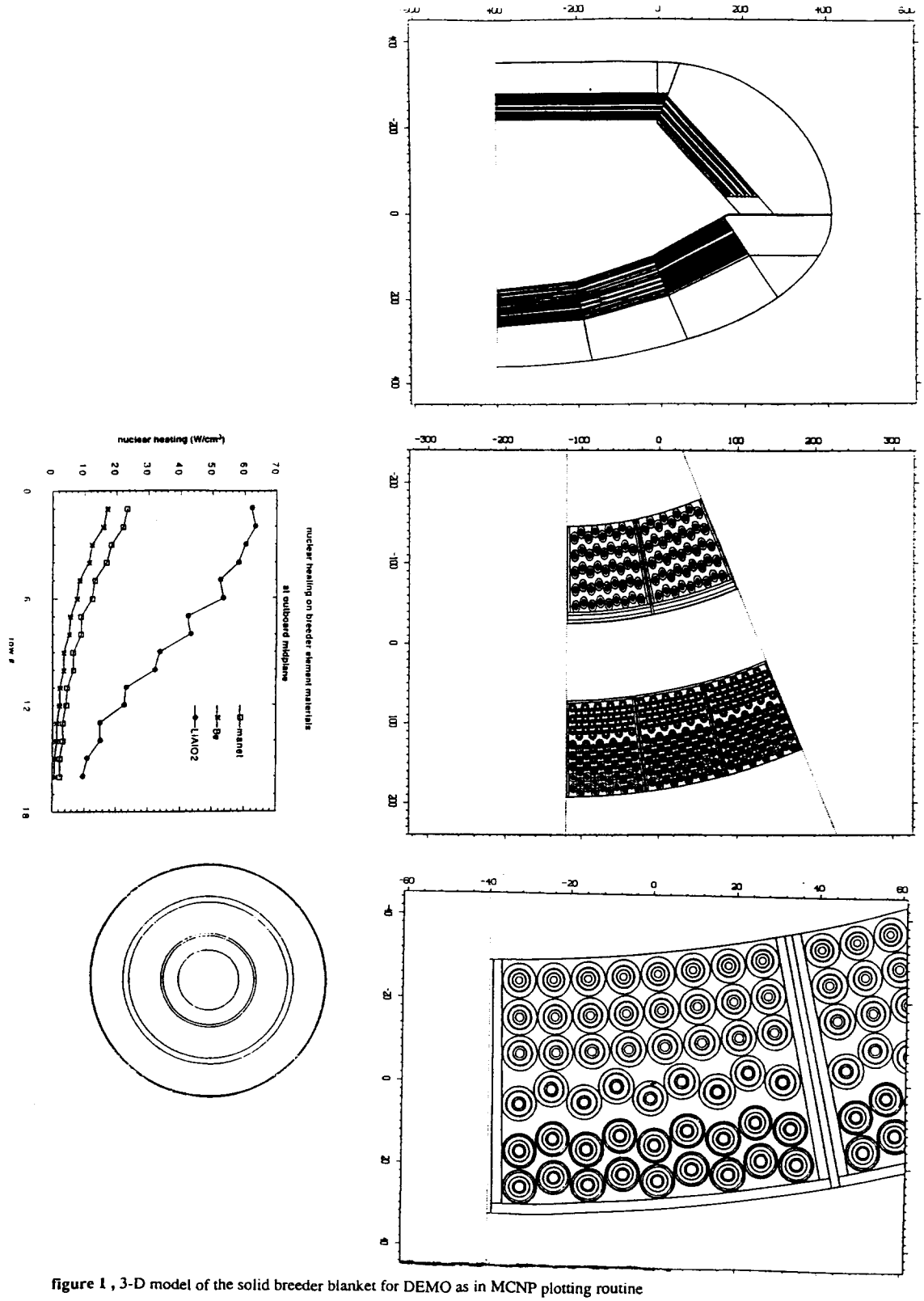

figure 1 , 3-D model of the solid breeder blanket for DEMO as in MCNP plotting routine

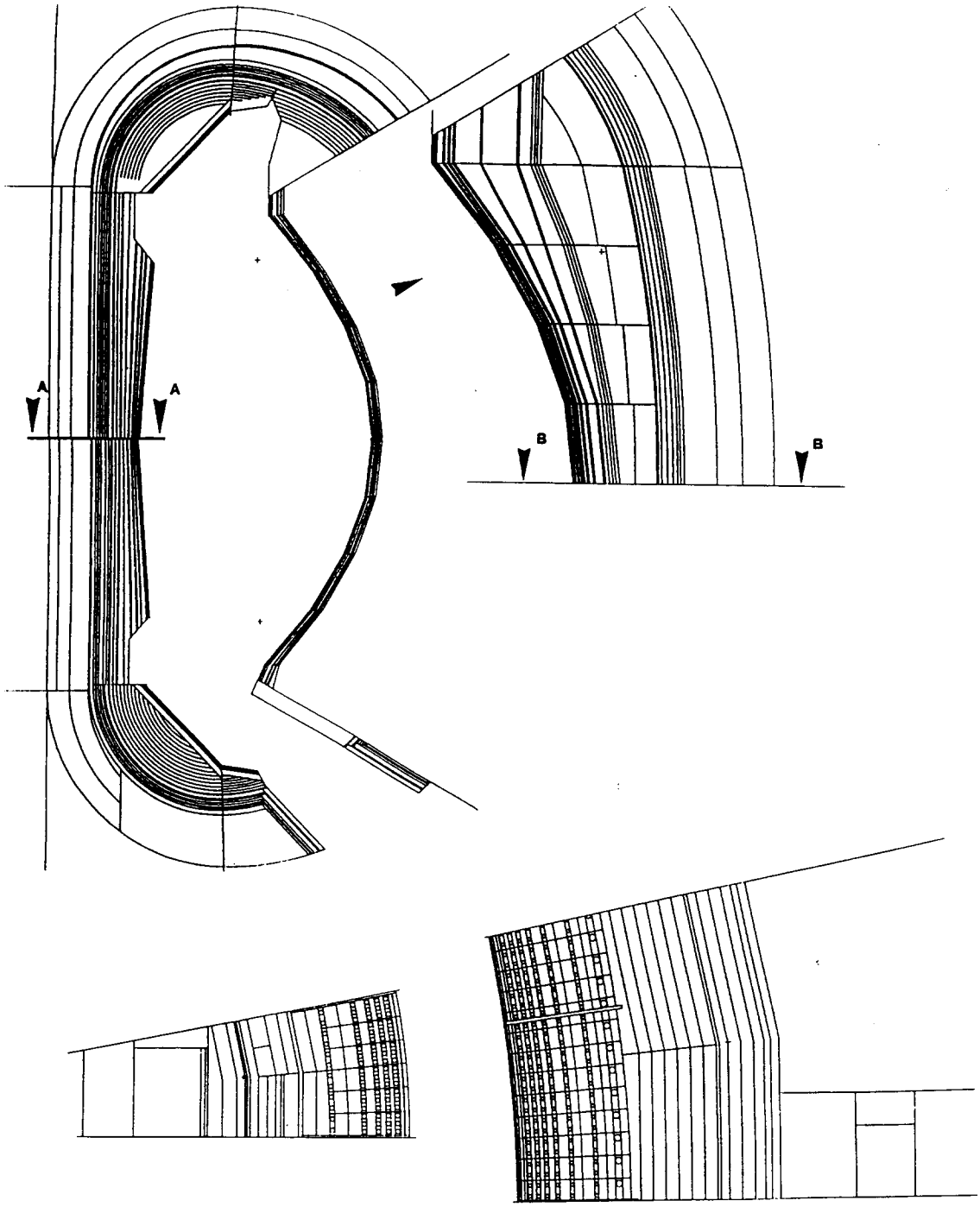

figure 2 , 3-D model of the shieding (ss+water) blanket for ITER as in MCNP plotting routine

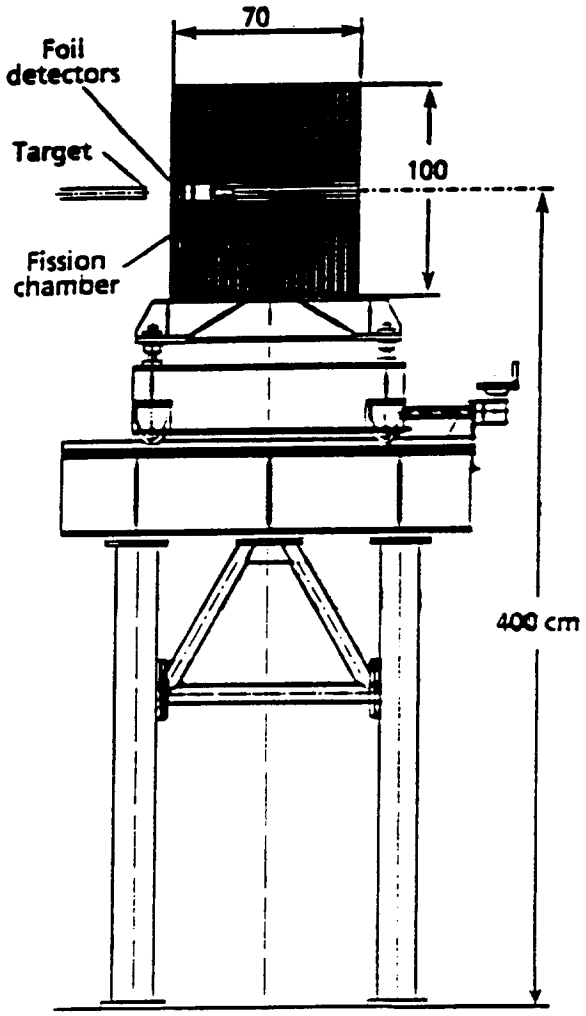

figure 3 , draft of FNG

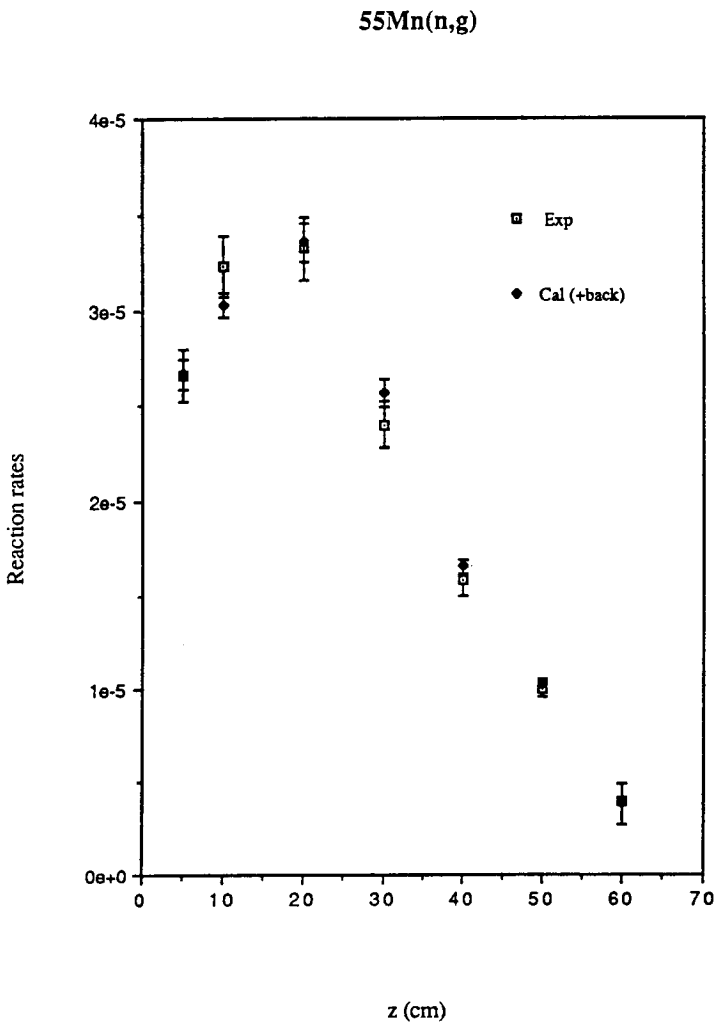

figure 4 , Experiment - calculation comparison for $Mn^{55}(n,\gamma)$

preliminary results

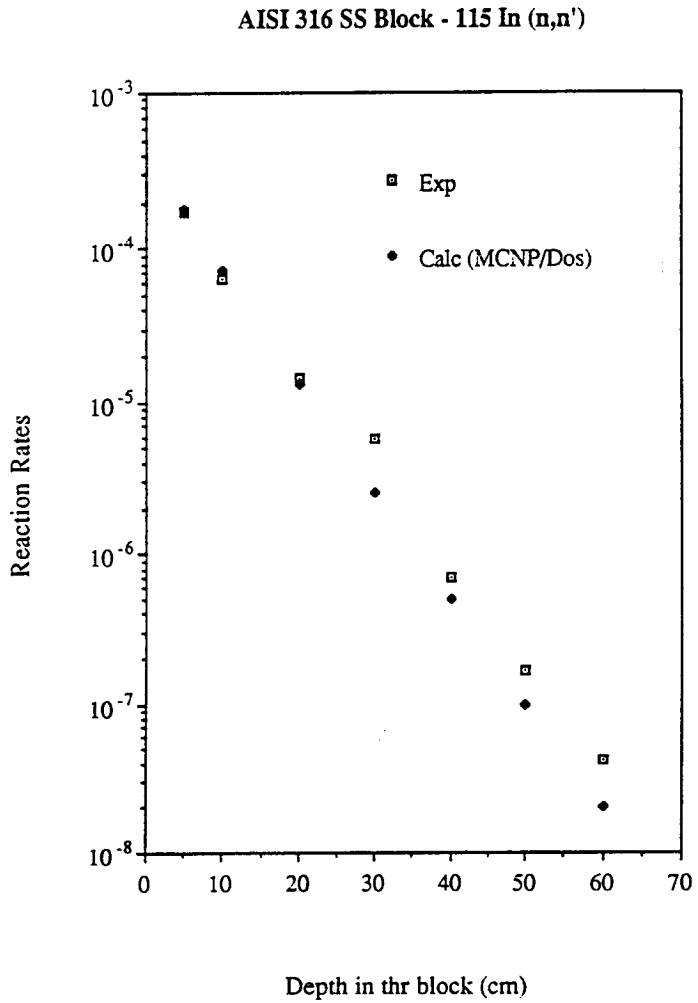

figure 5, Experiment - calculation comparison for $In^{115}(n,n')$

preliminary results

TABLE 1 NUCLEAR LOADS ON THE MAGNET - FUSION POWER 860 MW breeding blanket

zone	n(1)	poloidal length (cm)	power (Watt) case	winding pack	total	winding pack max. pw dens. (10^{-4} W/cm^3)	insulator max. dose (10^9 rads) (*)	10^{-3} dpa (*)
straight inboard	1	100	118.8(5)	111.1(5)	229.9	8.8(6)	2.74(6)	1.52(6)
	2	100	58.4(10)	51.0(9)	107.4			
	3	100	17.5(14)	17.8(13)	35.3			
	4	100	9.0(14)	8.6(14)	17.6			
	5	93.4	18.6(7)	20.5(8)	39.1			
			220.3	209.0	429.3			
divertor bottom	6	458.7	262.4(6)	35.0(8)	297.4			
bottom	7	70.0	793.9(3)	43.7(5)	837.6	5.2(4)	1.39(4)	0.65(5)
	8	37.6	366.2(4)	20.1(6)	386.3	4.7(6)	1.29(6)	0.52(7)
	9	53.1	187.0(4)	12.4(7)	199.4	1.8(8)	0.40(8)	0.19(9)
	10	111.2	206.4(5)	11.6(8)	218.0			
	11	102.8	38.7(11)	3.6(15)	42.3			
	12	252.5	12.1(17)	0.6(28)	12.7			
			1604.3	92.0	1696.3			
divertor top	6	458.7	193.6(6)	32.5(9)	226.1			
top	7	70.0	789.0(3)	42.3(5)	831.3			
	8	37.6	303.5(4)	17.3(7)	320.8			
	9	53.1	55.7(6)	5.7(10)	61.4			
	10	111.2	2.8(21)	0.2(30)	3.0			
	11	102.8	—	—	—			
	12	252.5	—	—	~2	overall nuclear heating		
			1151.0	65.5	1218.5	{2•inboard+bottom+top+2•outboard}•16=70.2KW		
outboard	13				52.4(30)			

In brackets are the fractional standard deviations (%). (*) 3 years full irradiation time.

TABLE 2 NUCLEAR LOADS ON THE TFC SYSTEM - FUSION POWER 860 MW shielding blanket

n	l m	C kW	W kW	T kW	MPD W/cm³	R Rad	D DPA	He Appm
INBOARD								
1	1.	.127	.095	.2222(3)	8.98-4(5)	2.40+9(5)	1.16-3(6)	2.05-1(9)
2	1.	.073	.057	.1300(4)	5.30-4(7)	1.46+9(8)	7.47-4(10)	1.50-1(14)
3	1.	.027	.023	.0503(5)	2.05-4(10)	5.54+8(11)	2.75-4(12)	7.46-2(24)
4	1.	.035	.023	.0577(4)	2.26-4(6)	5.18+8(7)	2.04-4(9)	3.93-2(27)
5	.92	.073	.051	.1239(2)	5.91-4(3)	1.28+9(3)	4.31-4(4)	4.61-2(9)
6	2.29	.048	.021	.0681(6)	7.17-5(12)	2.08+8(12)	1.07-4(13)	4.15-2(14)
				.652				
TOP								
7	2.36	.118	.019	.1368(5)	5.78-5(12)	1.34+8(14)	5.48-5(15)	3.60-2(16)
8	1.38	.670	.076	.7458(3)	4.82-4(7)	1.14+9(7)	4.20-4(8)	6.18-1(3)
9	.97	.161	.014	.1748(6)	9.88-5(13)	2.07+8(13)	1.27-4(10)	2.04-1(5)
10	1.22	.011	.002	.0129(15)				
11	.30	.001	.000	.0012(36)				
				1.072				
BOTTOM								
12	2.36	.119	.019	.1380(5)	6.11-5(12)	1.43+8(13)	5.69-5(14)	3.56-2(14)
13	1.38	.460	.061	.5207(3)	3.85-4(7)	7.44+8(6)	2.92-4(8)	3.13-1(4)
14	.97	.390	.038	.4281(4)	2.84-4(8)	5.56+8(8)	2.24-4(7)	4.58-1(6)
15	1.22	.105	.008	.1128(7)	3.51-5(17)	8.47+7(14)	4.09-5(16)	
16	.30	.011	.001	.0112(24)				
				1.211				
OUTBOARD								
	2m at mid-pln.			.013(19)				
	TOTAL			.021(18)				

TOTAL POWER=(2*INBOARD+TOP+BOTTOM+OUTBOARD)*16= 57.7 kW

n POLOIDAL ZONE NUMBER (SEE FIG.1)
l POLOIDAL LENGHT IN THE WINDING PACK
C NUCLEAR HEATING IN THE CASE (1 COIL)
W NUCLEAR HEATING IN THE WINDING PACK (1 COIL)
T C + W
MPD MAXIMUM POWER DENSITY IN THE WINDING PACK
R MAXIMUM DOSE IN THE INSULATOR FOR 3 FPY
D MAXIMUM DAMAGE IN Cu STABILIZER FOR 3 FPY
He HELIUM PRODUCTION IN THE VACUUM VESSEL (INNEST WALL) FOR 3 FPY
FRACTIONAL STANDARD DEVIATIONS IN BRAKETS (%)

Major characteristics of FNG

Energy of D+ (keV)	300 (230)
Current, D+ only (mA)	3 (0.8)
Power on the target (fixed target) (keV)	0.9 (0.3)
Neutron yield (s^{-1})	$5x10^{11}$ ($2x10^{11}$)
Tritium content in the target (Ci)	10
Target half-life (t full target) (h)	2
Diameter of the beam spot on the target (mm)	15

Table 3 in brackets the actually reached values at this moment

CALCULATION OF RADIATION FIELDS INSIDE AND OUTSIDE THE NET CRYOSTAT/BIOLOGICAL SHIELD DURING OPERATION

A. HOGENBIRK & K. VERSCHUUR
Netherlands Energy Research Foundation ECN

This paper presents the results of an analysis of the radiation fields inside and outside the NET cryostat/biological shield during operation. The calculations have been performed using both the Monte Carlo code MCNP and the discrete ordinates neutron/γ transport code DORT. Consistent nuclear data were used: for the Monte Carlo calculations data were taken from the EFF-1.3 library, for the discrete ordinates calculations data were taken from the MAT175 library. Both libraries are based on the JEF/EFF-1 evaluation. Care was taken to model the 2.0 cm wide gaps between two blanket segments, as the neutron flux behind the vacuum vessel is largely determined by neutrons streaming through these gaps.

The resulting neutron- and γ-flux spectra are in excellent agreement up to the end of the cryostat. It is noted that at this position the attenuation of the neutron flux is about eleven orders of magnitude. Due to precautions in the Monte Carlo calculations the uncertainty in neutron- and γ-flux spectra calculated by the MCNP is only small: the uncertainty in the integrated neutron spectrum amounts to approximately 15% at the end of the cryostat.

The dose rates as calculated by MCNP and DORT also agree well. Differencies occur when heating data, which are due to inconsistencies of the data on the libraries used, are compared.

1. Introduction

The work presented in this paper was devoted to an analysis of radiation fields inside and outside the NET cryostat/biological shield during operation. In the NET design of the shielding blanket of ITER, this blanket consists of segments, which are separated by slots with a width of 2.0 cm. It is clear that the radiation leakage through the blanket segments slots will determine the radiation fields outside the torus to a large extent.

It was therefore concluded that useful information on the radiation fields outside the torus could only be obtained by using at least a two-dimensional geometry in which the segment slots are properly modelled. Calculations were performed using the Monte Carlo code MCNP, [1], and the neutron/γ transport code DORT, [2].

Section 2 gives a description of the calculational model used in this analysis while information on the nuclear data used can be found in Section 3. Some details on the MCNP and DORT calculations are given in Sections 4 and 5, respectively, and the results of the calculations are discussed in Section 6. Finally the conclusions from this work are presented in Section 7.

2. Model Description

The two-dimensional model used in the calculations is given in Figure 1. The model of the blanket part used in the calculations is given in Figure 2. The model represents the NET shielding-blanket design inside the ITER torus design surrounded by the cryostat/biological shield as planned for NET.

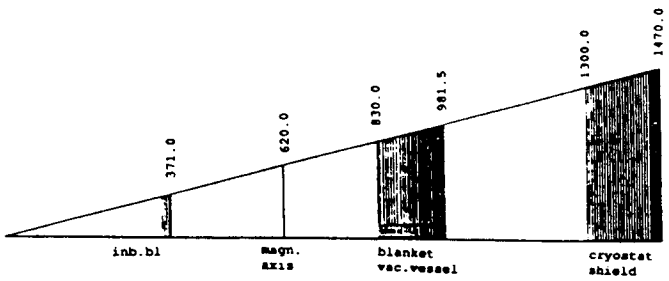

Figure 1: MCNP-model of the complete geometry. Note that the vertical direction has been magnified in order to increase the detail in this figure.

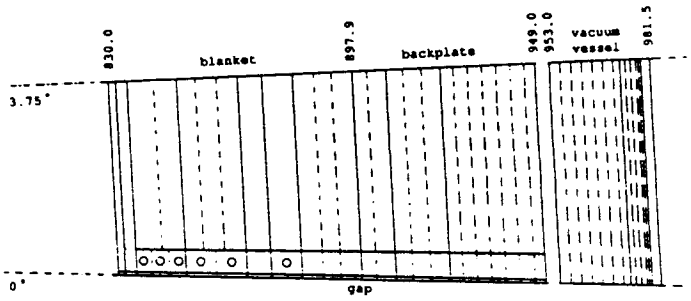

Figure 2: MCNP-model of the blanket-part of geometry.

According to the drawings obtained from the NET team, [3], the shielding blanket geometry consists of steel layers with incorporated cooling channels. These steel layers are oriented radially.

In our 2-D-model most blanket zones containing steel and cooling water have been homogenised into "onion-skin" wise material zones. The segment slot and the blanket layer nearest to the slot were modelled as accurately as possible, however, (correctly representing the cooling channels) as the main radiation leakage takes place in that region.

The blackplate was modelled in an analogous way. The second layer, consisting of vertical cooling pipes surrounded by steel pebbles, was homogenised. The material composition for this region was taken from a 1-D-model of the shielding blanket, [3].

A simple "onion-skin" type model of the inboard blanket / first wall was included in our model in order to obtain the correct backscatter contribution from the inboard region.

The cryostat/biological shield is a simple geometry consisting of a concrete wall lined at the inside with a steel layer of 6 mm thickness. The main function of the cryostat as a shield will be to reduce the γ dose rate outside the cryostat after shutdown. The thickness chosen (170 cm) is based on the results of preliminary MCNP calculations.

Our approximations made to the ITER torus result in additional toroidal symetry. Therefore our model could be restricted to a toroidal sector of 3.75°, which is 1/96th of the torus circumference.

The 14-MeV neutron source distribution of the plasma was represented by a homogeneous volume in an average wall loading of 1 MW/m^2 in our cylinder geometry.

3. Nuclear Data Libraries

In the MCNP calculations, scattering cross section data were taken from the EFF-1.3 library, [4], which is based on the basic nuclear data from the JEF/EFF-1 evaluation.

In the DORT calculations, the group cross section data were derived from the MAT175 (JEF/EFF-1) library, [5], (which is in the 175 group VITAMIN-J group structure) using the processing code TRAMIX, [6], for mixing, collapsing and self-shielding. A 33 neutron groups /12 γ group structure was used, which is a refinement of the 28 neutron groups /12 γ group structure that was used in [7].

The biological dose rates were calculated using the pointwise conversion factors from NCRP-38 as given in the MCNP manual, [1], which were converted to the required energy group structure for use in DORT.

Kerma data for MCNP were taken from the EFF-1.3 library. In the DORT calculations, use was made of kerma factors from the RFL-1 library, [8], which is also derived from JEF/EFF-1.

4. Two-Dimensional Calculations with MCNP

Neutrons streaming through the segment slots contribute significantly to response parameters outside the blanket region. Therefore an accurate estimate of the number of neutrons passing through these slots is required for a reliable calculation of these response parameters. The area of segment slots is only small compared with the total area of the outboard first wall (1.84%). Besides, the segment slots are narrow, which implies that only particles which are nearly exactly radially outward directed have a reasonable probability of passing through the slots. Therefore, a Monte Carlo calculation without biasing neutrons into the direction of the slots and, in the slots into the direction of the cryostat, will yield inaccurate results.

As it is required that a large number of neutrons start from the slot region of the surface of the outboard first wall, we chose to subdivide the complete geometry as given in Figure 1, in three separate regions:

1. the segment slot region,

2. the neighbouring blanket-slab region (in this region the water-cooling tubes are modelled explicitly),

3. the remaining blanket region.

Using this approach in the first step of the calculations, surface sources were produced on the outboard first wall for each of these three regions using the SSW-card in MCNP. These surface sources consist of neutrons and photons crossing the outboard first wall in the outward direction.

Simplified geometries were adopted in this step: only the first 22.75 cm of the inboard blanket and the first 18.9 cm of the outboard blanket were modelled, which is enough to take into account the backscatter contribution of the inboard and outboard blanket to the surface source on the outboard first wall.

The remaining calculations were devoted to the transport of neutrons and photons from the surface sources produced in the first step to the outside of the cryostat/biological shield. The weight-window technique was used in order to bias particles into the direction of the segment slot and also into the direction of the cryostat. The calculations were split up in two steps:

2. transport of neutrons and photons from the outboard first wall to the inside of the vacuum vessel, where again a surface source is produced;

3. transport of neutrons and photons from the surface source produced in step 2 to the outside of the cryostat/biological shield.

In step 2 the backscattering contribution from the complete vacuum vessel was taken into account while producing the surface source.

In order to transport neutrons through the concrete cryostat, biasing was applied using the exponential transform. The biasing parameter p was taken to be 0.7.

In oder to obtain statistically significant results care was taken to start with a surface source in which the statistical uncertainty is small enough. After preliminary calculations it was decided to start with a source in which the uncertainty in the integrated neutron flux spectrum was smaller than 0.65%.

On a series of locations response, parameters were calculated (fluxes, dose rates, heating). The energy group structure for representing the flux spectra was taken to be identical to the one used in the DORT calculations (see Section 5).

5. Two-Dimensional Calculations with DORT

Considerable time was spent to obtain the proper spatial-, angular- and energy-discretisation for this 2-D deep-penetration problem. The torus was modelled in R, θ geometry. Therefore the polygon-shaped blanket segments were approximated by ring sectors. Hence the segment slots in the DORT model are wedge-shaped rather than straight. As the slot width at the first wall practically determines the aperture of the slot, it was decided to take it to be equal to the correct width at the first wall (i.e. 2 cm). This approximation was not required in the MCNP calculations (see Section 4). Futhermore the cooling pipes in the first blanket layer (i.e. nearest to the segment gap) could not be modelled exactly. The spatial mesh was defined in such a way that each cooling pipe is enclosed by a spatial R, θ mesh, in which the amount of water and steel was homogenised.

Radial mesh intervals of 2- to 3-cm-thickness were used in the material zones and intervals with thickness up to 20 cm were used in the plasma- and void regions.

In the toroidal direction the geometry was subdivided in eleven intervals ($\tau = \tau_1$ to $\tau = \tau_{11}$), of which the first interval exactly spans the entrance gap.

For a proper calculation of the radiation leakage through the segment slots, a biased angular quadrature is required which is biased towards the R, Z plane to ensure a sufficient number of discrete directions passing through the slots. A strongly biased quadrature was used in the slot and in the first blanket layer. In this quadrature the number of directions is approximately ten times as large as in the normal S_8 quadrature whereas 35% of the directions pass through the whole slots. In the remaining part of the blanket a symetric S_8 quadature was used.

6. Intercomparison of MCNP and DORT Results

Figures 3 and 4 give radial distributions of the energy-integrated neutron fluxes. It is observed that despite the large attenuation of eleven decades over the whole geometry there is an excellent agreement between energy-integrated neutron fluxes as calculated by MCNP and DORT. The results from MCNP and DORT can be best compared, however, by studying the flux *spectra*. It is noted that the neutron spectra averaged over τ as calculated by both codes generally agree within the statistical accuracy of the MCNP results (see Figures 5, 6, 7). Due to the precautions taken in the MCNP calculations, also at the end of the cryostat (R = 1470 cm) the statistical uncertainty in the MCNP results is only very small ($\leq$ 15% in the energy-integrated spectra). At this location the DORT spectrum is approximately a factor of two lower over the whole energy range. This is most probably due to the fact that the DORT calculations were performed in a coarse energy group structure which may cause a too large flux attenuation. However, considering the large attenuation of eleven decades over the whole geometry, the agreement must be considered to be excellent. The γ-spectra averaged over τ are even in better agreement (see Figures 8, 9, 10). The importance of the slots between two

blanket segments is clearly demonstrated in Figure 11, in which a toroidal plot of the energy-integrated neutron flux at R = 949 cm (in front of the vacuum vessel) is given. Combining these results with the results of 1-D ANISN calculations, [9], (see Figure 11), which were performed as well, it can be derived that compared to the 1-D ANISN results the toroidally averaged fluxes are a factor of ten higher, the minimum fluxes (at $\tau = \tau_{,,}$) a factor of two to three higher and at the maximum (at $\tau = \tau_{,,}$) a factor of forty for the total neutron flux, a factor of a hundred for the fast neutron flux and a factor of two-hundred for the total γ-flux. It is observed as well that after the toroidal variation is levelled out, the total neutron- and total γ-fluxes remain a factor of ten higher throughout the rest of the geometry and that the fast neutron flux inside the cryostat becomes even three orders of magnitude higher.

The latter confirms that the presence of the slots reulsts not only in a larger but also harder fast neutron flux outside the vessel.

The results for the biological dose rates are given in Figure 12, from which it is observed that MCNP and DORT are in excellent agreement in this case.

Differences occur for the calculation of nuclear heating data: as can be seen in Figure 13, MCNP calculates lower values for the neutron heat in the vacuum vessel than DORT. The largest differences occur at $\tau = \tau_{,,,}$ farthest away from the slot where the neutron spectrum is softest. These large differences in calculated neutron heat are mainly due to differences in the kerma factors which are used by MCNP and DORT. On the EFF-1.3 library used by MCNP, only *prompt* local neutron heating values are given, which are based on the energy-balance method, [4]. However, on the RFL-1 library used with DORT, the *total* neutron kerma factors are given, including decay heat by prompt and delayed γ's, [10]. For fusion applications this latter approach seems to be most useful. For illustration, Figure 14 is included in which the kerma factors for ^{nat}Cu from both libraries are compared. The observed difference also occurs for other materials relevant in our case, such as ^{nat}Fe.

From the table below it is clear that if RFL-1 kerma data are used in MCNP as well, a good agreement is obtained between the results from MCNP and DORT. If kerma factors from EFF-1.3 are used in MCNP the neutron heat is lower by a factor of two to ten.

Neutron heat in W/cm^3 at R = 953cm.			
τ	MCNP (kerma factors from EFF1.3)	MCNP (kerma factors from RFL-1)	DORT
τ_1	$1.49 \cdot 10^{-2}$(11%)	$2.36 \cdot 10^{-2}$(6%)	$2.13 \cdot 10^{-2}$
τ_4	$2.00 \cdot 10^{-4}$(10%)	$4.98 \cdot 10^{-4}$(12%)	$5.93 \cdot 10^{-4}$
τ_7	$4.01 \cdot 10^{-5}$(9%)	$2.22 \cdot 10^{-4}$(14%)	$1.85 \cdot 10^{-4}$
τ_{11}	$1.44 \cdot 10^{-5}$(12%)	$1.11 \cdot 10^{-4}$(14%)	$7.56 \cdot 10^{-5}$

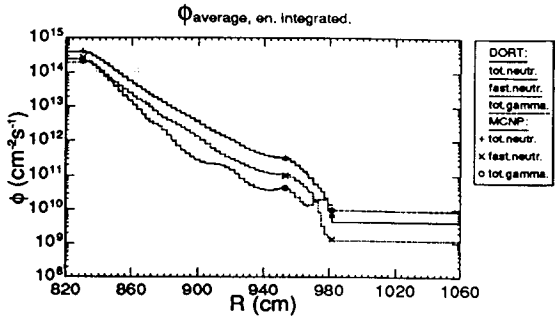

Figure 3: Energy-integrated neutron fluxes averaged over τ calculated by MCNP and DORT, radial distributions: R = 820 – 1060 cm.

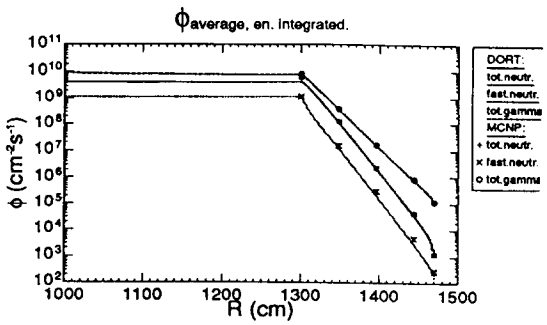

Figure 4: Energy-integrated neutron fluxes averaged ove τ calculated by MCNP and DORT, radial distributions R = 1000 – 1500 cm.

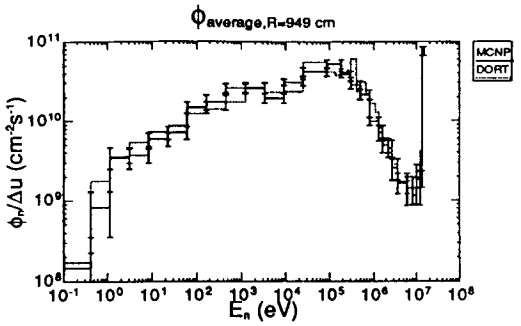

Figure 5: Neutron spectra calculated by MCNP and DORT at $R = 949$ cm.

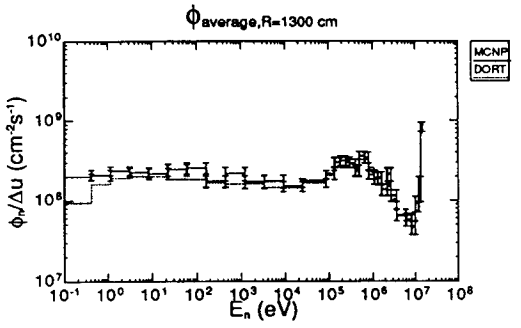

Figure 6: Neutron spectra calculated by MCNP and DORT at $R = 1300$ cm.

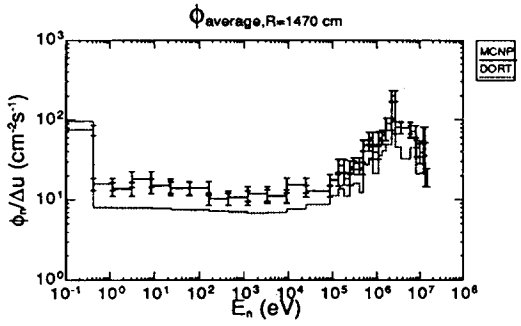

Figure 7: Neutron spectra calculated by MCNP and DORT at $R = 1470$ cm.

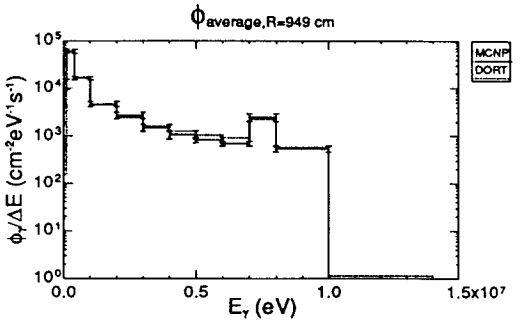

Figure 8: γ spectra calculated by MCNP and DORT at $R = 949$ cm.

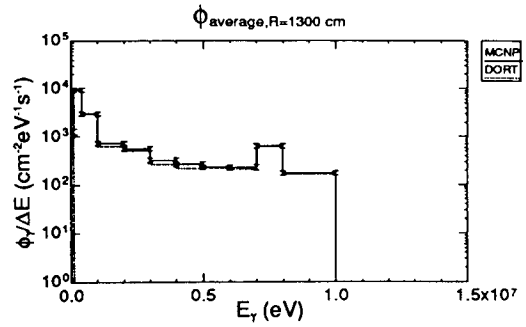

Figure 9: γ spectra calculated by MCNP and DORT at $R = 1300$ cm.

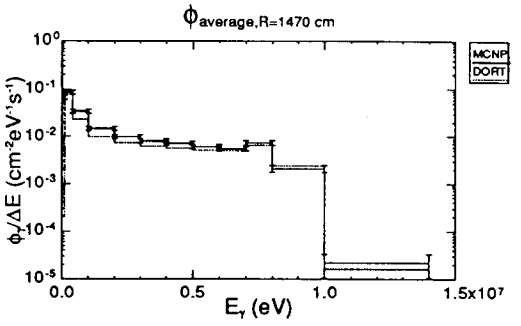

Figure 10: γ spectra calculated by MCNP and DORT at $R = 1470$ cm.

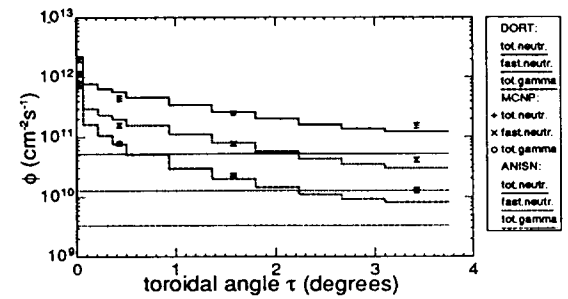

Figure 11: Energy-integrated neutron fluxes calculated by DORT, MCNP and ANISN, toroidal distribution at $R = 949$ cm.

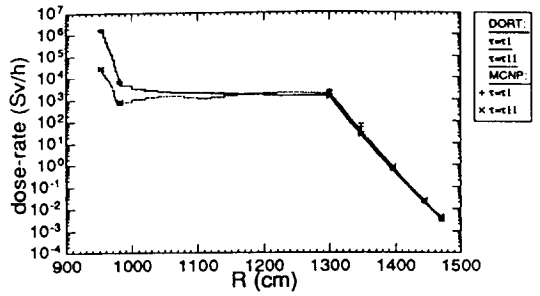

Figure 12: Total biological dose-rates calculated by MCNP and DORT, radial distributions: $R = 900 - 1500$ cm, at $\tau = \tau_1$ and τ_{11}.

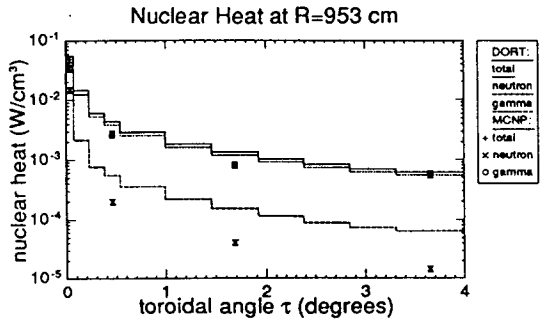

Figure 13: Total-, neutron- and γ- heat calculated by MCNP and DORT, toroidal distributions at $R = 953$ cm.

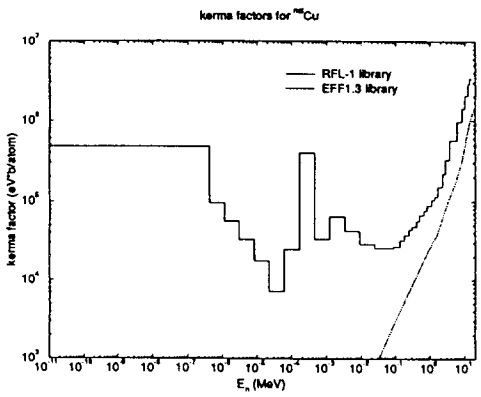

Figure 14: Comparison of kerma data for ^{nat}Cu from the EFF1.3 library and from the RFL-1 library.

7. Conclusions

The main conclusions of this work are the following:

- When suitable biasing techniques are applied, MCNP is a powerful tool to calculate responses in this slot-leakage/deep-penetration problem;

- In this work excellent agreement is obtained between MCNP calculations in which the JEF/EFF-1 based point cross section data library EFF-1.3, [4], was used and deterministic calculations, in which the JEF/EFF-1 based group cross section library MAT175, [5], was used;

- 90% of the radiation leaking into the vacuum vessel is due to the segment slots, thus increasing the fluxes averaged over the toroidal surface by a factor of ten, whereas directly behind the segment slot the fluxes are increased by two orders of magnitude. The increased radiation load of the vacuum vessel behind the segment slots may influence the design of the vessel with respect to the position of welds;

- The first order estimates of the effect of the blanket segment slots on the nuclear hea produced in the vacuum vessel and on the requirement for a biological shield around the torus, [11] are confirmed.

- To allow personal access outside the torus during reactor operation the total biologica dose rate should be as low as 25 μSv/h. This requires an attenuation of eight orders of magnitud behind the vacuum vessel, which will be achieved with a cryostat/shield of portland concrete with thickness of 230 cm (see Figure 12).

- Differences were observed between the neutron heat as calculated with MCNP using th point cross section data library EFF-1.3, [4], and the neutron heat as calculated with DORT usin kerma factors from the RFL-1 library, [8]. These differences are due to the fact that the kerma factor on both libraries are not consistent. The more conservative values of the neutron heat ar recommended. These values were calculated using kerma factors from RFL-1, in which th contribution of radioactive decay is taken into account.

References

[1] J. F. Briesmeister (ed.), "MCNP - A General Monte Carlo Code For Neutron and Photon Transport", Report LA-7396-M, Rev. 2, Los Alamos National Laboratory, September 1986

[2] W. A. Rhoades & R. L. Childs, "The DORT Two-Dimensional Discrete Ordinates Transport Code", Nucl. Sci. Eng. 99 (1988) 88, (RSIC code package CCC-484/DORT, March 1989)

[3] W. Dänner, 1989, private communication

[4] P. Vontobel, "EFF1LIB: A NJOY Generated Neutron Data Library Based on EFF-1 for the Continuous Energy Monte Carlo Code MCNP", PSI-Bericht Nr. 107, Paul Scherrer Institut, September 1991

[5] P. Vontobel & S. Pelloni, "JEF/EFF Based Nuclear Data Libraries", EIR-Bericht Nr. 636, Eidgenössisches Institut für Reaktorforschung, 1987, updated version used (obtained in 1989)

[6] J. Stepanek, "TRAMIX: A Code for Interfacing MATXS Cross Section Libraries to Nuclear Transport Code for all Type Fission Reactor, Fusion Blanket as well as Shielding Analysis", Paul Scherrer Institut (draft, 15-4-1988)

[7] K. A. Verschuur, "Poloidal variation of the NET blanket; nuclear response functions", Report EUR/FU/XII-80/88/82, Commission of the European Communities, Directorate General XII - Fusion Programme, January 1988

[8] G. C. Panini & P. Peerani, "RFL-1: A Library of nuclear response functions in Vitamin-J structure", Report EFF-Doc-130, 1992

[9] W. W. Engle Jr., "A users manual for ANISN", Report ORNL/K-1693, Oak Ridge National Laboratory, 1967

[10] M. Frisoni, G. C. Panini & P. Peerani, "Status report on the computation of kerma and photon production data for RFL-2", Report EFF-Doc-177, December 1992

[11] K. A. Verschuur, "Biological Shield required yes or no?", NET memo N/N/3400/1/A, October 1989

USE OF SPECIFIC PURPOSE MONTE CARLO CODES IN RADIATION APPLICATION PROBLEMS INVOLVING FINITE DETECTORS

Robin P. Gardner and Kuruvilla Verghese

Center for Engineering Applications of Radioisotopes
Department of Nuclear Engineering, Box 7909
North Carolina State University
Raleigh, North Carolina 27695-7909 USA

ABSTRACT

The authors have worked on specific purpose Monte Carlo codes for radiation applications such as gauges, analyzers, and tomographic devices for a number of years. These applications have in common the need to use talleys from finite radiation detectors which are often difficult to accomplish in the common general purpose Monte Carlo codes. Special techniques for handling this problem have been developed including: (1) exact statistical estimation, (2) the development and use of detector response functions, and (3) direction biasing methods. The methods developed are exact and very efficient for these problems. Results are given for a number of cases including nuclear well logging devices (neutron porosity, gamma-ray density, neutron lifetime, natural gamma-ray, and prompt gamma-ray logs); neutron moderation moisture content gauges, gamma-ray density gauges, energy-dispersive X-ray fluorescence gauges, neutron capture prompt gamma-ray gauges, and tomographic devices.

INTRODUCTION

The authors began using general purpose Monte Carlo codes for the simulation of radiation gauges such as the neutron moderation soil moisture content gauge with the O5R Code (Li69) and the gamma-ray backscatter soil density gauge with the OGRE-G Code (Ho73). Both of these codes gave only flux and/or current tallies of neutrons or gamma rays, so the required finite detector responses for the proportional counter filled with BF_3 gas and the NaI(Tl) scintillation detector had to be obtained by appropriate integrations over their surfaces. This difficulty, plus the lack of understanding of the Monte Carlo simulation obtained by the students when using these general purpose codes, led us to begin requiring that our students write their own *specific purpose* Monte Carlo codes when they wanted to use this kind of simulation.

Our experience in requiring this has been mostly very positive. In deriving their own codes the students learn Monte Carlo and the physics of their specific problem very well. In many cases they become the expert on their particular problem. And we have been surprised to find that many of these specific purpose codes are competitive with using the general purpose codes for the same problems. In particular, they are competitive in size, speed, and, above all, user-friendliness. This has led us to the development of specific

purpose codes for members of our Associate's Program.[1] Other codes have been developed that are sold outright to interested users. At present we often use the general purpose code MCNP to compare with the results of our specific purpose codes for benchmarking purposes (Lit89 and Ga91d).

The present paper describes our Monte Carlo work within the Center for Engineering Applications of Radioisotopes (CEAR). It starts with a review of some general Monte Carlo contributions, then discusses our specific contributions to user-friendliness, continues with a brief description and sample results of the specific purpose Monte Carlo codes that we have developed, and finishes with our anticipated future work.

GENERAL MONTE CARLO CONTRIBUTIONS

This section describes some of our work that we consider to have general interest for Monte Carlo practicioners. Some of this has been previously reviewed (Ga83b, Ve90, and Ga91c). It includes detector talley methods including reponse functions, direction biasing and statistical estimation methods, the complete composition and density correlated sampling method, geometrical approaches including the use of nested right circular cylinders and a general geometry approach, a special photon cross section treatment with cubic splines, the description of benchmark problems and results, and some ideas for future work.

Direct Detector Tallies and Detector Response Functions

In most of the specific purpose codes that we have developed we specify up to three separate detector zones and the interaction or interactions that are required for detection. In the case of the use of ^{3}He detectors for neutrons we specify that the ^{3}He(n,p)^{3}H reaction must occur in a detector zone in order that a detection event be recorded (Ch86b, Ga88b, Mi92, and Pr93b).

For gamma-ray detectors any of the three interactions Compton scatter, photoelectric effect interaction, or the pair production interaction yields a recorded detection event. In those cases where gamma-ray spectra are recorded, one of two methods is used. The first method is used when the detector has a length much larger than the diameter or when stringent detector collimation is employed. In this case each detected photon is followed individually within the detector and the total energy deposited in the detector by participating electrons is summed. This approach is described well and used by Ghanem in his McLDL code for the Monte Carlo simulation of the gamma-ray lithodensity oil well logging tools (Gh93). This was also used in the Monte Carlo McPNL code developed by Choi for the thermal neutron lifetime oil well logging tools (Ch86a, Ch87, and Ga88b).

The second method is the use of detector response functions. This method can be used when the the detector has about a one to one ratio of diameter to length so the detector has very little "directionality" and there is little or no shielding. In this case a detector

[1]The Associate's Program - Nuclear Techniques in Oil Well Logging that supports the Center for Engineering Applications of Radioisotopes presently consists of Amoco, ARCO, Conoco, Atlas Wireline Services, and Japan National Oil Corporation.

response function is used which spreads the interacting photon energy into the appropriate complete pulse-height spectrum. Optimum use is to store the incident interacting photon spectrum that is calculated by the Monte Carlo code and then use the detector response function to "convolve" it to obtain the pulse-height spectrum. This also accomplishes some natural "smoothing". This feature is included in the Monte Carlo NCSXRF code for energy-dispersive X-ray fluorescent programs (Do80, Do81, Do82a, Do82b, Ga79, Ga82a, Ya87, He91, He93, and Ve88a) and the neutron capture prompt gamma-ray Monte Carlo code (Cl82, Yu83, Yu87, Ji87, Sh88, Sh93, and Ve84).

Our group has done considerable work on detector response functions (Ga82b, Ga86, Ji86b, and Ya86b) including the use of Monte Carlo to generate detector response functions directly (Ar79, Be78, Ch86b, Du72, Ga86, Ji86a, and Gr92). However, our primary approach for detector response functions has been a semi-empirical one which identifies individual parts of the detector response function that can be described with simple analytical functions. Then linear least-squares techniques are used with a limited amount of experimental data from single energy sources to obtain the model parameters as a function of energy. This has been done for the Si(Li) detectors (Ga86 and Ya86b) and the high purity Ge detectors (Ga86, Ji86b, and Le87). We have almost finished the development of detector response functions for NaI scintillation detectors.

Direction Biasing and Statistical Estimation

The use of statistical estimation and direction biasing techniques are particularly valuable for problems involving the detection of radiation with finite radiation detectors. Since this type of problem has been of primary interest to our group, we have tried to use these approaches for a number of problems. Unfortunately, we found that these techniques had not been very fully developed - particularly for right circular cylindrical detectors which are the detectors almost always encountered. Therefore, we have endeavored to develop these methods more fully. In the area of direction biasing the authors (Ga88a) developed an approach to angle biasing that involves transforming the scattering pdf from the usual original direction of the radiation to a direction towards the center of the detector of interest. A simple general arbitrary pdf is then used in the new angle system to choose a direction toward the detector and the appropriate weight change is made for not using the true pdf. This technique is very attractive for those cases in which one has relatively simple pdf's like the Klein-Nishina distribution for gamma-ray scattering. It can also be used for neutron scattering when simple analytical forms can be used. The special problem of neutron scattering with hydrogen was treated in a later paper (Ga91a).

Statistical estimation techniques were also treated by the authors. The initial paper on this (Ga87a) developed the algorithms necessary to determine the limiting polar and azimuthal angles to spherical, planar circular, and right circular cylindrical detectors. This was done by transforming the axes so that the original interaction point is at the origin and the original radiation direction is along the new Z axis. Then the azimuthal limiting angles can be easily obtained first and the limiting polar angles next. This approach works quite well, but it was improved upon in a subsequent paper (Mi88b) in which the axes were transformed to a line from the radiation interaction point to the center of the sphere and a line parallel to the Z axis of the right circular cylindrical detector. These transformations provided

even simpler algorithms for determining the limiting polar and azimuthal angles and in this case it does not matter which limiting angles are determined first since they are independent.

Complete Correlated Sampling

In many radiation application problems that involve finite radiation detectors such as oil well logging devices and gauges and analyzers of various kinds, one is interested in interpreting the response of these devices when measurement interferences are present. In particular, one is often interested in the effects of small composition and density variations in the samples being analyzed. This type of calculation is done ideally by correlated sampling techniques. We have used what we call the complete composition and density correlated sampling method. In this approach the Monte Carlo simulation is carried out in the usual way for a *reference* sample and the identical path is forced to occur in any number of *comparison* samples by appropriate weighting. This approach has the advantage that the correlation between reference and comparison sample is complete within any radiation history. This approach is described and applied to several of our specific purpose Monte Carlo codes in a series of three articles (Ga89, Mi89b, Ga90, and Ga92).

Geometrical Considerations

Many of the oil well logging devices and some of the energy-dispersive X-ray fluorescence (EDXRF) and neutron capture prompt gamma-ray (NCPGR) analyzers can be described by a system of homogeneous nested right circular cylinders all oriented in the same direction. This allows one to geometrically describe these devices as a set of nested right circular cylinders of various compositions and densities. This is a very simple geometry system with very efficient tracking capability. This geometry system is described and applied to a number of our specific purpose Monte Carlo codes in a series of articles (Ch86a, Ch87, Mi88a, Mi89b, Ga83b, and Ve90).

Some of the oil well logging devices such as the gamma-ray lithodensity logs and the EDXRF secondary fluorescer type analyzers cannot be described by the simple nested right circular cylinder treatment. For these cases a general geometry package called HERMETOR was developed by T.H. Prettyman (Ga88c, Pr90, Pr93a, and Pr93b). This general geometry treatment is capable of treating very complex geometries and is relatively straightforward to use and computationally efficient. It has been applied to our gamma-ray lithodensity Monte Carlo code McLDL (Gh93), to our EDXRF Monte Carlo code NCSXRF (He91 and He93), and to our NCPGR Monte Carlo code NCSPGA (Sh88 and Sh93).

Photon Cross Section Treatments

Rather than use the usual technique of linear or log interpolation for photon cross sections, our group uses a cubic spline fitting technique that reduces both the storage requirements and computer access time. This approach was developed by A.M. Yacout (Ya84) and includes a novel idea of using cubic splines that can be functionally discontinuous at selected knot positions while still being continuous in the first and second derivatives at these knot

positions. This allows one to fit the photoelectric effect cross sections across the jump discontinuities for each element.

Yacout (Ya86a) also used linear least-squares techniques to obtain two-variable cubic splines for fitting cumulative probabilty distribution functions for Compton and Rayleigh scattering for differential angles and energies for use in Monte Carlo simulation programs.

Benchmark Problems

Our group recognized the need for realistic benchmark problems for the nuclear oil well logging devices. Benchmark problems are invaluable for checking Monte Carlo codes against one another and to see if modifications to the codes do not introduce bias. A set of benchmark problems was developed in consultation with members of our Associates Program - Nuclear Techniques in Oil Well Logging for the neutron porosity, thermal neutron lifetime, and gamma-ray lithodensity logs and were first introduced into the literature in an article in Progress in Nuclear Energy (Ga91c). A Seminar & Workshop on Monte Carlo Simulation for Nuclear Well Logging Applications was organized and held by our Center in October 1990 after submission of these benchmark problems to selected users of the general purpose Monte Carlo codes MCNP and McBEND. These benchmark problems, which were slightly modified from the original ones, were described in an article in Nuclear Geophysics (Ga91d) along with data obtained from the various Monte Carlo codes. Generally speaking the comparisons were quite good with two exceptions. One of these exceptions indicated a problem in the use of MCNP for simulating the gamma-ray pulse-height spectra of the gamma-ray lithodensity logs. These benchmark problems along with some additional problems will serve as the basis for an International Intercomparison of Monte Carlo Codes sponsored by Colin G. Clayton, Editor of Nuclear Geophysics.

Future Work

Some of the work we would like to pursue in the future includes: (1) application of the probability table method for accessing neutron cross sections, (2) developing several automatic biasing techniques including one based on artificial intelligence (AI) and several heuristic schemes, and (3) investigation of parallel processing schemes for improvement of calculational efficiency.

CONTRIBUTIONS TO USER-FRIENDLINESS

Many of the general contributions discussed in the previous section are also contributions to user-friendliness. Three of them are discussed specifically in relation to user-friendliness here.

The Use of Nested Right Circular Cylinders

This approach probably affects the user-friendliness of those of our codes that can use it the most. When this treatment is valid, the geometry input to the codes is simply a listing of the center coordinates, radii, and length of all the right circular cylinders. Then the composition in elemental weight fractions and densities of each zone and the total number of histories, random number seed, and zone numbers of the detector zones are input. This treatment is described in several articles for the various Monte Carlo codes that we have used it in (Ch86a, Ch87, Mi88a, Mi89b, Ga83b, and Ve90).

Automatic Use of Splitting, Direction Biasing, and Path Length Stretching

The first two specific purpose Monte Carlo codes developed for our Associates Program - Nuclear Techniques in Oil Well Logging had essentially fixed parameters for splitting (actually statistical estimation), direction biasing, and path length stretching. These were the codes for the neutron porosity (Mi88a and Mi89a) and thermal neutron lifetime logs (Ch86a, Ch87, and Ch89). The first of these codes also used implicit capture and Russian Roulette while the second had a maximum neutron lifetime which was used to kill histories. Both of these codes also contained the complete correlated sampling composition and density feature (Ga89 and Mi89b). The fixed biasing parameters used in these two codes yielded Figures of Merit (FOM's) of the order of 10 to 20 larger than analog Monte Carlo, but were somewhat problem dependent. Factors of two to four in FOM's were obtained for formations with much different porosities. Subsequently this approach has been temporarily abandoned to use a method of automatic generation of importance maps with splitting and Russian Roulette, similar to the technique employed in the general purpose codes MCNP and McBEND. This is described in the next section.

Automatic Generation and Use of Importance Maps with Splitting and Russian Roulette

M.W. Mickael (Mi92) developed a specific purpose Monte Carlo code for the neutron porosity logs and later another for the thermal neutron lifetime log that contains an excellent automatic biasing feature. It consists of a short analog Monte Carlo run at the beginning of these codes to determine the average neutron model parameters for an adjoint one-dimensional multigroup neutron diffusion model (and coupled gamma-ray model for the second case). Then the diffusion models are used to calculate an importance map for the problem and the splitting and Russian Roulette utilized in the codes are controlled by these importances. These codes have very high FOM's compared to analog Monte Carlo and are very user-friendly. These codes belong to Atlas Wireline Services.

The approach used by Mickael was also used in a slightly modified form by T.H. Prettyman (Pr93b) in the present versions of our neutron porosity, epithermal neutron lifetime, and thermal neutron lifetime Monte Carlo codes.

Future Work

Our group is presently working on a number of automatic biasing approaches including the use of artificial intelligence (AI) and a number of heuristic methods, some involving direction biasing and path length stretching rather than splitting.

SPECIFIC PURPOSE CODES DEVELOPED - DESCRIPTION AND SAMPLE RESULTS

Our group presently maintains and continually improves five specific purpose Monte Carlo codes for nuclear oil well logging devices and three specific purpose Monte Carlo codes that have been developed independently of that program for EDXRF analyzers, NCPGR analyzers, and industrial photon tomography systems. These are briefly described in the following subsections.

McDNL - Neutron Porosity Log

This log is one of the two most important nuclear oil well logs in that it detects oil (or water) in rock formations surrounding boreholes. It consists of a fast neutron source (usually ^{241}Am-Be) and two ^{3}He-filled proportional counters located at different distances from the source. The fast neutrons slow to thermal speeds and are detected largely as a function of the hydrogen content of the formation. Our specific purpose Monte Carlo code McDNL was described earlier as one that utilizes an automatic biasing method that consists of a short analog Monte Carlo program run at the beginning of a case to calculate the average parameters for an adjoint one-dimensional multigroup neutron diffusion model. Then this model is used to calculate a continuous importance map for the problem which is used to control the splitting or playing of Russian Roulette at each neutron interaction. This code has a very high FOM and is very user-friendly. It is being supplied to members of our Associates Program - Nuclear Techniques in Oil Well Logging. It has been extensively benchmarked against the other general purpose Monte Carlo codes on our benchmark problems and with proprietary data on actual commercial logging devices from test pits. A number of successful checks have been made for a generic model with published results on the CNL tool (Ga92). The early version of this code that primarily used direction biasing and path length stretching was described in an earlier article (Mi88a) and the present version is very similar to that described by Mickael (Mi92). Results with this code are given in several articles (Mi88a, Mi89a, Ga89, Ga90, Ga91c, Ga91d, and Ga92).

McENL - Epithermal Neutron Lifetime Log

This is a very new log that was originally developed by Mobil. It consists of an accelerator source of fast (14 MeV) neutrons that are detected by ^{3}He-filled proportional counters covered with a suitable thermal neutron filter like gadolinium so that primarily epithermal neutrons are detected. A burst of fast neutrons is made at fixed time intervals after which the epithermal neutrons are detected at fixed time intervals after these bursts. The "dieaway" curve so obtained can be related to the epithermal neutron absorption cross section of the rock formation. Our code McENL (Pr93b) uses the same approach as that for McDNL except that the neutron diffusion models are time dependent. This code has a very high FOM and has been checked with proprietary data on a prototype device designed by Mobil (Pr93b). This code also contains complete composition and density correlated sampling.

McPNL - Thermal Neutron Lifetime Log

This is also an important nuclear oil well logging device. It is an established log and is very similar to the epithermal neutron lifetime log. It differs in that the detectors used are NaI scintillation crystals and the prompt gamma rays are detected that arise from thermal neutron radiative capture events that occur in the rock formation and borehole fluid. Our McPNL code is very similar in design to the McENL code just discussed with the exception that gamma-ray diffusion models are coupled to the neutron diffusion model groups. This code is currently undergoing modifications, but the present code has a very reasonable FOM. The earlier version was developed by H.K. Choi and is described in a number of articles (Ch86a, Ch87, Ch89, Ga88b, Ga89, Ga90, Ga91c, Ga91d, Mi89a, and Mi89b). The most recent version is adequately described by Mickael (Mi92). This code has been extensively benchmarked against other general purpose codes with our benchmark problems and with proprietary data from Welex (now Halliburton). This code also contains complete composition and density correlated sampling.

McLDL - Gamma-Ray Lithodensity Log

This is one of the two most important nuclear oil well logs. It consists of a gamma-ray source of ^{137}Cs and two collimated NaI detectors at different distances from the source. It primarily is a function of formation density, but a low-energy pulse-height window is also sensitive to the formation lithology. It is important in that it also gives an independent measurement of porosity. This code has a general geometry package since the right circular cylinders treatment is not sufficient to describe this log. Our first generation McLDL code is somewhat slower and has a somewhat lower FOM than we would like. This version is based on self-automated statistical estimation methods used in conjunction with direction biasing and path length stretching. This code has been benchmarked against the general purpose MCNP code with our benchmark problems and compared to proprietary data supplied by Atlas Wireline Services. While it is within predicted standard deviations, these standard deviations are quite high and we are presently not satisfied with the performance of this code with the exception of the complete composition and density correlated sampling feature which gives adequate results. We are presently working on two modifications of this code - one using artificial intelligence methods for automated variance reduction and the other using a heuristic approach to automated variance reduction.

McNGR - Natural Gamma-Ray Log

This is a fairly important nuclear oil well log in that it is useful in detecting shaly layers. This log consists of a long uncollimated NaI detector that is used to detect the natural gamma rays of potassium, uranium, and thorium that emanate from the formation. This is the most recent specific purpose Monte Carlo code that our group has worked on and the present version is probably the fastest of all. It is completely self automated and uses a special type of direction biasing that is very efficient. This first involves assuming a very long *pseudo* NaI detector. Counts are accumulated and stored as a function of position along this long detector from radioactive emissions chosen randomly according to assumed homogeneous concentrations within the formation. Whenever the polar angle chosen subtends this long detector the azimuthal angle is biased strongly to intersect the detector. Then a special kind of correlated sampling is available for this code. The log can be moved independently down the borehole with a fixed active detector length equal to the actual detector length. At each position of the log only those detected events that fall within the actual detector length are detected at that position. In this way a highly correlated response versus log depth can be generated from the previous data on the *pseudo* long detector and thin layers of shale can be detected. Results of this method were reported at a recent SPWLA meeting (Ga92). At present this code is being extensively benchmarked against laboratory data on a ^{24}Na source in a controlled laboratory experiment and against proprietary test pit data provided by Atlas Wireline Services on their commercial tool. This code will also contain complete composition and density correlated sampling when first released.

NCSXRF - Energy Dispersive X-Ray Fluorescence Analyzers

Our group has worked on this specific purpose Monte Carlo code for quite a long time (Ga75, Ha75a, Ha75b, Ha75c, Ha77, Ga78, Ga79, Do80, Do81, Do82a, Do82b, Ga82a, Ya87, He91, and He93). The present NCSXRF code is capable of simulating the entire pulse-height spectrum detected by a Si(Li) detector from a multielement sample that is excited by an X-ray machine source or a radioisotope source and it has a general geometry capability. It also has a special capability to solve the inverse problem - given the pulse-height spectrum it can estimate the elemental amounts present in the sample. This is done by what we call the Monte Carlo - Library Least-Squares Principle (MCLLS). This principle consists of first assuming a particular composition of the sample of interest. Then the complete pulse-height spectrum and all the spectra from each individual element (the library spectra) are generated by the Monte Carlo code NCSXRF. Next the linear library least-squares method is used with the calculated library spectra and the experimental sample spectrum to obtain estimates of the elemental amounts. If these amounts are not sufficiently close to the initial assumed values that a linear relationship exists, the entire procedure is iterated until it does. It has been found that one or two iterations are almost always sufficient. A typical result (the first figure) from our most recent paper (He93) shows that the Monte Carlo code NCSXRF matches the experimental pulse-height spectrum of a stainless steel sample almost exactly. This code has been extensively benchmarked against a number of NIST samples and has been found to be quite accurate (He93).

NCSPGA - Neutron Capture Prompt Gamma-Ray Analyzers

Our group has worked on the development of this specific purpose Monte Carlo code for slightly less time than the NCSXRF code (Cl82, Yu83, Yu87, Sh88, and Sh93). This code describes the complete pulse-height spectrum obtained from the prompt gamma rays excited by thermal neutron radiative capture events in a bulk sample and detected by a high purity Ge detector. It also has general geometry capability and contains the MCLLS approach. It has been extensively benchmarked against laboratory data on four coals of various compositions and found to be quite accurate. In this case also only one or two iterations of the MCLLS approach were always found to be adequate for convergence. A typical Monte Carlo model result (the second figure) versus experimental data for a coal is shown from our most recent publication (Sh93). It is obvious from this result that the code is very accurate.

NCSTOM - Tomographic Simulator

This is a recent endeavor by our group and represents the work of T.H. Prettyman (Pr90). A novel approach of *pathway sampling* and the use of extensive splitting and biasing games are utilized in this code to handle the simulation of highly collimated photon beams. The code is set up in such a way that it can be used to investigate the extent of selected photon pathways and the effect of multiple interaction pathways. It has the general geometry capability (HERMETOR) developed by Prettyman (Ga88c). It has been extensively benchmarked against laboratory experiments (Pr93a).

FUTURE WORK

Our group will continue to try to improve all of the Monte Carlo codes described in the previous section - especially the first five that are supplied to members of our Associates Program - Nuclear Techniques in Oil Well Logging. We intend to continue to develop subroutines for doing specific jobs that will make the future design of Monte Carlo codes easier. We also will continue to investigate and try to develop better automatic variance reduction techniques.

ACKNOWLEDGEMENTS

The authors gratefully acknowlege the technical and financial support of the members of our Associates Program - Nuclear Techniques in Oil Well Logging that presently includes Amoco, ARCO, Conoco, Atlas Wireline Services, and Japan National Oil Corporation.

REFERENCES

Ar79 F. Arinc and R.P. Gardner, "Monte Carlo Simulation of the Backscatter Region in Photon-Excited Energy Dispersive X-Ray Fluorescence Spectra", Journal of Radioanalytical Chemistry, 54 (1-2), pp. 221-234 (1979).

Be78 G.R. Beam, L. Wielopolski, R.P. Gardner, and K. Verghese, "Monte Carlo Calculation of Efficiencies of Right-Circular Cylindrical NaI Detectors for Arbitrarily Located Point Sources", Nuclear Instruments and Methods, 154, pp. 501-508 (1978).

Ch86a H.K. Choi, R.P. Gardner and K. Verghese, "Monte Carlo Simulation of the Neutron Lifetime Logging Tool", Transactions of the American Nuclear Society, 52, 354-356(1986).

Ch86b H.K. Choi, B.W. Wehring, K. Verghese, and R.P. Gardner, "Monte Carlo Simulation of Neutron Response for ^{3}He Spectrometers Transactions of the American Nuclear Society, 52, pp. 639-640(1986).

Ch87 H.K. Choi, K. Verghese, and R.P. Gardner, "Monte Carlo Simulation of the Temporal and Spectral Responses of the Pulsed Neutron Logging Principle", Nuclear Geophysics, 1 (1), 71-81 (1987).

Ch89 H.K. Choi, K. Verghese, and R.P. Gardner, "Experimental Benchmarking of the Specific Purpose Monte Carlo Code McPNL/v. 1.0 for Simulating Pulsed Neutron Logging Tool Response", Nuclear Geophysics, Vol. 3, No. 3, 167-177(1989).

Cl82 T. Chris Clark, Robin P. Gardner, and Kuruvilla Verghese, "A Monte Carlo Model for in Situ Prompt Gamma-Ray Analysis Probes", Nuclear Instruments and Methods, 193, pp. 365-370(1982).

Do80 J.M. Doster and R.P. Gardner, "Monte Carlo Simulation of Sample Scattering Effects from Homogeneous Samples Excited by Monoenergetic Photons", Advances in X-Ray Analysis, 23, pp. 117-124 (1980).

Do81 J.M. Doster and R.P. Gardner, "Monte Carlo Studies on the Design of Radioisotope Source Holders and Shields for EDXRF Analyzers", Advances in X-Ray Analysis, 24, pp. 413-415 (1981).

Do82a Joseph M. Doster and Robin P. Gardner, "The Complete Spectral Response for EDXRF Systems - Calculation by Monte Carlo and Analysis Applications. 1. Homogeneous Samples", X-Ray Spectrometry, 11, (4), pp. 173-180 (1982).

Do82b Joseph M. Doster and Robin P. Gardner, "The Complete Spectral Response for EDXRF Systems - Calculation by Monte Carlo and Analysis Applications. 2. Heterogeneous Samples", X-Ray Spectrometry, 11, (4), pp. 181-186 (1982).

Du72 W.L. Dunn and R.P. Gardner, "The Determination of Intrinsic Gamma-Ray Detection Efficiencies for Cylindrical Geiger-Muller Tubes by Monte Carlo Methods", Nuclear Instruments and Methods, 103, pp. 373-384 (1972).

Ga75 R.P. Gardner and A.R. Hawthorne, "Monte Carlo Simulation of X-Ray Fluorescence from Homogeneous Samples Including Tertiary Interelement Effects", X-Ray Spectrometry, 4, pp. 138-148 (1975).

Ga78 R.P. Gardner, L. Wielopolski, and J.M. Doster, "Adaptation of the Fundamental Parameters Monte Carlo Simulation to EDXRF Analysis with Secondary Fluorescer X-Ray Machines", Advances in X-Ray Analysis, 21, pp. 129-142 (1978).

Ga79 R.P. Gardner and J.M. Doster, "The Reduction of Matrix Effects in X-Ray Fluorescence Analysis by the Monte Carlo Fundamental Parameters Method", Advances in X-Ray Analysis, 22, pp. 343-356 (1979).

Ga82a Robin P. Gardner, Joseph M. Doster, and Kuruvilla Verghese, "On the Development of a Calibration Method for X-Ray Fluorescence and Prompt Gamma-Ray Analyzers Based on Monte Carlo Simulation", Transactions of the American Nuclear Society, 43, pp. 250-251(1982).

Ga82b Robin P. Gardner and Joseph M. Doster, "Treatment of the Si(Li) Detector Response as a Probability Density Function", Nuclear Instruments and Methods, 198, pp. 381-390(1982).

Ga83a Robin P. Gardner and Kuruvilla Verghese, "Nuclear Data Requirements for Monte Carlo Simulations of Radioisotope-Excited Gauges and Analyzers", Transactions of the American Nuclear Society, 44, pp. 190-191 (1983).

Ga83b R.P. Gardner and K. Verghese, "Use of Monte Carlo Methods in the Calibration and Design Optimization of Radiation Gauges and Analyzers", Isotopenpraxis, 19, pp. 329-335 (1983).

Ga86 R.P. Gardner, A.M. Yacout, J. Zhang, and K. Verghese, "An Investigation of the Possible Interaction Mechanisms for Si(Li) and Ge Detector Response Functions by Monte Carlo Simulation", Nuclear Instruments and Methods in Physics Research, A242, 399-405(1986).

Ga87a R.P. Gardner, H.K. Choi, M. Mickael, A.M. Yacout, Y. Jin, and K. Verghese, "Algorithms for Forcing Scattered Radiation to Spherical, Planar Circular, and Right Circular Cylindrical Detectors for Monte Carlo Simulation", Nuclear Science and Engineering, 95, 245-256 (1987).

Ga87b R.P. Gardner, W. Haq, and K. Verghese, "A Monte Carlo Model for the Pulsed Neutron Activation Method of Flow Measurement", Transactions of the American Nuclear Society, Vol. 55, 711-712 (1987).

Ga88a R.P. Gardner, M. Mickael, and K. Verghese, "A New Direction Biasing Approach for Monte Carlo Simulation", Nuclear Science and Engineering, 98, 51-63 (1988).

Ga88b R.P. Gardner, K. Verghese, H.K. Choi, and M. Mickael, "Specific Purpose Monte Carlo Modelling of Nuclear Well Logging Tool Responses", IEEE Transactions on Nuclear Science, Vol. 35, No. 1, 882-885, February (1988).

Ga88c R.P. Gardner, T.H. Prettyman, M. Mickael, and K. Verghese, "Some Geometric Modelling and Tracking Codes for Monte Carlo Particle Transport Including Direction Biasing Techniques", Transactions of the American Nuclear Society, Vol. 57, 115-116 (1988).

Ga89 R.P. Gardner, M.W. Mickael, and K. Verghese, "Complete Composition and Density Correlated Sampling in the Specific Purpose Monte Carlo Codes McPNL and McDNL for Simulating Pulsed Neutron and Neutron Porosity Logging Tools", Nuclear Geophysics, Vol. 3, No. 3, 157-165(1989).

Ga90 R.P. Gardner, M.W. Mickael, C.W. Towsley, C.M. Shyu, and K. Verghese, "Correlated Sampling in the McDNL and McPNL Codes for Neutron Porosity and Neutron Lifetime Log Corrections", IEEE Transactions on Nuclear Science, Vol. 37, No. 3, 1360-1366 (1990).

Ga91a R.P. Gardner, M. Mickael, M. Oraby, and K. Verghese, "A Monte Carlo Direction Biasing Approach in the Laboratory System for Isotropic Neutron Center-of-Mass Scattering Including Hydrogen", Nuclear Science and Engineering, **108**, No. 3, 240-246 (1991).

Ga91b R.P. Gardner and K. Verghese, "Nuclear Data for Well Logging", Transactions of the American Nuclear Society, **63**, 167-168 (1991).

Ga91c R.P. Gardner, M.W. Mickael, and K. Verghese, "Specific Purpose Monte Carlo Code Development for Nuclear Well Logging Applications", Progress in Nuclear Energy, Vol. 25, No. 2-3, 245-264 (1991).

Ga91d R.P. Gardner and K. Verghese, "Monte Carlo Nuclear Well Logging Benchmark Problems with Preliminary Intercomparison Results", Nuclear Geophysics, Vol. 5, No. 4, 429-438 (1991).

Ga92 R.P. Gardner, Q. Ao, Y. Xie, P. Guo, T.H. Prettyman, and K. Verghese, "Iterative Convolution Augmented with Monte Carlo Simulation: Preliminary Formation Layer Results for Neutron Porosity and Natural Gamma-Ray Logs", SPWLA Thirty-Third Annual Logging Symposium, Paper R, 25 pages, June (1992).

Gh93 S.A. Ghanem, R.P. Gardner, and K. Verghese, "Monte Carlo Simulation of the Gamma-Ray Backscatter Lithodensity Logging Tool Response", accepted for publication in Nuclear Geophysics (1993).

Gr92 G. Griffith, R.P. Gardner, and K. Verghese, "NaI Gamma-Ray Detector Response Functions Using Semi-Emprical Monte Carlo Modelling", Transactions of the American Nuclear Society, Vol. 65, Supplement No. 1, 10-11 (1992).

Ha75a A.R. Hawthorne and R.P. Gardner, "Monte Carlo Models for the Inverse Calculation of Multielement Amounts in XRF Analysis", Transactions of the American Nuclear Society, Supplement No. 3, 21, pp. 38-39 (1975).

Ha75b A.R. Hawthorne and R.P. Gardner, "Monte Carlo Simulation of X-Ray Fluorescence from Homogeneous Multielement Samples Excited by Continuous and Discrete Energy Photons from X-Ray Tubes", Analytical Chemistry, 47, pp. 2220-2225 (1975).

Ha75c A.R. Hawthorne, R.P. Gardner, and T.G. Dzubay, "Monte Carlo Simulation of Self-Absorption Effects in Elemental XRF Analysis of Atmospheric Particulates Collected on Filters", Advances in X-Ray Analysis, 19, pp. 323-379 (1975).

Ha77 A.R. Hawthorne and R.P. Gardner, "Chapter 18. Monte Carlo Applications to the X-Ray Fluorescence Analysis of Aerosol Samples", in X-RAY FLUORESCENCE ANALYSIS OF ENVIRONMENTAL SAMPLES, T. G. Dzubay (ed.), Ann Arbor Science Publishers, Inc., Ann Arbor, Michigan, 1977, pp. 209-220.

Ham93 Y.S. Ham, J.C. Russ, R.P. Gardner, and K. Verghese, "Three-Dimensional Differential Absorption X-Ray Cone-Beam Microtomography Using Balanced Filters and Algebraic Reconstruction", accepted for publication in Nuclear Geophysics (1993).

He91 T. He, R.P. Gardner, and K. Verghese, "NCSXRF: A General Geometry Monte Carlo Simulation Code for EDXRF Analysis", Advances in X-Ray Analysis, Volume 35B, pp. 727-736 (1991).

He93 T. He, R.P. Gardner, and K. Verghese, "The Monte Carlo - Library Least-Squares Approach for Energy-Dispersive X-Ray Fluorescence Analysis", accepted for publication in Nuclear Geophysics (1993).

Ho73 W.C. Hopkins and R.P. Gardner, "Monte Carlo Simulation of Gamma-Ray Backscatter Soil Density Gauges", Nuclear Engineering and Design, 24, pp. 332-343 (1973).

Ji86a Y. Jin, K. Verghese, and R.P. Gardner, "Monte Carlo Simulation of the Scattered Component of Neutron Capture Prompt Gamma-Ray Analyzer Responses", Transactions of the American Nuclear Society, 52, pp. 353-354(1986).

Ji86b Y. Jin, R.P. Gardner and K. Verghese, "A Semi-Empirical Model for the Gamma-Ray Response Function of Germanium Detectors Based on Fundamental Interaction Mechanisms", Nuclear Instruments and Methods in Physics Research, A242, 416-426(1986).

Ji87 Y. Jin, R.P. Gardner and K. Verghese, "A Monte Carlo Model for the Complete Pulse-height Spectral Response of Neutron Capture Prompt γ-Ray Analyzers for Bulk Media and Borehole Configurations", Nuclear Geophysics, 1 (2), 167-178 (1987).

Le87 M.C. Lee, K. Verghese, and R.P. Gardner, "Extension of the Semi-Empirical Germanium Detector Response Function to Low Energy Gamma Rays", Nuclear Instruments and Methods in Physics Research, A262, 430-438 (1987).

Li69 W.L. Lippold, A. Carnesale, and R.P. Gardner, "A Monte Carlo Simulation of the Surface-Type Neutron Moisture Gauge", Nuclear Engineering and Design, 10, pp. 373-380 (1969).

Lit89 R.C. Little, M. Mickael, K. Verghese, and R.P. Gardner, "Benchmark Neutron Porosity Log Calculations: A Comparison of MCNP and the Specific Purpose Code McDNL", IEEE Transactions on Nuclear Science, Vol. 36, No. 1, 1223-1226(1989).

Mi88a M. Mickael, R.P. Gardner, and K. Verghese, "McDNL: A New Specific Purpose Monte Carlo Code for Simulation of Dual-Spaced Neutron Porosity Logs", SPWLA Twenty-Ninth Annual Logging Symposium, Paper MM, 17 pages, June (1988).

Mi88b M. Mickael, R.P. Gardner, and K. Verghese, "An Improved Method for Estimating Particle Scattering Probabilities to Finite Detectors for Monte Carlo Simulation", Nuclear Science and Engineering, 99, 251-266 (1988).

Mi89a M. Mickael, H.K. Choi, R.P. Gardner, and K. Verghese, "Specific Monte Carlo Code Development for Nuclear Well-Logging Tool Responses", Nuclear Geophysics, Vol. 3, No. 4, pp. 339-350 (1989).

Mi89b M. Mickael, K. Verghese, and R.P. Gardner, "Correlated Sampling Added to the Specific Purpose Monte Carlo Code McPNL for Neutron Lifetime Log Responses", IEEE Transactions on Nuclear Science, Vol. 36, No. 1, 1220-1222 (1989).

Mi92 M.W. Mickael, "Importance Estimation in Monte Carlo Modelling of Neutron and Photon Transport", Nuclear Geophysics, Vol. 6, No. 3, pp. 341-350 (1992)

Pr90 T.H. Prettyman, R.P. Gardner, and K. Verghese, "MCPT: A Monte Carlo Code for Simulation of Photon Transport in Tomographic Scanners", Nuclear Instruments and Methods in Physics Research A299, pp. 516-523 (1990).

Pr93a T.H. Prettyman, R.P. Gardner, J.C. Russ, and K. Verghese, "A Combined Transmission and Scattering Approach to Composition and Density Imaging", accepted for publication in Nuclear Geophysics (1993).

Pr93b T.H. Prettyman, R.P. Gardner, and K. Verghese, "The Specific Purpose Monte Carlo Code McENL for Simulating the Response of Epithermal Neutron Lifetime Well Logging Tools", accepted for publication in IEEE Transactions on Nuclear Science (1993).

Ro79 R.S.C. Rogers and R.P. Gardner, "A Monte Carlo Method for Simulating Dispersion and Transport through Horizontal Rotating Cylinders", Powder Technology, 23, pp. 159-167 (1979).

Sh88 C.M. Shyu, T. He, K. Verghese, and R.P. Gardner,"Monte Carlo - Library Least-Squares Principle for Nuclear Analyzers", Transactions of the American Nuclear Society, Suppl. 3, Vol. 56, 44-46 (1988).

Sh93 C.M. Shyu, R.P. Gardner, and K. Verghese, "Development of the Monte Carlo - Library Least-Squares Method of Analysis for Neutron Capture Prompt Gamma-Ray Analyzers", accepted for publication in Nuclear Geophysics (1993).

Ve84 K. Verghese, R.P. Gardner, Y.L. Yuan, and A. Almasoumi, "Monte Carlo Models for On-Line Neutron Capture Prompt Gamma-Ray Analysis", Preprint No. 84-128, Annual Meeting of the Society of Mining Engineers of AIME, Los Angeles, February 26-March 1, 1984.

Ve88a K. Verghese, R.P. Gardner, M. Mickael, C.M. Shyu, and T. He, "The Monte Carlo - Library Least-Squares Analysis Principle for Borehole Nuclear Well Logging Elemental Analyzers", Nuclear Geophysics, Vol. 2, No. 3, 183-190 (1988).

Ve88b K. Verghese, M. Mickael, T. He, and R.P. Gardner, "A New Analysis Principle for EDXRF: The Monte Carlo - Library Least-Squares Principle", Advances in X-Ray Analysis, Vol. 31, 461-469 (1988).

Ve90 Kuruvilla Verghese and Robin P. Gardner, "A Generalized Approach to Designing Specific-Purpose Monte Carlo Programs: A Powerful Simulation Tool for Radiation Applications", Nuclear Instruments and Methods in Physics Research A299, pp. 1-9 (1990).

Wa80 D.W. Wall and R.P. Gardner, "A Monte Carlo Simulation of the Rate of Breakage in Ball Mills", Proceedings of Powder and Bulk Solids Conference, Chicago, Illinois, May 13-15, 1980, 4 pages.

Ya84 A.M. Yacout, R.P. Gardner, and K. Verghese, "Cubic Spline Techniques for Fitting X-Ray Cross Sections", Nuclear Instruments and Methods in Physics Research, 220, 461-472 (1984).

Ya86a A.M. Yacout, K. Verghese and R.P. Gardner, "Cubic Spline Representation of the Two-Variable Cumulative Distribution Functions for Coherent and Incoherent X-Ray Scattering", X-Ray Spectrometry, 15, 259-265(1986).

Ya86b A.M. Yacout, R.P. Gardner and K. Verghese, "A Semi-Empirical Model for the X-Ray Si(Li) Detector Response Function", Nuclear Instruments and Methods in Physics Research, A243, 121-130(1986).

Ya87 A.M. Yacout, R.P. Gardner, and K. Verghese, "Monte Carlo Simulation of the X-Ray Fluorescence Spectra from Multielement Homogeneous and Heterogeneous Samples", Advances in X-Ray Analysis, Vol.30, 121-132 (1987).

Yu83 Yih-Liang Yuan, Kuruvilla Verghese, and Robin P. Gardner, "A Specific Monte Carlo Model for the Neutron-Capture Prompt Gamma-Ray Analyzers for Bulk Media", Transactions of the American Nuclear Society, 45, pp. 219-221 (1983).

Yu87 Y.L. Yuan, R.P. Gardner, and K. Verghese, "A Monte Carlo Model for for On-Line Neutron Capture Prompt Gamma-Ray Analysis of Coal in Transmission Grometry", Nuclear Technology, 77 (1), 97-109 (1987).

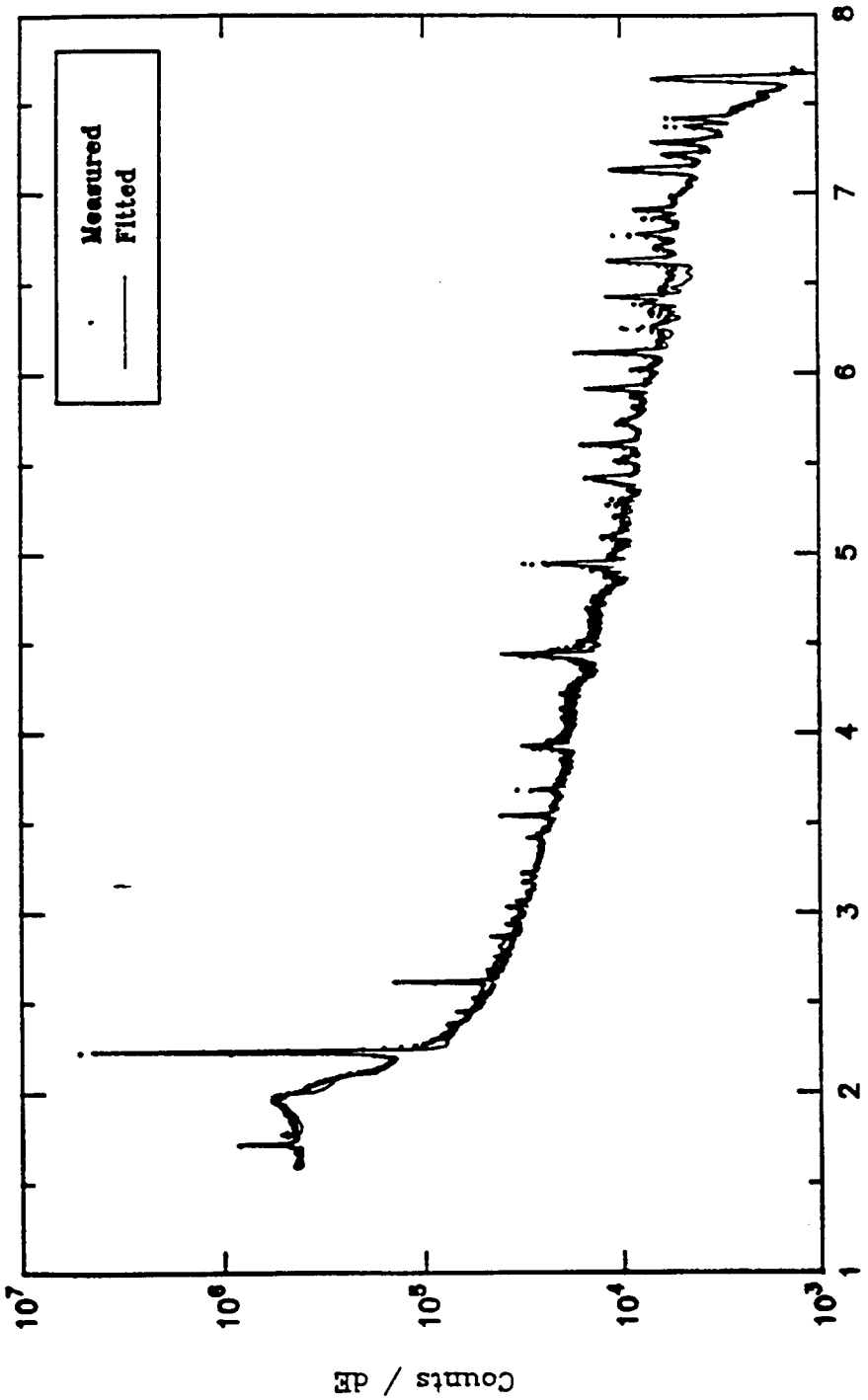

Figure 7.22 Comparison Between Experimental and Fitted Spectra of Coal Sample III

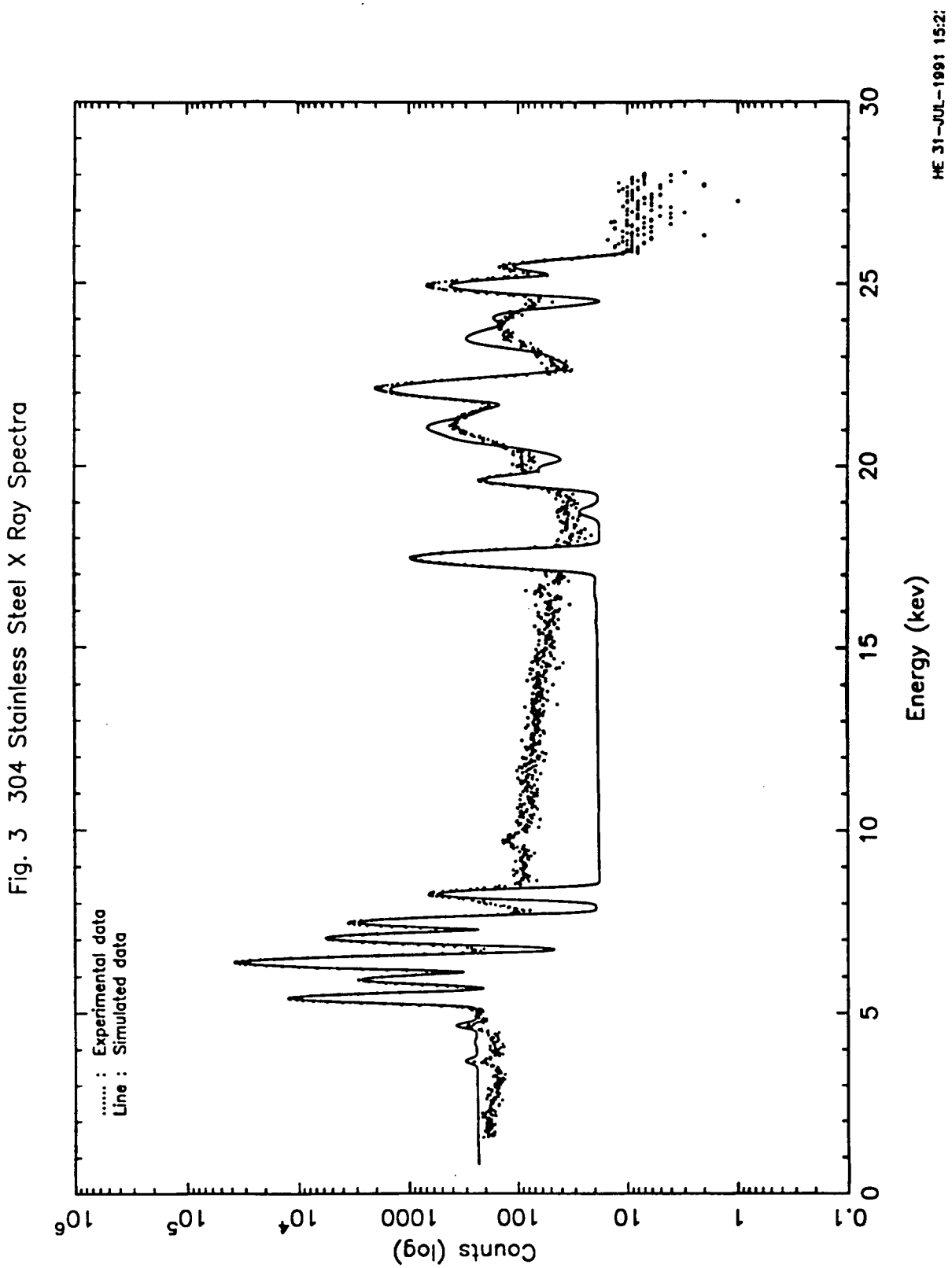
Fig. 3 304 Stainless Steel X Ray Spectra
..... : Experimental data
Line : Simulated data
Counts (log)
Energy (kev)
0.1
1
10
100
1000
10^4
10^5
10^6
0
5
10
15
20
25
30
HE 31-JUL-1991 15:2

Activity at ENEA-DRI, Bologna, Italy, on Monte Carlo Electron Transport

R.Guaraldi, F.Padoani, ENEA-DRI,Via Martiri di Monte Sole, 4, 40129 Bologna, Italy

1. Activity up to present

A code named MCNPE-BO has been developed for the coupled transport of neutrons, γ rays and electrons /1/,/2/. As far as the neutron and γ transport is concerned, the code is based on MCNP (ver.3a), whilst the electron transport is based on the Molière theory. The idea behind the work was to develop a code including electron transport that had the reliability and user-friendliness of MCNP. The work was started before MCNP version 4, which contains electron transport, became available. Notwithstanding, because the development at ENEA has concentrated on the Molière theory, whilst MCNP-4 used Goudsmit-Saunderson theory, the development may be regarded as complementary to the latest MCNP developments.

The particular model based on Molière theory adopted, has been developed and implemented by A. Ferrari and P. Sala at INFN, Milan. This model is substantially more complex with respect to the simple model employed by EGS, and has been tested and validified down to quite low energies /3/.

The γ-e, e-e and e-γ data are generated in a pre-processing step using a modified form of PEGS, whilst the rest of the data is MCNP based.

The practical energy range of application of MCNPE-BO at present is from about 1 keV (depending on the ionization potential) to 100 MeV.

2. Physics

At the moment only the following basic interactions concerning electron production and transport are considered: Knock-on (Moller and Bhabha), Bremsstrahlung, Annihilation, as well as Compton and pair production. Still missing are detailed shell treatment and other minor effects (X-ray emission, straggling, Auger, etc.).

Interaction events with a secondary energy above the cut-off are treated singularly ("catastrophic events"). Instead if the secondary energy is below the cut-off, multi-scattering theory is used and the energy loss of the primary is calculated with the continuous slowing down approximation model.

At the moment we are considering whether to insert a correction to the Molière single scattering cross-section to take into account the spin-relativistic effect, based on the Mott theory, which should be important in the calculation of backscattering.

3. The new, extended multiscattering model based on Molière theory (/3/)

The path length correction (ratio of the real path to the straight line path) has been calculated in a precise fashion and supplied in tabular form /2/.

Two angles are applied to the track: one at the beginning of the track that controls the lateral displacement, and the other at the end of the track that gives the final direction of the electron. The correlation between the two angles is ignored /2/,/3/.

The included correlation between step length and the two above angles allows a more accurate calculation of the backscattering compared with the simple EGS model. Furthermore the angles are corrected in an appropriate fashion according to the step length using tables of data.

For boundary crossings, as the electron nears the boundary, the size of the step is progressively decreased, and *vice versa* as the electron moves away from the boundary.

For segmented tallies, the decrease in energy along the step length is taken into account.

The variables that are a function of the energy are averaged along the step length, taking into account in a consistent fashion the degradation in energy along the step.

4. Results

An extensive effort has been expended on benchmarking the code with respect to other codes and with respect to experimental results /4/ (see for example figs. 1 and 2). In general the results obtained are comparable with those from codes based on Goudsmit-Saunderson (ACCEPT, MCNP4). However it seems that MCNPE-BO with its boundary crossing algorithm allows a better treatment of heterogeneities (near voids, boundaries between materials, etc.).

Disadvantages: MCNPE-BO runs slower than MCNP4; at present the electron x-sec pre-processing step is required.

Advantages: the results seem slightly better than MCNP4. All normal MCNP tallies are allowed as well as tally segmentation.

5. Goals

The new code will be made available to the community to allow easy and relatively clean comparisons between the two electron transport models. Our opinion is that an extended model based on Molière gives good results also at low energies.

6. Future activity

We are working on a patch to MCNP4 containing the new electron transport model. At the same time we are working on improving the CPU time. We are also improving the low energy physics (shell structure in the range 1-100 keV).

7. References

1. Guaraldi R., Padoani F., Burn K.W. and Gualdrini G.F., "Monte Carlo Applications to Photon Radiation Protection and Dosimetry at ENEA", *Progress in Nucl. Energy* **24** 365 (1990)

2. Guaraldi R. and Padoani F., "MCNPE-BO: A New Version of MCNP for the Coupled Transport of Neutrons, Photons and Electrons. User Manual", to be published

3. Ferrari A., Sala P., Guaraldi R. and Padoani F., "An Improved Multiple Scattering Model for Charged Particle Transport", *Nucl. Instruments and Methods* **B71** 412 (1992)

4. Guaraldi R. and Padoani F., "Benchmarking of the code MCNPE-BO", to be published

Figure 1. **Calculated and experimental absorbed-dose distributions from 1-MeV electron source in AL-Au-Al**

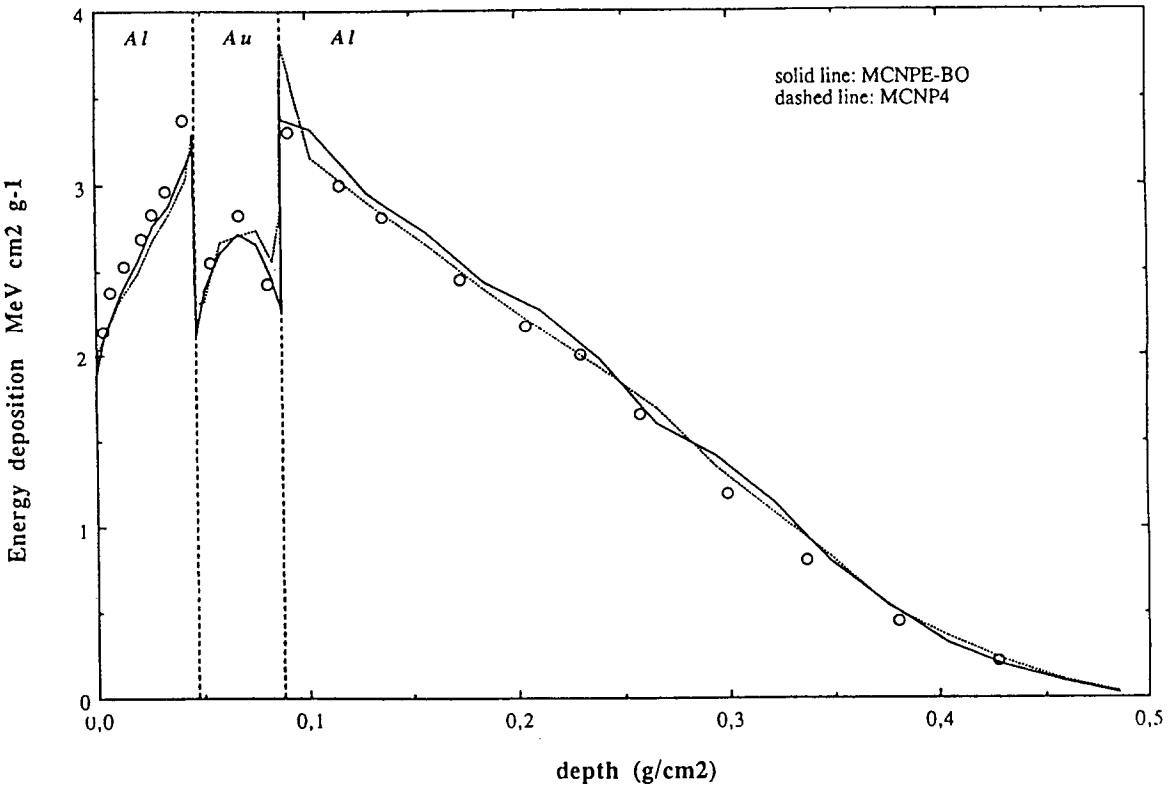

Figure 2.

Depth-dose distributions from a 20MeV electron source on a water phantom

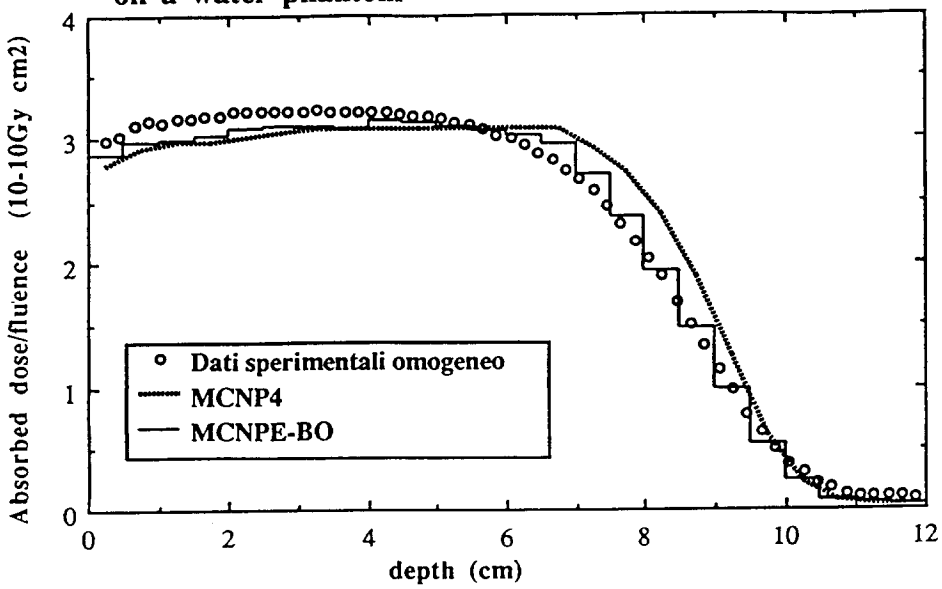

CASCADE-5 MONTE CARLO CODE FOR CALCULATION OF AVERAGE AND FLUCTUATION CHARACTERISTICS OF ELECTRON-PHOTON TRANSPORT

A.V.Lappa, +D.S.Burmistrov
Chelyabinsk State University, +Urals Research Center for Radiation Medicine
Russia

General purpose: calculation of both the average and fluctuation characteristics of electron, photon and positron coupled transport in an axial-symmetric multi-zone heterogeneous media including arbitrary substances; the particles energy range is 0.01 - 10^9 MeV.

Characteristics under calculations: particle interaction data; fluence distributions in space, direction and energy; absorbed dose distributions in space; albedo characteristics; probability distributions and moments of energy absorbed in arbitrary volumes of the media, in small and optically thin volumes among them; average and fluctuation characteristics of high and extra-high energy electromagnetic cascades, etc.

Calculation methods: various schemes of Monte Carlo method, including analog simulation of particle histories taking into account particle multiplication and transformation; the technique of condensation of charged particle collisions with a low energy transfer [1]; variance reduction biasing schemes speeding up calculations in the case of very low or very high number of secondary particles; new high-efficient non-analog Monte Carlo methods for calculation of fluctuation characteristics: "Fluctuation Detector Method" and "Fluctuation Weighting Scheme" (see the last item of the paper).

User interface. There are two levels of code operation. At the first level the user's abilities are restricted to a set of user's modules included in CASCADE-5. At this level the code is under the control of a set of parameters, their input is made in a dialogue. The user does not need to know any programming language or any detail of CASCADE-5 operation. He can either start a new calculation or continue calculations started earlier. At the second level CASCADE-5 gives an opportunity to include new user's modules according to documented simple rules. At this level the users should be familiar with FORTRAN and have a notion of Monte Carlo method and radiation transport theory.

Analogs and advantages. The main analog of CASCADE-5 is EGS-4 Code [2]. CASCADE-5 includes more correct simulating procedures at low and high energies. For example, it does not require an assumption of cross section monotonicity; it simulates Auger-electron production and fluorescent yield in the main spectrum lines; it takes into account Landau-Pomeranchuc "suppression effect" in pair production and bremstrahlung at high energies; the particle angles in the collisions are simulated using continuous distributions; more detail scheme of multiple scattering simulation is implemented in CASCADE-5. As concerns the methods of fluctuation characteristic calculations, CASCADE-5 is unique.

Development history. The base version of CASCADE code system was created in 1982 by A.V.Lappa and A.V.Plyasheshnikov [3] using elaborations of A.M.Kolchuzhkin's research group from Tomsk Polytechnic Institute (USSR) [1]. The present version CASCADE-5 was created by A.V.Lappa and D.S.Burmistrov.

Documentation: There is detailed description of the base version CASCADE [3], user manual and help system for CASCADE-5 (in Russian).

Hardware required: IBM compatible PC (AT-286 and higher), about 3Mb of hard disk space and 300Kb of memory.

Contact address: Dmitry Burmistrov, Urals Research Center for Radiation Medicine, Medgorodok FIB-4, 454076, Chelyabinsk, Russia, e-mail: dima@urcrm.chel.su , fax: (3512) 344-321. Alexander Lappa, Chelyabinsk State University, Br.Kashirinikh 129, 454136, Chelyabinsk, Russia, e-mail: nig@cgu.chel.su , fax: (3512) 421-547.

Applications. Intensive exploitation of a few CASCADE code versions at several institutions in Russia testifies to reliability of the algorithms and programs. The results of original and test calculations have been published in 3 monographs, in the proceedings of the Soviet Radiation Protection Conferences, a large number of reports and papers (in Russian). Some results of calculations by CASCADE-5 have been published in [4]. To illustrate the CASCADE-5 capabilities two problems solved recently are outlined here.

1. The image of a small defect in a radio-graphic or introscope device is a spot on the film or on scintillation screen, which is masked by noise due to random nature of radiation energy absorption. To investigate the degree of defect discovering it is necessary to calculate the probability distribution or, at least, the mean and variance of random energy absorbed in mm-size volumes in the sensitive screen placed behind a thick layer of material under test. That is a hardly realizable task for analog Monte Carlo because only very small fraction of the particles contributes to absorbed energy in the small volume. Conventional biasing (weighting) schemes are inapplicable for calculation of the desired values, since these methods are designed to calculate the means only. This task has been solved by CASCADE-5 using the "Fluctuation Detector Method" [5].

2. One of the methods of cosmic ray energy determination is the emulsion chamber method of particle shower registration. It requires the knowledge of both average and fluctuation characteristics of showers in the atmosphere and chamber. The analog Monte Carlo fails to solve this problem for high enough shower energy due to a huge number of secondaries in such a shower. Making use of the CASCADE-5 and "Fluctuation Weighting Scheme" (by introducing the "killing" of shower secondaries) we have calculated the mean and variance of charged particle number in several elements of the chamber. In many respects these are record calculations: 0.1 - 10^9 MeV energy range from cut-off energy to initial energy; heterogeneous media including realistic not uniform atmosphere, and lead chamber; all the main particle interactions are taken into account including Compton scattering and photoelectric effect; Landau-Pomeranchuk effect is taken into account; fluctuation characteristics were calculated; each calculation was carried out without any intermediate steps using PC-AT(386). We compared the effectiveness of the weighting and analog schemes. In the most difficult calculations the weighting scheme provided a thousand-fold gain in computation time. The result is to be published.

Remark on the non-analog fluctuation methods. The Monte Carlo methods deal conventionally with the linear radiation characteristics, i.e., the characteristics that can be expressed as linear functionals of the solution of the transport equation. Every linear characteristic is, in a probabilistic sense, the mean of random variable additive over particle trajectories. The variables of that "additive" kind are, for example, the absorbed energy in some phase-space region over a definite time, the number of interactions in the region, the number of particles at a fixed time moment, etc. However, there are numerous applications of microdosimetry, radiobiology, cosmic ray physics, the nuclear reactor noise problem, radiation flaw detection, etc., that makes us consider fluctuation characteristics, in particular, the probability distributions and higher moments of the additive variables. In general, the fluctuation characteristics are not linear, and the conventional Monte Carlo techniques can not be used to calculate them. They can be calculated (and they are calculated in practice) by analog Monte Carlo, but this approach is often ineffective or even unrealizable.

The available non-analog Monte Carlo methods for the fluctuation characteristics can be subdivided into two groups: 1) the schemes based on special probabilistic models for the fluctuation characteristics, some generalizations of well known representation of linear characteristics in the direct, adjoint and "contributon" forms, and 2) weighting schemes, that are in a sense a generalization of conventional biasing schemes. All the methods have been elaborated by means of the stochastic radiation transport theory.

The "Fluctuation Detector Methods" (FD methods) [6,7] belong to the first group. The methods are especially efficient in calculating the distributions and moments of the absorbed energy and interaction number in a small target. The methods have been successfully applied for solving some problems of microdosimetry [8], and radiation flaw detection [5].

The "Fluctuation Weighting Schemes" belong to the second group. Three different kinds of weighting estimators for the moments have been proposed in [9-11]. The estimators are defined on biased branching trajectories of the particles, the mean value of each estimator is equal to a certain higher moment. The methods are efficient in the same cases, when conventional biasing schemes are efficient.

REFERENCES

1. A.M. Kolchuzhkin, V.V Uchaikin, "An Introduction in the theory of particle transport through media", Moskva:Atomizdat, 1978 (in Russian).

2. W.R.Nelson, H.Hirayama, D.W.O.Rogers, "The EGS-4 Code System", SLAC-265, 1985.

3. A.V.Lappa, A.V.Plyasheshnikov,"The code for Monte Carlo calculations of electron-photon transport characteristic in heterogeneous media", VNTIC, 1982, No 02825030754 (in Russian).

4. "5th Allunion Scientific Conference on Radiation Protection of Nuclear Devices", Protvino, 1990, P.109-114, 115-127, 148-152 (in Russian).

5. A.V.Lappa, D.S.Burmistrov, "Method for calculation of quantum fluctuations and degree of defect discovering in radio-graphic and introscope systems", Defectoscopiya, 1989, No.11, P.29-37 (in Russian).

6. Lappa A.V.,"Mathematical description and method for calculation of energy absorption fluctuations in small volumes of a substance irradiated by ionizing particles", Izvestia vuzov SSSR. Fizika., 1984, No 9, P.13-18. (in Russian).

7. Lappa A.V., Vasilyev O.N., Burmistrov D.S., "Mathematical description and calculation method for fluctuation characteristics of ionizing particles influence on small sensitive volumes in irradiated systems", VINITI, 1987, No 4650-B87 (in Russian).

8. A.V. Lappa, E.A. Bigildeyev, D.S. Burmistrov, O.N. Vasilyev, "TRION code for radiation action calculations and its application in microdosimetry and radiobiology", Radiat. Environ. Biophys., 1993, V.32, P.1-19.

9. A.V.Lappa, "The estimators for higher moments of additive quantities in cascade processes of particles transport", Metody Monte Karlo v vychisl. matem. i matem. fizike, 1985, P.301-304 (in. Russian).

10.A.V.Lappa, "The weighting Monte Carlo estimator for calculation of higher moments of additive characteristics of particles transport with a multiplication", Jurnal vychislit. matam i matem. fiziki, 1990, v.29, P.122-134 (in Russian).

11.A.V.Lappa, D.S.Burmistrov, "Basic estimator for higher moments of additive functionals in cascade particle transport processes", Metody Monte Karlo v vychisl. matem. i matem. fizike, 1991, v.2, P.73-76 (in. Russian).

APPENDIX A

PROGRAMME AND INDEX

27 April 1993

Registration of Participants

Welcome - Announcements

Session I. ***General presentation of key features of advanced Monte Carlo programs including their validation.***

Chair: J.C. Nimal

J.S. Hendricks
MCNP4A: Features and Philosophy

T. Vergnaud
Overview of Monte Carlo Methodologies in TRIPOLI-3

M.B. Emmett
Status of the MORSE Multigroup Monte Carlo Radiation Transport Code

N.R. Smith, R.J. Brissenden, M.H. Watmough
The Development of the MONK and MCBEND Codes within the New Monte Carlo Modular Code Scheme MCANO

J.A. Halbleib, R.P. Kensek, G.D. Valdez, T.A. Mehlhorn S.M. Seltzer, M.J. Berger
ITS Version 3.0: The Integrated TIGER Series of Coupled Electron/Photon Monte Carlo Transport Codes

Luncheon

Session II. Automatic/semiautomatic biasing schemes, their performance and benchmarking

Chair: G. Ledanois

K.W. Burn
Present State of the Direct Statistical Approach (cell model) to Semi-automatic Variance Reduction

B. Morillon
Automatic Biasing Techniques in Monte Carlo

J.S. Tang, B.L. Broadhead
Development and Application of the Automated Monte Carlo Biasing Procedure in SAS4

M. Caillaud
Automatic Biasing in the KAISSA Computer Program

P.C. Miller, S.J. Chucas, I.J. Curl - presented by E. Shuttleworth
The Advanced Features of the Monte Carlo Code MCBEND

Refreshments

Chair: K.W. Burn

C. Oliveira, J. Salgado
Some results of the Effect of Variance Reduction Techniques on the Figure of Merit of Monte Carlo Calculations

J.E. Hoogenboom, J.L. Kloosterman
Automatic Generation of Biasing Parameters for MORSE Shielding Problems

K.N. Abotel, E.W. Larsen, W.R. Martin
Local Exponential Transform Methods for the Monte Carlo Simulation of Multigroup X,Y-Geometry Transport Problems

J.A. Halbleib, R.P. Kensek, G.D. Valdez
Variance Reduction Unique to Coupled Electron/Photon Monte Carlo Transport

Benchmark Session Benchmarks on Variance Reduction Schemes

Chair: K.W. Burn

K.W. Burn
Some Preliminary Remarks concerning the Proposal of an International Benchmark on Variance Reduction Schemes employed in Monte Carlo Neutron and Photon Transport Codes

K.W. Burn
Summary of Discussion on Variance Reduction Benchmark Proposal

Cocktail offered by CEA/DRN/DMT/SERMA

28 April 1993

Session III. Impact of New Computer Architectures, Special Monte Carlo Games

Chair: W.R. Martin

K. Higuchi
MONTE-4 for Monte Carlo Simulations with High Performance

G.W. McKinney
Distributed Processor Monte Carlo: MCNP Results on a 16-node IBM Cluster

M. Nakagawa, T. Mori
Capability and Performance of Vectorized Monte Carlo Codes for Neutron and Photon Transport Calculations

J.P. Both
A Communication Library for TRIPOLI-4

J. Wood
Monte Carlo Calculations on a Parallel Computer Using MORSE-CG

Refreshments

Chair: H. Rief

Y. Uenohara
Parallelism in Continuous Energy Monte Carlo Method for Neutron Transport

W.R. Martin, A. Majumdar, J.A. Rathkopf, M. Litvin
Experiences with Different Parallel Programming Paradigms for Monte Carlo Particle Transport Leads to a Portable Toolkit for Parallel Monte Carlo

Session IV. Monte Carlo Perturbations, Hybrid Methods, Geometry Modelling - Any New Monte Carlo Development

Chair: H.U. Barz

H. Rief
Monte Carlo Perturbation Algorithms Exploit New Computer Architectures

R.S. Baker
Hybrid S_n Monte Carlo Research and Results

Luncheon

Chair: E. Hoogenboom

S.N. Cramer
Recent Developments and Applications of the MORSE Code

J.O. Johnson, R.T. Santoro
The MASH 1.0 Code System: Utilization of MORSE in the Adjoint Mode

R.A. Forster, S.P. Pedersen, T.E. Booth
A New Method to Assess Monte Carlo Convergence

G. Ledanois
The MCNP Photon Benchmark Problems Revisited

N.R. Smith, E. Shuttleworth, M.H. Watmough
A new Approach to Geometry Modelling and Visualisation for MONK and MCBEND

T. Twardowski
The Development of a New Collision Processing Module for MONK/MCBEND Codes

W. Matthes
Monte Carlo Calculation of a Quadratic Average $\int q(x)\, W^2(x)\, dx$

Refreshments

Session V. Presentation of User Experience, Applications, Performance with Emphasis on New Aspects.

Chair: J. Halbleib

Various Applications

P. Andreo
A Comparison between the ITS-3 and EGS-4 Monte Carlo Codes in Radiation Physics

D. Paul
Presentation of the FIRAM Association. Intercomparison Exercise with the EGS-4 Code

K.J. Leliveld
Development of a Simulator for X-ray Computerized Tomography using Monte Carlo Techniques

B. Dahl
Monte Carlo Activities at the Department of Reactor Physics, Chalmers University of Technology

29 April 1993

Session V. Presentation of User Experience, Applications, Performance with Emphasis on New Aspects (Cont.)

Chair: R.A. Forster

Various Applications (Cont.)

T. Eurajoki
User Experience of the MCNP Code in NPP Radiation Safety Analyses and Design

N. Cerullo, M. Bogliardi, R. Guzzardi, P. Riscossa
PETSI, a Package Based on Monte Carlo Techniques to Simulate the Positron Emission Tomography

M. Sumini, J. Fernandez
Comments on Polarization Effects in Photon Transport

B. Laboudigue, G. Beurton - oral presentation only
Optimization of Neutron Interrogation Techniques for Analysing Bauxite

F.W. Schultz, J. Geleijns, J.Th.M. Jansen, J. Zoetelief
Calculation of Organ and Effective Doses for PA Chest Radiography Using Anthropomorphic Phantoms and MCNP

J.Th.M. Jansen, N.J.P. de Wit, F.W. Schultz, J. Zoetelief
Comparison Measured and Calculated Depth-Dose Distributions in Phantom Consisting of Three Cubes (PMMA, air, PMMA) Irradiated with Cs-137 Gamma Rays

L.E. De Geer
Comparison of MCNP Simulated and Measured Dose Rates from Depth Distributed Chernobyl Cesium-134/137 in Russia and Ukraine

G. Minsart
Study of Neutron Spectra and Dose Rates Distribution in the VENUS Reactor Building with the Monte Carlo Code TRIPOLI-2

H.P. Jacquet - oral presentation only
Application of TRIPOLI to Neutron Diagnostics

Refreshments

J.C. Gommé - oral presentation only
Application of TRIPOLI to Studies on Radiation Effects from Nuclear Weapons

J.Ch. Sublet - presented by Ch.M. Diop
Fusion Power Reactor Neutronic Analysis with TRIPOLI-3

L. Levitt - oral presentation only
Experience using MCNP4 on 486/66 PC's at Fluor Daniel, Inc.

Chair: Ch.M. Diop

Cross Sections and Detectors

S.H. Zheng, P. Ribon, J.C. Nimal
Probability Tables Cross Sections in Monte Carlo TRIPOLI-3

H. Tellier, M. Coste, C. Raepsaet, M. Soldevila, C. Van der Gucht
Monte Carlo Validation of Self-shielding and Void Effect Caculations

A.G. Sboev, M.B. Tsitovich
Statistical Generating the Neutron Cross Sections in the Unresolved Resonance Energy Region for Monte Carlo Calculations

J.J. Steyaert
Anomalies in Gamma-Ray Spectra at 68 keV and 170 ke V

Luncheon

Chair: J.S. Hendricks

Cross Sections and Detectors (Cont.)

P. Battistoni, L. Petrizzi, M. Pillon, V. Rado
Use of MCNP in Fusion Blanket Design, ITER Magnet System Shielding Analysis, Benchmark of the EFF (European Fusion File) Neutron Data with the FNG (Frascati Neutron Generator) 14 MeV Neutron Facility

A. Hogenbirk, K.A. Verschuur
Calculation of Radiation Fields Inside and Outside the NET Cryostat/Biological Shield during Operation

F. Mathy - oral presentation only
The Use of ITS Codes in Designing X- or gamma-ray Semiconductor Detectors working as Photoconductors or Spectrometers for some Medical or Non-destructive Testing Applications

R.P.Gardner, K. Verghese
Use of Specific Purpose Monte Carlo Codes in Radiation Application Problems Involving Finite Detectors

V. Mares, H. Schraube - oral presentation only
MCNP Calculated Neutron Response of a Bonner Sphere Spectrometer with Scintillation Detector

J. Arkuszewski - oral presentation only
Stroggling with MCNP - Applicability to Small Size Geometry

R. Guaraldi, F. Padoani
Activity at ENEA-DRI (Bologna, Italy) on Monte Carlo Electron Transport

A.V. Lappa, D.S. Burmistrov
CASCADE-5 Monte Carlo Code for Calculation of Average and Fluctuation Characteristics of Electron-Photon Transport

Closing

APPENDIX B

ORGANISING COMMITTEE AND SUPPORT STAFF

Shielding Laboratoty of CEA, France	**Jean-Claude NIMAL**
	Gilberte CARON
	Mohamed EID
EPIC Radiation Shielding Information Center, USA	**Robert W. ROUSSIN**
OECD/NEA	**Enrico SARTORI, Secretary**
	Michèle FAURE
	Marsha BEAUDOIN-MAYER

LIST OF PARTICIPANTS

AUSTRIA

WOLOCH, Franz

Oesterr. Forschungszentrum
Seibersdorf Ges.m.b.H.
2444 SEIBERSDORF

Tel +43 (2254) 80 2723
Fax +43 (2254) 80 2118
Telex 047000 14353

BELGIUM

MINSART, Georges

Centre d'Etude de l'Energie Nucléaire
200 Boeretang
2400 MOL

Tel +32 (14) 33 2278
Fax +32 (14) 31 5021
Telex 31922

RENARD, Alfred

Belgonucléaire
Avenue Ariane 2-4
1200 BRUXELLES

Tel +32 (2) 774 0634 OR 0511
Fax +32 (2) 774 0547

STEYAERT, Jacques J.

Institut de Physique Nucléaire
Univ. Catholique de Louvain
Ch. du Cyclotron 2
1348 LOUVAIN-LA-NEUVE

Tel +32 (10) 473 273
Fax +32 (10) 452 183

FINLAND

EURAJOKI, Tapani

IVO International Ltd
Nuclear Power Engineering
Safety and Fuel
SF-01019 IVO

Tel +358 (0) 8561 4460
Fax +358 (0) 8561 3403

FRANCE

BAJAC, Jean

Centre d'Etudes de Limeil-Valenton
CEL-V
B.P. 27
94190 VILLENEUVE ST GEORGES

BEURTON, Gabriel

Centre de Recherches de Voreppe S.A.
Péchiney - CRV
B.P. 27
38340 VOREPPE

Tel +33 76 57 80 00
Fax +33 76 56 89 75
Telex 320783

BIOUX, Philippe

EDF/DER/RNE/PhR
Etudes et Recherches
1, av. du Général de Gaulle
92141 CLAMART CEDEX

Tel +33 (1) 47 65 39 08
Fax +33 (1) 47 65 34 99
Telex 204 426 F

BORDY, Jean-Marc

IPSN/DPHD/SDOS
CE FONTENAY-AUX-ROSES
B.P. no. 6
92265 FONTENAY-AUX-ROSES CEDEX

Tel +33 (1) 46 54 742 42
Fax +33 (1) 47 46 97 77

BOTH, Jean-Pierre

CE Saclay
DRN/DMT/SERMA/LEPP
Bat. 470
91191 GIF/YVETTE CEDEX

Tel +33 (1) 6908 8478
Fax +33 (1) 6908 4572

BRESARD, Isabelle

CE Saclay
IRDI/DEDR/DEMT/SERMA/LEPP
Bat. 470
91191 GIF/YVETTE CEDEX

Tel +33 (1) 69 08 56 87
Fax +33 (1) 69 08 23 81

CAILLAUD, Michel

CEA/CEL-V
Service Mathématiques et Codes Numériques
94145 Villeneuve-St.Georges Cedex

Tel +33 (1) 4595 6527
Fax +33 (1) 4595 9555

CARON, Gilberte

CE Saclay
IRDI/DEDR/DEMT/SERMA/LEPP
Bât. 470
91191 GIF/YVETTE CEDEX

Tel +33 (1) 69 08 59 18
Fax +33 (1) 69 08 45 72
Telex 604641

DAYMARD, Nadia

Centre de Recherches Nucléaires
Groupe Strasbourgeois de Neutrothérapie
CHIMIE NUCLEAIRE
B.P.20
67037 STRASBOURG CEDEX 2

Tel +33 88 28 64 15
Fax +33 88 28 64 31

DEJONGHE, Gérard

C.E. de Limeil
DAM/DMA-AIM
B.P. 27
94190 Villeneuve-Saint-Georges

Tel +33 (1) 45 95 62 88
Fax +33 (1) 45 95 95 55

DIOP, Cheikh M'Backe

CE Saclay
DRN/DMT/SERMA/LEPP
Bât. 470
91191 GIF-SUR-YVETTE CEDEX

Tel +33 (1) 6908 5676
Fax +33 (1) 6908 4572
Telex 604641

DOUCET, Michel

Société Framatome
Tour Fiat
92084 PARIS LA DEFENSE

Tel +33 (1) 4796 45 56
Fax +33 (1) 4796 37 43

EID, Mohamed

CE Saclay
IRDI/DEDR/DEMT/SERMA/LEPP
Bât. 470
91191 GIF/YVETTE CEDEX

Tel +33 (1) 69 08 31 75
Fax +33 (1) 69 08 45 72
Telex 604641

GOMME, Jean Claude

CEA/CESTA
BP No. 2
33114 LE BARP

Tel +33 5668 4209
Fax +33 5668 5121

GONNORD, Jean

Centre d'Etudes Nucléaires de Limeil
DAM/DMA-AIM
B.P. 27
94190 VILLENEUVE ST GEORGES

Tel +33 (1) 4595 6576
Fax +33 (1) 4595 9555

HOFFMANN, Alain

DRN-DMT
CE SACLAY
91191 GIF SUR YVETTE CEDEX

Tel +33 (1) 69 08 24 53
Fax +33 (1) 69 08 66 42
Telex 604 641 F ENERG

JACQUET, Henri-Patrick

CE Bruyères le Chatel
Service CEM
B.P. 12
91680 BRUYERES LE CHATEL

Tel +33 (1) 69 26 54 34
Fax +33 (1) 69 26 60 65

KODELI, Ivo

C.E. de Saclay
DRN/DMT/SERMA/LEPP
Bâtiment 470
91191 GIF-SUR-YVETTE CEDEX

Tel +33 (1) 69 08 32 87
Fax +33 (1) 69 08 45 72

LABOUDIGUE, Bruno

Centre de Recherches de Voreppe S.A.
Péchiney - CRV
B.P. 27
38340 VOREPPE

Tel +33 76 57 80 00
Fax +33 76 56 89 75
Telex 320783

LE DAIN, Loic

Centre d'Etudes de Vaujours
CIT/R
BP. No. 7
77181 Courtry

Tel +33 (1) 4936 8005
Fax +33 (1) 4936 7513

LEDANOIS, Guy

CEA/CEL-V
94195 Villeneuve-St.-Georges Cedex

Tel +33 (1) 4595 6617
Fax +33 (1) 4595 9555

LELONG, Henri

Centre d'Etudes Nucléaires de Limeil
CEL-V, Service PG/NME
B.P. 27
94190 VILLENEUVE ST GEORGES

Tel +33 (1) 45 95 69 55
Fax +33 (1) 49 86 50 70

MATHY, Francoise

Fax +33 76 88 51 64

C.E. de Grenoble
LETI/DSYS/SCSI
17, rue des Martyrs
38054 GRENOBLE CEDEX 9

MATTEI, Michel

Tel +33 (1) 45 95 65 73

Centre d'Etudes Nucléaires de Limeil
B.P. 27
94190 VILLENEUVE ST GEORGES

MORILLON, Benjamin

Tel +33 (1) 6908 8040
Fax +33 (1) 6908 4572
Telex 604641

CE Saclay
DRN/DMT/SERMA/LEPP
Bât. 470
91191 GIF-SUR-YVETTE CEDEX

NIMAL, Jean-Claude

Tel +33 (1) 69 08 59 18
Fax +33 (1) 69 08 45 72
Telex 604641

CEN Saclay
IRDI/DEDR/DEMT/SERMA/LEPP
Bât. 470
91191 GIF/YVETTE CEDEX

NOURI, Ali

Tel +33 46 54 89 15
Fax +33 46 57 29 98
Telex 270049

C.E.A.
IPSN/DRS/SEC
B.P. No 6
92265 FONTENAY AUX ROSES CEDEX

PAUL, Didier

Tel +33 (1) 46 54 72 44
Fax +33 (1) 46 57 97 77
Telex 270049 SURIN

CEA/IPSN/DPHD/SDOS
CE Fontenay-aux-Roses
B.P. No. 6
92265 FONTENAY-AUX-ROSES

POULLOT, Gilles

Tel +33 (1) 46 54 85 66
Fax +33 (1) 46 57 29 98
Telex 270049 SURIN

CEA/IPSN/DRS/SEc
CE Fontenay-aux-Roses
B.P. No. 6
92265 FONTENAY-AUX-ROSES

ROSHD, Mustapha

ENS/Cachan
18, rue Paul Verlaine
78860 Saint-Nom-La-Bretèche

Tel +33 (1) 30 80 04 08

SALVATORES, Massimo

Directeur de Recherche
Dir. des Réacteurs Nucléaires
Bât. 707 - CE/CADARACHE
13108 ST. PAUL LEZ DURANCE CEDEX

Tel +33 4225 3365
Fax +33 4225 4142
Telex 440678

SOUBEYRAN, Amaury

Division Système
MATRA Espace Toulouse
31 rue des Cosmonautes
Z.I. du Palays
31077 TOULOUSE CEDEX

Tel +33 62 24 75 12
Fax +33 62 24 77 90
Telex 530980

TELLIER, Henri

CE Saclay
DPRMA/SERMA/LENR
91191 GIF/YVETTE CEDEX

Tel +33 (1) 69 08 31 79
Fax +33 (1) 69 08 23 81

VERGNAUD, Therèse

DEMT/SERMA/LEPP
C.E. SACLAY
91191 GIF SUR YVETTE CEDEX

Tel +33 (1) 69 08 59 40
Fax +33 (1) 69 08 45 72

ZHENG, Song Hui

CE Saclay
DRN/DMT/SERMA/LEPP
Bât. 470
91191 Gif sur Yvette Cedex

Tel +33 (1) 6908 8040
Fax +33 (1) 6908 4572

GERMANY

BARZ, Hans-Ulrich

Forschungszentrum Rossendorf
Inst. Sicherheitsforschung
Postfach 19
O-8051 DRESDEN

Tel +49 (351) 591 3370
Fax +49 (351) 36 069
Telex 2167

HOSSEINI, M.M. Qasim

Bundesamt für Strahlenschutz
Albert Schweitzerst. 18
Postfach 100149
3320 SALZGITTER 1

Tel +49 (531) 592 7643
Fax +49 (531) 592 7616

LEMBCKE, Reiner

Siemens Aktiengesellschaft
Unternehmensbereich KWU
Berliner Str. 295-303
Postfach 10 10 63
6050 OFFENBACH AM MAIN

Tel+49 (69) 807 3324
Fax +49 (69) 807 2484
Telex 041000 4152990

MARES, Vladimir

GSF - Forschungszentrum für Umwelt u. Gesundheit
Gmbh Neuherberg
Postfach 1129
85758 Oberschleissheim

Tel +49 (89) 3187 2652
Fax +49 (89) 3187 3323

NOACK, Klaus

Forschungszentrum Rossendorf
Inst. Sicherheitsforschung
Postfach 19
D O-8051 DRESDEN

Tel +49 (351) 591 3239
Fax +49 (351) 36 069

ISRAEL

PEREL, R.

Racah Institute of Physics
The Hebrew University
JERUSALEM 91009

ITALY

BURN, Kenneth W.

VEL-PRO-NEUT
ENEA
Via Martiri di Monte Sole 4
40129 BOLOGNA

Tel +39 (51) 6098 486
Fax +39 (51) 6098 629

CERULLO, Nicola

Dipartimento Ingegneria Energetica
Via all'Opera Pia 15A
16145 GENOVA

Tel +39 (10) 353 2869
Fax +39 (10) 311 870

FERNANDEZ, Jorge E.

Laboratorio di Ingegneria Nucleare Montecuccolino
Univ. degli Studi di Bologna
Via dei Colli, 16
40136 BOLOGNA

Tel +39 (51) 58 11 05
Fax +39 (51) 58 11 08
Telex 043000 520620 ING BO I

NEUHOLD, Piero

ANSALDO
Corso Perrone 25
16161 GENOVA

Tel +39 (10) 655 8690
Fax +39 (10) 655 8890

PETRIZZI, Luigi

FUS/INGFUS
ENEA Frascati
Via Enrico Fermi 27
00044 FRASCATI

Tel +39 (6) 9400 5741
Fax +39 (6) 9400 5250

SUMINI, Marco

Laboratorio di Ingegneria Nucleare Montecuccolino
Univ. degli Studi di Bologna
Via dei Colli, 16
40136 BOLOGNA

Tel +39 (51) 58 11 05 /06 /07 /08
Fax +39 (51) 58 11 08
Telex 043000 520620 ING BO I

JAPAN

HIGUCHI, Kenji

JAERI / SISC
Tokai Research Establishment
TOKAI-MURA, Naka-gun
Ibaraki-ken 319-11

Tel +81 (292) 82 5369
Fax +81 (292) 82 6070

NAKAGAWA, Masayuki

Dept. of Reactor Engineering
JAERI
Tokai Research Establishment
TOKAI-MURA, Naka-gun
Ibaraki-ken 319-11

Tel +81 (292) 82 5337
Fax +81 (292) 82 6122
Telex 3632340

UENOHARA, Yuji

Nuclear Engineering Lab.
TOSHIBA Corporation
4-1, Ukishima-cho
Kawasaki-ku,
Kawasaki 210

Tel +81 (44) 288 8130
Fax +81 (44) 299 2853

NETHERLANDS

HOGENBIRK, Alfred

Nuclear Analysis Group
B.U. Nuclear Energy
ECN
Postbus 1
1755 ZG PETTEN

Tel +31 (2246) 4051
Fax +31 (2246) 3490
Telex 044000 57211 REACP NL

HOOGENBOOM, J. Eduard

Delft University Technology
Interfaculty Reactor Institute (IRI)
Mekelweg 15
2924 VK DELFT

Tel +31 (15) 786962
Fax +31 (15) 786422

Telex 38214 IRI NL

JANSEN, Jan

Center for Radiation Protection and Dosimetry
TNO
Lange Kleiweg 151
P.O.Box 1585
2280 HV RIJSWIJK

Tel +31 (15) 84 27 50
Fax +31 (15) 84 39 98

LELIVELD, Kees-Jan

KSEPL/FOM/TUD
P.O.Box 60
2280 AB RIJSWIJK

Tel +31 (70) 311 2447
Fax +31 (70) 311 3110

POLAND

DABROWSKA, Joanna

Environmental & Radiation Transport Physics Dept.
Institute of Nuclear Physics
ul. Radzikowskiego 152
31-342 KRAKOW

Telex 322461 ifj pl

LOSKIEWICZ, Jerzy

Institute of Nuclear Physics
ul. Radzikowskiego 152
31-342 KRAKOW

Tel 19 48 37 02 22 (EXT. 345)

Telex 063000 0322 461 ifj

PORTUGAL

OLIVEIRA, Carlos

INETI/ICEN
Physics Department
Estrada Nacional N. 10
2685 SACAVEM

Tel +351 (1) 955 0021
Fax +351 (1) 955 0117
Telex 040400 12727

RUMANIA

TISEANU, I.

Institute for Atomic Physics
IFTAR, Lab. 22
Bucharest-Magurele
P.O. Box MG-7, R-76900

Fax +401 312 1154

RUSSIAN FEDERATION

ROGOV, Anatoli

Joint Institute for Nuclear Research (JINR)
Head Post Office,
P.O. Box 79
101000 MOSCOW

Telex 064000 MSK DUBNA 412621

SBOEV, Alexander G.

I.V. Kurchatov Institute for Atomic Energy
I.V. Kurchatova Proshchad
123182 MOSCOW D-182

Fax +7 (095) 196 66 39 / 190 5171

SLOVENIA

RANT, Joze

Institut "Jozef Stefan"
Reactor Centre
Jamova 39
61111 LJUBLJANA, p.p. 100

Tel +386 (61) 1885 357 OR 450
Fax +386 (61) 374 919
Telex 062000 31296 JOSTIN YU

SOUTH AFRICA

TAVIV, Eugene

Electricity Supply Commission
(ESKOM)
P.O. Box 1091
2000 JOHANNESBURG

Tel +27 (11) 800 8111
Fax +27 (11) 800 5771
Telex 095000 4-24481 SA

SPAIN

GARCIA DE VIEDMA, Luis

Deputy Director, Computing
Consejo de Seguridad Nuclear
C/ Justo Dorado, 11
28040 MADRID

Tel +34 (1) 3460 124, 178
Fax +34 (1) 3460 588
Telex 05200 49051 CSNM E

SWEDEN

ANDREO, Pedro

Dept. of radiation Physics
University of Lund
22185 Lund

Tel +46 (46) 17 31 31
Fax +46 (46) 13 61 56

DAHL, Ingolf

Dept. of Reactor Physics
Chalmers University
412 96 Goteborg

Tel +46 (31) 772 3079
Fax +46 (31) 772 3079

DAHL, Berit

Dept. of Reactor Physics
Chalmers University of Technology
412 96 Goeteborg

Tel +46 (31) 772 3084
Fax +46 (31) 772 3079

DE GEER, Lars-Erik

FOA National Defence Research
Establishment
Dept. Weapon Systems, Effects and Protection
172 90 SUNDBYBERG

Tel +46 (8) 663 15 00
Fax +46 (8) 628 55 64
Telex 10366 foa s

SWITZERLAND

ARKUSZEWSKI, Jacek J.

Paul Scherrer Institute
5232 VILLIGEN PSI

Tel +41 (56) 99 20 83
Fax +41 (56) 98 23 27 PSI CH
Telex 045000 82 74 17 PSI CH

UNITED KINGDOM

CURL, I.J.

WINFRITH TECHNOLOGY CENTRE
Reactor Physics Division
DORCHESTER
Dorset DT2 8DH

Tel +44 (305) 203 109
Fax +44 (305) 202 746
Telex 41231 ATOMWH G

SHUTTLEWORTH, E.

AEA Reactor Services
Winfrith Technology Centre
DORCHESTER
Dorset DT2 8DH

Tel +44 (305) 25188
Fax +44 (305) 202 746

SMITH, Nigel R.

AEA Technology Winfrith
DORCHESTER
Dorset DT2 8DH

Tel +44 (305) 203 260
Fax +44 (305) 202 746

THORNTON, D.A.

Nuclear Electric
Berkeley Nuclear Labs.
BERKELEY
Gloucestershire GL13 9LA

Tel +44 (453) 810451
Fax +44 (453) 812590
Telex 051000 43227

TWARDOWSKI, Timothy

British Nuclear Fuels plc
Advanced Methods, Nuclear Technology Section
Risley, Warrington
Cheshire WA3 6AS

Tel +44 (925) 83 30 59
Fax +44 (925) 83 32 67

WOOD, James

Queen Mary College
Nuclear Group
Dept. of Mechanical Engineer
Mile End Road
LONDON E1 4NS

Tel +44 (71) 975 52 84
Fax +44 (81) 981 75 17
Telex 051000 893750

UNITED STATES OF AMERICA

BAKER, Randal S.

Los Alamos National Laboratory
Radiation Transport Group
X-6, MS B226
Los Alamos, NM 87545

Tel +1 (505) 667 3041
Fax +1 (505) 665 5538

CRAMER, S. Noel

Engineering Physics Information Center
Oak Ridge National Laboratory
Post Office Box 2008
Oak Ridege, TN 37831-6362

Tel +1 (615) 574 6176
Fax +1 (615) 574 6182
Telex 854467 ORNL EPIC UD

EMMETT, Margaret B.

Building 6011, MS 6370
Oak Ridge National Laboratory
Post Office Box 2008
Oak Ridge, TN 37831-6370

Tel +1 (615) 574 5276
Fax +1 (615) 574 3527

FORSTER, R. Arthur

Group X-6, MS B226
Radiation Transport Group
Los Alamos National Lab.
Los Alamos, NM 87545

Tel +1 (505) 667 5777
Fax +1 (505) 667 5538

GARDNER, Robin P.

Center for Engineering Applications of Isotopes
North Carolina University
Box 7909
Raleigh, NC 27695-7909

Tel +1 (919) 515 3378
Fax +1 (919) 515 5115

HALBLEIB, John A.

Sandia National Laboratories
Simulation Technology
Org. 9341
Albuquerque,
New Mexico 87185-5800

Tel +1 (505) 845 7064
Fax +1 (505) 845 7841

HENDRICKS, John S.

Los Alamos National Laboratory
Radiation Transport Group
X-6, MS B226
Los Alamos, NM 87545

Tel +1 (505) 667 6997
Fax +1 (505) 665 5538

JOHNSON, J. O.

Building 6011, MS 6370
Oak Ridge National Laboratory
Post Office Box 2008
Oak Ridge, TN 37831-6370

Tel +1 (615) 574 5280
Fax +1 (615) 576 3513
Telex 023000 854467

LEVITT, Leo

Fluor Daniel, Inc.
3333 Michelson Drive
IRVINE
California 92730

Tel +1 (714) 975 6952
Fax +1 (714) 975 5747 OR 5004

MARTIN, William R.

UNIVERSITY OF MICHIGAN
Dept. of Nuclear Engineering
225 Cooley Building, North Ca
ANN ARBOR, MI 48109-2104

Tel +1 (313) 764 55 34
Fax +1 (313) 763 45 50

McKINNEY, Gregg W.

Los Alamos National Laboratory
Radiation Transport Group
X-6, MS B226
Los Alamos, NM 87545

Tel +1 (505) 665 8367
Fax +1 (505) 665 5538

TANG, Jabo S.

Building 6011, MS 6370
Oak Ridge National Laboratory
Post Office Box 2008
Oak Ridge, TN 37831-6370

Tel +1 (615) 574 5266
Fax +1 (615) 576 3513
Telex 023000 854467

INTERNATIONAL ORGANIZATIONS

Joint Research Centre

MATTHES, Wilhelm

Joint Research Centre
I-21020 ISPRA

RIEF, Herbert W.

Sector Head
Info.Analysis & Handling Div.
Joint Research Centre
Ispra Establishment
I-21020 ISPRA

Tel +39 (332) 789 746
Fax +39 (332) 785 584
Telex 043000 43380058

OECD Nuclear Energy Agency

BEAUDOIN-MAYER, Marsha

OECD-NEA
12 boulevard des Iles
F-92130 Issy-Les-Moulineaux

Tel +33 (1) 45 24 10 16
Fax +33 (1) 45 24 11 10
Telex 630668 AEN-NEA

FAURE, Michèle

OECD-NEA
Section Conference
12 boulevard des Iles
F-92130 Issy-Les-Moulineaux

Tel +33 (1) 45 24 10 22
Fax +33 (1) 45 24 11 10
Telex 630668 AEN-NEA

SARTORI, Enrico

OECD/NEA Data Bank
Le Seine-Saint Germain
12 boulevard des Iles
F-92130 Issy-Les-Moulineaux

Tel +33 (1) 45 24 10 72
Fax +33 (1) 45 24 11 10

SAVELLI, Philippe

Deputy Director
OECD/Nuclear Energy Agency
Le Seine Saint Germain
12, Bd. des Iles
F-92130 Issy-Les-Moulineaux

Tel +33 (1) 45 24 10 06
Fax +33 (1) 45 24 11 10

MAIN SALES OUTLETS OF OECD PUBLICATIONS
PRINCIPAUX POINTS DE VENTE DES PUBLICATIONS DE L'OCDE

ARGENTINA – ARGENTINE
Carlos Hirsch S.R.L.
Galería Güemes, Florida 165, 4° Piso
1333 Buenos Aires Tel. (1) 331.1787 y 331.2391
Telefax: (1) 331.1787

AUSTRALIA – AUSTRALIE
D.A. Information Services
648 Whitehorse Road, P.O.B 163
Mitcham, Victoria 3132 Tel. (03) 873.4411
Telefax: (03) 873.5679

AUSTRIA – AUTRICHE
Gerold & Co.
Graben 31
Wien I Tel. (0222) 533.50.14

BELGIUM – BELGIQUE
Jean De Lannoy
Avenue du Roi 202
B-1060 Bruxelles Tel. (02) 538.51.69/538.08.41
Telefax: (02) 538.08.41

CANADA
Renouf Publishing Company Ltd.
294 Algoma Road
Ottawa, ON K1B 3W8 Tel. (613) 741.4333
Telefax: (613) 741.5439

Stores:
61 Sparks Street
Ottawa, ON K1P 5R1 Tel. (613) 238.8985
211 Yonge Street
Toronto, ON M5B 1M4 Tel. (416) 363.3171
Telefax: (416)363.59.63

Les Éditions La Liberté Inc.
3020 Chemin Sainte-Foy
Sainte-Foy, PQ G1X 3V6 Tel. (418) 658.3763
Telefax: (418) 658.3763

Federal Publications Inc.
165 University Avenue, Suite 701
Toronto, ON M5H 3B8 Tel. (416) 860.1611
Telefax: (416) 860.1608

Les Publications Fédérales
1185 Université
Montréal, QC H3B 3A7 Tel. (514) 954.1633
Telefax : (514) 954.1635

CHINA – CHINE
China National Publications Import
Export Corporation (CNPIEC)
16 Gongti E. Road, Chaoyang District
P.O. Box 88 or 50
Beijing 100704 PR Tel. (01) 506.6688
Telefax: (01) 506.3101

CZECH REPUBLIC – RÉPUBLIQUE TCHÈQUE
Artia Pegas Press Ltd.
Narodni Trida 25
POB 825
111 21 Praha 1 Tel. 26.65.68
Telefax: 26.20.81

DENMARK – DANEMARK
Munksgaard Book and Subscription Service
35, Nørre Søgade, P.O. Box 2148
DK-1016 København K Tel. (33) 12.85.70
Telefax: (33) 12.93.87

EGYPT – ÉGYPTE
Middle East Observer
41 Sherif Street
Cairo Tel. 392.6919
Telefax: 360-6804

FINLAND – FINLANDE
Akateeminen Kirjakauppa
Keskuskatu 1, P.O. Box 128
00100 Helsinki
Subscription Services/Agence d'abonnements :
P.O. Box 23
00371 Helsinki Tel. (358 0) 12141
Telefax: (358 0) 121.4450

FRANCE
OECD/OCDE
Mail Orders/Commandes par correspondance:
2, rue André-Pascal
75775 Paris Cedex 16 Tel. (33-1) 45.24.82.00
Telefax: (33-1) 49.10.42.76
Telex: 640048 OCDE
Orders via Minitel, France only/
Commandes par Minitel, France exclusivement :
36 15 OCDE

OECD Bookshop/Librairie de l'OCDE :
33, rue Octave-Feuillet
75016 Paris Tel. (33-1) 45.24.81.67
(33-1) 45.24.81.81

Documentation Française
29, quai Voltaire
75007 Paris Tel. 40.15.70.00

Gibert Jeune (Droit-Économie)
6, place Saint-Michel
75006 Paris Tel. 43.25.91.19

Librairie du Commerce International
10, avenue d'Iéna
75016 Paris Tel. 40.73.34.60

Librairie Dunod
Université Paris-Dauphine
Place du Maréchal de Lattre de Tassigny
75016 Paris Tel. (1) 44.05.40.13

Librairie Lavoisier
11, rue Lavoisier
75008 Paris Tel. 42.65.39.95

Librairie L.G.D.J. - Montchrestien
20, rue Soufflot
75005 Paris Tel. 46.33.89.85

Librairie des Sciences Politiques
30, rue Saint-Guillaume
75007 Paris Tel. 45.48.36.02

P.U.F.
49, boulevard Saint-Michel
75005 Paris Tel. 43.25.83.40

Librairie de l'Université
12a, rue Nazareth
13100 Aix-en-Provence Tel. (16) 42.26.18.08

Documentation Française
165, rue Garibaldi
69003 Lyon Tel. (16) 78.63.32.23

Librairie Decitre
29, place Bellecour
69002 Lyon Tel. (16) 72.40.54.54

GERMANY – ALLEMAGNE
OECD Publications and Information Centre
August-Bebel-Allee 6
D-53175 Bonn Tel. (0228) 959.120
Telefax: (0228) 959.12.17

GREECE – GRÈCE
Librairie Kauffmann
Mavrokordatou 9
106 78 Athens Tel. (01) 32.55.321
Telefax: (01) 36.33.967

HONG-KONG
Swindon Book Co. Ltd.
13-15 Lock Road
Kowloon, Hong Kong Tel. 2376.2062
Telefax: 2376.0685

HUNGARY – HONGRIE
Euro Info Service
Margitsziget, Európa Ház
1138 Budapest Tel. (1) 111.62.16
Telefax : (1) 111.60.61

ICELAND – ISLANDE
Mál Mog Menning
Laugavegi 18, Pósthólf 392
121 Reykjavik Tel. 162.35.23

INDIA – INDE
Oxford Book and Stationery Co.
Scindia House
New Delhi 110001 Tel.(11) 331.5896/5308
Telefax: (11) 332.5993

17 Park Street
Calcutta 700016 Tel. 240832

INDONESIA – INDONÉSIE
Pdii-Lipi
P.O. Box 4298
Jakarta 12042 Tel. (21) 573.34.67
Telefax: (21) 573.34.67

IRELAND – IRLANDE
Government Supplies Agency
Publications Section
4/5 Harcourt Road
Dublin 2 Tel. 661.31.11
Telefax: 478.06.45

ISRAEL
Praedicta
5 Shatner Street
P.O. Box 34030
Jerusalem 91430 Tel. (2) 52.84.90/1/2
Telefax: (2) 52.84.93

R.O.Y.
P.O. Box 13056
Tel Aviv 61130 Tél. (3) 49.61.08
Telefax (3) 544.60.39

ITALY – ITALIE
Libreria Commissionaria Sansoni
Via Duca di Calabria 1/1
50125 Firenze Tel. (055) 64.54.15
Telefax: (055) 64.12.57

Via Bartolini 29
20155 Milano Tel. (02) 36.50.83

Editrice e Libreria Herder
Piazza Montecitorio 120
00186 Roma Tel. 679.46.28
Telefax: 678.47.51

Libreria Hoepli
Via Hoepli 5
20121 Milano Tel. (02) 86.54.46
Telefax: (02) 805.28.86

Libreria Scientifica
Dott. Lucio de Biasio 'Aeiou'
Via Coronelli, 6
20146 Milano Tel. (02) 48.95.45.52
Telefax: (02) 48.95.45.48

JAPAN – JAPON
OECD Publications and Information Centre
Landic Akasaka Building
2-3-4 Akasaka, Minato-ku
Tokyo 107 Tel. (81.3) 3586.2016
Telefax: (81.3) 3584.7929

KOREA – CORÉE
Kyobo Book Centre Co. Ltd.
P.O. Box 1658, Kwang Hwa Moon
Seoul Tel. 730.78.91
Telefax: 735.00.30

MALAYSIA – MALAISIE
University of Malaya Bookshop
University of Malaya
P.O. Box 1127, Jalan Pantai Baru
59700 Kuala Lumpur
Malaysia Tel. 756.5000/756.5425
Telefax: 756.3246

MEXICO – MEXIQUE
Revistas y Periodicos Internacionales S.A. de C.V.
Florencia 57 - 1004
Mexico, D.F. 06600 Tel. 207.81.00
Telefax : 208.39.79

NETHERLANDS – PAYS-BAS
SDU Uitgeverij Plantijnstraat
Externe Fondsen
Postbus 20014
2500 EA's-Gravenhage Tel. (070) 37.89.880
Voor bestellingen: Telefax: (070) 34.75.778

NEW ZEALAND
NOUVELLE-ZÉLANDE
Legislation Services
P.O. Box 12418
Thorndon, Wellington Tel. (04) 496.5652
Telefax: (04) 496.5698

NORWAY – NORVÈGE
Narvesen Info Center – NIC
Bertrand Narvesens vei 2
P.O. Box 6125 Etterstad
0602 Oslo 6 Tel. (022) 57.33.00
Telefax: (022) 68.19.01

PAKISTAN
Mirza Book Agency
65 Shahrah Quaid-E-Azam
Lahore 54000 Tel. (42) 353.601
Telefax: (42) 231.730

PHILIPPINE – PHILIPPINES
International Book Center
5th Floor, Filipinas Life Bldg.
Ayala Avenue
Metro Manila Tel. 81.96.76
Telex 23312 RHP PH

PORTUGAL
Livraria Portugal
Rua do Carmo 70-74
Apart. 2681
1200 Lisboa Tel.: (01) 347.49.82/5
Telefax: (01) 347.02.64

SINGAPORE – SINGAPOUR
Gower Asia Pacific Pte Ltd.
Golden Wheel Building
41, Kallang Pudding Road, No. 04-03
Singapore 1334 Tel. 741.5166
Telefax: 742.9356

SPAIN – ESPAGNE
Mundi-Prensa Libros S.A.
Castelló 37, Apartado 1223
Madrid 28001 Tel. (91) 431.33.99
Telefax: (91) 575.39.98

Libreria Internacional AEDOS
Consejo de Ciento 391
08009 – Barcelona Tel. (93) 488.30.09
Telefax: (93) 487.76.59

Llibreria de la Generalitat
Palau Moja
Rambla dels Estudis, 118
08002 – Barcelona
(Subscripcions) Tel. (93) 318.80.12
(Publicacions) Tel. (93) 302.67.23
Telefax: (93) 412.18.54

SRI LANKA
Centre for Policy Research
c/o Colombo Agencies Ltd.
No. 300-304, Galle Road
Colombo 3 Tel. (1) 574240, 573551-2
Telefax: (1) 575394, 510711

SWEDEN – SUÈDE
Fritzes Information Center
Box 16356
Regeringsgatan 12
106 47 Stockholm Tel. (08) 690.90.90
Telefax: (08) 20.50.21

Subscription Agency/Agence d'abonnements :
Wennergren-Williams Info AB
P.O. Box 1305
171 25 Solna Tel. (08) 705.97.50
Téléfax : (08) 27.00.71

SWITZERLAND – SUISSE
Maditec S.A. (Books and Periodicals - Livres et périodiques)
Chemin des Palettes 4
Case postale 266
1020 Renens VD 1 Tel. (021) 635.08.65
Telefax: (021) 635.07.80

Librairie Payot S.A.
4, place Pépinet
CP 3212
1002 Lausanne Tel. (021) 341.33.47
Telefax: (021) 341.33.45

Librairie Unilivres
6, rue de Candolle
1205 Genève Tel. (022) 320.26.23
Telefax: (022) 329.73.18

Subscription Agency/Agence d'abonnements :
Dynapresse Marketing S.A.
38 avenue Vibert
1227 Carouge Tel.: (022) 308.07.89
Telefax : (022) 308.07.99

See also – Voir aussi :
OECD Publications and Information Centre
August-Bebel-Allee 6
D-53175 Bonn (Germany) Tel. (0228) 959.120
Telefax: (0228) 959.12.17

TAIWAN – FORMOSE
Good Faith Worldwide Int'l. Co. Ltd.
9th Floor, No. 118, Sec. 2
Chung Hsiao E. Road
Taipei Tel. (02) 391.7396/391.7397
Telefax: (02) 394.9176

THAILAND – THAÏLANDE
Suksit Siam Co. Ltd.
113, 115 Fuang Nakhon Rd.
Opp. Wat Rajbopith
Bangkok 10200 Tel. (662) 225.9531/2
Telefax: (662) 222.5188

TURKEY – TURQUIE
Kültür Yayinlari Is-Türk Ltd. Sti.
Atatürk Bulvari No. 191/Kat 13
Kavaklidere/Ankara Tel. 428.11.40 Ext. 245
Dolmabahce Cad. No. 29
Besiktas/Istanbul Tel. 260.71.8
Telex: 43482

UNITED KINGDOM – ROYAUME-UNI
HMSO
Gen. enquiries Tel. (071) 873 001
Postal orders only:
P.O. Box 276, London SW8 5DT
Personal Callers HMSO Bookshop
49 High Holborn, London WC1V 6HB
Telefax: (071) 873 820
Branches at: Belfast, Birmingham, Bristol, Edinburgh, Manchester

UNITED STATES – ÉTATS-UNIS
OECD Publications and Information Centre
2001 L Street N.W., Suite 700
Washington, D.C. 20036-4910 Tel. (202) 785.63
Telefax: (202) 785.03

VENEZUELA
Libreria del Este
Avda F. Miranda 52, Aptdo. 60337
Edificio Galipán
Caracas 106 Tel. 951.1705/951.2307/951.12
Telegram: Libreste Carac

Subscription to OECD periodicals may also be placed through main subscription agencies.

Les abonnements aux publications périodiques de l'OCDE peuvent être souscrits auprès des principales agences d'abonnement.

Orders and inquiries from countries where Distributors have not yet been appointed should be sent to: OECD Publications Service, 2 rue André-Pascal, 75775 Paris Cedex 16, France.

Les commandes provenant de pays où l'OCDE n'a pas encore désigné de distributeur peuvent être adressées à : OCDE, Service des Publications, 2, rue André-Pascal, 75775 Paris Cedex 16, France.

OECD PUBLICATIONS, 2 rue André-Pascal, 75775 PARIS CEDEX 16
PRINTED IN FRANCE
(66 95 05 1) ISBN 92-64-14376-9 - No. 47740 1995